170(3), 2017

COMBUSTION ENGINES


BUS
OF THE YEAR
2017
U12 CNGSOLARIS
PO 899 B
SOLARIS
WSPÓLNY
KIERUNEK ›
Zmieniamy oblicze komunikacji miejskiej
www.solarisbus.com

PTNSS Supporting Members
Członkowie wspierający PTNSS

BOSMAL Automotive Research and Development Institute Ltd
Instytut Badań i Rozwoju Motoryzacji BOSMAL Sp. z o.o

Motor Transport Institute
Instytut Transportu Samochodowego

The Institute for Sustainable Technologies
Instytut Technologii Eksploatacji

Institute of Aviation
Instytut Lotnictwa

Automotive Industry Institute
Przemysłowy Instytut Motoryzacji

The Rail Vehicles Institute TABOR
Instytut Pojazdów Szynowych TABOR

Institute of Mechanised Construction and Rock Mining
Instytut Mechanizacji Budownictwa i Górnictwa Skalnego

Institute of Logistics and Warehousing
Instytut Logistyki i Magazynowania

Industrial Institute of Agricultural Engineering
Przemysłowy Instytut Maszyn Rolniczych

AVL List GmbH

Solaris Bus & Coach S.A.

Air Force Institute of Technology
Instytut Techniczny Wojsk Lotniczych

COMBUSTION ENGINES

A Scientific Magazine

2017, 170(3)

Year LVI

PL ISSN 2300-9896

Editor:

Polskie Towarzystwo Naukowe Silników Spalinowych
43-300 Bielsko-Biała, Sarni Stok 93 Street, Poland
tel.: +48 33 8130402, fax: +48 33 8125038
E-mail: sekretariat@ptnss.pl
WebSite: http://www.ptnss.pl
Papers available on-line: http://combustion-engines.eu

Editorial:
Institute of Combustion Engines and Transport
Poznan University of Technology
60-965 Poznan, Piotrowo 3 Street
tel.: +48 61 2244505, +48 61 2244502
E-mail: papers@ptnss.pl

Prof. Jerzy Merkisz, DSc., DEng. (Editor-in-chief)
Miłosław Kozak, DSc., DEng. (Editorial Secretary for Science) – papers@ptnss.pl
Ireneusz Pielecha, DSc., DEng. (Technical Editor)
Krystyna Bubacz, MSc. (Proofreading Editor)
Wojciech Serdecki, DSc., DEng. (Statistical Editor)
and Associate Editors

Contents

Editor
Polish Scientific Society of Combustion Engines
43-300 Bielsko-Biała, Sarni Stok 93 Street, Poland
tel.: +48 33 8130402, fax: +48 33 8125038
E-mail: sekretariat@ptnss.pl
WebSite: http://www.ptnss.pl

Subscriptions
Send subscription requests to the Publisher's address.
Cost of a single issue PLZ30 + VAT.

Preparation for print
ARS NOVA Publishing House
60-782 Poznań, ul. Grunwaldzka 17/10A

Circulation: 700 copies.

Printing and binding
Zakład Poligraficzny Moś i Łuczak, sp. j., Poznań, ul. Piwna 1

The journal is registered in the Polish technical journals content database – **BAZTECH** www.baztech.icm.edu.pl

The journal is listed in the international database **IC Journal Master List** – **Index Copernicus** www.indexcopernicus.com

Declaration of the original version
The original version of the Combustion Engines journal is the printed version.

Papers published in the ***Combustion Engines*** quarterly receive 13 points as stated by the Notification of the Minister of Science and Higher Education dated 31 December 2015.

Cover
I – Infiniti Twin-Turbo V6 Engine (*fot. www.infinitiusa.com*), background (© VIGE.co – *pl.fotolia.com*)
IV – Variable Compression Ratio by FEV (*fot. vcr.fev.com*)

Article citation info:
TULWIN, T., WENDEKER, M., CZYŻ, Z. The swirl ratio influence on combustion process and heat transfer in the opposed piston compression-ignition engine. *Combustion Engines*. 2017, **170**(3), 3-7. DOI: 10.19206/CE-2017-301

Tytus TULWIN
Mirosław WENDEKER
Zbigniew CZYŻ

CE-2017-301

The swirl ratio influence on combustion process and heat transfer in the opposed piston compression-ignition engine

In order to maximise engine heat efficiency an engines charge flow must be properly designed -especially its swirl and tumble ratio. A two-stroke compression-ignition opposed piston engine reacts to engine swirl differently compared to a standard automotive engine with axially symmetric combustion chamber. In order to facilitate direct fuel injection, high-pressure injectors must be positioned from the side of combustion chamber. Depending on the combustion chamber geometry the swirling gases impact greatly how the injection stream is formed. If the deformation is too high the high temperature combustion gases can hit the piston surface or get into gaps between the pistons. This greatly affects the heat lost to the pistons and raises their local temperature. More atomised injection stream is more prone to swirling gas flow due to its reduced droplet size and momentum. The paper presents simulation results and analyses for different intake process induced swirl ratios and different types of combustion chambers in an experimental aviation opposed piston engine.

Key words: *opposed, two-stroke, combustion, heat, diesel*

1. Introduction

The compression ignition engines are more thermodynamically efficient than the SI engines, even though the theoretical thermodynamic cycle seems less efficient at first glance (heat capacity is higher for the constant pressure heat addition). Higher efficiency is achieved because of the lean combustion and higher compression ratio – not feasible in SI engines due to knock combustion phenomena. Lean combustion in an CI engine ensures better isolation of hot combustion gases from cold combustion chamber walls. This is the reason why proper injection, intake, exhaust and combustion process design is important for the heat loses. Additionally, some energy can be recuperated with turbocompressor. In order to isolate hot combustion gases from chamber walls an indentation in the piston is introduced. During the injection, nearly all gas mixture is enclosed by that indentation. Additionally, squeezing all gas into small confined volume creates a "squish" phenomena which amplifies swirling motion and turbulence properties. The smaller the combustion chamber active area the smaller the heat flux will be. This is why it is favourable to make more spherical combustion chamber as sphere has the best volume to surface ratio

The swirling motion of the gas is defined by axial swirl and radial swirl called "tumble". In order to estimate the swirl ratio, an axis of rotation have to be known. The swirl ratio can be calculated with formula:

$$R_s = \frac{60}{2\pi n} \frac{-\sum_i m_i[(x_i - x_C)v_i - (y_i - y_C)u_i]}{\sum_i m_i[(x_i - x_C)^2 - (y_i - y_C)^2]} \quad (1)$$

where C = (x_c, y_c, z_c) represents the center of mass of the whole combustion chamber gas region [1].

2. Materials and Methods

The paper presents the simulation results of thermodynamic CFD hypothetical two stroke compression ignitions opposed engine simulations, that is being designed for use in light aircraft. High power to weight ratio and thermal efficiency are the key values of the engine. Designing a new engine is bound to many uncertainties and variables. In order to investigate engine working cycle phenomena, the simulation is split into combustion and intake/exhaust parts (Fig. 1).

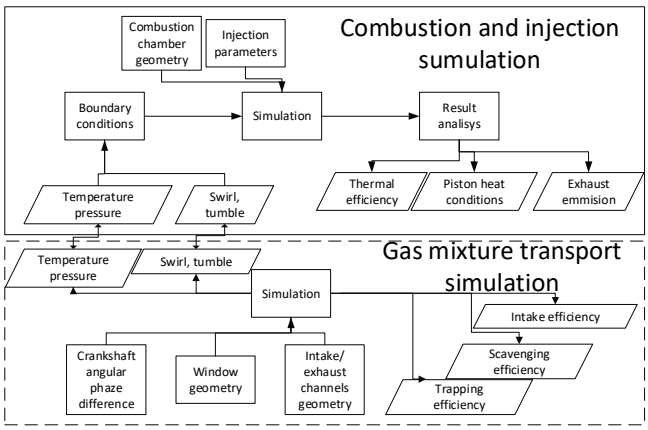

Fig. 1. Information flow diagram for engine work cycle optimization simulations

The gas transport simulation is intended to find optimal intake and exhaust windows geometry for a required mass that needs to be transported into combustion chamber, required swirl, tumble and minimal energy loses. In order to find out what swirl ratio will be best for a given load a combustion simulation is conducted with variable swirl ratio as an initial condition. The combustion simulation therefore stars after intake windows close and finishes before the exhaust windows open. It allows for combustion chamber geometry and injection parameters optimization, maximising engine heat efficiency and minimizing heat flux through chamber walls. This paper presents mainly the impact of varying swirl ratio on combustion process. The simulations were performed in the AVL Fire software. Throughout the optimization process many combustion chamber geometries were developed. Some of them are presented in Fig. 2. Geometry v4 is the simplest one with

symmetry in all perpendicular planes. Geometries v4, v7 and v8 are further improvements, with increased sphericity of piston bowl and with flow disturbing edges deformations.

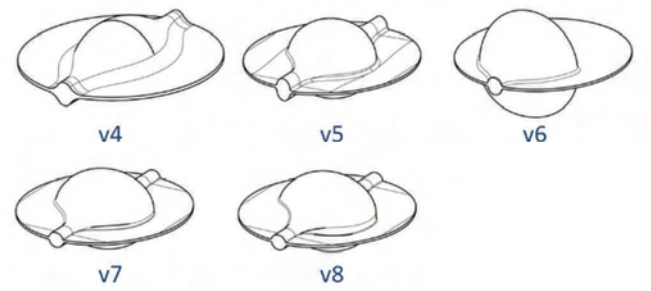

Fig. 2 Geometry versions of the combustion chamber

They intend to change the rotation axis of initially cylinder axial swirl. Geometry v6 is designed for only one injector. Table 1 shows engine parameters. Study [2] presents similar engine with swirl ratio analysis.

Table 1. Engine parameters

Bore	65.5 mm
Stroke	76.4 mm
Displacement volume	514607 mm^3
TDC comb. cha. volume	21850 mm^3
Compression ratio	24.5
Connecting rod	125 mm
Crankshafts axis distance	325.1 mm
Crank angle shift	24° CA
Crankshaft rotational speed	4000 min-1

The simulation starts at angle 610° CA and ends at 800° CA. The initial parameters presented in Table 2 are set for angle 610° CA.

Table 2. Simulation parameters and initial conditions

Parameter	Value
Simulation range	610-800° CA (720°=TDC)
Pressure	194634 Pa
Temperature	428 K
Turbulent kinetic energy	30 m^2/s^2
Turbulence length scale	0.0013 m
Turbulent dissipation rate	20769.2 m^2/s^3
Laminar flame speed	Maghalchi & Keck
EGR composition	0.63
Lower heating value	43,400 MJ/kg
Cylinder temperature boundary condtition	373 K
Piston temperature boundary condtition	443 K
Heat transfer wall model	Standard wall function

3. Results

The increase of axial swirl rotational speed tends to higher redirection of the fuel stream from its axial hole direction due to higher local tangential velocities. Also, higher turbulence provides better atomization of the fuel droplets and higher combustion flame front area. This leads to faster combustion and higher thermodynamic efficiency. On the other hand, if the swirl ratio is too negative effects can occur. Increasing high swirl increases the pumping loses. The hot post combustion gases can be scattered throughout the colder combustion regions, intensifying the heat transfer to the combustion chamber walls. During the combustion and gas expansion phase the increased heat transfer leads to decreased thermodynamic cycle efficiency. The heat addiction process is not as isochoric and the gas expansion process is not as adiabatic. Additionally, high swirl ratio means higher local gas velocity close to the chamber walls. This increase the heat transfer coefficient what also increase the heat transfer. Similar conclusions were drawn studies [3, 4].

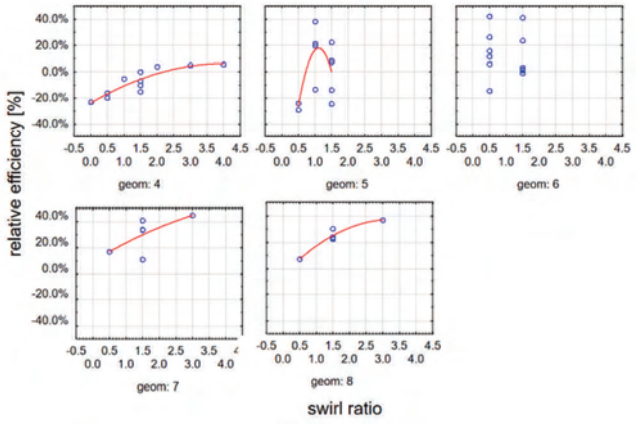

Fig. 3. Relative efficiency and swirl ratio for different geometries

Around 60 cases were calculated for different combustion chambers and injection parameters. Some trends can be distinguished when we compare the results. Figure 3 presents how relative efficiency changes with the change of swirl ratio. All Geometries show similar trend, where increasing swirl ratio increases the relative efficiency up to certain maximum point and any further increase decreases the efficiency. This happens because after certain point the increased convective heat transfer has bigger impact than increase of turbulent flame speed and reaction rate.The heat loses seem to follow a linear trend with the increase of swirl ratio. This is because the heat transfer coefficent is fairly proportional to the increase of tangenal near wall velocity. All geometries follow a steady linear trend of relative heat loss vs. swir ratio.

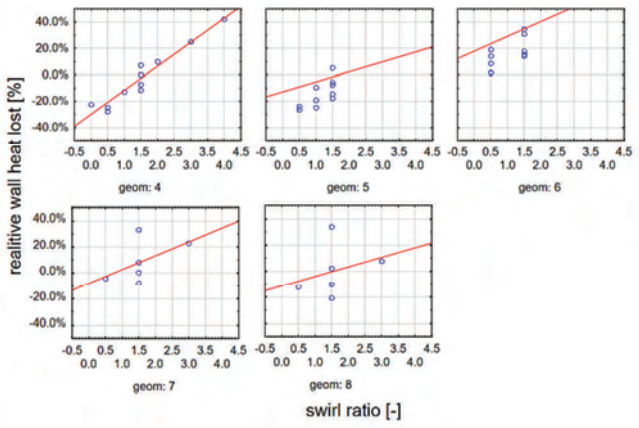

Fig. 4. Relative efficiency and swirl ratio for different geometries

Figure 5 presents simulation results for geometry v4. Swirl ratio = 0 result in poor flame surface propagation, low flame velocity and poor injection atomisation. Two injection streams meat at the middle of combustion chamber and expand uniformly in all directions. Increasing the swirl ratio causes the injection streams to deflect from their axial direction. This causes an increased flame front surface and faster combustion.

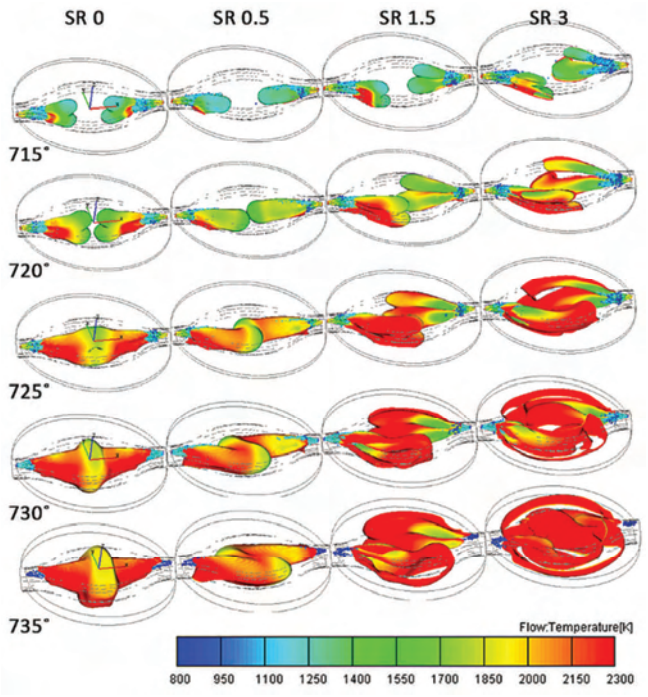

Fig. 5. Injection and combustion visualisation for 4 different swirl ratios and different crank angle potions

Increasing the swirl ratio higher cause the hot gases to flow between the in-between pistons gaps increasing heat loses to pistons and cylinder walls. Therefore, it is important to choose the optimal swirl ratio for a given case. Another study of an opposed piston dual injection engine also shows that there is an optimal swirl ratio for maximum IMEP [5].

Figure 6 shows that increasing the swirl ratio leads to faster combustion process and to higher maximum rate of heat release. This is the biggest factor for the thermal efficiency increase. The values of heat release are high compared to study [6] where lower compression ratio engine is investigated but the trend of swirl ratio impact is similar.

Piston heat load

In order to analyse the heat load in comparative way the heat flux was recorded (Fig. 7). It is clearly visible that the increase of swirl ratio increase the heat transfer rate throughout the whole cycle. The heat rate peaks near the end of the injection process when nearly all fuel is burned and hot gases come close to combustion chamber walls.

The time integration of heat flux gives the total cumulative energy transferred via convection through the chamber walls (Fig. 8). The increase of swirl ratio increases the total chamber walls heat transfer as the gas temperature and heat transfer coefficient increase. Most heat is transferred through the piston walls, as they compose most surface area of the combustion chamber during the combustion phase. There is no cylinder head so instead most heat is loaded on the pistons. This is the main reason why it is essential to predict convective heat transfer loads in the design process of the engine.

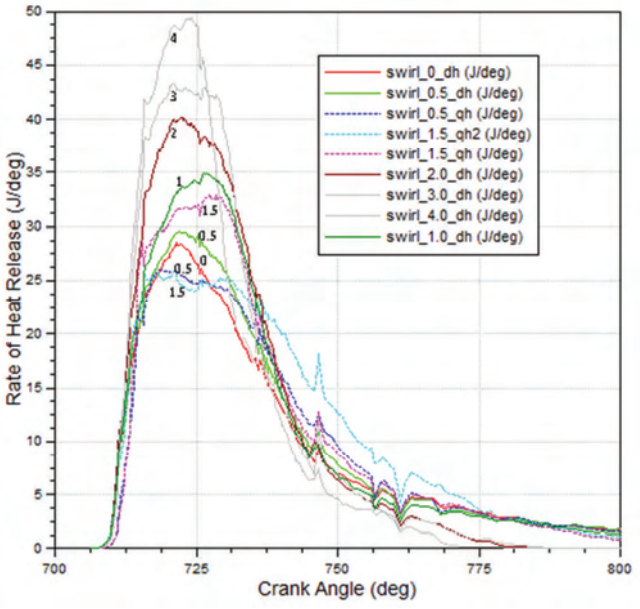

Fig. 6. Rate of heat release in respect to the crank angle for different swirl ratios

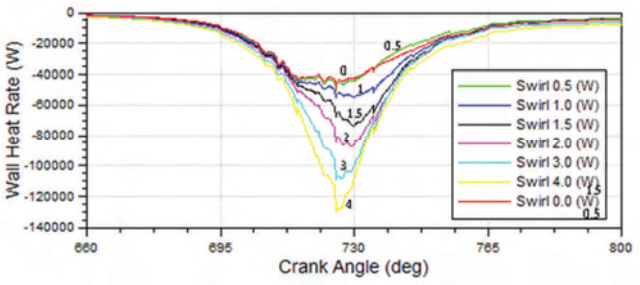

Fig. 7. Heat rate through combustion chamber walls at different crank ankle positions

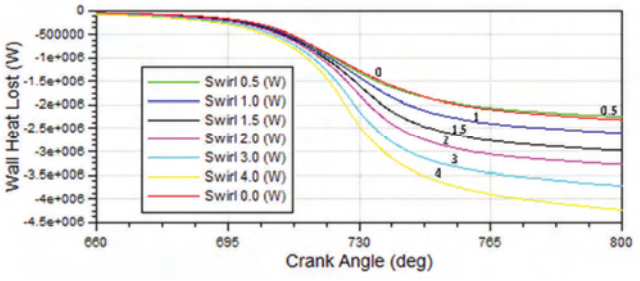

Fig. 8. Cumulative heat transferred through combustion chamber walls at different crank angle positions

The results show that the heat flux can vary vastly with the change of swirl ratio, injection parameters and combustion chamber geometry. It is very important not to exceed the temperature limits if the piston materials. The temperature affects piston strength limits and its thermal expansion.

Also, if the temperature is too high the oil density and its lubrication abilities decrease. This causes high cylinder wear what decreases engines service life.

Emmision

The ECFM-3Z+ combustion model allows detailed post flame chemistry, especially the NOx emission. Figure 9 presents the NO mass fraction against the crank angle for different swirl ratios. The increase of swirl ratio leads to more turbulent therefore faster combustion further increasing the in-cylinder peak gas temperature. Therefore, the increase in swirl ratio tend to increase the NO emission. Following studies show similar trend [7, 8].

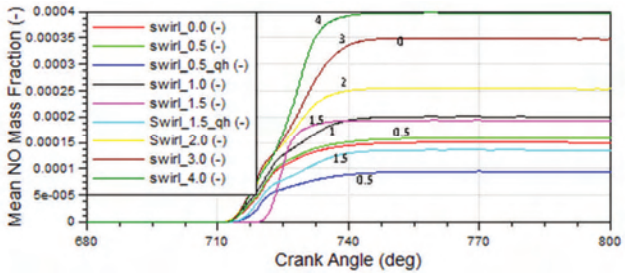

Fig. 9. Mean NO mass fraction at different crank angle positions and different swirl ratios

Soot deposes in the regions of rich mixture in certain temperatures. Because in CI engines diffusion flame is dominant, soot forms in the local rich regions. Due to the high temperature and lean conditions soot a vast amount of soot burn long after the injection process (Fig. 10).

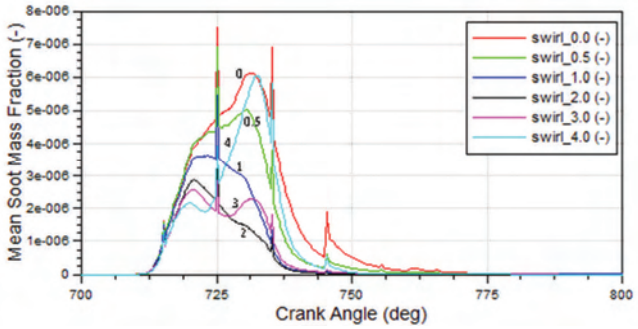

Fig. 10. Mean soot mass fraction in respect to the crank angle for different swirl ratios

Increasing the swirl ratio decreases the amount of soot formed, because better mixture turbulization increases the chance of succesfull post flame combustion. The soot levels are high for all cases when we compare it to european automotive standards.

Study [9] shows an opposite trend for a different engine, because the injection fuel has much higher contact with combustion chamber bowl walls. The main idea of chamber being designed is to limit this contact as much as possible. Figure 11 shows that with the increase in swirl the CO emission decreases both for a maximum value and final value after combustion and expansion process. Increasing swirl ratio has negative effect on NO emission and positive effect on soot and CO formation. Similar considerations can be found in [10, 11].

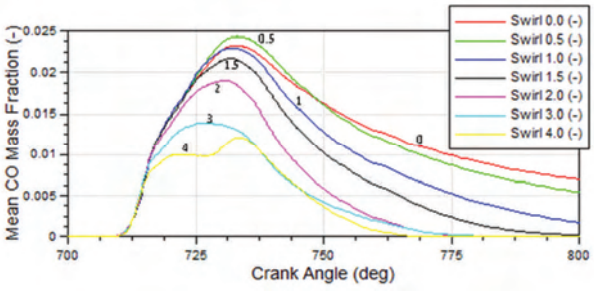

Fig. 11. Mean CO mass fraction against crank angle position for different swirl ratios

4. Discussion

The distance between the injection stream and chamber walls has a big impact on combustion process. If the fuel meets cold chamber wall before it evaporates it may not be combusted leading to incomplete combustion. This has negative effect on exhaust emission and indicated power. Even during combustion when the flame front meets cold chamber walls the heat efficiency drops dramatically, as the heat is inevitably lost via cooling. The shape of combustion chamber also induces swirl, tumble and squish. The swirling flow has a big influence on fuel stream trajectory, fuel atomisation and evaporation and combustion process itself including the turbulent flame speed. Piston induced squish forces the mixture into small spherical piston bowl. Decreased gas inertia increases the swirl rotational velocity. After heat addition with increased temperature the gas kinematic viscosity increases too. This makes the swirl dissipate faster and further decrease its rotational velocity through the gas expansion process. Higher swirl makes the injection fuel stream deflect more (fig. 5). The fuel droplet atomisation is better and the flame surface area increases. The larger the flame surface area the faster the combustion process, making the thermal efficiency higher. If the swirl ratio is too high the efficiency decreases. As the heat loses to the walls linearly increase with the swirl ratio, the combustion speed increases with decreasing gradient until its maximum. Also, high swirl ratio tends to force the hot gases to the gap between the pistons, decreasing the heat that is transformed into pressure. When we increase the swirl ratio the combustion process is faster and makes the heat addition process more isochoric and the overall heat efficiency is higher. The increased heat transfer coefficient negatively impacts the engine conditions. Increased heat transfer increases the heat load on the pistons. In such engine, it is important to maintain piston temperature below its limits. High Hotspots can occur in some locations, intensifying soot and hydrocarbons emission. To sum up:

- for simulated cases swirl ratio between 1 and 1.5 gives best efficiency with acceptable amount of heat load to the pistons,
- increasing swirl ratio has negative effect on NO emission and positive effect on soot and CO formation,
- for the perpendicular to cylinder axis injectors orientation the swirl ratio has a big influence on the injection trajectory.

5. Acknowledgments

Prepared in collaboration with WSK PZL-Kalisz S.A design office.

Nomenclature

CI compression ignition
DI direct injection
CA crank angle
EGR exhaust gas recirculation
SI spark ignition
TDC tom dead center
IMEP -indicated mean effective pressure.

Bibliography

[1] PERIN, F., MILES, P.C., REITZ, R.D. A comprehensive modeling study of in-cylinder fluid flows in a high-swirl, light-duty optical diesel engine. *Computers & Fluids*. 2014, **105**, 113-124.

[2] MA, F., ZHAO, C., ZHANG, F. et al. Effects of scavenging system configuration on in-cylinder air flow organization of an opposed-piston two-stroke engine. *Energies*. 2015, **8**, 5866-5884.

[3] OLMEDA, P., MARTIN, J., GARCIA, A. et al. A combination of swirl ratio and injection strategy to increase engine efficiency. *SAE Technical Paper*. 2017, **10**(3).

[4] KOCSIS, M.C., JOO, S., BRIGGS, T., ALGER, T. Impact of swirl ratio on combustion performance of a non-pent roof combustion chamber engine. *SAE Technical Paper*. 2015.

[5] ZHANG, Z., ZHAO, C., XIE, Z. et al. Study on the effect of the nozzle diameter and swirl ratio on the combustion process for an opposed-piston two-stroke diesel engine. *Energy Procedia*. 2014, 542-546.

[6] PERINI, F., DEMPSEY, A., REITZ, R.D. et al. A computational investigation of the effects of swirl ratio and injection pressure on mixture preparation and wall heat transfer in a light-duty diesel engine. *SAE Technical Paper*. 2013.

[7] GAFOOR, A., GUPTA, R. Numerical investigation of piston bowl geometry and swirl ratio on emission from diesel engines. *Energy Conversion and Management*. 2015, **101**, 541-551.

[8] KOOK, S., KOOK, S., MILES, P.C. et al. The effect of swirl ratio and fuel injection parameters on CO emission and fuel conversion efficiency for high-dilution, low-temperature combustion in an automotive diesel engine. *SAE Technical Paper*. 2006, 2006-01-0197.

[9] WEI, S., JI, K., LENG, X. et al. Numerical analysis on the effect of swirl ratios on swirl chamber combustion system of DI diesel engines. *Energy Conversion and Management*. 2013, **75**, 184-190.

[10] SU, L., LI, X., HE, X. LIU, F. Experimental research on the diffusion flame formation and combustion performance of forced swirl combustion system for DI diesel engines. *Energy Conversion and Management*. 2015, **106**, 826-834.

[11] LIA, X., ZHOUA, H., SUB, L. et al. Combustion and emission characteristics of a lateral swirl combustion system for DI diesel engines under low excess air ratio conditions. Fuel. 2016, 184, 672-680.

Tytus Tulwin, MEng. – Faculty of Mechanical Engineering at Lublin University of Technology.

e-mail: *T.Tulwin@pollub.pl*

Prof. Mirosław Wendeker, DSc., DEng. – Faculty of Mechanical Engineering at Lublin University of Technology.

e-mail: *M.Wendeker @pollub.pl*

Zbigniew Czyż, MEng. – Faculty of Mechanical Engineering at Lublin University of Technology.

e-mail: *Z.Czyz@pollub.pl*

Article citation info:
BIAŁY, M., PIETRYKOWSKI, K., TULWIN, T., MAGRYTA, P. CFD numerical simulation of the indirect cooling system of an internal combustion engine. *Combustion Engines*. 2017, **170**(3), 8-18. DOI: 10.19206/CE-2017-302

Michał BIAŁY
Konrad PIETRYKOWSKI
Tytus TULWIN
Paweł MAGRYTA

CE-2017-302

CFD numerical simulation of the indirect cooling system of an internal combustion engine

The paper presents an analysis of the fluid flow in the cooling system of an internal combustion engine with oposite pistons. The purpose of the work was to optimize the flow of fluid through the channels located in the engine block. Simulation studies and subsequent iterations were performed using Ansys Fluent software. Two-equation k-epsilon turbulence model was used in the simulation model. Boundary and initial conditions were taken from previously made simulations conducted in AVL Boost software. The average wall temperature of the cylinder and the temperature of the outer walls of the cylinder were assumed for simulations. The results of the analyzes were graphically illustrated by the speed streamline distribution of velocity fields and temperature.

Key words: *Ansys Fluent, combustion engine, computational fluid dynamics CFD, cooling system*

1. Introduction

CFD method is one of the most rapidly growing nowadays. It is used in all areas of life. Beginning with medicine, by simulating blood flow in major arteries and finishing with the engineering activities, i.e. simulations of the flow around the obstacle. CFD allows to reduce the cost of producing an item. Rather than producing and testing an object by experimentation, it can be tested using the simulation tools. CFDs provide the opportunity for modification of geometry, changing boundary conditions and observing their impact on the key parameters. Both fluid and energy flows can be analyzed [1, 3].

The internal combustion engine generates the energy contained in the gas pressure and the heat from the combustion of the fuel in each cycle. On one hand the energy of the gas pressure is converted to mechanical energy. On the other hand, heat energy must be drained out of the system.

Cumulating of heat energy can lead to an increase in the thermal loads of individual engine components, thus accelerating their wear and tear. Too low or too high heat energy directly affects the combustion process, significantly worsening it. Therefore, it was decided to carry out a numerical studies using the CFD method to calculate the amount of heat flowing from the combustion chamber to the cooling system, through the fluid jacket placed in the engine block. As a research object, a research three cylinder engine with a opposite pistons was used [5].

2. CFD simulations

The element that receives the heat from the system in the internal combustion engine is the fluid (working medium). There are two different methods of receiving the energy: forced or gravitational, air or coolant. In the presented engine with opposing arrangement of the pistons (Fig. 1) the cylinders are placed in the block (wet bushings). In each of the cylinders between intake and outlet windows, the cylinder wall is in contact with the cooling fluid. The heat generated during the combustion of the fuel is transported to the outlet manifold (through the outlet windows) along with the hot exhaust gases and to the cylinder walls. Then the energy is taken over by the cooling fluid and then transported to a radiator in which the energy is dispersed into the environment [6, 8].

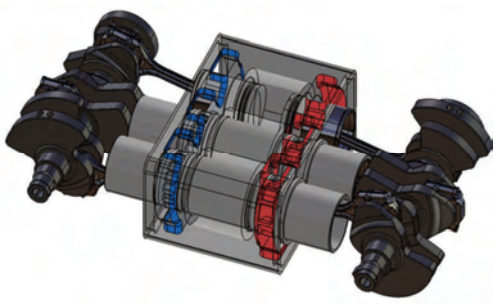

Fig. 1. CAD model of the engine

The engine with opposing pistons is a three-cylinder unit that will be used to drive lightweight gyrocopters. The engine will be characterized by a power of 100 kW, with a capacity of about 1600 cm^3, with a diesel cycle. The unit will have three cylinders with opposing pistons positions and two crankshafts facing each other. The engine will be equipped with a piston timing system and a direct diesel injection system to the inside of the cylinder.

CFD computer method was used to calculate the efficiency of a fluid jacket (Fig. 2) of the designed engine. The jacket geometrical model was created by "subtract" operation from the previously designed engine block, the "empty" part of the cooling channel was removed.

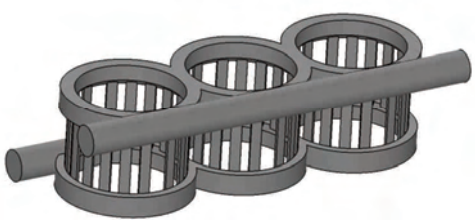

Fig. 2. CAD Model of fluid jacket

Computer fluid mechanics simulations were performed using ANSYS software in ver. 13.0.

The preparation of a simulation model using ANSYS software consisted of the following steps [7]:
- geometry preparation in CAD environment,
- geometry importing into the Geometry module,
- computational grid generation in Mesh module,
- assumption of the initial and boundary conditions,
- carrying out simulations of the heat flow,
- analysis of results.

2.1. Grid generation

The CAD model of the fluid jacket (Fig. 2) was transferred from CATIA V5 software in STP format. This is a standard format for exchanging product model data. STP files are used to store 3D image data in ASCII format, in accordance with ISO 10303-21 standards. Thus obtained geometry was imported to the Geometry module. This module allows for preparation of a model to generate a calculation grid and to modify the geometry, or perform boolean operations. In addition, the module can be coupled with CAD software, enabling live geometry updating in ANSYS after changes made in CAD model. Figure 5 shows the geometry model of the jacket in Geometry module [2].

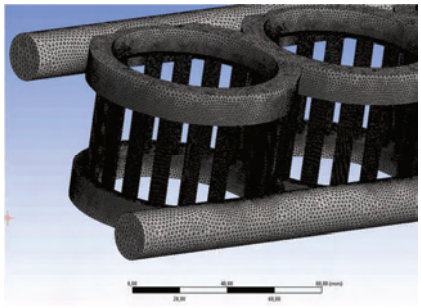

Fig. 3. Computational grid of fluid jacket model, with a minimum element size of 0.4 mm

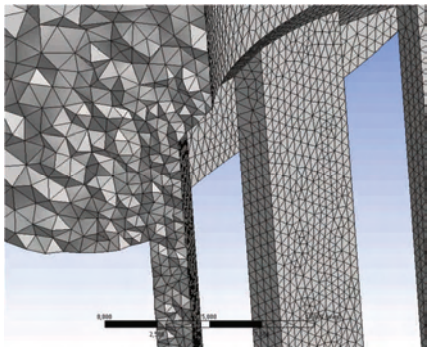

Fig. 4. Cross-section of computational grid of fluid jacket model, with a minimum element size of 0.4 mm

Such prepared geometry was imported into the Mesh module. This module allows to generate a computational grid based on the finite element method FEM. It is one of the most important steps in creating a CFD simulation. It depends on the correct definition of resolution, dimensions and number of calculation elements. This stage should be carefully analyzed as it is a parameter that has a measurable impact on the accuracy of the obtained results and the time of calculations. Optimal selection of grid resolution depends largely on the complexity of the analyzed object, its size and the thickness of the walls. Figure 3 shows the target grid of the model consisting of over 6,000,000 elements, and Fig. 4 shows the cross-section of the grid through the rib (channel along the cylinder axis).

2.2. Initial and boundary conditions

Simulation studies of the amount of heat received from the combustion chamber to the cooling system were made using ANSYS software in FLUENT module. Calculations were based on pressure-based solver. It is used for calculating the streams of incompressible and slightly compressible flows, with low flow velocity. In this approach, the obtained solution of the equation of pressure or equation of pressure correction is obtained from the equations of continuity and momentum. The model also includes the energy equations that allows the flow of heat energy and temperature recording at selected points. A k-omega (2 equ), SST viscosity model was also selected. This model (k-omega), well reflects the turbulent flow in the boundary layer, but is very sensitive to turbulent magnitudes in free flow. As a coolant fluid, water was assumed, but as the material of engine block the aluminum was selected and the as the material of cylinder a steel was chosen.

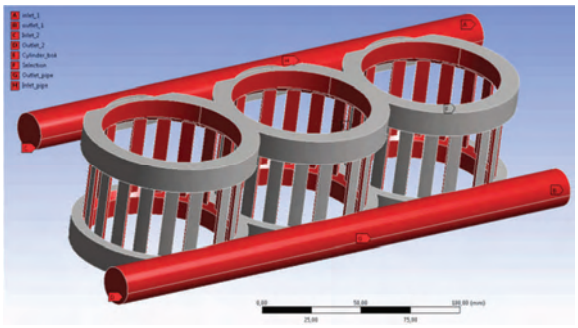

Fig. 5. The geometry model of the jacket in geometry module in Ansys Fluent

Boundary and initial conditions were taken from previously conducted simulations using AVL Boost software. The engine work was simulated for the state of operation of full load for a 4,000 rpm crankshaft rotational speed. The folowing assumptions were made:
- the cylinder wall surface:
  - wall temperature: 480 K (average cycle temperature),
  - wall thickness: 5 mm,
- engine block surface:
  - wall temperature: 323 K,
  - wall thickness: 5 mm,
- injectors placement surface („injectors” selection):
  - wall temperature: 480 K,
  - wall thickness: 5 mm,
- inlet surface („inlet” selection):
  - temperature: 363 K,
  - mass flow rate of the coolant: 0.3 kg/s,
  - turbulence intensity: 5%,
  - turbulence viscosity coefficient: 5%,
- outlet surface („outlet” selection):
  - temperature: 368 K (value assumed as the starting parameter),
  - turbulence intensity: 5%,

– turbulence viscosity coefficient: 5%,
– jackets surface outer/inner of cooling channels in block („wall" section):
  – walls temperature: 323 K,
  – wall thickness: 5 mm.

2.3. Calculations models

2.3.1. Influence of computational grid

In order to verify the influence of the size of the computational grid elements on the results of the simulations, a number of elementary mesh grid were developed for the geometry of the basic model. In all cases, the number of the elements was changed. Because of the flow phenomena, the most important place, with the smallest cross-sectional area, has been found, to be ribs running along the smooth surface of the cylinder.

Simulations were started with a mesh size of approximately 2 mm in the rib area, resulting in a total number of elements less than 600,000, ending in a 0.4 mm element size, resulting in a total number of approximately 6 million elements. Figure 4 shows the calculation grids with a minimum element size of 0.4 mm and figure 6 shows an intermediate mesh of 0.8 mm.

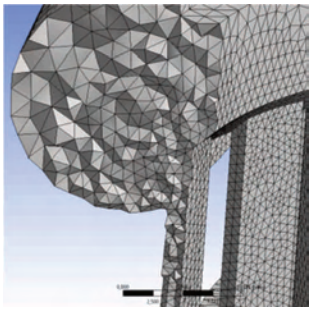

Fig. 6. Computational grid of fluid jacket model, with a minimum element size of 0.8 mm

2.3.2. Influence of turbulence

During the simulation a momentum equations and two-equation k-epsilon turbulence model were used. The k-epsilon model was adopted, with standard wall functions. Implicit coefficients such as were assumed [4]:
– C2-Epsilon = 1.9,
– TKE Prandtl Number = 1,
– TDR Prandtl Number = 1.2,
– Energy Prandtl Nubmer = 0.85.

In order to verify the effect of turbulence on the quality of simulation results, the turbulence intensity factor was changed. This ratio was in the range of 5 to 10%.

2.3.3. Geometrical calculations models

In order to optimize the flow of thermal energy during combustion of the fuel dose and transfer it to the cooling fluid, more than 20 geometric models were used for simulation tests. The different models differed in the intake and outlet diameters, the inlet and outlet manifold inclination angle, the water jacket splits individually for each cylinder, the enlargement and reduction of the fluid capacity above and below the ribs, the gradual gradation of the intake outlet channels, as to achieve a uniform flow in each of the cylinders or the assembly of the two inlet and outlet nozzles.

Among all analyzed models, the following versions can be distinguished:
– basic model used to determine the effect of calculating grid size and turbulence (Fig. 5),
– individual cylinder flow model (Fig. 7).

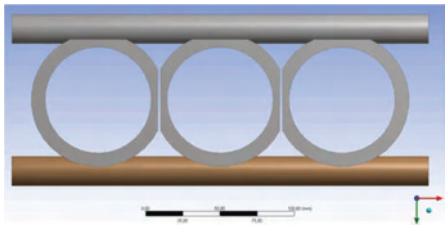

Fig. 7. Model with individual cylinder flow

– model with variable geometry of the intake and exhaust channels (Fig. 8),

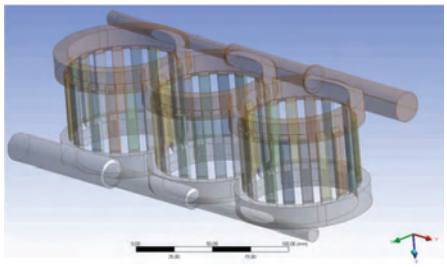

Fig. 8. Model with variable geometry of the intake and exhaust channels

– model for reducing flow resistance (Fig. 9),

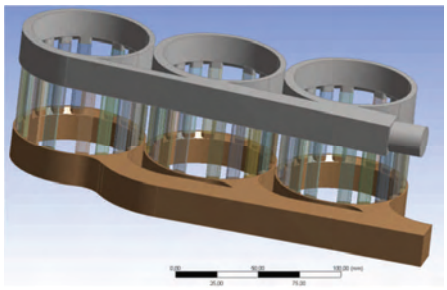

Fig. 9. Model for reducing flow resistance

– final model with the variable cross-section of the intake manifold at the cylinder inlet, double outlet channels with integrated joint outlet and inclination inlets of all ribs (Fig. 10).

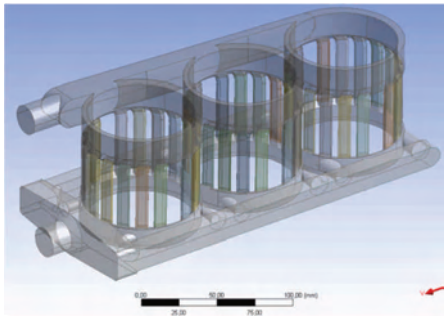

Fig. 10. Final model

2.4. Simulations results

Figures 11 to 17 show the results of the simulation studies in the form of the distribution of velocity fields of the working medium and the temperature fields on the model walls in the cylinder region.

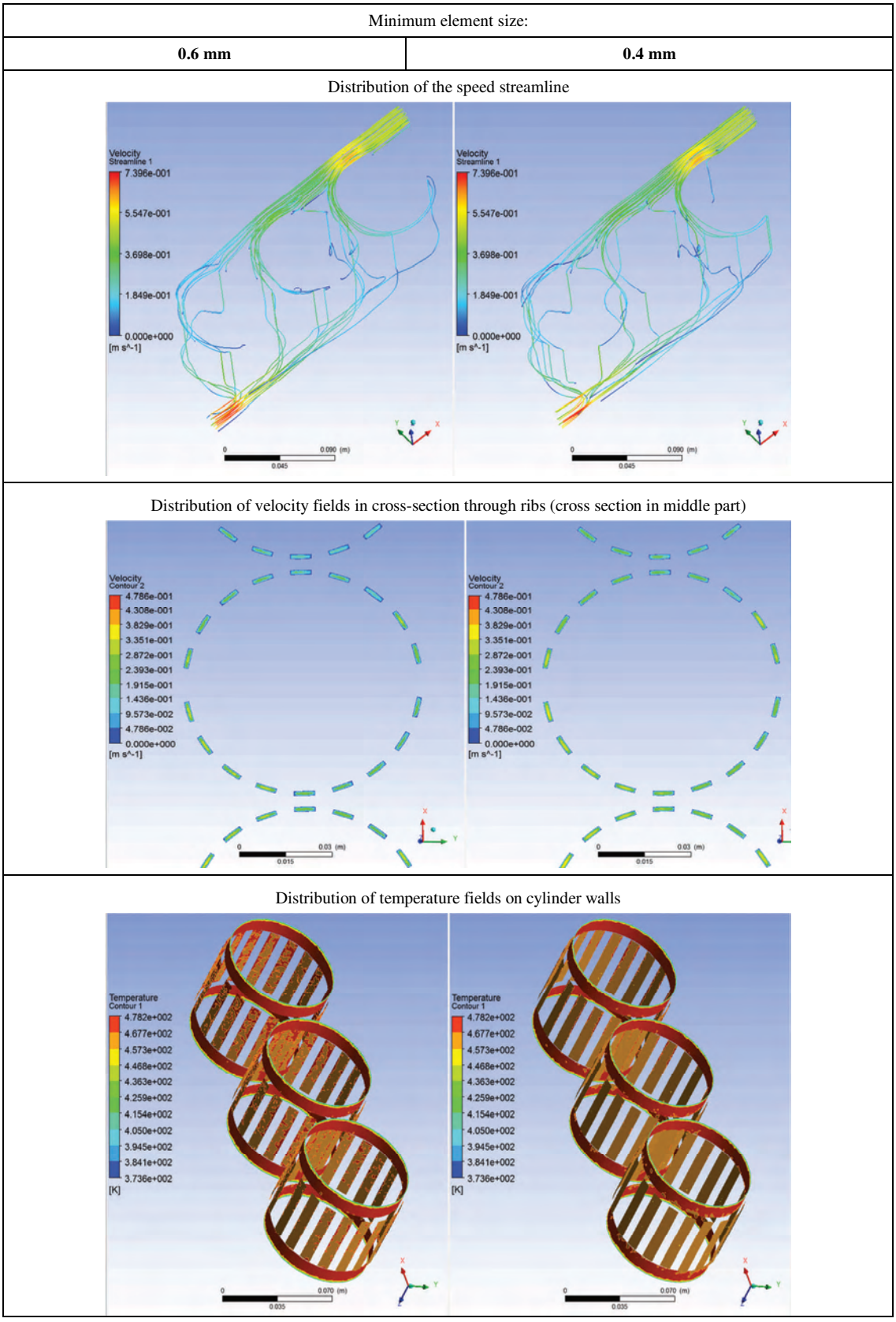

Fig. 11. Distribution of velocity and temperature fields for the computational grid with a minimum element size of 0.8 mm (left side) and 0.6 mm (right side)

Turbulent Intensity **5%**	Turbulent Intensity **10%**
Distribution of the speed streamline	
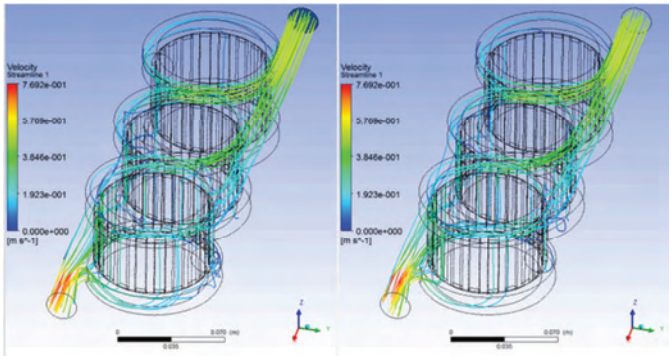	
Distribution of velocity fields in cross-section through ribs (cross section in middle part)	
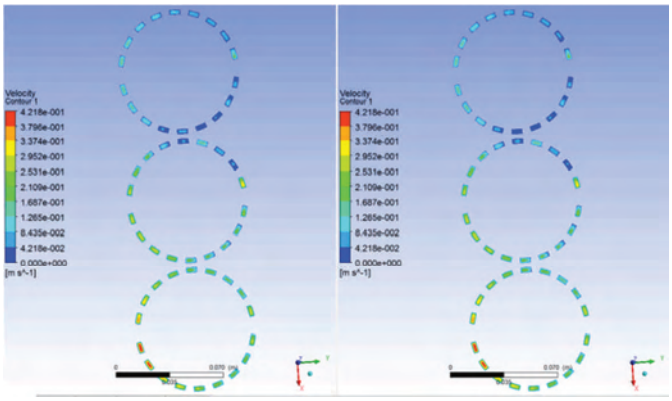	
Distribution of pressure fields in cross-section through ribs (cross section in middle part)	
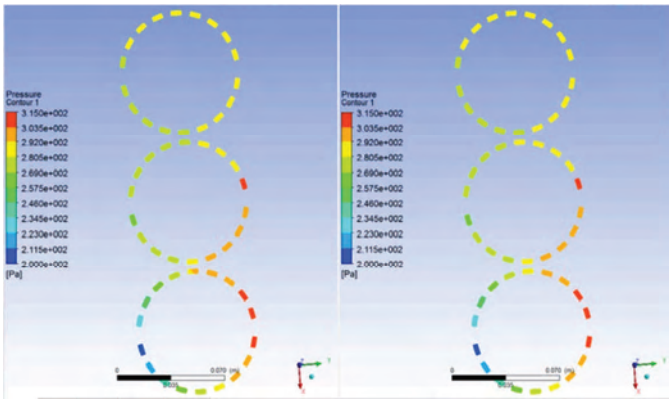	
Distribution of kinetic energy of turbulence	
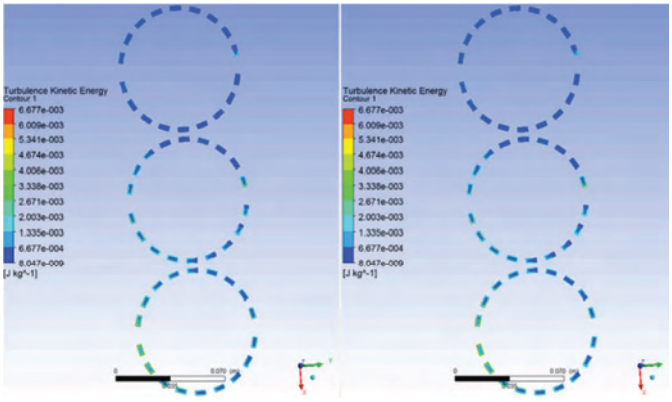	

Fig. 12. Visualization of the effect of turbulence intensity on the computational model

Basic model	
1 inlet / 1 outlet	**2 inlets / 2 outlets**

Distribution of the speed streamline

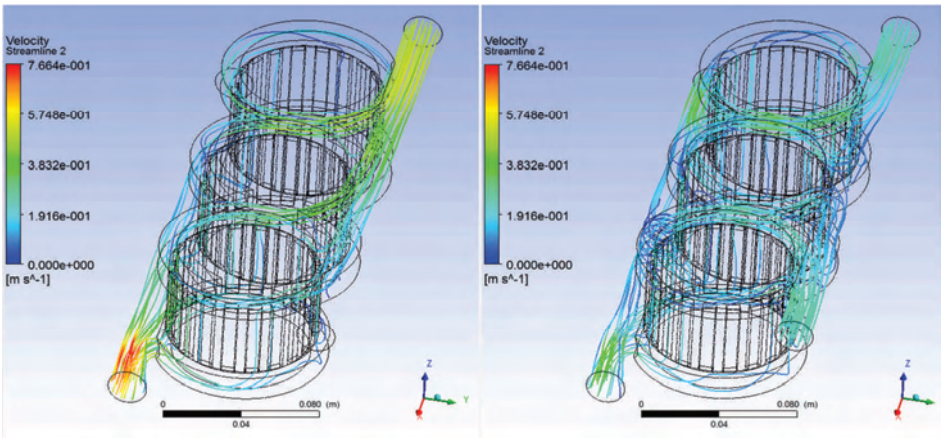

Distribution of velocity fields in cross-section through ribs (cross section in middle part)

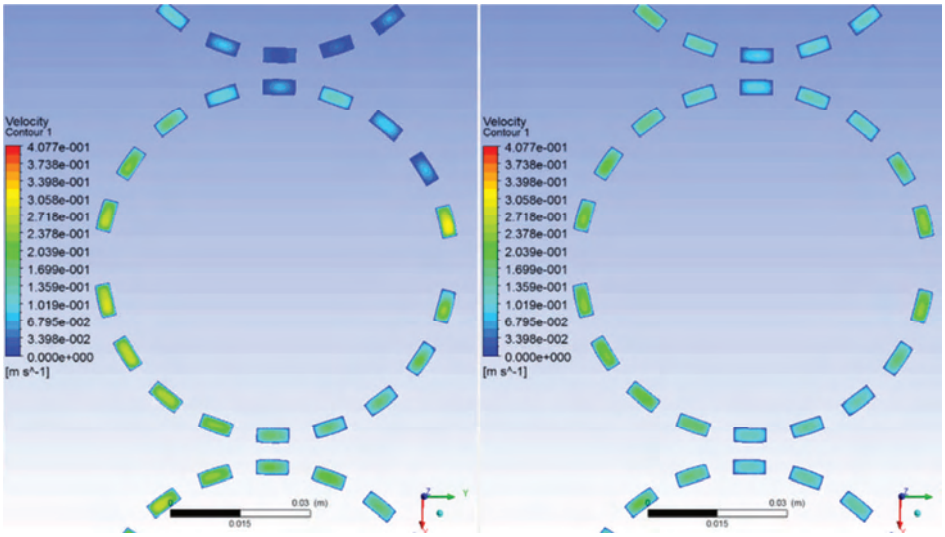

Distribution of temperature fields on cylinder walls

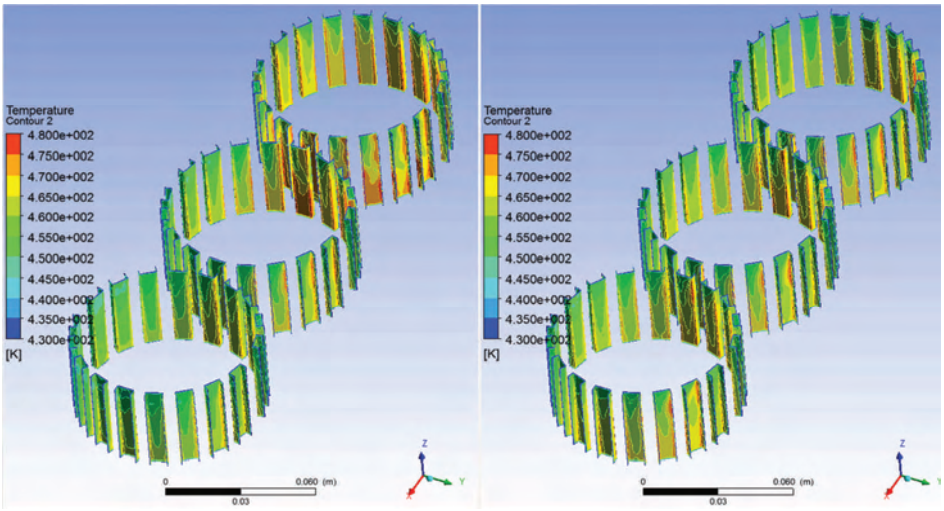

Fig. 13. Comparison of distribution velocity fields across the ribs and temperature fields for the basic model, one inlet and outlet (left side) and two inlets and outlets (right side)

Model with individualized flow in cylinders	
1 inlet / 1 outlet	**2 inlets / 2 outlets**
Distribution of the speed streamline	
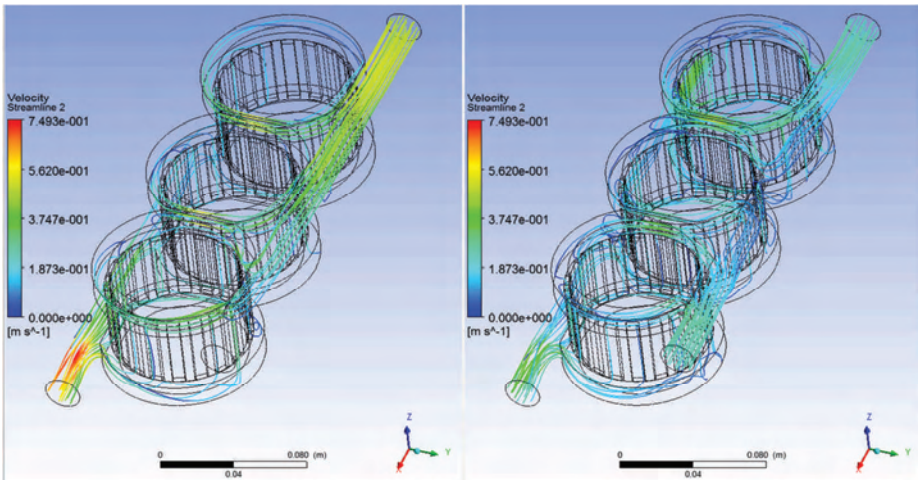	
Distribution of velocity fields in cross-section through ribs (cross section in middle part)	
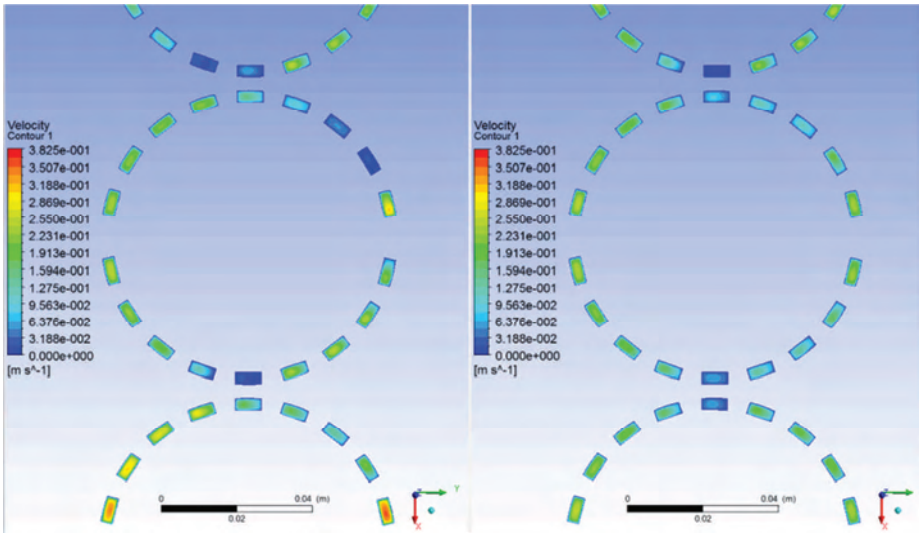	
Distribution of temperature fields on cylinder walls	
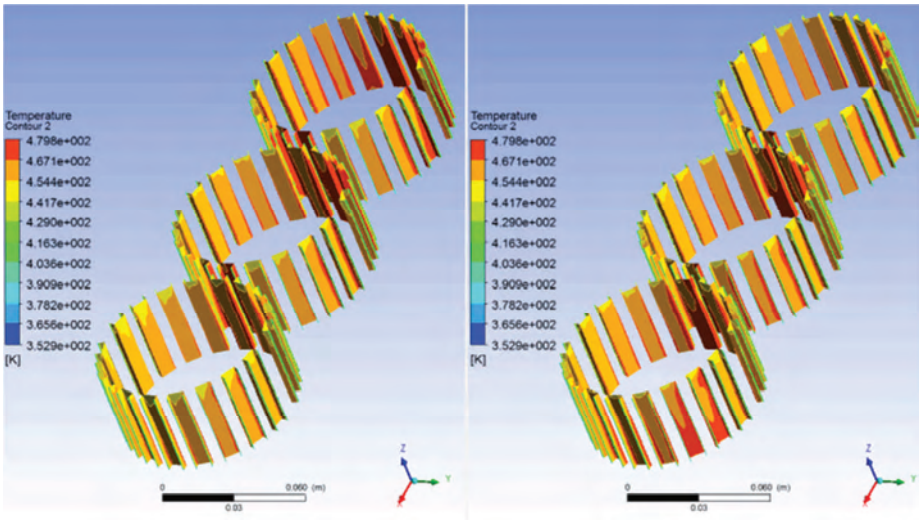	

Fig. 14. Comparison of distribution of velocity fields across ribs and temperature fields for model with individualized flow in cylinders, one inlet and outlet (left side) and two inlets and outlets (right side)

Model with the variable geometry of the intake and outlet channels	
Graduated collectors	**Graduated collectors, split cylinders**

Distribution of the speed streamline

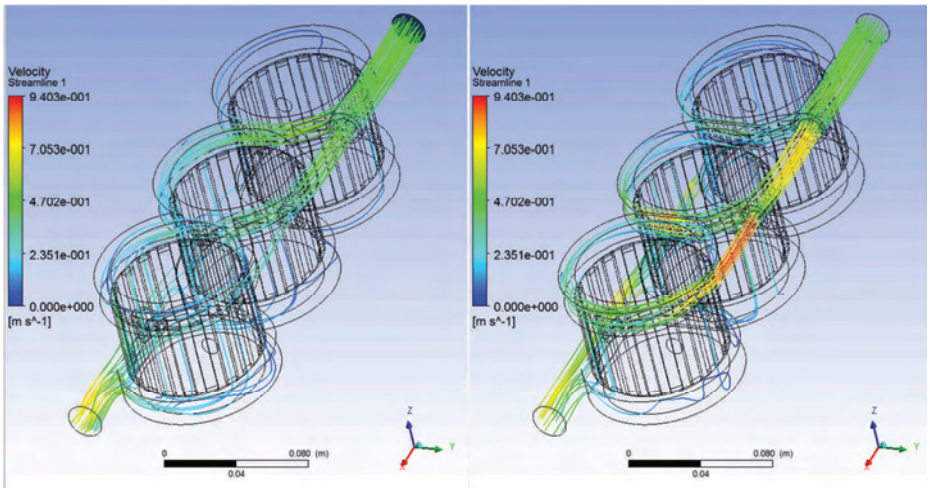

Distribution of velocity fields in cross-section through ribs (cross section in middle part)

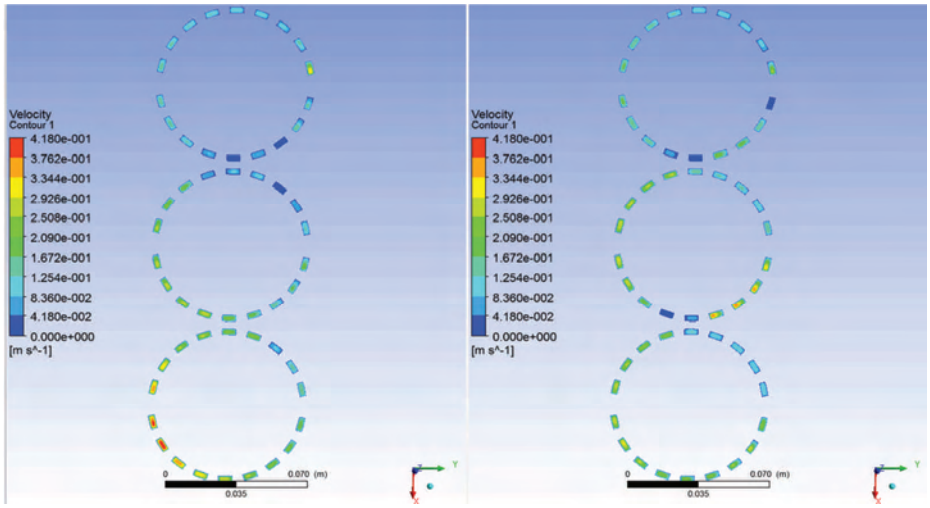

Distribution of temperature fields on cylinder walls

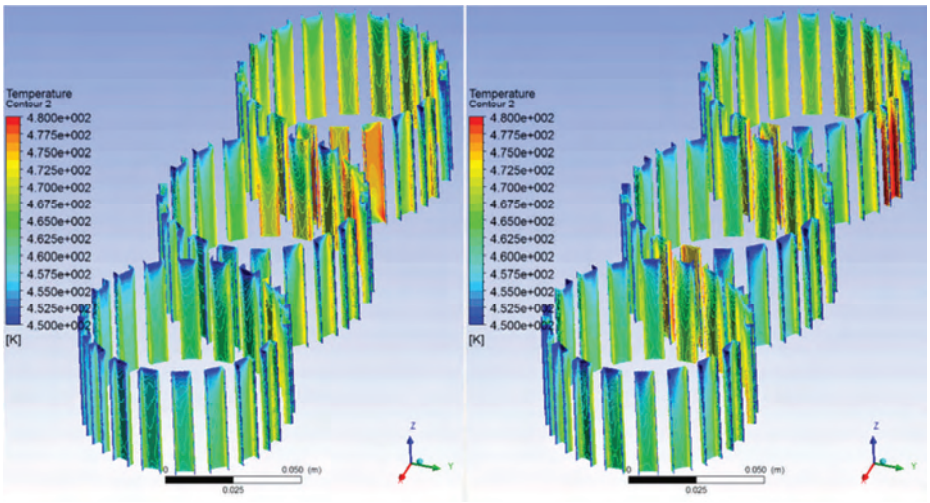

Fig. 15. Comparison of distribution of velocity field across ribs and temperature fields for model with variable geometry of the intake and outlet channels

Model with reduction of flow resistance	
Without splitting the cylinders	**With cylinder splitting**
Distribution of the speed streamline	
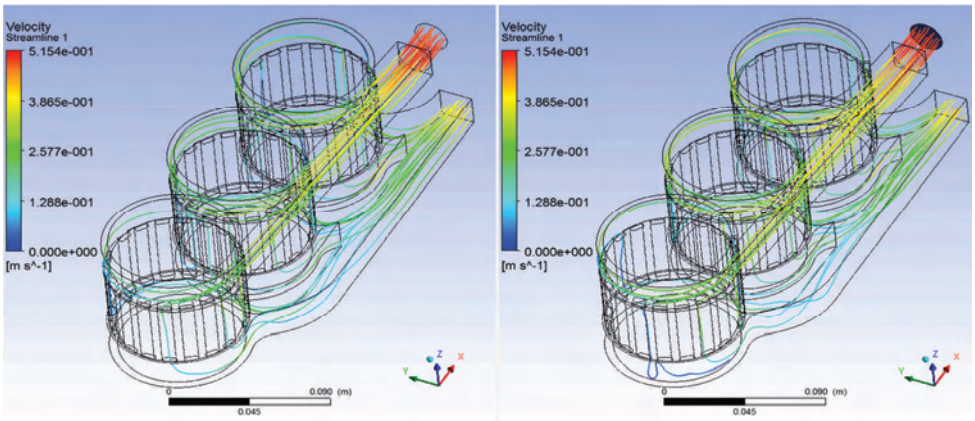	
Distribution of velocity fields in cross-section through ribs (cross section in middle part)	
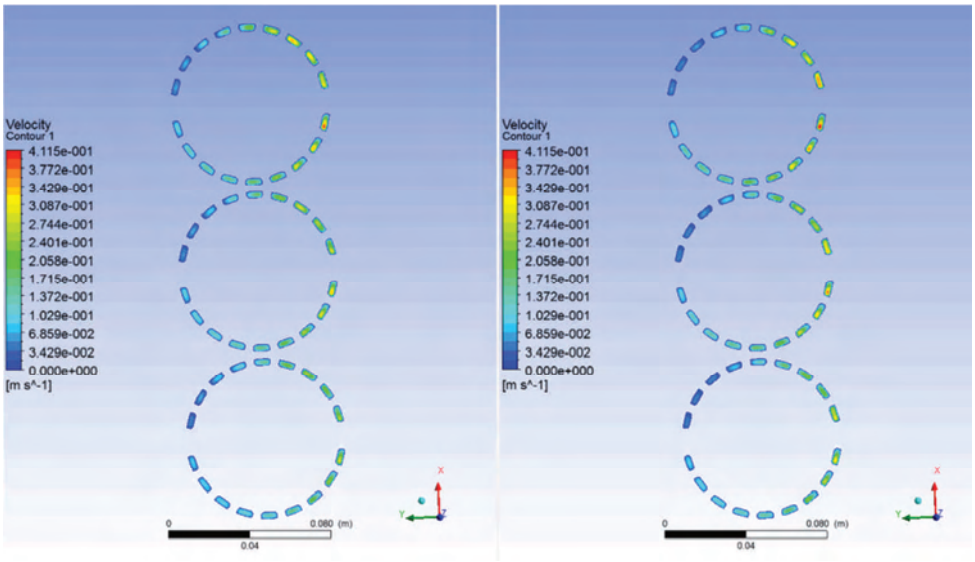	
Distribution of temperature fields on cylinder walls	
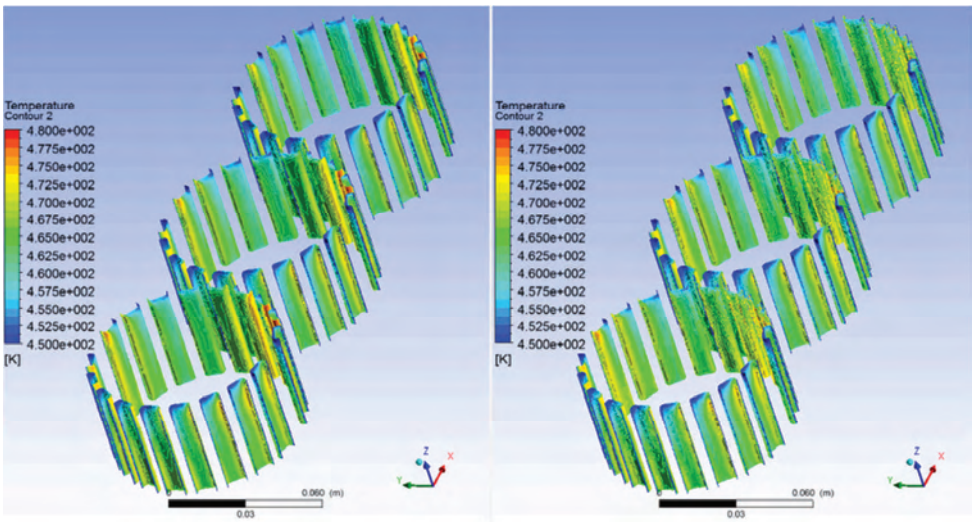	

Fig. 16. Comparison of the distribution of velocity fields across the ribs and the temperature fields for the model with reduction of flow resistance

Final model	
m = 0.15 kg/s	**m = 1.5 kg/s**
Distribution of the speed streamline	
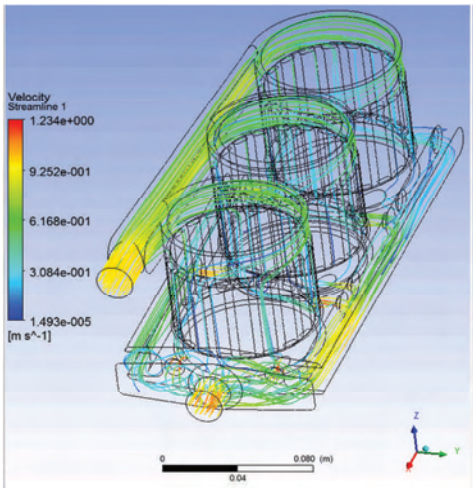	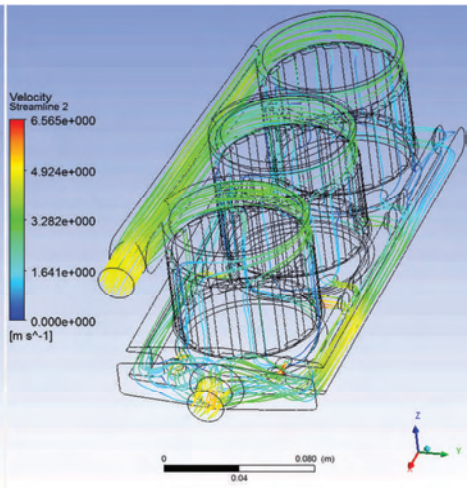
Distribution of velocity fields in cross-section through ribs (cross section in middle part)	
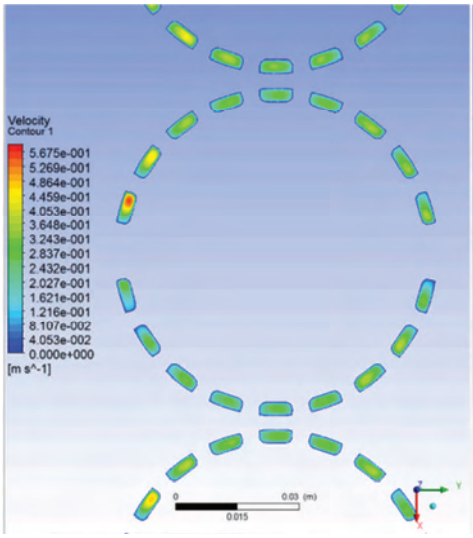	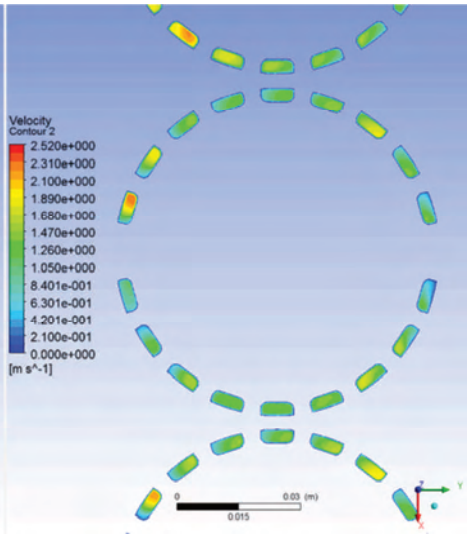
Distribution of temperature fields on cylinder walls	
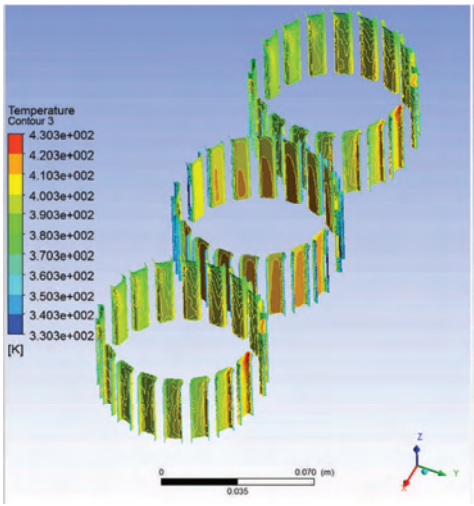	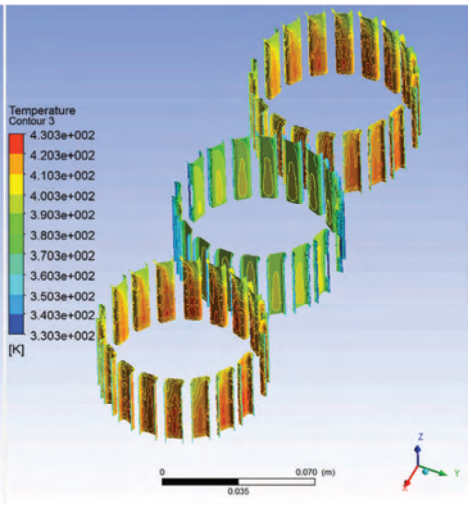

Fig. 17. Comparison of distribution of velocity fields across the ribs and temperature fields for the final model, for two mass flow rates

3. Summary and conclusions

During the simulations tests of the heat flow from chemical reactions that's occurs during the fuel combustion, more than twenty different channel designs were analyzed in the engine cooling system. Each model was analyzed in the range of two to four design variants, i.e. for different flow rates and different combinations of inlet and outlet of the working medium. This article presents five representative models. These models were constructed using CAD software, using CATIA V5. Subsequent versions differed in shape and size of the inlet, outlet channels, number of inlets and outlets channels, arrangement of inlet and outlet channels (on one and other side of the model), shape of channels along the cylinder axis etc.

Using ANSYS software, a computational grid was developed, numerical research was performed and results were transformed into color graphs. During the numerical tests for all models, identical initial and boundaries conditions and the size of the computational grid in the critical elements, as in the basic model, were assumed. Boundary and initial conditions were established on the basis of previously conducted research.

Based on the analysis of the results of the simulation tests, it can be stated that the distribution of the flow of the working medium is not evenly distributed in the heat transfer space from the cylinder (vertical ribs). This condition can be observed in different velocities distributions for all investigated cases. Depending on the calculation version, the most intensive flow occurs in the area of the intake channel and in the ribs between the intake and outlet channels (between the cylinders) the velocity of the medium drops almost to zero. This directly translates into uneven temperature distribution on the cylinder walls, where for the extreme case, the difference for a single cylinder reaches almost 50°C.

The unevenness of the heat transfer from the cylinder wall will result in an increase in mechanical stress between the same wall in different thermal conditions.

The smallest spread of velocity values (and thus the increase in thermal stability - the reception of heat energy from the walls) is observed in the channels located along the cylinder axis for the last, final case. Therefore, this version seems to be the most optimum version. The smallest spread of the velocity fields between cylinders reflects in the smallest temperature difference on the cylinder walls. This state will directly result in an even mechanical stress distribution in the cylinder block in the area of the individual cylinders.

Acknowledgement

This work has been realized in the cooperation with The Construction Office of WSK "PZL-KALISZ" S.A." and is part of Grant Agreement No. POIR.01.02.00-00-0002/15 financed by the Polish National Centre for Research and Development.

Nomenclature

CAD computer aided design
CFD computational fluid dynamics
FEM Finite Elements Method

Bibliography

[1] CHOUGULE, A.B., SURESH, R. Pusher configured turboprop engine oil cooler ejector performance: CFD analysis and validation. *Proceedings of the 6th International and 43rd National Conference on Fluid Mechanics and Fluid Power*. December 15-17, 2016, MNNITA, Allahabad, U.P., FMFP2016–PAPER NO. 35.

[2] CZYŻ, Z., PIETRYKOWSKI, K. CFD model of the CNG direct injection engine. *Advances In Science And Technology Research Journal*. 2014, **23**(8), 45-52.

[4] CZYŻ, Z., ŁUSIAK, T., MAGRYTA, P. Badania numeryczne CFD wpływu usterzenia na charakterystyki aerodynamiczne. *Transactions of The Institute of Aviation – Prace Instytutu Lotnictwa*. 2013, **232**, 3-14.

[4] FOGLA, N., BYBEE, M., MIRZAEIAN, M. et al. Development of a K-k-E phenomenological model to predict in-cylinder turbulence. *SAE International Journal of Engines*. 2017, 3.

[5] GRABOWSKI, Ł., CZYŻ, Z., KRUSZCZYŃSKI, K. Model numeryczny układu chłodzenia zespołu napędowego wiatrakowca. *Logistyka*. 2014, **6**, 4169-4178.

[6] GRABOWSKI, Ł., CZYŻ, Z., KRUSZCZYŃSKI, K. Numerical analysis of cooling effects of a cylinders in aircraft SI engine. *SAE 2014 International Powertrain, Fuels & Lubricants Meeting*. 20-23, October 2014, Birmingham.

[7] NURSAL, R.S., HASHIM, A.H., NORDIN, N.I. et al. CFD analysis on the effects of exhaust backpressure generated by four-stroke marine diesel generator after modification of silencer and exhaust flow design. *ARPN Journal of Engineering and Applied Sciences*. 2017, **12**(4).

[8] ROMANOV, V. A., KHOZENIUK, N.A. Experience of the diesel engine cooling system simulation. International Conference on Industrial Engineering, ICIE 2016, *Procedia Engineering*. 2016, **150**, 490-496.

Michał Biały, MEng. – Faculty of Mechanical Engineering at the Lublin University of Technology.

e-mail: *M.Bialy@pollub.pl*

Tutus Tulwin, MEng. – Faculty of Mechanical Engineering at the Lublin University of Technology.

e-mail: *T.Tulwin@pollub.pl*

Konrad Pietrykowski, DEng. – Faculty of Mechanical Engineering at the Lublin University of Technology.

e-mail: *K.Pietrykowski@pollub.pl*

Paweł Magryta, MEng. – Faculty of Mechanical Engineering at the Lublin University of Technology.

e-mail: *P.Magryta@pollub.pl*

Article citation info:
DZIUBIŃSKI, M., DROZD, A., KORDOS, P., SYTA, A. Diagnosing the automobile starting system. *Combustion Engines*. 2017, **170**(3), 19-23. DOI: 10.19206/CE-2017-303

Mieczysław DZIUBIŃSKI
Artur DROZD
Paweł KORDOS
Arkadiusz SYTA

CE-2017-303

Diagnosing the automobile starting system

This article presents a new method for analysing the torque of an internal combustion engine using registered electromechanical runs and magnetic field distribution in a starter. The aim of the study was to develop a model of the starting current of an internal combustion engine and carry out verification tests on real objects. The developed model allows to simulate the shutdown of individual cylinders. Experimental research was conducted using the Bosch FSA 740 equipment for four internal combustion engines under variable operating conditions. During testing, the starting current and relative compression in cylinders were recorded. Simulating the variable load of the starter, the magnetic induction distribution of the magnetic induction was recorded in the feed slot. The research will be used to develop a method of diagnosing the starter and determining the torque of the internal combustion engine.

Key words: *starter, starting current, diagnostics, Matlab, engine torque*

1. Introduction

Because of the growing environmental requirements of the automotive industry, a lot of attention is paid to maintaining the engine and its equipment in proper technical condition, guaranteeing air pollution as low as possible. In addition, new technical solutions are introduced to reduce emissions. In the case of the starter system, it is commonly used in new vehicles with a start-stop system that reduces fuel consumption and the emission of toxic components into the environment, while increasing the number of starter starts by 50%.

The starting system is the only device in the vehicle that is not monitored as a pilot light or information on the on-board computer. Damage to it affects the ecology in terms of the start-up phase and passenger safety when the engine is stopped [4, 5]. It is therefore desirable to develop models and diagnostic patterns that allow the in-service supervision of the starting system.

A frequent damage to starters is the wear of brushes and bushes. In the works [1, 7, 8], the authors attempted to diagnose the boot system using neural networks. The results confirm the possibility of diagnosing the condition of the starter brushes using a single-directional neural network. In reference [2] a wear model of the starter bearing system is developed. This model can be used to describe and interpret the actual operating processes as well as evaluate the durability of the starter bearings. The vibroacoustic studies of the starter [6] have confirmed the possibility of using a vibroacoustic signal to assess the technical condition of the pacemaker. Work [9] analyses the effect of engine torque variations on the engine startup process using electric and pneumatic starters. The relationship between the momentary torque values and the crankshaft rotational speed was determined. It has been found that the degree of non-uniformity of instantaneous speed is dependent on the value of the torque component of the number of engine cylinders and the power of the starting system.

2. Analysis of engine torque

Movement resistance associated with the operation of the internal combustion engine significantly limits its technical indicators. When calculating the torque moments of the internal combustion engine, the resistance torque generated by the individual engine functionalities must be taken into account.

The total anti-torque of the motor can be represented by the pattern:

$$M_{a\text{-}t} = M_f + M_g + M_i + M_{aux} \tag{1}$$

adding up the moment values of: M_f – friction, M_g – gas forces, M_i – inertia forces of the internal combustion engine, M_{aux} – auxiliary devices.

An important component of the torque is the friction torque M_f, resulting from the frictional forces accompanying the engine, including the piston travel and the rings mounted on the cylinder liners, as well as the frictional forces associated with the pivot movement with respect to the pan in the main and the main bearing.

The moment of friction can be expressed as:

$$M_f = \frac{V_e}{4\pi \cdot p_f} \tag{2}$$

V_e – engine displacement, p_f – friction force acting on the piston with respect to the surface unit.

Variability of the torque during one engine cycle is due to the compression of the load in the individual cylinders and is caused by the gas pressure acting on the surface of the piston crown, connecting rod bearings and the main crankshaft bearings. Changes in resistance torque values from gas forces follow the formula:

$$M_g(\alpha) = -Sr\left(\sin\varphi + \frac{\lambda\sin\varphi + \mu\cos\varphi}{\sqrt{1-(\lambda\sin\varphi+\mu)^2}}\right)$$
$$(p_1(\alpha) + p_2(\alpha + 2\pi) + p_3(\alpha + 3\pi) + p_4(\alpha + 4\pi) - 4p_0) \tag{3}$$

S – piston head surface area, r – crankshaft crank radius, φ – angle of rotation of the crankshaft, p_i (I =1, 2,3,4) – instantaneous pressure in individual cylinders, p_0 – ambient pressure.

Coefficients:

$$\mu = \frac{e}{l} \qquad \lambda = \frac{r}{l} \tag{4}$$

e – mischievousness, l – length of connecting rod, r – connecting rod radius.

The moment of inertia, which accompanies changes in engine speed, also has a significant effect on the resistance of the engine. The moment of inertia of the internal combustion engine can be represented by the formula:

$$\frac{I\omega_r^2}{2} = \frac{I_r\omega_r^2}{2} + \frac{I_{zr}\omega_r^2}{2} + \frac{2m_tV_t^2}{2} + \frac{2m_kV_k^2}{2} + \frac{I_b\omega_k^2}{2} \quad (5)$$

I – torque reduced to the axis of the starter rotor, I_{zr} – moment of inertia of the rotary masses of the internal combustion engine reduced to the axis of the crankshaft, I_b – moment of inertia of the connecting rod relative to the axis passing through the centre of gravity and perpendicular to the connecting rod plane, I_r – moment of inertia of the starter, m_t – mass of the piston and the piston pin, m_k – mass of the connecting rod, V_k – instantaneous linear velocity of the centre of gravity of the connecting rod, ω_k – instantaneous angular velocity of the connecting rod, V_t – instantaneous linear velocity of the piston, ω – angular velocity of the crankshaft, ω_r – angular velocity of the starter

At the moment of resistance there is also the moment resulting from the work of auxiliary equipment, necessary for the proper functioning of the engine: cooling, lubrication and fuel systems. In order for auxiliaries to function, they must be supplied with sufficient energy. During normal operation of the engine, this energy reduces the available power of the engine, while the start-up of the engine must be provided by the start-up system, which must balance it, and the excess power generated by the engine is expected to result in effective movement. Calculations based on empiric engine attachments relate to established operating conditions (temperature and load), their use for startup conditions may be misleading because of differences in the assumptions for which they were designated.

The moment of the auxiliary devices can be represented by the formula:

$$M_{UP} = M_{wp} + M_{op} + M_{inj} + M_{al} + M_{ca} + M_{opr} \quad (6)$$

where M is, respectively, the moment of: M_{wp} – the water pump, M_{op} – the oil pump, M_w – the injection pump, M_{al} – the alternator resistance, M_{sk} – the compressor air, M_{pow} – the oil pump resistance.

The tangential forces for different motor states are shown in Figures 1–3.

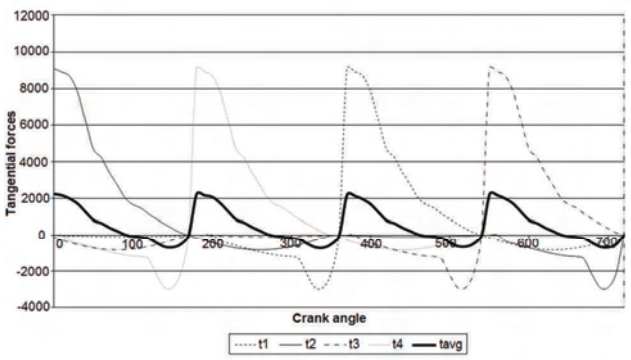

Fig. 1. Crank tangential forces in a smooth-running motor

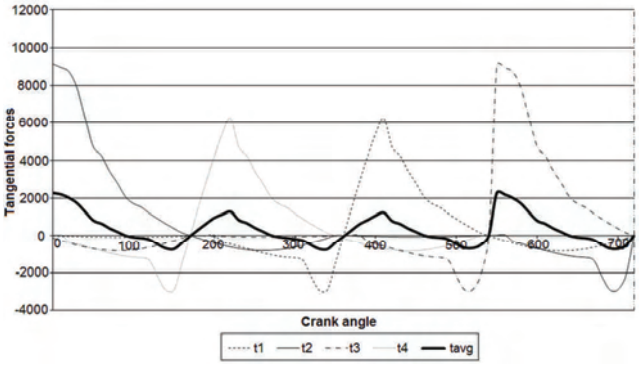

Fig. 2. Crank pin effort – no burning in two cylinders

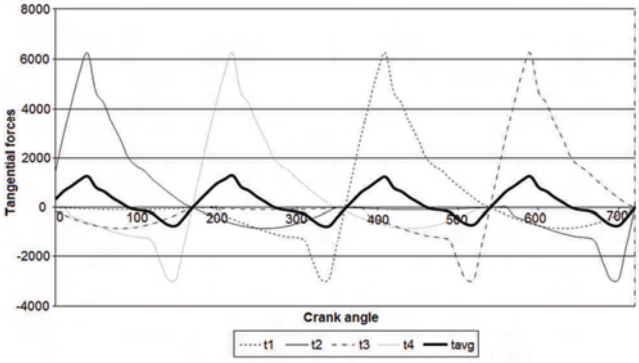

Fig. 3. The tangential force – no burning in four cylinders

3. Equations of the electric starter circuit of the car

Diagnostics is based on the analysis of the start and stop torque components of the engine. The equations describing the moment include the following.

The electric piston equation takes the form:

$$E_B = (R_a + R_B) \cdot i_a(a) + \left(z_a \cdot \frac{\delta\phi_t}{\delta i_t}\right) \cdot \frac{di_t}{dt} + c_E \cdot \phi_a \cdot \omega(a) \quad (7)$$

where: E_B – electromotive force unloaded battery [V], R_a – resistance of the armature winding [Ω], R_B – internal resistance of the battery [Ω], $d\Psi_a/dt$ – voltage induced in the armature windings [V], i_a – current of the armature [A], z_a – number of coil windings of the armature, ϕ_a– main magnetic flux of the armature circuit [Wb].

The mechanical system consisting of a starter rotor, gear and crankshaft has one degree of freedom. Therefore it is possible to describe it in one equation by reducing all the forces and moments to the axis of the starter rotor. The basis for determining the form of the equation is Formula 8, resulting from the principle of the conservation of mechanical energy:

$$\frac{dE}{dt}A = N \quad (8)$$

E – mechanical energy of the whole system, N – the resulting power of the driving and thrust forces

$$E = \frac{I\omega_r^2}{2} \quad (9)$$

$$N = M \cdot \omega_r \quad (10)$$

where: I – the incident moment of inertia of all the masses in motion reduced to the starter axis, M – the resulting

torque of the drive and thrust forces reduced on the starter axis

$$\frac{d}{dt}\left(\frac{I\omega_r^2}{2}\right) = M \cdot \omega_r \tag{11}$$

or:

$$\frac{dI}{d\varphi_r} \cdot \frac{\omega_r^2}{2} + \frac{d\omega_r}{dt} \cdot I = M_e + M_{a-t} + M_{loss} \tag{12}$$

M_e – magnetic moment produced in the starter, M_{a-t} – engine torque, reduced to the starter axis, M_{loss} – moment of mechanical and magnetic losses of the starter, φ_r – angle of rotation of the starter rotor.

A system of differential equations (12), describing at any time the process of starting a combustion engine:

$$\begin{cases} \dfrac{d\varphi_r}{dt} = \omega_r \\ \dfrac{di}{dt} = \dfrac{U_0 - ki - iR - c\omega_r\phi_a}{z_a\dfrac{\delta\phi_a}{\delta i} + z_w\dfrac{\delta\phi_w}{\delta i}} \\ \dfrac{d\omega_r}{dt} = \dfrac{c\phi_a i - M_{a-t} - M_{loss} - \dfrac{\omega_r^2}{2}\dfrac{dI}{d\varphi_r}}{I(\varphi_r)} \end{cases} \tag{13}$$

Assuming that: $\phi_r = y_1$, $i = y_2$, $\omega_r = y_3$

$$\begin{cases} \dfrac{dy_1}{dt} = y_3 \\ \dfrac{dy_2}{dt} = \dfrac{U_0 - ky_2 - R(y_2,T) - cy_3\phi_a(y_3)}{z_a d\phi_a(y_2) + z_w d\phi_m(y_2)} \\ \dfrac{dy_3}{dt} = \dfrac{c\phi_t(y_2)y_2 - M_{a-t}(y_3,y_1,T) - \dfrac{y_3^2}{2}\dfrac{dI(y_1)}{dy_1} - M_{loss}(y_3,y_2)}{I(\varphi_r)} \end{cases} \tag{14}$$

In order to solve the system of differential equations, a program was written in the Matlab environment, on the basis of which the angular velocity, magnetic flux and current waveforms were derived, as shown in Fig. 5.

In this study, the current drawn by the starter during power-up is analysed. The simulation of the current flow on the PC is similar to that obtained from direct measurements. Using the data obtained from the above program regarding the starting current as a function of time, the curve I = f(t) was analysed. After feeding the data into "starter.exe.", waveforms were plotted. Figure 4 shows the value of current changes during start-up obtained by computer simulation. The first part of the chart, which represents the maximum current increase (Fig. 6), deserves special attention.

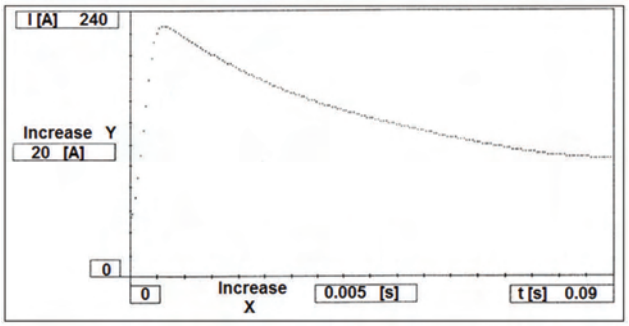

Fig. 4. Graph of the current drawn by the starter as a function of time

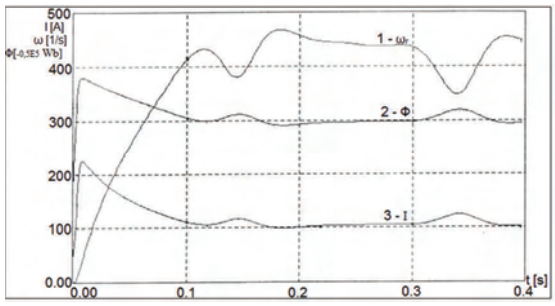

Fig. 5. Solution of the system of differential equations (1 – angular velocity, 2 – magnetic flux, 3 – current waveform)

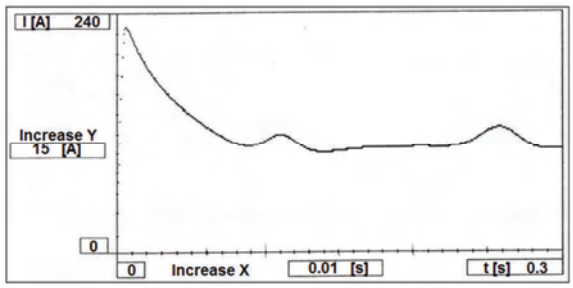

Fig. 6. Initial start-up phase

With a function that approximates the starting current, a definite integral can be calculated in the time interval of 0–0.09 s. The starting current size can be a characteristic parameter for various starter faults, as confirmed in the research part of the work.

4. Modelling the characteristics of the starting current in Matlab

The analysed system of first order differential equations was discretised, and then decoded numerically by means of the fourth-order Runge-Kutta method with the integration step. This method is commonly considered to be effective and corresponds to a compromise between the accuracy of solutions and the time of numeral simulations. In this case, the method was implemented in the Matlab environment.

A program was written that allows modelling current consumption by the starter for the engine's variable anti-torque. The program includes equations describing anti-torque in a four-cylinder internal combustion engine.

A characterisation of the starting current is shown in Fig. 7.

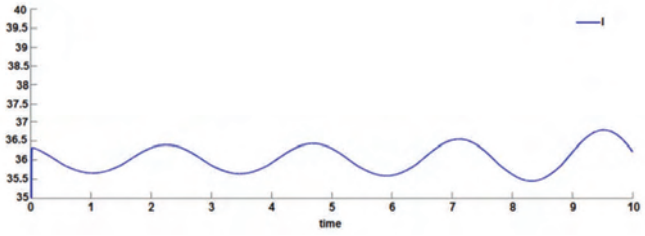

Fig. 7. Starting current characterisation for a four-cylinder engine

5. Experimental verification tests

In experimental research, the size of the starter circuit was measured using the BOSCH FSA 740 apparatus. Using the FSA device, the starting current measurements and indirect pressure measurements in individual cylinders

(relative compression) were performed. The results of the measurements are shown in Figures 8–13.

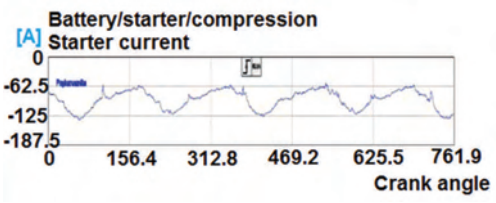

Fig. 8. Starting current for all spark plugs

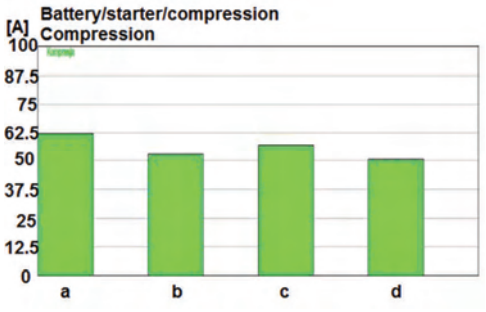

Fig. 9. Relative compression for all spark plugs

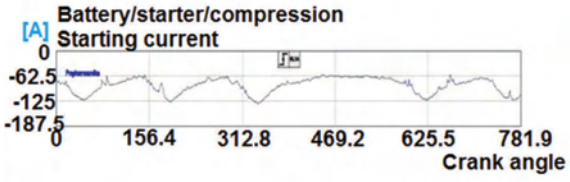

Fig. 10. Starting current with one spark plug removed

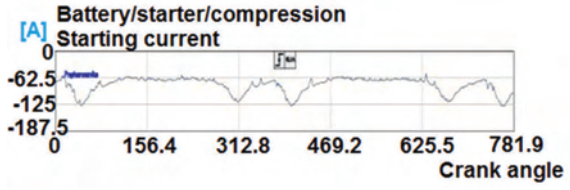

Fig. 12. Starting current for two spark plugs

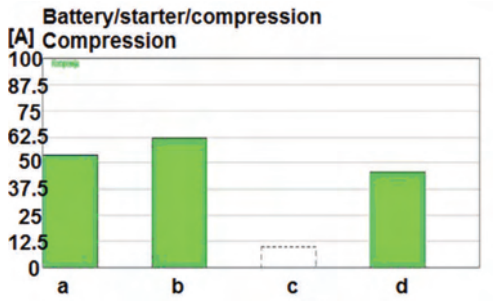

Fig. 11 Relative compression for one spark plug current for two spark plugs

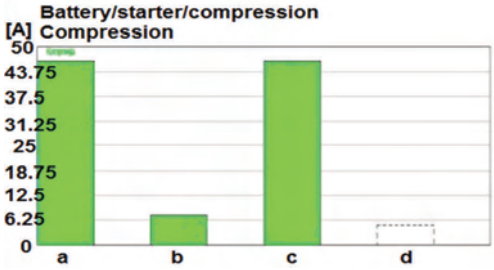

Fig. 13. Relative compression for two spark plugs

6. Summary

Analysis of the effect of starter failure can correct the indirect pressure measurement of the compression. Experimental research has allowed the results to be verified from the model thanks to the simulated changes in the tightness of the individual cylinders.

The registered starting current for one spark plug was confirmed by the absence of compression pressure in the unsealed cylinder. When two cylinders are unsealed, there is a change in the starting current, which confirms change of the torque in individual cylinders.

Nomenclature

CI compression ignition
CNG compressed natural gas
DI direct injection
LPG liquified petrolum gas
SI spark ignition

Bibliography

[1] BAY, O., BAYIR, R. A fault diagnosis of engine starting system via starter motors using fuzzy logic algorithm. *Gazi Journal University of Science*. 2011, **24**(3), 437-440.

[2] BURCAN, J., SICZEK K. The durability and reliability of bearing of car starter. *Tribology*. 2003, **4**, 69-78.

[3] DUDZIKOWSKI, I., JANISZEWSKI, S. Analysis of car rmanent-magnet starters. *Scientific Papers of The Institute of Electrical Machines, Drives and Measurements of the Wrocław University of Science and Technology Series: Studies and Research*. 2000, **20**, 167-174.

[4] DZIUBIŃSKI, M., DROZD, A., ADAMIEC, M., SIEMIONEK, E. Simulation tests of the starting system. *Poznań University of Technology Academic Journals. Electrical Engineering*. 2016, **88,** 89-100.

[5] DZIUBIŃSKI, M. Modeling and experimental testing of starting system in means of transport. *Monograph, Lublin University of Technology*, ISBN 978-83-7947-205-5, Lublin 2016.

[6] EBRAHAMI, E., MOLLAZDADE, K. Intelligent fault classification of a tractor starter motor using vibration monitoring and adaptive neuro fuzzy inference system. *Insight-Non-Destructive Testing and Condition Monitoring*. 2010, **52**(10), 561-566.

[7] FUVESI, V., KOVACS, E. Diagnoses of additive faults of serial wounded motor using artificial intelligence methods. *Recent Innovations in Mechatronics*. 2014, **1**(1).
[8] GAD, S., PAWLAK, M. The artificial neural networks as the tool for diagnostics of automotive vehicles. *Electrotechnical Review*. 2004, 7(8), 693-697.
[9] PSZCZÓŁKOWSKI, J., TRAWIŃSKI, G. Engine crankshaft driving with the help of electric and pneumatic starter. *Logistics*. 2011, **6**, 3499-3508.
[10] ZENG, S., SUN, B., TONG, CH. A modified model of electronic device reliability protection. *Maintenance and reliability*. 2009, **4**, 4-9.

Mieczysław Dziubiński, DEng. – Faculty of Mechanical Engineering at Lublin University of Technology, Poland.

e-mail: *m.dziubinski@pollub.pl*

Paweł Kordos, DEng. – Faculty of Mechanical Engineering at Lublin University of Technology, Poland.

Arkadiusz Syta, DEng. – Faculty of Mechanical Engineering at Lublin University of Technology, Poland.

Artur Drozd, MEng. – Faculty of Mechanical Engineering at Lublin University of Technology, Poland.

Article citation info:
ŻÓŁTOWSKI, A. Influence of after-treatment systems on NO_2 emissions in diesel engines. Combustion Engines. 2017, **170**(3), 24-29. DOI: 10.19206/CE-2017-304

Andrzej ŻÓŁTOWSKI

CE-2017-304

Influence of after-treatment systems on NO_2 emissions in diesel engines

The article discusses the results of bench tests that monitor the increase of NO_2 emissions in the heavy duty vehicles engines' exhausts as a result of the use of particulate matter filters. The use of passive particulate matter filters inevitably leads to an increase in NO_2 emissions from the engine. The particularly intensive increase in the emissions occurs when SCR reactors are shut off, which is still a common practice among drivers. NO_2 concentrations in exhaust gases of DPF-equipped engines reach concentration dangerous for human health and life. The causes of the NO_2 formation in the vehicles' exhaust systems, the harmfulness of this chemical, and the results of NO_2 measurements in different tests, are discussed. In addition, the effect of the presence of this compound on the accuracy of opacity measurement is discussed.

Key words: *emissions measurements, after-treatment system, particulate filters*

1. Introduction

The systematic decrease in pollutants emissions limits in Heavy Duty vehicles engines has led to significant expansion of the exhaust after-treatment systems in these type of engines. A number of systems designed to reduce the selected exhausts component may be included in the exhaust system of an engine compliant with the Euro VI limit. The most popular are the Diesel Oxidation Catalyst (DOC), which reduces CO and THC concentrations in the exhaust gases, Selective Catalyst Reactors (SCRs) that reduce NO_x emissions in the exhaust gas by the chemical reaction that occurs on the catalytic converter between NO_x and the urea solution fed from the outside to the converter. SCRs type reactors are equipped with Ammonia Slip Catalyst (ASC), which is a system for reducing excess ammonia produced in SCR.

Another exhaust after-treatment system is the Diesel Particulate Filters (DPF) that reduce the particulate number emissions and the mass of solid particles contained in the exhaust gases. Heavy Duty vehicles usually are equipped with kind of them as so-called, passive filters. Passive particulate filters are coated with a catalyst layer to facilitate the oxidation of the soot particles contained in the exhaust gases. Typically, in such processes, the reaction (1) between the soot particles and the NO_2 contained in the exhaust gases, is used:

$$C + 2NO_2 \rightarrow CO_2 + 2NO \quad (1)$$

For this reason, the proper amount of NO_2 is needed for the proper functioning of the DPF filter. Nitrogen oxides (NO_x) contained in the raw exhaust gases coming from outlet port of cylinder head consist mainly of nitrogen oxide (NO). This is an unstable compound formed at high temperatures during the combustion process in the cylinder. At ambient temperature NO is gradually converted to NO_2, which is a form of nitrogen oxides that is more natural to lower temperatures. The exhausts, having left the engine outlet port are immediately cooled which favours conversion of NO into NO_2, especially in the presence of ozone. We may notice that in the engine without exhaust after-treatment system, the predominant majority of the emitted nitrogen oxides leaves the engine exhaust pipe as NO and the share of NO_2 in the NO_x emitted is only a few percent.

For engines equipped with DPF, the systems need more NO_2 for their operation. This makes it easier by the catalyst layer on PDF core converting part of NO formed during fuel combustion in the cylinder into NO_2. The share of NO_2's created that way in the NO_x amounts to tens of percent. For this reason, NO_x leaving the DPF-equipped engine's exhaust system, owing to the high NO_2 content, may be completely unlike the NO_x composition measured before DPF. On the other hand, in the shorter scale of time and in the NO_x concentrations measured in street conditions, a DPF-equipped engine and one not equipped with this system will emit nitrogen oxides with completely different toxic properties. When comparing NO and NO_2, the properties of the latter one should be considered more toxic. Especially unpleasant are its irritating properties and the ability to create aerosols with droplets of condensed moisture in the cooled exhaust gases. So far, because of low NO_2 content in NO_x, no significance attention has been paid to the toxic properties of this gas, considering the NO toxic properties as representative for NO_x.

2. NO_2 properties

NO contained in the exhaust gases is generated in the combustion chamber of the engine, where the high temperature during fuel combustion and the oxygen excess contribute to its formation. As a result of the decrease of the temperature of the exhaust gases in the expansion stroke, there occur conditions for oxidation of the part of NO contained in the exhaust gas, to the NO_2 form according to the reaction (2). However, this reaction is slow enough, compared to the duration of the expansion and exhaust stroke, that only a small fraction of NO may be oxidized at this time.

$$2\,NO + O_2 \rightarrow 2\,NO_2 \quad (2)$$

At ambient temperature NO_2 it is a brown, strongly toxic gas with a sharp odour reminiscent of chlorine gas.

Nitrogen dioxide can irritate the lungs and cause less resistance to respiratory infections such as influenza. Prolonged or frequent exposure to concentrations that are significantly higher than normal in the air can cause an increased incidence of acute respiratory illness in children. It contributes to reducing the immune system and increasing the risk of lung infections, as well as exacerbating asthmatic symptoms and conjunctivitis. Air pollution from vehicle

engines contributes to serious health problems such as chronic respiratory diseases, bronchial asthma, allergies, cancer, and even an increased mortality rate.

Road transport, power industry and local heating systems are the main sources of nitrogen dioxide emissions. In large urban areas, characterized by heavy traffic and the absence of power industry, the predominant importance for NO_2 emissions has vehicle exhaust gases; therefore, the highest pollution most often occurs in the vicinity of busy roads.

Gaseous NO_2 diffuses into the epithelial lining fluid (ELF) of the respiratory epithelium and dissolves, and chemically reacts with antioxidant and lipid molecules in the ELF; NO_2's health effects are caused by the reaction products or their metabolites, which are reactive nitrogen species and reactive oxygen species that can drive bronchoconstriction, inflammation, reduced immune response, and may have effects on the heart.

Acute harm due to NO_2 exposure is only likely to arise in occupational settings. Direct exposure to the skin can cause irritations and burns. Only very high concentrations of the gaseous form cause immediate distress: 10–20 ppm can cause mild irritation of the nose and throat, 25–50 ppm can cause edema leading to bronchitis or pneumonia, and levels above 100 ppm can cause death due to asphyxiation from fluid in the lungs. There are often no symptoms at the time of exposure other than transient cough, fatigue or nausea, but over hours inflammation in the lungs causes edema. Chronic exposure to NO_2 can cause respiratory effects including airway inflammation in healthy people and increased respiratory symptoms in people with asthma.

NO_2 is classified as an extremely hazardous substance in the United States as defined in Section 302 of the U.S. Emergency Planning and Community Right-to-Know Act (42 U.S.C. 11002), and it is subject to strict reporting requirements by facilities which produce, store, or use it in significant quantities[2]. The U.S. EPA has set safety levels for environmental exposure to NO_2 at 0.1 ppm, averaged over one hour, and 0.053 ppm, averaged annually.

However, NO_2 concentrations in exhaust gas of vehicles and near roadways are appreciably higher than the ones measured in considerable distance from the road. In fact, in-vehicle concentrations can be 2–3 times higher than measured at nearby area-wide monitors. Near-roadway (within about 50 m) concentrations of NO_2 have been measured to be approximately 30 to 100% higher than concentrations away from roadways. Individuals who spend time on or near major roadways can experience short-term NO_2 exposures considerably higher than measured by the current network. Approximately 16% of U.S. housing units are located within 91 m of a major highway, railroad, or airport (approximately 48 million people). Studies show a connection between breathing elevated short-term NO_2 concentrations, and increased visits to emergency departments and hospital admissions for respiratory issues, especially asthma.

3. Testing of engines

3.1. NO_2 emissions

In order to determine the NO_2 emissions from the average diesel engine, the engine was tested on engine test bench. Basic technical data of the tested engine are shown in Table 1.

Table 1. Technical data of tested engine

Number of cylinders	6 in-line
Displacement [dm^3]	12,8
Rated power	380 kW
Maximum torque	2300Nm
Fuel injection system	Common Rail
Exhaust after-treatment system	SCR, DOC, DPF, ASC
Fuel type	Diesel oil
Emissions limit	Euro VI
Date of engine manufacture	2014

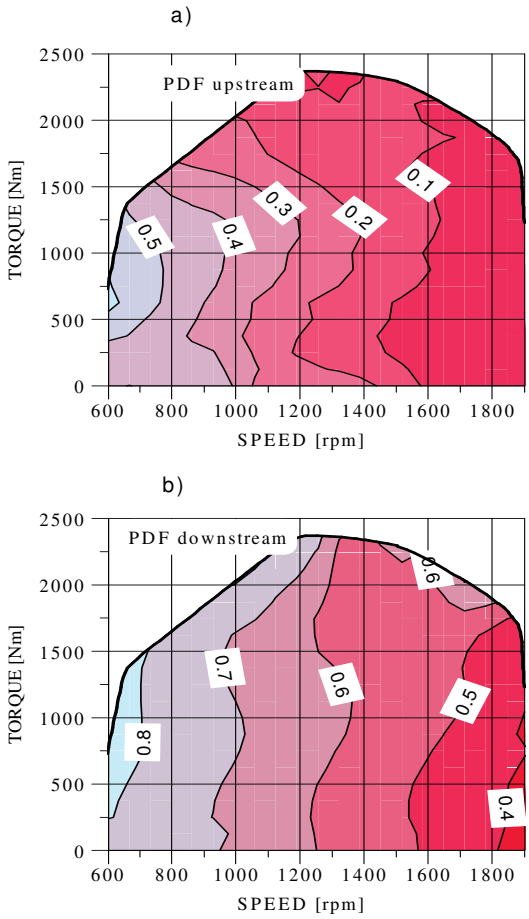

Fig.1. NO_2/NO_x ratio in tested engine

The tests were carried out on a typical test bench equipped and designed for the engine type-approval tests of the pollutants emissions from the engine outlet system. Figure 1 shows the course of the NO_2 concentration share in the NO_x concentration on the general characteristics of an engine operating in the ETC cycle. This graph shows that NO_2/NO_x ratio (NO_2 share in NO_x) increases with decreasing engine speed. This is primarily due to the decrease of the exhaust gas temperature with the reduction of the engine speed and the increasing the time of the exhaust gas flow from the combustion chamber to the point at which the NO_2 concentration was measured. Greater flow times of the expanded and cooled exhaust gas through the engine exhaust system favored a greater conversion of NO to NO_2. The meridian-like character of the isolines shown in Figure 1 indicates that the conversion rate of NO to NO_2 is little dependent on the change in engine load. Apparently, the rise in exhausts temperature caused by the increase of en-

gine loading is compensated by a drop in the air-fuel ratio and lower oxygen content in the exhaust gas. This can be traced on the Figure 2. It is clear from this figure that the main factors influencing the conversion intensity of NO to NO_2 are the temperature of the exhaust gas and the air-fuel ratio.

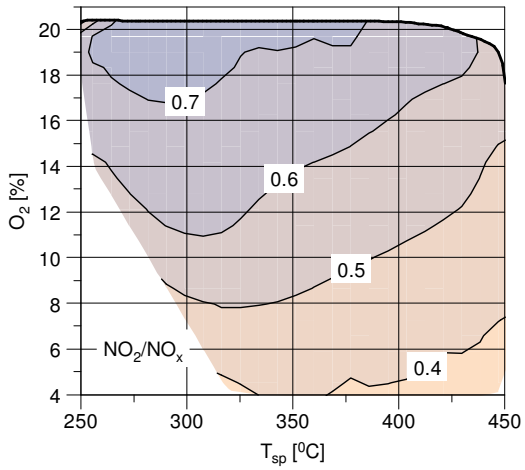

Fig.2. NO_2/NO_x ratio versus exhaust gas temperature (T_{sp}) and O_2 concentration

It is clear from Figs 1 and 2 that the best conditions for the formation of NO_2 in exhaust gases are at high concentrations of O_2 in the exhausts and their low temperature. Such conditions exist when the engine is running on idle. Their opposite state to the idle is where the exhaust gas temperatures reach the highest values and the concentration of oxygen in the exhausts reaches the lowest possible value. Then NO_2/NO_x ratio reaches the lowest values.

The courses shown in Fig. 1 were measured in an engine with a non-functioning SCR system caused by the cutting off the flow of urea solution into the reactor. This was intended to simulate the operating state of the engine, which we deal with when drivers of vehicles, in wrongly perceived savings, decide on such a step. By analysing the NO_2 concentration in the exhaust system of the tested engine, it can be seen that as a result of PDF use, it increased (Fig. 3) from an average of 29 ppm before PDF to 230 ppm after PDF, thus nearly eight times. In section 1 on this article there was written that NO_2 concentration greater than 100 ppm can cause death.

On Figure 1 are shown the results of tests with the SCR reactor inoperative. For comparison, on Figure 4 are shown the results of NO_2 testing in the engine with a functioning SCR reactor. Comparing Figures 1a) and 4, it can be seen that the NO_2 share in NO_x has been noticeably reduced. The nature of the NO_2/NO_x relationship from the engine speed and torque has not changed, but the ratio has decreased by about 30%.

On Figs 5 and 6 are shown the results of NO_2 concentration measurement and the specific emissions of this engine operating as in the conditions shown in Fig. 1b. Comparing Figures 1b and 5, we find that the highest concentrations of NO_2 in the tested engine are near the rated rotational speed, i.e. near the highest occurring exhaust temperatures. The impact of the engine loading on the NO_2 concentration is rather secondary. It appears that despite the significant degree of NO-NO_2 conversion at low engine speeds, the highest NO_2 concentration is obtained at the highest speeds that are precisely where the tested engine has the highest concentrations of NO_x emissions. In terms of the similarity of NO_2 and NO_x, courses, the graphs of these concentrations are quite similar.

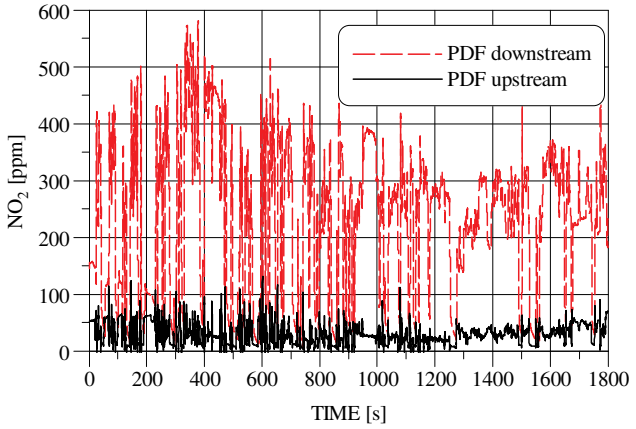

Fig. 3. Concentration of NO_2 in ETC cycle

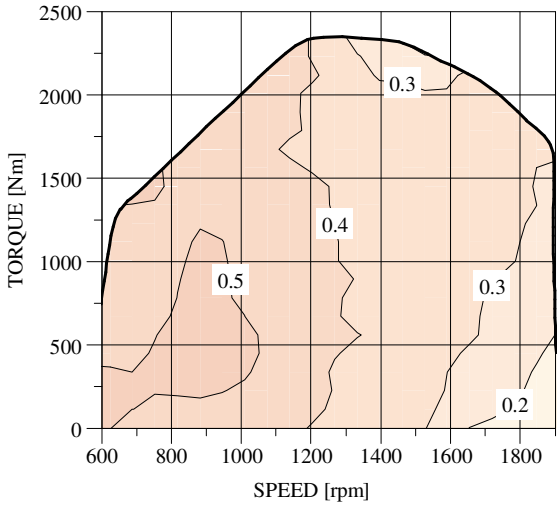

Fig.4. NO_2/NO_x ratio versus speed and torque of the engine equipped with SCR

On Fig. 7 there are compared two speed characteristics of the NO_x and NO_2 concentration measured at a constant engine load. This figure clearly shows how both of these exhaust components depend on engine speed.

On Fig. 6 are drawn NO_2 specific mass emissions. This figure is a reversal of the trend shown on the NO_2/NO_x ratio graph (Fig. 1b). Where the NO_2/NO_x ratio is the highest (high engine loading at low engine speed), the NO_2 specific emissions is the smallest. And vice versa - where the NO_2/NO_x ratio is the smallest (low engine loading at high speed) the NO_2 specific emissions is the highest.

In order to determine the actual emissions of nitrogen oxides, tests were carried out in the cycles foreseen for this purpose in Euro V and Euro VI standards. The results of these tests are summarized in Tables 2–5. By analysing the NO_2/NO_x ratio in each cycle, it can be seen that the ratio is

0.5 to 5.5% for raw (untreated) exhaust gases, from 42 to 52% at the PDF outlet (without SCR) and 30 to 53% in the exhaust gases purified by PDF and SCR. The differences between the NO_2/NO_x ratios measured for each cycle result primarily from different engine operating conditions, producing, inter alia, close to twofold greater work performed by the engine in the ETC cycle compared to the WHTC cycle.

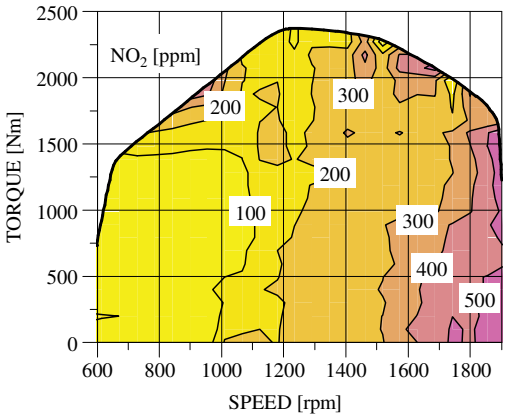

Fig. 5. NO_2 concentration in exhaust gas measured downstream of afertreatment system (without SCR)

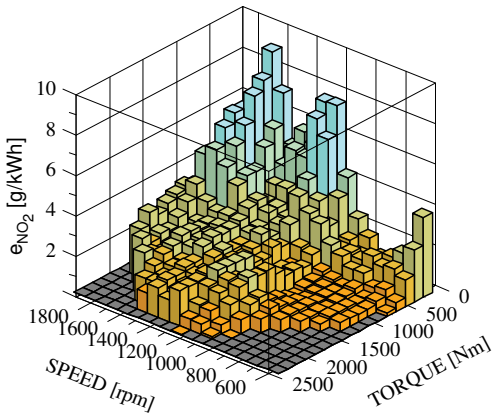

Fig. 6. Specific emission of NO_2 in the engine not equipped with SCR

Table 2. Emissions in ETC cycle [g/kWh]

Pollutant	Without DPF and SCR	With DPF and without SCR	With DPF and SCR
NO_x	5,747	5,089	0,080
NO_2	0,030	2,651	0,024
CO	1,150	0,010	0,011
N_2O	0,085	-	0,070
THC	0,162	0,005	0,015

Table 3. Emissions in ESC cycle [g/kWh]

Pollutant	Without DPF and SCR	With DPF and without SCR	With DPF and SCR
NO_x	5,730	5,548	0,265
NO_2	0,190	2,317	0,096
CO	0,374	0,001	0,014
N_2O		0,007	0,096
THC	0,095	0,001	0,037

Table 4. Emissions in WHSC cycle [g/kWh]

Pollutant	Without DPF and SCR	With DPF and SCR
NO_x	7,326	0,102
NO_2	0,229	0,036
CO	0,538	0,019
N_2O		0,107
THC	0,146	0,002

Table 5. Emissions in WHTC cycle [g/kWh]

Pollutant	Without DPF and SCR	With DPF and SCR
NO_x	6,663	0,051
NO_2	0,367	0,027
CO	2,628	0,013
THC	0,189	0,003

The NO_2 concentration in the exhaust gases of an engine equipped with SCR reached 2 ppm. In the engine without SCR this level exceeded 200 ppm. In both cases, these are multiple times the EPA limit laid down in [2]. For this reason, the NO_2 concentration in the engine exhaust gas system should be considered hazardous to human health and should be monitored by appropriate regulations.

3.2. Effect of NO_2 on the exhausts opacity

NO_2 is a reddish-brown gas whose absorption band of electromagnetic radiation is in the visible region. Its molar light absorption coefficient as a function of wavelength λ [4] ranges from 5.5×10^{-23} m^2/molecule at λ = 400 nm, to 0.5×10^{-23} m^2/molecule at λ = 600 nm. A slight effect of temperature on the absorption coefficient was observed in the range from -30 °C to + 124 °C. In the commercial

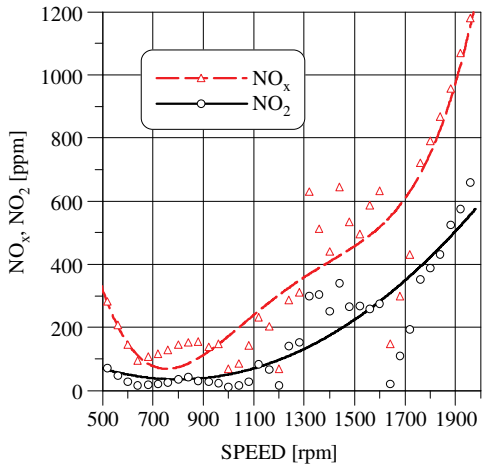

Fig.7. Engine speed characterystic at constant loading T=1000 Nm

opacimeters using tungsten filament lamps and normal UV-absorbing optical glass, we can expect light absorption by NO_2 in the range $(0.5–5) \times 10^{-23}$ m^2/molecule.

Due to the low level of the exhausts opacity in the low-emissions CI engines, the resolution of the conventional opacimeter, the stability of the indications and the noise must be adjusted to allow for measurements in these engines. The catalytic exhausts after-treatment systems such as oxidation reactors (DOCs) or particle filters (DPFs) may cause an increase of NO_x concentration in NO_x. The NO_2

absorbs the green light that is used in traditional opacimeters. The presence of NO_2 in the exhaust gases increases the indications of the current opacimeters from 0.00016 to 0.00024 m^{-1}/ppm NO_2, depending on the width of the band transmitted by the sensor [4].

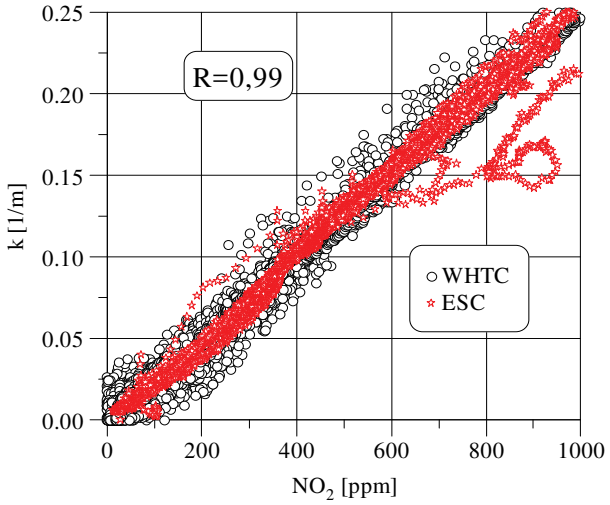

Fig. 8. Opacity versus NO_2 concentration in exhaust gases in ESC and WHTC cycles

In the tested engine, the NO_2 concentration many times exceeded the value of 1000 ppm, hence the values of the light absorption coefficient should be reduced by the corresponding correction. The values of these coefficients are close to the coefficient of the polynomial describing the regression line shown in Fig. 8, which shows the relationship of the light absorption coefficient *k* and the concentration of NO_2 contained in the exhaust gases determined during the ESC cycle. The AVL 439 opacimeter was used in the study. Very high correlation coefficient R = 0.994 between NO_2 concentration and k value was noted. For comparison, in the same test, the correlation coefficient between NO and k was 0.05 and between NO_x and k – 076.

The light absorption coefficient measured by the opacimeter consists of the component associated with the presence of particulate matter in the exhaust gases and the component associated with the presence of NO_2 in the exhausts. Fig. 8 shows the dependence of the exhausts opacity coefficient on the concentration of NO_2 contained in the exhaust gases. The subject tested was an Euro III engine equipped with DPF. The high value of the correlation coefficient obtained indicates that the value of the light absorption coefficient *k* measured by the opacimeter depends primarily on the concentration of NO_2 in the exhausts rather than on the concentration of the light-absorbing particles in the opacimeter. With some approximation it can be assumed that the field shown under the diagram (Figure 8) represents the opacity component associated with the presence of NO_2 in the exhaust gases while the component representing the correct opacity of the exhausts is presented as the width of the graph shown in Fig. 8. From the Fig. 8 it appears that for low concentrations of NO_2 (up to a dozen of ppm) that are encountered in the case of the engines without PDF and SCR–equipped engines, the presence of NO_2 in the exhaust gases does not have practical significance for the measurement of the exhausts opacity. The problem begins with engines equipped with PDF but without SCR. In the tested engine, for the ETC cycle, the average concentration of NO_2 in the test was 230 ppm, which means that for this NO_2 concentration the exhausts opacity was 0.06 1/m (Fig. 8), while the opacity component caused by the presence of NO_2 in the exhaust gases was about 0.04 1/m. This means that the exhausts opacity measurement in these conditions was subject to a 66% error. For this reason the opacimeters indications should be corrected for the presence of NO_2 in the exhaust gases. Looking at Figure 8, we can infer that the opacimeter correction coefficient used in the test should be no more than 0.00024 m^{-1}/ ppm NO_2.

4. Conclusions

1. The use of passive particulate filters in the engine exhaust system results in an increase in NO_2 emissions in exhaust gases
2. NO_2 concentrations in exhaust gases of DPF-equipped engines reach life and human health threatening values reported by EPA. For this reason, this exhaust gas component should become a major concern for ecologists and environmentalists.
3. The presence of NO_2 in the exhaust gases can cause significant measurement errors during measuring exhausts opacity.
4. In order to avoid any possibility of making an error during opacity measurement, it is necessary to use previously developed correction factor.

Nomenclature

CI	compression ignition
DI	direct injection
DOC	diesel oxidation catalyst
ESC	European stacionary cycle
ETC	European transient cycle
PDF	particulate diesel filter
SCR	selective catalyst reactor
WHSC	world harmonized stacionary cycle
WHTC	world harmonized transient cycle

Bibliography

[1] ŻÓŁTOWSKI, A., TAUBERT, S., WIŚNIOWSKI, P. Ograniczenie emisji cząstek stałych z silników o zapłonie samoczynnym oraz opracowanie metodyki wyznaczania macierzy emisji masy i liczby cząstek stałych. *Work No. 6503/COŚ of Motor Transport Institute*, 2017.

[2] 40 C.F.R. Appendix A to Part 355 – The list of extremely hazardous substances and their threshold planning quantities. (July 1, 2008 ed.). *Government Printing Office.* Retrieved October 29, 2011.

[3] BISHOP, G.A., STEDMAN, D.H. Emissions of nitrogen dioxide from modern diesel vehicles. *WIT Transactions on Ecology and the Environment*. 2008, **116**.

[4] DAVIDSSON, J.A., CANTRELL, C.A., MCDANIEL, A.H. et al. Visible-ultraviolet absorption cross sections for NO_2 as a function of temperature. *J. Geophys. Res.* 1988, **93**, 7105.

[5] ŻÓŁTOWSKI, A. Badania skuteczności filtru CRT w silnikach pojazdów ciężkich. *Combustion Engines*. 2009-SC1, 391-397.

[6] ŻÓŁTOWSKI, A. Analiza porównawcza testów badawczych emisji zanieczyszczeń. *Transport Samochodowy*. 2008, 2, 63-74.

Andrzej Żółtowski, DEng. – Environmental Protection Center in Motor Transport Institute.

e-mail: *Andrzej.Zoltowski@its.waw.pl*

Article citation info:
WORSZTYNOWICZ, B., UHRYŃSKI, A., BORKOWSKI, B., PLUTA, M. The analysis of thermal state of catalytic converter depending on fuel supply and engine load using thermo-vision. *Combustion Engines*. 2017, **170**(3), 30-36. DOI: 10.19206/CE-2017-305

Barbara WORSZTYNOWICZ
Andrzej UHRYŃSKI
Bartłomiej BORKOWSKI
Marek PLUTA

CE-2017-305

The analysis of thermal state of catalytic converter depending on fuel supply and engine load using thermo-vision

The paper discusses the problem of thermal state of three-way catalytic converter depending on engine load with spark ignition fueled with gasoline and natural gas. The measurements on the test bench were performed, during which the temperature of the exhaust gases in the exhaust system was measured with the help of thermocouples, and at the same time, the track of the thermal state of the catalytic converter was monitored using thermo-vision camera. The stable work of engine with different rotation speed and values of load was considered together with transient states. The results of the measurements were presented in forms of charts and selected thermo-grams, qualitatively presenting the issue of thermal state of the catalytic converter.

Key words: *catalytic converter, thermo-vision, thermal state, emissivity*

1. Introduction

The degree of conversion of the toxic exhaust gas components by the catalytic converter depends primarily on the composition of the fuel-air mixture and catalytic converter temperature. For proper operation of the catalytic converter it is required to heat it up to 300°C [1, 7, 8]. The operating time is also important, because chemically aggressive fumes and variable temperature values cause aging of the converter which results in a decrease in conversion rate and increase of light-off temperature [7, 8].

The thermal state of the catalytic converter results from the engine's operating parameters, such as the load and the rotational speed. In the first phase, after the engine's cold start, there occurs high heat loss in the exhaust fumes resulting from increased heat exchange between the cold engine elements located in the exhaust gas flow path and exhaust gases. Because of its high heat capacity, the catalytic converter causes a significantly greater temperature reduction of fumes than the conduit between the outlet manifold and the catalytic converter [12, 14]. Measurements made during engine warm-up, both idle and under load, showed a constant fumes temperature of 50°C behind the catalytic converter for about 50–60 seconds after starting the engine, despite a very rapid rise in exhaust fumes temperature before the catalytic converter. This relationship indicates the intense heat transfer of the fumes into the converter cores. At this time there are no exothermal reactions of oxidation of CO and HC [14]. The catalytic converter warm- up period to operating temperature is dependent on the operating conditions of the engine and may last up to several minutes [14]. However, even after the engine has been warmed up, the operating conditions of the converter are not stable. This is directly due to the characteristics of the engine's performance in the vehicle, which is characterized by frequent changes in rotational speed and load, which directly affects the exhaust gas temperature.

Therefore, continuing previous work, the catalytic converter's thermal state was measured using a thermo-vision camera, taking into account the different load conditions of the engine, as well as the fuel supply with petrol and natural gas. During the experiment, the acoustic data was collected and will be analyzed in a separate article.

2. Measurement stand

The measurements were performed on an engine dynamometer fitted with a straight four-cylinder spark ignition engine (Fiat 170A1.00) of the displacement of 900 cm^3. The engine has a maximum power of 30 kW (at rotation speed 5500 rpm) and a maximum torque of 65 Nm (at rotation speed 3000 rpm). The engine exhaust system was fitted with a serially manufactured three-way catalytic converter. In an insulated catalytic converter casing, two ceramic support monoliths were fitted of a circular cross-section (diameter of approx. 90 mm) and the length of approx. 75 mm each, divided by a gap of approx. 8 mm. The distance between the exhaust manifold and the catalytic converter was 250 mm. During the measurements, the engine was fueled with unleaded fuel (LO 95) and natural gas.

Due to the specific purpose of the investigations the temperature was measured at exhaust manifold and behind the catalytic converter. The coolant temperature in the cylinder head was also measured serving the purpose of validation of the engine temperature and intake air temperature monitoring the ambient conditions (engine operating conditions). The temperature measurements were performed with K thermocouples and the results were continuously recorded by NI card with the measurement resolution of 2 s.

At the same time the recording of the thermal state of the catalytic converter was realized with a thermo-graphic camera (Flir T335). Prior to the measurement, the following parameters were set in the camera: emissivity of the object under investigation, ambient temperature (reflected apparent temperature), atmospheric temperature, air humidity and distance from the object tested [6]. That is why the main measurements were preceded by preliminary measurements consisting of the determination of the thermal emission rate on the surface of the elements on which the thermal state was recorded (the determined emission coefficient on the surface of the catalytic converter was $\varepsilon = 0.75$) and determining appropriate temperature ranges and operating parameters of the thermo-graphic camera.

Additionally, the excess air coefficient λ was measured and recorded along with the exhaust gas composition downstream of the catalytic converter with a 5 – gas analyzer Capelec CAP 3201.

Besides that, acoustic data was collected using the SVAN 948 sound level meter and the Zoom H4n recorder. Equivalent sound pressure level in 1/3 octave bands and audio signal was recorded. The time interval using a sound level meter was set at 30 s, thus obtaining 6 samples from each engine cycle.

3. Thermo-graphic measurements

Thermo-vision (thermo-graphy, thermal imaging) deals with the detection, registration, processing and visualization of infrared radiation [11]. It is currently considered one of the most interesting diagnostic and observation methods. It is used in the power industry, construction, metallurgy, environmental research, medicine, scientific research and many other fields [2, 3, 4, 9, 10]. The wide use of thermo-vision is due to a number of advantages of measuring systems based on thermal analysis of the tested objects. One of such important advantages is the non-contact and non-invasive measurement of the examined objects, which in most applications, is a fundamental criterion for the use of thermal imaging.

Devices for measuring the energy of the examined object are thermo-vision cameras, consisting of an optical system, an infrared radiation detector, an electronic amplification path, a processing and a visualization. Flir T335 thermo-vision cameras are used for measurements that are included in the work. The camera's operating temperature range is –20 to +650°C and the temperature measurement error is ±2°C or ±2% of the measured value. The camera used is equipped with a microbolometric matrix with a resolution of 320 x 240 pixels, a 25 x 18.75° lens and is characterized by a sensitivity of N.E.T.D. 0.05°C.

In thermo-vision measurements we use the emission of electromagnetic radiation by every object whose temperature is greater than absolute zero. The electromagnetic spectrum is divided into a number of wavelength areas that are distinguished by the methods used for radiation detection. There is no fundamental difference between radiation in different bands of electromagnetic spectrum. All of them are subject to the same laws and differ only in wavelength. In thermo-graphic studies, part of the electromagnetic spectrum is used in the infrared range. The value of the emitted energy increases with the increase in the object temperature, which allows it to measure its temperature by measuring the emitted energy value, especially in the infrared radiation band. The intensity of electromagnetic radiation depends on the temperature and features of the surface of the object [13]. The resulting thermo-gram is a representation of the temperature distribution on the surface of the observed object.

Unfortunately, this method is endangered by a very wide range of errors, which are due both to human factors, measurement conditions, and the nature of measurement as well as to the technology used. Despite such great possibilities of thermo-vision, it is extremely easy to make wrong measurements or misinterpret the received thermo-grams. That is why it is crucial to optimize the selection of parameters to eliminate measurement errors. The energy received by the thermo-vision device does not only depend on the object's temperature but also on the emissivity of the surface. Radiation comes also from the environment and is reflected by the object tested. To measure the temperature accurately using a thermo-vision camera one should make up different sources of radiation by entering specific parameters such as (Fig. 1):

- emissivity of the object,
- ambient temperature (reflected apparent temperature),
- atmospheric temperature,
- relative humidity,
- distance of the object tested from the camera.

Emissivity is the most important, from a practical point of view, parameter of the object necessary to carry out proper measurement of the thermo-vision device. This is a measure of the intensity of the radiation (surface area) emitted by the object to the radiant intensity of the black body surface at the same temperature [5, 11]. Although emissivity depends on many factors, there are tables of values for this parameter in the literature for different materials. In this case it should be noted that the values given in the tables are only guidelines and may differ from the object being measured. In order to obtain the exact emissivity value for a specific study it becomes necessary to determine it oneself.

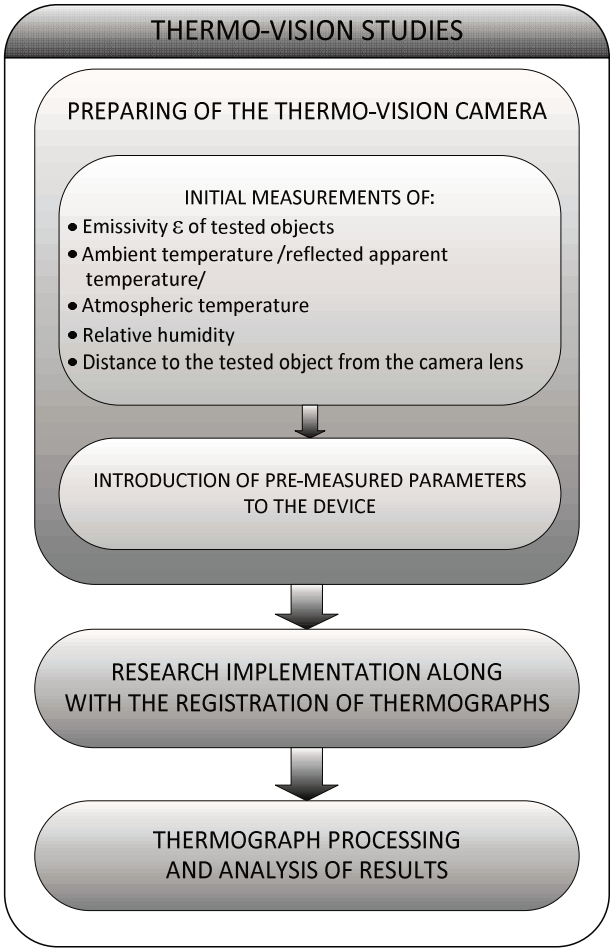

Fig. 1. Thermo-graphic measurement algorithm

During the measurements the emissivity of the test surfaces was determined using a thermo-vision device. In order to determine the emissivity of a given surface, a tape of known emissivity (ε = 0.95) should be placed on its fragment, which will constitute the measurement base. At the same time, the tape's emissivity is entered into the camera's settings. After waiting for some time to warm up a given surface (the material emissivity is measured at a temperature higher than the ambient temperature), the temperature on the tape surface is measured by the thermo-vision camera. This value will be the actual temperature. In the next step, the emissivity is being changes until the values measured on the tape and the test surface are the same. The emissivity set in this way corresponds with the emissivity of the surface of the object being measured

The ambient temperature (reflected apparent temperature) is the reflected radiation from the test object or objects in its environment. Proper compensation of reflected radiation is particularly important for objects of low emissivity and when there is a strong heat source near the object [5, 11].

Distance is the distance separating the object from the camera. It serves to compensate both the influence of the radiation of the atmosphere itself, but also for absorption and diffusion of radiation through the atmosphere between the camera and the object tested [5, 11].

4. Results and analysis

For each kind of fuel the measurements started in the same ambient conditions, while the thermal state of the catalytic converter was recorded after the engine was warmed up. On the basis of preliminary measurements, for the main measurements, the engine working with a constant speed of 3000 rpm was selected. The load was changed from 40 Nm to 10 Nm and then from10 Nm to 40 Nm, with a 10 Nm measurement step. For each engine load, the measurement duration was approximately 5 minutes. Registration of results was conducted continuously. All of the graphs presented in the work include the measurement results as a function of time.

The coolant temperature values in the cylinder head and the intake air of the engine for the two series are shown in Fig. 2. These measurements were used to verify the repetition of the engine conditions on the stand and the engine's thermal state.

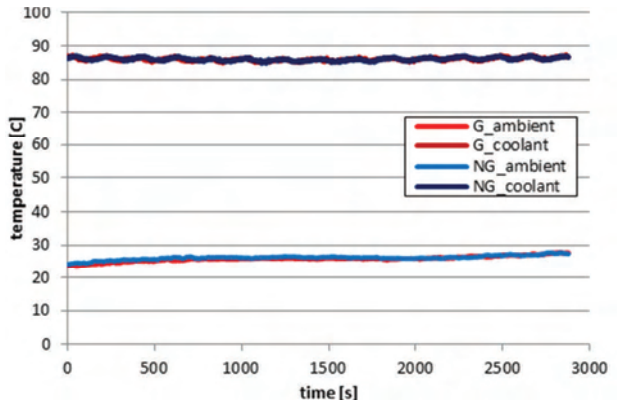

Fig. 2. Air temperature in intake manifold and coolant temperature in the cylinder head

During the supply of the engine with petrol, the exhaust gas temperature in the exhaust manifold varied between 730°C and 660°C, while in the pipe behind the catalytic converter from 660°C to 550°C. During the supply of the engine with natural gas, adequate temperature ranges were 710°C to 630°C for the exhaust manifold and 630°C to 520°C for the exhaust pipe. Changing the load, both for smaller and larger ones, resulted in a 20 K change in exhaust manifold temperature for a petrol powered engine and about 30 K for a gas powered engine for about 10–14 seconds. During the next few minutes of engine working with constant load a further slow change in temperature followed of about 10 K. Changes in the exhaust gas temperature behind the catalytic converter are considerably higher than in the exhaust manifold and are much slower, as illustrated in Fig. 3.

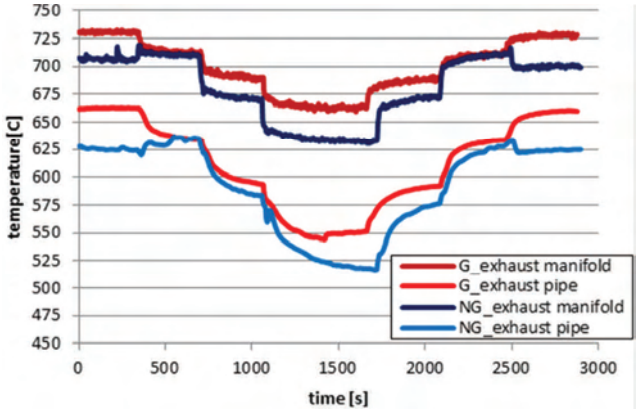

Fig. 3. Exhaust gas temperature in the exhaust manifold and in the pipe behind the catalytic converter

The smaller the engine load is, the higher the exhaust gas temperature difference is between the exhaust manifold and the pipe behind the catalytic converter. This is directly related with the mass of exhaust gases flowing through the exhaust system and therefore with their velocity which results in the time at which heat is exchanged between exhaust gases and exhaust system components.

As the load is reduced in the range of 30 to 10 Nm, the difference between the exhaust gas temperature values for the petrol and natural gas powered engine increases a can be seen both in the exhaust manifold and in the pipe behind the catalytic converter. This is due to the constant value of the air excess coefficient (λ = 1) of the air – gas mixture (Table 2) and the decreasing air excess coefficient from 1.16 to 1.08 for the petrol – air mixture (Table 1) together with decreasing load in this range. The types of fuel used are characterized by a significant difference in the stoichiometric constant (which was taken into consideration during the gas analyzer calibration for each type of fuel). If the petrol powered engine was powered with Lambda sensor feedback, the exhaust gas temperature difference for both fuels would be similar for different loads. For a 40 Nm load, the natural gas supply system was not sufficiently efficient and the Lambda was 1.18–1.28, which was also reflected in the exhaust gas temperature values.

At the same time, recording of the temperature distribution across the surface of the entire catalytic converter allows you to observe the differences in the degree of heating of its components. The amount of emitted energy results, among other things, from the materials used and the number of layers. There are insulating mats on the surface of both cores which limit the amount of radiation, but the occurrence of the same layers does not affect the value of the temperature difference. Therefore, the analysis of images from the thermo-vision camera gives the possibility of conducting a comparative analysis of a qualitative nature.

Table 1. Emissions of exhaust components measured behind catalytic converter – petrol powered engine

Load	CO [% vol]	CO_2 [% vol]	HC [ppm vol]	O_2 [% vol]	NO_x [ppm vol]	Lambda
40 Nm	0	13.3	3	2.30	1893	1.121
30 Nm *	0	13	0	2.77	1061	1.149
30 Nm	0	13	1	2.77	913	1.150
20 Nm *	0	13.3	1	2.25	684	1.119
20 Nm	0	13.3	1	2.24	603	1.118
10 Nm *	0	13.7	0	1.58	395	1.081
10 Nm	0	13.7	1	1.57	328	1.080
20 Nm *	0	13.3	6	2.29	542	1.121
20 Nm	0	13.3	2	2.32	556	1.122
30 Nm *	0	12.9	4	2.96	673	1.161
30 Nm	0	12.9	0	2.95	714	1.160
40 Nm *	0	13.2	7	2.41	1318	1.128
40 Nm	0	13.3	4	2.36	1440	1.125

*right after load change

Table 2. Emission of exhaust components measured behind catalytic converter – natural gas powered engine

Load	CO [% vol]	CO_2 [% vol]	HC [ppm vol]	O_2 [% vol]	NO_x [ppm vol]	Lambda
40 Nm	0	10.2	10	2.61	1062	1.179
30 Nm *	0	11.5	13	0.10	923	1.005
30 Nm	0	11.6	12	0.04	482	1.001
20 Nm *	0	11.6	14	0	44	0.999
20 Nm	0	11.6	12	0	41	0.999
10 Nm *	0	11.6	12	0.03	187	1.001
10 Nm	0	11.6	11	0.08	212	1.004
20 Nm *	0	11.6	12	0.06	497	1.003
20 Nm	0	11.6	13	0.05	511	1.002
30 Nm *	0	11.6	13	0.07	795	1.004
30 Nm	0	11.6	12	0.03	689	1.001
40 Nm *	0	9.6	9	3.68	615	1.269
40 Nm	0	9.5	10	3.82	560	1.282

*right after load change

The curves in Figures 4 and 5 show the minimum, maximum and average temperatures read from the thermo-grams according to the procedure described in [14] for the first and second catalytic converter cores for both fuels respectively. The temperature values on the surface of the first core are higher, and so the minimum is about 15–30 K, the maximum is about 40–55 K, and the average is 25–30 K, regardless of the fuel used. Similarly, for both fuels and on both cores, the mean difference between the minimum and average values is 50–60 K. On the other hand, the delta for the average and maximum values for the first core is between 90–110 K and the second is about 70–90 K. The thermograms show the causes of numerical differences (Fig. 6). The temperature distribution on the surface of the first core is very different, while for the second it is evenly distributed, with much lower temperature gradients. The maximum intensity of the maximum values, resulting in large differences between cores, occurs in the initial part of the first core, where, despite the sealing mat, there is a direct contact between the incoming exhaust gas and the core housing and its heating.

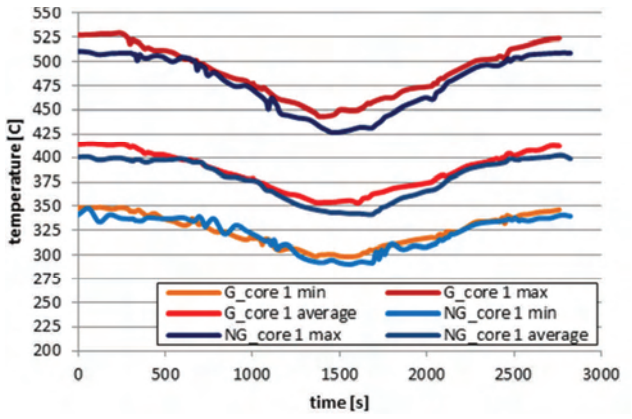

Fig. 4. Temperature values on the surface of the first core derived from thermo-grams

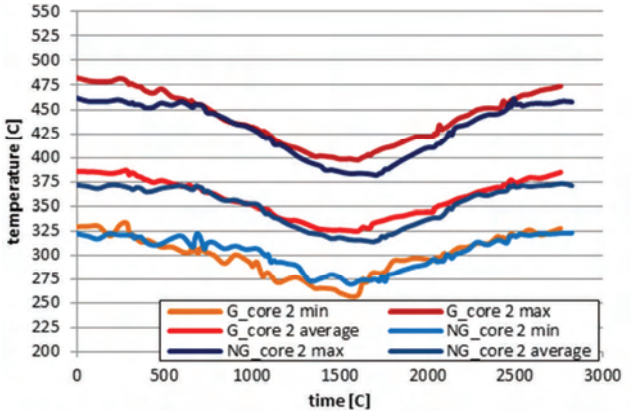

Fig. 5. Temperature values on the surface of the second core derived from thermo-grams

Considering the influence of the fuel used in the engine and the composition of the fuel – air mixture on the exhaust gas temperature, the thermo-grams of the exterior surfaces of the catalytic converter show much less difference in temperature than the thermocouples measured in the interior of the exhaust system. In addition, the curves of minimum values are characterized with high fluctuations that makes it impossible to determine the difference clearly. On the other hand, for the other curves, the tendency associated with the load and composition of the fuel – air mixture described for the thermocouple value occurs, though without clear demarcation.

The exhaust gas behind the catalytic converter (Fig. 3) and the surface of the catalytic converter (Fig. 4, Fig. 5) during the whole measurement obtained values that clearly indicate that the catalytic converter reached the correct temperature for proper operation. The carbon dioxide content of the exhaust gas reflects the chemical composition of the fuels (Table 1 and Table 2). Due to the different composition of the mixture, it is not possible to compare directly the emissions of toxic components of the exhaust gases with the environment depending on the fuel that the engine

was powered with. In both cases of measurement, there was no carbon monoxide emission behind catalytic convertor to the atmosphere, while emission of hydrocarbons was very low, however, higher values were obtained when the engine was supplied with natural gas. This can result from the composition of the mixture and the main constituent of natural gas, i.e. methane, whose conversion rate in the catalytic converter is considerably lower than that of the higher hydrocarbons [15]. Emission of nitric oxides correlates with engine load and mixture composition.

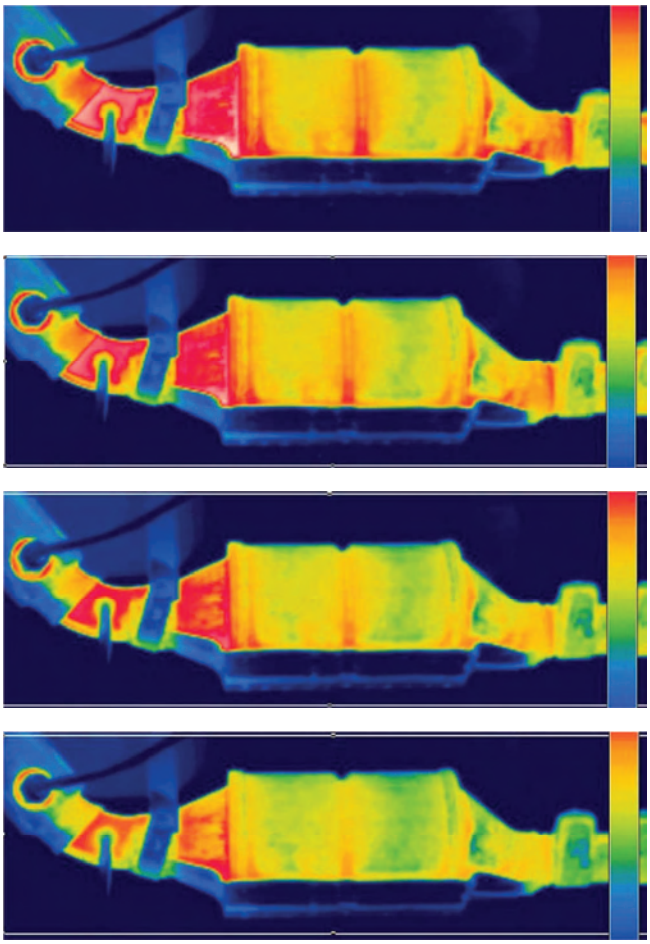

Fig. 6. Thermo-graphic images selected from the measurements – petrol supply, load: 40 Nm, 30 Nm, 20 Nm, 10 Nm

During the analysis of the thermo-grams, besides the temperature values for the individual converter cores, the maximum temperature for the entire catalytic converter was also read. This value was present on the diffuser, which is the first element on the flow path of the exhaust gas through the catalytic converter, and in addition, the exhaust gas has direct contact with the walls. In addition, there is a change of shape, and in the immediate vicinity of the area with the highest temperature there is the cover, also occurs a sheltered section (a kind of recess), where radiation is reflected between the adjacent surfaces. Due to the shield also the impact of ambient conditions is limited. As a result, the maximum temperature is significantly higher than the temperature on the converter cores casing. That is why this temperature was compared to the temperature measured by the thermocouple behind the catalytic converter (Fig. 7 and Fig. 8). The values obtained are less than 5 to 28 K. Because of the lack of insulating elements, the nature of the curve is more consistent with the exhaust gas temperature than the cylindrical surface in which the cores are.

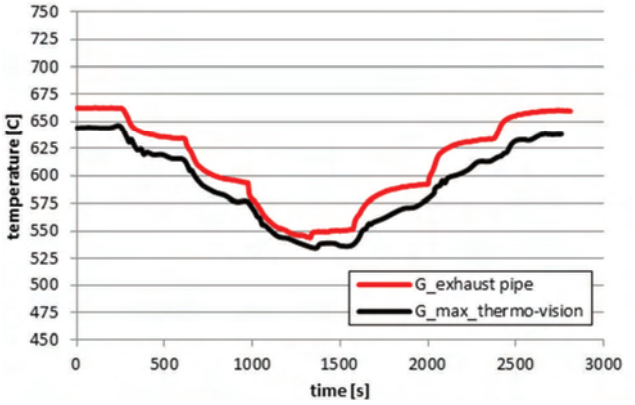

Fig. 7. Comparison of temperature values in the pipe behind the catalytic converter with the maximum from thermo-grams – for petrol

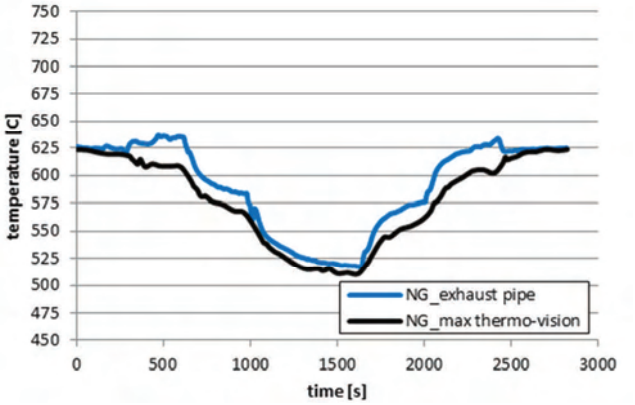

Fig. 8. Comparison of temperature values in the pipe behind the catalytic converter with the maximum of thermo-grams for natural gas

The intensity of electromagnetic radiation depends on the temperature and characteristics of the surface of the observed object. Therefore, for each object the emissivity should be individually determined. The measurements presented in this paper were focused on the heat state of the catalytic converter, so during the preliminary measurements the surface emissivity of the catalytic converter was set at $\varepsilon = 0.75$. As the temperature in the exhaust manifold was also measured using a thermocouple, it was reasonable to compare thermo-grams for the exhaust manifold surface as well. The use of the thermo-vision camera settings for the catalytic converter concerning other parameters (ambient temperature, atmospheric temperature, relative humidity, distance of the examined object from the camera) was appropriate because the tested objects were in the same atmospheric conditions and distance from the measuring device. Using the same emissivity, however, would result in a serious measurement error. The surface of the cast iron exhaust manifold is much more dull than the surface of the steel sheet converter housing, therefore the emissivity of the manifold is $\varepsilon = 0.93$. Use of the emissivity of the converter relative to the exhaust manifold results in a difference in temperature results of about 15%. Figure 9 shows the com-

parison between the exhaust gas temperature at the exhaust manifold and the maximum temperature read from the thermo-gram (Fig. 10) with the specific emissivity for the manifold (ε = 0.93) and the catalytic converter (ε = 0.75).

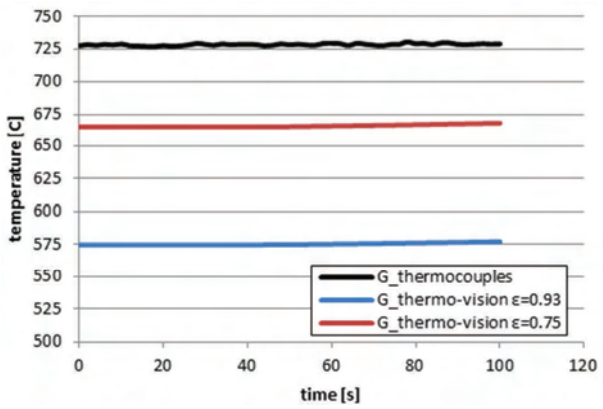

Fig. 9. Comparison of temperature values for exhaust manifold derived from thermocouple and thermo-graphic images (different emissivity)

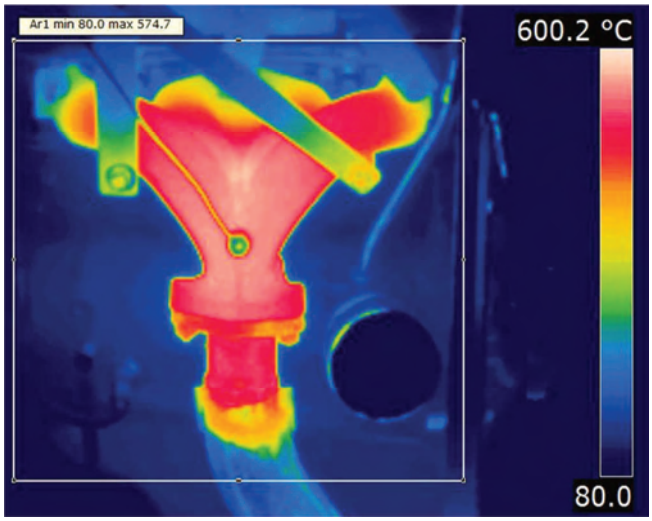

Fig. 10. Thermo-graphic image of the engine exhaust manifold (emissivity ε = 0.93)

5. Conclusions

The exhaust temperature depends primarily on the load on the engine, but also on the composition of the fuel - air mixture and the type of fuel used. Measurements of the thermal state of the catalytic converter at the engine bench were made after the engine was warmed up. The exhaust gas temperature behind the catalytic converter and the catalytic converter surface indicate that during the entire measurement the converter reached the correct temperature for proper operation. However, taking into account the effect of the engine load on the difference between exhaust gas temperature between the exhaust manifold and the pipe behind the catalytic converter, the distance between the exhaust manifold and the device will be of great importance for the conversion rate achieved in the converter. Especially during the operation of the vehicle in urban conditions when most of the time the engine is running at low load or idle speed. The use of ceramic monolith is advantageous in this case because of its lower thermal conductivity and greater specific heat compared to the metal monolith.

The amount of heat radiated outside will always be smaller than the actual amount inside the device being tested, therefore, thermo-vision measurements are a qualitative and not quantitative method whose main advantage is being non-invasive. In the case of a catalytic converter, the insulating mats between the converter cores and the casing also have an effect on the temperature distribution on the surface of the converter. Nevertheless, the nature of the changes recorded by the thermocouples and the thermo-vision camera was the same; resulting from the conditions of the engine operating . The thermo-grams show differences in the degree of heating of the individual parts of the catalytic converter depending on the conditions set.

A very important aspect during thermo-vision measurements is to determine the correct operating parameters of the camera which depend on the ambient conditions and the emissivity of the tested objects. However, despite many parameters affecting the quality of thermo-vision, this technique proves useful in the thermal analysis of various objects, including engine components.

Bibliography

[1] BIELACZYC, P., MERKISZ, J., PIELECHA, J. Stan cieplny silnika spalinowego a emisja związków szkodliwych. *Wydawnictwo Politechniki Poznańskiej*. Poznań 2001.

[2] DAMIJAN, Z., UHRYŃSKI, A. Systemic cryotherapy influence of low temperatures on selected physiological parameters. *Acta Physica Polonica A*, Polska Akademia Nauk. Instytut Fizyki, Warszawa ; ISSN 0587-4246. 2012, **121**(1-A). *Acoustic and biomedical engineering*, A-38–A-41.

[3] DAMIJAN, Z., UHRYŃSKI, A. The influence of driver's working environment on thermical changes of their organism. *Acta Physica Polonica A,* Polska Akademia Nauk. Instytut Fizyki, Warszawa ; ISSN 0587-4246. 2010, **118**(1), 35-40.

[4] DAMIJAN, Z., UHRYŃSKI, A. The effect of general low frequency vibration on energy balance of a human being. *Acta Physica Polonica.* A, ISSN 0587-4246. 2013, **123**(6). *Acoustic and biomedical engineering,* 970-973.

[5] FLIR. Instrukcja obsługi. 2010.

[6] JAKUBOWSKA, T., PESZYŃSKI-DREWS, C., WIĘCEK, B. Standaryzacja w badaniach termograficznych w zastosowaniu praktycznym na przykładzie pracowni termograficznej w Centrum Diagnostyki i Terapii Laserowej Politechniki Łódzkiej. *Acta Bio-Optica et Informatica Medica*. 2006, **2**(12), 81-84.

[7] KRUCZYŃSKI, S. Trójfunkcyjne reaktory katalityczne. *Wydawnictwo ITE*, Warszawa-Radom 2004.

[8] KRUCZYŃSKI, S. Eksploatacja trójfunkcyjnych reaktorów katalitycznych – dezaktywacja termiczna. *Eksploatacja i Niezawodność*. 2012, **14**(3).

[9] LEPIARCZYK, D., GAWĘDZKI, W., UHRYŃSKI, A., TARNOWSKI, J. Usage of thermo-vision in research concerning kinematic pair of friction in machines and mechanical devices. *Vísnik Kïvs'kogo Nacional'nogo Universitetu Tehnologij ta Dizajnu*. 2012, **3**, 190-195.

[10] LEPIARCZYK, D., UHRYŃSKI, A. Thermo-vision analysis of iron foundry production process concerning secondary usage of heat. *Polish Journal of Environmental Studies*. 2014, **23**(3), 1017-1023.
[11] MADURA, H. at al. Pomiary termowizyjne w praktyce. Warszawa: *Agenda Wydawnicza PAKu*, 2004.
[12] RYBARZ, M., BRZEŻAŃSKI, M. Zagadnienia tworzenia się kondensatu w układzie wylotowym silnika spalinowego. *Czasopismo Techniczne Mechanika*. 2008, **8-M**.
[13] WIŚNIEWSKI, S. Wymiana ciepła, *WNT*, Warszawa 1997.
[14] WORSZTYNOWICZ, B., UHRYŃSKI, A. The analysis of heating process of catalytic converter using thermo-vision. *Combustion Engines*. 2015, **162**(3), 41-51.
[15] WORSZTYNOWICZ, B. Influence of the mixture composition on the conversion degree of catalytic conventer during power supply of the engine with natural gas. *Journal of Polish Cimac. Diagnostic, reliability and safety.* 2013, **8**(2).

Barbara Worsztynowicz, DEng. – AGH University of Science and Technology in the Faculty of Mechanical Engineering and Robotics.

e-mail: *Worsztyn@agh.edu.pl*

Bartłomiej Borkowski, DEng. – AGH University of Science and Technology in the Faculty of Mechanical Engineering and Robotics.

e-mail: *bborkow@agh.edu.pl*

Andrzej Uhryński, DEng. – AGH University of Science and Technology in the Faculty of Mechanical Engineering and Robotics.

e-mail: *uhrynski@agh.edu.pl*

Marek Pluta, PhD – AGH University of Science and Technology in the Faculty of Mechanical Engineering and Robotics.

e-mail: *Pluta@agh.edu.pl*

Article citation info:
STRUŚ, M., POPRAWSKI, W., REWOLTE, M. Testing of the fleet of the vehicles with diesel engines fed by BIOXDIESEL fuel. *Combustion Engines*. 2017, **170**(3), 37-41. DOI: 10.19206/CE-2017-306

Mieczysław STRUŚ
Wojciech POPRAWSKI
Mariusz REWOLTE

CE-2017-306

Testing of the fleet of the vehicles with diesel engines fed by BIOXDIESEL fuel

The paper presents results of testing of the fleet of the parcel delivery vehicles, equipped with the Diesel engines fed by biofuel BIOXDIESEL, manufactured on the way of the ethanol esterification process of the waste vegetable and animal fats, with the addition of the standard diesel fuel and pure ethanol. The comparison results of the vehicles test bed on the beginning of the testing and at the end of the testing, when vehicles were fueled with standard diesel and testing biofuel. The results of the testing at non-stationary states are also presented. The paper presents also results of the drivers evaluation of the performance of the vehicles based on the questionnaire. Presented results show that the BIOXDIESEL fuel is fully replaceable to the standard diesel fuel.

Key words: *biodiesel, fatty acid ethyl esters, compression ignition engines*

1. Introduction

According to Polish and European law, it is allowed to add to the fuel specified for Diesel engines, up to 7% of biocomponents, according to calorific value. Such biocomponents currently are only the fatty acid methyl esters (FAME). Current standards and legal acts regarding quality of biofuels, as well as from tax point of view, require only FAME.

From the other hand, the other type of biocomponents, especially fatty acid ethyl esters FAEE, manufactured from waste animal and vegetable fats, and fully renewable bioetanol, are at least as valuable from engine performance, environmental aspects, and quality point of view.

Currently methanol, which is used as a feedstock to produce FAME is obtained from fossil resources. It is also worth to mention, that methanol and its vapors are toxic.

Replacement of methanol with ethanol allows production of FAEE, which chemical and physical properties are beneficial from fuel point of view. Also the products of combustion of FAEE are less harmful to the environment in comparison with FAME [1].

According to the current Polish law, the selected fleet of the vehicles is defined as a group of at least 4 vehicles, agriculture tractors or other off-highway machines or group of locomotives or ships, equipped with the engines which can be fueled with liquid biofuel. The vehicles should be used by the same user. The law allows, that the properties of the fuel can be different than stated in standards or other legal requirements.

2. Description of the testing fuel

For testing of the fleet vehicles the experimental fuel BIOXDIESEL has been used. This new fuel is a blend of the Fatty Acid Ethyl Esters (FAEE) with addition of standard Diesel fuel and bioethanol. There are also additives, which are improving cold flow properties of the fuel.

Due to lack of the standards in Poland and in Europe regarding FAEE, the physical and chemical properties of the BIOXDIESEL fuel are compared with the PN-EN 590:2013 standard, which describes diesel fuel quality parameters. FAEE quality is also compared with the PN-EN 14214 standard, which regards FAME only.

In the USA, Brasil and India the methyl or ethyl esters are not distinguished in the standards, which are describing fuel parameters. The biofuel just has to meet standard requirements, eg. ASTM D6751 in the USA, ANP 42 in Brasil or IS15607:2005 in India.

Table 1 presents selected quality parameters of the BIOXDIESEL fuel (results obtained by the authors) compared with PN-EN 590 and PN-EN 14214+A1.

Table 1. Selected quality parameters of the BIOXDIESEL fuel compared with standards for Diesel fuel and for FAME

Parameter	Units	Properties of BIOXDIESEL fuel	PN-EN 590:2013 requirement		PN-EN 14214+A1 requirement	
			min	max	min	max
Cold Filter Plugging Point	[°C]	–17	Season dependent eg. intermediate –10°C		Season dependent eg. intermediate –10°C	
Cetane number		51.9	51		51	
Density at 15°C	kg/m^3	868	820	845	860	900
Flash point	°C	24	55		101	
Viscosity at 40°C		2.33	2	4.5	3.5	5
Calorific value	MJ/kg	38.5	42.8		38	

The fatty acid ethyl esters were obtained on the way of transesterification of the waste animal (pork and poultry) fats, waste vegetable fats, eg. used frying oils and small addition of fresh rapeseed oil with bioethanol in the presence of alkali catalyst (KOH). The selection of feedstock for production of FAEE used for BIOXDIESEL fuel is described in [6].

The application of waste animal fats as a feedstock for biodiesel production is a subject of an intensive research also around the world, eg. [2, 3].

The BIOXDIESEL used for feeding the engines of the fleet vehicles used for the testing is a blend mate of about 70% of biocomponents (FAEE and bioethanol) and about 30% of diesel fuel with additives.

3. Description of the fleet vehicles used for testing

The fleet used for testing consisted of 15 parcel delivery vehicles. The vehicles have been used on different duty cycles: 5 vehicles were operated in the cities, 5 in long distances and 5 vehicles in the mixed duty cycles. Table 2 describes the fleet vehicles and their engines.

Table 2. Description of vehicles and engines used for fleet testing

Make, model	Year of build	Engine displacement [ccm], no of cylinders	Max engine power [BHP]	Max engine torque [Nm]
Citroen Jumper	2011	2200, 4 cyl	100	250
Citroen Berlingo	2011	1560, 4 cyl	75	185

4. Testing procedures of the fleet vehicles fed with BIOXDIESEL fuel

The vehicles have been thoroughly examined before start of the testing.

On the day of fuel replacement, the engine performance was evaluated on the vehicle test bed, when vehicles were fed with standard Diesel fuel. Also the engine performance in non-stationary condition was measured according to the procedure described in [1] and [5].

Just before filling the vehicles' fuel tanks with BIOXDIESEL fuel the oil, oil filters and fuel filters were replaced with the new ones.

Then the vehicles were tested with in non-stationary conditions according to [1] and [5] again with the experimenttal fuel. Also the vehicles engine performance was tested on the vehicle test bed.

In the middle of the test the vehicles engine performance was measured in non-stationary states.

Then at the end of the test vehicles were tested in non-stationary conditions and on the vehicle test bed with BIOXDIESEL fuel and after replacement with standard Diesel fuel.

4.1. Description of the testing in non-stationary conditions

The testing procedure is described in details in [1] and [5]. The testing in non-stationary conditions consists the set of rapid acceleration and deceleration of the engine from idling to maximal speed, back to idling. The engine is loaded by the moment of inertia of moveable parts of the engine.

The cyclodynes are the curves drawn on the engine torque – engine revolution plane. It is possible to draw cyclodynes in the angular acceleration – engine crankshaft rotational velocity, when the information about polar moment of inertia of the engine is not known. For comparison purposes it is possible to use the angular acceleration - engine speed plane.

The cyclodynes remain loops, which positive part is drawn when accelerating and negative part during deceleration. The area of the positive part of cyclodynes is related to the energy generated by the engine during acceleration (depend calorific value of the fuel and efficiency of burning of the fuel), while negative part of the cyclodyne depends on overall condition engine and quality of lubrication oil in the engine.

4.2. Description of the on the vehicle test bed

The performance of the vehicles was evaluated in co-operation of ECU-PROJECT company, on the 4DW test bed manufactured by Dynoproject. This test bed is able to test the vehicles with maximum power of 1000 BHP and maximum torque of 1000 Nm and results are corrected according to DIN 70020.

The torque and power vs. engine crankshaft revolution graphs have been obtained for each of the vehicles.

5. Description of the vehicles performance evaluation based on the questionnaire

The drivers of the vehicles were obliged to fill in the questionnaire describing their subjective opinion about vehicle's performance. They had to provide their opinion about following vehicles' performances:

- Traction of the vehicles (acceleration of the vehicles and driving with load);
- Engine performance (cold start, hot start, engine noise and exhaust evaluation);
- Vehicle's tachometer at the beginning of each drive, date and type of the duty (urban, extra urban, mixed);
- Information about amount of the fuel filled;
- Information about the service or repair activities.

The engine and vehicle's performance was evaluated based on the 3 grades: low, middle and high.

6. Results

The results consisted a set of data obtained on the vehicle test bed and also results of the data coming from the testing in non-stationary conditions.

6.1. Results of the vehicles performance measured on the vehicle test bed

Table 3 presents results of measurement of peak engine power and peak engine torque measured on the test bed for selected vehicles at the end of the test. It is noticeable, that the maximum power for Berlingo vehicles is about 8% lower when fueling with BIOXDIESEL fuel in comparison with standard diesel fuel. Similar trend can be observed for torque measurement. This can be explained with the fact, that the calorific value of BIOXDIESEL fuel is 10% lower than standard Diesel fuel.

Table 3. Examples of results of the vehicle test bed obtained for selected Citroen Berlingo vehicles, obtained at the end of the test

	Standard diesel fuel		BIOXDIESEL fuel	
	Max Power	Max torque	Max Power	Max torque
	BHP(RPM)	Nm	BHP(RPM)	Nm
Berlingo_1	76(3135)	187.7(2256)	69.6(3030)	173.3(2200)
Berlingo_2	76.6(3096)	186.9(2255)	68.2(2993)	170.6(2213)
Berlingo_3	77.9(3067)	191.8(2181)	68.8(3058)	169.9(2173)
Berlingo_4	76.8(3080)	188.5(2222)	68.4(3045)	167.1(2194)
Berlingo_5	74.9(3112)	180(2253)	66.9(3035)	160.8(2243)
Berlingo_6	76.3(3087)	188.4(1964)	68.7(3033)	166.3(2266)
Berlingo_7	73(3054)	179.7(1981)	66.3(3157)	164.5(2229)
Berlingo_8	75.3(3061)	187.8(2205)	69(3012)	172.6(2172)
Average	75.6(3204)	185.6(2177)	68.0(3041)	167.8(2213)

In Table 4 results of measurement of the peak power and torque measured on the test bed for are presented. It is

noticeable, that the maximum power for Jumper vehicles is about 7% lower when fueling with BIOXDIESEL fuel in comparison with standard diesel fuel. Similar trend can be observed for torque measurement, the torque drop when fueling with experimental fuel is about 8% lower in comparison with standard Diesel fuel, even though the calorific value of BIOXDIESEL is lower by 10% than Diesel fuel.

Table 4. Examples of results of the vehicle test bed obtained for selected Citroen Jumper vehicles, obtained at the end of the test

	1 ON		2 BIOXDIESEL	
	Max Power	Max torque	Max Power	Max torque
	BHP(RPM)	Nm	BHP(RPM)	Nm
Jumper_1	116.5(3146)	279.4(2709)	105.4(3350)	244.6(2733)
Jumper_2	113.5(3050)	282(2627)	102.7(3142)	248.9(2659)
Jumper_3	115.6(3014)	283.5(2691)	109.3(3000)	270.5(2618)
Jumper_4	109.8(3208)	266.8(2638)	105.1(3171)	259.3(2607)
Jumper_5	116.7(3045)	285.5(2666)	108.8(3252)	259.9(2725)
Average	114.42(3092.6)	279.44(2666.2)	106.26(3183)	256.64(2668.4)

6.2. Results of the vehicles performance measured in non-stationary conditions

Due to shorter measurement procedure the testing in the non-stationary condition took place also in the middle of the long term test.

Figure 1 shows examples of cyclodynes obtained for one of Citroen Berlingo vehicles in the beginning of the test (start day), while figure 2 shows the results of the measurement obtained at the end of the test.

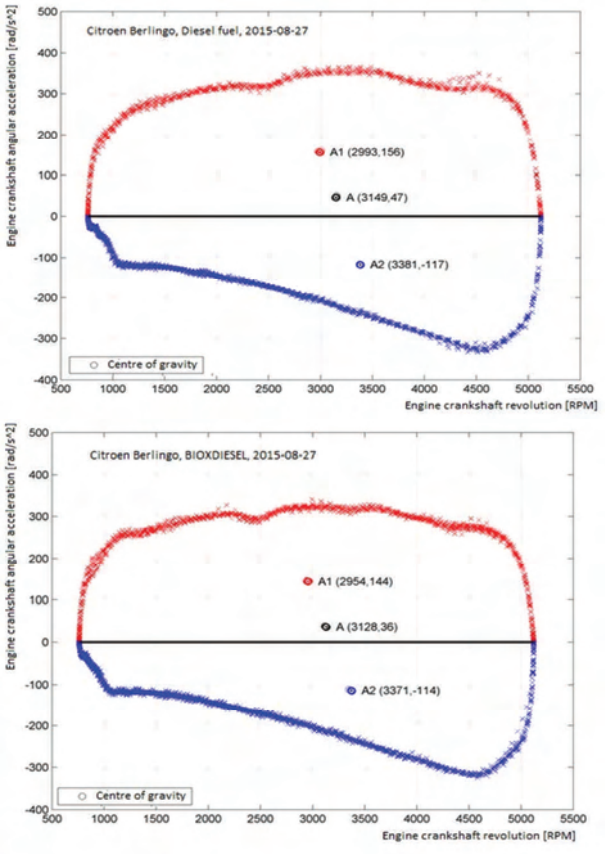

Fig. 1. Results of the testing in non-stationary conditions, start day of the testing; top – standard Diesel fuel, bottom – BIOXDIESEL fuel

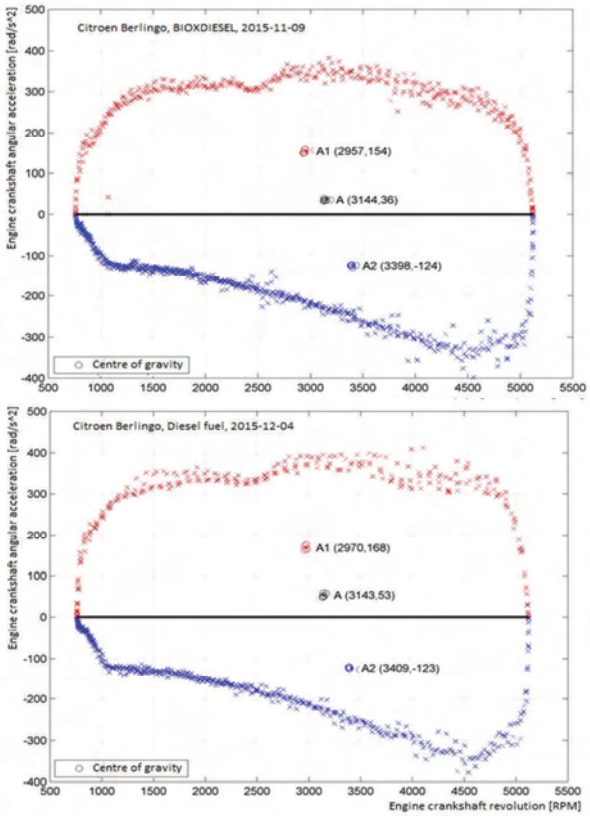

Fig. 2. Results of the testing in non-stationary conditions, end of the testing; top – BIOXDIESEL fuel, bottom – standard Diesel fuel

The outcome of the test in non-stationary condition is the value of the area of the positive part of the cyclodyne loop. The area is proportional to energy conversion of the fuel. Tables 5 and 6 present the area of the cyclodynes obtained at different stages of the test for Berlingo and Jumper vehicles. One can notice, that similarly to the results of the vehicle test bed measurements, the performance of the vehicles was about 8% lower when using the BIOXDIESEL fuel than standard diesel fuel.

Table 5. Results of the testing the group of Citroen Berlingo vehicles in non-stationary conditions – area of cyclodynes

Vehicle	1 ON	2 BIOXDIESEL	3 BIOXDIESEL	4 BIOXDIESEL	5 ON
	P_1	P_1	P_1	P_1	P_1
	[rad/s^2] [1/min]	[rad/s^2] [1/min]	[rad/s^2] [1/min]	[rad/s^2] [1/min]	[rad/s^2] [1/min]
Berlingo_1	1316313	1213310	–	1274083	1418216
Berlingo_2	1280899	–	–	1251420	1391665
Berlingo_3	1351733	1265174	0	1255458	1341255
Berlingo_4	1307915	1237558	1286056	1270063	1376368
Berlingo_5	1316467	1222883	1215428	341941	1462068
Berlingo_6	1328186	-	–	1189034	1346919
Berlingo_7	1302171	1182546	–	–	–
Berlingo_8	1338380	1226060	1267457	1300205	1368112
Berlingo_9	–	–	1270898	1286918	1387675
Average	1317758	1224588	1259959	1271140	1386535

Table 6. Results of the testing the group of Citroen Jumper vehicles in non-stationary conditions – area of cyclodynes

Vehicle	1 ON	2 BIOXDIESEL	3 BIOXDIESEL	4 BIOXDIESEL	5 ON
	P_1	P_1	P_1	P_1	P_1
	[rad/s^2] [1/min]	[rad/s^2] [1/min]	[rad/s^2] [1/min]	[rad/s^2] [1/min]	[rad/s^2] [1/min]
Jumper_	1214621	1163422	1241925	1349096	1340930
Jumper_2	1357113	1138616	1459679	1391904	1509587
Jumper_3	1261361	1183280	1228581	1315499	1263977
Jumper_4	1336754	1246477	1303827	1365905	1377638
Average	1292462	1182949	1308503	1355601	1373033

6.3. Description of the vehicles performance evaluation based on the questionnaire

The numerical values describing maximal engine power or maximal engine torque are not giving the full image of the vehicle performance in everyday operation. It was also necessary to collect the opinions of the drivers about driving the vehicles fueled with standard and experimental fuel.

In order to make the subjective opinions comparable the drivers had to evaluate the vehicle's performance on the base of the questionnaire:

– Traction of the vehicles (acceleration of the vehicles and driving with load);
– Engine performance (cold start, hot start, engine noise and exhaust evaluation);

Above questions were evaluated in three grades: low, middle and high.

The questions below were additional, which helped analyzing the data:

– Vehicle's tachometer at the beginning of each journey, date and type of the duty (urban, extra urban, mixed);
– Information about amount of the fuel filled;
– Information about the service or repair activities.

Assuming, that the 'law' value is scored by 0 points, 'medium' as 50 points and 'high' as 100 points, the results of the evaluation for the group of Citroen Berlingo are presented in Table 7.

Table 7. Results of drivers' evaluation of Citroen Berlingo when fuelling with BIOXDIESEL (averaged)

Vehicle	Accelera-tion	Drive with load	Cold start of the engine	Hot start of the engine	Noise	Exhaust
Berlingo_1	100%	100%	100%	100%	100%	100%
Berlingo_2	100%	100%	100%	100%	100%	100%
Berlingo_3	50%	50%	50%	50%	50%	50%
Berlingo_4	100%	100%	94%	100%	98%	97%
Berlingo_5	50%	100%	100%	100%	50%	48%
Berlingo_6	100%	99%	100%	100%	100%	42%
Berlingo_7	51%	52%	90%	100%	100%	100%
Berlingo_8	50%	50%	100%	100%	100%	50%
Berlingo_9	100%	100%	86%	100%	88%	94%
Berlingo_10	100%	51%	69%	94%	51%	94%
Average	**80%**	**80%**	**89%**	**94%**	**84%**	**78%**

Evaluation of the vehicles' performance during the fleet testing was very positive. The drivers did not observe a lack of power, poor acceleration of the vehicles or excessive fuel consumption. No major problems were observed with the cold start of the engine (the test was carried from August to December), this means the end of the test took place in colder weather conditions. There were no problems with hot start of the engines. The drivers did not observe s in exhaust gases smoke during acceleration or during driving with heavier load.

Table 8. Results of drivers' evaluation of Citroen Jumper performance with fueling with BIOXDIESEL (averaged)

Vehicle	Accelera-tion	Drive with load	Cold start of the engine	Hot start of the engine	Noise	Exhaust
Jumper_1	100%	100%	29%	85%	71%	81%
Jumper_2	89%	94%	94%	100%	100%	100%
Jumper_3	100%	100%	7%	67%	50%	100%
Jumper_4	100%	100%	100%	100%	100%	100%
Jumper_5	94%	86%	77%	89%	78%	83%
Average	**97%**	**96%**	**61%**	**88%**	**80%**	**93%**

Table 9. Comparison of fuel consumption of the selected Citroen Berlingo and Citroen Jumper before the test (standard diesel fuel) and with BIOXDIESEL fuel

Vehicle	Diesel fuel			Diesel fuel		
	August - December 2014			February - July 2015		
	amout of fuel [dm^3]	Covered distance [km]	Fuel consumption [dm^3/100km]	amout of fuel [dm^3]	Covered distance [km]	Fuel consumption [dm^3/100km]
Berlingo 1	271	2824	9,6	124	1073	11,6
Berlingo 2	312	3531	8,8	-	-	-
Jumper 1	1901	18795	10,1	546	4235	12,9
Jumper 2	1037	10611	9,8	1129	12505	9,0
Vehicle	BIOXDIESEL			BIOXDIESEL		
	August - December 2015			February - April 2016		
	amout of fuel [dm^3]	Covered distance [km]	Fuel consumption [dm^3/100km]	amout of fuel [dm^3]	Covered distance [km]	Fuel consumption [dm^3/100km]
Berlingo 1	173	1460	11,9	175	1738	10,1
Berlingo 2	312	3503	8,9	276	2812	9,8
Jumper 1	-	-	-	389	3152	12.3
Jumper 2	-	-	-	538	4598	11.7

Table 9 presents comparison of fuel consumption recorded one year before the start of the test, using standard Diesel fuel and during the test with BIOXDIESEL fuel.

7. Summary and conclusions

Unlike the vehicles performance measurement on the vehicle test bed or testing the engines in non-stationary conditions, the drivers did not see a drop of performance of the vehicles when fueling with the BIOXDIESEL fuel. The difference of the maximal engine power and torque did not influence the daily operation of the vehicles. No major maintenance problems were observed. It is worth to mention, that the parcel delivery vehicles are operated in difficult duty cycle: high number of start and stop of the engine per day, driving mainly in urban conditions.

It is worth to notice, that in case of the Berlingo's, the maximum power of the engines appears in lower engine speed when fueling with BIOXDIESEL in comparison with the standard diesel fuel.

Also the fuel consumption of the BIOXDIESEL fuel is not significantly different to standard Diesel fuel.

Presented results of testing the engines fueled with the BIOXDIESEL and Diesel show:

- similar efficiency engine feeding BIOXDIESEL and Diesel,
- fuel consumption, vehicles behaviour in everyday natural operation remained the same for standard Diesel and BIOXDIESEL;
- lack of linear relations between calorific value of biofuel and the peak power of the engine related to the standard diesel fuel confirms more efficient combustion of BIOXDIESEL fuel.

Analysis of presented in this paper results of the road testing, vehicle test bed measurement, testing in non-stationary conditions and evaluation of vehicle performance by the drivers in day by day operation entitle to state, that the BIOXDIESEL fuel is very advanced, and can be used as an alternative fuel for all Diesel engines.

Nomenclature

FAEE – fatty acid ethyl esters
FAME – fatty acid methyl esters

Bibliography

[1] STRUŚ, M.S. Ocena wpływu biopaliw na wybrane właściwości eksploatacyjne silników o zapłonie samoczynnym. *Oficyna Wydawnicza Politechniki Wrocławskiej*, Wrocław 2012.

[2] RAMALHO, E., SANTOS, I., MAIA, A. et al. Thermal characterization of the poultry fat biodiesel, *Journal of Thermal Analysis and Calorimetry*. 2011, **106**, 825-829.

[3] CHAKRABORTY, R., GUPTA, A.K., CHOWDHURY, R. Conversion of slaughterhouse and poultry farm animal fats and wastes to biodiesel: parametric sensitivity and fuel quality assessment, *Renewable and Sustainable Energy Reviews*. 2014, **29**, 120-134.

[4] STRUŚ, M.S. Efektywność silników spalinowych o zapłonie samoczynnym zasilanych paliwem Bioxdiesel z komponentami całkowicie odnawialnymi. *Inżynieria Maszyn*. 2014, **2**(19), 108-115.

[5] STRUŚ, M.S. The biofuel Bioxdiesel with ethyl components in feeding Diesel engines. *Silniki Spalinowe*. 2011, **3**, 1-9.

[6] STRUŚ, M.S., POPRAWSKI, W., REWOLTE, M. Efficiency of raw material selection for the second generation BIOXDIESEL biofuel for Diesel engines. *Combustion Engines*. 2015, **144**(3), 1053-1059.

[7] STRUŚ, M.S., POPRAWSKI, W., REWOLTE, M., KARDASZ, P. Feeding the engines of fleet vehicles with BIOXDIESEL fuel and heavy alcohols. *Journal of KONES*. 2016, **23**(4), 495-503.

Mieczysław Struś, DSc., DEng. – Faculty of Mechanical and Power Engineering, Wrocław University of Technology.

e-mail: *Mieczyslaw.Strus@pwr.edu.pl*

Wojciech Poprawski, DEng. – Faculty of Mechanical and Power Engineering, Wrocław University of Technology.

e-mail: *Wojciech.Poprawski@pwr.edu.pl*

Mariusz Rewolte, MEng. – Proagroenergia Przedsiębiorstwo Innowacyjno-Wdrożeniowe sp. z o.o.

e-mail: *Mariusz.Rewolte@proagroenergia.pl*

Acknowledgement

This research has been funded under INNOTECH II Programme, project no. INNOTECH-K2/INZ/88/182607/NCBiR/13.

Article citation info:
STELMASIAK, Z., LARISCH, J., PIETRAS, D. Selection of an algorithms controlling operation of supercharged compression ignition engine with additional fueling with CNG gas. *Combustion Engines*. 2017, **170**(3), 42-48. DOI: 10.19206/CE-2017-307

Zdzisław STELMASIAK
Jerzy LARISCH
Dariusz PIETRAS

CE-2017-307

Selection of an algorithms controlling operation of supercharged compression ignition engine with additional fueling with CNG gas

The article presents an issues concerning selection of controlling algorithms for operation of supercharged compression ignition engine fueled additionally with CNG gas, including implemented control procedures, adjustment algorithms and operational algorithms. As the result, the engine which is run in dual fuel system operates under control of two controllers, factory ECU controller, governing fueling with the base fuel (Diesel oil) and all fueling parameters, and the second controller for gaseous fuel supply. Priority of operation of the controllers relates to fueling with Diesel oil, while the gas is treated as supplementary fuel. Due to possibility of usage of factory-made original ECU controller as used with Diesel oil supply; it has been presented proposal of its software in form of array algorithms.

Key words: *compressed natural gas, dual fuel engine, work parameters, toxicity, smoke, engine controlling*

1. Introduction

The main objective of the study was to assess a possibility of reducing smoke in exhaust gases by small additive of CNG natural gas. Reduction of the smoke in exhaust gases leads to reduction of emission of PM particulate matter, component of exhaust gases considered as highly toxic and the most severely restricted by international regulations concerning the problem of toxicity of exhaust gases [1, 3–6, 11–13, 16]. At the same time, the smoke comprising soot as its main component, is actually generating a big problem in operation of compression ignition engines in transient, urban driving conditions, especially during winter season [2, 10, 12, 15]. Excessive smoke, and thus emission of particulate matter under these conditions result in increased frequency of DPF filter regeneration, what reduces its service life and generates emission of toxic compounds during the regeneration. The utilitarian objectives of the study were to evaluate potential for partial substitution of liquid fuel by gas, to determine what are safe shares of the gas assuring correct operation of the engine and maintaining its service life, as well as developing of a map with control parameters of dual fuel engine in scope of fueling with Diesel oil and gas, which would be possible to be implemented in traction engines. Developed maps can be used to programming of already existing control systems, governing operation of EUS engine, or to construction of a new systems during adaptation of traction engines to dual fuel supply, provided that these engines are equipped with electronic injection systems of liquid and gaseous fuel.

The research was performed within framework of the Project No. PBS1/A6/13/2012 funded by NCB&R on a serial engine of Fiat 1.3 MJT type. The study assumes that the main control parameters for dual fuel engine supply should be:

- division method of unit dose of Diesel oil in range of quantity and size of partial doses;
- injection advance angle of the first initial dose and delay angles of remaining doses;
- size of the dose and injection parameters of natural gas.

These parameters were investigated in complete range of engine operation, what results from its destination as a traction engine. It has been assumed that total dose of Diesel oil should vary from nominal dose of traditional fueling within limits of about 40% for minimal engine load, and up to about 70% in area of maximal engine loads. Assumed dose resulted from necessity to ensure knocking-free engine operation in complete field of engine operation, and to maintain temperature of exhaust gases within acceptable limits. Such assumptions should assure failure-free operation of dual fuel engine over a long period of time. High energetic shares of natural gas at partial engine loads, up to 60%, should ensure a significant operational exchangeability of liquid fuel by gas, what due to difference in price of the both fuels should bring significant operational savings of the engines.

2. Research stand

As object of the research work was used supercharged compression ignition engine of FIAT 1.3 MJT type, destined to powering of passenger cars from compact class. The engine is equipped with second generation, direct injection system Common Rail (CR) with division of the dose, so called Multi Jet. The Multi Jet injection technology enables active changing of injection characteristic of Diesel oil, resulting in reduction of engine noise, reduction of harmful emissions and improved engine performance. In this engine is used turbocompressor with constant geometry. Controlling of boost pressure is performed with use of wastegate valve, based on pressure of intake manifold. The supercharged air is cooled. The FIAT 1.3 MJT engine complies with EURO 4 emission standards, owing to EGR valve with cooler of recirculated exhaust gases. Technical parameters of this engine are presented in the Table 1.

Table 1. Technical specification of Fiat 1.3 MJT engine [19]

Engine type	1.3 MJT
Bore x stroke	69.6 x 82 mm
Displacement	1248 cm^3
Number of cylinder	4
Compression ratio	18
Maximum power	51 kW przy 4000 rpm
Maximum torque	180 Nm przy 1750 rpm
Injection system	Common Rail
Number of valve per cylinder	4
Timing system	DOHC
Exhaust gas recirculation	EGR valve

a)

b)

Fig. 1. Intake manifold and test stand of Fiat 1.3 MJT engine:a) intake manifold, b) engine Fiat 1.3 MJT

The engine was adapted for simultaneous combustion of two fuels – natural gas and Diesel oil. It was used a prototype inlet manifold with four injectors of gas, enabling sequential injection of gas in area close to inlet valves. Moreover, it have been installed additional pipes (with coolant, supplying gas and air), and wiring harness connecting gas supply installation with the ECU and with the engine [17, 18, 20]. View of prototype manifold and the engine is shown in the Fig. 1.

Commercially available system of Oscar-N Diesel SAS type was used in adaptation of the engine [20]. It is a system of sequential ignition of gas (CNG or LPG) developed by EuropeGas Company, destined to compression ignition engines. The main components of this system are presented in the Fig. 2.

In result, the engine run in dual fuel supply system operated under control of two controllers: factory-made ECU_{DO}, controlling the neat fuel (Diesel oil) and all parameters of the supply, and ECU_{CNG} controller for fueling with gas. Operational priority of the controllers concerns fueling with Diesel oil, while the gas is treated as a supplementary fuel [18].

3. Selection of algorithms to controlling operation of dual fuel engine

Additional controllers used with dual fuel systems in compression ignition engines are generally of all-purpose character and are dedicated to various engines. Such controllers comprise necessary software for strategic and controlling procedures, but in practical application they can differ in their availability, with suitable interfaces to these procedures and their abilities to shaping appropriate operational characteristics. The control system used in the research work required usage of two controllers, factory made ECU_{DO} controller, governing injection of Diesel oil and other fueling parameters, and ECU_{CNG} controller, to feeding with gas and performing injection of gas in accordance with programmed operational characteristics. The controller enables displaying of the following messages about exceeded preset parameters. Below is the list of all monitored messages:

- maximal temperature of exhaust gases,
- maximal level of knocking,
- lacking thermo-couple,
- high or low temperature of the reducer,
- low pressure of gas,
- low or high MAP pressure,
- low or high voltage of battery,
- low temperature of gas,
- low rotational speed of the engine,

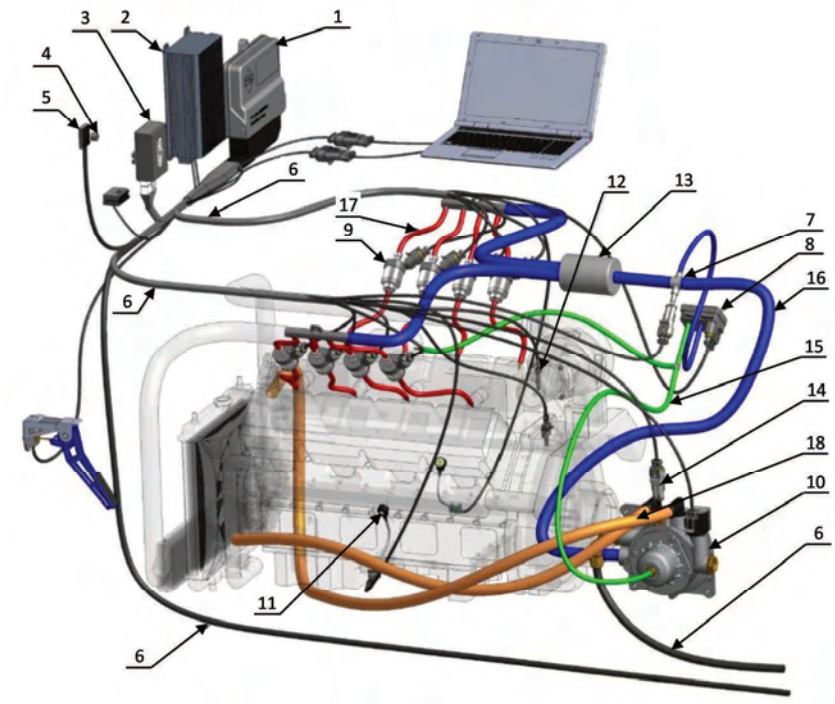

Fig. 2. Scheme of installation of CNG supply of OSCAR-N Diesel SAS type [20]: 1 – controller, 2 – power supply of the system- inverter 24V/12V – DC/DC, 3 – emulator TPS, 4 – buzzer, 5 – switch, 6 – wiring harness, 7 – measuring Tee, 8 – MAP sensor, 9 – injectors, 10 – reducer, 11 – knocking sensor, 12 – thermocouple, 13 – filter of violate phase, 14 – sensor of reducer's temperature, 15 – pipe – pressure in the manifold, 16 – pipe – low pressure of gas, 17 – pipe – low pressure of gas, 18 – pipe – heating of reducer, 19 – high-pressure pipe – supply of gas from bottle

– high rotational speed of the engine,
– high outlet temperature of exhaust gases,
– high level of knocking,
– lacking rotational speed,
– braking with engine,
– too short injection times of gas,
– too long injection times of gas,
– electro-valves switched on,
– pilot injection,
– emergency switch-off the system,
– recorded errors of the system, (message is displayed when in the controller's memory are written errors),
– emulators active.

Obviously, it would be possible to develop a single controller which would govern program of engine fueling, but it would require stipulations with many engine manufacturers, and due to it, such method of controlling would not be all-purpose. The Oscar-N Diesel SAS system, along with the controller, features many advantages such as: precise and safe supply with gas, easy installation of gaseous system, sequential mode of injection, short injection times, control of injection pressure of the gas, and ability of emulation of "accelerator pedal", programmable control algorithms of array type, and operational algorithms, which in all states and conditions of engine operation can jointly control injection of gas in dual fuel engine with compression ignition. Control of Diesel oil injection was accomplished on the basis of factory controller without interfering with its controlling parameters. Such approach in the research process should reflect commonly used, classical way of accomplishment of commercial dual fuel installations in compression ignition engines.

Selection of parameters of the control algorithms to dual fuel engine has comprised the following control functions:

- Control of opening times of injectors and values of injection advance angle for individual portions of Diesel oil: Pilot, Pre, and Main;
- Control of fuel pressure value in Common Rail and value of boost pressure inside inlet manifold (accomplished by control of turbocompressor unit),
- Control of opening time of CNG gas injectors.

Above mentioned parameters were controlled in function of position of accelerator lever (ACC – accelerator) and rotational speed of the engine (n).

The tables of the above algorithms have 81 fields in 9 x 9 coordinate system. Tables 2–4 show values of the control algorithms of opening times of injectors for individual portions of the dose of Diesel oil at dual fuel supply. Specified values take into consideration reduction of total quantities of injected Diesel oil due to additive of gas, in relation to the engine run on neat Diesel oil. Using colours are marked in the tables such areas of the control parameters having influence on reduction of beneficial effects resulting from additive of CNG gas.

Tables 5–7 show values of the control algorithms of injection advance angle for each portions of Diesel oil dose at dual fuel supply. These values are similar to the values used in the engine run on Diesel oil only. There was none possibility to change value of this parameter in course of the investigations. It resulted solely from algorithms written and executed for supply with Diesel oil by factory-installed controller of the engine. As in case of the previous arrays, with colour are marked areas of control parameters having influence on reduction of beneficial effects resulting from additive of CNG gas.

Table 2. Control algorithm of opening time of Diesel oil injectors for Pilot dose at dual fuel supply of the engine

Pilot injection timing – diesel oil [μs]									
100	320	350	0	0	0	0	0	0	0
75	220	350	0	0	0	0	0	0	0
55	315	350	0	0	0	0	0	0	0
40	315	345	0	0	0	0	0	0	0
30	310	0	0	0	0	0	0	0	0
20	310	0	0	0	0	0	0	0	0
15	310	325	0	0	0	0	0	0	0
10	320	330	0	0	0	0	0	0	0
5	320	330	0	0	0	0	0	0	0
ACC [%]	**1000**	**1500**	**2000**	**2500**	**3000**	**3500**	**4000**	**4500**	**5000**
	Engine speed n [rpm]								

Table 3. Control algorithm of opening time of Diesel oil injectors for Pre dose at dual fuel supply of the engine

Pre injection timing – diesel oil [μs]									
100	290	290	277	274	240	0	0	0	0
75	290	290	277	274	240	0	0	0	0
55	290	295	277	274	240	255	215	0	0
40	290	295	278	275	255	265	215	0	0
30	295	300	285	278	275	265	220	0	0
20	295	320	280	280	275	270	220	0	0
15	295	325	288	300	280	275	225	0	0
10	325	335	300	320	330	280	230	0	0
5	330	340	310	330	335	285	235	0	0
ACC [%]	**1000**	**1500**	**2000**	**2500**	**3000**	**3500**	**4000**	**4500**	**5000**
	Engine speed n [rpm]								

Table 4. Control algorithm of opening time of Diesel oil injectors for Main dose at dual fuel supply of the engine

Main injection timing – diesel oil [μs]									
100	780	830	910	910	860	725	670	655	605
75	750	780	850	810	790	725	670	625	600
55	630	680	730	705	685	620	620	610	590
40	595	600	670	660	640	585	575	565	540
30	555	570	620	630	600	535	540	545	530
20	505	525	590	560	540	495	495	490	480
15	475	500	545	510	495	460	470	480	465
10	440	460	500	460	450	430	440	450	430
5	345	355	390	380	380	360	355	415	400
ACC [%]	**1000**	**1500**	**2000**	**2500**	**3000**	**3500**	**4000**	**4500**	**5000**
	Engine speed n [rpm]								

Table 5. Control algorithm of injection advance angle of Diesel oil for Pilot dose at dual fuel supply of the engine

Angle advance of injection pilot [°]									
100	12	48	–	–	–	–	–	–	–
75	10	48	–	–	–	–	–	–	–
55	8	19	–	–	–	–	–	–	–
40	8	19	–	–	–	–	–	–	–
30	7	–	–	–	–	–	–	–	–
20	8	–	–	–	–	–	–	–	–
15	8	16	–	–	–	–	–	–	–
10	8	19	–	–	–	–	–	–	–
5	8	18	–	–	–	–	–	–	–
ACC [%]	**1000**	**1500**	**2000**	**2500**	**3000**	**3500**	**4000**	**4500**	**5000**
	Engine speed n [rpm]								

Table 6. Control algorithm of injection advance angle of Diesel oil for Pre dose at dual fuel supply of the engine

Angle advance of injection Pre [º]									
100	8	8	10	17	25	–	–	–	–
75	8	8	10	17	22	–	–	–	–
55	6	7	9	14	20	28	32	–	–
40	6	7	8	12	19	28	30	–	–
30	5	7	8	11	19	26	29	–	–
20	5	7	8	12	18	25	29	–	–
15	5	7	9	12	18	25	29	–	–
10	6	7	10	13	18	25	29	–	–
5	6	7	10	13	18	25	29	–	–
ACC [%]	**1000**	**1500**	**2000**	**2500**	**3000**	**3500**	**4000**	**4500**	**5000**
	Engine speed n [rpm]								

Table.7. Control algorithm of injection advance angle of Diesel oil for Main dose at dual fuel supply of the engine

Angle advance of injection Main [º]									
100	3	3	5	9	15	21	24	27	28
75	2	3	4	9	13	20	23	25	27
55	2	2	3	6	10	17	21	24	26
40	1	2	2	4	10	16	19	22	25
30	1	2	2	3	9	15	18	21	25
20	1	1	2	4	9	15	17	20	25
15	1	2	2	5	9	15	17	20	23
10	2	2	3	6	9	15	17	20	23
5	2	2	3	6	9	15	17	20	23
ACC [%]	**1000**	**1500**	**2000**	**2500**	**3000**	**3500**	**4000**	**4500**	**5000**
	Engine speed n [rpm]								

Table 8 shows values of control algorithms of fuel pressure in Common Rail of Diesel oil at dual fuel feeding.

Table 8. Control algorithm of fuel pressure in Common Rail at dual fuel supply of the engine

Fuel pressure [bar]									
100	750	830	1000	1100	1210	1380	1590	1590	1590
75	730	810	990	1100	1200	1360	1580	1550	1520
55	690	790	980	1105	1200	1310	1370	1360	1360
40	630	740	960	1090	1180	1200	1200	1190	1140
30	580	680	930	1040	1090	1100	180	1050	1040
20	490	520	750	930	1020	1000	980	910	910
15	440	470	620	790	910	920	880	840	840
10	390	430	500	650	750	790	790	780	780
5	300	390	440	540	610	690	680	660	650
ACC [%]	**1000**	**1500**	**2000**	**2500**	**3000**	**3500**	**4000**	**4500**	**5000**
	Engine speed n [rpm]								

Table 9 presents values of control algorithms for opening time of CNG gas injectors. Although values of the opening times are practically at the same level, in practice the value of injected gas has undergone a bigger change. It results from fact of continuous correction of injection pressure of the gas based on pressure change in the intake manifold. Despite such adjustment, share of the gas in total quantities of supplied fuel varies significantly. At low engine loads share of the gas is bigger and decreases with increasing engine load.

It was very important to develop an algorithm to control value of air boost pressure in the intake manifold. In order to restrict emissions of the particulate matter and smoke, it was necessary to verify operation of turbocharger assembly, and its controlling to assure supply of the same mass of the air at dual fuel supply as in case of fueling with Diesel oil only. Values of control algorithm of the boost pressure are presented in Table 10.

Table 9. Control algorithm of opening time of CNG gas injectors at dual fuel supply of the engine

Pilot injection timing – CNG [ms]									
100	1,0	1,0	1,0	1,5	2,0	2,0	2,0	2,0	2,0
75	1,0	1,0	1,0	1,5	2,0	2,0	2,0	2,0	2,0
55	1,0	1,0	1,5	1,5	2,0	2,0	2,0	2,0	2,0
40	1,0	1,5	1,5	2,0	2,0	2,0	2,0	2,0	2,0
30	1,0	1,5	1,5	2,0	2,0	2,0	2,0	2,0	2,0
20	1,5	1,5	2,0	2,0	2,0	2,0	2,0	2,0	2,0
15	1,5	2,0	2,0	2,0	2,0	2,0	2,0	2,0	2,0
10	2,0	2,0	2,0	2,0	2,0	2,0	2,0	2,0	2,0
5	2,0	2,0	2,0	2,0	2,0	2,0	2,0	2,0	2,0
ACC [%]	**1000**	**1500**	**2000**	**2500**	**3000**	**3500**	**4000**	**4500**	**5000**
	Engine speed n [rpm]								

Table 10. Control algorithm of fuel pressure in Common Rail at dual fuel supply of the engine

Boost pressure [mbar]									
100	1700	1840	1880	2000	2000	1960	1900	1780	1700
75	1580	1760	1860	2000	1920	1880	1860	1720	1660
55	1440	1580	1620	1820	1860	1840	1820	1680	1620
40	1280	1400	1520	1750	1700	1640	1620	1600	1540
30	1200	1260	1400	1640	1620	1600	1540	1520	1450
20	1120	1140	1320	1500	1440	1500	1480	1480	1360
15	1050	1100	1280	1360	1400	1440	1430	1420	1320
10	980	1050	1200	1280	1380	1400	1390	1380	1280
5	900	1000	1100	1190	1240	1220	1210	1200	1200
ACC [%]	**1000**	**1500**	**2000**	**2500**	**3000**	**3500**	**4000**	**4500**	**5000**
	Engine speed n [rpm]								

As seen from performed studies, system of additional supply with gas, co-acting with factory controller of Diesel oil, for which the control algorithms are presented above, has got several disadvantages limiting full usage of beneficial effect of addition of CNG gas. The disadvantages include, among others: division of dose into three partial doses Pilot, Pre and Main, too small size of Pre dose, incorrect injection advance angle of Pre dose, too big delay in injection of Main dose, lacking control over recirculation of exhaust gases and lacking possibility of control over supercharging (volumes of supplied air) [18]. Supply of additional fuel in form of gas is resulting, as a rule, in shift of operational point of the engine in control algorithms of Diesel oil to direction of lower loads, as a result of smaller amount of air supplied to the engine (reduction of boost pressure and simultaneous increase of EGR). Since two fuels (Diesel oil + CNG) are supplied to the engine for proper engine load in conditions of reduced quantity of supplied air, it results in increased level of smoke in exhaust gases at some points of engine operation [16, 17]. Also in case of additional fueling with CNG gas, division methods of Diesel oil dose as implemented in the factory controllers, as well as advance angle of individual portions of the dose, are unsuitable for system of the dual fuel supply. In the control algorithms of Diesel oil, shown in Tables 2 to 7, using colour are marked areas of incorrect control parameters.

The above mentioned drawbacks necessitate interfering with software of the factory controller, or developing controller of gas in such way as to allow such overlapping correction of control parameters of Diesel oil, which would allow proper method of dual fuel supply of the engine. These changes are aimed at full use of positive effect of addition of gas in combustion process of Diesel oil. Below

are presented control algorithms of Diesel oil, taking into account proposed changes in parameters of control algorithms contained in the Tables 2 to 7, in tables marked with colour. They concern the following changes:

- completely switched off Pilot dose,
- increased size of portion of Pre fuel dose.

In Tables 11 to 12 are presented proposed values of the control algorithms of opening times of injectors for individual portions of Diesel oil for dual fuel supply (Table 11). Whereas, increase in value of switched off Pilot dose was seen in area marked with more dark colour in the Table 3. Proposed value of opening time of injectors is not the sum of the values from Tables 2 and 3, because in these Arrays are included values of control times, while during evaluation of the times from Table 11, mass of injected fuel per cycle was summed up. Considering specifics of control process of injectors operation, control time of injector operation after summation of the doses will always be lower than sums of the times. In turn, in area marked in lighter colour in the Table 3, increase in value of portion of the dose Pre occurred at the expense of reduced value of portion of the dose Main. Hence, are seen differences in control times both in Table 11 and Table 12, relative to the values specified respectively in Tables 3 and 4.

Table 11. Corrected control algorithm of opening time of Diesel oil injectors for Pre dose at dual fuel supply of the engine

Pre injection timing – CNG [µs]									
100	400	405	375	375	370	0	0	0,0	0,0
75	400	415	375	375	375	0	0	0,0	0,0
55	380	400	380	380	375	375	365	0,0	0,0
40	365	395	380	380	375	375	365	0,0	0,0
30	360	390	385	380	380	375	370	0,0	0,0
20	375	390	380	380	380	375	370	0,0	0,0
15	385	400	385	385	380	380	375	0,0	0,0
10	400	405	390	390	380	380	380	0,0	0,0
5	405	405	400	390	385	380	380	0,0	0,0
ACC	**1000**	**1500**	**2000**	**2500**	**3000**	**3500**	**4000**	**4500**	**5000**
[%]	**Engine speed n [rpm]**								

Table 12. Corrected control algorithm of opening time of Diesel oil injectors for Main dose at dual fuel supply of the engine

Main injection timing – CNG [µs]									
100,0	780	830	865	865	815	725	670	655	605
75,0	750	780	795	760	745	725	670	625	600
55,0	630	680	675	655	640	620	620	610	590
40,0	595	600	615	625	605	585	530	565	540
30,0	555	535	585	585	565	500	505	545	530
20,0	505	500	555	525	515	475	475	490	480
15,0	475	500	515	485	475	445	450	480	465
10,0	440	460	465	440	410	410	405	450	430
5,0	345	355	365	365	355	335	325	415	400
ACC	**1000**	**1500**	**2000**	**2500**	**3000**	**3500**	**4000**	**4500**	**5000**
[%]	**Engine speed n [rpm]**								

In Table 13 are presented proposed values of control algorithms of injection advance angle for individual portions of Diesel oil dose at dual fuel supply. The same as it was occurred in case of value of Pilot dose of liquid fuel, when the Pilot dose is switched off, the algorithm will not include value of injection advance angle. Presented here, proposed values of injection advance angle for the dose Pre were unchanged in relation to the values presented in Table 6. In order to accelerate combustion process of portion of dose Main it was proposed a slight increase of the injection advance angle for this portion of the dose (Table 13) in relation to the values included within coloured area of Table 7. In addition, due to extended injection time of the dose Pre, real interval between end of the injection for portion of dose Pre, and beginning of injection of portion of dose Main will be much shorter than it would be resulted only from correction of the injection advance angle for portion of dose Main. Such approach was taken to restrict unfavorable phenomenon of „reduction of oxygen concentration" by combusted gas contained in combustion chamber (ignition of gas occurs practically at beginning of self-ignition of dose Pre) before start of combustion of dose Main. This phenomenon has an effect on result of combustion of portion of dose Main in reduced concentration of oxygen, what leads to increased smoke in exhaust gases.

In case of numerical values of the algorithms: controlling fuel pressure in Common Rail, opening time of injectors of CNG gas, and air boost pressure inside intake manifold, none corrections were introduced for dual fuel supply in relation to Tables 8, 9 and 10. In particular, the control algorithm of air boost pressure inside intake manifold was especially developed during the experimental research, and the values presented in the Table 10 are values modified with respect to values programmed in the factory controller of Diesel oil.

Table 13. Proposed control algorithm of injection advance angle of Diesel oil for Main dose at dual fuel supply of the engine

Angle advance of injection Main [°]									
100	4	4	6	11	17	21	24	27	28
75	3	4	5	11	15	20	23	25	27
55	3	3	4	8	12	20	24	24	26
40	2	3	3	6	12	19	22	22	25
30	2	3	3	5	11	18	21	21	25
20	2	2	3	6	11	18	20	20	25
15	2	3	3	7	11	18	20	20	23
10	3	3	4	8	11	18	20	20	23
5	3	3	4	8	11	18	20	20	23
ACC	**1000**	**1500**	**2000**	**2500**	**3000**	**3500**	**4000**	**4500**	**5000**
[%]	**Engine speed n [rpm]**								

Use of additive of gas and discussed changes in controlling of dual fuel engine resulted in significant changes in smoke in exhaust gases and emission of particulate matter, which was the primary objective of the research work performed within framework of the Project No. PBS1/A6/13/2012 financed by NCB&R. changes in the smoke were investigated in static conditions, at the points determined by Mo-n (torque – rotational speed) representative for NEDC driving test [14].

Relative changes in the smoke, in comparison with Diesel oil, obtained at the points of NEDC test, were calculated from the formula:

$$\delta S_{DF} = 100 \cdot \frac{S_{DF} - S_{DO}}{S_{DO}} [\%] \tag{3}$$

where: δS_{DF} – relative change in smoke in exhaust gases with correction of air output and with opening time of gas

injector of 2.0 ms, S_{DF} – smoke in exhaust gases from dual fuel engine at opening time of gas injector of 2.0 ms, S_{DO} – smoke in exhaust gases from engine run on Diesel oil.

Relative changes in smoke shown in the Fig. 3 show at a big reduction of smoke both in conditions of urban driving Point 1-15, as well as extra-urban driving Point 16-20. Reduction of the smoke in urban conditions, especially when driving in low temperatures, will contribute to prolonged periods between successive regenerations of PDF filter, what will reduce emissions of toxic compounds generated during purification of this filter [9, 12, 15]. In addition, signaled by a drivers failure rate of engines with assembled DPF filters will be decreased, while operational periods between successive purifications of the DPF filter will be extended.

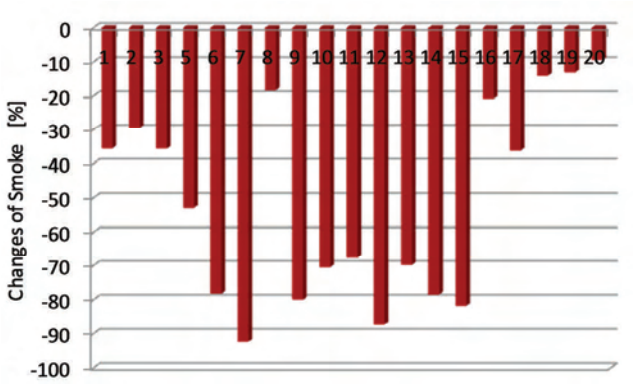

Fig. 3. Changes of smoke in exhaust gases of dual fuel engine at points simulating NEDC test in relation fueling with pure Diesel oil: correction of air output, opening time of gas injector 2.0 ms

Reduction of the smoke is accompanied by reduced emission of particulate matter, what is shown in the Fig. 4. Especially high differences are present at a higher engine loads, Points 19 and 20, when the absolute emissions of exhaust gases are the highest. Relatively lower changes in the PN number of emitted particulate matter at partial engine loads, simultaneously with big changes in smoke shown in the Fig. 3, suggest that additive of gas causes emission of particulate matter with smaller mass (diameter) with respect to emission at traditional fueling. However, these issues require another detailed investigations.

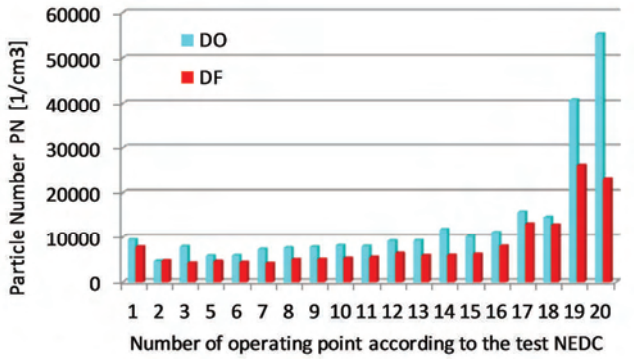

Fig. 4. Comparison of total PN number of particulate matter in exhaust gases of Fiat 1.3 MJT engine fueled traditionally and in dual fuel system: correction of air output, opening time of gas injectors 2.0

To important issues in operation of dual fuel engines belongs replacement of Diesel oil by gas. With constant opening time of gas injectors, such replacement is dependent on engine load, what is seen in the Fig. 5. Increase in share of gas at a higher engine loads would require active change in opening times of gas injectors, what complicates control of dual fuel engines. In addition, possibility of knocking combustion at maximal engine loads should also be taken into considerations. These issues were considered as the main assumptions adapted to the accomplished research work, in which share of gas at maximal engine loads was consciously limited.

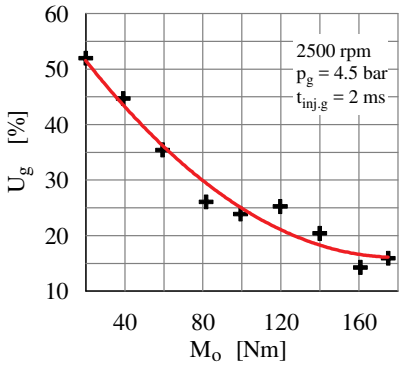

Fig. 5. Changes of gas energy share depending on engine load by fueling with diesel oil and dual fuel: gas injectors opening times 2 ms, fixed gas supply pressure 4.5 bar

4. Summary

In the presented research work on dual fuel supply it have been used two controllers, factory made ECU controller for Diesel oil and additional controller for gas of Oscar-N Diesel SAS type, produced by Europe Gas Company. Control algorithms for gas as presented above were used in controlling of gas. Controlling of Diesel oil dose requires reprogramming of the factory controller or usage of additional controller for Diesel oil with proposed control algorithms, which will take over governing function over injection of liquid fuel after switching to dual fuel supply.

A special patch-type controller can be also produced for simultaneous control of injection of Diesel oil and gas. The basic functions of the Oscar-N Diesel SAS controller can be utilized in control section of gas, which have been tested and have confirmed correct and safe operation of the engine at gaseous fueling.

In adaptations of the engines to dual fuel supply, it is recommended to supply gas to intake manifold as close as possible to inlet valves. The system should be functional both with LPG gas and CNG or LNG. Depending on a type of used gas, a suitable components of the system like tank, reducer, high-pressure pipes, refueling valves and gas flow shut-off electro-valves should be used.

Performed research work has shown that there are real possibilities of reduction of the smoke and particulate matter in modern, high-speed compression ignition engines at low adaptation costs and small modifications in design of the engine. Additional aspect of proposed adaptation is possibility of alternate operation on Diesel oil or in dual fuel system, while maintaining all performance parameters

of the engine, what could have important meaning in case of insufficient number of gas filing stations.

Obtained results of the research work show that dual fuel supply systems with small additive of gas can be also successfully used in future in low capacity engines, used as power units in passenger cars. It can be confirmed by results of the research work performed on Fiat 1.3 MJT engine.

Acknowledgment

The study was performed within framework of Research Project No. PBS1/A6/13/2012 „Reduction of smoke and particulate matter in exhaust gases of automotive engines with compression ignition, accomplished with use of CNG gas addition" financed by NCBiR.

Bibliography

[1] BARROSO, P., RIBAS, X., DOMINGUES, J. et al. Study of dual-fuel (diesel+natural gas) particle mater and CO_2 emissions of a heavy-duty diesel engine during transient operation. *Combustion Engines*. 2013, **153**(2), 28-39.

[2] BEROUN, S., MARTINS, J. The development of gas (CNG, LPG and H2) engines for buses and trucks and their emission and cycle variability characteristics. *SAE Technical Paper*. 2001, 2001-01-0144.

[3] CLARK, N.N., ATKINSON, C.M., ATKINSON, R.J. et al. Optimized emission reduction strategies for dual fuel compression ignition engines running on natural gas and diesel. www.cemr.wvu.edu, 2002, 1-6.

[4] DAISHO, Y., TAKAHASHI, K. Controlling combustion and exhaust emissions in a direct-injection diesel engine dual fueled with natural gas. *SAE Technical Paper*. 1995, 952436.

[5] EHSAN, M., BHUIJAN, S. Dual fuel performance of a small diesel engine for applications with less frequent load variations. *International Journal of Mechanical & Mechatronics Engineering IJMME*. 2011, **9**(10).

[6] FRIEDEMAN, Z. Gasmotoren. *Vogel Buchverlag* Wurzburg, 2001.

[7] GEBERT, K., BECK, J., BARKHIMER, R.L., WONG, H.C. Strategies to improve combustion and emission characteristics of dual-fuel pilot ignited natural gas engines. *SAE Technical Paper*. 1997, 971712, 79-87.

[8] KOWALEWICZ, A. Adaptacja silnika wysokoprężnego do zasilania gazem naturalnym. *Czasopismo Techniczne Wydawnictwo Politechniki Krakowskiej*. 2008, **7-M**, 67-78.

[9] KOZAK, M. Studium wpływu komponentów tlenowych oleju napędowego na emisję toksycznych składników spalin z silników o zapłonie samoczynnym. Monografia habilitacyjna, *Wydawnictwo Politechniki Poznańskiej*, Poznań 2013.

[10] MATYJASIK, M. Aktywizacja procesu spalania mieszaniny gaz-powietrze w silnikach dwupaliwowych przez podział dawki inicjującej oleju napędowego. *Praca doktorska.* Bielsko-Biała 2012.

[11] MERKISZ, J., DASZKIEWICZ, P., IDZIOR, M. et al. Analiza ograniczenia emisji toksycznych składników spalin dwupaliwowego silnika o zapłonie samoczynnym. *Logistyka*. 2014, **6**, 7260-7269.

[12] MERKISZ, J., PIELECHA, J. Emisja cząstek stałych ze źródeł motoryzacyjnych. *Wydawnictwo Politechniki Poznańskiej*. 2014, 309.

[13] MERKISZ, J., PIELECHA, J., ŁABĘDŹ, K., STOJECKI, A. Badania emisji spalin pojazdów o różnej klasie emisyjnej zasilanych gazem ziemnym. *Prace Naukowe Politechniki Warszawskiej. Transport*. 2013, 98, 463-472.

[14] PIETRAS, D., SOBIESZCZAŃSKI, M., ŚWIĄTEK, A., PAJDOWSKI, P. Dobór parametrów pracy silnika 1.3 multijet charakterystycznych dla testu jezdnego NEDC do badań rozwojowych. *PTNSS P05-C065*, PTNSS Kongres 2005.

[15] STELMASIAK, Z., LARISCH, J., PIETRAS, D. Wpływ dodatku gazu ziemnego na zadymienie spalin samochodowego silnika ZS. *Combustion Engines*.2015, **3**.

[16] STELMASIAK, Z., LARISCH, J., PIETRAS, D. Wpływ dodatku gazu ziemnego na wybrane parametry pracy silnika Fiat 1.3 MultiJet zasilanego dwupaliwowo. *Combustion Engines*. 2015, **3**.

[17] STELMASIAK, Z., LARISCH, J., PIETRAS, D. Wybrane problemy adaptacji samochodowego silnika o zapłonie samoczynnym do zasilania dwupaliwowego. *Combustion Engines*. 2015, **3**.

[18] STELMASIAK, Z., LARISCH, J., PIETRAS, D. Some problems of controlling the car diesel engine powered dual fuel. *Combustion Engines*. 2015, **162**(3), 1070-1081.

[19] Materiały firmy FIAT AUTO POLAND, 2014.

[20] Materiały techniczne firmy EuropeGAS, 2013.

Prof. Zdzislaw Stelmasiak, DSc., DEng. – Faculty of Mechanical Engineering and Computer Science at University of Bielsko-Biala.

e-mail: *ZStelmasiak@ath.bielsko.pl*

Jerzy Larisch, DEng. – Faculty of Mechanical Engineering and Computer Science at University of Bielsko-Biala.

e-mail: *JLarisch@ath.bielsko.pl*

Dariusz Pietras, DEng. – Faculty of Mechanical Engineering and Computer Science at University of Bielsko-Biala.

e-mail: *Pietras@ath.bielsko.pl*

Article citation info:
KNEBA, Z., STRASZAK, P., JAKÓBCZYK, K. The effectiveness of fault detection in common rail injectors examination methods. *Combustion Engines*. 2017, **170**(3), 49-56. DOI: 10.19206/CE-2017-308

Zbigniew KNEBA
Paweł STRASZAK
Klaudia JAKÓBCZYK

CE-2017-308

The effectiveness of fault detection in common rail injectors examination methods

The article presents the effectiveness tests of fault detection in common rail injectors. 40 injectors with different wear levels were tested. Testing was made on two test benches of a completely different design. Research includes comparison of accuracy, reproducibility and testability to detect specific defects. A device was created for visualization of the fuel injector spraying steam.

Key words: *injector testing, common rail, injector test stand, measurement methods, injection spray pattern*

Introduction

The aim of the following article is to evaluate the workshop methods of testing injectors used in modern compression ignition engines. Various test benches and devices for fuel atomization process visualization were used to evaluate the effectiveness of the damage detection. Not only injectors are evaluated in terms of fuel dosage but also in the shape of the stream or atomization of droplets. A widely used automatic test in 4 operating points may lead to confusion when deciding about the reconditioning of the injector. The examinations expanded with injector characteristics in a wide range of parameter changes coupled with experience of machine operator leads to more precise diagnostics and can even indicate malfunction of other engine components or improper engine maintenance.

1. Injector testers

Test bench is a device designed for, among others, injector examination. It provides conditions necessary for injector to work and allows its working properties measurement. Test Benches are used in injector repair workshops in several stages of injector reconditioning process such as:

- Introductory examination of injector in purpose of defect verification
- Regulation of injector
- Check operation after repair
- IMA code assignment

Injector testers are also useful in car workshops. In many cases it is impossible to set a clear engine diagnosis. Testing benches are tools that help to determine, whether the defect is caused by injectors and which one exactly. Another application of test benches are science researches and development works.

In purpose of testing of injectors, instead of using diesel oil, required calibration fluid is used. Its properties are precisely determined by ISO 4113 standard or other standards created by producers on a basis of ISO 4113.

The injected fuel quantity, and the return quantity are basic quantities measured by the test benches. The most common method of testing injectors is measuring the injector parameters in 4 operating points. The first operating point is a full load dosage, which simulates work of the injector during engine's full load. The second parameter is an emission dosage, which corresponds to the medium load of the engine. The next measured dose is an idle dose (LL). The last measured dose is a pre injection dose. The manufacturer of injectors determines conditions for those tests, like fuel pressure and actuation time. The ranges of correct dosage values are also provided. This kind of test is relatively fast and allows to diagnose most of injector's malfunctions. However, the diagnose of some of the malfunctions is impossible, since in the real operation injectors work in the whole range of pressures and actuation times. More precise method is to determine the characteristics of injector working with many operating points. In this case, a problem with interpretation of the results appears, because manufacturer does not share characteristics of injectors in working order. Moreover, such measurement may even take couple of hours, so it's problematic in case of workshop use. The additional test, carried out as the first one, is the leak test. It is carried out with maximum operating pressure and without actuation. This test enables to check the nozzle and control valve tightness. Leaks flowing through fuel return port are measured automatically, while other leaks, especially the nozzle leak, are supposed to be checked visually by the machine operator.

Two test benches were used in order to carry out this research. The first one is STPiW 3. It is available in the laboratory of Gdańsk University Of Technology. The second device is Bosch EPS 200, provided through courtesy of Motogab injectors reconditioning workshop. These machines differ when it comes to their research capabilities. The main difference is the method of measurement of a fuel quantity. This measurement in case of Bosh EPS 200 is performed with a turbine flowmeter. The advantage of this device is a real time measurement, which speeds up the time of a test. In case of STPiW 3 fuel quantity is measured indirectly through measurement of hydrostatic pressure of calibration fluid injected to the measuring cylinders.

1.1. Bosch EPS 200

The Bosch EPS 200 (Fig. 1) is an automatic injector tester. It has a compact design but allows to test only one injector at a time. It consists of a high pressure pump Bosch CP3, which pumps the test oil to a rail. The rail is equipped with a piezoelectric pressure sensor and a pressure control valve.

The built-in two-chamber calibration fluid reservoir has a capacity of approximately 7 litres. The fluid used in the test is drained into the first chamber where larger impurities

are deposited. In the second chamber, the test oil is brought to the correct test temperature and then fed to the high pressure pump. The most important element of the device is the turbine flowmeter, because it directly reflects on the accuracy of measurements.

Fig. 1. Bosch EPS 200

The flowmeter measures the injected fuel quantity or the return quantity, depending on the setting of the valves directing the streams flowing out of a tested injector.

Measurements are possible only in an automatic mode, which is controlled according to the test procedure specified for each kind of injector. This makes the workshop test, comfortable and fast, and greatly limits the possibility of human error. On the other hand, in laboratory conditions, it also limits testing capabilities. [2]

In the case of piezo injectors, to ensure their proper operation, it is important to determine the threshold voltage for the piezo actuator. During exploitation, the nature of the piezo stack and the components directly associated with it may be changed and the ISA code designated at the factory may become wrong. The Bosch EPS can check the adequacy of this code and take it into account when the impulses are generated during the test. Furthermore, the construction of the piezo injectors requires increased return back pressure (approximately 10 bar) which EPS provides.

1.2. STPiW 3

STPiW 3 is designed for testing pumps, injectors, pressure sensors and control valves which occur in common rail systems and systems with distributor pump. Construction of the test bench allows simultaneous testing of four injectors. Figure 3 shows the layout of the device. The fuel system has all the elements that can be found in a system of a car. The electric feed pump (1) supplies calibration fluid through the filter (2) to the high pressure pump (PO1). This is the 3-plunger radial-piston pump Bosch CP1H. It is driven through toothed belt by the induction motor (SIL). The motor is powered by the inverter (FAL) that provides smooth and precise speed control. The pump is controlled by the cut-off valve (ZAW2) and the pressure regulator valve (ZAW3). The rail (K) is equipped with the pressure sensor (CC1) and the pressure control valve (ZAW1). Pressure value in a high pressure system is controlled by the electronic module (D2) which controls all valves on the basis of a sensor reading. Tested injectors connected by flexible cables are placed in the injected fuel quantity measuring cylinders (H). On the right side, there are cylinders that measure the return quantity (I). All return pipes are connected to the return collector (9) from which the liquid flows into the main tank (4). Injectors control the pulse generator (D1), which is set by the software on the computer connected to the device. In order to maintain accuracy of the tests and comparability of the results, it is necessary to keep the fluid temperature constant. This is done by the system, marked by dotted line, consisting of the heater (6), the electric pump (7) and the cooler with the fan (WEN1).

Fig. 2. STPiW 3

Quantity measurement begins with the measurement of hydrostatic pressure of the liquid in the measuring cylinders (H). Subsequently, the motor driving the pump is started. When the pump speed is stabilized, the pressure is adjusted to the setpoint. In the next stage, the injectors starts injecting the calibration fluid into the measuring cylinders. The standard measuring cycle is set to 1000 injections. At the end of the series of injections, the hydrostatic pressure is measured again. Based on the pressure difference, before and after a test, the software calculates the amount of liquid that has increased during the test. Afterwards the volume is divided by the amount of injections which determines the injected fuel quantity.

The great advantage of this device is capability of setting parameters such as:

– fuel pressure,
– actuation time,
– frequency of injections,
– amount of injections,
– pump speed,
– fuel temperature.

This allows to examine the injectors at every point of operation and allows to determine the characteristics according to different parameters. Because of the reasons mentioned above, the STPiW device has bigger testing capabilities and a wider use in research.

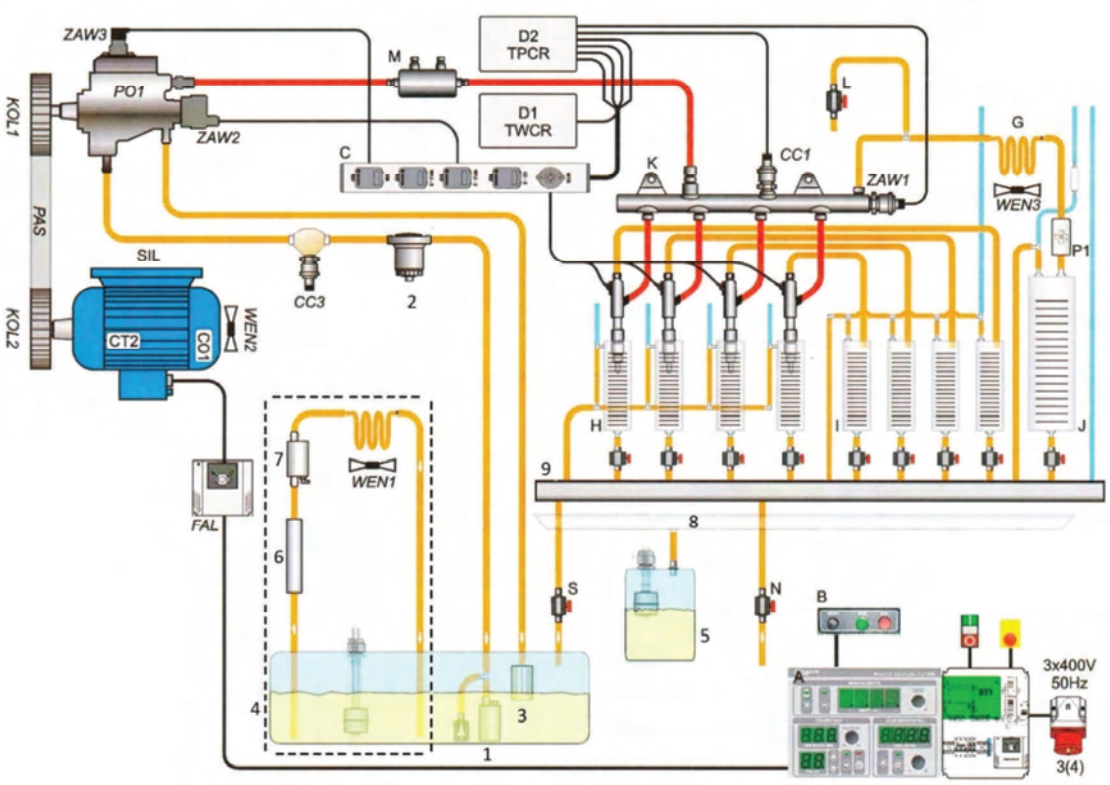

Fig. 3. Scheme of STPiW device

2. Observed causes of measurement errors

2.1. Measurement error of pre injection test

During examination in automatic mode, according to the injector card, measurement inaccuracy was noticed while performing the VE test. The measurements was carried out with the Bosch injector number 0445110021. Settings, according to the injector card, were as follows:

- Pressure 80 MPa,
- Actuation time 160 µs,
- Number of impulses 1000,
- Frequency 20 Hz

The results of 20 measurements that were performed under the conditions shown above, are presented in the Fig. 4.

Standard deviation was relatively high and amounted: $\sigma = 0.266$.

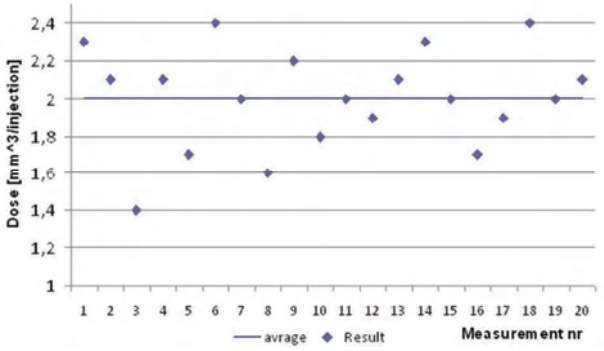

Fig. 4. Outlines of VE test before test modification

During those tests, little amount of fluid (about 2 ml) was injected to the measuring cylinder in time of one measurement. Precision of the test would be better if the number of impulses in time of one test was increased. Such modification would lead to increase of a measured volume. During consecutive examinations the number of impulses was increased to 4000. The distribution of results after the test modification is presented in the Fig. 5.

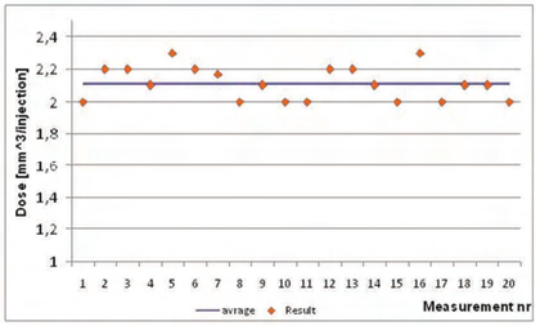

Fig. 5. Outlines of VE test after test modification

In that way the standard deviation decreased more than twice to the value $\sigma = 0.103$.

The change of parameters has given expected results, so the following VE measurements was performed with 4000 impulses.

2.2. Error of the first measurement

In order to increase accuracy of measurements, every test was repeated several times. It was noticed that the result of the first measurement, which was carried out immediately after setting the injector on the test bench, in many cases was significantly different from the other results in many cases. The first hypothesis to explain this

phenomenon was an influence of the injector and its components' temperature on injected fuel quantity. It was thought that results stabilized after the injector was heated to the calibration fluid temperature. In order to examine influence of the temperature on the injector operation, the injector was cooled down to the temperature of 5°C, afterwards it was mounted on a bench. The injected fuel quantity was measured as the components were warming up. The measurement of temperature was carried out with a digital pyrometer in two places. In the upper part, near the fluid supply connector, and in the lower part, near the nozzle nut. The calibration fluid temperature was stabilized at 40°C. Table 1 shows the measurement outcomes.

Table 1. Influence of the injector's temperature on injected fuel quantity

No	temp. top [°C]	temp. bottom [°C]	dose [mm^3/injection]
1	5.5	5.5	51.2
2	10.2	7.5	51.4
3	14.8	11.1	51.3
4	23	17.4	51.2
5	27.1	25.9	50.9
6	29.4	27.7	51.3
7	31.3	29.5	51.2
8	34.8	30.4	51.1
9	35.2	30.7	51.4

As it is presented in the Table 1, the temperature of the injector has no recognizable influence on the fuel quantity and has nothing to do with the error mentioned above.

It was also noticed that if the injector had previously been examined on the test bench, the error of the first measurement did not occur. Due to the fact that the injectors have not been used for a long time, such results could be caused by accumulation of deposits and slight corrosion which reduced the ease of movement of the injector components.

2.3. Devices comparison

Main differences between researched devices are presented in the Table 2.

Table 2. Main differences between test benches

Bosch EPS	STPW
Quantity measurement with the turbine flow meter	Quantity measurement indirectly through measurement of hydrostatic pressure of calibration fluid injected to the measuring cylinders
Automatic measurement mode only	Automatic measurement mode
Abilities to increase return pressure and to generate impulses based on IMA code (piezo injectors)	Lack of these abilities
Possibilities to test 1 injector at a time	Possibilities to test 4 injector at a time

In order to compare the accuracy and reproducibility of the measurements, a series of 12 measurements was carried out on both devices. The solenoid injector with a catalogue number 0 445 110 021 was used to carry out the tests. The following graphs (Figs 6–9) presents the results of the tests. Green lines indicate results obtained on the Bosch EPS and grey lines stand for the STPiW device. The minimum permissible quantity is marked with a black line, while the red is the maximum. If injector test results are within the range between these lines, the injector retain its correct work parameters.

The first VL result is vitiated by a gross error, which is marked with a red point (Fig. 6). It will not be considered in calculations.

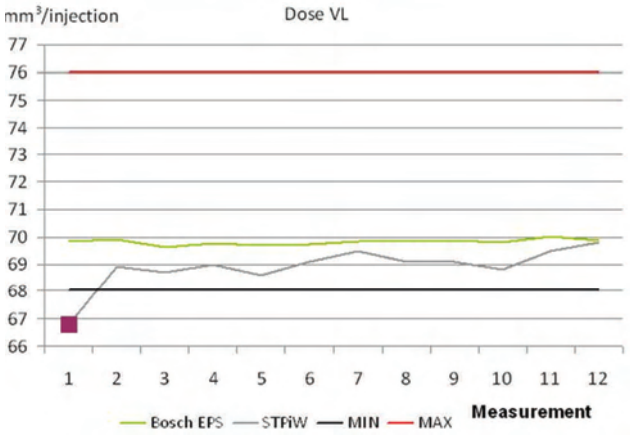

Fig. 6. VL test (actuation time 1300 µs, pressure 130 MPa)

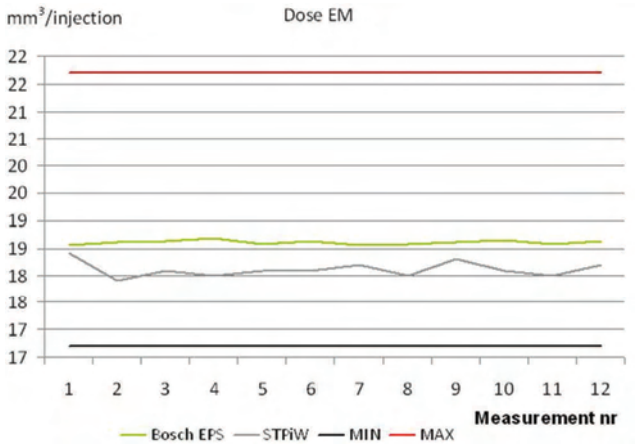

Fig. 7. EM test (actuation time 500 µs, pressure 80 MPa)

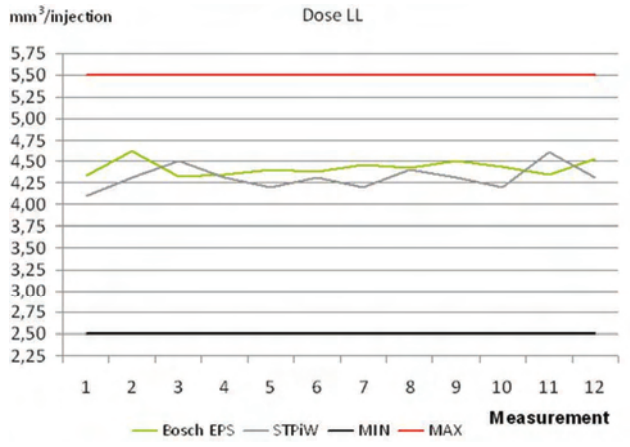

Fig. 8. LL test (actuation time 600 µs, pressure 25 MPa)

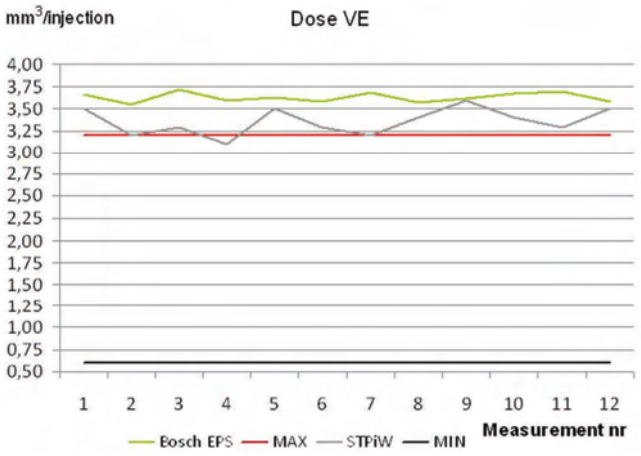

Fig. 9. VE test (actuation time 160 µs, pressure 80 MPa)

Table 3 shows the juxtaposition of standard deviations of the measurement series depending on the device and the type of test. The arithmetic mean of the standard deviations, which is a measure of the precision, is in the last row of the table. It is very clear that the tests performed with Bosch EPS are more precise and more reproducible. It is also noticed that the standard deviations for the VL tests performed on both devices is much higher than the standard deviations for the other tests. The difference is not due to lower precision of testers in these conditions, but rather to lower precision in the injector dosage at such high pressures and injection times, as the flow process inside the injector is more turbulent.

Table 3. Standard deviations of measurements

		Bosch EPS	STPiW
Standard deviation	VL	0.1088	0.3688
	EM	0.0386	0.1404
	LL	0.0894	0.1380
	VE	0.0526	0.1505
Average standard deviation		0.0724	0.1994

Table 4 presents the results of average injected fuel quantities. It is clear to see that the results of tests performed by these machines differ insignificantly. In the case of the examined injector, STPiW always indicates slightly lower values. However, considering the other injector's tests, this dependence is not a rule.

Table 4. Average results of measurements

		Bosch EPS	STPiW
Average dose [mm^3/injection]	VL	69.82	69.10
	EM	18.61	18.12
	LL	4.42	4.31
	VE	3.63	3.36

Return quantity was considered in the case of mentioned comparison. This quantity has no direct influence on the engine's operation, so there is no requirement for the injector dosage to be precise. For this reason, the discrepancies in the measurement results do not reflect the precision of the measuring equipment because they are caused by the nature of the injector work. Therefore, the measurement accuracy of the devices cannot be compared. Fig. 10 presents the distribution of the return quantity measurement results during the VL test.

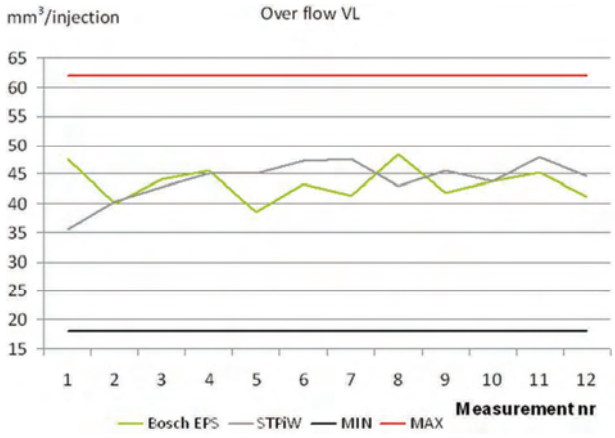

Fig. 10. Return quantity in VL test (actuation time 1300 µs, pressure 130 MPa)

3. Description of the complete injector characteristics interpretation

The test method at 4 operating points is fast and able to detect most of the faults. However, considering the fact that the injector is operating over the entire span of actuation times and pressures, some defects may remain undetected during the standard test. It often happens after improper injector reconditioning, in which not all of damaged parts have been replaced, and the injector was adjusted just to pass the test. Determining the characteristics in many operating points is much more time-consuming than the standard test.

Full characteristics allows detection of any injector work area where the injector works improperly. On the other hand this measuring method requires testing the injector at multiple operating points leading to a significant prolongation of the test time.

Due to a lack of comparative characteristics, the evaluation of correctness of obtained characteristics consist on checking the parallelism of the sections between two operating points. Owing to the fact that these sections correspond to short time difference, they are treated as straight lines. They should be as parallel to each other as possible. However, in some cases, significant deviations and even intersections are visible, what is unacceptable. The excessive deviations or the line intersection testify to malfunction of the injector.

The test performed on the injector with number 0 445 110 200 is an example which shows the influence of the complete characteristics interpretation on the injector diagnosis. The injector passed short 4-points test. However, complete characteristics, as shown in Fig. 11, excluded a positive result of injector diagnosis.

The characteristics clearly illustrate the areas of operation where intersections of the pressure lines occurred. As already mentioned, this is an unacceptable failure.

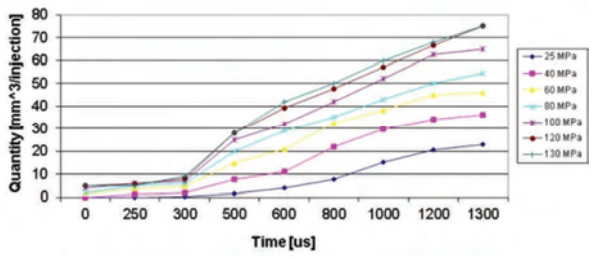

Fig. 11. Characteristic of improper injector work 0 445 110 200

The characteristics above shows that the injector's malfunctions occur especially in the actuation time between 200 and 300 μs and 450 and 600μs.

This is proof that the basic test may be insufficient in many cases. In practice, even if the injector completed the first test successfully, an improper working range of the engine could occurred.

Close attention should also be paid to situations in which the characteristics have disturbances especially at high pressures. Due to a leakage of the injector and an excessive return of fuel, the pump is unable to produce high pressure in the fuel rail. Hence the results are falsified (characteristic overlap of high pressure lines corresponding to too low fuel quantities) (Fig. 12). In order to obtain required pressure for the injector, a need to increase the rotational speed of a pump appeared (Fig. 13).

The following characteristics present the situation described above while testing the Denso RF7J 13H50 injectors.

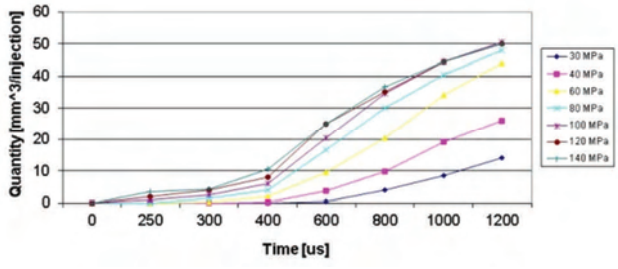

Fig. 12. Characteristic with pump speed 800 rpm

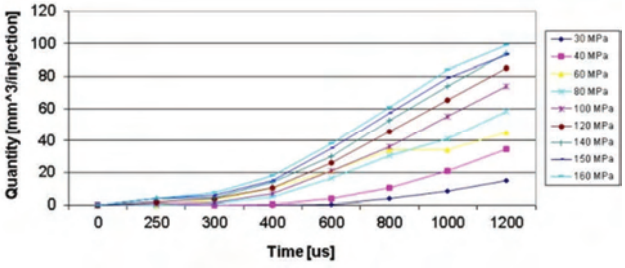

Fig. 13. Characteristic with pump speed 1100 rpm

4. Examination of the Bosch 0 445 110 084 injectors

The objects of the study in this section are Bosch CRI 1 solenoid injectors with number 0 445 110 084. The injectors derive from the Renault Laguna with a 2.2 dCi engine. The engine failure occurred at around 220,000 km. The first symptoms of the failure was loss of power, then it was and then impossibility to start the engine.

The examination of the injectors was carried out on the STPiW test bench. The outcomes of the tests are presented in Tab. 5.

Table 5. Test results of injectors no 0 445 110 084

Test		Injection time	Presure	Dose [mm^3/injection]		
				Measurement		Reqired
				Injector no		
		μs	MPa	1	2	
Tightness		0	140	210.7	295.2	35 ±35.0
VL	Dose	1100	135	67	71	72.1 ±4.0
	Return			167.9	182.5	40.0 ±22.0
EM		500	50	13.5	13.2	8.3 ±2.5
LL		500	30	4.9	4.8	3.4 ±2.0
VE		260	50	3.9	3.3	1.8 ±1.3
Test result				Negative	Negative	

It can be seen clearly that the injector fault can be already identified during the leak test. The injector number 1 has the return quantity 3 times bigger than the maximum permissible value, while the injector number 2 exceeds that value more than 4 times. This first test may already exclude the injector from further examination because this test is sufficient to determine its fault. Despite this fact, further tests have been carried out in order to observe the effect of leaks on the injected fuel quantity. During a full-load test with a standard pump drive setting at 800 rpm, it was not possible to reach a preset pressure of 135 MPa because of too little pump flow in relation to the sum of the injected fuel quantity and the leaks. The pump had been set at 1100 rpm, what increased the pump's output and allowed to maintain the preset pressure.

By analysing the results from tab. 5, it can be stated that the injector malfunction did not affect the results of full load test. The idle dosage has been slightly increased, but within permissible limits. On the other hand, the emission dosage and the pre-injection dosage were too high.

Inability to start the engine was caused by too big fuel leakage through the injectors, which consequently did not allow the pump rotating with low rotational speed (resulting from the rotational speed of the starter) to build up the pressure in the rail necessary for proper injector activation and engine start-up.

a) b)

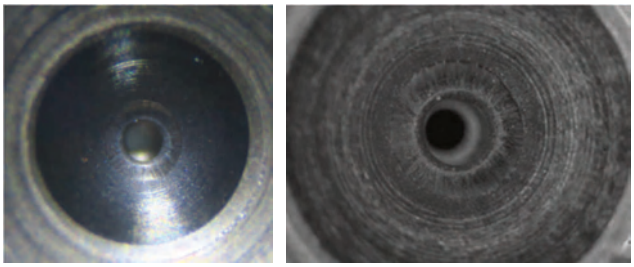

Fig. 14. Damage of the valve seat a) injector no 1, b) injector no 2

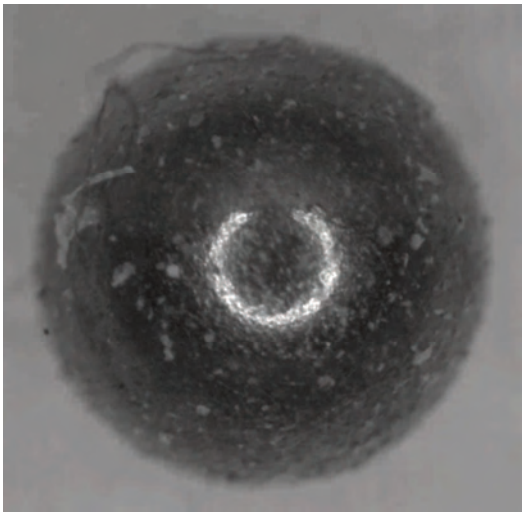

Fig. 15. Damage of the valve ball

Figure 14 presents the control valve seat. The ring around the hole is the sealing surface. The quality of this surface is crucial to maintain valve tightness. The pictures show radial grooves caused by cavitation erosion. In addition, Figure 15 shows the ball of the first injector. The irregularity of the ball's surface ~~is~~ also causes leaks. These are the main causes of the injectors' malfunction the large return quantity.

a) b)

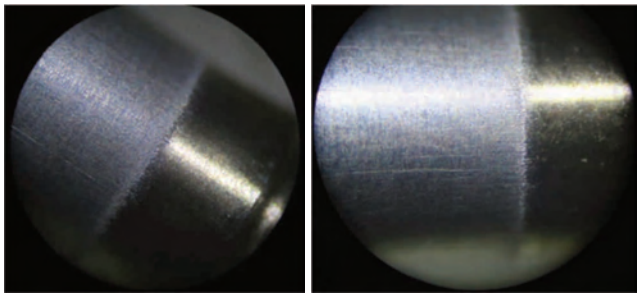

Fig. 16. The guiding surface of needle a) injector no 1, b) injector no 2

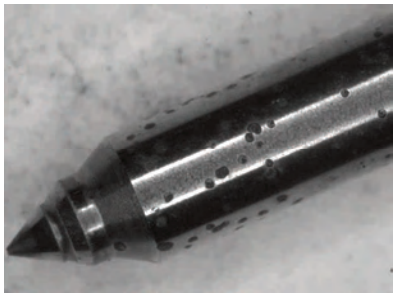

Fig. 17. Needle corrosion

Fig. 16 presents the needles of both injectors, specifically their guiding surfaces. There is a strong abrasive wear at the place where the co-operation with the nozzle occurs and deep dents caused by contamination. These impurities could be caused by corrosion of the needle surface, where pitting spots are visible (Fig. 17). Wear of the cooperation surface resulted in greater clearance of the precision pair such as needle and nozzle. In consequence the clearance caused additional leaks and increased ~~in~~ the return quantity. Analogous wear can be observed in the case of the second precision pair, i.e. the control valve body and the plunger. Fig. 18 shows damage of plungers.

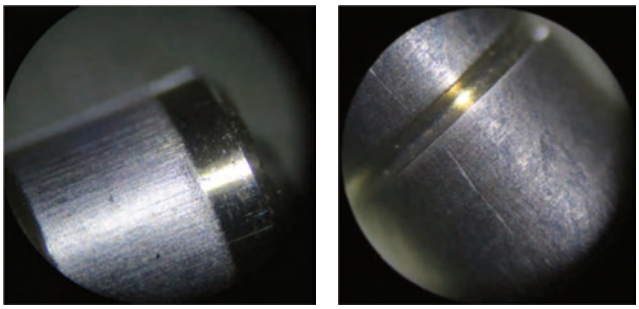

Fig. 18. Damages of valve plungers

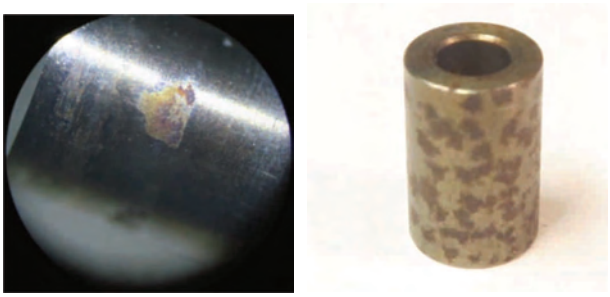

Fig. 19. Corrosion of the needle and the guiding sleeve

Figure 19 shows the corrosion damage of the upper part of the needle and the guiding sleeve. Corrosion has occurred in places that do not work with other parts, so it has no effect on the operation of the injector. On the other hand, further corrosion can lead to fuel contamination with corrosion products and damage other components.

Fig. 20. Fuel spray pattern of a damaged injector

In addition, the spray pattern of the injector number 1 was documented (Fig. 20). The streams formed by the two upper holes are characterized by a larger cone angle than the others. Considering the amount of reflected light from these streams it can be inferred that they contained a higher injected fuel quantity. The spraying from the lower hole is

severely opened from the beginning, while the sprayed droplets have not yet reached the wall of the visualization chamber. This means that spreading speed of the droplets flowing from the lower hole is smaller than those from the remaining holes. The reason for such phenomenon is because the flow through this channel is disturbed by the unevenness of its geometry, which may be due to internal sediments.

Conclusions

The standard 4-point injector test can detect most of the faults. Sometimes, however, it is required to have a full feature consisting of multi-point measurements, because in actual conditions the injector is operating and must perform at full pressure and opening times.

Comparative testing of test benches has shown that Bosch EPS is characterized by greater accuracy and precision of measurements, while STPiW has wider research capabilities and allows for arbitrary parameter setting during testing. Differences in the method of measuring the fuel dose and the course of the control pulses influence the divergence of the results obtained with these devices.

The visualization station, despite the simplicity and low cost of execution, allowed to observe and document the macro structure of the fuel spray jet. The instrument has made it possible to diagnose faults related to the quality of fuel spraying and to integrate it with the test bench in a laboratory of the Faculty of Mechanical Engineering, the device also has a didactic value. In spite of listed above wear an corosion demages the main injector problem are deposites [3]. The best method to limit the occurrence of the above phenomena is the application of effective detergent fuel addetives.

Nomenclature

VE	pilot dosage	LL	idle dosage
EM	emission load dosage	VL	full load dosage

Bibliography

[1] BOGUŚ, P., GRZESZCZYK, R., WRONA, A. et al. The possibility of applying wavelet analysis for diagnostics of the validity of injection process of diesel engine fuel injector based on selected parameters of the reactive cylinder vibration process. PTNSS–2015–3397.
[2] Instrukcja obsługi Bosch EPS 200.
[3] STĘPIEŃ Z. Investigation of injector deposits in modern diesel engines. *Combustion Engines*. 2016, **165**(2), 9-20.

Zbigniew Kneba, DSc., DEng. – Faculty of Mechanical Engineering at Gdańsk University of Technology.

e-mail: *ZKneba@pg.gda.pl*

Klaudia Jakóbczyk, BEng.

e-mail: *Jakobczyk.Klaudia@gmail.com*

Paweł Straszak, BEng.

e-mail: *PawelStraszak@op.pl*

Article citation info:
SIDOROWICZ, M., PIELECHA, I. Inflammability evaluation of hydrocarbon fuels mixtures formed directly in the combustion chamber. *Combustion Engines*. 2017, **170**(3), 57-65. DOI: 10.19206/CE-2017-309

Maciej SIDOROWICZ
Ireneusz PIELECHA

CE-2017-309

Inflammability evaluation of hydrocarbon fuels mixtures formed directly in the combustion chamber

The proposed article involves an investigation of the processes taking place during the preparation of mixed fuels that are combined directly before combustion. The fuel dose formed in this way must take into account the qualitative and quantitative composition of the fuels and the amount of air in the process. Given that liquid fuels similar to gasoline (e.g. methanol, ethanol, butanol) are characterized by different properties, their comparison would be useful in order to use their ratio to influence the combustion process. The process of fuel preparation plays a decisive role in this issue.

The article describes abilities of modelling the injection of various fuels simultaneously to the combustion chamber for creating fuel mixture directly before ignition. First part of the article consists of analysis of light hydrocarbon fuels mixing abilities, supported with present research data. Next part describes the evaluation of execution of the assumed system – two fuel injectors with analysis of spray penetration. The modelling of the injection and spray was performed in the AVL FIRE 2014.2 environment and the results were presented. The injection possibility was proven by injecting the fuel to the combustion chamber model. Local values of air-fuel ratio, density and ambient pressure were presented to better understand the potential in mixing fuels directly before ignition. The conclusion includes description of fuel mixing abilities, influence of various fuels on creation of a stratified mixture and definition of controllability of charge ignition.

Key words: *fuel injection, mixing fuels, hydrocarbon fuels, combustion chamber*

1. Introduction

Combustion processes are considered mainly in terms of a mono-fuelled combustion. Processes of preparation and combustion of gasoline-like fuels are widely described in literature.

Dual-fuel mixtures are crated mostly in the earlier process (for example, a mixture of ethanol and gasoline or petrol and methanol [12, 17]) and are burned most often in stoichiometric conditions. The way of preparing such a mixture causes it to have specific physico-chemical properties (viscosity, surface tension and density closely define specific contents of different hydrocarbon groups) [12, 22]. In such a situation, sprays of drops with small, homogeneous dimensions are obtained. Figure 1 shows a typical process of fuel flow from the injector [2].

The air with high temperature is "incorporated" into the fuel spray. The hot air causes fuel evaporation, and as a result the length of the spray is reduced. After the initiation of combustion, a slight reduction of the spray takes place and then its length stabilizes before the end of the injection. The diffusion flame is formed in the areas where the mixture reaches a value close to stoichiometric. The rich flammable mixture zone is an area in which the formation of particulate matter is initiated. This results in a significant concentration of soot in the diffusion flame of the burned fuel. The pre-flame zone (outer) is "responsible" for the formation of nitrogen oxides [3].

Gasoline is a mixture of over 100 different hydrocarbons having different molecular structure and different boiling points. Most often the structure of gasoline consists of about 55% paraffins (single-bond C–C), around 35% aromatic hydrocarbons (benzene rings) and a maximum of up to 20% olefins (double bond C=C). Paraffins are complex components with low molar mass: these are e.g. n-butane, 2-methyl-pentane and 2,2,4-trimetyl-pentane (iso-octane). Aromatic hydrocarbons contain 4 to 8% toluene and around 4% xylene.

The oxidizing additives used in gasoline increase its octane number. The influence of additives on the octane number is dependent on the fuel composition. Gasoline is enriched with alcohols (R-O-H, where R is the HC group) and ethers (R-O-R). Alcohols are mainly methanol (MeOH), ethanol (EtOH), isopropanol (IPA) and t-butanol (TBA). Due to the weak solubility of methanol in gasoline in the presence of water, it must be used together with TBA as a co-solvent. Ethers used as additives include mainly: methyl tert-butyl ether (MTBE), tert-amyl methyl ether (TAME) and ethyl tert-butyl ether (ETBE).

Use of previously proposed fuels to determine the properties of the mixtures, requires knowledge of their physico-chemical properties. Physical properties of such fuels should play an important role in the mixing processes.

The distillation curve of gasoline, taking into account that gasoline is a mixture of different hydrocarbons, is shown against the background of basic fuels (Fig. 1).

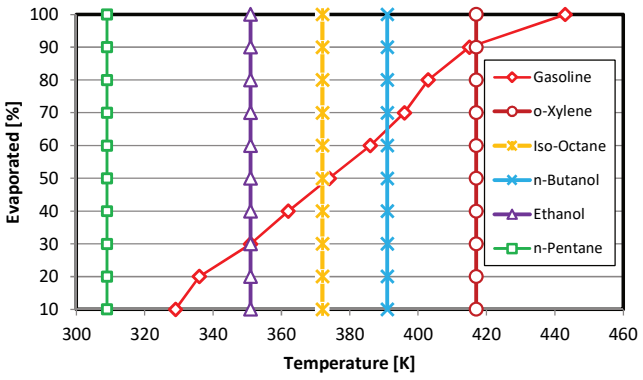

Fig. 1. Distillation curve of gasoline and other fuels [1]

Also the physico-chemical properties of all the analysed fuels are known. Although o-xylene, presented in Figure 2, has a boiling point close to the last value of boiling point for gasoline, it was also qualified in the study as a stand-alone fuel submitted to mixing. The coefficients for determining fuel vapour pressure were presented e.g. by [7] and they can be used in the equation [1]:

$$\ln(p_i) = A - B/(T_i + C) \tag{1}$$

where A, B, and C are Antoine constants for pure components (e.g. water, methanol or ethanol) obtained from literature data.

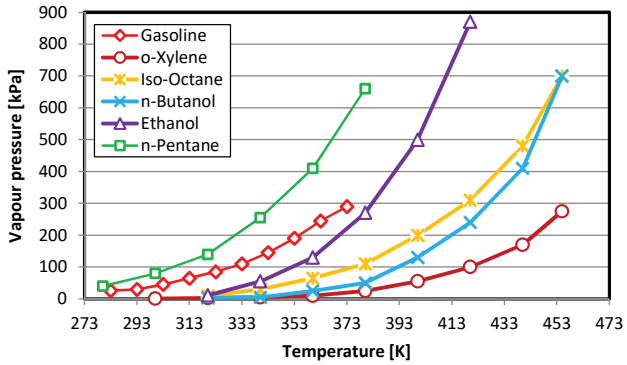

Fig. 2. Fuel vapours pressure

The exchange of mass between the surface of the fuel drop and the gaseous medium (air) occurs due to molecular and turbulent diffusion. The molecular diffusion is the spontaneous mixing of fuel and air particles as a result of concentration gradient dc/dr, which excites the flow of heat and, induced by this, the flow of mass (thermo-diffusion). In case of creating a flammable mixture diffusion caused by a gradient of concentration of components is of crucial significance. Molecular diffusion, characterised by diffusion coefficient (D_M), is of vital importance in case of the lack of flow or laminar flow. In this case, mixing of the components is caused by random movement of their particles. In case of turbulent flow, the mass exchange is more intense due to the movements of particles in normal direction. The turbulent diffusion coefficient (D_T) has much higher value than the D_M coefficient. During the diffusion of vapour from the surface of the drop of fuel, surrounded by turbulent air jet, the surface layer δ consists of the first sub-layer, contacting the surface of the liquid, and the second layer located on the outside of the first. In the first sub-layer a molecular diffusion takes place, and on the other layer – it's mainly turbulent diffusion.

Many publications [e.g. 1, 20] claim that penetration of sprays chosen for testing fuels shows a similar linear scope. This indicates similar physical properties of these fuels. At the same time, it should be noted that such similarity is a positive feature, as it can alter the properties of ignition of mixtures without a significant change in parameters of their atomisation. These changes are visible only during significant heating of fuels (above 373 K). Then the penetration of pentane and ethanol is lower by about 10% [1].

The effect of flow turbulence can be characterized by the Reynolds number (Fig. 3):

$$\mathrm{Re} = \rho \cdot u \cdot d/\mu \tag{2}$$

where ρ – is density, μ – kinematic viscosity of liquids, d – diameter of the injector aperture, u – flow rate.

The lowest Reynolds number (at constant flow parameters) can be observed for butanol (laminar flow at low temperatures of the fuel).

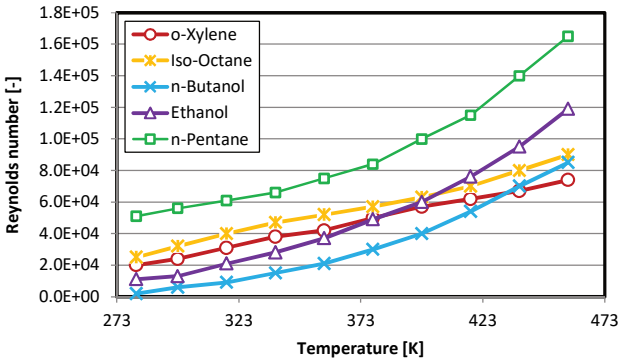

Fig. 3. Reynolds number of selected fuels [1]

The fuels selected for analysis are characterized by a Weber number above 50. With the increasing temperature, this value also increases: for o-xylene it is 120 and for the remaining fuels much more (for iso-octane – 230) at a temperature of about 453 K. These figures result from the specificity of the adopted characteristic values, requiring calculation of We number [1].

In publication [15] it was shown that the Weber numbers for ethanol and gasoline are similar for fuel temperatures ranging from 275-450 K. Further increase of the temperature causes an increase of Weber number for ethanol above 500 (in temperature of 500 K), while for petrol it is about 300 (temperature 500 K). This means that at high temperatures of the fuel the so-called catastrophic breakdown of ethanol drops occurs.

Ohnesorge number is convergent with the data contained in the publications [4, 8] and amounts to about $6 \cdot 10^{-3}$ to $1.6 \cdot 10^{-2}$ at the temperature of about 283 K, and decreases to a value of about $6 \cdot 10^{-3}$ for temperature of 463 K.

Indication of these differences is a basis for the conclusion that the created drops of fuel will also have different diameters, which will contribute to their diversified evaporation.

Combustion in dual-fuel systems of fuel mixtures created immediately before ignition makes it possible to determine the combustion air factor, which will be the resultant of the ratio of both fuels:

$$\lambda = \frac{m_{air}}{L_1 m_1 + L_2 m_2} \tag{3}$$

where: L_1 and L_2 are stoichiometric air requirements for combustion of fuel 1 and 2, m – is weight of fuel, respectively 1 and 2, m_{air} – is the weight of air. The share of one of the fuels can be calculated from the following:

$$U_{m2} = \frac{W_{op2} m_2}{W_{op1} m_1 + W_{op2} m_2} \tag{4}$$

Determination of inhomogeneity of the mixtures created immediately before combustion leads to the assessment of

production of soot originating from the inhomogeneity of the charge in the process of mixing the air-fuel charge. The global index of uniformity is referred to as [18]:

$$U_I = 1 - \sigma/\sigma_{v,\eta} \tag{5}$$

where σ determines the standard deviation of the fuel mass distribution, and $\sigma_{n,h}$ is defined as the standard deviation of the completely inhomogeneous charge (fuel and air):

$$\sigma_{n,h} = \frac{\sqrt{A/F}}{1+A/F} \tag{6}$$

However, the U_I parameter is not fully representative of the possibility of determining the distribution of fuel vapour with division into rich and lean zones. Also the analysis associated with post-processing of the images from such a process is required. This index takes the maximum value equal to 1 for completely homogeneous mixtures. It is a good indicator of mixing fuels proposed for tests in the current research.

2. Motivation

The process of combustion of liquid fuels (gasoline, ethanol, methanol, n-butanol and its mixtures) is characterized by high variability of the thermodynamic conditions. The process of combustion of liquid fuels may be continuous or cyclical. In the first case there are stabilized thermodynamic conditions, and in the other case – the conditions are changing. Due to significant changes in combustion conditions (temperature, pressure), the process of preparing the mixture is short, which is one of the main causes of its unrepeatability. In such a short time the initial physical processes of mixing fuel with air and the pre-flame processes take place (chemical evaporation of fuel and its thermal decomposition). During this period the reactions and processes leading to formation of toxic components also begin take place. Some scientists assume [27] that oxidation and products of thermal decomposition of the liquid fuel molecules can be important intermediate stages in the formation of particulate matter.

The dominant trend concerning combustion of liquid fuels is delivering them in the form of previously created mixtures: e.g. gasoline-ethanol or gasoline-methanol in various proportions. It is justified from chemical perspective to create mixtures with very specific proportions in order to ensure the homogeneity of such a mixture.

However, there are no descriptions in the literature of possibilities of creating mixtures of fuels directly before their combustion in open or closed chambers. Knowing that liquid hydrocarbon fuels (similar to gasoline) have different properties, it is reasonable to mix them in such a way that the proportions can influence the combustion process. Currently this is not possible, because the composition of fuels (proportions) is strictly defined prior to combustion. Different parameters of volatility, vapour pressure or octane number can provide a method of controlling the process of their combustion in a wide range. However, before such combustion can take place, it is necessary to recognize both the physical and chemical processes of mixing such fuels immediately before ignition.

3. Research methodology

The research was performed by means of computer aided simulation using the AVL Fire 2014.2 software environment.

The combustion chamber used in the research was modeled to comply with the assumed engine parameters, listed in the Table 1.

Table 1. Modeled engine technical data

Parameter	Unit	Value
Type	-	Piston engine, 4-stroke, spark ignition
Cylinder number	-	1
Displacement	cm^3	385
Compression ratio	-	10.2
Bore	mm	83
Stroke	mm	71.2

The research consisted of performing the direct fuel injection events into the modeled combustion chamber through two separate injectors. The indicative view of the injectors positioning in the combustion chamber is presented in Fig. 4.

Three combinations of fuels injected with separate injectors were used:
– gasoline from both injectors,
– gasoline and methanol,
– gasoline and iso-pentane.

The injectors were oriented so their axes formed a 45° angle with the cylinder axis. Each simulation included single injections of constant mass of fuel. The injections were open for a constant amount of time (CA-wise) and were initiated with the same timing. The injectors' and spray parameters are listed in Table 2.

Table 2. The parameters of injectors and spray

Parameter	Unit	Value
Injectors type	–	Outward opening
Nozzle apex angle	deg	95
Spray angle	deg	10
Nozzle outer diameter	mm	2
Nozzle inner diameter	mm	1.5
Spray type	–	hollow cone
Injection beginning	deg CA	35 before TDC
Injection end	deg CA	25 before TDC
Injected mass per event	mg	30
Drag law model	–	Schiller-Naumann
Fuel evaporation model	–	Dukowicz ('Gasoline') Multi-component (others)
Fuel breakup model	–	Wave

The Schiller-Naumann drag law model Cd is an empirically evaluated equation for calculating drag coefficient in drag force acting on the flowing particles in fluid with Re ranging from 0.2 to 1000. It is described with the equation:

$$Cd = \frac{24}{Re}(1 + 0.15Re^{0.687}) \tag{7}$$

where Re is the Reynolds number. For the Re > 1000 the Cd has the constant value of 0.44 [5].

The Dukowicz evaporation model describes the heat and mass transfer processes on the droplet-fluid border. The model is based on the following assumptions:
– spherical symmetry,
– quasi steady gas-film around the droplet,

– uniform droplet temperature along the drop diameter,
– uniform physical properties of the surrounding fluid,
– liquid-vapor thermal equilibrium on the droplet surface.

The vapor mass flux ($\dot{f}_{vs}$) to local surface heat flux ($\dot{q}_s$) ratio is, according to the Dukowicz model, calculated as per formula (8):

$$\frac{\dot{f}_{vs}}{\dot{q}_s} = \frac{-B_y}{h_\infty - h_s - (h_{vs} - h_{gs})(Y_{v\infty} - Y_{vs})} \tag{8}$$

where B_y is mass transfer number, h_∞ is enthalpy in particle far-field condition, h_s is enthalpy at particle surface, h_{vs} is enthalpy in vapor conditions at droplet surface, h_{gs} is enthalpy in ambient gas conditions at droplet surface, $Y_{v\infty}$ is vapor mass fraction in particle far-field condition, Y_{vs} is mass fraction in vapor conditions at droplet surface [5].

The Multi-component evaporation model is the extension of the Abramzon-Sirignano approach. The difference to single-component cases is that the mass transfer of every component is taken into account separately, whereas the heat transfer remains a global mechanism. The resulting mass flow rate then is the sum of the single contributions:

$$\dot{m} = \sum_{i=1}^{N} \dot{m}_i \tag{9}$$

The distribution of the components inside the droplet is assumed to be homogeneous [5]. This model is required to be used in multi-fuel spray calculations.

The Wave breakup model describes the spray into droplet breakup behaviour. Initial spray assumption is that the blob injection is realized (initial droplet size is similar to the nozzle diameter). The quasi-continuous fuel stream is broken up to droplets as per Wave model. It assumes that the growth of an initial perturbation on a liquid surface is linked to its wavelength and toother physical and dynamic parameters of the injected fuel and the domain fluid. For the high pressure injection systems (high spray velocity) the size of the product (parent) droplets is set equal to the wavelength of the fastest growing or most probable unstable surface wave. For lower velocities, the Rayleigh type breakup is applied [5].

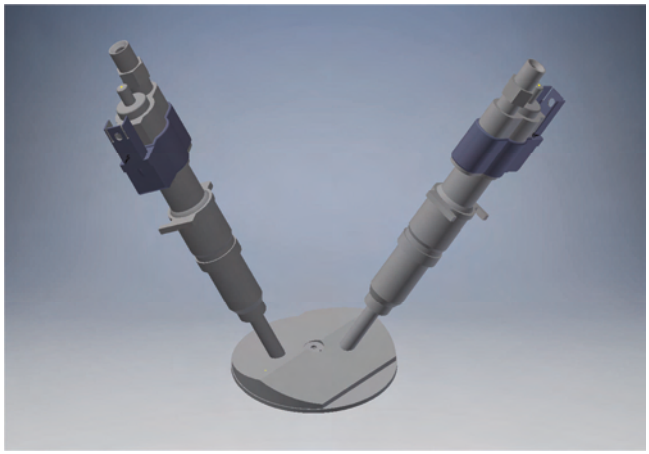

Fig. 4. The indicative view of positioning the direct injection fuel injectors

The model engine data are presented in Table 1, whereas the combustion chamber view with positioned injectors in it in Fig. 4. The visible two injectors are mounted instead of valves. Such configuration of the fuel injection into the area of centrally positioned spark plug (Fig. 5) allows the execution of spray-guided type mixture creation.

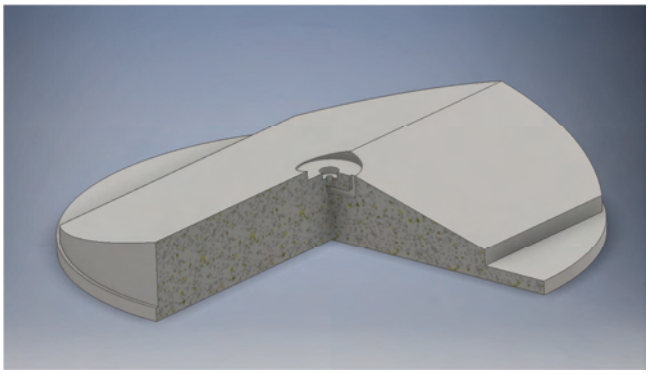

Fig. 5. The part-section view of the combustion chamber with outlined spark plug in the centre of the chamber

In the AVL Fire 2014.2 software using the Fame Engine+ module the displaceable mesh was created (Fig. 6), in which the following selections were assigned:
– piston buffer,
– piston moving
– piston non_moving.

The created mesh of size of 211 thousand cells (Table 3) served as the model for injection and spray analysis of various fuels.

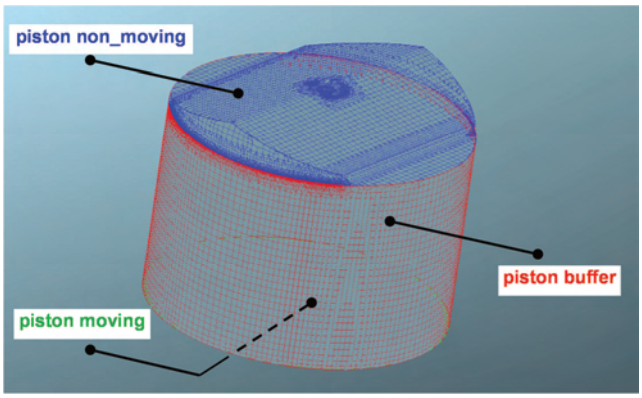

Fig. 6. The displaceable mesh of combustion volume for fuel spray simulation

Table 3. The computational mesh parameters

Mesh info	Value
Number of nodes	203732
Number of surface faces	40240
Number of tet cells	2200
Number of hex cells	160022
Number of pyramid cells	15908
Total number of cells	211406
Surface area	0.027 m^2
Volume	0.0003362 m^3

4. The fuels' injection and spray processes analysis

The presented simulations concerning fuels' spray cover the injection analysis of gasoline, ethanol and iso-pentane in various configurations of their delivery to the combustion chamber. Varied properties of these fuels, presented in point 2 and Table 4, point at possibilities of air excess ratio

shaping in combustion chamber during their direct mixing before ignition.

Table 4. Physical and chemical properties of fuels

Parameter	Unit	Fuel		
		Gasoline	Ethanol	Iso-pentane
Chemical formula	–	C_8H_{15}	C_2H_5OH	C_5H_{12}
Composition (C,H,O)	%	86,14,0	52,13,35	87,13,0
Research octane number	–	95 [29]	106 [14]	100 [21]
Density@ 20°C	kg/m^3	744.6 [29]	790.9 [29]	616 [28]
Lower heating value	MJ/kg	43.5 [11]	27.0 [11]	44.91 [10]
Viscosity @25°C	mm^2/s	0.4–1 [16]	1.32 [19]	0.35 [23]
Dynamic viscosity @ 25°C	mPa s	5.29 [26]	1.104 [25]	0.22
Surface tension	N/m	0.022 [9]	0.0223 [25]	0.016[6]
Enthalpy of evaporation	kJ/kg	373 [29]	840 [29]	342 [23]
Stoichiometric A/F ratio	–	14.6 [11]	9.0 [11]	38.1 [6]
Saturation pressure at 38 deg C	kPa	31 [11]	13.8 [11]	128 [13]
Flash point	°C	–45 to–38 [11]	21.1 [11]	–50 [23]
Auto-ignition temp.	°C	420 [11]	434 [11]	468 [23]
Boiling point	°C	32.8 [29]	78.4 [29]	27.9 [28]

The conducted research, due to its basic character, is aimed at identification of the air-fuel mixture creation changes during simultaneous injection of both fuels. In this research only the conditions of combustible spray build-up in the spark plug area are analyzed. The charge creation conditions were analyzed mainly in the aspect of the time required for the creation of combustible mixture as well as spacious relations in the combustion chamber concerning the fuel sprays' range. Due to the assumed method of fuel supply (direct injection with outward-opening injectors) the mixture creation is being considered through the fuel movement (*spray-guided*). Because of this, the assumed fuel injection is at 685°CA (35° before TDC).

The stoichiometric mixture creation was based on the assumption, that in dual-fuel injection, this coefficient is referred to the value for gasoline. Thus during ethanol or iso-pentane injection the air demand for these fuels' combustion was not included.

The fuels' spray analysis with two injectors participating begun with simultaneous injection of gasoline only (Fig. 7). The fuel spray analysis was conducted in the range from the start of injection to the point of piston's TDC. The area around the spark plug was subjected to research (the section of combustion chamber was selected to allow for the observation of the fuel spray) referred to fuel droplets distribution and air excess ratio of the A/F mixture (defined as equivalence ratio). The gasoline injection and spray effects in uniform A/F mixture creation on both sides of the combustion chamber (diverse areas in Fig. 7 result from the lack of symmetric section of combustion chamber). At 5° CA before TDC the conditions which correspond to the stoichio-

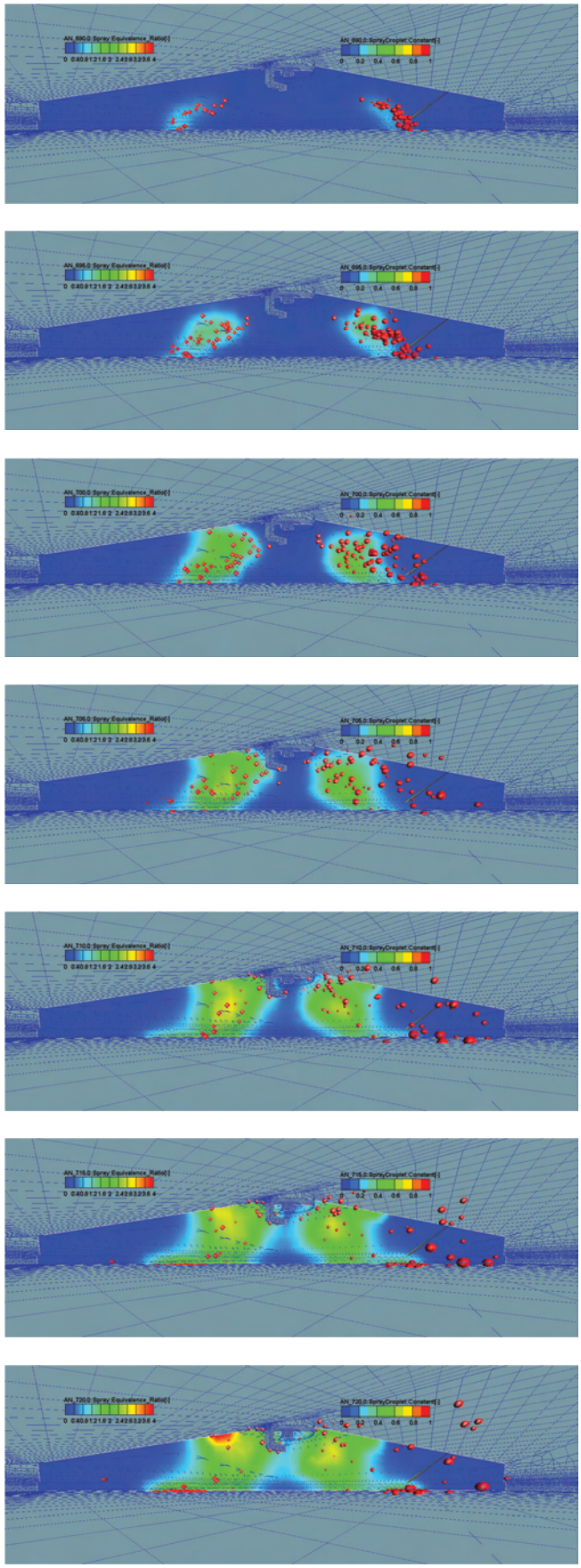

Fig. 7. The development of the gasoline streams in the two-injectors system (combustion chamber section concerns the 1/λ quantity); the droplet color indicates its type of fuel (gasoline)

metric mixture flammability are reached (air excess ratio corresponding to the value of 1). The specific position of the injectors in the combustion chamber causes the A/F mixture to not cover the whole combustion chamber. Such distribution of mixture results in the creation of stratified charges, thus allowing for lean mixtures combustion.

The combustion analysis of various fuel mixtures (gasoline and ethanol) implies that the method of creating the mixture is conditioned by its physicochemical properties. Higher density of ethanol, thus lower fuel outflow velocity from the injector nozzle (Figs 8 and 9) results in the retardation of the A/F mixture creation for this fuel. Thus, the gasoline and ethanol mixture creation should be more effective compared to gasoline only. Such mixture creation characteristics was observed during the analysis of gasoline and ethanol injection (Fig. 10).

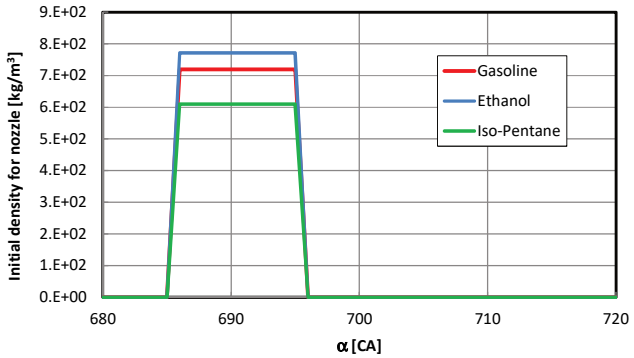

Fig. 8. The effect of the initial fuel droplet density during outflow from the injector on the fuel type during injection

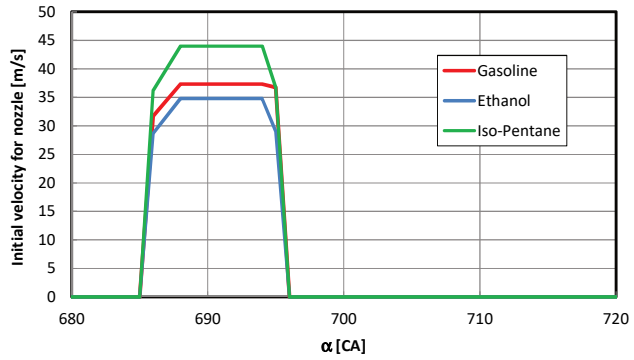

Fig. 9. The effect of the initial fuel droplet velocity during outflow from the injector on the fuel type during injection

The analysis of dual-fuel spray (gasoline and ethanol) points to the gasoline spray reaching the spark plug area quicker. In addition, the spayed ethanol remains more compact, because the created mixture covers much less space in the initial spraying period than the gasoline-air mixture. This indicates that the mixture creation in the spark plug area (the air excess ratio enhancing flammability) including gasoline and ethanol is performed with a significant gasoline advance. To minimize these differences, a correction would be required for the injection timing of ethanol.

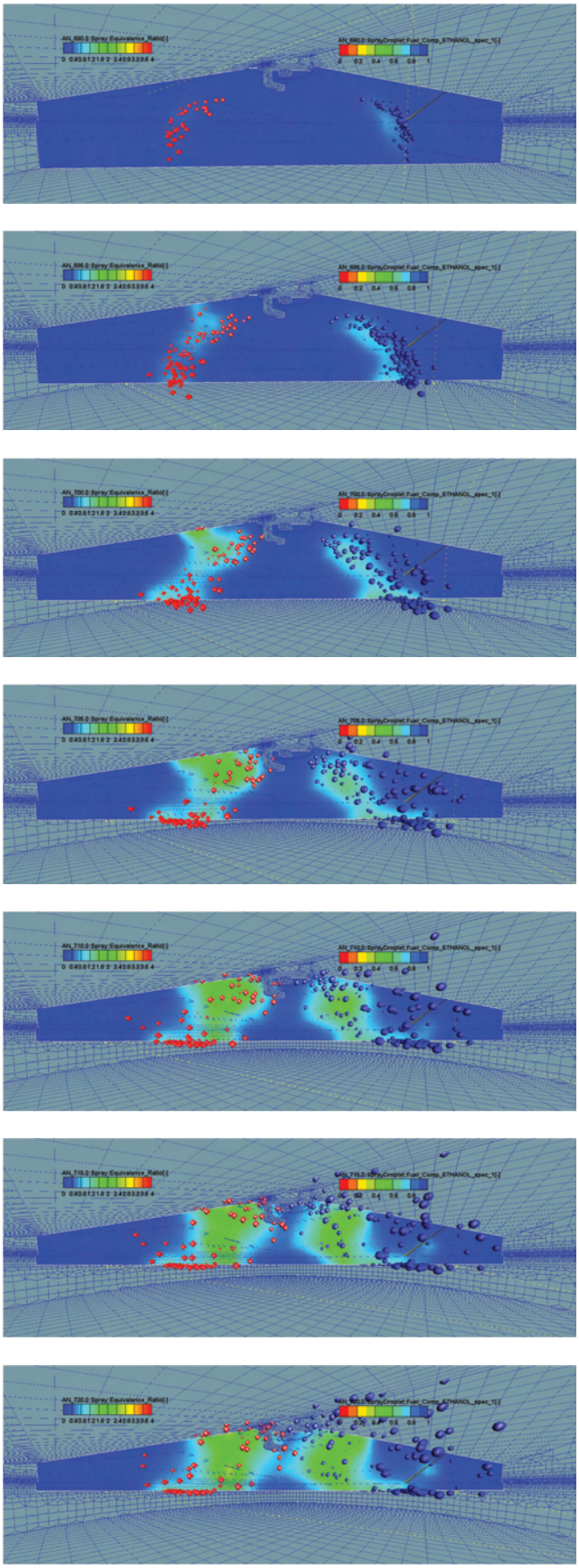

Fig. 10. The development of the gasoline (red spheres) and ethanol (blue spheres) streams in the two-injectors system (combustion chamber section concerns the 1/λ quantity

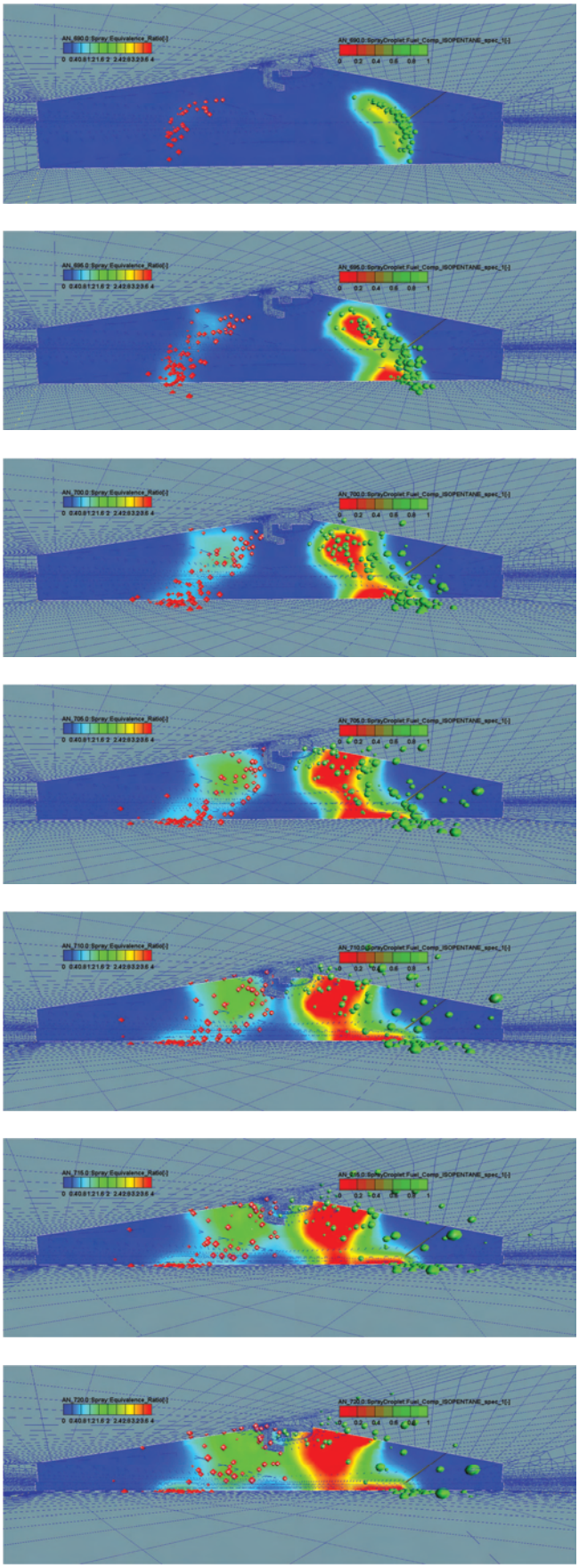

Fig. 11. The development of the gasoline (red spheres) and iso-pentane (green spheres) streams in the two-injectors system (combustion chamber section concerns the 1/λ quantity

The injection of isopentane, whose physicochemical properties are different from previous fuels, will result in different spray. The isopentane density is lower than that of gasoline, meaning that its mixing with air already starts after a few degrees of CA from the injection initiation. The isopentane spray area is significantly larger than the area of gasoline spray (Fig. 11). In the area of spark plug at 5° CA before TDC the isopentane dictates what flammability point of the mixture will be achieved. Its evaporation at this time is significantly higher than of gasoline as can be seen on the section of combustion chamber around the spark plug.

Based on the above analysis it was determined, that the injection and mixing of both fuels directly before ignition lets spatially shape the air excess ratio in the spark plug area. The injection of two different fuels significantly changes these relations.

5. Fuel mixing analysis

Successive analysis conducted in this area concerns the quantitive coefficients of mixture creation. They contain the global values of analyzed variables. Due to the various values of injected fuels evaporation enthalpy, the temperature values inside the cylinder are subject to changes (Fig. 12). The temperature value change at gasoline and ethanol injection is approximately 3 K (circa 0.5% difference at 715° CA, indicating theoretical ignition point) versus gasoline-only injection. Even higher temperature changes were noted during gasoline and isopentane injection. In this case the temperature drop is of 10 K was registered, and its share is about 2%. These are the mean values related to the whole combustion chamber, which points to significant temperature drop around the spark plug area.

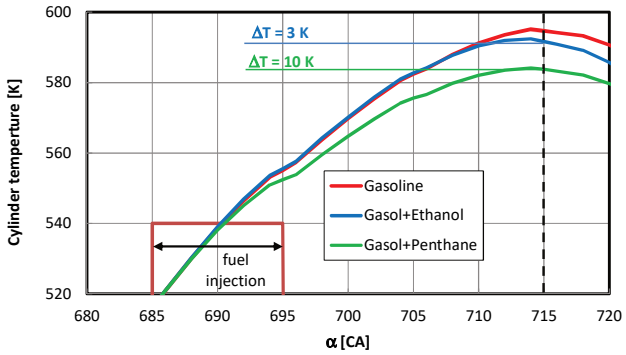

Fig. 12. The cylinder pressure and temperature value course during compression and decompression strokes

Diverse coefficients of fuels' spray are the result of their properties. Due to its lower density, isopentane shows a greater range in typical fuel injection phase (up to 715° CA) (Fig. 13), what was confirmed in spatial research of the atomized fuel spray. The value of isopentane spray range is higher at about 8%, and of ethanol at 2% versus that of gasoline (at 715° CA).

In following part of the spraying process the range decreases, because a significant part of the isopentane fuel dose already evaporated.

The analysis of the absolute value of these fuels evaporated mass confirms the previous results (Fig. 14). It was stated that the mass of evaporated fuels (gasoline and etha-

nol) is 31% lower than the evaporated mass of gasoline alone, whereas the mass of evaporated fuels: gasoline and isopentane is 31% higher than the evaporated mass of gasoline. Absolute mass values of evaporated fuels point at the twice as high value of evaporated gasoline and isopentane (20.9 mg) versus evaporated gasoline and ethanol (10.8 mg). The amount of evaporated gasoline is at 14.3 mg.

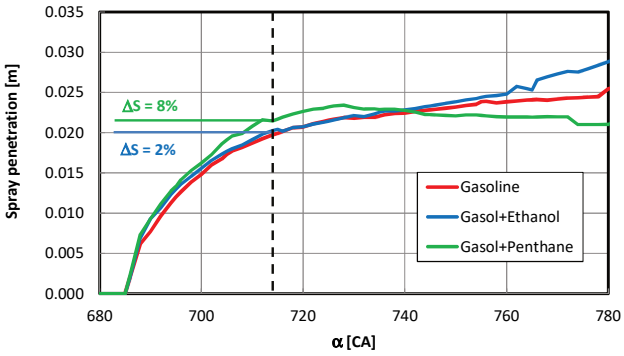

Fig. 13. The effect of the fuel stream range changes on the fuel type during injection and spray to the combustion chamber

Obtained results of evaporated fuel mass allow to determine its total share in injected fuel dose. At 715° CA the shares of evaporated mixtures are:

a) gasoline – 32%
b) gasoline and ethanol – 18%
c) gasoline and isopentane – 34%.

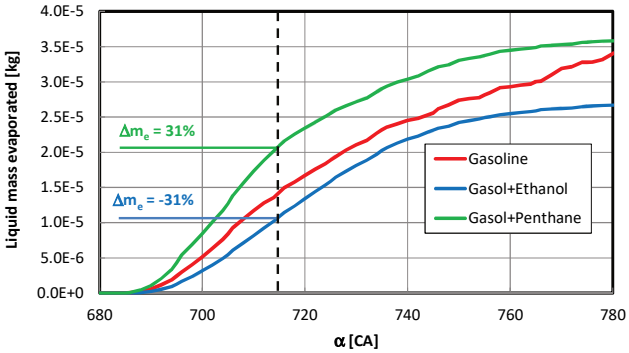

Fig. 14. The effect of the evaporated dose quantity in the combustion chamber on the fuel type during its injection and spray

This implies that mixing fuels before ignition allows for reducing the fuel evaporation speed by 25% (gasoline and ethanol) or increasing this speed by 46% (gasoline and isopentane) versus the standard gasoline injection. This means that gasoline-isopentane mixture lets achieve almost double (92%) the evaporated mass than the gasoline-ethanol mixture.

The analysis of the above results allows to determine the amount of evaporated fuel during injection (Fig. 15). Due to the gasoline-ethanol mixture properties, its evaporation is the slowest and during injection 2% less fuel evaporates than during gasoline-only injection. The gasoline-isopentane mixture evaporates quicker and at the end of the injection the evaporated fuel value is 4% higher compared to gasoline-only injection (almost 5% to gasoline-ethanol mixture).

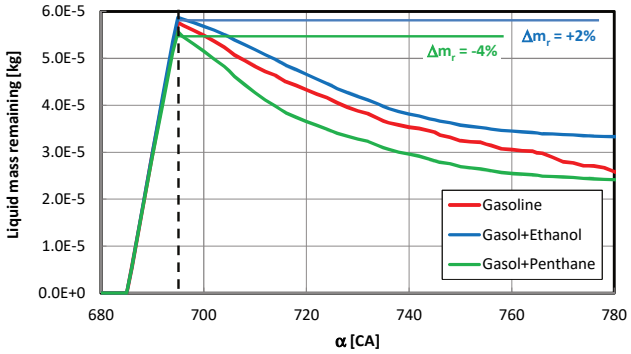

Fig. 15. The effect of the unevaporated dose quantity in the combustion chamber on the fuel type during its injection and spray

Different fuel properties mean that it is important to create the fuel mixture before its combustion directly in the combustion chamber. The analysis presented above points to the significance of this issue in the aspect of searching for solutions lowering the fuel consumption and limiting the CO_2 emission.

6. Summary

The paper describes the research conducted in AVL Fire calculation environment, which is focused on a new direct fuel injection solution. The current knowledge about internal combustion initiated by direct injection fuel supply systems was considered and the dual direct injection fuelling system was introduced.

The research concerns the effects of using three different fuels in combination with gasoline for separate direct injection on spray and flammability of the created mixture directly before ignition.

It was shown that it is possible to shape the air excess ratio in the area of the spark plug by injecting different fuels. Isopentane and ethanol injected through a separate injector than the gasoline have various effects on the air-fuel mixture in the area of combustion initiation. The quantitative properties of the spray were presented and the effects described.

The air excess ratio value in the spark plug area depends on:

– fuel density – its increase causes limitation of the fuel outflow from the injector nozzle, and as a result – the limitation of fuel spray range,
– injection timing of different fuels – different fuel properties, which means: enthalpy of evaporation, density, specific heat and stoichiometric A/F ratio cause different flammability condition in the spark plug area.

Further research directions include:

– various injection crank angles analysis of both fuels in order to find required flammability in the area of spark presence,
– proper injectors positioning in order to find feasible and optimal solution to execute the dual fuel injection,
– effects on combustion by using described fuel supply system in combination with different fuels.

Acknowledgements

The study presented in this article was performed within the statutory research.

Nomenclature

A/F	air-fuel ratio
CA	crank angle
CI	compression ignition
CNG	compressed natural gas
DI	direct injection
LPG	liquified petrolum gas
m_e	fuel mass evaporated
m_r	fuel mass remaining
S	penetration
SI	spark ignition
T	temperature
TDC	top dead center

Bibliography

[1] ALEIFERIS, P.G., VAN ROMUNDE, Z.R. An analysis of spray development with iso-octane, n-pentane, gasoline, ethanol and n-butanol from a multi-hole injector under hot fuel conditions. *Fuel*. 2013, **105**, 143-168.

[2] ARGACHOY, C., PIMENTA, A.P. Phenomenological model of particulate matter emission from direct injection diesel engines. *Journal of the Brazilian Society of Mechanical Sciences and Engineering*. 2005, **27**(3).

[3] ASAY, R., SVENSSON, K., TREE, D. An empirical, mixing-limited, zero-dimensional model for diesel combustion. *SAE Technical Paper*. 2004, 2004-01-0924.

[4] ASHGRIZ, N. Handbook of atomization and sprays. *Springer*, New York 2011.

[5] AVL Fire 2014.2, AVL AST Documentation.

[6] CAMEO Chemicals. cameochemicals.noaa.gov (accessed 19.03.2017).

[7] CHEN, Z., GU, F., HU, W. Chemical engineering thermodynamics. *Chemical Industry Press*, Beijing, 2006.

[8] CHEN, H., REUSS, D.L., SICK, V. Analysis of misfires in a direct injection engine using proper orthogonal decomposition. *Experiments in Fluids*. 2011, **51**.

[9] DECHOZ, J., ROZÉ, C. Surface tension measurement of fuels and alkanes at high pressure under different atmospheres. *Applied Surface Science*. 2004, **1-4**(229), 175-182.

[10] DEMIREL, Y. Energy, green energy and technology. *Springer-Verlag* London, 2012.

[11] ELFASAKHANY, A. Investigations on performance and pollutant emissions of spark-ignition engines fueled with n-butanol–, isobutanol–, ethanol–, methanol–, and acetone–gasoline blends: A comparative study. *Renewable and Sustainable Energy Reviews*. 2017, **17**, 404-413.

[12] FOURNIER, S., SIMON, G., SEERSET, P. Evaluation of low concentrations of ethanol, butanol, BE, and ABE blended with gasoline in a direct-injection, spark-ignition engine. *Fuel*. 2016, **181**, 396-407.

[13] GARG, P., KUMAR, P., SRINIVASAN, K., DUTTA, P. Evaluation of isopentane, R-245fa and their mixtures as working fluids for organic Rankine cycles. *Applied Thermal Engineering*. 2013, **1-2**(51), 292-300.

[14] HUANG, Y., HONG, G. Investigation of the effect of heated ethanol fuel on combustion and emissions of an ethanol direct injection plus gasoline port injection (EDI + GPI) engine. *Energy Conversion and Management*. 2016, **123**, 338-347.

[15] HUANG, Y., HUANG, S., HUANG, R., HONG, G. Spray and evaporation characteristics of ethanol and gasoline direct injection in non-evaporating, transition and flash-boiling conditions. *Energy Conversion and Management*. 2016, **108**, 68-77.

[16] JONES, J.J. Hydrocarbons. Physical properties and their relevance to utilization. *C Jones &Ventus Publishing*. bookboon.com, 2010.

[17] LIU, S, CUTY CLEMENTE, E.R., HU, T., WEI, Y. Study of spark ignition engine fueled with methanol/gasoline fuel blends. *Applied Thermal Engineering*. 2007, **27**(11-12), 1904-1910.

[18] LUCCHINI, T., D'ERRICO, G., ONORATI, A., BONANDRINI, G. et al. Development and application of a computational fluid dynamics methodology to predict fuel–air mixing and sources of soot formation in gasoline direct injection engines. *International Journal of Engine Research*. 2014, **5**(15), 581-596.

[19] MOOSAVI, M., DANESHVAR, A., SEDGHAMIZ, E. et al. Shear rate-, temperature- and composition-dependencies of viscosity behavior of mixtures of {[bmim]NO3+ethanol}. *Journal of Molecular Liquids*. 2017, **199**, 257-266.

[20] PIELECHA, I. Modeling of gasoline fuel spray penetration in SIDI engines. *International Journal of Automotive Technology*. 2014, **15**(1), 47-55.

[21] Refining online. www.refiningonline.com (accessed 19.03.2017).

[22] SCHIFTER, I., GONZÁLEZ, U., GONZÁLEZ-MACÍAS, C. Effects of ethanol, ethyl-tert-butyl ether and dimethylcarbonate blends with gasoline on SI engine. *Fuel*. 2016, **183**, 253-261.

[23] Shell Chemicals, Isopentane Q1111, www.shellcom (accessed 19.03.2017).

[24] SHEN, C., LI, X.-M., LU, Y.Z., LI, C.X. Effect of ionic liquid 1-methylimidazolium chloride on the vapour liquid equilibrium of water, methanol, ethanol, and {water + ethanol} mixture. *Journal of Chemical Thermodynamics*. 2011, **43**(11), 1748-1753.

[25] STORCH, M., KOEGL, M., ALTENHOFF, M. et al. Investigation of soot formation of spark-ignited ethanol-blended gasoline sprays with single- and multi-component base fuels. *Applied Energy*. 2016, **181**, 278-287.

[26] Thermal-Fluids Central, www.thermalfluidscentral.org (accessed 20.03.2017).

[27] TURNS, S.R. An introduction to combustion: concepts and applications. *McGraw-Hill*, New York 1996.

[28] WEI, J. Molecular symmetry, rotational entropy, and elevated melting points. *Industrial & Engineering Chemistry Research*. 1999, **38**(12), 5019-5027.

[29] ZHUANG, Y., HONG, G. Primary investigation to leveraging effect of using ethanol fuel on reducing gasoline fuel consumption. *Fuel*. 20132, **105**, 425-431.

Maciej Sidorowicz, MEng. – Faculty of Machines and Transport at Poznan University of Technology.

e-mail: *Maciej.Sidorowicz@doctorate.put.poznan.pl*

Ireneusz Pielecha, DSc., DEng. – Faculty of Machines and Transport at Poznan University of Technology.

e-mail: *Ireneusz.Pielecha@put.poznan.pl*

Article citation info:
MERKISZ, J., RYMANIAK, Ł. Determining the environmental indicators for vehicles of different categories in relation to CO_2 emission based on road tests. *Combustion Engines*. 2017, **170**(3), 66-72. DOI: 10.19206/CE-2017-310

Jerzy MERKISZ
Łukasz RYMANIAK

CE-2017-310

Determining the environmental indicators for vehicles of different categories in relation to CO_2 emission based on road tests

The article discusses the possibility of determining the environmental indicators for vehicles of different categories in relation to CO_2 emissions. These are called toxicity indicators because they concern the compounds: CO, THC and NO_x. Three Euro V compliant vehicles with different propulsion systems types were used for the study: a 0.9 dm^3 urban passenger car with a SI engine and a start-stop system, a 2.5 dm^3 off-road vehicle with a CI engine, and a city bus with a hybrid drive system in series configuration and a CI engine with a displacement of 6.7 dm^3. Measurements were made in actual operating conditions in the Poznan agglomeration using a portable emissions measurement system (PEMS). The paper presents the characteristics of the operating time shares of vehicles and propulsion systems as well as CO_2 emissions depending on the engine load and crankshaft rotational speed for individual vehicles. The determined toxicity indicators allowed to indicate their usefulness, to make comparisons between tested vehicles, and to identify directions for further work on the application and interpretation of these indicators.

Key words: *CO_2 emission, combustion engines, PEMS, RDE, toxicity indicators*

1. Introduction

Combustion engine pollutant emission tests are no longer conducted exclusively on engine dynamometer stations. Research conducted on emissions in real operating conditions, referred to as RDE – real driving emissions, is essential. For heavy-duty vehicles (HDVs) these tests have been a part of their type approval for several years [3]. They are required for service conformity assessment. For passenger cars (PC) the road measurements will become required from 1 September 2017 in accordance with the Euro 6c [2]. Testing in real driving conditions allows a thorough assessment of the ecological indicators in the full range of the internal combustion engine's operating parameters, which has not been previously tested in laboratory measurements [4, 7, 8]. In addition, these tests allow for the performance assessment of not only the internal combustion engine but also the entire drive system (e.g. hybrid). The drive system ecology depends on two main factors: the type and effectiveness of the exhaust aftertreatment system and the combustion process in the cylinder.

The emissivity and efficiency of the combustion engine depends to a large extent on the exothermic oxidation reaction quality. Its course is complex because it deals with issues described in organic chemistry (fuel), inorganic chemistry (combustion products) and physical chemistry (equilibrium and speed) [6]. Piston engines are most often powered with liquid fuels (diesel, petrol). For this reason, in the combustion process it is important not only to mix the fuel with the oxidizer, but also to ensure quick fuel evaporation. In this aspect gaseous fuels, such as natural gas (NG), are preferred because they are already in the form of a volatile gas [5]. However, gaseous fuels are generally characterized by lower caloric content.

According to the theory of absolute rate of combustion [1], each chemical reaction proceeds according to a scheme which will be described by the simplest elementary reaction between the two reactants A and BC. If reactants A and BC are involved in the reaction and AB and C are produced as a result of the reaction, the A-B-C complex, referred to in the literature as the transitional complex, is always present on the path. This scheme is written as:

$$A + BC \rightarrow \text{active complex A-B-C} \rightarrow AB + C \qquad (1)$$

The basic condition for the process (1) is the contact during particle collisions. In addition, the appropriate spatial orientation and also for the particles to possess the energy of activation E. During combustion the rate of reaction depends exponentially on the temperature. This relation is expressed by the Arrhenius equation in the form:

$$k = A \cdot \exp\left(-\frac{E}{RT}\right) \qquad (2)$$

where there are two constants: the pre-exponent A and the activation energy E. The physical meaning of both constants is due to existing theories of matter construction [2]. Nevertheless, because of the complexity of these theories the values of these constants are usually determined experimentally.

Affecting the combustion process in a combustion engine can have a positive impact on its environmental indicators and performance parameters. Therefore, modern engineered constructions use many advanced technical solutions to improve the combustion process. These are primarily: high pressure direct injection systems with staggered dose, variable valve timing systems, turbocharging, as well as inlet manifold solutions that ensure adequate swirling when filling cylinders with the fuel dose [9]. Frequently mentioned systems have a smooth adjustment of their operating settings and operate interdependently.

2. Use of CO_2 emissions in the assessment of toxic emissions

The ecological indicators of the vehicle are based primarily on specific emissions – the mass of the harmful substance that is released relative to the work performed (also used in the assessment of machines with internal combustion engines) and the road emission – the mass of the harmful compound that is released relative to the distance traveled. Special indicators of the emitted flue gas

component mass in relation to the work performed are more commonly being adopted for operated machinery (e.g. plowed area, truncated tree volume, etc.). The emission indicators determined in such a way sometimes make it difficult to compare between vehicles, as it depends on the type of drive system used (e.g. hybrid), the operating conditions (e.g. urban or highway drive), driving style, etc.

The primary combustion product in an internal combustion engine is CO_2, which is classified as a harmful compound. Its content in the flue gas depends on the amount of fuel burned and the quality of the oxidation process. Other harmful compounds in exhaust gases, also characterized as toxic, are formed during incomplete or imperfect combustion, and in the presence of high temperatures and pressures. The emission limits included in the type approval standards refer to the CO, THC (NMHC + CH_4), NO_x, PM, PN, and also NH_3 in vehicles equipped with SCR (selective catalytic reduction). The only product that does not affect air pollution is water vapor.

By analyzing the characteristics of the piston engine operation, the fuel oxidation mechanism and the formation of toxic compounds, it can be assumed that the CO_2 emission rate is a measure of the combustion process efficiency. Comparing the emissions of toxic compounds with CO_2 emissions, it is possible to determine the toxicity indicators M_j that characterize a particular engine or drive system (if non-exhaust gas purification systems are also used in the system). Such ecologically defined indicators enable an efficient comparison between different combustion engines. The quantitative toxicity indicator is defined as:

$$M_j = b \cdot \frac{e_{RDE,\,j}}{e_{CO_2}} \tag{3}$$

where: M – dimensionless toxicity indicator [–], j – the toxic compound, for which the emission indicator has been determined, b – a constant (for CO, THC and NO_x = 10^3, for PM = 10^5), $e_{RDE,\,j}$ – specific or road emission or emitted mass of the toxic compound j determined as a result of emission testing [g/(kW·h); g/(km); g], e_{CO_2} – specific or road emission, or CO_2 mass determined as a result of emission testing (same as $e_{rzecz,\,j}$) [g/(kW·h); g/(km); g].

3. Research methodology

Research in the actual vehicle operating conditions is becoming more and more common. This type of research is useful in assessing both the ecological indicators and the operating parameters of the drive systems, e.g. in construction or optimization. Road tests have been carried out to assess the validity of the discussed considerations for the determination of toxicity indicators from motor vehicles. Three Euro V compliant vehicles were used for the measurements, with different types of drive systems (Table 1, Fig. 1). A passenger car with a 0.9 dm^3 two-cylinder SI engine and an active start-stop system was designated as vehicle A. The second test vehicle (vehicle B) was an off-road 2.5 dm^3 CI engine pick-up. Vehicle C was a city bus with a CI engine and a hybrid drive in series configuration. The engine's displacement was 6.7 dm^3, and the power of the electric traction motor used was 240 kW.

Testing of vehicles A and B in real traffic conditions was performed on the same test route No. 1 (Fig. 2a). New European Driving Cycle (NEDC) guidelines were included in its selection. In some parts of the route there were a number of intersections, which made it possible to map the highly urban driving conditions. In addition, sections on which the vehicle could accelerate to higher speeds were selected, which allowed to simulate suburban travel and to the main communication arteries. The total length of the test route was 11.6 km. The third vehicle was tested on Route 2 selected according to its purpose (Fig. 2b). The route covered

Table 1. Vehicle technical parameters

Parameter	Tested vehicle		
	Vehicle A	Vehicle B	Vehicle C
Engine type/fuel	4-stroke, SI/Gasoline	4- stroke, CI /Diesel	4- stroke, CI/Diesel
Displacement [dm^3]	0.9	2.5	6.7
Compression ratio	10	15	17
Max. power [kW]/[rpm]	64/5500	140/4000	209/2300
Max. torque [N·m]/[rpm]	145/1800	400/2000	1008/1200
Aftertreatment system	TWC	DOC/DPF	DOC/SCR/DPF
Drive system	Start–stop system	Conventional	Series hybrid drive, electric motor with a power of 240 kW
Vehicle curb weight [kg]	1 300	2 500	24 000

Fig. 1. Tested vehicles: a) vehicle A, b) vehicle B, c) vehicle C

Fig. 2. Routes used in RDE tests: a) route No. 1 for vehicle A and B, b) route No. 2 for vehicle C [11]

the urban operating conditions, including bus stops. The total route distance was 12.2 km. All measurements were made on weekdays, in the morning. This was to achieve similar and comparable traffic and congestion conditions.

SEMTECH DS mobile device was used in the evaluation of the toxicity indicators. It is used in real operating conditions and is classified as a portable emissions measurement system (PEMS). The analyzer kit allows measuring emissions from both SI and CI engines that meet the norms Euro 3 and above. Its principle of operation is shown in Fig. 3. The exhaust gases are sampled out of the exhaust gasses main mass flow, the sample's temperature is kept at 191°C. Then they are directed to the set of analyzers: flame ionization detector (FID) – for THC measurement, non-dispersive detector ultra violet (NDUV) – NO_x measurement, non-dispersive detector infra red (NDIR) – CO_x measurement. In the last stage, the measurement of the oxygen content of the exhaust gas by electrochemical method is carried out. The instrument enables synchronization with the GPS positioning system, LAN connection and meteorological data system, as well as communication with the vehicle's OBD [10].

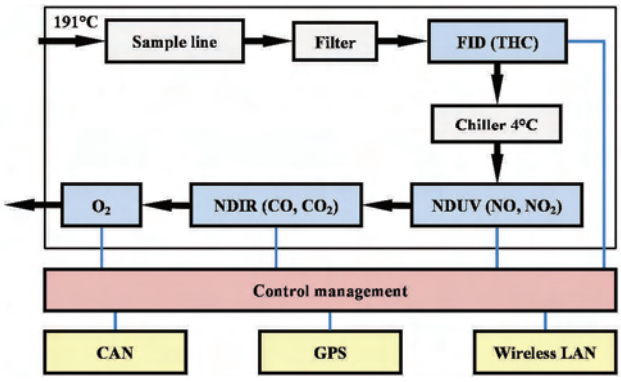

Fig. 3. SEMTECH DS operating schematic [10]

4. Real driving emissions results

4.1. Analysis of the vehicles and combustion engines operating conditions

Based on the recorded speed profiles of the individual vehicles, their operating time share characteristics in the speed-acceleration (V–a) parameters were determined. Vehicles A and B were tested on the same route at a similar time of day, resulting in similar characteristics. The registered average speeds of these cars were 44.3 km/h and 37.4 km/h respectively. Therefore, Figure 4 shows the distribution of the vehicle A's operating time share only. The total time spent stationary for passenger cars in the test reached the same value of 13.7%. Maximum speed reached during test did not exceed 22 m/s (79.2 km/h). The greatest share of operating time occurred in the speed intervals (8 m/s; 20 m/s⟩ for acceleration ⟨–0.8 m/s^2; 0 m/s^2) and (0 m/s^2; 0.8 m/s^2⟩, where the recorded share of operating time for vehicle A was – 19.1% and 29%; and vehicle B – 16.3% and 28.7%. For driving at a constant speed in the interval (16 m/s; 20 m/s⟩ the time share was 11% and 5.9% respectively.

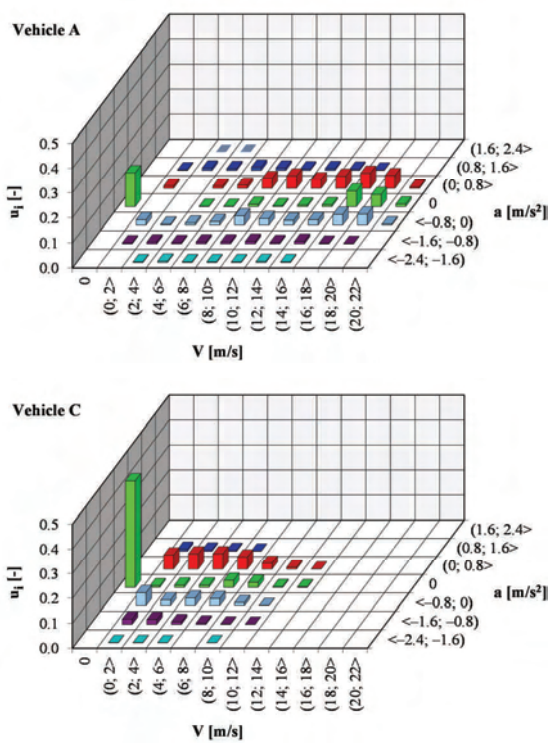

Fig. 4. Shares of vehicles operating time in speed and acceleration compartments during road tests

In the study of the city bus, the maximum share of operating time of 43% was recorded for vehicle being stationary, which was due to the vehicle's operation characteristics (servicing bus stops) and the traffic conditions in the city center. The maximum speed recorded on the measurement route was 12.2 m/s (43.9 km/h). The highest share of operating time occurred in the speed ranges of (0 m/s, 8 m/s⟩ for acceleration ⟨–0.8 m/s^2, 0 m/s^2) and for (0 m/s^2, 0.8 m/s^2⟩. In the remaining speed and acceleration ranges, the determined time share values did not exceed 2.8%.

When analyzing the emission of the tested vehicles, it is important to know the internal combustion engines operating parameters, as shown in Fig. 5. The time share characteristics are shown in coordinates of the crankshaft rotation speed to engine load. The petrol vehicle had the highest share of 50% operating time for rotational speeds in the range of (1800 rpm, 2600 rpm⟩ with the engine load not exceeding 20%. In the load range of more than 80%, the assigned value of operating time share was 12%. The engine characteristic had an effect on the resulting distribution of the work area of the engine, especially the torque curve, which is characterized by small values in the engine speed range of less than 1600 rpm.

The compression ignition engine used in vehicle B had the largest variation of operating parameters. The highest share of operating time was recorded for engine speeds not exceeding 1000 rpm at engine loads of up to 20%, which constituted 29.1% of the total operating time. For the same load in the speed range (1000 rpm, 2600 rpm⟩ the operating time share of 44.7% was determined. The large value of this time share was derived from the characteristics of the internal combustion engine – high torque is reached from the idle speed already. In the remaining single compartments, the shares of operating time did not exceed 3%.

The hybrid drive used in vehicle C had a significant influence on the obtained distribution of the engine operating time share characteristics for that vehicle. Moreover, the engine was loaded with additional torque associated with the operation of functional systems (e.g. pneumatic system and the air conditioning). The highest value of 40.6% was found for the lowest engine speed range of (20%; 40%⟩. In the performed test conditions, the speed range of (1000 rpm, 1400 rpm⟩ for load range ⟨0%; 80%⟩, in which the total time share value of 31% was registered, had the most significant impact on the overall results. This was mainly due to the interaction with the electric motor in the hybrid drive, which converted the engine torque into electric power. For the same reasons the lowest rotational speed and load range the time share was only 2%.

4.2. Ecological results analysis

In order to determine the tested engines toxicity indicators, it is useful to determine their CO_2 emissions depending on the operating conditions of the internal combustion engines (Fig. 6). Based on the characteristics, it can be stated that the analyzed harmful compound emission intensity of vehicle A depends primarily on the load. For speeds above 1400 rpm with loads in the range (80%, 100%⟩ as well as speed (1800 rpm, 3400 rpm⟩ and loads ⟨60%, 80%⟩ CO_2 emissions are greater than 7.4 g/s (maximum 14.2 g/s). For vehicles labelled B and C, equipped with CI engines, the emission characteristics are clearly dependent on engine speed and load. In both cases, the maximum CO_2 emission occurred at engine load above 80%: for vehicle B it was 29.7 g/s at speed (3000 rpm, 3400 rpm⟩ and for vehicle C it was 32.4 g/s for maximum crankshaft rotational speed. However, it should be noted that the engine operating time shares in these compartments were below 3%. In single compartments where the registered maximum engine operating time share was recorded, the emissions were respectively: A (u_i = 35%) – 2.9 g/s; B (u_i = 29.1%) – 1.1 g/s and C (u_i = 40.6%) – 3.2 g/s.

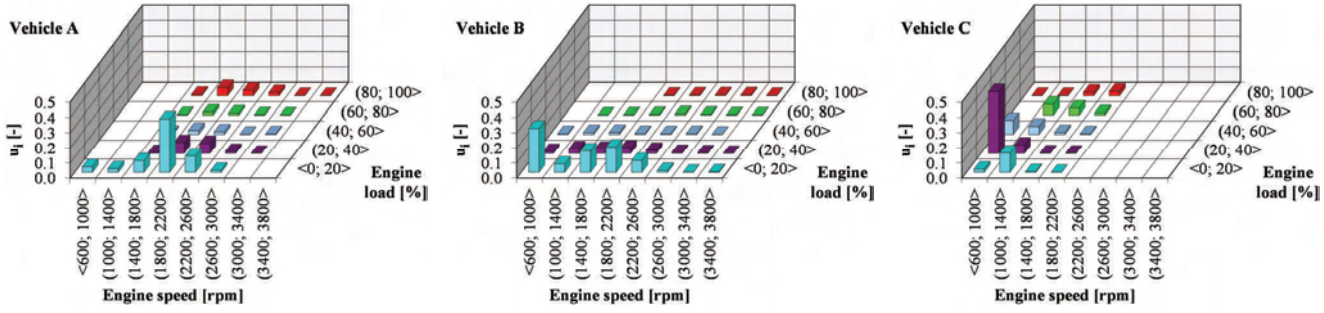

Fig. 5. Operating time shares of internal combustion engines in crankshaft speed and load ranges obtained in road tests

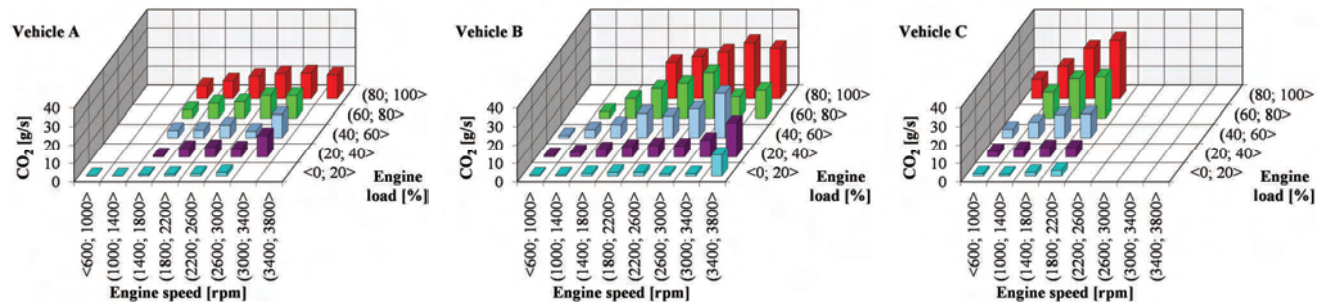

Fig. 6. CO_2 emissions concentration in the speed and torque compartments during road tests

In order to assess the dependence of NO_x emissions on CO_2, the recorded values of emission intensity of these compounds were compared, taking into account time compliance (Fig. 7). Based on the obtained characteristics it can be stated that their distribution is strongly dependent on the exhaust gas aftertreatment system used. In vehicle A, the three-way catalytic reactor was characterized by a high degree of conversion, and NO_x reduction. For CO_2 emissions of up to 6 g/s, the value of the toxic compound compared did not exceed 0.01 g/s. During the entire study cycle the maximum value reached was 0.06 g/s that occurred during dynamic acceleration. For vehicle B, where no notible NO_x reduction systems have been used, a dependence has been obtained – with the increase in CO_2 emission intensity, the NO_x emission values also increased. The resulting distribution was undoubtedly influenced by the exhaust gas recirculation system (its effect was to reduce NO_x emissions in exchange for higher CO_2 emission values). The maximum NO_x emission of 0.22 g/s was recorded for corresponding CO_2 emissions of 23 g/s.

The least regular dependence of NO_x on CO_2 emissions occurred for the city bus. This was due to both the exhaust gas recirculation system and the selective catalytic reduction system. In this system, the conversion rate depends primarily on the temperature and mass flow rate of the exhaust gas – with a higher flow rate, the conversion rate is lower. Urea is added in doses, depending on the thermodynamic parameters present in the catalytic reactor. The absence of linear NO_x reduction resulted in a CO_2 emission intensity of about 32 g/s when the NO_x emission intensity was in the range of 0.05–0.43 g/s. It should be noted that the combustion engine of this vehicle, due to the interaction with the electrical components, has been operating in the range of high efficiency (high temperature in the combustion chambers), which has a very high impact on NO_x emissions compared to other toxic compounds.

As illustrated by the previous example the engine exhaust aftertreatment systems have a very significant impact on the values of the analyzed toxicity indicators. For a vehicle with an SI engine, the excess air ratio λ, which directly affects the performance of a three-way catalytic converter, is undoubtedly also significant. Figure 8 shows the recorded speeds of the tested vehicles as a function of the distance travelled, along with the values of the M_CO/CO_2 toxicity indicators. Recorded mileage for vehicle A clearly indicates that the vehicle acceleration dynamic has a significant impact on the toxicity indicator. Dynamic speed increase results in a M_CO/CO_2 value of above 15. During constant speed motion and braking, this indicator does not exceed the value of 3. This was caused by the high engine load – a small heat unit was heavily loaded during intense acceleration, which could have led to an enrichment of the fuel mixture and thus change the value of the excess air ratio, which guarantees the effective operation of TWC.

For the other researched vehicle the relation between the toxicity indicator curve and the velocity curve were noted. The increase in M_CO/CO_2 was recorded during braking, especially during slight decelerations using engine braking. In this process, the CO_2 emission (being the denominator of the coefficient) tends towards 0. Therefore, even a small

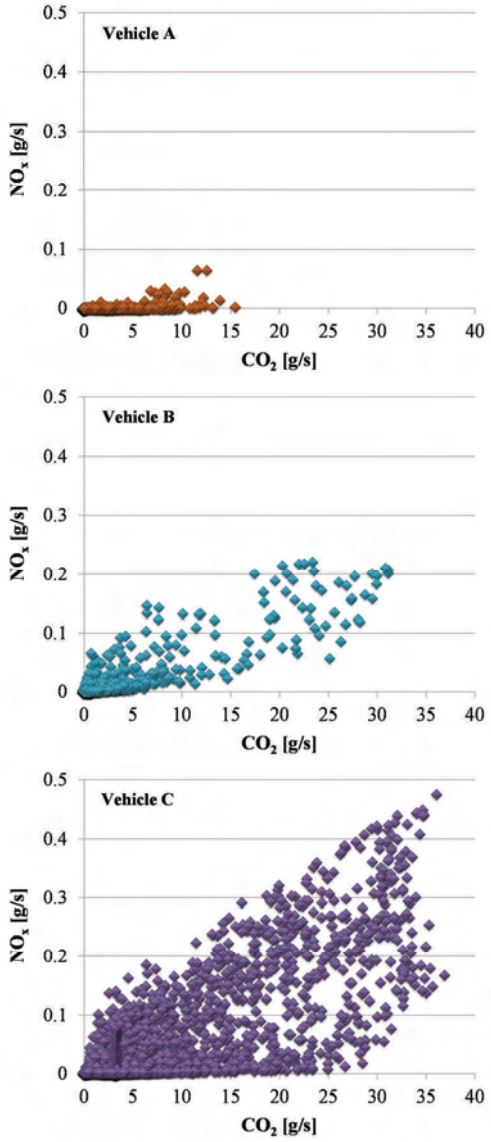

Fig. 7. Comparison of NO_x and CO_2 emissions during road tests with respect to time compliance

CO emission results in high values from the calculations. In addition, the resulting curves indicate incomplete combustion in the cylinders. The indicator reached a maximum value of 40. Whereas during acceleration, the indicator did not exceed the value of 4. Similar tendencies were observed for the vehicle C. The M_CO/CO_2 ratio depends primarily on braking. Despite the hybrid system, vehicle movement had a significant impact on the characteristics. It should also be noted that the maximum toxicity indicator values were even five times greater than in the vehicle B tested. This is due to the difference in the combustion engines used (power and displacement) and the type of vehicle (mass and purpose) and operating conditions. In the acceleration process, the factor obtained only a small value – in this vehicle, the propulsion system was boosted by a supercapacitor system storing the energy recovered in vehicle braking.

Based on the analysis of the results obtained for the M_THC/CO_2 indicators, very close correlations were obtained as were found with the M_CO/CO_2. For the first test vehicle its values depended primarily on acceleration,

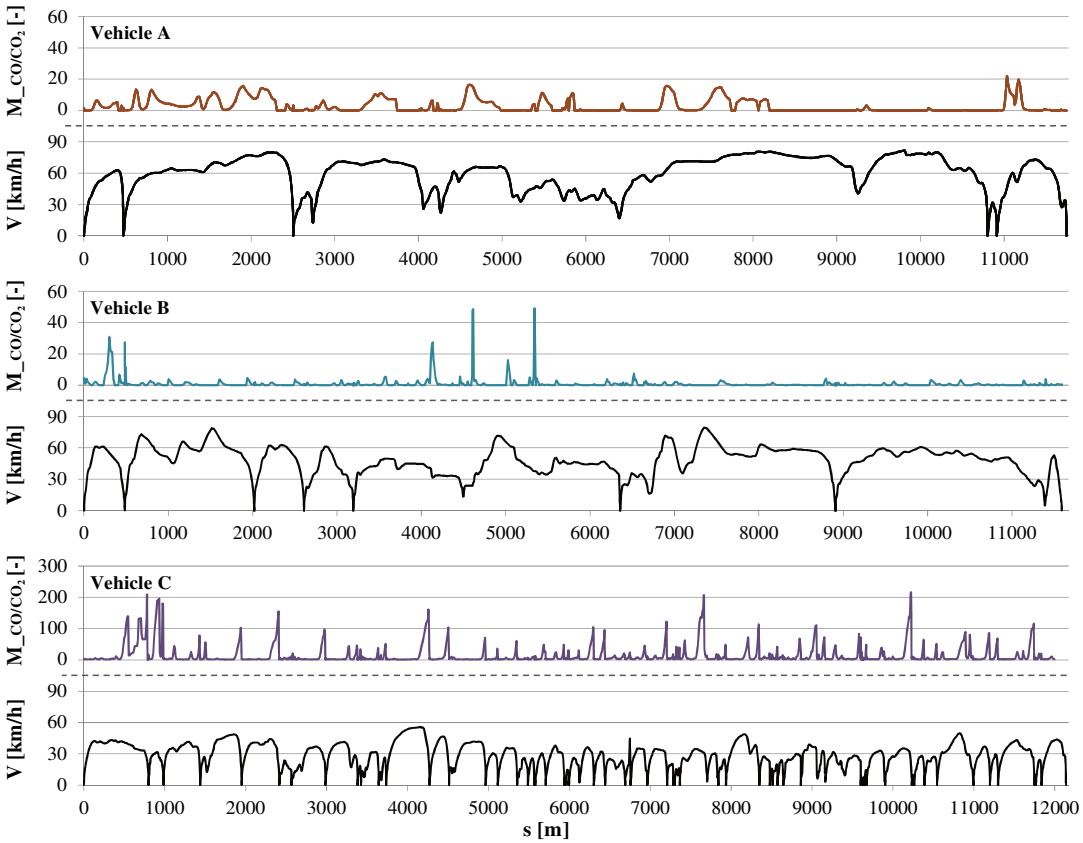

Fig. 8. Vehicle speed curves and the M index for the CO emission values recorded during road tests

while for vehicles with CI engines the maximum values was obtained during braking. This is due to the fact that THC emissions are somewhat similar in origin to CO emissions and oxidation of these compounds uses a single exhaust aftertreatment system with one or more catalysts.

Taking into account the entire emission of pollutants recorded in the road tests, total toxicity indicators for CO, THC, and NO_x were determined (Fig. 9). The largest value was achieved for the pick-up, while the smallest for the urban passenger car with an SI engine. The most significant differences occurred with the M_CO/CO_2, where the value for vehicle C – 2.51, was 5.5 times that of vehicle A and 3.8 times that of vehicle B. With respect to M_NO_x/CO_2, vehicle A reached 0.35 – while the indicator for vehicle B was t 14.7 times greater and for vehicle C more than 21 times greater. The low M_NO_x/CO_2 ratio for the first vehicle was primarily due to the highly efficient exhaust gas aftertreatment system that significantly reduced the amount of the analyzed toxic compound. A relatively small internal combustion engine was used in the test bus due to the development and capabilities of the hybrid system. However, this solution caused the engine to work more frequently in the areas of higher load (higher efficiency, high cylinder temperatures during combustion), which had a significant effect on the results obtained in the road measurements. Taking into account the considerations made, it must be stated that, during the analysis and assessment of ecological toxicity indicators, it is also necessary to take into account the purpose and design of the vehicles together with the exhaust gas aftertreatment systems used.

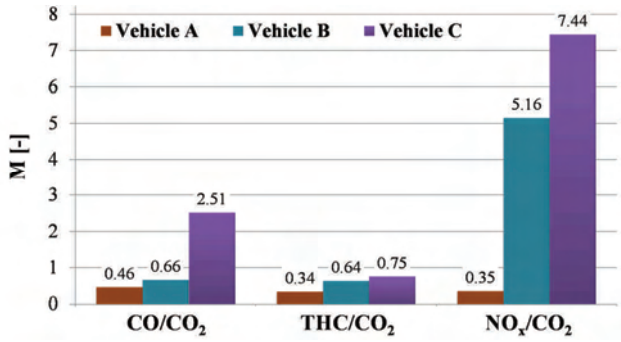

Fig. 9. Summary of toxicity index M for CO, THC, and NO_x

5. Conclusion

The research presented in the study was of an urban passenger vehicle, an off-road vehicle and a city bus. The only difference in the measurement procedures was the other test route used for the third vehicle – this resulted in the need for reliable operating conditions complemented by the servicing of the bus stops. In order to compare the results obtained from the two routes, the performance characteristics of the vehicles and their internal combustion engines were calculated. This allowed to indicate the differences between the trips, which were influenced mainly by the types of drive systems used and the traffic conditions. For vehicles A and B, the highest share of operating time occurred in the load range of up to 20%, while for the bus they were in the range of (20%, 40%⟩. The CO_2 emission distribution for each vehicle in terms of engine load and the crankshaft speed was then presented and discussed for given combustion engines.

The presentation of the NO_x emissions as a function of CO_2 has allowed to determine the environmental performance of the tested vehicles for those exhaust components, and to assess the impact of the exhaust gas aftertreatment systems applied. The most effective in this respect was a gasoline-powered vehicle equipped with a three-way catalytic reactor. The calculated M_CO/CO_2 toxicity indicators made it possible to conclude that in gasoline vehicles their values depend primarily on acceleration parameters, whereas in vehicles with CI engines their value depends mainly on engine braking. Based on the analysis of toxicity indicators, it can be concluded that they are useful in ecological assessment of vehicles of different categories and their comparison. The presented and discussed research results show that the use of a toxicity indicator, which is the emission ratio of a particular toxic component relative to the corresponding CO_2 emission, makes it possible to consider conventional and hybrid solutions together. The indicator shown is in a way a measure of the fuel's combustion efficiency and a tool for evaluating the performance of exhaust gas aftertreatment systems. When determining the environmental indicators based on the assumed model, the results are independent of the distance traveled and the work performed by the drive system in the test. However, when analyzing and evaluating ecological toxicity indicators, it is also necessary to take into account the purpose and design of vehicles together with the exhaust gas aftertreatment systems used. For these reasons, its use can be particularly useful when evaluating drives in the design and construction phase and in future type approval operations.

Acknowledgements

The research was funded by project co-financed by the European Regional Development Fund in the Regional Program – Lubuskie 2020 (contract No. RPLB.01.01.00-08-0055/16-00).

Nomenclature

a	acceleration
b	a constant of the toxicity indicator
DOC	diesel oxidation catalyst
DPF	diesel particulate filter
e	emission of harmful exhaust components
FID	flame ionization detector
GPS	global positioning system
k	rate constant
LPG	liquefied petroleum gas
M	toxicity indicator (dimensionless)
NDIR	non-dispersive infrared
NDUV	non-dispersive ultraviolet
NEDC	New European Driving Cycle
NG	natural gas
OBD	on-board diagnostic
PEMS	portable emission measurement system
R	universal gas constant
RDE	real driving emissions
s	distance
SCR	selective catalytic reduction
T	temperature
TWC	three way catalyst
u	share coefficient
V	velocity

Bibliography

[1] ATKINS, W.P. Physical chemistry. *Wydawnictwo Naukowe PWN*. Warszawa 2003.
[2] Commission Regulation (EU) 2016/427 of 10 March 2016 amending Regulation (EC) No 692/2008 as regards emissions from light passenger and commercial vehicle (Euro 6).
[3] Commission Regulation (EU) No 582/2011 of 25 May 2011 implementing and amending Regulation (EC) No 595/2009 of the European Parliament and of the Council with respect to emissions from heavy duty vehicles (Euro VI) and amending Annexes I and III to Directive 2007/46/EC.
[4] FUC, P., LIJEWSKI, P., ZIOLKOWSKI, A., DOBRZYNSKI, M. Dynamic test bed analysis of gas energy balance for a diesel exhaust system fit with a thermoelectric generator. *Journal of Electronic Materials*. 2017, **46**(5), 3145-3155.
[5] KAKAEE, A.H., PAYKANI, A., GHAJAR, M. The influence of fuel composition on the combustion and emission characteristics of natural gas fueled engines. *Renewable and Sustainable Energy Reviews*. 2014, **38**, 64-78.
[6] KORDYLEWSKI, W. (red.) Spalanie i paliwa. *Oficyna Wydawnicza Politechniki Wrocławskiej*. Wrocław 2005.
[7] MERKISZ, J., BAJERLEIN, M., RYMANIAK, Ł., SIEDLECKI, M. Development of road test to evaluate the fuel consumption in the urban cycle for city buses equipped with hybrid powertrain. *Combustion Engines*. 2015, **3**(162), 587-592.
[8] MERKISZ, J., PIELECHA, J. The possibilities of conversion of pollution emission values from combustion engines in heavy-duty vehicles. *Journal of Polish CIMEEAC*. 2016, **11**(1), 139-150.
[9] PULKRABEK, W.W. Engineering fundamentals of the internal combustion engine. *Pearson Prentice Hall*. Upper Saddle River, 2014.
[10] Sensors Inc. Emissions Measurement Solutions. SEMTECH DS On Board In-Use Emissions Analyzer. Erkrath 2010.
[11] gpsvisualizer.com (access: 19.03.2017).

Prof. Jerzy Merkisz, DSc., DEng. – Faculty of Machines and Transport at Poznan University of Technology.

e-mail: *Jerzy.Merkisz@put.poznan.pl*

Łukasz Rymaniak, DEng. – Faculty of Machines and Transport at Poznan University of Technology.

e-mail: *Lukasz.Rymaniak@put.poznan.pl*

Article citation info:
ROGÓŻ, R., JAWORSKI, P., KAPUSTA, Ł.J., TEODORCZYK, A. The influence of the injection frequency on the selective catalytic reduction systems performance. *Combustion Engines*. 2017, **170**(3), 73-77. DOI: 10.19206/CE-2017-311

Rafał ROGÓŻ
Piotr JAWORSKI
Łukasz Jan KAPUSTA
Andrzej TEODORCZYK

CE-2017-311

The influence of the injection frequency on the urea selective catalytic reduction systems performance

This study presents the influence of the UWS injection frequency on a close coupled SCR systems performance. The investigation was performed with the CFD tool AVL Fire. In the paper the analysis of four different UWS injection frequencies in the three different operating points of diesel engine was shown. The assessments of the system performance was referred to the ammonia distribution at catalyst intake and wall film formation inside the investigated geometry, as these are considered as crucial in such a configuration. The results showed that injection frequency affects both factors on different level depending from the flow conditions. In addition, the wall film crystallization risk was discussed basing on the obtained wall film characteristics.

Key words: *AVL FIRE, selective catalytic reduction, uniformity index, UWS, wall-film*

1. Introduction

The SCR is the most widely used technique for nitrogen oxides control in the automotive industry. Successive emission regulations put increasingly stringent limits on NO_x content in an exhaust gases. Those restrictions are especially demanding for a diesel engines, for which NO_x emission was reduced over 85% in Europe, compering the Euro 5 and Euro 6 standards [1]. Thus, the SCR systems are objects of intensive research work.

The urea-water-solution (UWS), containing 32.5% of the urea, is injected directly in to the hot exhaust gas stream. The reducing agent ammonia (NH3) is produced by UWS decomposition described by three steps [2]:

1. Evaporation of water,

$$(NH_2)_2CO(aq) \rightarrow (NH_2)CO(s \quad or \quad l) + 6.9H_2O(g) \tag{1}$$

2. Thermolysis of urea into ammonia and isocyanic acid,

$$(NH_2)CO(s \quad or \quad l) \rightarrow (NH_3)(g) + HNCO(g) \tag{2}$$

3. Hydrolysis of isocyanic acid,

$$HNCO(g) + H2O(g) \rightarrow NH_3(g) + CO_2(g) \tag{3}$$

Subsequently passing through these three steps 1 mol of the urea generates 2 mols of ammonia. The UWS mass flow is usually determined to give the same number of NH_3 and NOx mols upstream the catalyst.

The typical diesel after-treatment system, to meet last regulations, consist of Diesel Oxides Catalyst (DOC), Diesel Particular Filter (DPF) and SCR in different configurations. However, as further even stringent emission restrictions are expected, an improvement of this particular technology could be challenging. The newest approach is to combine the DPF and SCR functions by wash-coating the SCR on the DPF, what is called SCRoF (Selective Catalytic Reduction on Filter). Due to the fact, that such a solution occupied less space it can be placed closer to the engine, what reduces thermal loses, backpressure, packaging space, weight and costs at least [3]. On the other hand, the placement of the systems and its packaging results in smaller space for the UWS decomposition and mixing what directly affects the main benchmark of the SCR systems which is even ammonia distribution at catalyst intake described by Uniformity Index (UI). The common solution to improve the ammonia UI is installing a static mixing device, which generates swirls before SCRoF. Nevertheless, it means that spray-wall interactions should be expected, therefore undesired by-products like biuret, cyanuric acid, melamine and ammeline could occur and form solid deposit. The urea crystallization can lead to decreased SCR systems efficiency and higher ammonia slip simultaneously. What is more, the formed deposit results in higher backpressure, and in highly unfavorable conditions may log whole system and simply destroy it [4]. Due to the above, the knowledge about urea wall-film formation risk, uniformity index and pressure drop is crucial already at early stage of the product development process.

Number of research works proof usefulness of the Computational Fluid Dynamics (CFD) tools for a SCR applications. For instance it was shown that a numerical simulations could be used for developing the static mixers design in case of an ammonia distribution and a pressure-drops [5], an assessment of the spray-wall interaction [6] and an UWS injection [7]. Moreover, CFD tools offer functionality, cost effectiveness and increasing credibility. At the early stage of the product development, when a variety of a different concepts and configurations are taken into consideration, CFD calculations helps to choose the most promising design, or upgrade already existing idea. Therefore, it is widely used in automotive industry.

In this work, investigation into SCR systems performance using numerical simulations was carried out. Within the presented paper, the influence of the injection frequency on the ammonia distribution and wall-film formation was analyzed. Considered geometry refers to the DOC+SCRoF architecture in the close coupled solution. The calculations were conducted for variety of flow conditions corresponding to the different exhaust mass flow of the diesel engine.

2. Geometry and numerical setup

For the comparison purposes four different injection frequencies from 1 Hz up to 8 Hz, for three different exhaust gases mass flow rates corresponding to idle, light and medium load of diesel engine were calculated. The results

for 4 Hz injection were treated as the reference value in each condition. The full matrix of the calculations is shown in the Table 1.

Table 1. Calculations matrix

Injection Frequency / Operating Point	1 Hz	2 Hz	4 Hz	8 Hz
Idle	Case 1	Case 2	Case 3	Case 4
Light	Case 5	Case 6	Case 7	Case 8
Medium	Case 9	Case 10	Case 11	Case 12

The geometry resembles typical closed coupled solution for light duty vehicles with the cylindrical DOC and SCRoF connected by transfer cone. The inlet section of the DOC was extruded by 10 cm in order to make so called dummy inlet which provided stable flow at catalyst intake, the same operation was repeated on the SCRoF outlet, where 10 cm long dummy outlet was created. In the middle of the transfer cone static mixer device is placed. The injector is located at the top of the section and its axis passes through the mixer. Whole geometry setup is shown in the Fig. 1.

The computational mesh (Fig. 1) was built by hexahedral elements in a few steps. Firstly, the transfer cone was meshed, using the AVL Fame Hexa tool, with base size of the elements equal to 3 mm. Due to the irregular shape of the design, the injector and mixer section were refined by 1.5 mm and 0.75 mm cell respectively. The DOC mesh were extruded from the inlet selection of the transfer cone and afterwards dummy inlet from the DOC. The same

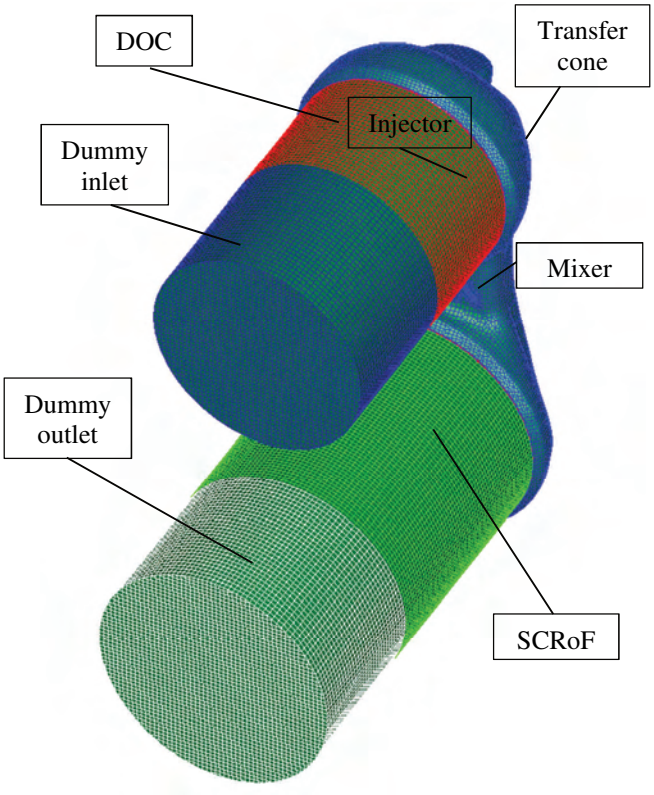

Fig. 1. The geometry and mesh

meshing strategy was applied to the SCRoF and dummy outlet. Thanks to this meshing methodology the structural grid before and after transfer cone was obtained and moreover conformal matching of the parts was possible. Finally, the total size of the domain was equal to 643132 cells.

All of the simulations were conducted using the AVL Fire 2014.2 CFD software, with Species Transport, General Gas Phase Reactions, Porosities, Spray and Wallfilm modules activated. The flow, consisted of diesel combustion products: CO_2, CO, H_2O, O_2, NO, NO_2, N_2 was treated as compressible and turbulent. Timestep was set to dt = 5 ms and dt = 0.5 ms for the flow when injection did not occur and for injection time, respectively. All walls were treated as adiabatic, static pressure outlet was set for the outlet selection.

Both, DOC and SCRoF were modeled as the direct porous media zones. The pressure drop for them were calculated from the Forchheimer formula [8] which described pressure drop as a linear viscous loses corrected by quadratic inertial loses in the function of the velocity inside the zone. Note that, the porous media zones were used only to obtain desirable pressure drops and flow distribution. The chemistry inside the catalyst was not included as it does not have impact on specific objectives of this work.

The UWS spray was represented using the Discrete Droplet Method (DDM). In this approach droplets of the similar size and properties are grouped in the parcels and as a unity treated in the equations. For the UWS decomposition the Birkhold model was used [2], in which it is assumed that urea decompose through thermolysis directly from the solid or liquid phase and its evaporation could be neglected. Thus, due to the fact that water has lower boiling temperature than urea, the model assumed that firstly water evaporates until in droplet remains only urea (1) and then thermolysis occurs (2) [9]. The influence of the dissolved urea in the water on its evaporation rate is modeled basing on Aramzon-Sirignano approach, where heat mass transfer of each component is taken account separately, while heat transfer is a global mechanism [9]. It is assumed that there is no urea crystallization and droplet remain spherical through evaporation and crystallization. Finally, the hydrolysis of the HNCO into ammonia (eq. 3) is resolved by General Gas Phase reaction module with CHEMKIN input chemistry. The UWS injection is realized by three nozzle commercial injector, which works under the pressure of 4 bar with static the mass flow of 1g/s. As the spray is represented with the DDM method, the volume based Rosin-Rammler distribution were applied. The dosing of the UWS were recalculated for each operating condition for keeping constant ammonia to NO_x ratio, the injected mass was controlled by duration of the injection. The injection was started after 0.3 s from the simulation start, when the flow was fully developed.

Spray-wall interaction was implemented with AVL Fire Wallfilm module. With this approach Kuhnke model is implemented, hence software distinguishes four interactions regimes basing on dimensionless droplet velocity and dimensionless wall and saturation temperature ratio. With those quantities dependences rebound, thermal breakup, deposition or splash could occur [10].

For the turbulent conditions the k-zeta-f model was chosen. This model, developed Hanjalic et al. [11, 12], according to the authors, improves the numerical stability of the origin model by solving the velocity scale ratio $\overline{v^2}/k$ transport equation instead of velocity scale $\overline{v^2}$. Due to the more convenient formulation of the equation it is more robust and less sensitive to non-uniformities and clustering of the computational grid [13].

3. Results and discussion

3.1. Ammonia distribution

The pictures presented below (Figures 2–4) show the comparison of the time averaged ammonia uniformity index at the SCRoF inlet for set of the injection frequency in each operating condition. The distinct dependency between UWS injection frequency and the course of the uniformity over the time can be seen for idle operating point (Fig. 2). Here, along with the injection frequency increase the value of the uniformity index is respectively smaller in whole range of the simulation time. At the end of the simulation

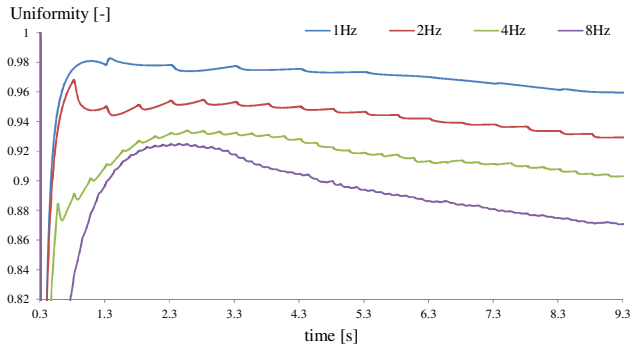

Fig. 2. Uniformity index at SCRoF inlet for idle load

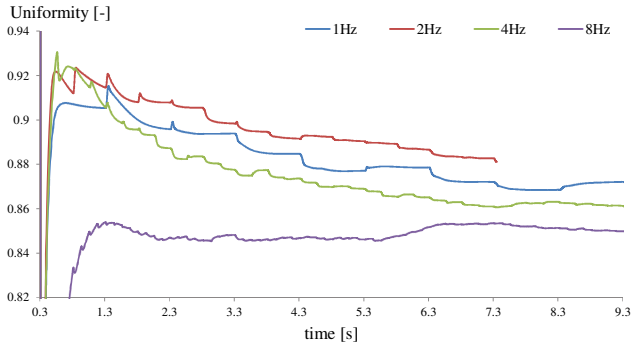

Fig. 3. Uniformity index at SCRoF inlet for light load

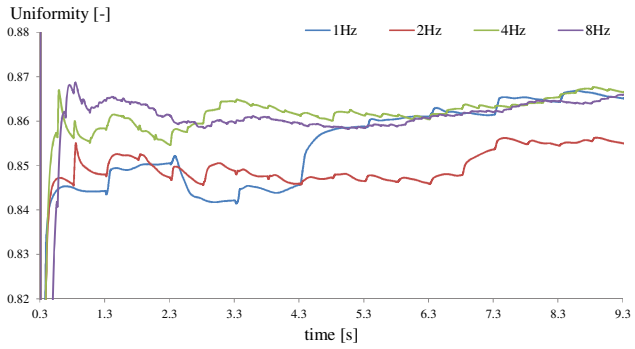

Fig. 4. Uniformity index at SCRoF inlet for medium load

the difference between extreme values is equal approximately 10%. Moreover, the higher rate of rise of the graph after first injection could be noticed for the lower injector frequencies.

The observed dependencies for idle conditions are not so apparent for light and medium loads. Figure 3 shows that the differences in final uniformity result decreasing, in comparison with idle load, and the maximum deviation is circle about 4%. It is also characteristic for this graph that the best performance is given by 2 Hz injector. Despite the fact that calculations for 2 Hz injector were conducted for shorter time, it was assumed that the general trend of the line should be kept up to 9.3 s.

For the middle engine load (Fig. 4), the uniformity index graphs convergence to the approximately same value, with the exception of 2 Hz injector line, which again distinguish at the overall trend. Nevertheless, the difference does not exceed 1%, hence it is legitimatized to claim that the distinction between final results declines with higher combustion products and UWS mass flow through the system.

3.2. Wall film formation

Next analysis refers to the wall film formation. Figures 5–7 depict accumulated total film mass on the transfer cone walls, including mixer device. It could be noticed that with higher injection frequency, the wall film fluctuations have smaller amplitude. For the idle engine load (Fig. 5) the dependencies are clear, the extreme points of one injection pulse of the higher frequency are placed inside the lower frequencies. It is also visible that regardless of case the total amount of wall film at the ends of the injection cycle is close to zero. The situation is slightly different for further engine loads. At the Figure 6 one can observe that 8Hz case does not fit overall trend. The maximum points in each cycle are above maximums of 4 Hz injector. It means that due to short time between subsequent injections capability of the evaporation from the walls was exceed compering to the lower frequencies. The confirmation of this conclusion could be found at the medium load wall film graph (Fig. 7), where even local minimums of the 8Hz curve cross 4 Hz curve at the end of the simulation. It could be also deducted from the graphs behaviour that with longer computational time 2 Hz case extreme points will lie under the 8 Hz case for medium operating point. What is also distinctive, lower frequencies give better wall film performance. As shown at the Fig. 6, 1 Hz case, as the only one, reaches values near zero at the ends of injection pulses.

Nevertheless, in the conducted numerical research, no wall film crystallization model was applied, hence wall film mass could not be treated as only benchmark in those cases. As it is shown at Figures 5–7, despite the fact that with lower frequency less wall film is deposited at walls at the end of the each cycle, the attention also ought to be pay for maximum points. Those peaks could be responsible for local wall cooling and crystallization as the consequence. Therefore, in order to better assessment of the risk, additional Film coefficient (FC), given by equation (4), describing the mass concentration at wall surface, was introduced.

$$FC = \frac{\text{Wallfilm mass}}{\text{Wetted area}}\left[\frac{\text{mg}}{\text{mm}^2}\right] \tag{4}$$

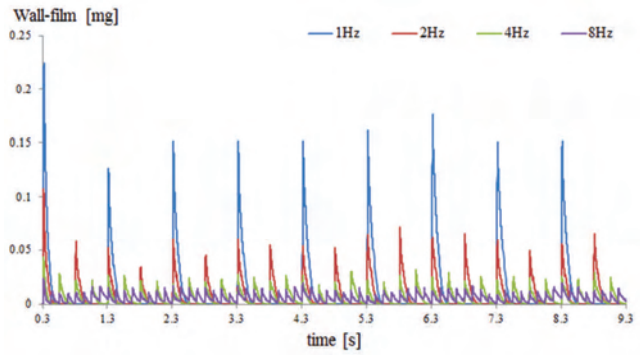

Fig. 5. Total wall film mass for idle load

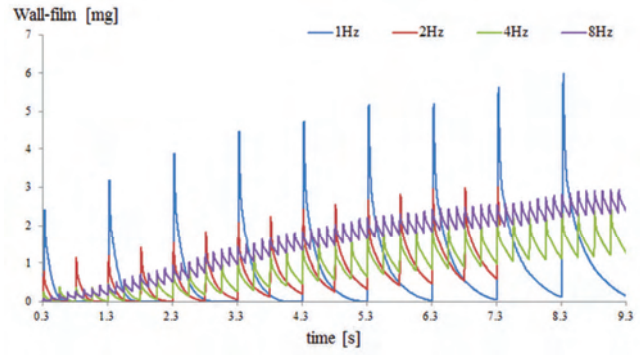

Fig. 6. Total wall film mass for light load

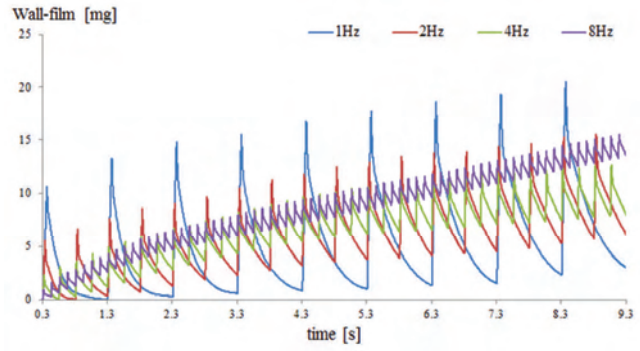

Fig. 7. Total wall film mass for medium load

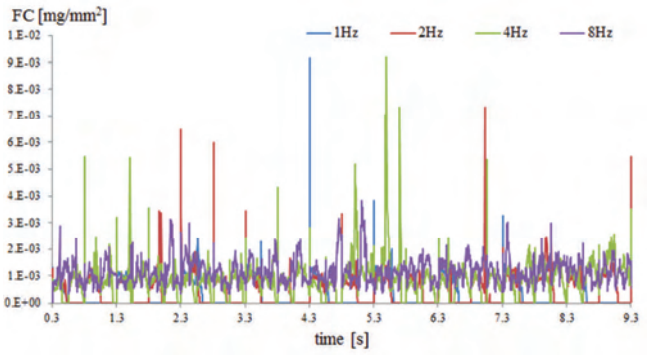

Fig. 8. Film coefficient for idle load

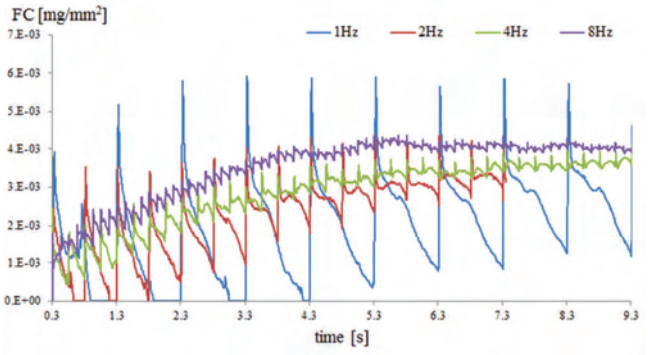

Fig. 9. Film coefficient for light load

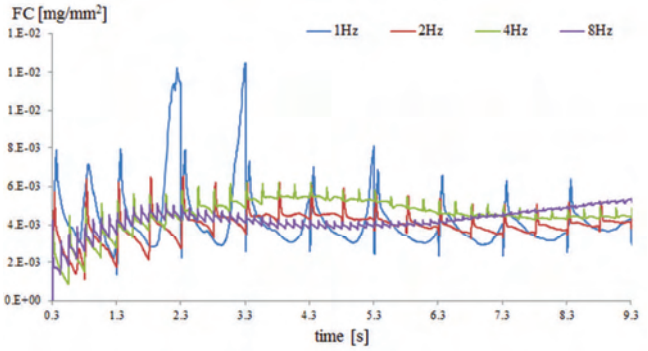

Fig. 10. Film coefficient for medium load

Figures 8–10 presents FC course over the time in each operating condition. For the idle condition (Fig. 8), due to the small UWS flow the graphs behave in stochastic way and it could be say that mean values of the coefficient in calculated cases are approximately equal. Next, the values for the idle conditions are at the similar order magnitude with those from the light and medium operating point (Figs 9–10). The explanation among other could be that for the lower operating point the momentum of the gas is not high enough to influence the spray droplets, hence only the area in the spray direction is affected by the spray. On the other hand, along with mass flow increase more droplets are taken by the stream, thus wall film is distributed on the bigger area. For this series it is also visible that FC amplitude decreases with the time, and purses to the quasi stable value.

The risk of the wall film crystallization could be directly associate with value of the FC, as more heat will be taken from the same unit of the surface. Basing on the graphs, independently from the operating point, due to the highest peaks, the bigger risk comes from the 1 Hz frequency, and then from the 8 Hz.

4. Conclusions

This paper presents the numerical research of the close coupled SCRoF and numerical capabilities of simulating physical phenomena occurring in such systems . The influence of the injection frequency on the SCR system performance was investigated for different diesel engine operating conditions corresponding to idle, light and medium load of diesel engine. The analysis referred to the ammonia distribution at SCR inlet and wall film formation on the SCR system walls including mixing device.

The results showed that, especially for the idle and light engine loads, the best UI index is given by low frequency injections. The differences could be up to 10%, what is quite big amount when considering that engineers and designers put a lot of effort for each one percent of UI value. What is more, wall film analysis indicates that for the idle operating point the risk of the wall film crystallization

ought to be approximately same for each injection frequency. Nevertheless, for rest of the simulated operating points, research showed distinctly that lowest frequency gave the higher crystallization risk.

Acknowledgements

Current work was supported by the European Smart Growth Operational Programme 2014-2020 through the project "Development of mixing and urea-water solution conversion unit in SCR systems in order to start production of exhaust system for compression ignition engine that meets the Euro 7 emission standards", number POIR.04.01.04-00-0060/15-02.

This work has been done under AVL University Partnership Program.

Nomenclature

CFD	computational fuid dynamic
DDM	discrete droplet method
DOC	diesel oxidation catalyst
DPF	diesel particulate filter
FC	film coeficient
SCR	selective catalytic reduction
SCRoF	selective catalytic reduction on filter
UI	uniformity index
UWS	urea water solution

Bibliography

[1] European Union, REGULATION (EC), 2007, 715.
[2] BIRKHOLD, F., MEINGAST, U., WASSERMANN, P., DEUTSCHMANN, O. Modeling and simulation of the injection of urea-water-solution for automotive SCR DeNOx-systems. *Appl. Catal. B Environ.* 2007, **70**(1-4), 119-127.
[3] GUAN, B., ZHAN, R., LIN, H., HUANG, Z. Review of state of the art technologies of selective catalytic reduction of NO_x from diesel engine exhaust. *Appl. Therm. Eng*. 2014, **66**(1-2), 395-414.
[4] BRACK, W. et al. Kinetic modeling of urea decomposition based on systematic thermogravimetric analyses of urea and its most important by-products. *Chem. Eng. Sci.* 2014, **106**, 1-8.
[5] SUNG, Y., CHOI, C., KIM, T. et al. Effect of geometric structure of static mixers on mixing characteristics and pressure drop in marine SCR applications. 2013, **2**, 1-7.
[6] NOCIVELLI, L., MONTENEGRO, G., LIAO, Y. et al. Modeling of aqueous urea solution injection with characterization of spray-wall cooling effect and risk of onset of wall wetting. *Energy Procedia*. 2015, **82**, 38-44.
[7] STRÖM, H., LUNDSTRÖM, A., ANDERSSON, B. Choice of urea-spray models in CFD simulations of urea-SCR systems. *Chem. Eng. J*. 2009, **150**(1), 69-82.
[8] AVL Fire ® version 2014.2. Porous Module. 2014.
[9] AVL Fire ® version 2014.2. Spray Module. 2014.
[10] AVL Fire ® version 2014.2. Wallfilm Module. 2014.
[11] HANJALIĆ, K., POPOVAC, M., HADŽIABDIĆ, M. A robust near-wall elliptic-relaxation eddy-viscosity turbulence model for CFD. *Int. J. Heat Fluid Flow*. 2004, **25**(6), 1047-1051.
[12] POPOVAC, M., HANJALIC, K. Compound wall treatment for RANS computation of complex turbulent flows and heat transfer. *Flow, Turbul. Combust*. 2007, **78**(2), 177-202.
[13] KAPUSTA, Ł.J., TEODORCZYK, A. Numerical simulations of a simultaneous direct injection of a liquid and gaseous fuel into constant volume chamber. *J. Power Technol.* 2012, **92**(1), 12-19.

Rafał Rogóż, MEng. – Division of Aircraft Engines at Warsaw University of Technology.

e-mail: *Rafal.Rogoz@itc.pw.edu.pl*

Łukasz Jan Kapusta, DEng. – Faculty of Power and Aeronautical Engineering at Warsaw University of Technology.

e-mail: *Lukasz.Kapusta@itc.pw.edu.pl*

Piotr Jaworski, MEng. – Division of Aircraft Engines at Warsaw University of Technology.

e-mail: *Piotr.Jaworski@itc.pw.edu.pl*

Prof. Andrzej Teodorczyk, DSc., DEng. – Faculty of Power and Aeronautical Engineering at Warsaw University of Technology.

e-mail: *Andrzej.Teodorczyk@itc.pw.edu.pl*

Article citation info:
HENNEK, K., GRABA, M., MAMALA, J. The influence of the throttle position regulation characteristics of a SI engine on the fuel consumption in driving cycles. *Combustion Engines*. 2017, **170**(3), 78-83. DOI: 10.19206/CE-2017-312

Krystian HENNEK
Mariusz GRABA
Jarosław MAMALA

CE-2017-312

The influence of the throttle inclination characteristics of a SI engine on fuel consumption in driving cycles

This dissertation shows the analysis of the selected indicators of the work of a passenger vehicle drivetrain designated with the use of the Road Load Engine Simulator. In a digital simulation, an internal – combustion engine is saved in a form of numerical speed characteristics in the computers memory. Basing on a virtual vehicle, some indicators of the drivetrain of a passenger vehicle have been determined, while driving with five electronic throttle inclination regulator settups. The simulation results of e.g., throttle repeal speeds and fuel consumtion are summarized in a tabular and graphic form and some of them are expressed per 100 kilometer of the distance covered. Both synthetic and real driving cycles were analyzed during the study and their influence on the egines fuel consumption was also shortly described.

Key words: *fuel consumption, driving cycle, NEDC, throttle inclination regulator, simulation*

1. Introduction

The increase in human mobility and the ways of using internal combustion engines contribute to the progress of environmental pollution. The high technical standard of modern vehicles is partly forced by the aspect of the cleanliness of our environment. Together with the mass automobile production it caused the access to vehicles with combustion engines to be easy for a great part of the population (Fig. 1). The increase in global fuel consumption, noticed in the last twenty years, results with an increase of toxic exhaust gases emissions, which have a destructive influence on our environment.

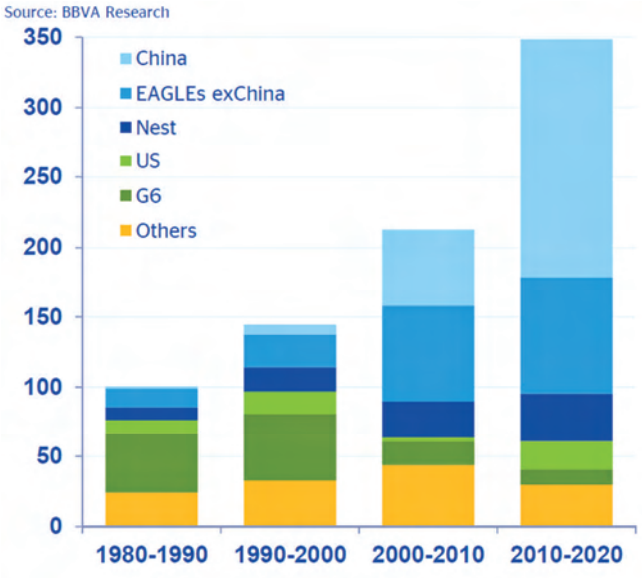

Fig. 1. Global amount of vehicles (in million pieces) [1]

One way to reduce the emissions is to minimize the fuel consumption. There are several methods to achieve it according to the combustion engine, i.a.:

1. through controlling the drivetrain working properties in a way, which makes it possible for the engine to work in its maximum effectivity field,
2. through reducing the fuel volume dosed to the engines combustion chambers; it may cause a reduction of the vehicles traction properties and increase in emissions.

Within this research, a series of virtual rides with a passenger vehicle in driving cycles were performed. To achieve the simulation the Road Load Engine Simulator was used. The Simulator is one of the research stands of the Chair of Road and Agricultural Vehicles in the Opole University of Technology. Binary readings of the engine characteristics and velocity profiles of the driving cycles are downloaded to the Simulator to enable the test to run without the actual vehicle model or its drivetrain.

The rides were performed in five variants of engine throttle inclination regulator settings, in real and synthetic driving cycles. The chosen velocity profiles were measured in real suburban driving conditions near the Opole city. During those on-the-road measurements the driver was controlling the vehicles load with an intention of achieving maximum driving dynamics (cycle 1) and the lowest possible fuel consumption (cycle 2). For comparison purposes a synthetic cycle NEDC (New European Driving Cycle) was used. Figure 2 depicts the examples of driving cycles velocity profiles, which were used in the simulation.

2. The influence of the regulator settings on the throttle repeal speed

The vehicles momentary velocity depends on one hand on the will of the driver, and on the other hand on the conditions deriving from the environment (i. a.: the road topography, atmospheric conditions, and other driver maneuvers). The driver using the acceleration pedal choses the proper engine torque amount, which is delivered to the wheels in accelerating, engine braking or constant velocity driving processes.

Modern drivetrains based on a combustion engine are often equipped with the ETC (Electronic Throttle Control) system. In ETC the acceleration pedal is connected with the throttle by electrical wires. The input signal derived from the pedal is converted by the engine control unit according to an algorithm and sent to the throttle electronical actuator. While the system is working, the throttle plate and accelera-

tion pedal inclinations are checked frequently. It allows an almost immediate diagnosis of any eventual malfunction of the system parts.

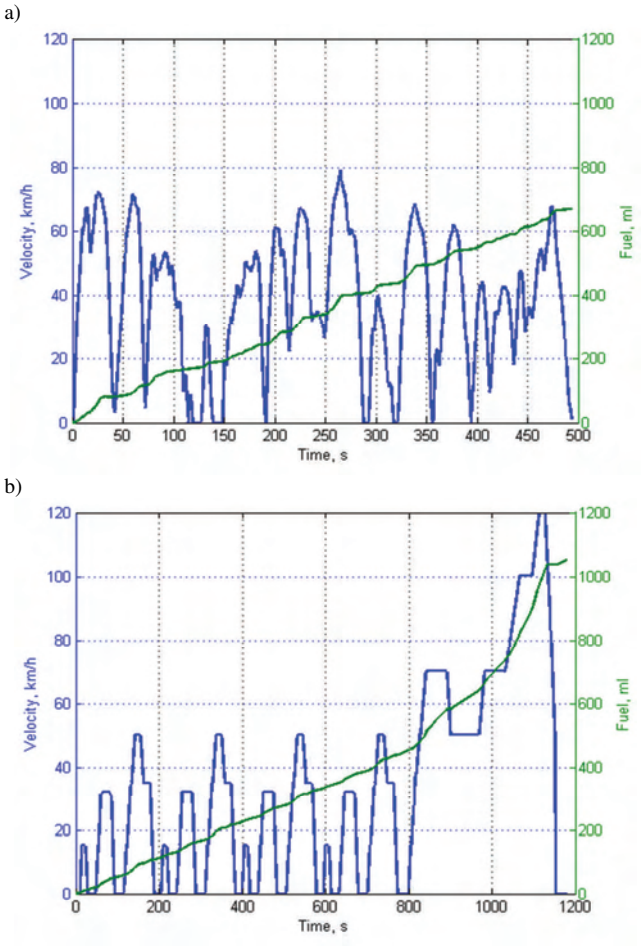

Fig. 2. Exemplary driving cycles, which were used in the simulations: a) driving cycles measured in real suburban driving conditions, b) NEDC

The Simulators software allows changing the settings of the throttle inclination regulator. Modifications of the settings influence the rapidity of the throttle reaction on the inducing acceleration pedal signal. Figure 3 depicts the noted momentary repeal speeds of the throttle plate. The results derived from the rides in V1, V2, V4, V5 regulator settings variants were compiled with the base V3 setting result. According to figure 3 the throttle repeal speed increases subsequently in the order of the variants numbers (starting with V1, ending with V5). The dense clouds of points, characterizing the mostly noticed repeal speeds, occupy even wider surfaces, which demonstrate that the inclinations of the throttle plate were changing more and more dynamic.

The influence of the velocity profile on the throttle working parameters is also noticeable. Simulation of a dynamic suburban cycle was marked with higher throttle plate repeal dynamics, than the economic cycle simulation. This fact confirms the achievement of aims in the real driving measurements. In this case the higher throttle repeal speed is an evidence of higher repeal speed of the acceleration pedal and more sudden use of the vehicles acceleration potential.

The clouds shape should also be considered. In the real driving cycles the highest point dense can be noticed in the center of the plot and becomes the shape of a straight line (V1). In the next plots it becomes more and more the shape of a rhombus (V5). In the synthetic cycle the shape of the V1 cloud reminds a straight line and in the next plots becomes more and more a rectangle in the V5 variant. The highest point concentration occurs in the summits and in the middle of the sidewalls of the rectangle. Such velocity distribution of the throttle plate indicates the cyclicality of the movement phases, which is typical for the synthetic NEDC driving cycle. In contrast to the real driving cycles, in the NEDC the processes of acceleration and velocity decreasing are led with the same intensity in all cycle modules and the constant driving velocities are held at the same level (in the city traffic part of the cycle).

3. The influence of regulator settings on the positioning of the mostly used area of the engine characteristic

According to the changing conditions of the vehicles engine, its useful efficiency is changing in a high range of values. It is determined not only by the properties of the engine, but also by its working parameters, which are forced by the movement of the power receiver, as is the vehicle.

The changes of the throttle plate inclination have an effect in the intake manifold air pressure. As a result, there occur changes of the volume of air and fuel mixture provided to the cylinder, influencing the torque value, which the engine generates in given conditions. It follows that the settings of the throttle inclination regulator affect the momentary power supply while driving with often changes in the inclination of the power supply control component, thus in the so-called undefined states.

Diversification of possible undefined states inducements is an important issue in the development of a universal method for building the engine characteristics as appropriate to the specific transition phases of a vehicle. Unstable conditions of the engine operation occur mainly in the powering phase, while changing the travel velocity.

Figure 4 depicts the isoclines of the velocity characteristic of torque, used by the virtual engine. Additionally the in-cycle mostly noticed points of the characteristic were marked. The changes in throttle inclination regulator settings didn't cause radical differences in the points positions on the graphs plotted for the same driving cycle. The percentage magnitudes, which describe the use summits were changing, what is shown in the a) part of the Fig.e 5.

The velocity profile course of the driving cycle determines the engine load during the test. As shown in Fig. 4, during the simulation of dynamic driving, the engine worked mostly in conditions of high or low load and low and medium engine speeds. In the simulation of economical driving, the engine load is lower at similar engine rotation speeds. In NEDC simulations, the engine load is focused around about 30 Nm and the rotation speeds are between 2000 and 2500 rotations per minute.

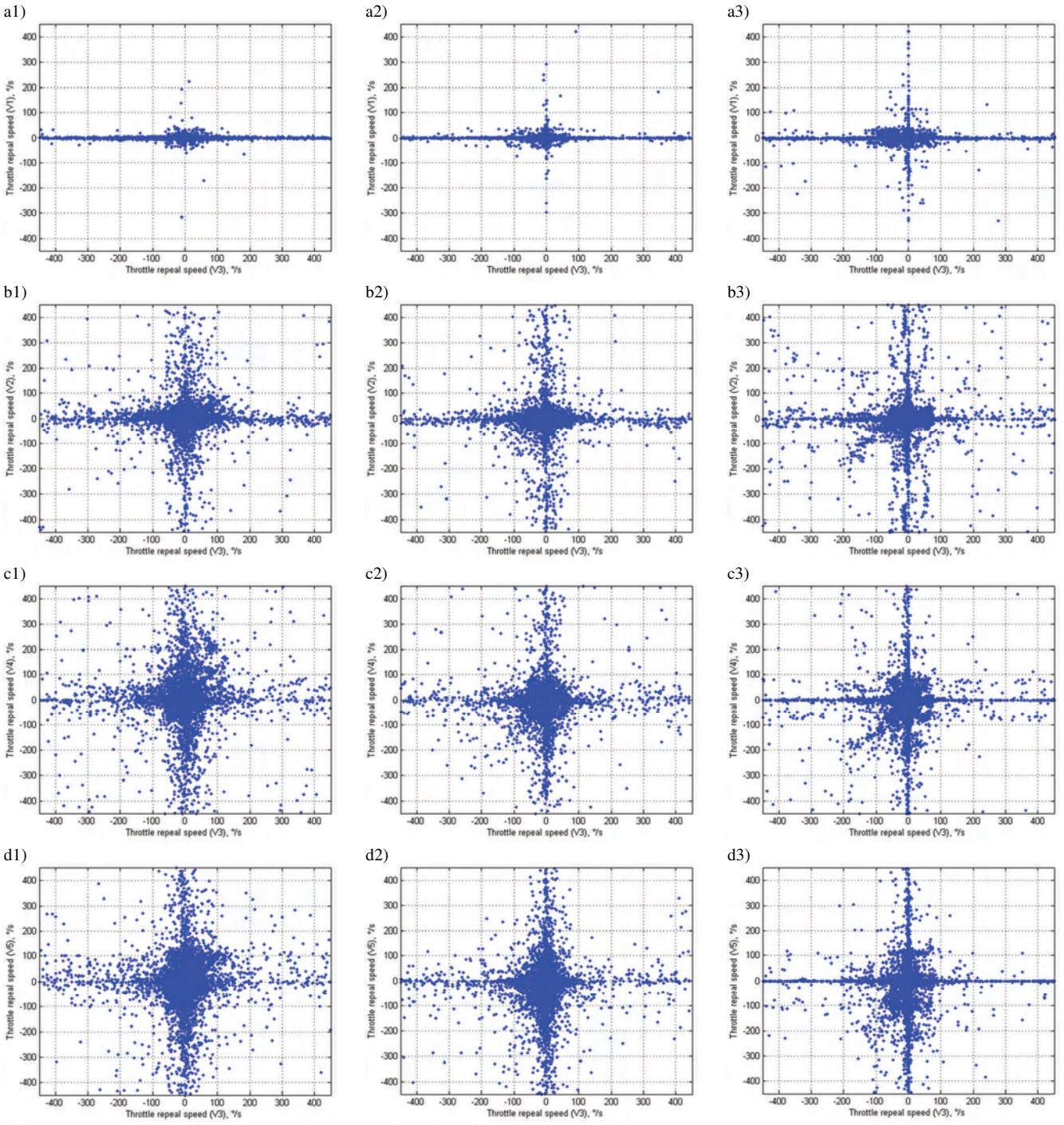

Fig. 3. Comparison of angular velocity of throttle movement for the individual variants of controller settings with the base variant (V3): a) – V1, b) – V2, c) – V4, d) – V5; 1 – cycle 1, 2 – cycle 2, 3 – NEDC cycle

It can be derived from Figure 4, that the most commonly used range of engine rotation speeds starts with the idling velocity and ends within 2500 rpm. According to the most commonly used low load (5.5–16.5 Nm) it should be noted, that this area of engine's load characteristic is highly unfavorable, because of its low overall efficiency.

The results of such tests, along with the use of the velocity characteristics of the useful efficiency, may allow the selection of such throttle plate working parameters which will allow the engine to work as close the point of its maximum efficiency as possible. A considerable part of the mileage fuel consumption and exhaust gasses emissions is generated during the acceleration processes. At the same time the torque development depends on the throttle inclination changes. It may be wise to select the optimal throttle inclination regulator settings algorithm for all these parameters.

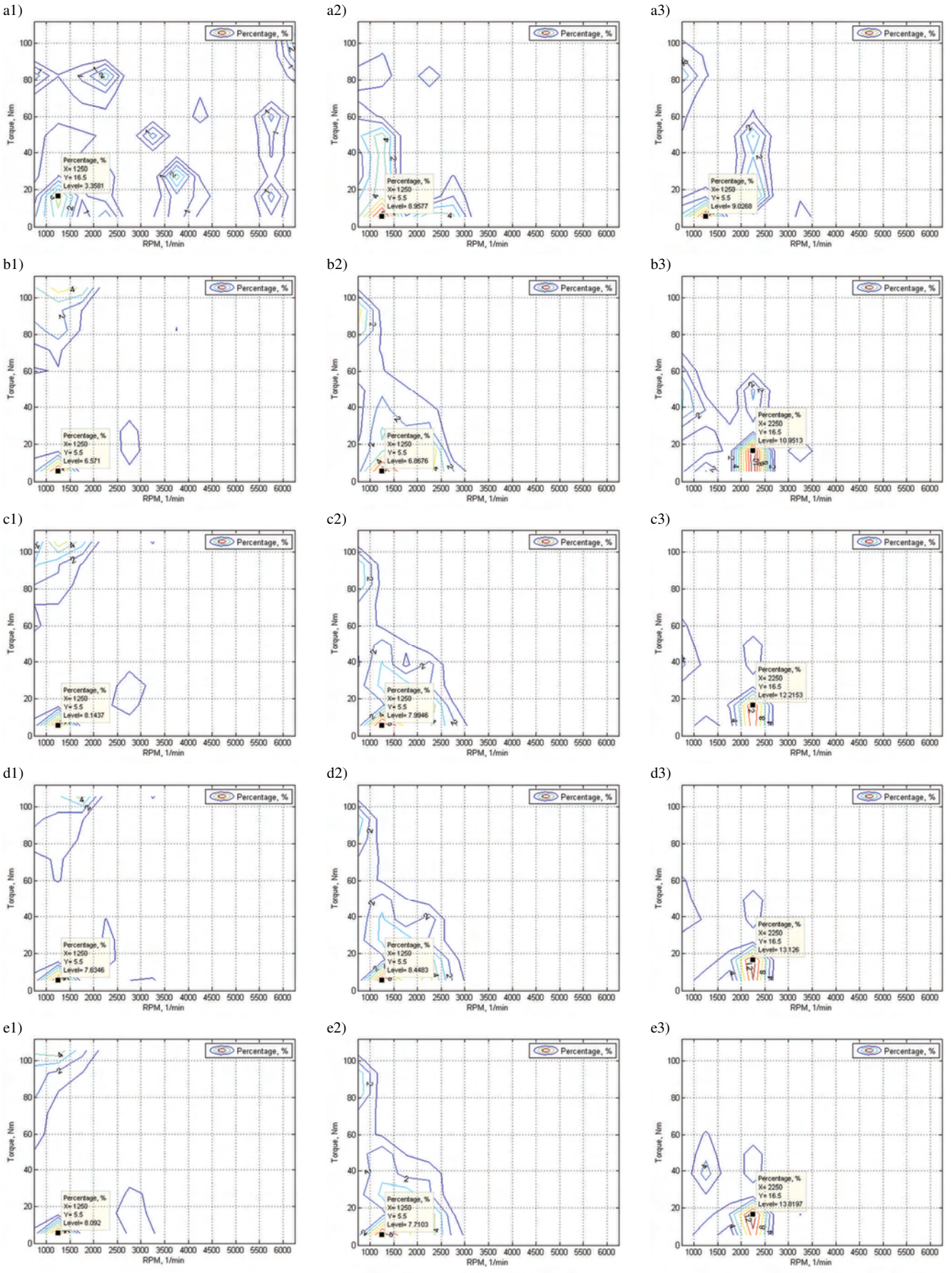

Fig. 4. Most commonly used points of the speed characteristic of engine torque: a) – V1, b) – V2, c) – V3, d) – V4, e) – V5; 1 – cycle 1, 2 – cycle 2, 3 – NEDC

4. Effect of regulator setup on fuel consumption in driving cycles

The basic energetic trait of a vehicle engine is its fuel consumption. It is dependent on engine and drivetrain efficiency and motion energy consumption, which describes the amount of energy at the drive wheels needed to traverse given length of the road. Factors which most significantly affect fuel consumption are the frequency and intensity of acceleration phases, which decide the mean value of acceleration, and the engine idling time. There are potential possibilities to reduce fuel consumption in city driving by minimizing the energy dissipated during braking and shortening the engine idling time.

Partial characteristic of engine power, torque and specific fuel consumption in the function of engine speed are applicable for the analysis of vehicle motion characteristics and its energy consumption. They are prepared for selected power supply mechanism positions (mostly given as percentage values). Such curve courses usually show some characteristic traits. Maximum spark ignition engine power is usually situated at lower than top engine speed. Maximum torque engine speed is always lower than maximum engine power speed. On the other hand, minimum specific fuel consumption is situated at the engine speed higher than maximum torque speed and lower than maximum power speed.

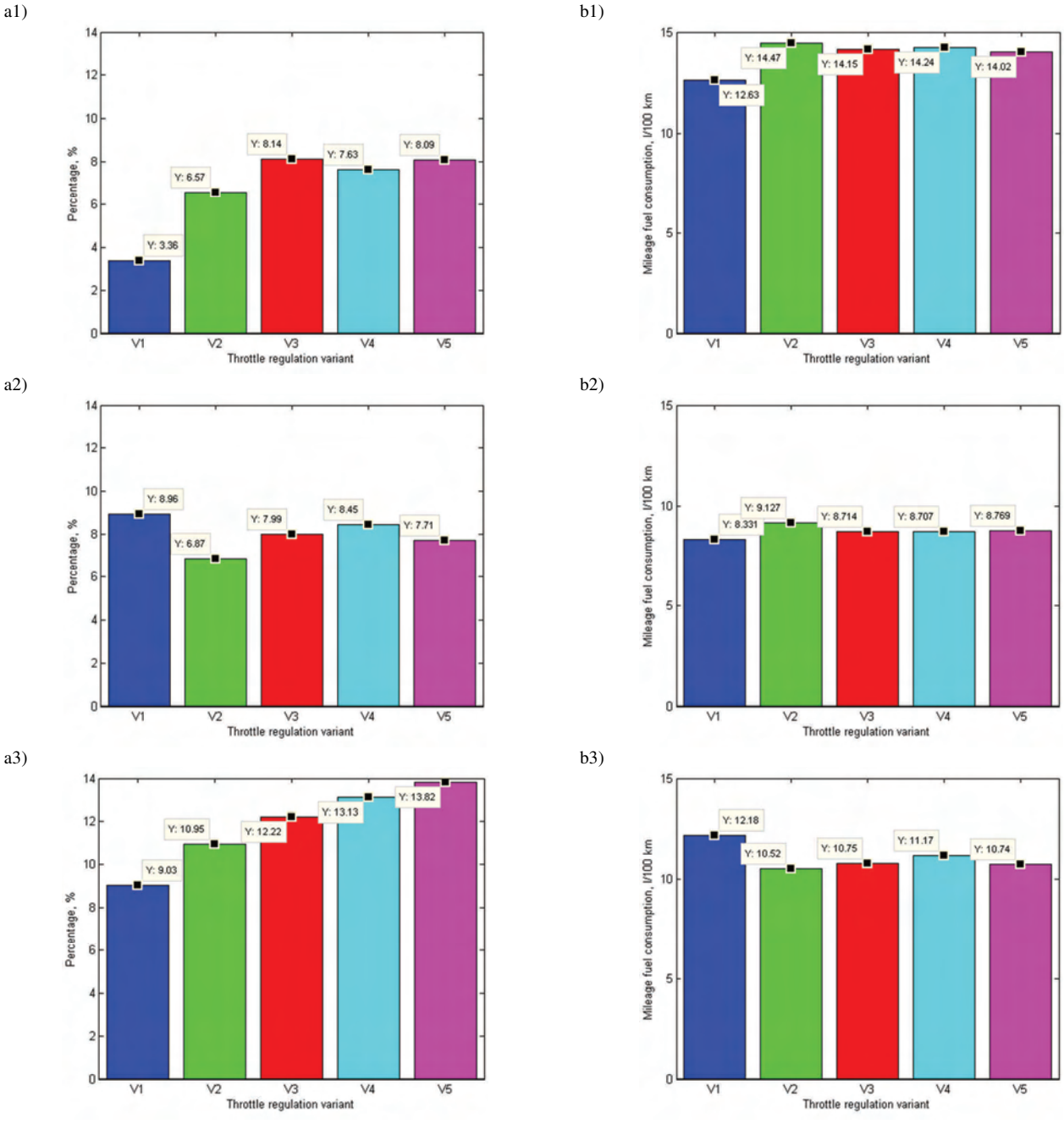

Fig. 5. Summaries of: a) – percentage values of mostly used points of the engine torque characteristic, b) – mileage fuel consumption; 1 – cycle 1, 2 – cycle 2, 3 – NEDC

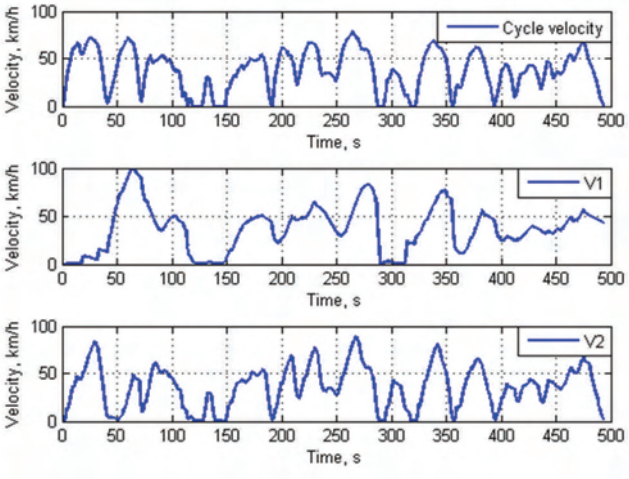

Fig. 6. Velocity courses versus time curves: on the top – the velocity profile of the Opole city dynamic cycle, in the middle – the velocity profile carried out for the V1 setup, at the bottom - the velocity profile carried out for the V2 setup

Comparisons of mileage fuel consumption in Fig, 5 b) show values of virtual fuel consumption obtained in drive cycles in relation to a length of 100 kilometers. The lowest fuel consumption in real drive cycles was achieved for V1 throttle regulation setting, while in synthetic cycles the V1 setting showed the highest fuel consumption. In the same synthetic cycle, the lowest value of fuel consumption was measured for V2 variant, which yielded the highest fuel consumption for real drive cycles. The remaining versions of regulator settings generated comparable results for both cycle types. It is worth noting that for V1 variant the throttle was repealed at very low speeds, which significantly impaired acceleration capabilities. The reason for this is a poor adherence of realized velocity profile in comparison to the assumed one, as is shown in Fig. 6. The V2 variant showed a much better adherence of velocity profiles. The effect of driving cycle velocity profile on mileage fuel consumption is also noticeable. Dynamic driving was characterized by 50% larger fuel consumption than economical driving.

5. Summary

By analyzing the obtained research results it can be seen, how significant is the effect of throttle inclination management method on vehicle dynamics, fuel consumption and driving safety. Slow regulation of throttle plate inclination helps to reduce fuel consumption; however it impairs dynamic properties of the drivetrain. On the other hand, quick regulation of throttle plate inclination causes a significant clipping of the induced repeal angle – in response to this, the ECU starts increasing the fuel dosage, which in turn causes the mileage fuel consumption to increase significantly. However, as can be noted from the conducted research, it is difficult to clearly point out which of the proposed throttle inclination regulator settings would allow to minimize fuel consumption while maintaining adequate vehicle drive dynamics. The analysis of simulated drive cycles allows to assume that conventional regulators only partially fulfill the requirements of minimizing fuel consumption while retaining adequate vehicle drive dynamics. Therefore, while using this class of throttle regulators it is required to achieve a certain compromise between low fuel consumption and good drivetrain dynamics. Velocity profile and road conditions have a substantial effect on fuel consumption; however driver behavior is the most important factor affecting it. The driver-dependent style of application of throttle inclination change is the factor that has the biggest effect on fuel consumption. In this case, an adaptive regulator has to be used in the throttle plate management system to correct its settings depending on driver behavior. This solution would allow to keep fuel consumption as low as possible, while retaining satisfying vehicle drive dynamics. Only this control strategy would allow to control throttle inclination for all road conditions and driver behaviors in a way that would minimize fuel consumption and retain drive dynamics that could be deemed satisfying for each driver. The use of adaptive regulators in throttle inclination control systems will be the further scope of the authors' research.

Bibliography

[1] BBVA Research: The Future of World Car Fleet: The Road Ahead, 2012.

[2] SIŁKA, W. Teoria ruchu samochodu. Skrypt 192. *Dział Wydawnictw Politechniki Opolskiej*, Opole 1996.

[3] MAMALA, J. Kompensacja niedostatku siły napędowej w procesie rozpędzania samochodu osobowego. Zeszyt 290, *Oficyna Wydawnicza Politechniki Opolskiej*. Opole 2011.

[4] MAMALA, J., BROL, S., GRABA, M. Engine control unit testing by hardware-in-the-loop simulation, *Solid State Phenomena*. 2014, **214**, 67-74.

[5] BIENIEK, A., GRABA, M., LECHOWICZ, A. Sterowanie układem wtryskowym silnika ciągnika rolniczego w aspekcie poprawy jego własności ekologicznych. *Combustion Engines*. 2011, **146**(3), 1-8.

Krystian Hennek, MEng. – Faculty of Mechanical Engineering at Opole University of Technology.

e-mail: *K.Hennek@po.opole.pl*

Mariusz Graba, DEng. – Faculty of Mechanical Engineering at Opole University of Technology.

e-mail: *M.Graba@po.opole.pl*

Jarosław Mamala, DSc., DEng. – Faculty of Mechanical Engineering at Opole University of Technology.

e-mail: *J.Mamala@po.opole.pl*

Article citation info:
MAGRYTA, P., PIETRYKOWSKI, K., BIAŁY, M., SZLACHETKA, M. The influence of load distribution in kinematic constraints of connecting rod on the results of the stress simulation. *Combustion Engines*. 2017, **170**(3), 84-87. DOI: 10.19206/CE-2017-313

Paweł MAGRYTA
Konrad PIETRYKOWSKI
Michał BIAŁY
Marcin SZLACHETKA

CE-2017-313

The influence of load distribution in kinematic constraints of connecting rod on the results of the stress simulation

The article presents the results of simulations research carried out, using Finite Element Method. The simulations were made in the Abaqus software. Calculations were made on the connecting rod of opposed piston engine. The connecting rod was subjected to a compression tests. Different versions of the boundary conditions in the form of load forces and pressure distribution acting on the small end of the connecting rod were presented. Depending on the load distribution acting on the connecting rod small end, different distributions of stresses in the connecting rod geometry were obtained. All studies were performed for the same geometry, the same mesh grid, and for the same value of compressive force (research could be considered as comparable). Changing the size and distribution of stresses in the connecting rod, evidence the impact of the adopted boundary conditions of the load distribution on the calculation results. It is important for the use of modern simulation tools in the design process of new mechanical parts.

Key words: *connecting rod, simulation, FEM, Abaqus, Catia v5*

1. Introduction

Within the research project realized with WSK "PZL-KALISZ" S.A., the design of the aircraft engine with opposing pistons is being developed. This engine will be used in ultralight aircraft. This type of engine has many advantages:

- lower fuel consumption than other piston engines (better efficiency),
- reduced heat losses because of the small area of the combustion chamber (no engine head),
- leaner combustion (Diesel operation),
- faster and earlier combustion at the same pressure rise rate (large flame front surface),
- lower pollutant emission compared to turbine engines,
- lower costs (small number of parts and simple design).

At present, due to environmental requirements and dealing with climate change, it is beneficial to develop aircraft piston engines and adopt the achievements of automotive engineering such as computer controlled common rail high pressure injection systems and variable pressure turbochargers.

For this reason, modern simulation tools have been used to analyze the various design solutions used in such an engine. One good example are FEM analysis, which allows to estimate stress values in main engine components. This article focuses on the connecting rod stress calculations. It should be emphasized, that in order to obtain the simulated results as close as possible to reality, the conditions defined during the simulations have to be identical to the real ones. Sometimes it is impossible or difficult to estimate these conditions. In such a case, committing a non-major error in the initial calculation phase may result in erroneous results of the simulation calculations. Therefore, the authors of the article decided to examine the effect of boundary conditions of the connecting rod compression simulations on the obtained results of the simulation.

2. Research simulations – introduction

Strength tests of the connecting rod were made using Finite Element Method in the Abaqus software. This is a software commonly used for this type of analysis. The geometry of the connecting rod was taken from opposite piston engine. This model was designed by geometry changing, resulting from the previously performed optimization calculations. This article presents the target model, which was the 8th analyzed model. The article identifies the same boundary conditions as in model previously described in [5].

From the studies conducted in [5], it was found that the results of the simulation tests of the tested model were strongly dependent to the load conditions that were applied to the connecting rod model. Despite the same conditions of restraint and the same values of forces acting on the model, the size and the distribution of stresses were influenced by the method of load distribution [6]. In addition, all the models used the same material data. It should be noted, that the connecting rods that are discussed where analyzed only for the compression, while the same differences have been observed for the connecting rod stretching simulations [6]. As a result of noticeable changes in stress distribution, it was decided to expand this discussion and perform several simulations with different load distributions for the connecting rod [1, 2, 4].

3. Load boundary conditions

This section presents the variable boundary conditions for several analyzed models.

3.1. Load 1 version

In the first version, the boundary conditions were determined by giving a fixation at one point in the center of the connecting rod, where all degrees of freedom were fixed. The load was realized by connecting the first reference point to the lower surface of the rod bushing and connecting the second reference point to the top surface of the upper rod bearing insert. The compression forces acting in the vertical direction were applied to the reference points. This way of defining the load has resulted in the distribution shown in Figure 1.

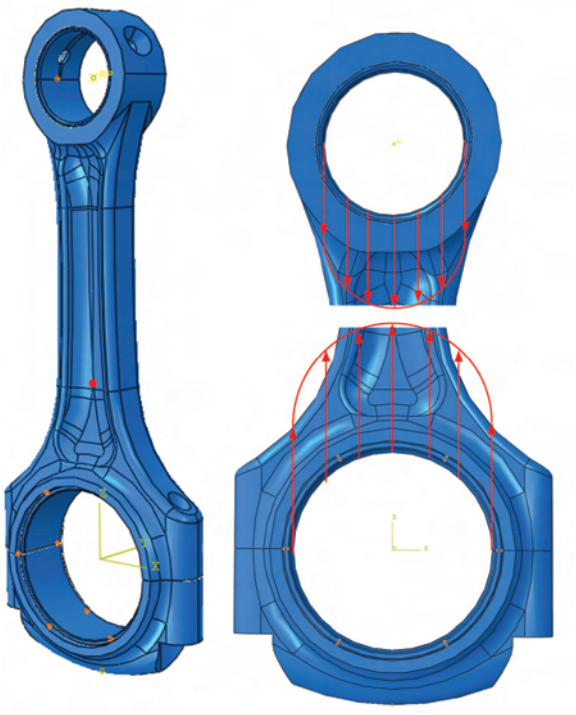

Fig. 1. Fix and load 1 version

3.2. Load 2 version

In the second version, the boundary conditions were determined by assigning a fixation at one point of the center of the connecting rod, where all degrees of freedom were fixed. The load was realized by defining the pressures identical to the forces values from version 1. Those pressures were applied perpendicularly to the bottom surface of the rod bushing and the top surface of the upper rod bearing insert. This way of defining the load has resulted in the distribution shown in Figure 2.

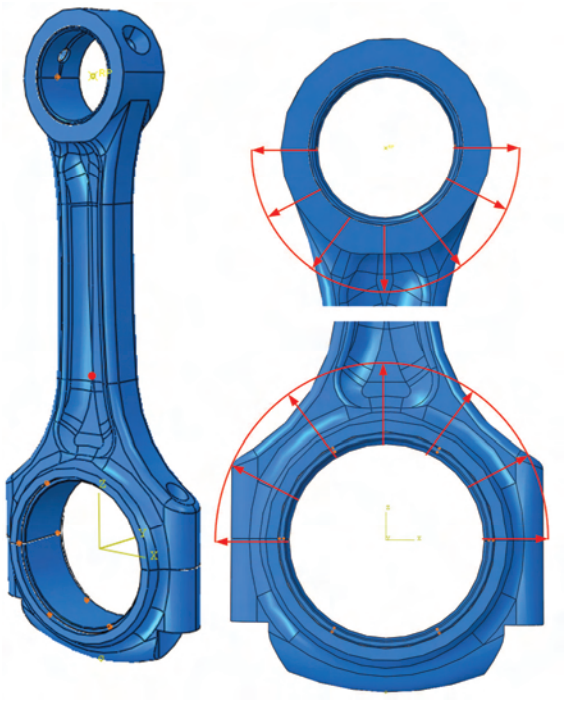

Fig. 2. Fix and load 2 version

3.3. Load 3 version

In the third version, the boundary conditions were determined by assigning only one center point of the connecting rod, where all degrees of freedom were fixed. However, the load was realized by defining pressure on two surfaces. On the bottom surface of the rod bushing and on the top surface of the upper rod bearing insert. The load values were identical to the force from version 1 and 2. The pressure was defined by the distribution of pressure from the sinusoidal function depending on the length of the arc. This way of the load defining has resulted in the distribution shown in Figure 3.

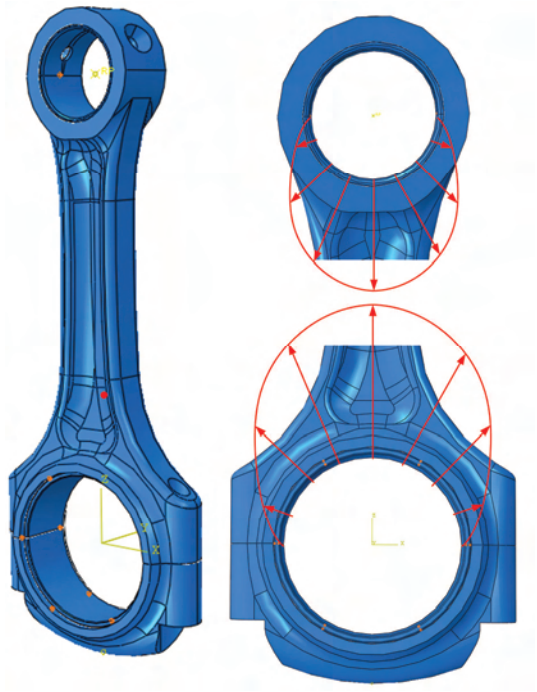

Fig. 3. Fix and load 3 version

In this version of the calculations, it was decided to determine the pressure distribution on the rod bushing (connecting small end) and the upper rod bearing insert (connecting rod big end) depending on the coordinate x. The pressure distribution was based on the force acting on these surfaces. It was decided to use the function determining the most real pressure distribution in case of sliding contact.

$$p = \frac{F}{a \cdot b} \cos\left(\operatorname{asin}\left(\frac{x}{y}\right)\right)$$

where: p – pressure, F – force, a, b – width and length of the surface projection of the surface of the rod bushing/upper rod bearing insert on the transverse plane to the main axis of the connecting rod, x – distance value perpendicular to the main axis of the connecting rod, r – inner rod bushing/upper rod bearing insert radius.

The graph of the above function is presented in Figure 4. The horizontal axis shows the dimension in [mm] corresponding to the length of the surface projection of the surface of the rod bushing on the transverse plane to the main axis of the connecting rod, while the vertical axis represents the dimensionless pressure value for which 1 corresponds

to the maximum pressure value. The function was chosen in such a way, that the sum of the vertices values of the pressure (acting along the connecting rod main axis) was identical to the same values in versions 1 and 2.

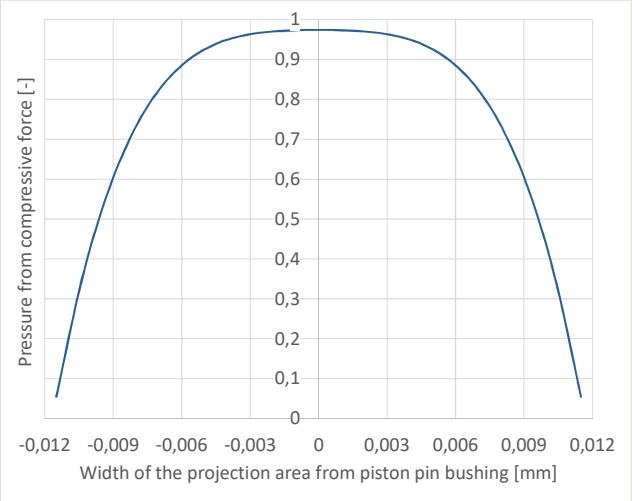

Fig. 4. Function graph describing the pressure distribution on the surface of the rod bushing

4. Simulation research

This part of the paper presents the results of the simulation tests for all three versions of the connecting rod loads.

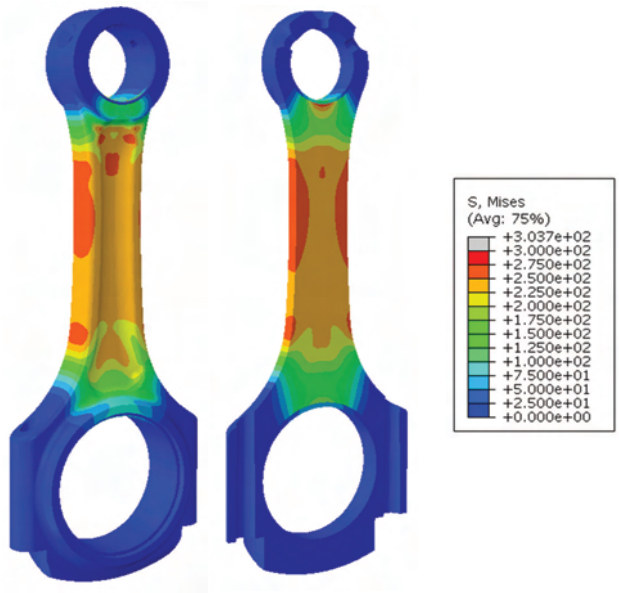

Fig. 5. Results of simulation tests, connecting rod compression 1 version

In the case of version 1, the maximum stresses values are the smallest. Also their range on the rod small end and big end are the smallest (blue color). The highest stresses values are in version 2 (3 times bigger). This is due to the fact that in case 1, there is only vertical component of the compression force. In other cases also horizontal components of forces occurs, of which in the second version they are the largest. This causes additional bending of the connecting rod small end to the outside. The loads in case 3 are most similar to the real distribution because the force applied decreases to 0 for a distance equal to the radius of the rod bushing, measured from the main axis of the connecting rod. In this case, the maximum stresses are slightly higher than in version 1. The location of the areas with the highest stress values are different. In case 1, they occur near the rod small end and big end, which results from the tensile force acting sideways.

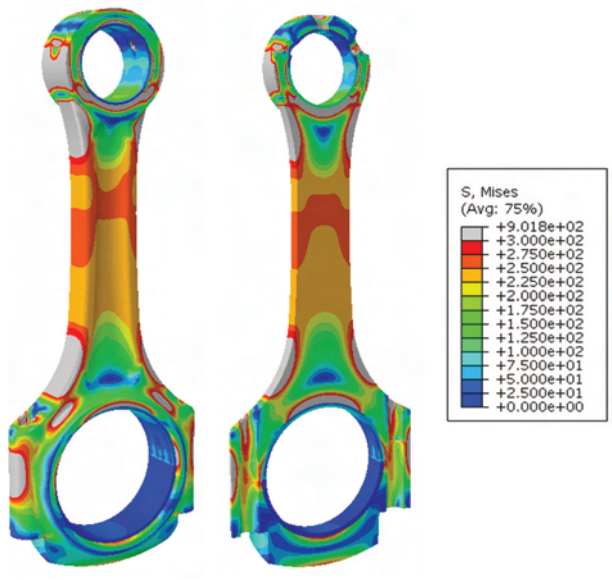

Fig. 6. Results of simulation tests, connecting rod compression 2 version

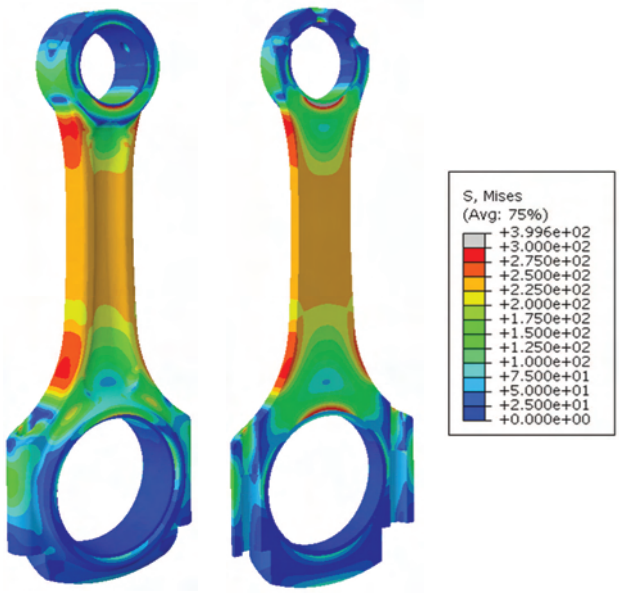

Fig. 7. Results of simulation tests, connecting rod compression 3 version

5. Summary

FEM modeling allows to get quick results without having to carry out costly and laborious occupational testing. However, depending on the degree of simplification of the boundary conditions, the results may vary in small or to a large extent from reality. In the case of connecting rod stress calculations, it is therefore essential to correctly define the distribution of applied forces or pressures. The calculation results show that the maximum stresses can be 3 times greater than the real ones, which can lead to overdimensioning of the element.

The closest to the real distribution of forces is presented in the version 3. However, the determination of such case is a little difficult, because it is necessary to apply pressure rather than direct force to the model. In the case of version 1, the results do not differ significantly from case 3. It is therefore not a great mistake to assume such a force distribution, which is a common practice. However, it is not possible to assume boundary condition presented in case 2, as they are not identical with the actual load distribution and result in a false values.

Acknowledgement

This work has been realized in the cooperation with The Construction Office of WSK "PZL-KALISZ" S.A." and is part of Grant Agreement No. POIR.01.02.00-00-0002/15 financed by the Polish National Centre for Research and Development.

Nomenclature

FEM finite element method

Bibliography

[1] ABBEY, T. Understanding Load Paths, www.digitaleng.news/de/understanding-load-paths/

[2] DASSAULT SYSTEMES, ELFINI Structural, Analysis *CATIA V5 Training Exercises* Version 5 Release 19, 2009.

[3] ZHUA, J.-C., ZHUA, H.-H., FANA, S.-D. et al. A study on the influence of oil film lubrication to the strength of engine connecting rod components, *Engineering Failure Analysis*. 2016, **63**, 94-105.

[4] KURDI, O., MAT NORMAN, M.A.B., YULIANTI, I., MD RASHID, M.N.B. Simulation of fatigue life prediction and enhancement of connecting rod of car engine. *Advanced Materials Research*. 2012, **557-559**, 2410-2414.

[5] MAGRYTA, P., PIETRYKOWSKI, K., MAJCZAK, A. Optimizing the geometry of the connecting rod in opposite pistons engine. *Combustion Engines*. 2017, **168**(1), 191-196.

[6] TIWARI, A., TIWARI, J.K., CHANDRAKAR, S.K. Fatigue, analysis of connecting rod using finite element analysis to explore weight and cost reduction opportunities for a production of forged steel connecting rod. *International Journal of Advanced Mechanical Engineering*. 2014, **4**(7), 782-802.

Paweł Magryta, MEng. – Faculty of Mechanical Engineering at the Lublin University of Technology.

e-mail: *P.Magryta@pollub.pl*

Konrad Pietrykowski, DEng. – Faculty of Mechanical Engineering at the Lublin University of Technology.

e-mail: *K.Pietrykowski@pollub.pl*

Michał Biały, MEng. – Faculty of Mechanical Engineering at the Lublin University of Technology.

e-mail: *M.Bialy@pollub.pl*

Marcin Szlachetka, DEng. – Faculty of Mechanical Engineering at the Lublin University of Technology.

e-mail: *M.Szlachetka@pollub.pl*

Article citation info:
BIENIEK, A., MAMALA, J., GRABA, M., HENNEK, K. Impact of EGR control at in-cylinder pressure and ecological properties of CI off-road vehicle engine. *Combustion Engines*. 2017, **170**(3), 88-95. DOI: 10.19206/CE-2017-314

Andrzej BIENIEK
Jarosław MAMALA
Mariusz GRABA
Krystian HENNEK

CE-2017-314

Impact of EGR control at in-cylinder pressure and ecological properties of CI off-road vehicle engine

An attempt has been made to clarify the effect of wide-ranging control of the exhaust gas recirculation system on the cylinder pressure and ecological engine performance. This publication contains the results of tests performed on the CI (compression ignition) engine of the off-road vehicle mounted on the test bench. The study was based on advanced EGR control with a proportional valve and a very efficient exhaust gases cooling system. Analysis of the test results is based on the cylinder pressure and the concentration of NO_x and PM components at exhaust gases. The study included the influence of the exhaust gas recirculation system control on parameters such as differential pressure, MBF, and relative NO_x and PM emissions. As demonstrated by the analysis conducted, the EGR valve control method and the exhaust gas cooling intensity significantly affect the cylinder pressure and its ecological performance.

Key words: *exhaust gas recirculation, in-cylinder pressure, mass fraction burning, differential pressure, NO_x, particulate matter PM*

1. Introdution

Continuous increase in emissions requirements for internal combustion engines due to increasingly stringent emission standards for both road and off-road vehicles results in the need to improve methods to reduce emissions of nitrogen oxides, carbon monoxide, hydrocarbons, particulate matter and other compounds in the exhaust gases. In the case of non-road vehicles in the latest standards, there is a tendency for significant exacerbation of mainly NO_x and particulate matter (PM) emissions. Among the many methods used to reduce the emission of harmful substances, the methods used are in-cylinder and after treatment methods. It is of great importance to reduce emissions already at the stage of the generation of harmful exhaust gases, which can reduce or simplify the equipment belonging to the after treatment systems of reducing harmful substances in exhaust gases. Mechanisms for the formation of both NO_x and PM are related to processes occurring in the cylinder during the combustion process, so it is important to monitor them. One of the possibilities of evaluating the combustion process is to observe the pressure in the cylinder and then its thorough analysis. As a result, a number of engine performance indicators can be obtained to evaluate the course of the combustion process. In-depth analysis of the combustion process allows you to indicate areas of the engine where improvement of engine performance can be achieve by adjusting the control parameters to take a compromise between some of them, such as engine efficiency, engine performance.

Control of the internal combustion engine should be based on analysis of the combustion process occurring in the cylinder, so it is important to take into account a number of parameters resulting from the analysis of the in-cylinder pressure [1, 13, 17, 20]. Taking into account the increase curve of in-cylinder pressure, pressure peak and heat release, as well as other parameters, in controlling the combustion process in the cylinder can lead to improvement of combustion process. The expected effect of such control is to improve both ecological and economical engine properties.

In addition, it should be noted that the emission of particular harmful substances may be interdependent, which may lead to a slight reduction in emissions of one harmful substance to a significant increase in other. Commonly used in-cylinder limitation of harmful exhaust gas compounds are advanced fuel injection control with multiphase fuel injection and also exhaust gas recirculation. Huge influence on the pressure of the cylinder, and consequently exhaust emission has an injection control [4–6]. Also, the method of controlling the amount of exhaust gas recirculation, the cooling level of the recirculated exhaust gas is important not only for the ecological properties of the engine [2, 3, 7–10, 12, 19], but it also affects the performance indicators such as power or torque. Other aspects of engine performance, such as irregularity of engine speed [16], noise or fuel consumption [11] could be also taken into account during control process. Monitoring of the in-cylinder pressure and their analyzing allows, among other things, such control of the exhaust gas recirculation system to obtain the most favorable values of the individual engine performance indicators [1, 13, 15, 17, 20]. Information on the combustion process can be used to control both fuel injection and exhaust gas recirculation system.

2. Research methodology

2.1. Research object

In order to investigate selected engine operating indexes, the Z1505 engine used in agricultural tractors (Fig. 1) was mounted on a test bench. The tested research object has a maximum power of 92 kW at 2200 rpm. The engine is powered by diesel fuel by means of a prototype multiphase injection pump and equipped with a turbocharger with a relief valve and intake air cooler. The tested engine is also equipped with cooled EGR system. In addition, an advanced exhaust gas recirculation system, consisting of a gas-liquid heat exchanger, a proportional EGR valve and a feedback system, incorporates an integrated NO_x/O_2 sensor. The test stand is equipped with an AVL pressure sensor located in one of the test engine cylinders.

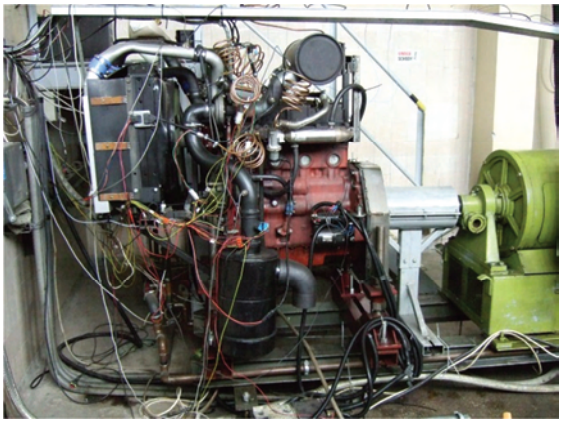

Fig. 1. Research engine mounted at test bench

Comparative studies have also been conducted for standard and modified (advanced) exhaust cooling systems. The modification of the cooling system was to increase the cooling level of the exhaust gas by using a refrigerant flowing through a gas-liquid heat exchanger with an inlet temperature of about 50 K lower than in the standard system during normal engine operation.

2.3. Research scope

Several engine cycles were registered, followed by averaging the pressure waveform, which, in view of some irregularities in subsequent cycles, minimizes the risk of selection for comparing accidental cylinder pressure. Determining the effect of exhaust gas recirculation on the cylinder pressure during engine operation there were required to select and averaged a series of stationary test cycles at selected speeds and torque loads.

Table 1. Main operating points of the tested engine - research scope

Group of points	Engine rotational speed rpm	Engine load, Nm
1	800	0–100
2	900	0–190
3	1000	0–190
4	1200	0–190
5	1400	0–190
6	1600	0–190
7	1800	0–190
8	2000	0–190
9	2200	0–190

Table 2. Operating points of EGR valve

No	EGR valve opening position, mm	EGR valve relative opening level, %
1	0	0
2	0.199	3
3	0.398	6
4	0.598	9
5	0.747	11
6	0.896	13
7	1.444	29
8	2.490	50
9	4.98	100

The tests were conducted for a full range of rotational speeds (800–2200 rpm) and torque loads ranging from 0–190 Nm (Table 1) and at different EGR valve opening level (Table 2).

3. Research problem

The main research problem is to clarify the effect of wide-ranging control of the exhaust gas recirculation system on the cylinder pressure and ecological engine performance.

The in-cylinder pressure profile contains a lot of information about the combustion process. The comparison of the in-cylinder pressure waveform without the fuel injection (motored in-cylinder pressure) with the pressure wave resulting from the initiated combustion process (Fig. 2) allows to determine the course of the differential pressure.

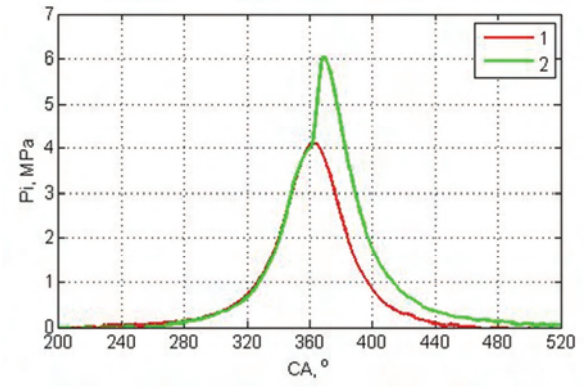

Fig. 2. In-cylinder pressure course at engine rotational speed 1000 rpm (1 – motored pressure, 2 – in-cylinder pressure at 190 Nm load)

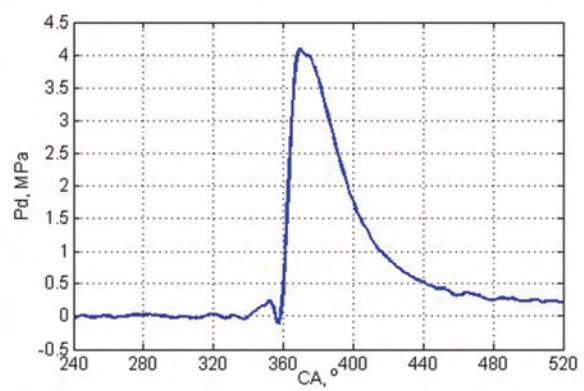

Fig. 3. Differential pressure at 100% EGR valve open (1000 rpm, 190 Nm)

Differential pressure is difference between motored in-cylinder pressure and in-cylinder pressure during combustion. Its variation allows for an overall assessment of the course of the combustion process, including, among other things, the rate of in-cylinder pressure increase resulting from fuel combustion, the occurrence of the maximum differential pressure ect.

$$p_{d(i)} = p_{comb(i)} - p_{motored(i)} \tag{1}$$

were: $p_{d(i)}$ – differential pressure at i-th interval, $p_{comb(i)}$ – combustion pressure at i-th interval, $p_{motored(i)}$ – motored pressure at i-th interval.

Mass fraction burned (MFB) is one of the important thermo dynamical engine indexes. In each individual engine cycle is a normalized quantity with a scale of 0 to 1, describing the process of chemical energy release as a function of crank angle [14, 18]. The determination of MBF is

based on burn rate analysis an there are many methods to evaluated it, but a procedure described by Rassweiler and Withrow [14] is a base method widely used because of its simplicity:

$$MFB = \frac{m_b(i)}{\sum_{0}^{N} m_b(i)} = \frac{\sum_{0}^{i} \Delta p_i}{\sum_{0}^{N} \Delta p_i} \tag{2}$$

were: m_b – mass burning, i – number of analysis interval, Δp_i – pressure rise at i-th interval, 0 – start of combustion, N – number of interval between start and end of combustion.

It can be assumed that in the range of the crankshaft angles in which the combustion process occurs takes place equality:

$$\Delta p_i = p_{d(i)} \tag{3}$$

From the work of many researchers it is clear that the use of the cylinder pressure analysis to control the combustion process in the engine allows many parameters to be improved. Thanks to the use of the pressure waveform analysis, both the efficiency of the operation and the environmental properties of the internal combustion engine can be improved. There are possibility to on-line supervision of fuel injection, feed forward of emission control, and feedback control of combustion process [17].

4. Influence of EGR control at engine operating indexes

4.1. Control of EGR valve opening

In order to understand the influence of the exhaust gas recirculation valve opening on the cylinder pressure, graphically the pressure waveforms at various openings of the exhaust gas recirculation valve for selected rotational speeds of 1000 and 1600 rpm with a 190 Nm load was presented.

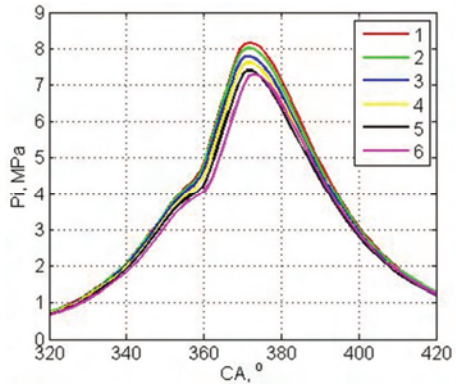

Fig. 4. In-cylinder pressure course at engine rotational speed 1000 rpm and 190 Nm load for different EGR opening level (1 – 0%, 2 – 3%, 3 – 8%, 4 – 15%, 5 – 50%, 6 – 100%)

Of the wide range of degrees of opening of the EGR valve for comparison, 6 open positions corresponding to relative valve lifting of 0, 3, 8, 15, 50 and 100% were selected. The in-cylinder pressure waveform are shown for 1000 rpm (Fig. 4) and 1600 rpm (Fig. 5) engine speed.

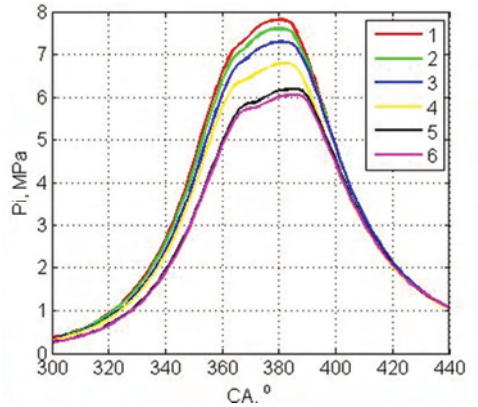

Fig. 5. In-cylinder pressure course at engine rotational speed 1600 rpm at 190 Nm load for different EGR opening level (1 – 0%, 2 – 3%, 3 – 8%, 4 – 15%, 5 – 50%, 6 – 100%)

One of the basic parameters describing in-cylinder pressure is its maximum value. The effect of the EGR valve opening on the maximum cylinder pressure is shown in Fig. 6.

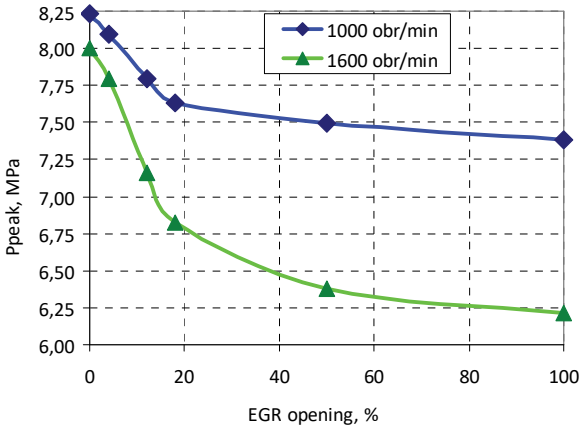

Fig. 6. Impact of EGR opening level at peak in-cylinder pressure

With the increase in the opening of the EGR valve, the maximum in-cylinder pressure drop can be observed. It is noteworthy that the greatest tendency of pressure drop is observed at the initial opening of the EGR valve, and at the same time this trend is more relevant for a higher rotational speed, which is accompanied by greater differences between the exhaust gas pressure and the intake manifold pressure, leading to an increase in the exhaust gas recirculation rate. Increasing the degree of EGR valve opening increases the rate of exhaust gas recirculation entering the cylinder. As a result, this will affect the combustion process, which takes place with less oxygen due to the increased share of exhaust gases entering the cylinder. There is a change in the dynamics of the combustion process, which manifests itself in differentiated MFB curves describing the dynamics of heat release in the cylinder.

Differential pressure variations for selected engine operating conditions at constant speeds of 1000 and 1600 rpm and 190 Nm load for various EGR valve opening stages are shown in Fig. 7 and Fig. 8.

As the differential pressure waveform analysis shows, the highest values are noticeable for the closed EGR valve, ie. without external recirculation. Maximum pressure values are: 4.774 MPa closed for full EGR valve (EGR 0%) and fully open (EGR 100%) 4.327 MPa respectively (Fig. 7) and with rotational speed of 1600 rpm and load of 190 Nm, the maximum differential pressure is between 5.213 MPa for the closed EGR valve (EGR 0%) and 4,007 MPa for the fully open valve (EGR 100%) (Fig.8).

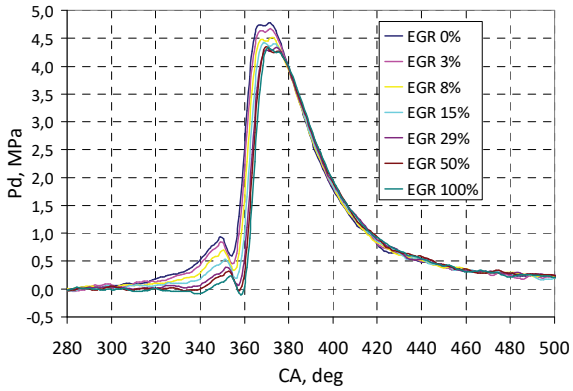

Fig. 7. Differential pressure at different EGR valve opening level (1000 rpm, 190 Nm)

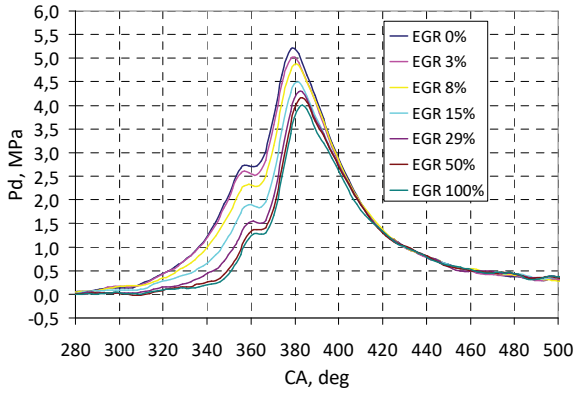

Fig. 8. Differential pressure at different EGR valve opening level (1600 rpm, 190 Nm)

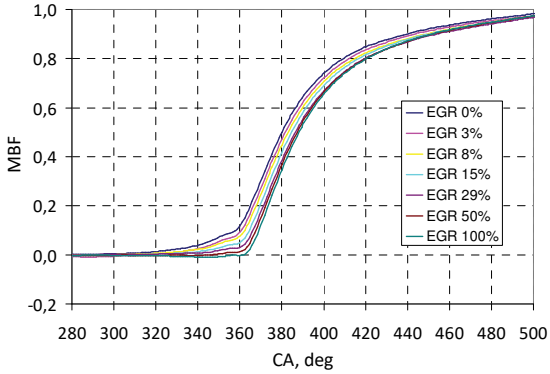

Fig. 9. Mass Fraction Burning course at different EGR valve opening level (1000 rpm, 190 Nm)

It can be noted that for a rotational speed of 1600 rpm, the variation in both maximum pressure and waveforms is significantly higher than with a rotational speed of 1000 rpm. This demonstrates the greater extent of the effect of exhaust gas recirculation with the same EGR valve settings. As the next index the heat dissipation patterns MFB were plotted for the same engine operating conditions (Fig. 9 – 1000 rpm, Fig. 10 – 1600 rpm. Also in this case, the influence of the EGR valve opening degree (exhaust gas recirculation rate) on the process of heat release in the cylinder was noticeable. Analysis of this graphs (Figs 9, 10) shows that dynamics releases heat in the case of high levels of exhaust gas recirculation is low in the first period of burning process, but intensifies as the combustion process progresses. Dynamics of heat release can be represented by the MFB values of 5%, 10%, 50% and 90% of the heat released during the combustion process, respectively mean as MFB 5%, MFB10%, MFB 50%, MFB90%. The graphs (Figs 11, 12, 13, 14) show the dependence of specific MFB values from the crankshaft angle for both engine speeds.

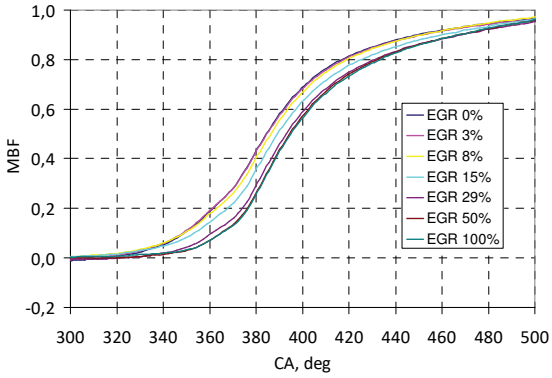

Fig. 10. Mass Fraction Burning course at different EGR valve opening level (1600 rpm, 190 Nm)

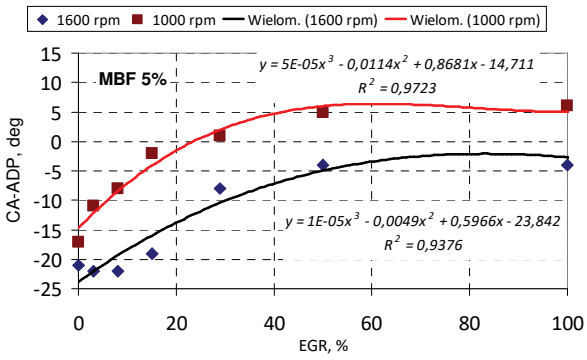

Fig. 11. Impact of EGR opening at MBF 5% value (190 Nm load)

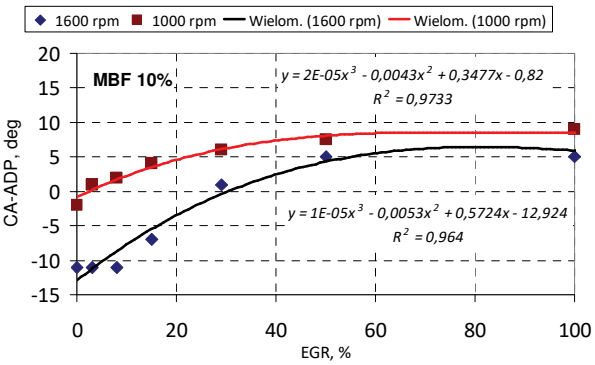

Fig. 12. Impact of EGR opening at MBF 10% value (190 Nm load)

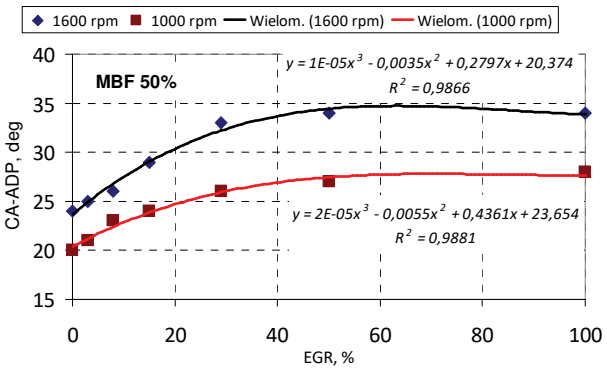

Fig. 13. Impact of EGR opening at MBF 50% value (190 Nm load)

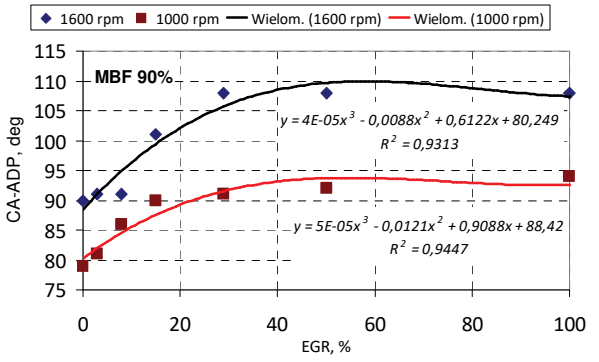

Fig. 14. Impact of EGR opening at MBF 90% value 190 Nm load)

Release of 5% or 10% of heat for both tested engine speed in case of significant opening of the EGR valve occurs much later, that is about 20 CA degrees later than in the absence of external exhaust gas recirculation. In turn, obtaining 50% of the MFB value is shifted by about 7–10 CA degrees, and for 90% MFB respectively 15–18 CA degrees. Duration to generate heat between 5% and 90% (Fig. 15) was also analyzed. Significant volume of exhaust gas returned to the cylinder does not significantly affect the duration of the value between MFB5% and MFB90%.

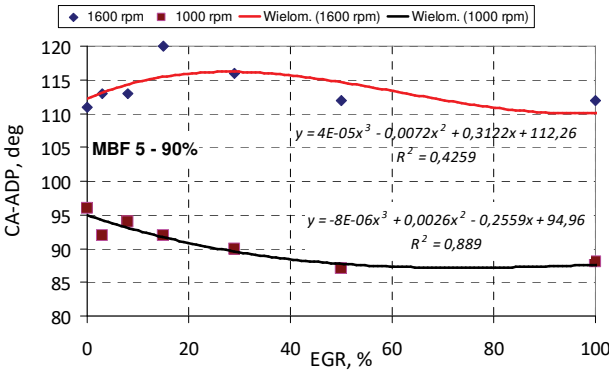

Fig. 15. Impact of EGR opening at duration of MBF 5% - 90 % value

In order to determine the effect of the EGR valve opening on the ecological properties of the test engine, the NO_x concentration and PM in the exhaust gas were analyzed. Figures 16 and 17 illustrate the effect of the opening of the EGR valve on NO_x and PM concentrations at exhaust gases at 1000 and 1600 rpm. There are also NO_x and PM concentrations expressed in absolute terms (Fig. 18).

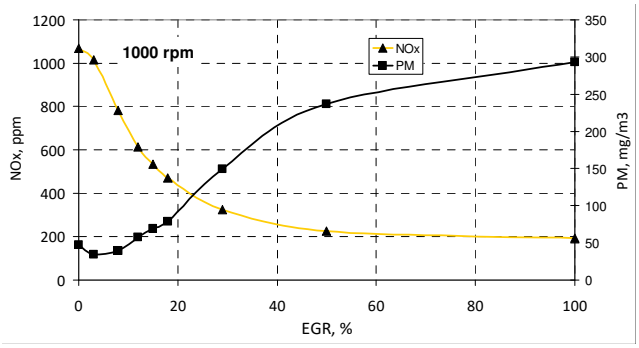

Fig. 16. Impact of EGR opening level at NO_x and PM concentration (1000 rpm, 190 Nm)

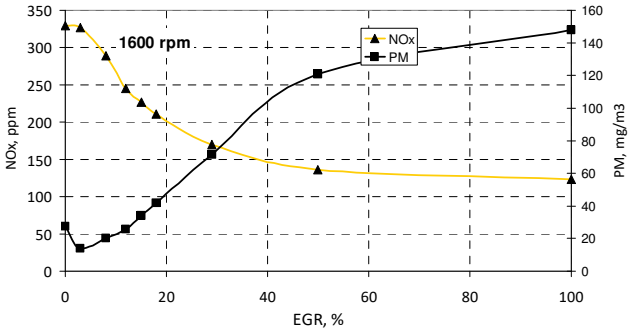

Fig. 17. Impact of EGR opening level at NO_x and PM concentration (1600 rpm, 190 Nm)

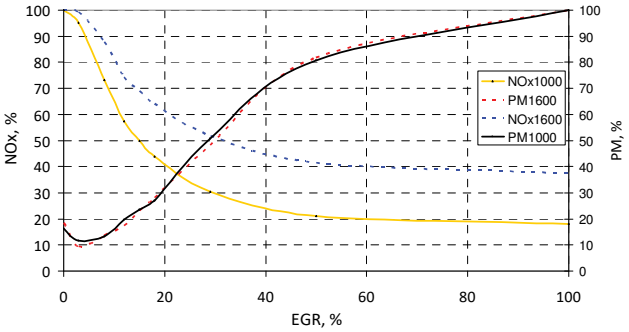

Fig. 18. Impact of EGR opening level at relative NO_x and PM concentration at 190 Nm load

The analysis shows the dependence of NO_x and PM concentration in the exhaust gases according to the EGR valve opening degree. Limiting emissions of one of the tested substances by controlling the EGR valve is associated with an increase in the emissions of the other substance. The PM relative emission curves for different engine speeds overlap, and for NO_x the curves are similar in shape, but the curve for higher rotational speeds is higher.

4.2. Modified advanced EGR cooling system

Finding the possibility of simultaneous reduction of both NO_x and PM emissions through exhaust gas recirculation, requires advanced control of the system, but at the same time a search for methods to influence temperature of the exhaust gas. One of the goals of the survey is to determine the effect of intensive exhaust cooling on both thermodynamic and ecological indicators. The modified cooling system of recirculated exhaust gas was characterized by a high cooling efficiency. This system is based on two heat

exchangers: the first gas-gas type and the second gas-liquid type. Increased cooling intensity was achieved by keeping the coolant temperature by about 50K lower than in the standard recirculated exhaust cooling system. Comparison of differential pressure for standard and advanced cooling systems is presented for selected engine operating points in Figs 19–21. The results of the study were compared by individual waveforms with fully open EGR valve (EGR 100%).

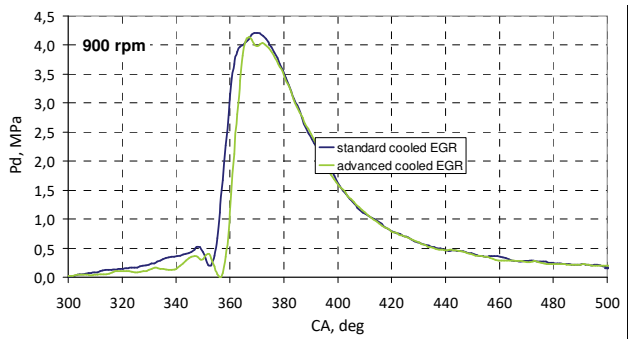

Fig. 19. Impact of EGR cooling system at differential pressure Pd (engine rotational speed: 900 rpm, 190 Nm load)

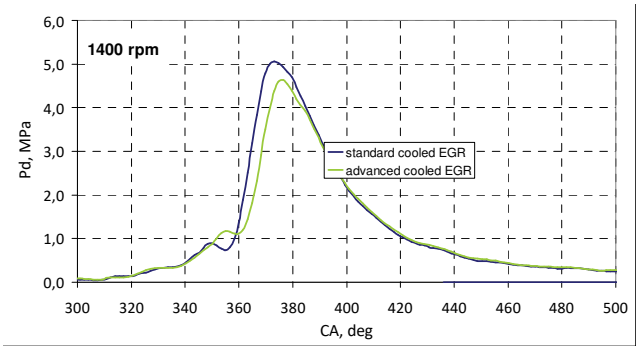

Fig. 20. Impact of EGR cooling system at differential pressure Pd (engine rotational speed: 1400 rpm, 190 Nm load)

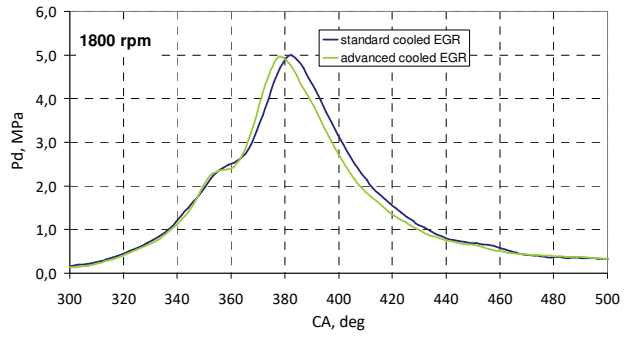

Fig. 21. Impact of EGR cooling system at differential pressure Pd (engine rotational speed:1800 rpm, 190 Nm load)

Analysis of selected waveforms shows that the use of intensive exhaust cooling system with a fully open EGR valve significantly influences the pressure in the cylinder, which results in a reduction in differential pressure. At the same time, the waveform offset for the advanced cooling system is noticeable. The intensive cooling of the recirculated exhaust gases reduces the maximum in-cylinder pressure resulting in a decrease in maximum differential pressure from 4.126 to 4.136 MPa for 900 rpm, 5.070 to 4.637 MPa for 1400 rpm and symbolically from 4.989 to 4.966 MPa for 1800 rpm.

The differences in the differential pressure waveforms has effect on the changes in the heat release dynamics shown in the form of the MBF curves (Figs 22–24). It is noticeable to grow the intensity of heat release especially during the first period of combustion process.

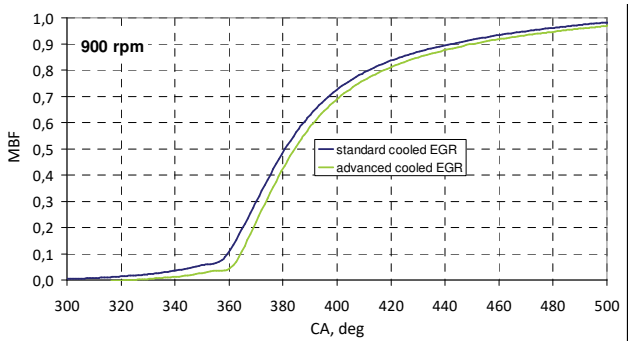

Fig. 22. Impact of EGR cooling system at MBF specific values (engine rotational speed: 900 rpm, 190 Nm load)

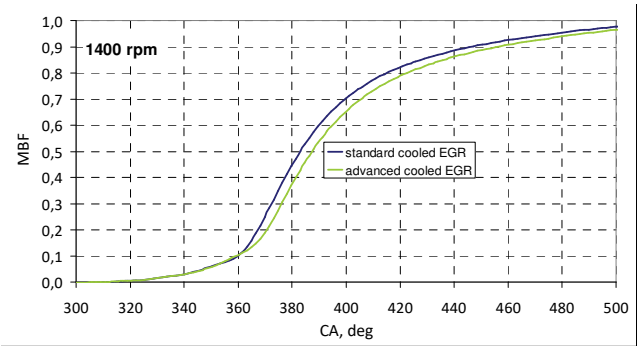

Fig. 23. Impact of EGR cooling system at MBF specific values (engine rotational speed: 1400 rpm, 190 Nm load)

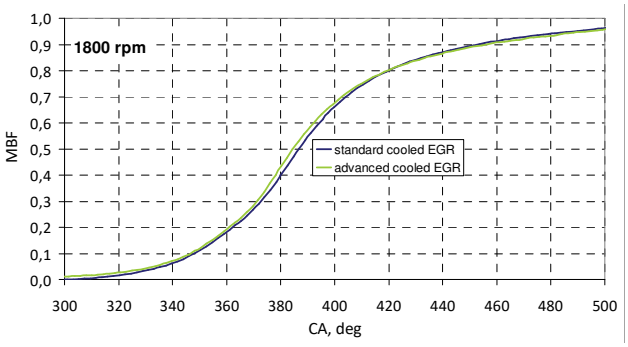

Fig. 24. Impact of EGR cooling system at MBF specific values (engine rotational speed: 1800 rpm, 190 Nm load)

This is most noticeable for the low engine rotational speeds, and the increase in this speed decreases the effect of the cooling intensity on the MBF curve.

More detailed analysis of the heat release dynamics in terms of the crankshaft angles (calculated relative to the crankshaft position corresponding to the piston position of the 1st cylinder at the upper dead center point – CA-AFD) corresponding to the specific MBF values, ie, respectively, 5%, 10%, 50% and 90% is presented on Fig. 25–27. The

differences are visible first for the lowest rotational speed of 900 rpm. There is a general trend towards greater heat release dynamics for advanced cooling systems especially in the first phase of the combustion process. Achieving a 5% or 10% MBF value, is recorded from 19 to 0 degrees crank angle with a tendency to decrease this value for higher rotational speeds. Achieving a 50% MBF value is usually a few degrees of CA later than with a standard cooling system. At the end of the combustion process, heat release dynamic slows down, resulting in achieving of MBF90% of about 3 to 10 degrees CA later than the standard cooling system. There is also a tendency to observe lower values of CA-AFD corresponding to higher rotational engine speeds.

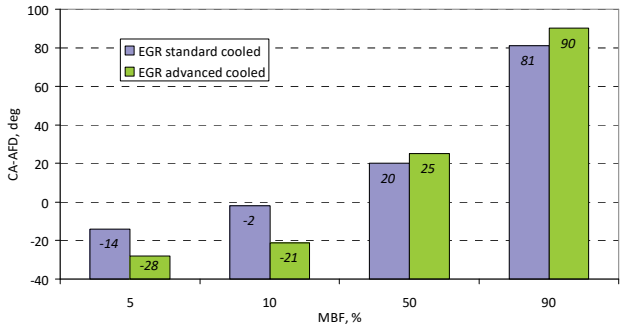

Fig. 25. Impact of EGR cooling system at CA – AFD of MBF specific value (engine rotational speed: 900 rpm, load: 190 Nm load)

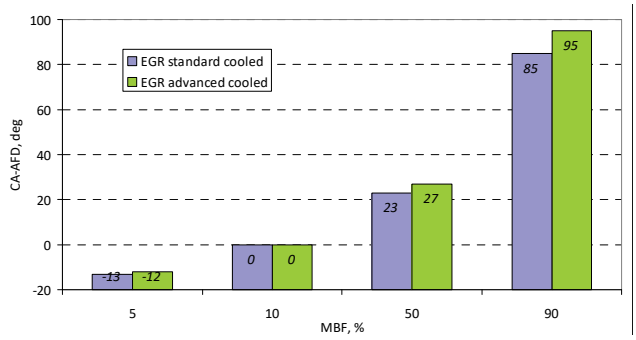

Fig. 26. Impact of EGR cooling system at CA –AFD of MBF specific value (engine rotational speed: 1400 rpm, load: 190 Nm load)

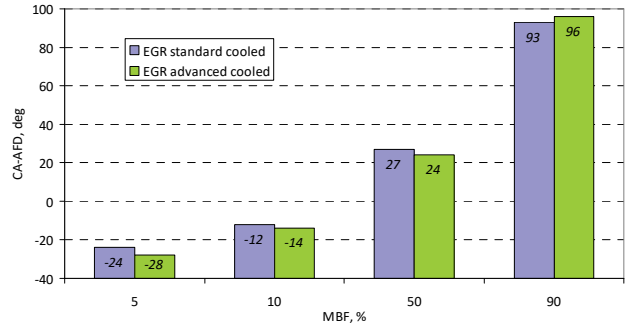

Fig. 27. Impact of EGR cooling system at CA –AFD of MBF specific value (engine rotational speed: 1800 rpm, load: 190 Nm load)

It is very important to determine the influence of application an advanced EGR system characterized by intense exhaust gas cooling on the exhaust gases concentration of NO_x and PM. Results of studies of such ecological properties are presented graphically in Figs 28–29. The recorded comparative curves of NO_x and PM concentrations in the exhaust gas corresponding to the different recirculated exhaust gas cooling levels show possibilities for simultaneous reduction of emissions of the two concerned substances.

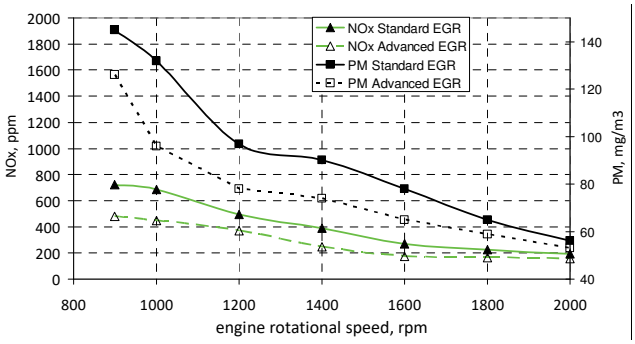

Fig. 28. Comparison of EGR cooling systems and NO_x and PM concentration at exhaust gasses

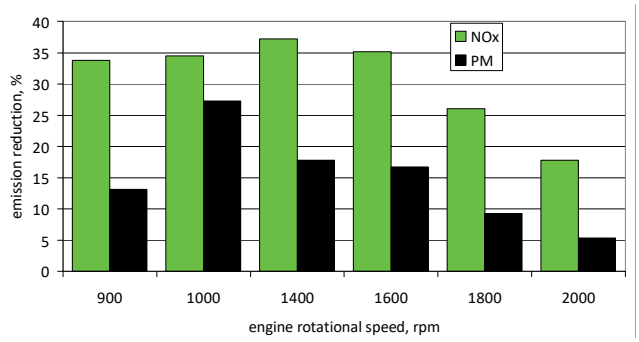

Fig. 29. Possibilities to emission reduction of NO_x and PM thru advanced exhaust gas cooling system

Reduction of emissions compared to the standard exhaust cooling system is possible from 15 to over 30% with NO_x, and at the same time the emission of PM can reduced at a range from 5 to almost 30%.

5. Conclusions

The study confirmed that controlling the EGR valve opening rate directly affecting the exhaust gas recirculation rate has a significant effect on the cylinder pressure. As a consequence, it results in changes in both thermodynamic and ecological engine properties. The studies have confirmed the significant effect of controlling the EGR valve opening rate on the differential pressure, obtaining the MFB specific values determining the method of heat release during combustion. Increasing the proportion of exhaust gas in the cylinder results in a reduction in maximum combustion pressure without reducing the torque available on the engine crankshaft. At the same time, the dynamics of heat release changes. The results of the studies also confirmed the correlation between the concentration of NO_x and PM in the exhaust gases. Increase in the opening of the ERG valve rate, affect of NO_x emissions reduction, but this results in a simultaneous increase in PM emissions. Controlling the degree of exhaust gas recirculation (through opening of the EGR valve rate) requires a compromise between the emission of these substances and consideration of the degree of extinction (emission reduction potential) of aftertreatment emission reduction systems. It has also been

shown that advanced recirculation exhaust gas cooling systems with significant cooling intensity can achieve significant and also simultaneous reduction of both NO_x and PM concentrations in exhaust gases. Emissions reductions with advanced EGR systems can exceed 30% at selected engine operating points.

Nomenclature

CI compression ignition
CA crank angle
CA-AFD crank angle after center deadpoint
EGR exhaust gas recirculation
MBF mass burning fraction/ mass burn fuel
NO_x nitrogen oxides
PM particulate matter

Bibliography

[1] BEASLEY, M. et al. Reducing diesel emissions dispersion by coordinated combustion feedback control. *SAE Technical Paper*. 2006, 2006-01-0186.

[2] BIENIEK, A., MAMALA, J., GRABA, M., LECHOWICZ, A. Control of advanced EGR system at nonroad diesel engine. *16th Asia Pacific Automotive Engineering Conference* – APAC Chennai India, *SAE India* M2010066, 1-6.

[3] BIENIEK, A., GRABA, M., LECHOWICZ, A. Adaptive control of exhaust gas recirculation at nonroad vehicle diesel engine, *Journal of Kones* 2011, **18**(4), 11-18.

[4] BIENIEK, A., GRABA, M., LECHOWICZ, A. Control of agricultural engine injection system in aspect of ecological property improvement. *Combustion Engines*. 2011, **SC-0192**, 1-8.

[5] BIENIEK, A., MAMALA, J., GRABA, M. Analysis of combustion process at multiphase injection at nonroad diesel engine, *Combustion Engines*. 2011, **4**, SC-190, 1-8.

[6] BIENIEK, A. Conception of cylinder pressure based Diesel injection control system. *Journal of Kones. Powertrain and Transport*. 2011, **18**(3), 27-35.

[7] BIENIEK, A., MAMALA, J., GRABA, M. Możliwości wstępnego ograniczenia emisji NO_x i PM silnika wysokoprężnego w aspekcie przyszłościowych norm emisji pojazdów pozadrogowych. *Zeszyty Naukowe Instytutu Pojazdów*. 2012, **1**(87), 75-86.

[8] BIENIEK, A. Wewnątrzsilnikowe ograniczenie emisji substancji szkodliwych w silniku wyposażonym w układ EGR pojazdu pozadrogowego. *Inżynieria Rolnicza*. 2013, **2**(143), 31-41.

[9] CIEŚLIK, W., BOROWSKI, P., PIELECHA, I. et al. Systemy recyrkulacji spalin we współczesnych konstrukcjach silnikowych. *Logistyka*. 2014, **3**, 1118-1127.

[10] GRABA, M., BIENIEK, A., MAMALA, J., LECHOWICZ, A. Sterowanie adaptacyjne zaworu recyrkulacji spalin w silniku o zapłonie samoczynnym w aspekcie obniżenia emisji substancji szkodliwych. *Inżynieria Rolnicza*. 2011, **5**(130), 73-80.

[11] GROMADKO, J., HONG, V., MILER, P. Applications of NRTC cycle to determine a different fuel consumption and harmful emissions caused by changes of engines technical conditions. *Maintaince and Reliability*. 2008, **4**, 63-65.

[12] GUEZENNEC, Y., CANNOVA, M., GARZARELLA, M. et al. Control-oriented modeling for HCCI combustion and multi-cylinder HCCI experimental activities. The Ohio State University. Center for Automobile Research, *Rapport* 2005, 1-9.

[13] HASEGAWA, M., SHIMASAKI, Y., et al. Study on ignition timing control for diesel engines using in-cylinder pressure sensor. *SAE Technical Paper*. 2006, 2006-01-0180.

[14] HEYWOOD, J.B. Internal combustion engine fundamentals. *McGraw-Hill*. 1988.

[15] KESSEL, J.-A., SCHMIDT, M., ISERMANN, R. Modelbasierte Motorsteuerung, Regelung und – Ueberwachung. *MTZ*. 1998, **59**, 240-246.

[16] KOWALSKI, D., BIENIEK, A., BROL, S. Irregularity of rotational speed Diesel engine with modified fuel injection system. *Journal of Kones, Powertrain and Transport*. 2011, **18**(4), 199-204.

[17] LEONHARD, S., MULLE,R N., ISERMANN, R. Methods for engine supervision and control based on cylinder pressure information. *IEEE-ASME Transactions on Mechatronics*. 1999, **3**(4), 235-245.

[18] MENDERA, K.Z., SPYRA, A., SMERECKA, M. Mass fraction burned analysis. *Journal of KONES Internal Combustion Engines*. 2002, **3-4**, 193-201.

[19] SOBIESZCZAŃSKI, M. et al. Wpływ parametrów regulacyjnych silnika ZS na zawartość składników toksycznych i zadymienie spalin. Nauka i technika. *Eksploatacja i niezawodność – Maintenace and Reliability*. 2008, **3**.

[20] SELLNAU, M., MATEKUNAS, F.A., BATTISTON, P. Cylinder-pressure-based engine control using pressure-ratio-management and low-cost non-intrusive cylinder pressure sensors. *SAE Technical Paper*. 2000, 2000-01-0932.

Andrzej Bieniek, DEng. – Faculty of Mechanical Engineering at Opole University of Technology.

e-mail: *A.Bieniek@po.opole.pl*

Mariusz Graba, DEng. – Faculty of Mechanical Engineering at Opole University of Technology.

e-mail: *M.Graba@po.opole.pl*

Jarosław Mamala, DSc., DEng. – Faculty of Mechanical Engineering at Opole University of Technology.

e-mail: *J.Mamala@po.opole.pl*

Krystian Hennek, MEng. – Faculty of Mechanical Engineering at Opole University of Technology.

e-mail: *k.hennek@po.opole.pl*

Article citation info:
KOZIOŁ-JAROSZ, M., BRZEŻAŃSKI, M. The role and tasks of the support mats in the construction of catalytic converters. *Combustion Engines*. 2017, **170**(3), 96-99. DOI: 10.19206/CE-2017-315

Magdalena KOZIOL-JAROSZ
Marek BRZEŻAŃSKI

CE-2017-315

The role and tasks of the support mats in construction of catalytic converters

The purpose of support mats used in catalytic converters as connecting element between the ceramic core and the metallic converter housing has been presented in article. The functional requirements and operating conditions have been discussed as well as support mat types and manufacturing methods. The support mat choice and basic design features have been also presented.

Key words: *support mat, exhaust system, catalytic converter, amorphous fibre, polycrystalline fibre*

1. Introduction

Different types of vehicles powered by internal combustion engines are from more than 100 years the primary means of transportation by land, water and air. A special role is played here by vehicles designed to land transport of people and goods and their operation affect the environment and human organisms directly.

Due to this reason, in the early 70s was introduced the limitation of toxic components in vehicle exhaust gases. Currently various types of catalytic converters in exhaust systems with spark ignition and compression ignition engines are used. The efficiency of these aftertreatment systems depends on the placement in the vehicle exhaust system depending mainly on the system geometry [1, 2, 3].

In the automotive industry the first elaborated and serial produced in 70s and 80s exhaust gas cleaning systems were oxidizing catalytic converters.

The three-way catalytic converter (TWC) in combination with a lambda sensor has become standard in vehicles with petrol engines. Due to an enhanced limitation of particle emissions the introduction of Gasoline Particulate Filters (GPFs) is on-going process. In the case of diesel engines, Diesel Oxidation Catalyst (DOC) and Diesel Particulate Filter (DPF) are standard to fulfil the carbon monoxide (CO), unburned hydrocarbons (HC) and soot particle limits. Enhanced NOx emission limitations require technologies like NSC (NOx trap catalyst) or the Selective Catalytic Reduction (SCR) technology.

The relevant regulations concerning both the conditions and operation lifetime, determine effectiveness of action of each system of exhaust gas purification. Hereby it has to be considered that these components have to fulfil challenging durability requirements. The efficient catalyst system operation has to be ensured through the entire life of the vehicle (for example in Europe – 12 years, in USA – 15 years). Operation lifetime is determined mostly by the design and installation of all elements, even those that from the viewpoint of objectives have additional aims. Such elements can include e.g. ceramic fibre mats whose function is to fix the core in the catalytic converter housing [4, 6].

2. Operating conditions of catalytic converters

For designing a robust converter layout it is mandatory to know the boundaries of the operating conditions. These are mainly:

- vibration – coming from the engine (high frequency) and interaction between terrain and vehicle body (low frequency),
- exhaust gas flow and temperature,
- chemical factors like exhaust gas condensate, ammonia or urea.

The inclusion of these three groups of factors has the greatest impact on design and selection of materials used for individual elements of the catalytic converter [1].

Generally the exhaust system can be divided into a so called “cold end” and a “hot end”. The cold end comprises mainly the vehicle underbody pipe routing, silencers and the tailpipe. The hot end contains mainly exhaust aftertreatment components which are located close to the engine. The exhaust gas temperature up to 1000°C can be achieved what put high requirements to all materials in this area, e.g. steel parts, support & insulation materials.

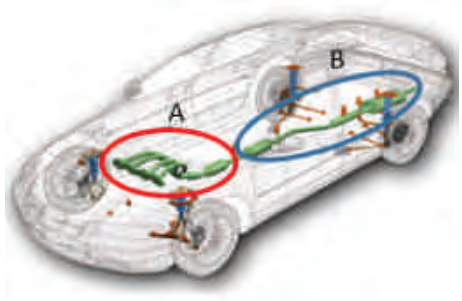

Fig. 1. Location of the exhaust system elements in a passenger car; A – "hot end", B – "cold end" [4]

High working temperature is one of the main factors that need to be taken into account while designing the catalytic converter, because it causes the formation of thermal stresses and changes in the structure of construction materials as well as their surface. Especially important is the heating-up period of the catalytic converter during which variable thermal stresses dependent on the heating rate and different characteristic of the materials used to construction of the catalytic converter are formed. The impact of thermal stress on components of the catalytic converter associated with changes in the geometry of the individual segments cause stresses and decrease of mechanical properties. It can cause micro- and macro-cracks which occur mostly at the transition area between heat affected zone (HAZ) of the weld seam and base material (significant difference in mechanical properties). The effect is enlarged by the mechanical vibrations coming from the suspension, the manifold gas pressure vibrations coming from the respective cylinders of the engine and the vibration of the entire exhaust

system comes from the irregularities of the surface on which the vehicle is moving. External vibrations are partially suppressed by the spring elements and elastic elements which mount the exhaust system under the car body, whereas the vibration inside the catalytic converter is suppressed mainly by a support mat. All of the above types of vibrations in combination with weakened mechanical properties of the material resulting from the manufacturing process, can cause the formation of cracks and destruction of the components of the catalytic converter [2, 5].

The TWC and DOC/DPF-assemblies are mainly located close to the engine whereas SCR-converters and GPFs are mainly located in a vehicle underbody position. For future emission levels these components will also be moved closer to the engine.

One of the structural components of catalytic converters which are particularly vulnerable to damage as described above is the core. Improper selection of support mats can lead to a shift of the core inside the catalytic converter housing and at worst case can lead to damage of it. In this case the appropriate choice of the mat material and the arrangement of the core in the reactor have a significant impact on the length of its life [4].

3. Support mats fibres overview

The operating conditions of the support mat used in production of catalytic converters create specific material design requirements.

The most frequently used materials to manufacture of support mats are inorganic synthetic fibres.

The fibres are divided into two groups:

1. Amorphous – mainly used for the production of support mats:
   - Mineral wools – e.g. Alkaline Earth Silicates (AES). These fibres are used for the production of biosoluble intumescent support mat. According to the regulations, both European and German, these fibres are classified as 0 i.e. "green fibres". AES fibres mainly consist of the following components: CaO, MgO, SiO_2, ZrO_2. The maximum allowed application temperature for this type of fibres is up to 850°C [1].
   - Refractory ceramic fibres (RCF) - belong to the classification 1B which is classified in Europe as potentially carcinogen. The use of this fibres type is restricted in EU. The chemical composition of RCF is based on SiO_2 and Al_2O_3 in proportions around 50:50%. The application temperature limit for this type of fibre is 1100°C [4].
2. Polycrystalline (PC) – the example of such fibres used in the production of support mats is:
   - Fibre consisting alumina belonging to subgroup oxide fibres. According to EU regulations these fibres belong to the category 0 – "green fibres", while according to German regulations these fibres belong to group 3 -suspected of being carcinogenic. PC fibres are made mainly of Al_2O_3 (more than 70%) and the remaining part of SiO_2. The maximum permissible temperature for this type of fibre is 1100°C [4].

Main manufacturing processes for fibres are produced by two methods (Fig. 2):

1. Melt spinning process – widely used in industry. Material from which fibre is produced is melted inductively in the crucible made of quartz or ceramics. The molten material is sprayed on a cooled roller rotating at a constant angular velocity. Cooling can take place on one roller or two rolls rotating in opposite directions. This method can produce amorphous fibres having a diameter of from 1 to 6 microns.

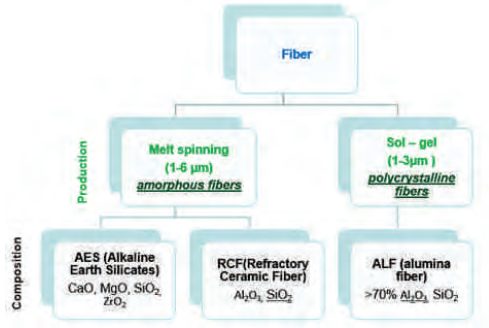

Fig. 2. Fibres materials used for manufacture of support mats [4]

By use of this method two types of amorphous fibres can be produced:

- Alkaline Earth Silicates (AES)
- Refractory Ceramic Fibre (RCF)

2. Method sol-gel – is to generate a gel from the colloidal solution (sol). Very important for this process is that the last three steps of heat treatment presented in Fig. 3 have to be conducted right after each other.

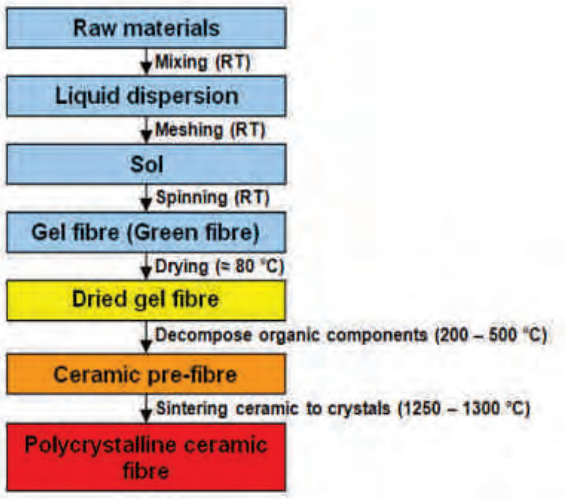

Fig. 3. Sol-gel process [4]

This method is mainly used for the production of polycrystalline fibres; the advantage is very constant and narrow fibre diameter of approximately 3 micrometres [4].

4. The support mat manufacturing process

Due to the build of the inner structure, the support mats are divided into three basic types:

1. Needled mat – needle felting method in which mat is formed in a dry air-lay process and then needled. In the first step, the bulk material is transformed into a blanket

of constant thickness through air-lay. Air-lay machines produce the blanket by disintegrating the fibre bulk with an air stream and settling it on a rotating drum. After the needling the felt is heat treated to convert the green sol-gel fibre into a ceramic fibre. The heat-treated mat is then cut in pieces and soaked in binder whereby the surplus is removed by a vacuum. After the bonding of the binder the product is cut into its final shape.

2. Paper mat – the earliest development of support mats. The paper mat production process starts with mixing fibres, binder raw material and a liquid to obtain a dispersion of slurry. The mat is then dried in an oven at moderate temperatures whereby the binder starts to bond the fibres together. The dried mat is then winded up to a big roll called jumbo. In case of production of blankets they are stacked upon each other. In the next step the blankets or jumbo rollers are cut with stamps into the shape of the final product.
3. Vermiculite mat – intumescing mats incorporate besides fibres also vermiculite whereby the content of vermiculite can be up to 65% mass. Fibres and vermiculite are bound together in a binder matrix. To produce intumescent mats vermiculite is added as a fourth component [4].

5. Support mat choice and layout

Main parameters for the right support mat choice and layout are:

- Local market regulations concerning fibre type permitted to use for catalytic converter support mat. In the EU support mat should belong to classification group of 0 i.e. “green fibre”.
- A very important parameter in the selection of the support mat is operating temperature of the catalytic converter. The choice is dependent not only on the place in which a catalytic reactor is mounted (near or far from the engine), but also on the exhaust gas temperature, which is dependent on the type and method of operation of the engine used.
- The borders of the mounting density called GBD (Gap Bulk Density) advised by the supplier.
- Safety factor of the designed support mat plate. It should be greater than or equal to 1 which means the system is robust.
- Customer requirements – in many cases customer has own support mat supplier.
- Support mat costs [4].

The support mat is placed between the catalytic reactor and the core. The main objective is to maintain the core in a fixed position and to prevent it from movement.

Based on the parameters mentioned above a layout calculation has to be performed to determine the required holding force of the mat according to allowed pressure to avoid destroying the fragile ceramic substrate or the support mat itself.

Beside the holding function the support mat acts as a bypass sealing and as an insulation material to keep the low outer housing surface temperature. The support mats are used exclusively to ceramic cores (Fig. 4), which are used as an input to the catalytic converter more often than the corresponding metal cores. The combination of ceramic substrate and support mat is good compromise between component costs and functional aspects.

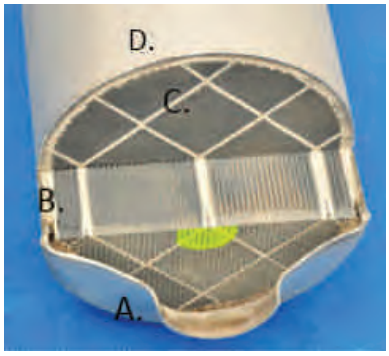

Fig. 4. Cross-section through a catalytic converter: A – cone, B – support mat, C – substrate, D – housing [4]

The disadvantage of ceramic cores is their fragile structure, worse thermal conductivity (longer heating time) and lower allowable temperature of their operation. For example, the TWC reactor operating temperature is in the range of 400-900°C because in this temperature range the coating have the best performance from the point of view of the operation of the catalytic converter [2, 3].

Depending on the core size, holding and surface temperature requirements the support mat thickness can vary. Therefore different ways of installation are available:

- One layer of the support mat (Fig. 5) – in this method the support mat is wrapped around the core and then subjected to a stuffing process. The canning technology is the most commonly used method.

Fig. 5. Support mat [4]

- Two layers of the support mat – this concept is used in case of a big support mat gap, e.g. due to enhanced surface temperature or holding requirements or big core diameter i.e. heavy duty applications. Disadvantageous is the increased handling effort due to the double layer.
- Multi wrapping mat - the process is applied in the case of a large gap. In the case of a single layer the holding force is not large enough to maintain the core. This applies to the support mat where the supplier does not offer a large enough dimension. In this process the core is wrapped two to four times with the support mat. Such prepared system is inserted into the steel housing which

has a constant diameter. This method is used in production of cylindrical catalytic converters for trucks [4].

An important issue in the case of the support mat is vibration as well as mechanical and thermal impact of exhaust gases that can lead to erosion. Erosion products in the form of detached fibres of the support mat can lead to partial or complete clogging of the channels of the core. Erosion of the support mat can take form of thin channels, by which exhaust gases can bypass the core. Any type of mat mass loss reduces its thickness and lead to changes in the structure of the mat. It can be a cause of displacement or damage of the substrate.

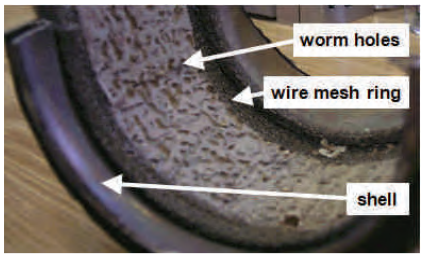

Fig. 6. Worm-holing effect by solid non fibrous material in the mat [4]

Proper support mat mounting and compression of it in the housing is very significant in case of intumescent mats. When the intumescent mat is compressed not enough the so called "worm-holing" effect (Fig. 6) can appear.

"Worm-holing" – occurs when lose particles like vermiculate in support mat can vibrate and oscillate freely after mounting the mat in housing.

Those particles damage the mat what cause erosion, less holding force and danger of not supporting the core properly. Due to a good progress in support mat design and the layout process it is possible to ensure reliable and durable construction in terms of holding function and erosion resistance [4].

6. Summary

The support mat is an important structural component of the design of aftertreatment systems which ensures a robust and durable fixation of the ceramic substrate in the exhaust line. For this reason, the correct choice of support mat material and the method of its installation inside the housing affect the proper functioning of the entire exhaust aftertreatment system. The main function of the support mat in a catalytic converter is to keep the core in the proper position and its protection against various types of internal and external damage. According to the modern requirements, assumed reliability and effectiveness of catalytic converters is from 10 to 15 years. During this period heat load and capacity of channels in the core should not be subject to significant changes. In practice however, the durability of catalytic converter is dependent on many different structural and operational factors. In this regard one of the most important elements that are responsible for the proper operation of the catalytic converter is support mat wrapped around the core in the housing. Therefore any research and development related to this topic is appropriate and very important. There is also a great demand for this research in the automotive industry.

Nomenclature

AES	alcaline earth silicates
CO	carbon monoxide
DPF	diesel particulate filter
DOC	diesel oxidation catalyst
GBD	gap bulk density
GPF	gasoline particulate filter
HAZ	heat affected zone
HC	hydrocarbon
NSC	NO_x trap catalyst
PC	polycrystalline
RCF	refractory ceramic fiber
SCR	selective catalytic reduction
TWC	tree-way catalytic converter

Bibliography

[1] KOZŁOWSKI, M. Mechanik pojazdów samochodowych. *Budowa i eksploatacja pojazdów*. Część 1. Wrocław, 2003.
[2] Wszystko o spalinach. *SmartDriver.pl*. www.smartdriver.pl (accessed: 02.01.2016).
[3] Zwalczanie emisji szkodliwych składników spalin. www.czasopismologistyka.pl (accessed: 06.01.2016).
[4] Tenneco Inc. – Factory information materials.
[5] MYSZKOWSKI, S. Układy wylotowe silników. Kompendium wiedzy praktycznej. *Dodatek techniczny do Wiadomości Inter Cars S.A.* 2009, **33**.
[6] BRZEŻAŃSKI, M., RYBARZ, M. Tworzenie się i oddziaływanie kondensatu w układzie wylotowym silnika spalinowego. *Wydawnictwo Politechniki Krakowskiej*, Kraków 2014.
[7] FILIPECKA, K., PAWLIK, P., WYSŁOCKI, J., GĘBARA, P. Nowoczesne metody wytwarzania materiałów amorficznych. dlibra.bg.ajd.czest.pl (accessed: 06.01.2017).

Magdalena Kozioł–Jarosz, MEng. – Rybnik Engineering Center (REC) Clean Air Europe. Tenneco Automotive Polska Sp. z o. o.

e-mail: *MKoziolJarosz@tenneco.com*

Marek Brzeżański, DSc., DEng. – Faculty of Mechanical Engineering at Cracow University of Technology.

e-mail: *MBrzez@pk.edu.pl*

Article citation info:
KNEBA, Z., WAJS, J., TYSZKOWSKI, K., BIEŃKOWSKI, S. The influence of settable parameters of switching gasoline/LPG on exhaust toxic emissions. *Combustion Engines*. 2017, **170**(3), 100-103. DOI: 10.19206/CE-2017-316

Zbigniew KNEBA
Jan WAJS
Karol TYSZKOWSKI
Sylwester BIEŃKOWSKI

CE-2017-316

The influence of settable parameters of switching gasoline/LPG on exhaust toxic emissions

The main objective of the studies shown in the paper was to develop a proper strategy for settable parameters of ECU to decrease total emission of toxic components in composition of exhaust during a cold start phase. The experimental research has been performed for engine running at idle and for engine running on the chassis dynamometer (performing European Driving Test NEDC).

Key words: *alternative fuels, LPG, toxic emissions, ECU parameters, calibration*

1. Introduction

Increasing air pollution in cities forces to consider every possible way of its reduction. Although the share of motor vehicles as a source of particulates PM2.5 to PM10 is small – less than 10% [5], actions taken by local governments for limiting vehicular traffic are much easier than remodelling home heating. Current engines, both self-ignition and modern spark ignition units, emit solid particles in the exhaust fumes during the heating phase. While it is true that methods of purifying exhaust gas from particulates has been very well developed especially those which are based on removing particulars of large size by exhaust gas filtration, but still smaller particles are passed through the filters. Alternatives to traditional diesel or gasoline fuel systems are fuel gases like methane gas or propane and butane mixture [3, 6]. No solid particles are generated when these gases are burned. However, it should be notated that those gases are fossil fuels and their reserves are limited. With 100% usage of LPG will reduce the cycle by cycle variations within the cylinder and, improves the combustion characteristics and combustion stability [7].

In the presented paper, the authors focus on heating phase of a passenger car engine supplied by propane and butane (LPG) mixture. The aim of the experimental research was to determine the proper settable parameters of engine's control unit and their influence on toxic emission. However, fuel consumption and fuel costs were not a priority for the control strategy. The adhibition of particulate matter reducing fuels, according to the authors, is less expensive than replacing vehicles with new models with extensive but often failing exhaust systems.

2. Approval requirements for dual fuel gasoline and LPG supply systems

Emissions of toxic exhaust gas components are tested for LPG and CNG gas installations intended for vehicles of class M1 and N1 in accordance with regulation no. 83 of directive 70/220 / EEC [4]. For the Type I (NEDC) test on a chassis dynamometer, a reference car is designated. Other vehicles in which the installation will be implemented must have many features in common with the reference car. Measurements start with cold start at 20-30 °C ambient temperature. The engine of the vehicle adapted for LPG at the beginning of the test engine is fuelled with gasoline. It happens in some vehicles that time of engine running on petrol is extended to ease meeting emissions requirements . In order to counter this, Regulation 692/2008 requires that the running time of the petrol engine must not exceed 60 seconds. In this paper authors tried to examine fuel systems in winter conditions when that time is difficult to reach. Examinations are being conducted using two reference fuels of very different composition The properties of fuels are given in Table 1 [4]. The authors used regular petrol from petrol station.

3. The settable parameters of supply controller deciding of fuel switching

The change of combusted fuel occurs in modern systems automatically on the basis of the measured thermodynamic parameters in the gas fuel supply system and the parameters that influence on the flexibility of the fuel change. Parameters characterizing the state of the gas in the installation are:

- temperature of evaporator-reducer;
- temperature in the gas fuel rail;
- pressure in the gas fuel rail.

Additional switch decision variables are:

- delay in cutting off gasoline supply;
- the time elapsed since the start of the engine;
- current speed;
- recognition of whether the rotational speed is increasing or decreasing;
- delay in switching individual cylinders from petrol to gas.

The parameters listed above represent the majority of all parameters used in engine control unit. Although manufacturers only use some of them. Authors' studies are focused on evaporator reducer temperature because this parameter is the most commonly used and has the greatest influence on the correct change of fuel during heating.

4. Phenomena affecting on proper fuel supply during heating phase of engine

The most important process while cold starting of engine with spark ignition, is evaporating of the fuel and mixing it with air. This process is transient in relation to changeable air temperature and temperature of engine walls. In indirect injection engines when the engine is

warmed up, the evaporation takes place largely on the hot surface of the intake valve head. In the cold engine this process is limited. Such evaporation is only possible for petrol supply because the optimum spray on the valve head is provided only for petrol injector. In the classic implementation of the supply system for the evaporated LPG , calibrated nozzles are screwed into the collector wall (Fig. 1).

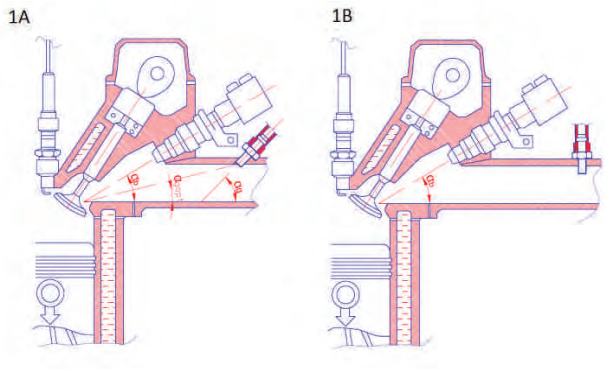

Fig.1. Placement of the gas inlet in the intake manifold: (1A) at an angle in the Al alloy manifold; (1B) perpendicular to the plastic collector

However, the best place for LPG nozzles is occupied by a gasoline injector. This creates the need to drive the gas from the solenoid valve to the nozzles trough the flexible conduit of thickness from ten to twenty inches. This solution is accompanied by unfavorable gas supply delays, bad angle of insertion of the stream into the collector, excessive distance from the nozzle to the inlet valve.

5. Engine starting temperature

The initial temperature of the engine coolant and the evaporator reducer, after a long standstill, are equal to the ambient temperature. At ambient temperature +20°C heat state of fully-heated engine requires 8 hours to return to its original state. If the standstill takes less, the liquid temperature is higher than the ambient temperature. The temperature drop over time is very dependent on the environmental conditions. The decrease in coolant temperature been investigated for standstill in open air winter conditions. The measurements done by author showed a significant influence of atmospheric conditions on the dynamics of liquid cooling (Fig. 2). The strength and direction of the wind is very important. Lesser is the effect of air temperature. At low temperatures, the cooling liquid expedites the heat more quickly to the environment, especially just after engine shut off because of the temperature difference. Then the cooling curves are approaching each other. The temperature drop in moderate weather conditions (–5 to +3ºC) in windless weather is around 35ºC in one hour. At the beginning of cooling about 30 minutes after stopping the temperature drops about 0.7ºC min and in the next half hour 0.5ºC/min. From Fig. 2 you can conclude that in winter conditions switching from petrol to gas will be almost instantaneous if the engine stop is less than an hour and a half. It would take about 6 hours to reach completely equal level out coolant temperature with ambient temperature in windless weather.

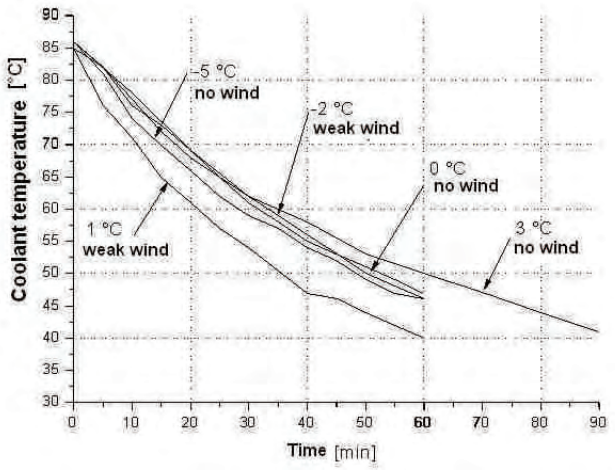

Fig. 2. Coolant temperature reduction after stopping Honda Accord 2.0 engine

6. The examination of times of fuel switching

During the winter, the engine starts at an unfavourably low temperature. To test the actual switching times from gasoline to evaporated gas, a test drive was performed with the registration of vehicle traffic parameters and operating parameters of fuel supply systems. The subject of research was Honda CRV 2.0 passenger car. For cold starts at 0° and 5°, ride on the same routes were recorded. In order to switch fuels without increased emissions of toxic compounds, especially hydrocarbons, the control of the composition of the mixture in the feedback loop must begin beforehand. The detection of this control was based on the registration of short-term fuel correction (STFT) included in the gas supply system. Table 1 lists the times that have elapsed since the start of the engine to reach the test condition. Figure 2 shows an example of the registration of the parameters listed in Table 1.

Table 1. LPG reference fuels [4]

Parameter	Unit	Fuel for light vehicles testing	
		fuel A	fuel B
Composition:			
content C3	%	30 ±2	85 ±2
content C4	%	rest	rest
content olefin	%	max. 12	max. 15
total sulphur content	mg/kg	max. 10	max. 10
Number of motor octane	–	min. 89	min. 89

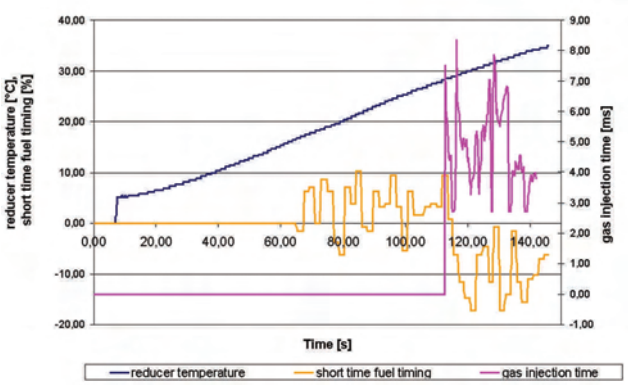

Fig. 3. Parameters related to fuel switching

7. Studies on emissions of toxic compounds during heating and fuels switching phase

As the main objective of this work is to investigate the change in the composition of the exhaust gases during the warm-up phase of the engine, series of cold start tests were performed. The cumulative emission of different exhaust components was measured. The subject was a Nissan Micra 1.2 passenger car. In the first stage of research the exhaust gas composition was measured during cold start phase only for engine running at idle. The results are shown in Figures 4 and 5.

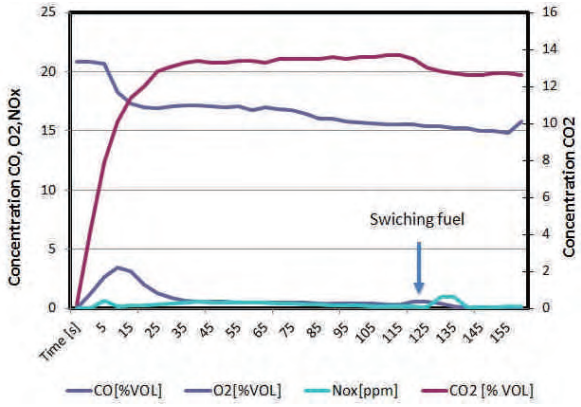

Fig. 4. Changes in the composition of toxic constituents and oxygen in the exhaust fumes during warm-up phase for engine at idle

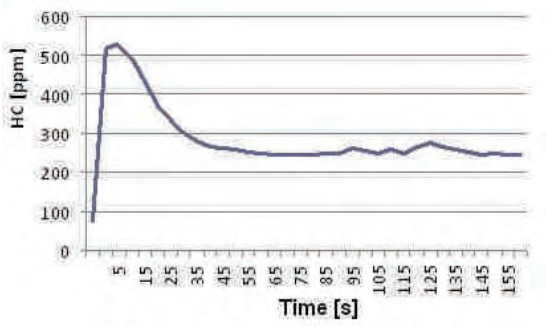

Fig. 5. Changes in the composition of hydrocarbons in the exhaust during warm-up phase for engine at idle

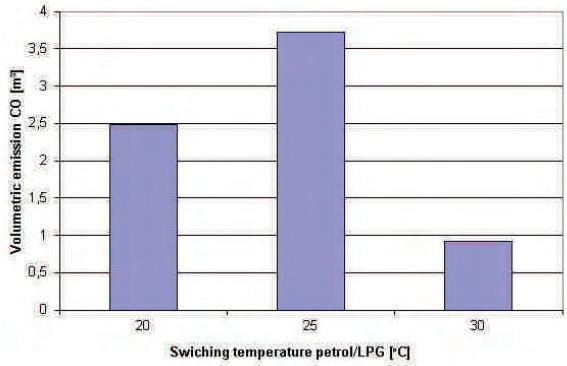

Fig. 6. Cumulative CO emissions in the fume gases from cold start to fuel switching moment

A typical phenomenon in the measurement is increased hydrocarbon emissions and reduced carbon monoxide emissions immediately just after fuel change. These elevated hydrocarbon emissions are the result of a lack of adequate mixing of the gas with low temperature air – are result of incomplete combustion.

The next stage of the study was the measurements on the chassis dynamometer during the implementation of the European type NEDC test. The composition of the exhaust gas was recorded during heating phase by setting the temperature of the evaporator reducer before each test as a decisive parameter for fuel's switch. Table 2 shows the switching times and total CO_2 emissions from the beginning of the test to fuel's switch moment

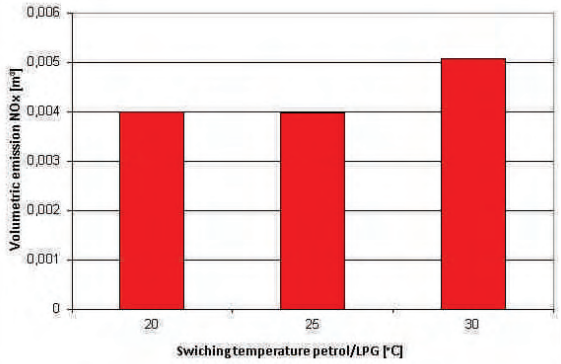

Fig. 7. Cumulative NOx emissions in the fume gases from cold start to fuel switching moment

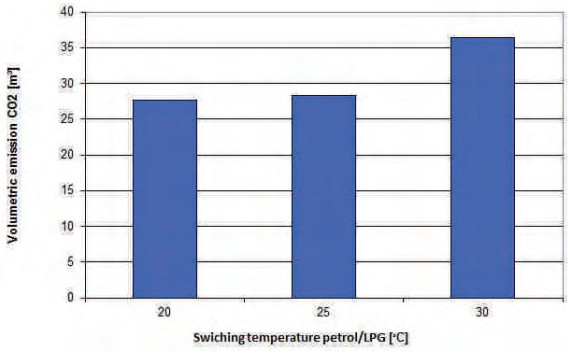

Fig. 8. Cumulative CO_2 emissions in the fume gases from cold start to fuel switching moment

Table 2. Running times of processes that determine effective switching of fuels

Starting temperature	0°C	5°C
Start-up of closed-loop fuel-air mixture control (STFT)	63 s	51 s
Reaching the temperature of evaporator reducer 25°C	94 s	75 s
Switchover of fuels	110 s	84 s

Table 3. Parameters related to the process of warming up the LPG supply system for switching from petrol to LPG – NEDC test

Adjustable petrol/LPG switching temperature	20°C	25°C (stand.)	30°C
Running time with gasoline	109 s	125 s	164 s
Change of CO emissions from baseline at 25°C	–33%	0	–75%
Change of HC emissions from baseline at 25°C	–12.7%	0	–47.4%
Change of NO_x emissions from baseline at 25°C	0%	0	+27.4%
Change of CO_2 emissions from baseline at 25°C	–2.5%	0	+29%

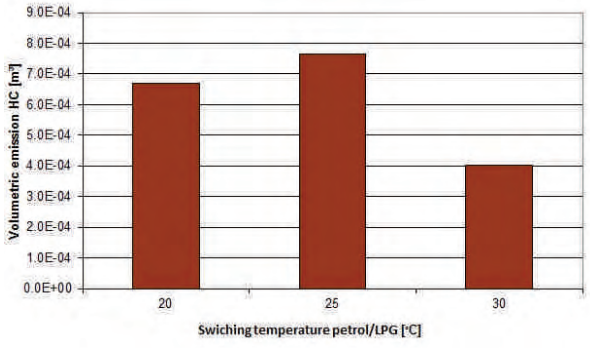

Fig. 9. Cumulative HC emissions in the fume gases from cold start to fuel switching moment

The test assumption was to set fuel switching temperatures that did not cause engine malfunction during the test run. The standard temperature has been set (temperature which is often chosen by installers) and two other one by five degrees higher and one five degrees lower than standard temperature. Based on the graphs, it can be stated that the reducer temperature settings for fuel switching in the range of 20-25°C do not significantly change the cumulative emissions of toxic compounds while engine working on petrol, except for carbon monoxide. Only increasing the switching temperature of reducer to 30°C results in a significant reduction in emissions especially of carbon monoxide and hydrocarbons.

8. Conclusions

Differentiated warm-up test of the propane and butane supply system were performed with a focus on the exhaust gas composition in this starting engine phase period. It has been found that the set-point (standard) switching temperature of reducer is not particularly beneficial due to the high emissions of carbon monoxide and hydrocarbons. Increasing the time of engine is running on gasoline result in reduction of toxic gas emissions and of course increasing the consumption of gasoline. Only nitric oxide emissions increase with engine's prolonged petrol working time. At low ambient temperatures cold start on petrol is significantly extending. For more general and up-to-date applications, similar measurements should be made using the WLTP test [2] for more cars at several starting temperatures.

Bibliography

[1] BIELACZYC, P., SZCZOTKA, A., PAJDOWSKI, P., WOODBURN, J. The potential of current European light duty LPG-fuelled vehicles to meet Euro 6 requirements. *Combustion Engines*. PTNSS-2015-3477.

[2] FUĆ, P., LIJEWSKI, P., ZIÓŁKOWSKI, A., SIEDLECKI, M. Trends in the type-approval regulations in terms of exhaust gas emissions for vehicles of category PC and LDV. *Combustion Engines*. PTNSS-2015-3365.

[3] MERKISZ, J., PIELECHA, I. Alternatywne napędy pojazdów. *Wydawnictwo Politechniki Poznańskiej*. Poznań 2006.

[4] MERKISZ, J., PIELECHA, J., RADZIMIRSKI, S. Pragmatyczne podstawy ochrony powietrza atmosferycznego w transporcie drogowym. *Wydawnictwo Politechniki Poznańskiej*. Poznań 2009.

[5] NIK: Raport Ochrona powietrza przed zanieczyszczeniami. 2014.

[6] ROMANISZYN, K. Alternatywne zasilanie samochodów benzyną oraz gazami LPG i CNG. *Wydawnictwo Naukowo-Techniczne*. Warszawa 2007.

[7] NAYAK, V., RASHMI, G.S., CHITRAGAR, P., MOHANAN, P. Combustion characteristics and cyclic variation of a LPG fuelled MPFI four cylinder gasoline engine. *Energy Procedia*. 2016, **90**, 470-480.

Zbigniew Kneba, DSc., DEng. – Faculty of Mechanical Engineering at Gdańsk University of Technology.

e-mail: *ZKneba@pg.edu.pl*

Jan Wajs, DEng. – Faculty of Mechanical Engineering at Gdańsk University of Technology.

e-mail: *Jan.Wajs@pg.edu.pl*

Karol Tyszkowski, MEng. – Faculty of Mechanical Engineering at Gdańsk University of Technology.

e-mail: *tyk3@wp.pl*

Sylwester Bieńkowski, MEng. – ELPIGAZ Sp. z o.o. Gdańsk.

e-mail: *dt5@elpigaz.com*

Article citation info:
KRZEMIŃSKI, A., KUSZEWSKI, H., LEJDA, K., USTRZYCKI, A. Effect of dodecanol additive on auto-ignition properties of diesel oil and ethanol blends. *Combustion Engines*. 2017, **170**(3), 104-107. DOI: 10.19206/CE-2017-317

Artur KRZEMIŃSKI
Hubert KUSZEWSKI
Kazimierz LEJDA
Adam USTRZYCKI

CE-2017-317

Effect of dodecanol additive on auto-ignition properties of diesel oil and ethanol blends

In order to increase the possibility of utilizing ethanol to propel the combustion ignition engines, ethanol or methanol blends with diesel oil or other similar fuels are used. However, ethanol has a low solubility index in diesel fuel especially at low temperatures, which requires the use of additives to improve this feature. The paper presents the results of comparative tests of the derived cetane number of diesel fuel blend with ethanol and the addition of dodecanol which is used to improve the miscibility of ethanol with diesel fuel. The results of tests indicate that the effect of dodecanol additive in blended diesel fuel-ethanol on the auto-ignition properties of such fuel is negligible.

Key words: *diesel fuel, ethanol, derived cetane number, alternative fuels*

1. Introduction

Introduction by the European Union of increasingly restrictive standards on toxicity of flue gases emitted by combustion engines necessitates the search for fuels that would be environmentally friendly and cost-competitive as compared with petroleum-based fuels. Alternative fuels having been tested in recent years are ethanol and methanol or their blends with diesel fuel. The following arguments support the use of alcohols as alternative fuels:

- they come from renewable sources,
- cheap and simple production process,
- possibility of reducing emission of solid particles.

The use of alcohols as a pure fuel for propulsion of compression ignition engines is not economical because it requires costly modifications of the propulsion system. In order to increase the ability of ethanol to propel this type of engines, ethanol or methanol blends with diesel fuel or other fuels are used [3]. As an engine fuel, ethanol is characterised by more favourable properties than methanol [10]. Unlike methanol, it is better blended with diesel fuel. Ethanol miscibility with diesel fuel is affected by the presence of water in fuel, even small quantity of which can cause a separation of blended components.

The use of a blended ethanol-diesel fuel as a fuel for the propulsion of compression ignition engines has some limitations, including among others lower viscosity compared to diesel fuel and relatively low stability and ability to blend with diesel fuel.

One of the additives that improves the stability of diesel fuel blend with ethanol and improves their miscibility is the dodecanol. It is characterized by good solubility in both of these fuels and its volume fraction in the blend may amount up to 3% [4]. However, it has a low pour point, which can lead to blend gelling [11].

One of the critical problems in the use of ethanol blends with diesel fuel is the very low susceptibility of ethanol to auto-ignition processes [8]. Fuel auto-ignition ability is determined by the cetane number (LC) or derived cetane number (DCN). The greater the value of these parameters, the greater the fuel susceptibility for auto-ignition. The following methods are used to determine the cetane number [9]:

- method consisting in calculating the value of derived cetane number based on the average value of ignition delay measured during fuel combustion in a constant volume combustion chamber,
- spectral analysis in the medium infra-red,
- method consisting in comparing the blends tested with analogous blends of known cetane number with a use of a test engine under standard test conditions.

The paper presents the results of the determination of derived cetane number of diesel fuel with different volume fractions of ethanol and for the same blends with the addition of dodecanol, which made it possible to determine its effect on DCN. In order to determine DCN value, the normative test method consisting in fuel combustion in a constant volume combustion chamber was used [1].

2. Test facility and test methodology

Determination of derived cetane number of diesel fuel and diesel fuel blend with ethanol with addition of dodecanol was conducted according to ASTM D7668 standard. This standard specifies accurately the determination of derived cetane number during the combustion of fuel in a constant volume combustion chamber.

CID 510 (Fig.1) was manufactured by Walter Herzog company by PAC (USA). This device meets the requirements of this standard and was used to determine the derived cetane number. In this device, determination of DCN is based on direct injection of fuel into a constant volume combustion chamber in which synthetic air is being heated. According to the standard procedure, a single measurement step consists of five initial combustion cycles and fifteen test cycles. Based on the test cycles, the ignition delay value (ID) and the combustion delay value (CD) are calculated. Triggering of the signal that controls the electromagnetic valve of fuel injector is assumed as the beginning of the auto-ignition delay period, while the increase of pressure in the combustion chamber over 0.02 MPa relative to the static pressure is assumed as the end of this period. The time between triggering of the signal that controls the electromagnetic valve of

fuel injector and the moment of reaching the half of the pressure increase in the combustion channel relative to initial pressure in the chamber is assumed as the combustion delay period. In the method discussed the injection time corresponds to duration of the injector control signal [8].

Determination of DCN value was carried out for seven samples with different volume fraction of ethanol in diesel fuel. Dodecanol additive was constant and amounted to 2%. Contaminated and dehydrated ethanol, the basic characteristics of which are shown in Table 1 was used for blends.

Table 1. Basic properties of ethyl alcohol [5]

Parameter	Value	Unit
Alcohol content at 20°C	99.9	%
Density	0.7897	g/cm^3
Esther content	< 0.2	mg/100 cm^3
Methanol content	< 0.6	mg/100 cm^3
Denatonium benzoate content	1	g/100 dm^3
Water content	<= 0.1	%(m/m)
Auto-ignition temperature	425	°C

Diesel oil used for tests could contain in accordance with the norm up to 7% FAME and up to 200 mg/kg water.

Selected dodecanol parameters are presented in Table 2. Determination of fuel samples is presented in Table 3.

Table 2. Basic properties of dodecanol [6]

Parameter	**Value**	**Unit**
Density at 16°C	0.9	g/cm^3
Water solubility at 25°C	0.037	g/l
Auto-ignition temperature	275	°C
Ignition temperature at 101.3 kPa pressure	134.8	°C
Melting/freezing point at 101.3 kPa pressure	24	°C

Table 3. Fuels used for auto-ignition tests

Fuel determination	Share % v/v		
	Diesel oil	Ethanol	Dodecanol
ON 100	100	0	0
ON+ET 5	95	5	0
ON+ET10	90	10	0
ON+ET15	85	15	0
ON+ET5+D	93	5	2
ON+ET10+D	88	10	2
ON+ET15+D	83	15	2

Fig. 1. Device for determination of derived cetane number CID 510

The prepared blends were stored in closed containers due to hygroscopicity of ethanol at room temperature of 20 ±2°C. Under these conditions, for 5% and 10% ethanol blends, homogeneous and clear blends were obtained. Whereas for a sample of 15% ethanol, it was not possible to obtain a homogeneous blend (Fig. 2).

The remaining samples were prepared by adding 2% (v/v) of dodecanol, maintaining the assumed ethanol content (5, 10 and 15%) and thereby reducing the content of diesel fuel in the sample.

Fig. 2. Diesel fuel blend with 15% volumetric content of ethanol

The use of dodecanol improved miscibility of ethanol with diesel fuel. For all ethanol contents in diesel fuel a homogeneous and stable blend was obtained. Figure 3 shows a comparison of diesel fuel with 15% (v/v) ethanol and 2% (v/v) dodecanol additive (1) and without dodecanol (2) at 20°C.

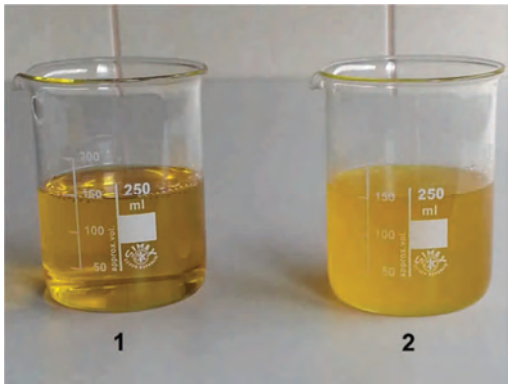

Fig. 3. Diesel fuel blend with 15% ethanol content: 1 – with dodecanol, 2 – without dodecanol additive

As one can see, the use of dodecanol has led to obtaining a homogeneous blend that has also been stable under conditions that cause the increase of water content in the sample.

3. Test results and their analysis

The results of determination of DCN for the blends tested. The graph shows that no blend of diesel fuel with ethanol, regardless of the fact whether dodecanol was added or not, has failed to meet the requirements in terms of derived

cetane number that cannot be less than 51 in accordance with PN-EN 590 standard. When adding the dodecanol, a slight increase in DCN may be observed, whereas the biggest increase (approx. 1.3%) was observed for blends with the lowest ethanol content amounting to 5%. Increasing the volume fraction of ethanol in diesel fuel resulted in a decrease in DCN. It has been also observed that with the increase in the volume fraction of ethanol, the effect of dodecanol additive on DCN decreases.

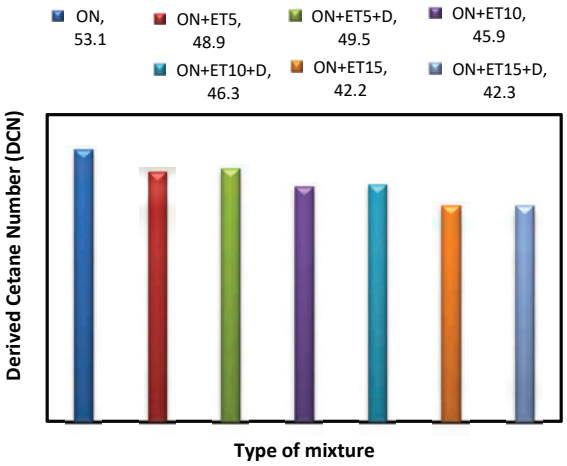

Fig. 4. DCN value for the blends tested

Figure 5 shows the results of auto-ignition delay (ID) for all the blends tested. As one can see, the use of dodecanol practically did not affect the value of this parameter.

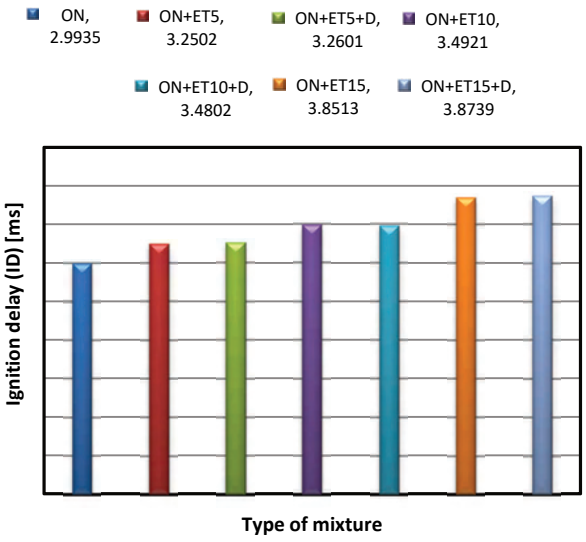

Fig. 5. Auto-ignition delay (ID) values for the blends tested

Figure 6 shows the results of combustion delay (CD) values. Along with the increase in ethanol volume fractions, the duration of this period increases and the use of dodecanol only results in a change of this parameter at the level not exceeding 1.5%. The biggest differences occur here, similarly as in the case of DCN, for a 5% ethanol blend.

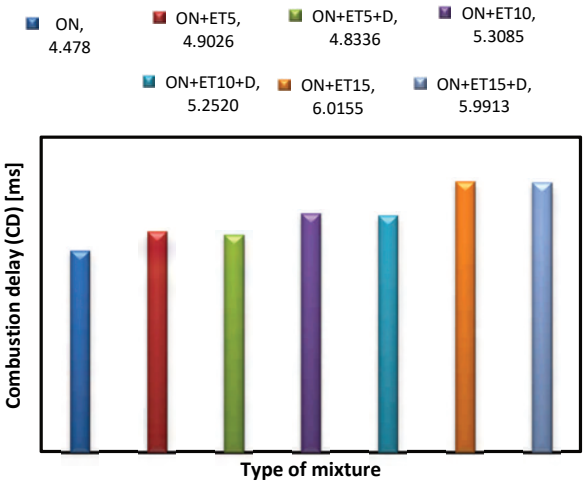

Fig. 6. Combustion delay (CD) values for blends tested

4. Conclusions

Addition of 2% (v/v) of dodecanol to diesel fuel blends with ethanol practically does not affect the DCN value. As can be seen from the above, in the applied concentration, dodecanol is a neutral additive with respect to auto-ignition properties of fuels.

Along with the increase in ethanol content in the blend with diesel fuel, the DCN value is being decreased. None of the tested diesel fuel blends with ethanol met the regulatory requirements for derived cetane value, which should amount to 51 according to EN-PN 590 standard. According to American ASTM D975 standard, the minimum cetane number is 40 [2]. Therefore, a blend containing up to 15% of ethanol meets the requirements specified in the above standard. The World Fuel Charter specifies the requirements for five diesel fuel categories from 1–5, for which the minimum cetane number is 48, 51, 53, 55 and 55, respectively [12]. The conducted tests of cetane number indicate that diesel fuel with 5% of ethanol meets the cetane number requirements for 1st category of diesel fuel. In order to allow for marketing of this type of fuel it is necessary to use the additives that would increase the DCN value in such a way that these blends could meet the current requirements for fuels for combustion ignition engines or change of regulatory requirements to the American model is needed.

The addition of dodecanol to blends of diesel fuel and dehydrated ethanol improves the miscibility of these fuels. It may be noticed in particular for higher concentrations of ethanol (15%) for which when preparing these blends some difficulties with miscibility and stability of this blend occurred. Already at a relatively high temperature (about 20°C), separation of blend components occurred, which is also demonstrated by test results presented in the study [7].

Dodecanol improves the miscibility of diesel fuel and ethanol and, what is important, remains neutral with respect to auto-ignition properties of these blends.

Bibliography

[1] ASTM D7668 – Standard test method for determination of derived cetane number (DCN) of diesel fuel oils – ignition delay and combustion delay using a constant volume combustion chamber method, 2014.

[2] ASTM D975 – standard specification for diesel fuel oils, 2014.

[3] CORKWELL, K.C., JACKSON, M.M. Lubricity and injector pump wear issues with e-diesel fuel blends. *SAE Technical Paper*. 2002, 2002-01-2849.

[4] DI, Y., CHEUNG, C.S., HUANG, Z. Experimental study on particulate emission of a diesel engine fuelled with blended ethanol–dodecanol–diesel. *Aerosol Science*. 2009, **40**.

[5] Karta charakterystyki: Alkohol etylowy całkowicie skażony. *Alpinus* 2016.

[6] Karta charakterystyki: 1-Dodekanol ≥98% do syntezy. *Carl Roth GmbH + Co KG*. Karlsruhe 2016.

[7] KRZEMIŃSKI, A., KUSZEWSKI, H., USTRZYCKI, A. Wpływ dodatku etanolu na lepkość kinematyczną oleju napędowego. *Monografia pod redakcją naukową K. Lejdy. Seria: Transport*. 2016, **7**, Rzeszów.

[8] KUSZEWSKI, H., JAWORSKI, A., LEJDA, K. et al. Badania pochodnej liczby cetanowej mieszanin oleju napędowego z etanolem. *Silniki Spalinowe*. 2015, PTNSS-2015-3488.

[9] KUSZEWSKI, H., JAWORSKI, A., LEJDA, K. et al. Oznaczanie pochodnej liczby cetanowej wybranych paliw na podstawie spalania w komorze o stałej objętości w aspekcie ich zastosowania w silniku o zmiennym stopniu sprężania VCR. *Mechanika Czasopismo Techniczne*. 2012.

[10] LAPUERTA, M., GARCIA-CONTERAS, R., CAMPOS-FRNAANDEZ, J., DORADO, M.P. Stability, lubricity, viscosity, and cold – flow properties of alcohol – diesel blends. *Energy Fuels*. 2010, **24**.

[11] LIU, H., HU, B., JIN, C. Effects of different alcohols additives on solubility of hydrous ethanol/diesel fuel blends. *Fuel*. 2016, **184**.

[12] Worldwide fuel charter. Fifth edition. September 2013.

Artur Krzemiński, MEng. – Faculty of Mechanical Engineering and Aeronautics at Rzeszów University of Technology.

e-mail: *ArtKrzem@prz.edu.pl*

Hubert Kuszewski, PhD – Faculty of Mechanical Engineering and Aeronautics at Rzeszów University of Technology.

e-mail: *HKuszews@prz.edu.pl*

Prof. Kazimierz Lejda, DSc., DEng. – Faculty of Mechanical Engineering and Aeronautics at Rzeszów University of Technology.

e-mail: *KLejda@prz.edu.pl*

Adam Ustrzycki, DEng. – Faculty of Mechanical Engineering and Aeronautics at Rzeszów University of Technology.

e-mail: *AUstrzyc@prz.edu.pl*

Article citation info:
BRZEŻAŃSKI, M., MARECZEK, M., MAREK, W. et al. The realized concept of variable chemical composition fuel gas supply systems, for internal combustion engines. *Combustion Engines*. 2017, **170**(3), 108-114. DOI: 10.19206/CE-2017-318

Marek BRZEŻAŃSKI
Michał MARECZEK
Wojciech MAREK
Tadeusz PAPUGA
Marek SUTKOWSKI

CE-2017-318

The realized concept of variable chemical composition fuel gas supply systems, for internal combustion engines

The article presents the results of industrial research, of mixer and injection gas supply systems of internal combustion engines, for fuel gas time-varying chemical composition. The publication presents an innovative injection system working by patent PL 222462, and obtained operating characteristics of power generators with the implemented system. In addition for comparison, the article presents the results of research a generator set with implemented an innovative system of the mixing gas fuel supply, with variable chemical composition.

Key words: *combustion engine, concepts of supply and control systems, post processing gases*

1. Introduction

In the era of the rationalization of the use of energy on strives for the smallest loss of energy at every stage of the production processes and exploitation activities. This also applies to the manufacturing processes in which different types of gases are used, including those that are energy carriers. For example, gases of this type of are used on a large scale in industrial processes carried out in the chemical industry, where a large part of them after utilization is post-production waste. In many cases, this creates environmental problems, because the waste gases composition is often very diversified and variable in time. This often does not allow for their further processing or use in standard combustion in heating systems. Only in very few cases their use possible in some systems by mixing the gaseous waste for example with natural gas. Therefore, waste post-processing gases, are usually subjected to utilization by burning flares, which involves not only the energy losses, but often also with environmental charges for heat and combustion gas emission.

At the Institute of Automobiles and Internal Combustion Engines there were developed innovative concepts for the use of various types of post processing gases with variable chemical composition, as fuel for internal combustion engines, used primarily to drive generators. This is a complex task, especially in the aspect of the need to preserve the constant speed of engine collaborated with a generator. In conventional reciprocating gas engines power system, a sudden change of the chemical composition of the fuel, which is usually accompanied also by changing of the calorific value of the incoming mixture, means a loss of control over the system speed and stability, what enables the procedure to stop the engine operation. These are the reasons due to which the producers of this type of engines do not provide for the possibility of their feeding with fuel, whose chemical composition change significant in a short period of time. The problem is also the use of fuels of low calorific value, compared to conventional fuels, such as for example: natural gas, because the intended parameters of the engine typically requires, the use of engines of large displacement and number of cylinders. It follows that, the greater cost of the investment and less total efficiency of the energy system, due to a greater share of mechanical power loss of engine, relative to its effective power. The other problem determining the possibility of post-processing gases engine feeding, are thermodynamic parameters of fuels and their resistance to detonation. In some industrial processes, particularly chemical, there are fairly large changes in pressure and temperature of the reagents, which also has a significant effect on the thermodynamic state of waste gases.

All of these features of post-processing gases, constitute a substantial barrier to their use as fuel for reciprocating internal combustion engines. Many renowned manufacturers of engines fed with gaseous fuels exclude the possibility of their exploitation for this type of fuels, and requirements usually put at first the condition of chemical composition constant parameters, and thermodynamic state of fuel. For this reason, concepts of waste fuels supply system developed at the Cracow University of Technology, proven in the laboratory and industrial applications, can be innovative considered.

2. General concepts of engines feeding systems with post processing gases

Standard gaseous fuel, used to feed the reciprocating internal combustion engines is usually natural gas. Many companies offer this type of industrial and traction engines on the market. Developed in Cracow University of Technology (CUT) concepts of post processing gas engines feeding systems, open up a new area of the use of these fuels for energy purposes. They shall take into account all of characteristics of these fuels, mainly the variability of their parameters in short time intervals and in particular: the chemical composition, the thermodynamic state and resistance to detonation.

The first of the systems was developed for industrial post-processing gases, from the chemical plant, which are available at a pressure greater than 3 bars. For this type of cases, the gas injection supply system was developed. It consisted of an innovative power and igniter control system, which took into account both the nature of the fuel,

and the volatility of its basic parameters. This system was subjected to laboratory tests in the CUT, and then had been verified in industrial research carried out in a pilot installation, located in one of the "AZOTY S.A." plants. These tests, carried out on the post-processing waste gases that contain a large share of hydrogen, have been launched in March 2014, and in continuous mode are still carried out. Power system was patented under the name: "Method to control regulation parameters in internal combustion engine with spark ignition Patent: PL 222462 B1-WUP 07/16, of 29. 07. 2016.

The second of the developed systems, being in the laboratory phase, is designed to feed the reciprocating internal combustion engines with gaseous fuels, which are available under the pressure close to ambient pressure. This group includes a number of flammable gases from industrial processes or processes of biological decomposition of organic substances. Among them may be mentioned e.g.: biogas, fermentation gas, carbon monoxide, mining gases, metallurgical blast furnace gas or coke oven gas. Developed system can be adapted to feed with one of the fuels or a mixture of gases composed in any proportions.

Total efficiency of engines equipped with developed control systems, to a large extent depends on the calorific value of the fuel and its resistance to detonation. It results among others from the participation of the mechanical losses in the engine, in relation to the achieved work parameters for the specific type of fuel.

Both systems have been adapted to engines that drive generators of electricity, where an extremely important parameters are to maintain constant speed and quick response system to load changing. These parameters are included in the relevant industry standards, and their meeting is a prerequisite for admission of power generators to service. Developed control systems meet the above requirements, also in the event of substantial changes of parameters of the supplied fuel, among others such as: chemical composition, calorific value, or resistance to detonation. In this scope, the created systems provide innovative solutions, which have not been used in products from reputable companies that producing power generators.

3. The concept of the engines feeding systems witch post-processing gases

3.1 General assumptions

The first realized task connected with the power of internal combustion engines with post-processing gases with changing parameters, was to develop a system that would allow the use of various types of flammable gases, which are waste products from chemical processes carried out in the installation of butanol, isooctanol and aldehydes, located in one of the "AZOTY S.A." plants. According to the factory specifications, the main component in the offered combustible gases, was industrial hydrogen, whose volume share was on average 60 to 90%, then volatile hydrocarbons, carbon monoxide and methane, and the whole was available in the form of mixture with other ingredients. In practice, the chemical composition of the offered gases, subject to rapid and significant change, and volume share of hydrogen often exceeded 90%.

The aim of the research was to develop the engine power and control system, using this type of fuel and adjust it to the requirements arising from the regulations allowing power generators into operation and providing them with the most favourable working conditions. For this reason, it became necessary to identify new issues related to engine cooperation with power generator and also achievement in research as good as possible, working and ecological parameters of engine. The study focused on determining the most favourable energy performance and emission of toxic components, for an engine running at a constant speed of 1500 rpm under changing load. This type of conditions corresponds to the work of the internal combustion engine in the power-plant generator.

Among the control parameters of the tested engine that had to be matched to the type of tested fuel, were belonged primarily: ignition timing and the air excess number.

Both of these parameters have a very significant impact on the process of combustion in the cylinder of the engine, hence both the value of the obtained energy performance and emission of toxic components. In addition, they affect the exhaust gas temperature intensively – directly through the combustion temperature and indirectly, due to the combustion process. It is important to place and time of heat release from the fuel. In the case of research this is crucial due to the raised by engine manufacturer criterion of the maximum value of exhaust gas temperature. In the case of the tested engine exhaust gas temperature may not exceed 700 C, due to the thermal strength of the turbocharger (turbine). This is relevant in determining the maximum power of engine fed with the given type of fuel. In addition, both the value of the air excess number, and especially the angle of ignition timing have a close relationship with the occurring phenomenon of the knock. For this reason, for the test fuel and for each engine operation (load) point, both of these regulatory parameters were set individually.

In the conducted analyses, three selection criteria of engine regulation parameters were assumed, for which the engine load was selected, when engine was powered by a particular fuel:

- max. engine exhaust gas temperature may not exceed 700 C,
- may not be an anomaly in the form of a knocking combustion,
- may not be the phenomenon of reverse flame to the intake manifold.

During the laboratory tests the value of concentration of: carbon monoxide (CO), hydrocarbons THC, nitric oxide, carbon dioxide CO_2 and oxygen O_2 have been studied and recorded. In addition, the impact of the test fuel to other engine parameters such as torque and power, fuel consumption, total efficiency, air excess coefficient and exhaust gas temperature have been also studied and recorded.

3.2 Research facility

As a laboratory investigation object, a 6-cylinder, supercharged MAN E2876 LE302 engine with a displacement Vs = 12.82 dm^3 was selected. The engine, which develops 200 kW of effective power, has a spark ignition system in its factory configuration and is fed with natural gas by use of air-gas mixer and designed to drive an electric current

generator. Hydrogen-fuelled engine laboratory tests were carried out at a special test stand at the Internal Combustion Engines Chair Laboratory at Cracow University of Technology.

The choice of this unit was resulted mainly due to the fact that MAN offered a 12-cylinder engine with the same geometric cylinder dimensions. Because the research program's assumptions envisaged the development of a single-cylinder power conversion concept, the modular design of the 6-cylinder and 12-cylinder engine fulfilled the stated condition. All elements of the developed concept of electronically controlled post-processing gas injection system as well as the control system itself were made at the Cracow University of Technology. Equipping of the power generators supplied by HORUS-Energia with all the elaborated and made elements of the system was made also here. After these operations, the aggregates were transported to a specially constructed facility, located in one of the "AZOTY S.A." plants. Fig. 1 shows the aggregates in enclosures during equipping with elements of the system in front of the Engines Laboratory of Cracow University of Technology.

Fig. 1. View of the power-generator set while equipping with elements of the electronically controlled fuel supply system of post-processing gas, in front of the building of Engines Laboratory of Cracow University of Technology

3.3 Control system

Practical implementation of the tasks required the design and construction of a special fuel system with a modular configuration similar to Common Rail. The gas fuel feeding system consists of a fuel rail divided into segments corresponding to the number of cylinders. Each segment is equipped with two electromagnetically controlled injectors, which facilitates precise fuel dosage control depending on engine load. There were used standard commercially available natural gas injectors that are used in automotive fuel supply installations. For the purpose of the project, they were modified by increasing the gaseous fuel flow rate and calibration was performed next. Each of the injectors was individually controlled by the control signal, allowing for individual adjustment of the air excess number in each cylinder. The ignition system has been significantly modified, providing the possibility of individually adjusting the ignition angle in each of the engine cylinders. The value of the ignition advance angle was dependent on the signals from the knock sensors, in which each of the cylinders was equipped. The fuel supply and ignition system of the 6-cylinder engine are shown in Figure 2 and the 12-cylinder engine in Figure 3.

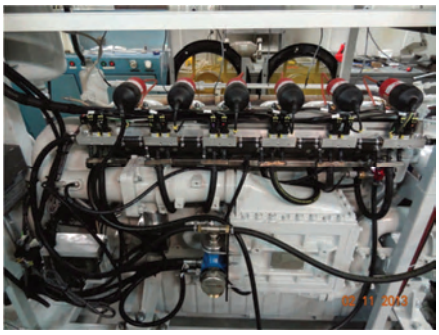

Fig. 2. Ignition system and post-process gas fuel supply system of 6-cylinder engine

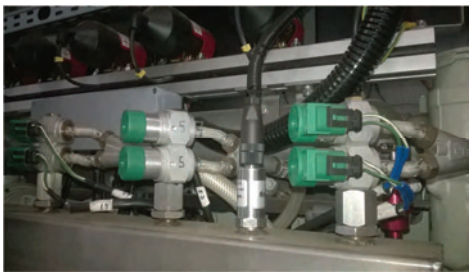

Fig. 3. Post-process gas fuel supply system of 12-cylinder engine

Original spark plugs, recommended by MAN during natural gas supply, were replaced by spark plugs where the spark channel of spark plug was more put out into the combustion chamber. This change has been made on the basis of experimental research and has resulted in a significant improvement of ignition initiation of fuel mixtures. This change was especially important when the engine was powered with a very lean air-gas mixture.

At Cracow University of Technology, a special controller was designed and manufactured to control the most important engine regulation parameters, such as: gaseous fuel dose, ignition angle, throttle opening, and the value of air excess number. This programmable engine controller was developed in LabView. The modular nature of the power and ignition system enabled the combustion process to be monitored in each of the cylinders. This was accomplished by measuring the exhaust gas temperature, individually measured by thermocouples, located in the outlet channel of each cylinder, directly at the exhaust gas outlet from the cylinder head. The individual measured exhaust temperature measured uniquely identifies the amount of heat generated in each cylinder, and is also a diagnostic tool that informs about combustion disturbances, such as chronic combustion effected by too lean an air-gas mixture, or misfire. In addition, the controller, in adaptive mode, continuously cooperated with knock sensors so and thanks to that it uniquely determined the knock limit for each cylinder in all analysed engine operating conditions. This type of supervision and regulation has allowed for high energy conversion efficiency in each of the engine cylinders. A control panel has been built into the control system, the external view of which is shown in Fig.4.

Fig. 4. General view of the control panel of the programmable controller

3.4 Operating industrial research

Based on the developed concept of engines injection feeding with post processing gases, at Cracow University of Technology was done the project, components of the system were made and three engines have been equipped with them: one 6-cylinder with a nominal power of 200 kW and two 12-cylinder engines with a nominal power of 400 kW. The total rated power of three motors prepared for exploitation tests was 1 MW, assuming the supply of natural gas, while the power output at the other chemical compositions feeding was respectively lower. The engines, after being equipped with the developed post-processing fuel supply system, were connected to the generators and placed in the HORUS-Energia unit. In such form, the units, marked with the symbols AK-1, AK-2 and AK-3, were put into operation in February 2014 in a facility, located in one of the "AZOTY S.A." plants. Up to now, engines run continuously, depending on the supply of gaseous post-processing fuel, as source of generating electricity and heat. During the operation a number of studies were conducted, the results of which confirmed the preliminary assumptions of the developed concept. Figure 5 shows the aggregates working in a specially built facility, located in one of the "AZOTY S.A." plants.

Fig. 6. Power generators with electronically controlled, post-processing gas injection system, located in one of the "AZOTY S.A." plants

Measurements made during the operational tests of the 6-cylinder AK-3 engine showed that in the case of waste gas fuelling, with hydrogen content of about 60%, it is possible to obtain 167 kW of apparent power. With respect to the internal combustion engine of this aggregate, a predicted cylinder power of about 30 kW was obtained. The corresponding fuel consumption was about 1 Nm^3/kWh. According to exploitation investigations, such level of performance from the cylinder is only obtainable in the case of an AK3 engine. However, under standard operating conditions, this unit was able to operate safely with a load of only 140 kW due to the limitations of peripheral equipment. For AK1 and AK2 engines with 12-cylinder engines under comparable operating conditions as for the AK3, 260 kW apparent power was obtained. Similarly to the AK3, under standard operating conditions, this unit, due to the limitations of peripheral equipment, was able to safely load up to 230 kW.

During the 8-month exploitation tests, the balance sheet was as follows:

AK1 – 3992 h, energy – 816 MWh, average load – 204 kW
AK2 – 3490 h, energy – 668 MWh, average load – 191 kW
AK3 – 3938 h, power – 470 MWh, average load – 119 kW

This data covers the entire exploitation period, hence the calculated average load of the individual aggregates is below the nominal value obtained currently during continuous operation.

The most spectacular effect of the use of high-hydrogen waste gaseous fuel was to obtain practically zero emissions of toxic exhaust gas components. Control measurements made during the operation of the 6-cylinder AK3 engine in a variable load field fully confirm the pro-ecological usefulness of such waste fuels. At the operating point of the engine, which corresponded at the given exploitation conditions a maximum value of 167 kW, only 0.3% v/v CO_2 and 59 ppm NO_x were found in the exhaust gas. The result was a combination of both the chemical characteristics of the fuel used and the way in which the mixture composition and engine power were controlled. The nominal 1MW power of three aggregates was determined by natural gas and so a fuel with high knock resistance and a calorific value of about 36 MJ/Nm^3. The operating parameters achieved by the engine depend obviously on the characteristics of fuel that power the engine. The fuel with hydrogen volumetric share of about 94% (by chromatographic analysis) has a calorific value of about 11 MJ/Nm^3. The AK3 generator of 200 kW rated power fed with this fuel has an apparent power of 167 kW and an active power of 162 kW with gas consumption of 44.6 m^3/h, which gives 165.5 Nm^3/h. The energy stream in this fuel is 506 kW, so the efficiency of electricity generation is 0.33.

The obvious effect is also the extremely low carbon dioxide emissions per unit of produced energy. On average, over a period of supervised operation of the aggregates, a value of slightly over 25 kg CO_2 per 1 MWh of produced energy was obtained, which is an incomparably less, than the emission achieved in electricity generated by coal-fired power plants, which can be as high as 1000 kg of CO_2 per 1 MWh. This extremely beneficial effect results from feeding the aggregates with fuel of high hydrogen volumetric share and very low carbon share, which is a characteristic feature of used waste post processing fuels.

The obtained engine working parameters, should be considered to be a great achievement on scientific, technical and economic scale if the properties of the fuel are taken into account. This system as so far has been working well correctly with very high variability of fuel composition and does not cause exploitation problems which positively pays for its further industrial applications.

3.5. Operational verification investigations during coke oven gas feeding

An additional element of verification of the innovative concept of the engines gas fuel supply systems, in which engine parameters adapts to the fuel properties was to carry out a coke oven gas feeding test. It is a gaseous fuel with a limited range of application for feeding engines mainly due to its physicochemical properties and constant impurities. In the conducted research at the "AZOTY S.A." plants, the coke oven gas was derived from the factory network and before being supplied to the engine was dried and cleaned in the installation developed by WT & T company.

Measurements made on an AK-3 engine equipped with a 6-cylinder engine. When powering the engine with coke oven gas with a hydrogen content of 50–60%, it was possible to obtain apparent power up to 202 kVA, which corresponded to the designed cylinder power at 35 kW. The corresponding unit consumption of fuel was about 0.6 Nm^3/kWh, corresponding to 33% efficiency of electricity generation. Performance tests were carried out over a period of 100 hours, while in continuous operation the aggregate was loaded at approximately 50% of the maximum value obtained in the measurements, which resulted from the constraints of the systems collaborating with the engine. On the basis of the measurements and results of earlier work, it can be predicted that under normal operating conditions, the aggregate can be safely loaded up to approximately 140 kW, due to the limitations of peripheral equipment. The significant effect of coke oven gas application is the very low emission of exhaust gas toxic components (Table 1).

Table 1. Selected values of concentration of exhaust gas components, during coke oven gas engine fuelling

Volumetric concentration of exhaust gas components (fuel – coke oven gas)								
No.	N_{effect} [kW]	N_{electr} [kW]	CO [%]	CO_2 [%]	HC [ppm]	O_2 [%]	NO_x [ppm]	λ
1.	200	196	0.02	4.4	6	9.2	139	1.70
2.	183	181	0.02	4.4	6	9.0	137	1.70
3.	162	160	0.02	4.4	7	9.1	130	1.70
4.	145	142	0.02	4.4	7	9.1	123	1.70
5.	124	122	0.02	4.4	7	9.1	138	1.70
6.	103	102	0.03	4.3	8	9.2	134	1.70

Control measurements made during operation of the AK3 aggregate in variable field of load, fully confirm the pro-ecological usefulness this type of fuel. At the operating point of the engine, which corresponded to the maximum operating conditions of 200 kW, only 0.02% v/v CO, 4.4% v/v CO_2, 6 ppm HC and 139 ppm NO_x were found in the exhaust gas. Almost identical results were recorded during engine operation in a 100-hour exploitation cycle. The result was a combination of the chemical characteristics of the fuel that was used, and the way in which the mixture composition, and engine power were controlled.

Studies have also shown that the use of coke oven gas as a fuel for generation of electricity has very good results in reducing carbon dioxide emissions per unit of produced energy. In this field, 677 kg CO_2 per 1 MWh of generated energy was obtained, while the value of this indicator for coal-fired power plants can be up to 1000 kg CO_2 per 1 MWh.

Verification studies have fully confirmed the design and operational features of the developed power and control concept, especially considering the "fuel flexibility" of the generating set, which can equally well be powered by natural gas, coke gas and postprocess gas. The obtained indicators for the tested cogeneration unit should be considered to be a significant achievement.

4. The concept of the gas fuelling mixer system

A large number of flammable gases are available in the economy, available at pressure close to ambient pressure. Preparing these gases for use in the above-mentioned injection power system requires compressing them to the required pressure of about 3 bars, which is not cost-effective and rationally justified from the point of view of the efficiency of the whole power system. Therefore in the Cracow University of Technology in cooperation with HORUS-Energia firm, an innovative, electronically controlled mixing system of various types of gaseous fuels, for powering the reciprocating combustion engines was developed. This system is currently undergoing laboratory testing, and the concept itself is being prepared to patent pending.

The study was conducted on the same type of 6-cylinder engine that was subjected to extensive laboratory testing during development of the injection fuelling concept described above. This makes it possible to compare both the concepts of power systems and the control of important engine parameters.

The developed electronically controlled mixer system has similar utility features and has a similar control system as the mentioned injection power system. In addition, it has the ability to simultaneous feed the engine with fuels of different physic-chemical characteristics and derived from different sources. It is very important possibility to attach another fuel with other properties to the feeding system without necessity to stop the engine. The developed concept has been adapted for engines that work with electric generators that maintain the condition of steady rotational speed and a fast response of the system to load change. These parameters are included in the relevant industry standards and their fulfilment is a condition for the admission of generators to operation.

Figure 6 shows the test stand at HORUS-Energia firm where the response of the developed control system to the rapid change of engine load parameters or to the change in the engine mixture parameters was investigated. The evaluated effect was the change of electrical quantities that characterize the operation of the generator.

Fig. 6. View of a part of a laboratory test stand with a electric current generator – Horus Energia

In the choice of fuel for combustion engines, the problem is often too low calorific value of fuel because in such cases a high share of engine power losses relative to its effective power results in a reduction of the total efficiency of the power generator unit. Therefore the concept of the system provides for the possibility of co-fuelling and co-firing of fuels with very different calorific values or very different knock resistance. In this range a study of the developed concept has been carried out to investigate the acceptable calorific values of the supplied gas at which the generator engine is able to operate properly.

In laboratory tests, the following gaseous fuels were selected:

– natural gas with carbon dioxide,
– natural gas with propane,
  propane with acetylene.

In the first phase of laboratory tests, the minimum calorific value of gas which guarantees stable engine operation was determined. The studies were conducted for natural gas mixtures with carbon dioxide with different proportions of these components, resulting in different fuel calorific values. The ability of the control system to match the engine's control parameters to the changing calorific value was examined.

The next phase of research concerned the so-called high calorific gases, composed for research purposes in different proportions from natural gas and propane. This part of the study was designed to investigate the limitations associated with the thermal load of the engine components, including mainly turbocharger.

The aggregate reaction to gaseous fuels with different knocking tendencies was also investigated. At this stage of the study, a mixture of technical propane and acetylene was used, i.e. an unsaturated hydrocarbon with a very high tendency to knock. In this case, the tests were carried out when the engine was fed with a mixture of these different acetylene gases to determine the reaction of the developed control system to change of the value of octane (methane) number of the fuel, which was used.

The main objective of the described laboratory tests was to determine the limits of the parameters of the fuel used which would be accepted by the developed electronic control system, and also meet all the conditions permitting the fuel to be supplied to the combustion engine.

To determine the dynamic characteristics of aggregate during the load change (which is one of the main evaluation parameters of the fuel supply system quality), only one electric current phase of the generator has been recorded during methane powering. Therefore, to determine the amplitude and frequency, it was necessary to reproduce artificially the voltages of the remaining phases and, in principle, the second voltage vector. This was possible with the assumption of symmetry of phase voltages. An example of the characteristics of the change in the electrical parameters produced in an aggregate equipped with the described power and control system, during a rapid increase in the generator load from 30 to 110 kW, is presented in Fig. 7.

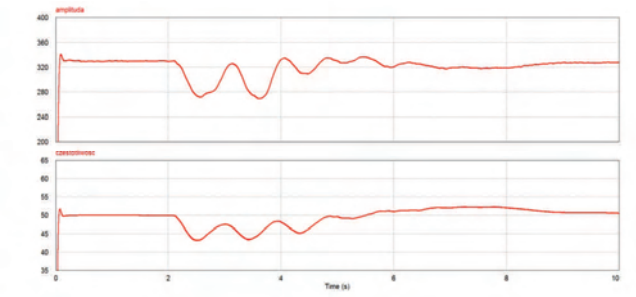

Fig. 7. Changes in generator current parameters with load increase: 30-110 kW

The graph shows that within about 4 seconds after the change of load the basic electrical parameters of the aggregate returned to nominal values. Accordingly, it can be estimated that the developed concept meets the requirements for such generators. Many of these characteristics were made during the change (increase or decrease) of the load, and also during the change of fuel parameters such as calorific value, octane (methane) number or change of thermodynamic parameters. The results of this type of measurement have fully confirmed the usefulness of the developed concept of electronically controlled mixing system of fuelling of reciprocating internal combustion engines with various types of gaseous fuels.

The developed concept can be intended to feed internal combustion engines with all types of gaseous fuels that are available at pressures close to ambient pressure. In practice, this group includes numerous flammable gases from industrial processes or biological decomposition processes. Among them can be mentioned e.g. biogas, fermentation gases, carbon monoxide, mining gas, metallurgical blast furnace gas or coke oven gas. An important feature of the developed concept is the possibility of supplying the engine with one of the mentioned fuels or a mixture of gases, created in any proportions.

5. Conclusions

The concepts of innovative power supply and control systems for internal combustion engines, developed in the Cracow University of Technology and in HORUS-Energia firm, designed for use on various types of gaseous fuels, have been made and put into operation. The experience gained during laboratory testing and industrial verification of these concepts allow us to formulate the following key findings:

1. Laboratory tests and industrial verification tests have demonstrated the usefulness of the developed concepts of power supply and control systems for internal com-

bustion engines designed for operation on various types of gaseous fuels for energetics purposes.
2. The developed concepts are highly flexible in relation to the fuels that are used and at the same time ensure their best energetic utilisation thanks to the system of current analysis and optimization of the most important engine parameters. Modern technical and programmatic tools are used to create a new quality in the discipline related to the design and operation of internal combustion engines.
3. The results of laboratory tests have shown that it is possible to significant extend the types and kind of gaseous fuels that can successfully be used to feed the internal combustion engines.
4. Proper operation of reciprocating engines for different types of gaseous fuels is the result of adopting and applying technical solution much more modern than the feeding and control systems used so far.
5. Much attention was paid to the selection of regulatory parameters including such ones as the ignition advance angle and the air excess number, resulting in favourable operating and ecological indicators of the engine when fuelled with different fuels.
6. The results of the research allowed defining the strategy of fuel supply and control of engine parameters, determining limit values of physic-chemical properties of applied fuels which can be accepted from the point of view of the correct operation of the engine and values of ecological parameters.
7. The obtained scientific and cognitive effects as well as the positive effects of industrial verification tests indicate the existing development potential and the need to seek new concepts of development work in the field of energetics. This type of work meets the postulates of sustainable development which in the energy sector concern mainly rationalizing of energy consumption by reducing losses. In the case of the conducted works the most important result is the energetic utilisation of various types of energy sources in the form of gaseous post-process fuels which have been so far in large part unproductively lost.

Bibliography

[1] BRZEŻAŃSKI, M., MARECZEK, M., MAREK, W., PAPUGA, T. Determination of operating parameters of industrial engine fuelled with post processing gases with high hydrogen content. *IOP Conference Series*, KONMOT 2016, Kraków 2016.

[2] BRZEŻAŃSKI, M., MARECZEK, M., MAREK, W., PAPUGA, T. Określanie parametrów ekologicznych stacjonarnego silnika spalinowego zasilanego różnymi paliwami. *Zeszyty Naukowe Instytutu Pojazdów*. Warszawa 2014.

[3] BRZEŻAŃSKI, M., CISEK, J., MARECZEK, M. et al. Investigation of the combustion engine fuelled with hydrogen. *Combustion Engines*. 2013-SC-192.

[4] BRZEŻAŃSKI, M., CISEK, J., MARECZEK, M., et al. Investigations of the fuel supply system of stationary combustion engine fed with natural gas. *Combustion Engines*. 2013-SC-192.

[5] BRZEŻAŃSKI, M., CISEK, J., MARECZEK, M. et al. Investigation of the combustion engine fuelled with hydrogen and mixed n-butanol with iso-butanol. *Combustion Engines*. 2013-SC-194.

[6] BRZEŻAŃSKI, M., MARECZEK, M., MAREK, W., PAPUGA, T. Zastosowanie odpadowych produktów przemysłu chemicznego w energetyce. *III Konferencja Naukowo-Techniczna, Współczesne Technologie i Urządzenia Energetyczne*. Kraków 2013.

[7] BRZEŻAŃSKI, M., MARECZEK, M., PAPUGA, T. Conception of utilization of the heat from cooling system to increase of the work and ecological parameters of the combustion engine. *Combustion Engines*. 2011-SC-113.

[8] BRZEŻAŃSKI, M., MARECZEK, M., MAREK, W., PAPUGA, T. Sposób sterowania parametrów regulacyjnych w silniku spalinowym o zapłonie iskrowym. *Opis Patentowy* nr PL 222 462 B1. WUP 07/16.

Marek Brzeżański, DSc., DEng. – Faculty of Mechanical Engineering at Cracow University of Technology.

e-mail: *MBrzez@pk.edu.pl*

Michał Mareczek, DEng. – Faculty of Mechanical Engineering at Cracow University of Technology.

e-mail: *Mareczek@pk.edu.pl*

Wojciech Marek, DSc., DEng. – Faculty of Mechanical Engineering at Cracow University of Technology.

Tadeusz Papuga, DEng. – Faculty of Mechanical Engineering at Cracow University of Technology.

e-mail: *TPapuga@pk.edu.pl*

Sutkowski Marek, DEng. – Senior Development Manager in Engine Portfolio Team within Technology & Solution, Wärtsila Finland Oy.

e-mail: *Marek.Sutkowski@wartsila.com*

Article citation info:
LUFT, S., SKRZEK, T. Effect of the boost pressure on basic operating parameters, exhaust emissions and combustion parameters in a dual-fuel compression ignition engine. *Combustion Engines*. 2017, **170**(3), 115-120. DOI: 10.19206/CE-2017-319

Sławomir LUFT
Tomasz SKRZEK

CE-2017-319

Effect of the boost pressure on basic operating parameters, exhaust emissions and combustion parameters in a dual-fuel compression ignition engine

The dual-fuel engine enables application of various fuels. One of such fuels is propane or its mixture with butane (LPG). Application of such fuels results in reduction of engine operation costs. The paper presents effect of application of such fuel in a turbocharged dual-fuel engine on basic operating parameters, exhaust emissions and basic combustion parameters. Test results in the form of load characteristics for various boost ratios obtained for dual-fuel engine were compared to corresponding results obtained for conventional engine operating on diesel fuel only. The obtained results indicate that it is possible a dual-fuel operation with the propane energy share of 70% for maximum engine loads.

Key words: *dual-fuel engine, propane, turbocharging, combustion process, exhaust emission*

1. Introduction

For many years in the Department of Automobiles and Internal Combustion Engines there are carried out investigations on dual-fuel compression ignition engine operating on various fuels (methanol, ethanol, LPG, propane and natural gas) [3, 6, 8, 9]. The majority of tests has been done on an naturally aspirated engine. Because the nowadays applied engines are mostly turbocharged compression ignition engines, authors have made an attempt to analyses the effect of boost pressure on basic parameters describing engine operation and combustion processes.

The tests have been carried out on a comprehensively equipped AVL test stand consisted of:

- single-cylinder compression ignition engine, Tab. 1.
- measurement system for basic operating parameters,
- boost system,
- system for exhaust gas analysis,
- system for combustion parameters registration.

The applied test equipment conforms the following regulations: Directive 1999/96/EC of the European Parliament and of the Council of 13 December 1999, Regulation (EC) No 715/2007 of the European Parliament and of the Council of 20 June 2007 and Commission Regulation (EC) No 692/2008 of 18 July 2008.

Table 1. Main specifications of the AVL 5402 engine

Number of cylinders	1
Bore	85.01 mm
Stroke	90.00 mm
Displacement	511.00 cm^3
Combustion type	Compression ignition
Valve system	4 valves
Valve overlap	60 deg
Compression ratio	17.5
Fuelling system	Common rail system
Maximum effective power, without supercharging	6 kW
Maximum effective power, with supercharging	16 kW
Rated engine speed	4200 rpm
Iniection pressure	180 MPa

To realize the task formulated in the title of this paper, the engine fuelling system has been modified in such a way to make possible a delivery of gaseous fuel into the intake manifold in a precisely controlled way (in both aspects: amount of fuel dose and correlation between the injection time and timing). The gaseous fuel used in the tests was propane. A schematic diagram of the modified fuelling system is presented in Fig. 1b.

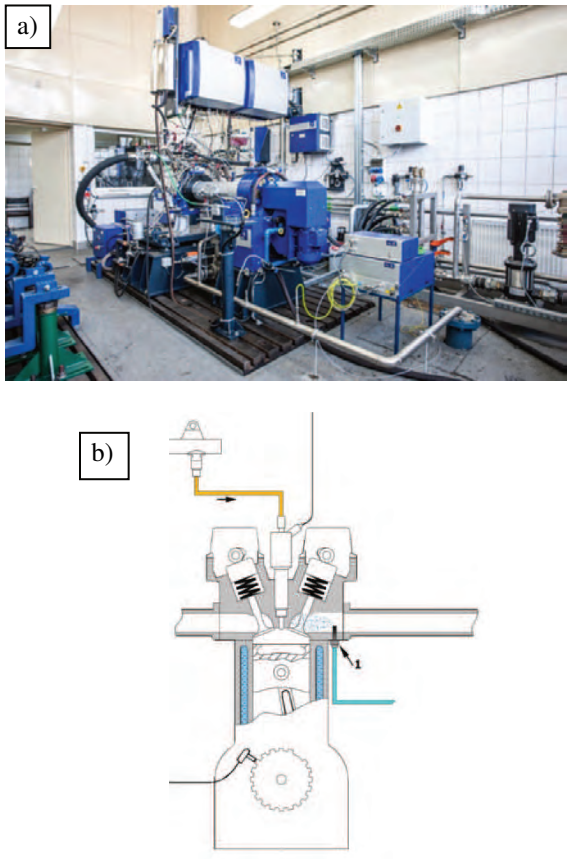

Fig. 1. a) General view of the AVL test bed, b) method of propane delivery into the engine

2. Investigation procedure

Commercial solutions based on dual-fuel compression ignition engines operating on gaseous fuels are more and more popular. Due to its well organized distribution network, LPG fuel is often applied in such solutions. The pri-

mary factor affecting interest in such solution is a competitive price of LPG compared to diesel fuel. The known and not yet very often applied solutions come down to a low LPG energy share (at the loads close to maximum ones, the LPG energy share does not exceed 30% of the total energy amount delivered by two fuels DF + LPG). Such a low energy share of LPG fuel arises from fear of unexpected negative results like: increase of maximum combustion pressure and increase of maximum and mean values of pressure rise rates [6]. These, generally, simple commercial solutions do not take into account the aspect of exhaust gas composition and changes in thermal and overall efficiencies. Commercial solutions do not apply results of investigations on the selection of diesel fuel dose injection parameters, particularly in modern solution where that dose is divided. Investigation from this field have been carried out in the Department of Automobiles and Internal Combustion Engines. The obtained results have been presented in [9].

The paper presents results of investigation on the effect of the boost pressure on basic operating parameters as well as the main exhaust emissions of a dual-fuel compression ignition engine. In each case, the obtained results have been compared to the corresponding results obtained for the standard version of the compression ignition engine operating on diesel fuel only.

The investigation procedure is based on the following assumptions:

- tests were carried out under conditions for load characteristic preparation at the constant engine speed n = 1200 rpm for both engine versions (standard operation on diesel fuel and dual-fuel operation on diesel fuel and propane),
- the air excess ratios (total in the case of dual-fuel operation) are comparable at each load point for both engine versions,
- energy share of diesel fuel versus the total energy of both fuels was from the range 25–30% (depending on the boost pressure from the range 0–400 mbar respectively) in conditions of maximum load,
- limitation of the maximum engine torque (maximum engine load) results from a limitation of the established maximum rate of pressure rise $(dp/d\alpha) \leq 10–12$ bar/CA, what has been recognized as a safe limit regarding the risk of knocking combustion,
- the boost pressure for both engine versions was equal to 0, 200, 400 mbar,
- standard adjustment of diesel fuel injection parameters in the case of conventionally operating engine for various engine load T [Nm],
- standard adjustment of injection timing of diesel fuel pilot and main doses in the case of dual-fuel operating engine for various engine load T [Nm],
- variable adjustment of the end of injection of the main diesel fuel dose in the case of dual-fuel operating (shortening of the time of injection aimed at a reduction of its quantity with an increase of the propane dose quantity).

3. Results of investigation on the effect of the boost pressure on the thermal and overall efficiencies and the achieved torque for investigated engine versions

Keeping the established and described in the 2nd paragraph assumptions, there were prepared load characteristics of thermal and overall efficiencies at the constant engine speed n = 1200 rpm. The results are presented in Fig. 2. Analysis of thermal efficiency characteristics obtained for dual-fuel and conventionally operating engines indicates that thermal efficiency of dual-fuel engine is slightly lower for all boost pressure values and engine loads. It is worth to notice, that this unfavorable difference decreases with the engine load. At the maximum load, this difference is very low and do not exceed 1% (at the minimum load reaching 5%). Similar trends are observed in the case of engine overall efficiency characteristics. Registered load characteristics of propane concentration in the exhaust gas of dual-fuel engine may be helpful in the interpretation of such trends (Fig. 4).

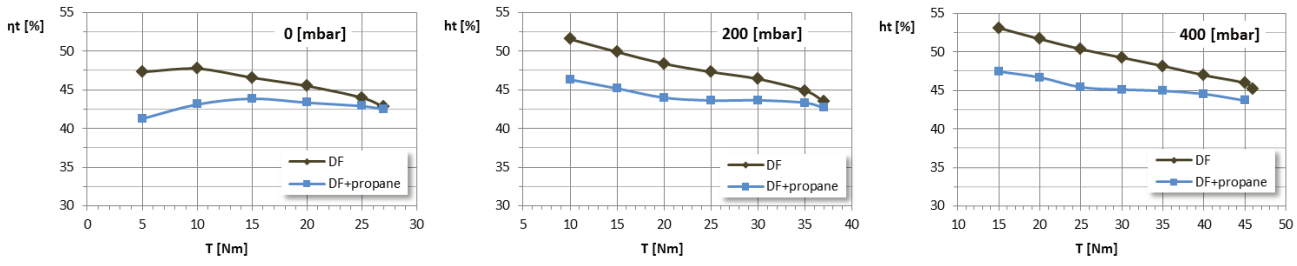

Fig. 2. Load characteristics of thermal efficiency for investigated engine versions

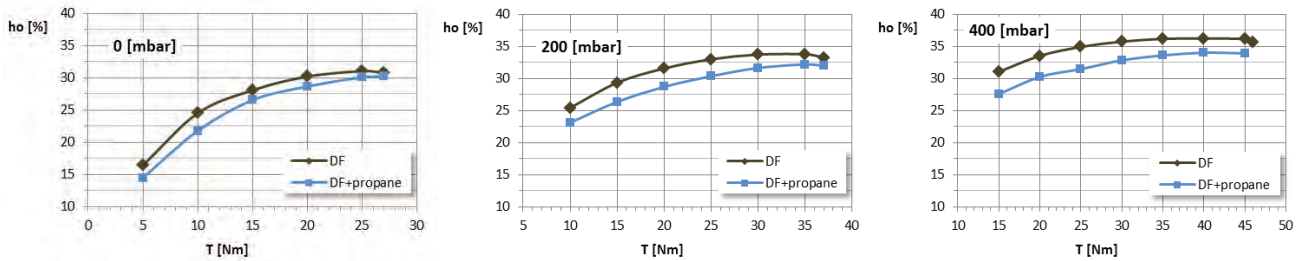

Fig. 3. Load characteristics of overall efficiency for investigated engine versions

Analysis of propane concentration in the exhaust gas leads to the following observation: propane concentration in the exhaust gas increases with load, reaches maximum at ca. 70% of the maximum load and then decreases. It should be noticed that the presence of propane in the exhaust gas results from fuel escape during the valve overlap as well as form the effect of incomplete combustion of this fuel (mainly in the area outside the diesel fuel spray for partial loads when the lean air-propane mixture does not undergo combustion). Increase of propane concentration in the exhaust gas of dual-fuel engine with load up to ca. 70% of the maximum load results from an occurrence of both described above phenomena. Slowing down this process for loads higher than 70% of the maximum load results from propane escape during the valve overlap period and better combustion with reaching the air-propane mixture (reduction of the incomplete combustion) [8]. The results presented in Fig. 4 allow to state that the dual-fuel engine reaches the same maximum torque as the engine operating in the conventional way for all applied boost pressures.

4. Results of investigation on the effect of boost pressure on some exhaust emissions from both investigated engine operating modes

The following emissions have been registered during preparation of load characteristics for both investigated engine operating modes for various boost pressures:

- unburned propane C_3H_8,
- particulate matter PM,
- nitrogen oxides NO_x,
- non-methane hydrocarbons NMHC.

The results are presented in Figs 4, 5, 6 and 7 respectively.

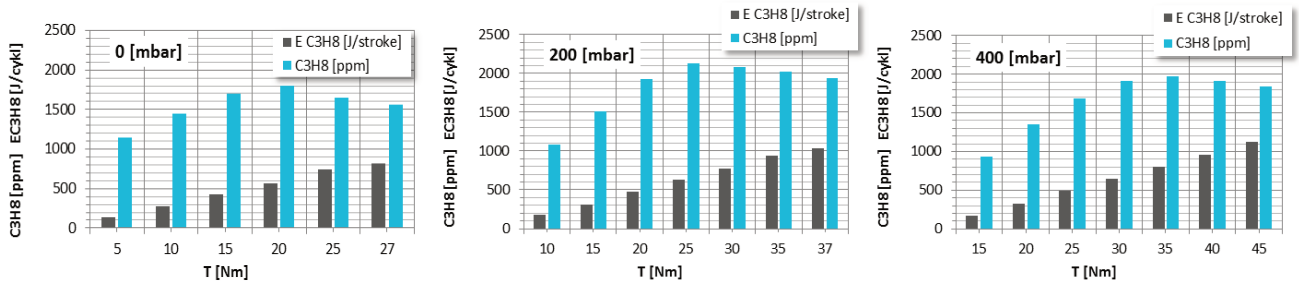

Fig. 4. Load characteristics of unburned propane (C3H8) concentration in the exhaust gas for both investigated engine operating modes

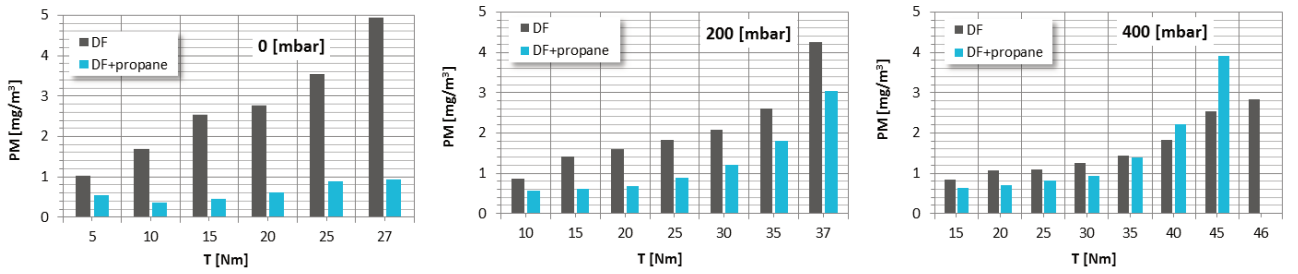

Fig. 5. Load characteristics of particulate matter (PM)concentration in the exhaust gas for both investigated engine operating modes

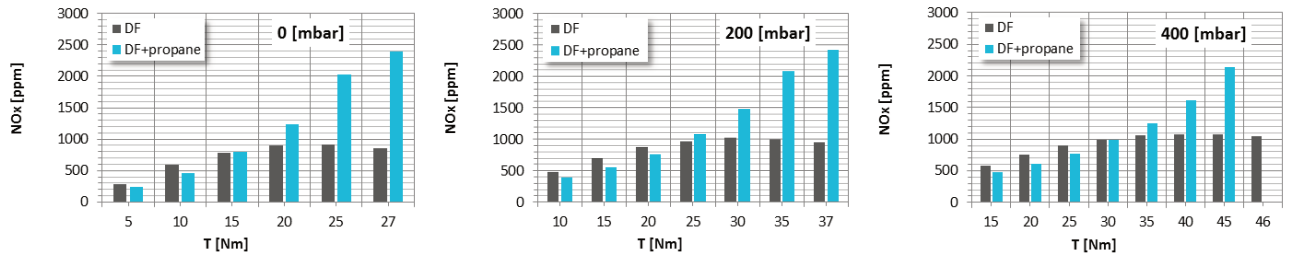

Fig. 6. Load characteristics of nitrogen oxides (NOx) concentration in the exhaust gas for both investigated engine operating modes

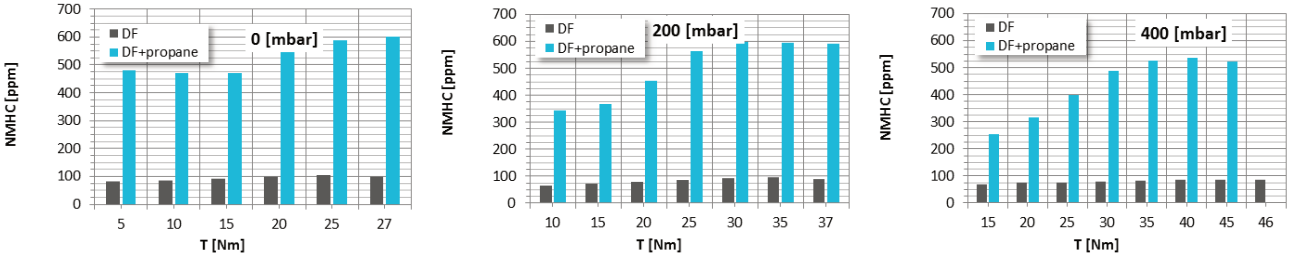

Fig. 7. Load characteristics of non-methane hydrocarbons (NMHC) concentration in the exhaust gas for both investigated engine operating modes

Analysis of characteristics presented in Figs 4, 5, 6 and 7 leads to the following remarks:

- presence of propane in the exhaust gas results from imposing of two phenomena: escape of a part of the propane charge into the exhaust manifold during the valve overlap and incomplete combustion of the air-propane mixture. Clarification of the course of propane concentration characteristic is described in the 3rd paragraph concerning overall and thermal efficiencies of both investigated engine operating modes,
- nitrogen oxides emission from dual-fuel engine is comparable with emission from conventionally operating engine in the range of low load for all applied boost pressures. In the range of load close to the maximum ones, a visible increase of this emission is observed from dual-fuel engine compared with the standard engine version. It results from higher obtained maximum pressures and thus higher combustion temperatures in dual-fuel engine in this range of load,
- non-methane hydrocarbons emission from dual-fuel engine is visibly higher than from conventionally operating engine in the whole range of load and for all applied boost pressures. It seems that increase of non-methane hydrocarbons emission from dual-fuel engine results mainly from the fact that diesel fuel combustion deteriorates. It should be remembered that the access to air is reduced when a diesel fuel charge in being injected into the air-propane mixture in this engine version.
- the observed increase of smoke emission from conventionally operating engine in proportion to the engine load is an effect well known and described in the literature [1, 3, 4]. Dual fuel operation, particularly in the case of considerable share of gaseous fuel should be characterized by visible reduction of that emission, what has been confirmed in many tests and has been observed for the investigated engine version but only without turbocharging (boost pressure equal to 0 mbar) and at the boost pressure of 200 mbar. The described differences in favour of dual-fuel engine are not observed just for the boost pressure of 400 mbar, whereas at maximum loads particulate matter emission from that engine is visibly higher than from conventionally operating engine. This may be explained referring to the phenomenon of pyrolysis. Probably, a considerable part of emitted particulate matter originates from the main diesel fuel charge injected into that part of the combustion chamber where combustion process is advanced. Injected diesel fuel particles are in the area with significantly reduced oxygen concentration as a result of combustion initiated by the pilot fuel dose as well as in effect of riching the air-gaseous fuel mixture with engine load. Diesel fuel particles injected in such conditions undergo coking and soot formation as a result of pyrolysis of hydrocarbons. In an injection system of the common rail type, the phenomenon favoring formation of particulate matter may be reduced mainly by delaying the start of injection of the main fuel charge. It will allow mixing the fuel charge in the combustion chamber, thus, better access to air. Moreover, significant delay of the start of injection of the main fuel charge will cause that the combustion chamber pressure in the moment of injection will be lower what, in effect, may result in better spraying and, in this way, better oxidation.

5. Results of investigation on the effect of boost pressure on basic operating parameters for both investigated engine operating modes

During preparation of load characteristics for both investigated engine operating modes there were registered combustion pressure courses for the applied boost pressures (Fig. 7). The registered courses served to calculate variability of maximum rate of pressure rise $(dP/d\alpha)_{max}$. (Fig. 8) and crank angle position at burning-out 50% of the fuel charge (Fig. 9).

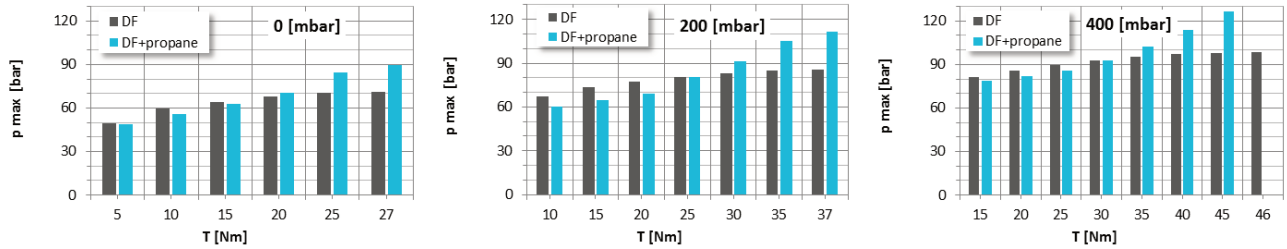

Fig. 8. Load characteristics of maximum combustion pressure courses pmax for both investigated engine operating modes

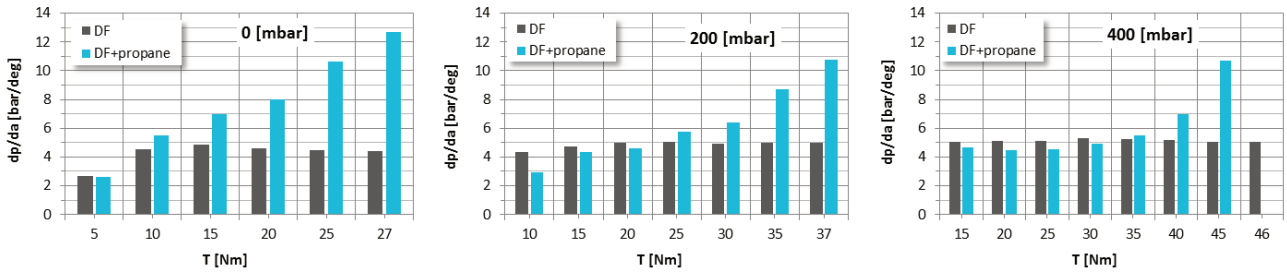

Fig. 9. Load characteristics of maximum rate of pressure rise $(dp/d\alpha)_{max}$ for both investigated engine operating modes

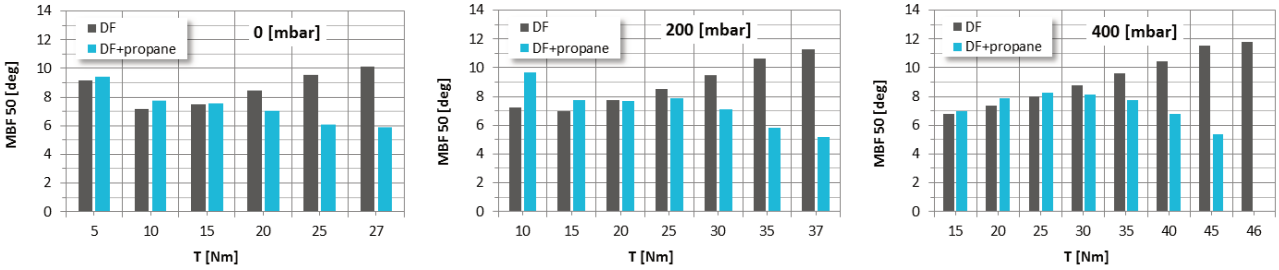

Fig. 10. Load characteristics of crank angle position at burning-out 50% of the fuel charge for both investigated engine operating modes

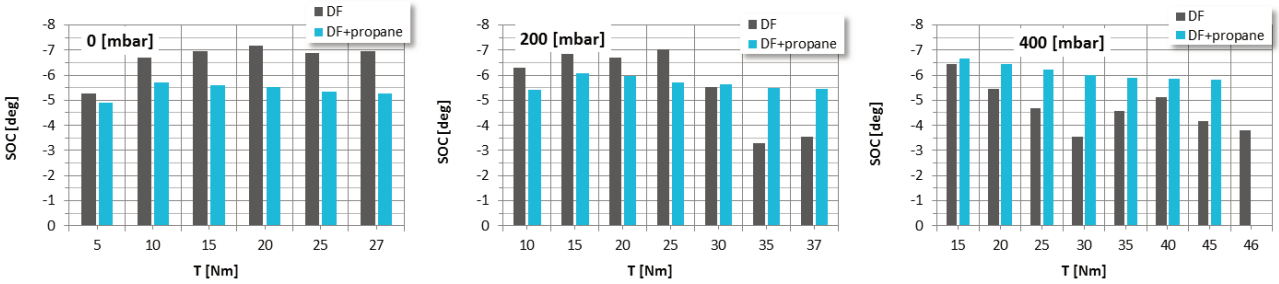

Fig. 11. Load characteristics of crank angle position at the start of combustion (C.A., BTDC) for both investigated engine operating modes

Analysis of maximum combustion pressure courses for both investigated engine operating modes indicates that in the range of partial loads, values of this parameter are comparable for all boost pressure values. In the range of loads close to the maximum ones values of this parameter are higher for dual-fuel operation. This is a result of higher rate of pressure rise in dual-fuel engine (particularly visible in the range of maximum loads, Fig. 8). This phenomenon leads to earlier burning-out 50% of the fuel charge (Fig. 9) at the crank angle position close to TDC. Therefore, intensive combustion occurs in small volume of the chamber and results in the observed increase of maximum combustion pressure. The observed phenomenon suggests that a different regulation of diesel fuel injection parameters should be applied in dual-fuel engine than in conventionally operating engine [2, 5, 7, 9–12]. Additionally, a proper selection of such regulation is justified by the fact that there are differences between ignition delay times and related to this – crank angle position at the start of combustion, what can be seen in Fig. 10.

6. Summary

Turbocharged dual-fuel engine compared to conventionally operating engine is characterized by:

- comparable obtained torque for all applied boost pressure values,
- slightly reduced value of overall efficiency for all applied boost pressure values,
- reduced particulate matter PM emission for lower boost pressure values and comparable emission for higher boost pressure values 400 mbar,
- increased nitrogen oxides NO_x emission for all applied boost pressure values,
- increased non-methane hydrocarbons NMHC emission for all applied boost pressure values,
- visibly increased maximum rates of pressure rise in the combustion process in the range of loads close to the maximum ones for all applied boost pressure values,
- 20–25% increase of maximum combustion pressure in the range of maximum loads for all applied boost pressure values.

The observed relationships have been obtained at 70%–75% energy share of propane in total energy amount delivered by both fuels. Some improvement, i.e. reduction of maximum pressures and in effect – maximum temperatures in the combustion process may be obtained introducing a change in diesel fuel injection parameters, what should result in reduction of nitrogen oxides NO_x emission from dual-fuel engine.

Nomenclature

CI compression ignition
LPG liquified petrolum gas
DF diesel fuel
TDC top dead center
SOC start of combustion
MBF mass burned fraction

Bibliography

[1] LEE, J., CHOI, S., KIM, H. et al. Reduction of emissions with propane addition to a diesel engine. *Int. J. Automotive Technol.* 2013, **14**(4), 551-558.

[2] LIU, J., YANG, F., WANG, H. et al. Effects of pilot fuel quantity on the emissions characteristics of a CNG/diesel dual fuel engine with optimized pilot injection timing, *Applied Energy*. 2013, **110**, 201-206.

[3] LUFT, S. Analysis of combustion process in a dual-fuel compression ignition engine fuelled with LPG in liquid phase. *J. KONES Power Train Transp*. 2007, **14**(4).
[4] OGAWA, H., ZHAO, P., KATO, T., SHIBATA, G. Improvement of combustion and emissions in a dual fuel compression ignition engine with natural gas as the main fuel. *SAE Technical Paper*. 2015, 2015-01-0863.
[5] PAPAGIANNAKIS, R.G., HOUNTALAS, D.T. Theoretical study of the effects of pilot fuel quantity and its injection timing on the performance and emissions of a dual fuel diesel engine. *Energy Convers. Manage*. 2007, **48**, 2951-2961.
[6] RÓŻYCKI, A. Analysis of performances of a dual-fuel turbocharged compression ignition engine. *Journal of KONES Powertrain and Transport*. 2010, **17**(3).
[7] SAYIN, C, CANAKCI, M. Effects of injection timing on the engine performance and exhaust emissions of a dual-fuel diesel engine. *Energy Conversion and Management*. 2009, **50**.
[8] SKRZEK, T. Assessment of the effect of gaseous fuel delivery mode on thermal efficiency and fuel losses during the valve overlap period in a dual-fuel compression ignition engine. *IOP Conf. Series: Materials Science and Engineering*. 2016, **148**, 012086.
[9] SKRZEK, T. Effect of the diesel fuel dose division and the injection angle on operating parameters of a dual-fuel compression ignition engine. *Combustion Engines*. 2015, **162**(3), PTNSS-2015-3480.
[10] STELMASIAK, Z., MATYJASIK, M. Exhaust emissions of dual fuel self-ignition engine with divided initial dose. *Combustion Engines*. 2013, **154**(3), 144.
[11] STELMASIAK, Z., The combustion controlling in the dual fuel CI engine by pilot dose division. *Combustion Engines*. 2011, **146**(3).
[12] WIERZBICKI, S. Effect of the parameters of pilot dose injection in a dual fuel diesel engine on the combustion process. *Journal of KONES Powertrain and Transport*. 2011, **18**(3), 499-506.

Sławomir Luft, DSc., DEng. – Mechanical Engineering Faculty at Radom University of Technology and Humanities.

e-mail: *S.Luft@uthrad.pl*

Tomasz Skrzek, DEng., – Mechanical Engineering Faculty at Radom University of Technology and Humanities.

e-mail: *T.Skrzek@uthrad.pl*

Article citation info:
BRZEZANSKI, M., PAPUGA, T., RODAK, L. Analysis of creation and combustion process of hydrogen-air mixtures by optical method in isochoric chamber. *Combustion Engines*. 2017, **170**(3), 121-125. DOI: 10.19206/CE-2017-320

Marek BRZEŻAŃSKI
Tadeusz PAPUGA
Łukasz RODAK

CE-2017-320

Analysis of creation and combustion process of hydrogen-air mixtures by optical method in isochoric chamber

The article considers the analysis of combustion process of hydrogen-air mixture of variable composition. Direct injection of hydrogen into the isochoric combustion chamber was applied and the mixture formation took place during the combustion process. The influence of the dose distribution of the fuel supplied before and after ignition on the formation of the flame front and the course of the pressure in the isochoric combustion chamber was discussed. The filming process and registration of pressure in the isochoric chamber during research of combustion process was applied.

Key words: *hydrogen-air mixture, isochoric combustion chamber, registration of pressure, filming of combustion process*

1. Introduction

The use of hydrogen as fuel in spark-ignition engines is becoming more and more up to date due to the ecological aspects of automotive industry. The combustion product of the hydrogen-air mixture is only water vapour and nitrogen oxides, which emerge under high loads and usage of poor mixture. The availability of hydrogen as an energy carrier is also not overestimated. In the case of hydrogen is supplied into the intake duct, hydrogen-powered engines feature lower specific power output compared to gasoline-powered engines. The reason for this is the reduction of the filling factor, due to the high volume of hydrogen in the mixture because the stoichiometric constant is 2.38 [Nm^3/Nm^3]. Combustion anomalies may also take place during engine power supply, and there is also a risk of uncontrolled ignition in the intake duct, as the mixture with such composition has explosive characteristics. The mixture formed in the intake channel, during the filling and compressing process, is heated from the valves and from the cylinder walls and undergoes a strong swirl. These phenomena lead to increased internal and kinetic energy of hydrogen-air mixture which promotes self-ignition.

These problems can be solved by feeding hydrogen directly to the engine combustion chamber by means of an injector. The authors of the article formulated thesis that using a very high diffusion coefficient of hydrogen can initiate the ignition of the mixture by spark discharge of spark plug at the end of the injection process. Reducing the formation time reduces the degree of advancement of pre-ignition reactions in front of the flame front, reducing the risk of combustion anomalies. During the initial motor tests, it became apparent that it is possible to form the pressure wave in the engine working space due to the desired pressure increase values $dp/d\alpha$. This effect depends on the initiation of ignition of part of the fuel dose, with respect to the rest of the dose delivered continuously during the combustion process. Also in this case, it was possible to regulate the engine power quantitatively and qualitatively due to the wide range of ignition of the hydrogen-air mixture.

Authors have conducted preliminary research in an isochoric chamber with the ability to record high quality pictures in high speed of frame rates and check pressure changes during the process of hydrogen-air mixture formation and combustion. The purpose of the study was to analyse the process of hydrogen-air mixture building and flame spreading depending on the method of distribution of the hydrogen dose and the initiation of combustion.

2. Method of research

The fixed volume chamber with the possibility of lighting and filming of its interior was used during research investigation. A pressure transducer for fast-change measurements was installed in the chamber. In addition, two manually operated valves were used to fill the chamber with air and to empty it from the exhaust. It provided the possibility of purging the chamber after each combustion cycle. In order to deliver fuel to the chamber, a standard high pressure gasoline injector was used. A spark plug was mounted into the chamber. The control system of fuel injection, ignition, pressure recording and camera was based on a specially written program in LabVIEW environment.
Figure 1 shows test bench, which the main object is a suitably equipped fixed-volume chamber, where the assumed combustion of the hydrogen-air mixture was realized.

Fig. 1. Test bench with isochoric combustion chamber

Schematic diagram of a constant-volume chamber with measurement systems: video footage, control of hydrogen supply and ignition system is presented in the Fig. 2.

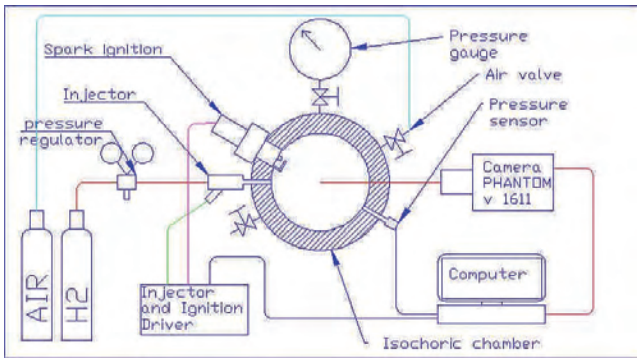

Fig. 2. Schematic diagram of the test bench

First, the amount of hydrogen supplied to the isochoric chamber was determined in one cycle. The amount of hydrogen injected per cycle was calculated using the gas state equation based on pressure variations in the chamber during one injection at a predetermined time. Hydrogen injection was applied to a chamber pre-filled with air at a pressure of 0.9 MPa. The injector was powered by hydrogen at a pressure of 5 MPa. Then the minimum dose of hydrogen injected into the test chamber was determined, which could be repeatedly initiated by the ignition spark. The research chamber was equipped with two glass windows in one axis. One window was used to illuminate the interior of the chamber and the second was to record the combustion in the chamber. Both windows are round and have a diameter of 79.5 mm. The injector and spark plug were mounted in axes perpendicular to the optical axis of the chamber. The injector and the spark plug were a short distance from each other. The injector was installed so that the output gas flowed almost tangentially to the chamber wall, which facilitated the swirling of the charge. As an illuminator, the LED matrix was used. Such a matrix illuminated the entire interior of the chamber evenly. A PHANTOM v 1611 camera with infrared filter lens was used for filming. The resolution of the camera's matrix was 768 x 768 pixels, the frame rate was 20000 and the exposure was 1 μs. Camera was equipped by lens type Macro Planar 100 mm f/2 with infrared filter from firm Carl Zeiss. The pressure measurement system in the chamber was by the OPTRAND pressure switch, model D21283-Q equipped. Pressure measurement was done at frequency 20 kHz. Pressure and image recording, fuel injection and ignition angle were synchronized. Such type of synchronization allows assigning a pressure value to a specific frame of the movie in the time.

3. Investigation of hydrogen-air mixtures combustion

In the chamber pre-filled with air at a pressure of 0.9 MPa, a hydrogen dose corresponding to a global air factor of $\lambda = 1.8$ was injected for an injection time of 65 ms and combustion and pressure profiles were recorded. Burning was initiated when the injector was closed. The course of pressure changes in the chamber is shown in Fig. 3.

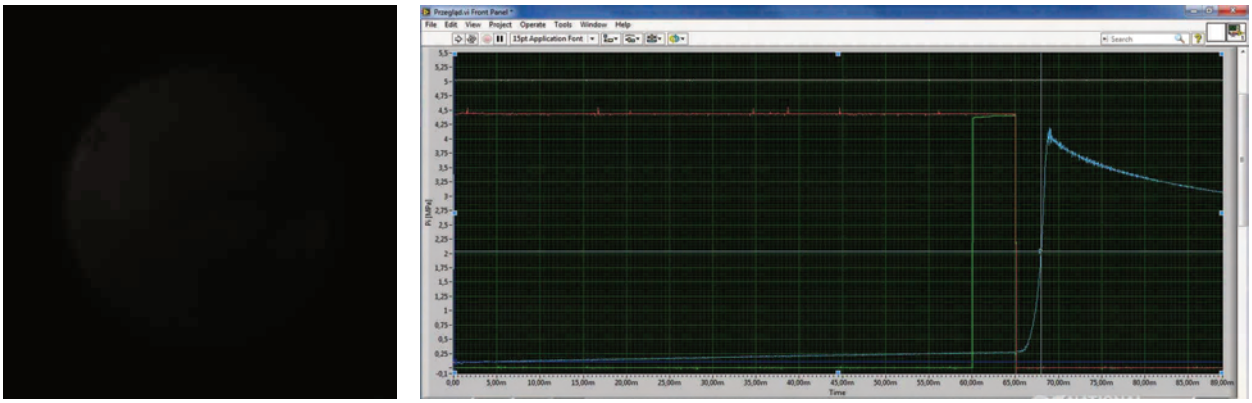

Fig. 3a. Photo of the combustion process and the pressure course with the marked pressure value. 3 ms after the combustion initiation

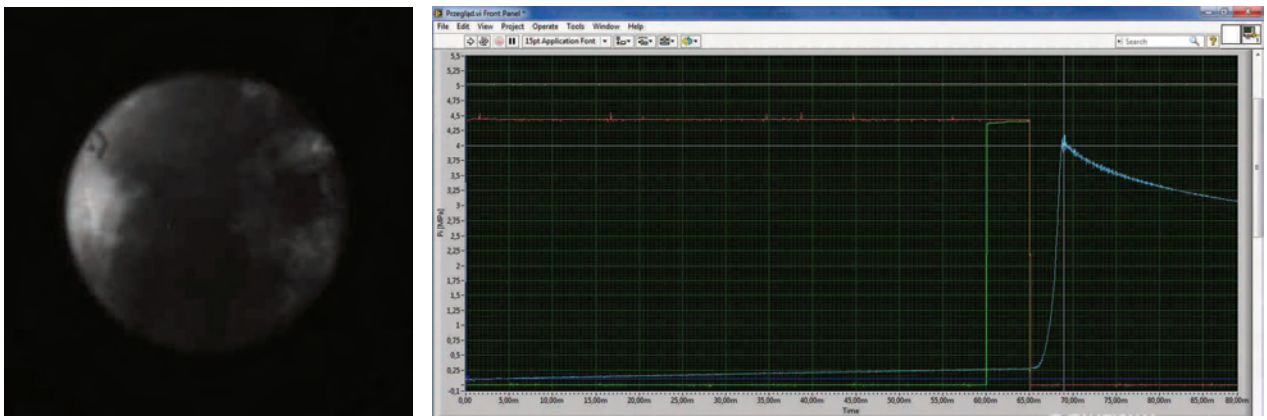

Fig. 3b. Photo of the combustion process and the pressure course with the marked pressure value 4 ms after the combustion initiation

Selected photographs show the stages of combustion evolution. The blue line represents the pressure in the isochoric chamber, the green line control signal of the ignition system, and the red line control signal of the injector. The combustion firing initiation corresponds to the moment of the falling edge of the control signal in the ignition system and the high level of the injection control signal corresponds to the opening of the injector.

Then an identical amount of hydrogen was supplied to the chamber, but the combustion initiation was followed during the fuel injection process and the fuel injection was continued during the combustion of the creating mixture. Pictures taken for the selected burning initiation time one can find below (Fig. 4 and Fig. 5).

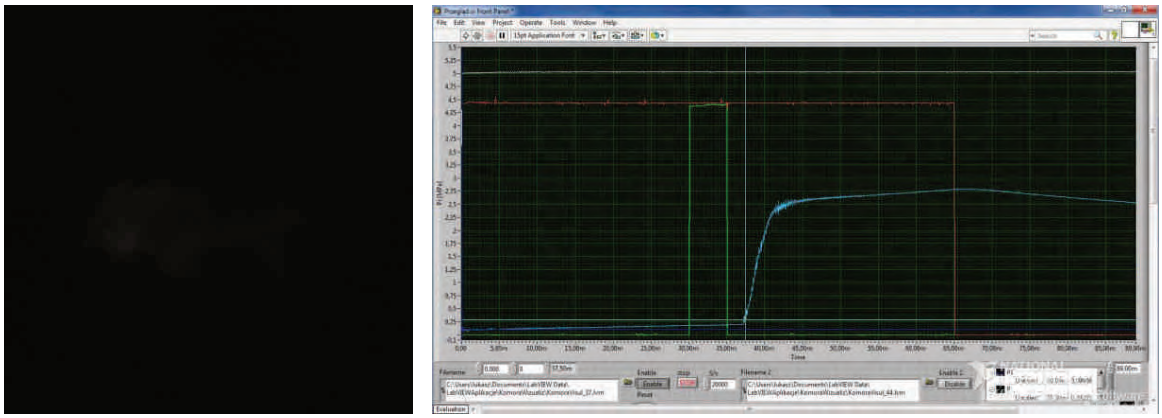

Fig. 4a. Photo of combustion advancement and pressure course with marked pressure value 2.5 ms after combustion initiation. Combustion initiation – 35 ms after opening of injector

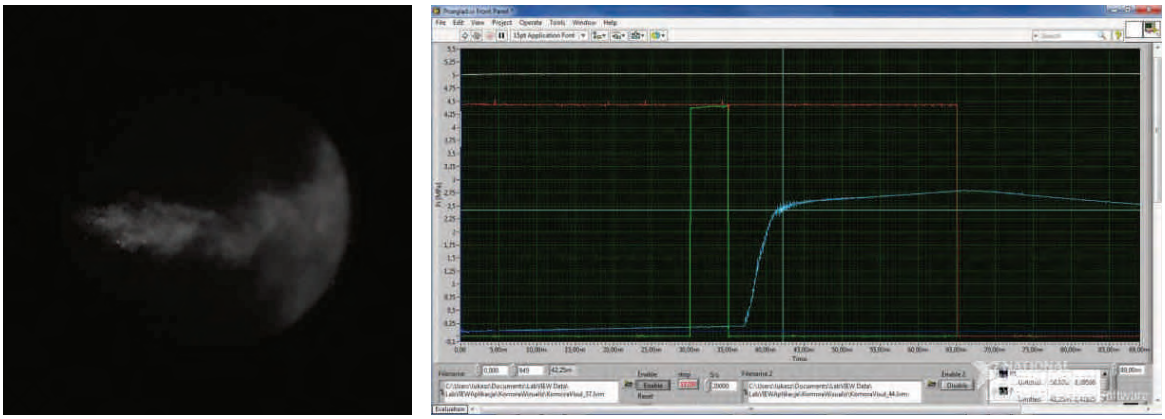

Fig. 4b. Photo of combustion advancement and pressure course with marked pressure value 7.25 ms after initiation of combustion. Combustion initiation – 35 ms after opening of injector

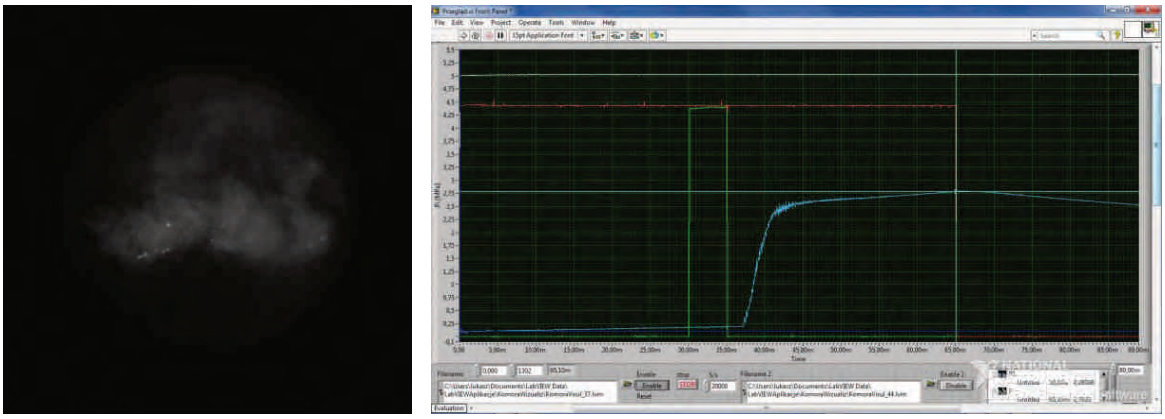

Fig. 4c. Photo of combustion progress and pressure course with marked pressure value 30.1ms after combustion initiation. Combustion initiation – 35 ms after opening of injector

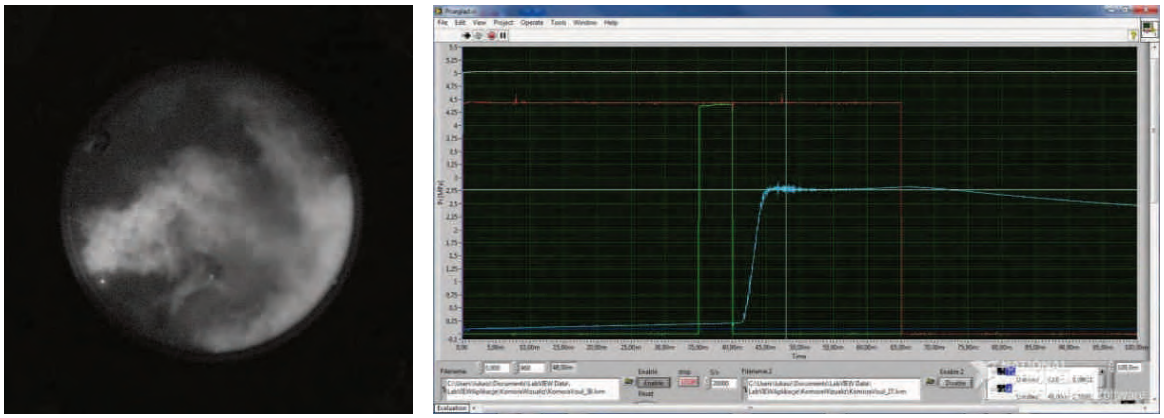

Fig. 5a. Photo of combustion progress and pressure course with marked pressure value 8ms after combustion initiation. Combustion initiation – 40 ms after opening of injector

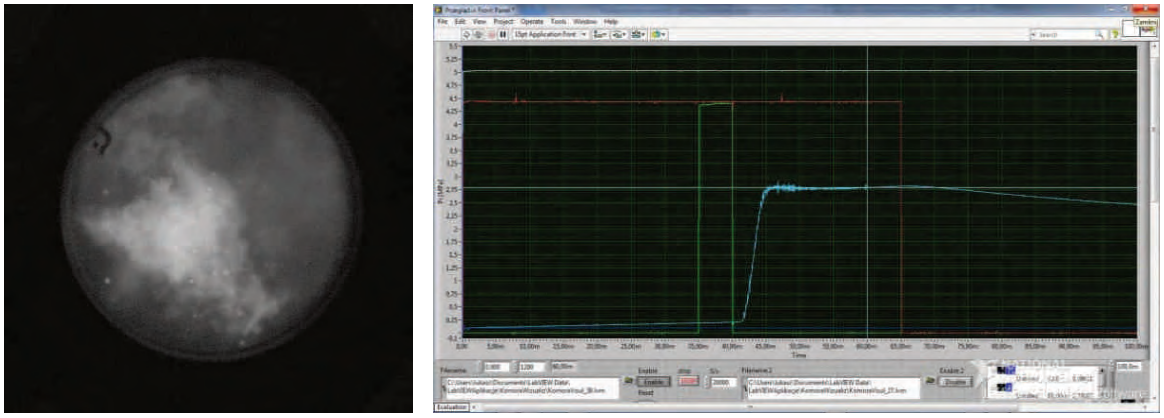

Fig. 5b. Photo of combustion stage and pressure course with marked pressure value 20 ms after combustion initiation. Combustion initiation – 40ms after opening of injector

4. Interpretation of research

The use of filming as a research method was aimed at preliminary recognition of the creating and burning process of hydrogen-air mixtures. These mixtures had a various compositions and were formed during the combustion process. Some photos were dark, but at this stage of the research it was not necessary to have them processed for analysis.

The authors were also aware that the processes filmed in the isochoric chamber did not fully correspond to the actual processes taking place in the engine combustion chamber.

In case of initiation of ignition at the end of hydrogen injection into the isochoric chamber, the flame front is formed after 50 μs at the spot of the spark on the spark plug electrodes, followed by rapid increase of pressure. After 3 ms from the injection end and the spark ignition, the pressure reaches half the maximum value. The maximum pressure is obtained after 4 ms from the initiation of combustion.

Figure 3a shows the formation of the flame 3 ms after the occurrence of a spark. Analysis of the film recorded during the experiment shows that the flame front spreads evenly from the spark plug into the chamber. This demonstrates the good mixing of hydrogen with air and the formation of homogeneous mixture throughout the volume of the chamber. When the peak pressure is reached, a rapid, short-term pressure change can be seen in the recorded pressure waveform. The reason for this is the reflection of the pressure wave from the wall of the chamber. This phenomenon is depicted in Figure 3b. In the case of initiation of ignition during injection (35ms), when the current value of the air excess number $\lambda = 3.15$, the combustion process is only visible after 2ms from the moment of ignition, as shown in Figure 4a. At the same time there is also an increase in pressure. Since the fuel is still being delivered, it is seen how the fuel stream from the injector burns using the remaining oxygen in the chamber. Figure 4a and 4b show the shape of a burning fuel stream. The burning fuel moves according to the axis of the fuel stream, which results from the construction of the injector. Figure 4b shows how the flame front reaches and bounces off the wall of the chamber. This phenomenon is accompanied by significant pressure pulsations. In this case, the highest value of pressure ~~is~~ occurs at the end of the fuel dosing (Fig.4c).

In the case of ignition initiation (40ms), when the current value of the air excess number is $\lambda = 2.86$, the combustion process is visible 1.5ms after the spark occurs, which means the beginning of the pressure increase and the noticeable combustion process in the video footage. The formation of the front and the shape of the flame is very similar to the one described earlier, but the geometric velocity of the flame front is greater. Reaching the front of the flame to the opposite wall of the chamber causes a strong reflection of the pressure wave and momentarily stopping the fuel flow from the injector. Figure 5a shows this situa-

tion. Decreasing the pressure in the chamber causes the fuel to re-inject from the injector. Figures 5a and 5b clearly show two local maxima of pressure values.

5. Summary

Control of the combustion process of the hydrogen-air mixture, mainly related to velocity of the flame front and heat release rat, is possible by using direct injection and initiating combustion during fuel injection. This way of initiating the combustion opens the way to supply the internal combustion engines with a mixture of stoichiometric composition. This way, you can significantly increase the amount of heat generated by the working process without entering the combustion anomaly area. This will allow for high engine power, in comparison to engines powered by a lean mixture.

The method used to record the combustion process has proven its usefulness in evaluating mixture formation and combustion.

Bibliography

[1] WHITE, C.M., KAISER, S., ROUX, M. Fuel-air mixing in a direct injection hydrogen fueled internal combustion engine. *14th-International Symposium on Applications of Laser Techniques to Fluid Mechanics*, Lisbon, .07-10 July, 2008.

[2] SUKUMARAN, S. Numerical study on mixture formation characteristics in a direct injection hydrogen engine. *Iowa State University*, Ames, Iowa 2010.

[3] GILLINGHAM, K. Internal combustion engine vehicles: a prudent intermediate step or a step in the wrong direction?, *Stanford University Department of Management Science & Engineering*, Global Climate and Energy Project Department of Management Science & Engineering, Stanford, CANADA, January 2007.

[4] WISŁOCKI, K. Studium wykorzystania badań optycznych do analizy procesów wtrysku i spalania w silnikach o zapłonie samoczynnym. Monografia habilitacyjna. *Wydawnictwo Politechniki Poznańskie*j. Poznań 2004

[5] WISŁOCKI, K. Optical methods in the research of internal combustion engines. *Thermal Processes Research Group, Instytut Silników Spalinowych i Transportu,* Politechnika Poznańska 2013.

[6] VANHAELST, R., THIELE, O., BERG, T. et al. Optical infrared-sensor inside the cylinder to determine the EGR- and residual gas rate in diesel engine. *Combustion Engines*. 2013, **154**(3), 3-11.

Marek Brzezanski, DSc., DEng. – Faculty of Mechanical Engineering at Cracow University of Technology.

e-mail: *MBrzez@pk.edu.pl*

Tadeusz Papuga, DEng. – Faculty of Mechanical Engineering at Cracow University of Technology.

e-mail*: TPapuga@pk.edu.pl*

Łukasz Rodak, MEng. – Faculty of Mechanical Engineering at Cracow University of Technology.

e-mail*: LRodak@pk.edu.pl*

Article citation info:
KRUCZYŃSKI, S., ŚLĘZAK, M., GIS, W. et al. Comparative studies of diesel engine powered by diesel and B100 fuel. *Combustion Engines*. 2017, **170**(3), 126-130. DOI: 10.19206/CE-2017-321

Stanisław KRUCZYNSKI
Marcin ŚLĘZAK
Wojciech GIS
Andrzej ŻÓŁTOWSKI
Maciej GIS

CE-2017-321

Comparative studies of exhaust emission from diesel engine fuelled with diesel fuel and B100 fuel

The article presents a comparative study of carbon monoxide, hydrocarbons, nitrogen oxides and the mass and number of particulate of diesel engine fulled with diesel and B100. B100 is a biofuel produced from vegetable oils for vehicles with compression-ignition engines. B100 fuel and diesel have similar physical-chemical characteristics which have been analyzed.

The research was carried out on an engine dynamometer in four cycles: ESC, ETC, WHSC and WHTC. The article provides an analysis of the research results, preceded by a discussion of the test cycles used.

Key words: *diesel fuel, B100 fuel, ecology, engine*

1. Introduction

With air pollution and increasingly restrictive requirements concerning the emission of harmful combustion substances, it is crucial to search for and use fuels from sources other than crude oil, including renewable sources, oilseeds, e.g. rape seed oil. Given the above, the self-ignition engine is suitable as it demonstrates a relatively low sensitivity to changes of fuel's physical & chemical properties.

Modern-day SI engines adapted to combust fuels derived from crude oils cannot be powered with natural rape seed oil due to problems relating to the immobilization of pressure elements, carbonisation of sprays, the occurrence of varnish in the combustion chamber and poorer lubricity properties of the engine oil [1, 10].

The content of glycerides in natural rape-seed oil accounts on average for 95-98%. Glycerides together with natural substances soluble in fat form a group of compounds known as lipids [2]. Large and heavy particles of rape-seed oil can be decreased by way of transesterification. Noteworthy results of the transesterification of natural rape-seed oil include considerable decrease of particles and significant reduction of viscosity (up to 10 times), the elimination of tri-glycerides (and thus reducing the varnish in the combustion chamber), as well as decrease of the cloud and solidification point and improved fuel volatility [1, 10].

B100 (methyl esters of fatty acids) is a biofuel produced in the country based on vegetable oils, intended for vehicles with SI engines.

The offered biofuel has a beneficial effect on the operation and durability of the engine; owing to good lubricity properties it protects the injection elements against excessive wear [5]. Greater content of oxygen compared to traditional diesel fuel manifests in "better" combustion, while a high cetane number ensures good engine performance. B100 biofuel meets the quality standards set forth bio-diesel according to PN-EN 14214 standard applicable on EU markets [7, 10]. Because of low-temperature characteristics (CFPP), there are three types of B100 biofuel: B, D and F (corresponding to fuels of temperate climate zones) and class 2 – corresponding to the fuel for arctic or harsh winter climate [12]:

- B100 type B with CFPP no greater than 0°C,
- B100 type D with CFPP no greater than –10°C,
- B100 type F with CFPP no greater than –20°C.

The last fuel continued to be available and was subject to evaluation, and its use in comparative studies covering commercial diesel fuel, in tests of IVECO engine allowed for comparing the emission of polluting combustion substances in the use of both fuels.

2. The purpose and scope of research

The purpose of the research was to perform comparative tests of emission of polluting combustion gases from a CI engine IVECO N60 ENT C, fuelled with diesel and B100 biofuel, in ESC, ETC, WHSC and WHTC cycles. The starting point for the tests was to define the advantages of using environmentally-friendly B100 biofuel in terms of emission of polluting combustion gases compared to conventional diesel fuel used in the same engine.

3. The tested objects

The tests comprised commercial diesel fuel and B100 fuel in N60 ENT C engine by IVECO.

The parameters of the tested fuels are presented in Table 1 (for diesel fuel) and in Table 2 (for B100 fuel).

Table 1. Parameters of diesel fuel [11]

Parameter	Unit	Range		Test method
		min.	max.	
Cetane number	–	51.0	–	PN-EN ISO 5165
Density at temp. 15°C	kg/m^3	820.0	845.0	PN-EN ISO 12185 PN-EN ISO 3675
Sulphur content	mg/kg	–	10.0	PN-EN ISO 20846 PN-EN ISO 20884
Ignition temperature	°C	56.0	–	PN-EN ISO 2719
Kinematic viscosity at 40°C	mm^2/s	2.000	4.500	PN-EN ISO 3104
CFPP temperature	°C	–	–20	PN-EN 116

The basic technical data of IVECO N60 ENT C engine are presented in Table 3, whereas the view of the engine installed in the testing unit is shown in Fig. 1.

Table 2. Parameters of B100 fuel [11]

Parameter	Unit	Range		Test method
		min.	max.	
Cetane number	–	51.0	–	PN-EN 14214
Density at temp. 15°C	kg/m^3	860.0	900.0	PN-EN 14214
Sulphur content	mg/kg	–	10.0	PN-EN 14214
Ignition temperature	°C	101.0	–	PN-EN 14214
Kinematic viscosity at 40°C	mm^2/s	3.500	5.000	PN-EN 14214
CFPP temperature	°C	–	–20	PN-EN 14214
Content of methyl ester of linoleic acid	%(m/m)	–	12	PN-EN 14214
Methyl alcohol content	%(m/m)	–	0.20	PN-EN 14214

Table 3. Technical data of the tested engine [11]

Engine type	N60 ENT C
Number of cylinders	6
Arrangement of cylinder	In-line
Engine displacement	5.9 dm^3
Nominal power	194 kW
Max. torque	1000 Nm at1400 rpm
Fuel injection system	direct, Common Rail
Combustion purification system	SCR
Type of fuel	Diesel fuel
Turbocharger system	TCA
Date of production	Maj 2012
Combustion gases standard	Euro V
Certificate of approval regarding emission of combustion pollutants	e3*2005/55*2008/74K*1035*05
Certificate of approval (power)	E3 85R-021218*01

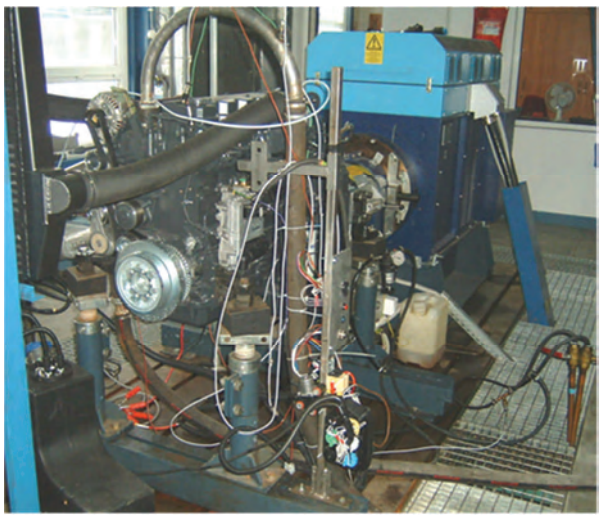

Fig. 1. IVECO N60 ENTC engine installed in the testing unit

4. Testing unit

The tests were conducted in the Motor Transport Institute in a testing unit equipped with an engine test bench, consisting of (Fig. 2, Fig. 3):

- an asynchronous electrical machine (capable of operating as an engine-generator) of AVL type AFA 100 4Z4/4 with a current frequency transformer; the unit allows for recreating dynamic tests and can be used for measuring the emission of combustion pollutants in line with the regulations currently in force;
- a digital rotation speed metering device Heidenham ROD 426 1024 27S12-03,
- a torque measuring shaft T10F 063230022 HBM installed on the shaft linking the engine with the brakes, which allows to eliminate – in dynamic position of the engine's operation – the impact of breakaway torque of the brake's rotor on temporary torque developed by the engine;
- a flow meter to measure fuel consumption – AVL 735, compatible with AVL 753, ensuring constancy of fuel's temperature during the measurement;
- a set of combustion analysers AMA i60 adapted to analyse undiluted combustions, consisting of a double set of analysers to gauge emission before and behind the combustion purification unit;
- an air flow-meter Sensyflow P to measure air consumption in the engine, effected by measuring the resistance of the heated wire;
- a set of thermometers and manometers to measure temperature and pressure of various media inside the engine (air, oil, coolant and combustion gases).

Fig. 2. A set of analysers AMA i60 R2 and CEB II

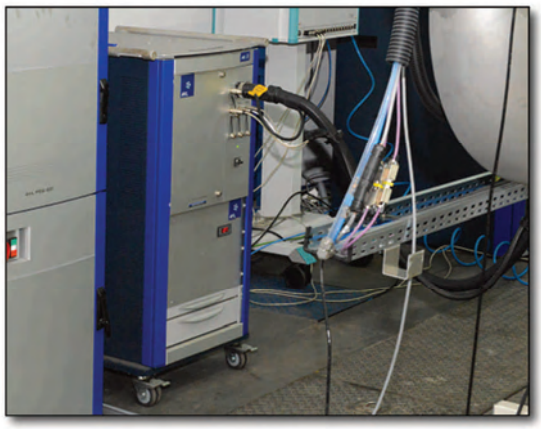

Fig. 3. AVL particulate matter measuring unit

5. Measuring cycles

The studies of emission of combustion pollutants generated by IVECO N60 ENTC engine fuelled with diesel and B100 were carried out with the engine test bench. The tests were performed in four cycles: ESC, ETC and WHSC and WHTC (Fig. 4, Fig. 5, Fig. 6, Fig. 7).

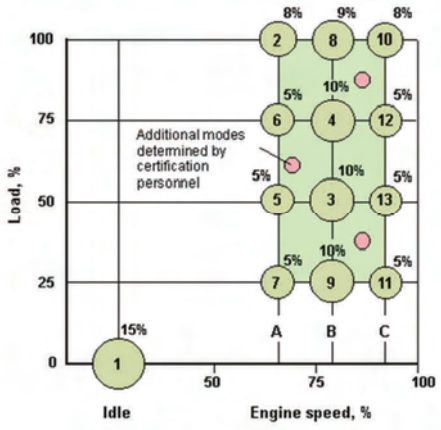

Fig. 4. European ESC cycle [9]

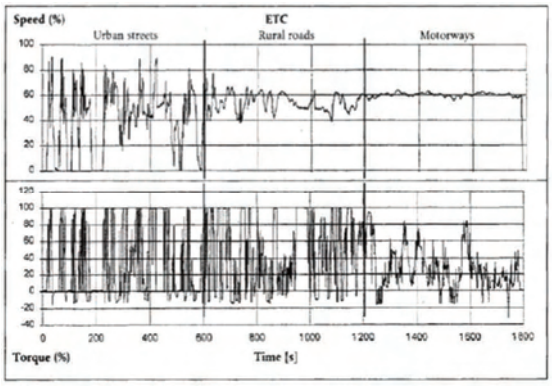

Fig. 5. ETC Transient Cycle – engine speed [9]

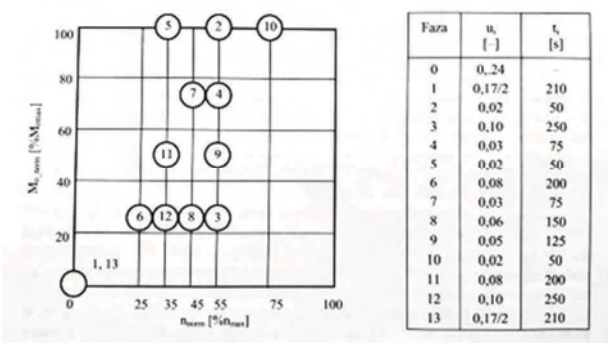

Faza	u_i [-]	t_i [s]
0	0,24	-
1	0,17/2	210
2	0,02	50
3	0,10	250
4	0,03	75
5	0,02	50
6	0,08	200
7	0,03	75
8	0,06	150
9	0,05	125
10	0,02	50
11	0,08	200
12	0,10	250
13	0,17/2	210

Fig. 6. Scheme of standardized WHSC cycle and coefficients participation phase [6]

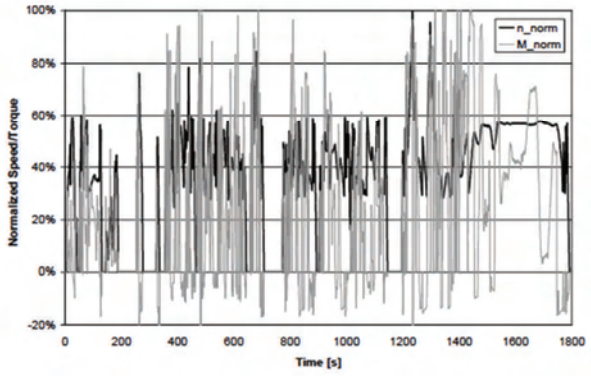

Fig. 7. European WHTC Cycle [8]

6. Testing process

The tested engine IVECO N60 ENTC was produced in May 2012 and therefore subject to approval as regards conformity with EURO V standard. It was certified with a certificate of approval no. e3*2005/55*2008/74K*1035*05 and the tests were performed pursuant to Directive 2005/55/EC [4] amended by Directive 2008/74/EC [3]. The abovementioned directives and the corresponding UN Vehicle Regulations – Rev. 05 did not envisage the method of approval as regards engines with bi-fuel system. The tests of bi-fuel engines were introduced on 06.08.2013 together with Rev. 06 of UN Vehicle Regulations 49. However, Review 06 describing the approval tests for engines with a bi-fuel system applies to engines that fulfil the limit of Euro VI requirements, thus engines tested in completely different cycles than Euro V engines. Euro V engines were tested in ESC and ETC cycles, whereas Euro VI engines are tested in WHSC and WHTC cycles.

Due to the above reasons, this study – which aimed at comparing the emissions of pollutants generated by the engine when fuelled with diesel and B100 compliant with Euro V regulations, in its basic versions fuelled with diesel – was based on methods described in Directive 2005/55/EC [4] and UN Vehicle Regulations – Rev. 05, making only necessary adjustments in the bi-fuel engine calculations, in accordance with UN Vehicle Regulations – Rev. 06, where required.

The tests were carried out in ESC, ETC in accordance with Directive 2005/55/EC, with the use of two different types of fuel. In the first case the engine was fuelled with diesel only, whereas in the second case with B100.

7. Analysis of test results

Table 4 presents results of tests of emission of combustion pollutants in the tested engine fuelled with diesel and B100, in different testing cycles applied in engine approval tests.

Table 4. Emission test results in different cycles [g/kWh]

Test	CO		NOx		THC		PN	
	ON	B100	ON	B100	ON	B100	ON	B100
ESC	0.509	0.340	1.728	2.300	0.024	0.030	10.906	2.699
ETC	0.694	0.541	1.811	2.345	0.022	0.028	13.973	10.308
WHSC	1.317	1.040	2.710	3.250	0.023	0.029	11.876	7.018
WHTC	1.926	1.473	5.136	5.718	0.063	0.061	9.317	18.516
WHTC COLD	3.375	1.336	8.459	5.867	0.137	0.045	43.168	8.464

According to Table 4 and Fig. 8 the unit emission of CO is lower when B100 fuel is used, compared to diesel fuel, in all test cycles.

THC emissions are practically analogous in ESC, ETC, WHSC and WHTC cycles when the engine is fuelled with diesel and B100, except for WHTC Cold, where the emission for diesel fuel is definitely greater (Fig. 9).

The level of particulate matter is clearly lower in ESC, ETC, WHSC and WHTC Cold cycles when fuelled with B100, except for WHTC (Fig. 11).

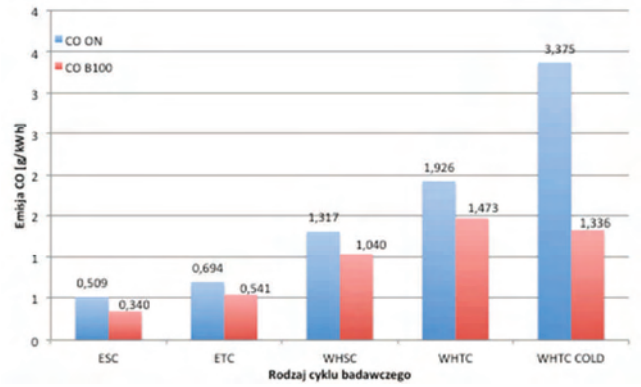

Fig. 8. Comparison of CO emission in an engine fuelled with diesel and B100, depending on the type of test

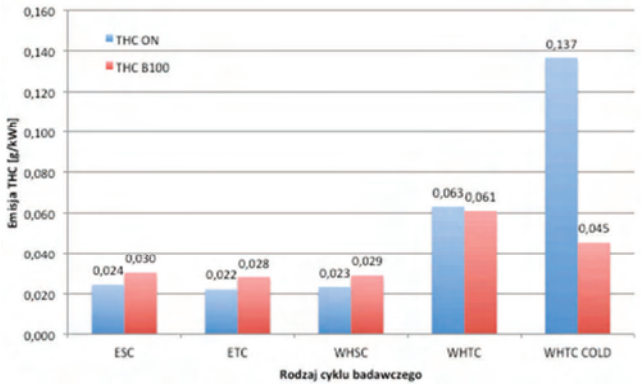

Fig. 9. Comparison of THC emission in an engine fuelled with diesel and B100, depending on the type of test

The unit emission of NOx is clearly greater in ESC, ETC, WHSC and WHTC cycles when fuelled with B100, except for WHTC Cold (Fig. 10).

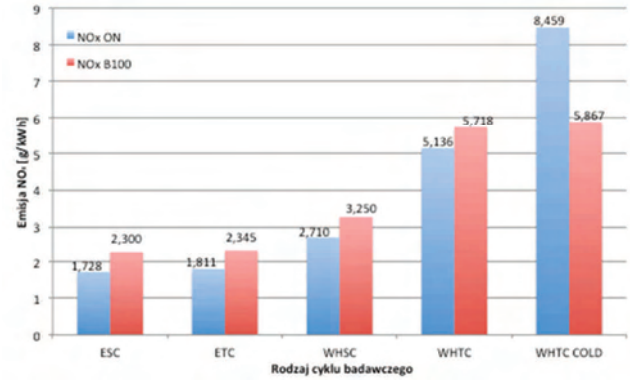

Fig. 10. Comparison of NO_x emission with engine fuelled by diesel and B100, depending on the type of test

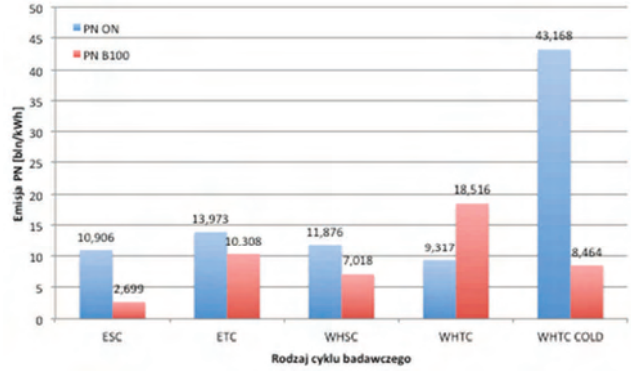

Fig. 11. Comparison of PN emission in an engine fuelled with diesel and B100, depending on the type of test

8. Summary

The tests lead to the following conclusions:

- the use of B100 to fuel a combustion engine in general has a positive impact on PM emission levels;
- the tendency to a lower emission is also noticeable in case of carbon oxide (CO) and to a lesser degree – also in the case of hydrocarbons (THC);
- the use of B100 to fuel a combustion CI engine affects the emission of nitrogen oxides (NOx);
- respective test cycles differ considerably in terms of emission levels with regard to all harmful substances. The lowest emissions have been achieved in ESC cycle and tend to increase in ETC, WHSC, WHTC and WHTC Cold cycles.

Nomenclature

CFPP	cold filter plugging point
CO	carbon monoxide
CO_2	carbon doxide
ESC	European Stationary Cycle
ETC	European Transient Cycle
NO_x	nitrogen dioxide
SI	spark ignition
PN	particular number
THC	total hydrocarbons
WHSC	World Harmonized Stationary Cycle
WHTC	World Harmonized Transient Cycle

Bibliography

[1] BACZEWSKI, K., KAŁDOŃSKI, T. Paliwa do silników o zapłonie samoczynnym. *WKŁ* 2004.

[2] CISEK, J., MRUK, A. Właściwości silnika ZS zasilanego naturalnym olejem rzepakowym. *Zeszyty Naukowe Instytutu Pojazdów*. 2012, **1**(87). Warsaw University of Technology.

[3] COMMISSION DIRECTIVE 2008/74/EC of 18 July 2008 amending, as regards the type approval of motor vehicles with respect to emissions from light passenger and commercial vehicles (Euro 5 and Euro 6) and access to vehicle repair and maintenance information, Directive 2005/55/EC of the European Parliament and of the Council and Directive 2005/78/EC (Text with EEA relevance).

[4] DIRECTIVE 2005/55/EC of the European Parliament and of the Council of 28 September 2005 on the approximation of the laws of the Member States relating to the measures to be taken against the emission of gaseous and particulate pollutants from compression-ignition engines for use in vehicles, and the emission of gaseous pollutants from positive-ignition engines fuelled with natural gas or liquefied petroleum gas for use in vehicles (Text with EEA relevance).

[5] KRUCZYŃSKI, W., KOŁODZIEJCZYK, K., OWCZUK, M. et al. Ocena zastosowania estrów metylowych różnego pochodzenia w silnikach o zapłonie samoczynnym. *Zeszyty Naukowe Instytutu Pojazdów*. 2012, **2**(88), Warsaw University of Technology.

[6] MERKISZ, J., PIELECHA, J., RADZIMIRSKI, S. Pragmatyczne podstawy ochrony powietrza atmosferycznego w transporcie drogowym. *Wydawnictwo Politechniki Poznańskiej*. Poznań 2009.

[7] PN-EN 14214. Ciekłe przetwory naftowe – Estry metylowe kwasów tłuszczowych (FAME) do użytku w silnikach samochodowych o zapłonie samoczynnym (Diesla) i zastosowań grzewczych – Wymagania i metody badań.

[8] REGULATION No. 49 Rev. 6. Uniform provisions concerning the measures to be taken against the emission of gaseous and particulate pollutants from compression – ignition engines and positive ignition engines for use in vehicles. E/ECE/324/Rev.1/Add.48/Rev.6 − E/ECE/TRANS/505/Rev.1/Add.48/Rev.6.

[9] REGULATION No. 49. Rev. 7. Uniform provisions concerning the measures to be taken against the emission of gaseous and particulate pollutants from compression-ignition engines for use in vehicles, and the emission of gaseous pollutants from positive-ignition engines fuelled with natural gas or liquefied petroleum gas for use in vehicles. E/ECE/324/Rev.1/Add.48/Rev.7−E/ECE/TRANS/505/Rev.1/Add.48/Rev.7

[10] SZLACHTA, Z. Zasilanie silników wysokoprężnych paliwami rzepakowymi. *WKŁ* 2002.

[11] TEST RAPORT NO 115520/COŚ. Badania emisji zanieczyszczeń silnika Iveco typ N60 ENT C zasilanego olejem napędowym oraz paliwem B100.

[12] www.orlen.pl

Kruczyński Stanisław, DSc., DEng. – Motor Transport Institute.

e-mail: *Stanislaw.Kruczynski@its.waw.pl*

Andrzej Żółtowski, DEng. – Motor Transport Institute.

e-mail: *Andrzej.Zoltowski@its.waw.pl*

Marcin Ślęzak, DSc., DEng. – Motor Transport Institute.

e-mail: *Marcin.Slezak@its.waw.pl*

Maciej Gis, MEng. – Protection Environment Center in Motor Transport Institute.

e-mail: *Maciej.Gis@its.waw.pl*

Wojciech Gis, DSc., DEng. – Motor Transport Institute.

e-mail: *Wojciech.Gis@its.waw.pl*

Article citation info:
BRZEŻAŃSKI, M., MĘŻYK, P. Heat balance of the military vehicle. *Combustion Engines*. 2017, **170**(3), 131-134. DOI: 10.19206/CE-2017-322

Marek BRZEŻAŃSKI
Przemysław MĘŻYK

CE-2017-322

Heat balance of the military vehicle

In modern combat vehicles there are very often used observation devices with the capability of operating in the infrared. They allow detecting heat emission. It is very important to reduce such situation on the battlefield; therefore generated heat masking or reducing systems are used. The article presents the heat balance of the military vehicle, impact of heat amount on detectability and solutions reducing or changing the thermal image which impedes recognition.

Key words: *heat balance, thermal energy storage, emission of heat, thermal image, IR device*

1. Introduction

The detection and proper identification of equipment on the modern battlefield is one of the basic military tasks. Over the past few years many solutions, which allow detection of a gathering of enemy forces based on weapon recognition including conveyance, have been developed. Recently most of the land, water and air vehicles use combustion engines which, during operation, emit a large amount of heat to the environment. This difficult to avoid feature is commonly used as an uncover factor. In military vehicles the heat emission issue is very important from the crew point of view. Effective reduction of heat emission is in many cases a condition for the survival of the crew of a combat vehicle on the battlefield. Optical devices which use infrared are currently standard equipment of observation and scouting units. They allow for quick detection and recognition not only of moving vehicles but also hidden, whose engines are switched off. Nowadays, we can find many different solutions that allow us to observe heat emission. Besides standard devices which present infrared images, image forming systems called fusion technology that rely on a combination of an image in visible light and image recorded in infrared are also used.

2. Heat balance of the military vehicle

Military land vehicles are usually propelled by piston or turbine internal combustion engines. Their characteristic feature is the very large stream of heat emitted along with the exhaust. A rough analysis proves that this stream depending on the type of engine, constitutes about 30% to 40% of total heat value emitted in the combustion process of the engine and that energy is compared to energy needed to move a vehicle. The second in terms of size heat flux dispersed in the vicinity of the vehicle is heat transferred in the cooling system and heat from other exchangers like oil coolers or air conditioning cooling systems. Therefore mentioned heat sources are the basic targets for detection systems on a battlefield. A simple technique using the infrared spectrum is becoming increasingly important during the operation of detection, identification and on the next step tracking and destroying a target. A typical view of a vehicles column, taking by standard observing systems using IR is presented in Fig. 1. From picture analysis it is possible to define a type and destination of the vehicle and operating state specifying temporary load of the engine.

Fig. 1. Combat vehicles' column in infrared image [9]

More complex recognition method, like the fusion technology mentioned earlier, allows for a thorough estimation of equipment, which visualize whether the device was used before so that it possible to evaluate e.g. the engine's thermal state relative to other systems of the vehicle, or the barrel's temperature after shot. The effects of this method are presented in Fig. 2, which allow for unambiguous analysis of the recorded image which has top priority in battlefield conditions.

Fig. 2. Comparing images (from left side) in visible light, in infrared and using fusion technology [1]

Factors affecting the thermal image of a military vehicle can be analysed by creating heat balance. This is a complex issue, because it is necessary to take into account a lot of factors. Employing literature [2] and [3] the following heat balance can be prepared for a combat vehicle, which includes the most important factors affecting heat emission outside the vehicle:

$$Q_u + Q_a + Q_s + Q_l = Q_n + Q_{ch} + Q_j + Q_w + Q_o \pm Q_f \quad (1)$$

where: Q_u – heat flux changed in the engine to mechanical energy, Q_a – heat flux provided from fire module (combustion of explosives), Q_s – heat flux provided from the sunlight, Q_l – heat flux secreted by people, Q_n – heat loss flux in power transmission system, Q_{ch} – heat loss flux in cooling system, Q_j – heat loss flux in traction system, Q_w – heat loss flux in exhaust system, Q_o – heat flux penetrated through vehicle's walls, Q_f – heat flux related with ventilation and air conditioning system.

In the above heat balance it is correct to assume that thermal efficiency of energy conversion systems is constant, all mechanical systems of the vehicle have a fixed thermal state, and ambient temperature is constant.

The biggest and the easiest to detect source of heat emission from contemporary combat vehicles is the heat stream from the propulsion unit. Only part of the thermal energy released from fuel combustion is processed on the mechanical energy used to move a vehicle, while most of the heat is emitted to the environment in the form of hot exhaust gases, heat transferred from exchanger of cooling system and in the form of radiation. Of course thermal energy converted to the mechanical energy is also consequently discharged into the environment, but it disperses considerably in power transmission system and it has less importance from the viewpoint of detection of a combat vehicle on the battlefield. In this aspect the most important is the heat stream from exhaust gases and from heat exchangers. The most important factors that will occur on a vehicle are listed here. Some of them could be written down in detail. For example heat stream from engine (Q_u) will have below form [2]:

$$Q_u = Q_p - Q_n - Q_r \quad (2)$$

where: Q_p – heat flux delivered to engine, Q_n – heat loss flux of incomplete combustion, Q_r – rest of balance includes other less significant errors and losses that are not included in other items of balance.

Heat flux Q_{ch} and Q_w should also be included but these factors occur in the main equation of balance, so they are omitted here. Military vehicles are designed for special tasks and it is hard to foresee all situations or factors influencing on the final heat balance. Therefore in the main equation (1) of heat balance it is worth to including additional factor Q_d which will be a sum of all heat profits and losses not included in main heat balance.

The final form of the equation is:

$$Q_u + Q_a + Q_s + Q_l = Q_n + Q_{ch} + Q_j + Q_w + Q_o \pm Q_f \pm Q_d \quad (3)$$

By analysing individual items of heat balance we can tell that reduction of heat emission from such a complicated construction as military vehicle is not so easy. It is necessary to carry out works aimed at hindering detection of heat emission from a vehicle. IR image of tank is presented in Fig. 3. The recognized tank has become a very easy target, which can be destroyed by a weapon with low power of destruction, because the thermal image allows identification of the most vulnerable, not protected points, areas or components of the vehicle. For example, mentioned above areas are the power transmission system and exhaust pipes presented in Fig. 3.

Fig. 3. Tank image in IR [7]

3. Reduction of heat emission and dispersion of heat stream

It is well known that total stoppage of heat emission from such a complicated mechanical construction as the military vehicle is impossible. Very important are the steps directed to reduce the biggest heat streams which are detected first from a long distance by standard IR detectors. Research therefore are carried out is on the possibility of temporary restriction of heat emission, heat storage and dispersion of heat stream.

In the Research and Development Centre for Mechanical Appliances "OBRUM" in Gliwice, the solutions that allow reducing heat emissions have been elaborated. One of them is a cooling system for multitask combat platform (Fig. 4.), which was designed for air streams from radial fans mixed with exhaust gases. Thanks to this exhaust gases are diluted and their temperature is reduced [4].

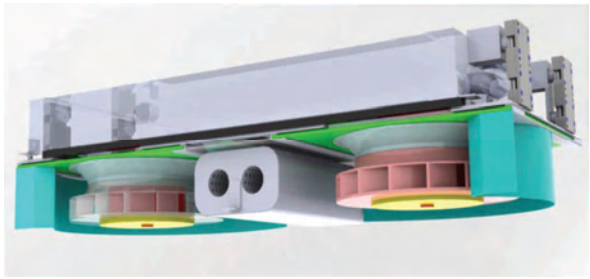

Fig. 4. Cooling system from Multitask Combat Platform (MCP) [5]

The above system has been used in combat platform called ANDERS (Fig. 5) thanks to this, the infrared thermal image is much weaker, and moreover dispersion of heat causes a blurring of thermal view and that make identification more difficult from long distance.

In special cases of protection of "big value" equipment like e.g. bombers masking methods are used, using the newest advanced technology in the field of optoelectronics and digital techniques. The first attempts of this kind were used in military aviation. The result of this was the "invisible" bomber Northrop B-2 Spirit. In the time when it was designed, new technology called Stealth had been used, that had begun in '60s of XX century [10].

Fig. 5. MCP „ANDERS" [OBRUM Ltd.]

This type of masking includes solutions which reduce visibility of the object for different detection systems like radars, sonars and all systems working by use of infrared spectrum [10]. Nowadays guidelines of Stealth technology are used more and more often in the design of military constructions. In OBRUM, concept works in that area were also carried out and as the effect of these works vehicle called "PL-01 Concept" was presented at the MSPO exhibition in 2013.

Fig. 6. „PL-01 Concept" vehicle on MSPO exhibition in 2013 [OBRUM Ltd.]

The method of forming of vehicle's thermal image taken by IR detection system exists as a separate issue. This kind of solution called ADAPTIV was developed in BAE Systems Company. It allows for hiding the vehicle from thermal vision detectors. This solution transforms heat emission and generates an environment temperature (Fig. 7) [8].

Fig. 7. Thermal masking method ADAPTIV from BAE Systems [8]

The system creates an opportunity of changing the thermal image of the vehicle and as a result, we can get a thermal imitation shape of something different e.g. a car or an animal [8]. This method also allows generation of a text on the side of the vehicle, what is useful for communication between the own forces (Fig. 8).

Fig. 8. Frame from advertisement movie, showing generated by ADAPTIV [8]

The system is built from hexagonal shape elements, mounted on the sides of the vehicle. The elements can heat up or cool down very quickly [8].

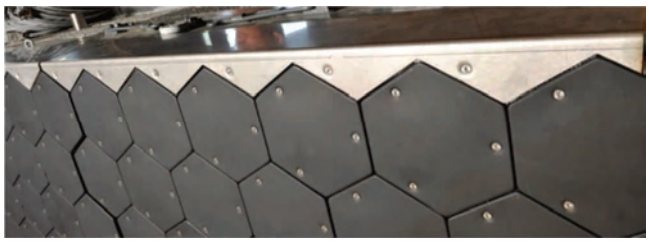

Fig. 9. Side of the vehicle with mounted elements of ADAPTIV [8]

4. Conception of heat management in combat vehicle

The total elimination of heat emission from the vehicle to the environment is impossible, but there are potential uses of these heat streams to active protection a combat vehicle by accumulating and forming emitted heat. One of the ways to use this method can be momentary stopping or reduction of heat emission by using heat storage. It is a thermally isolated vessel which contains an agent able to store heat. The shape of heat storage is usually cylindrical but it can be different and depend on free space in the vehicle's chassis. In first generation storages, thermal energy from exhaust system or cooling system was absorbed to a special phase-changeable substance. Because of problems with durability of this kind storages, which was a result of large chemical activity of used substances, so currently used heat storages use coolant which absorbs the engine heat. Periodically an accumulating agent can absorb a part of the emitted heat from an exhaust or cooling systems. Additionally, in certain cases, heat can be converted to cold e.g. in ice water installations. In this way, it is possible to periodically cool down selected elements of a vehicle and change its thermal image. In a dangerous situation when vehicle can be detected, exhaust gases can be quickly directed to heat exchangers in which the part of the heat is absorbed by coolant in heat storage. A properly planned heat control strategy of the military vehicle equipped in heat storage offers a wide variety of applications of stored heat. Opportune arrangement of heat storage's elements in

different places of the vehicle's chassis can change the thermal image of the vehicle which is scanned by IR detection devices. Momentary storage of heat significantly weakens the heat emission. The thermal image is blurred which makes identification very difficult. Heat storage used in the vehicle can have additional functions. The most important is the possibility to help start up a cold engine which is a big advantage in a combat vehicle [6]. In an emergency situation coolant from heat storage can be used to extinguish a fire and provide an additional protection layer. Beside additional volume of coolant inside heat storage can protect the cooling system from overload, resulting of combat vehicle's engine use or can be a system taking heat in case of damage to the cooling system. Additionally, storage heat can be used to warm up the crew area and also to maintain a hydraulic or transmission oil temperature. Besides the mentioned advantages, very important features of heat storage is capability of effective energy recovery, which is used to improve overall engine efficiency and use exhaust gases energy, which is usually irrevocably lost in conventional systems.

5. Summary

Heat management in a contemporary combat vehicle is very important, taking into account equipment's reliability and combat tasks. Presently, detecting devices working in infrared spectre had a significant impact on action tactics. Vehicles, which are not equipped with thermal covers (Fig. 3.) are tracked very quickly and destroyed by e.g. anti-tank missile equipped with IR detectors. An irrevocably lost heat, which emission is danger for the vehicle, can be reasonably used to different conditions of the vehicles work. Presented on the combat vehicle example issues related to the heat balance and various proposals for the heat use, show that necessary and purposeful is research in this field.

This article was conducted as part of the project Direct Support Vehicle founded by NCBiR under contract no DOBR-BIO4/017/13411/2013 dated 23.12.2013.

Nomenclature

IR infrared
MCP multitask combat platform

Bibliography

[1] www.flir.com/instruments/display/?id=60087; available: 03.2017.
[2] NIEWIAROWSKI, K. Tłokowe silniki spalinowe. *WKiŁ*, Warszawa 1968.
[3] OGRODZKI, A. Technika cieplna w pojazdach. *WKiŁ*, Warszawa 1982.
[4] SZAFRANIEC, A. Układ chłodzenia wielozadaniowej platformy gąsienicowej. *Biuletyn SPG*. 2011, **2**(28).
[5] HOLOTA, M., STACHURA, B. Wielozadaniowa platforma bojowa. *Zeszyty naukowe WSOWL*. 2011, **1**(159).
[6] BRZEŻAŃSKI, M., MĘŻYK, P. Starters of combustion engines in military vehicles. *Combustion Engines*. 2015, **162**(3), 491-497.
[7] www.defence24.com/company/pco-sa/gallery/thermal-imaging; available: 04.2017
[8] www.baesystems.com/en/feature/adativ-cloak-of-invisibility; available: 04.2017
[9] www.sofradir-ec.com/products-cooled.asp; available: 04.2017
[10] en.wikipedia.org/wiki/Stealth_technology; available: 04.2017

Przemysław Mężyk, MEng. – Research and Development Centre for Mechanical Appliances OBRUM Ltd. in Gliwice.

e-mail: *Przemyslaw.Mezyk@obrum.gliwice.pl*

Marek Brzeżański, DSc., DEng. – Institute of Automobiles and Internal Combustion Engines at Cracow University of Technology

e-mail: *MBrzez@usk.pk.edu.pl*

Article citation info:
GIS, W., KRUCZYŃSKI, S., TAUBERT, S., WIERZEJSKI, A. Studies of energy use by electric buses in SORT tests. *Combustion Engines*. 2017, **170**(3), 135-138. DOI: 10.19206/CE-2017-323

Wojciech GIS
Stanisław KRUCZYŃSKI
Sławomir TAUBERT
Andrzej WIERZEJSKI

CE-2017-323

Studies of energy use by electric buses in SORT tests

In article the market for electric buses in the world and in Poland have been discussed. The test methods for energy consumption of citi buses in Poland and the appropriate measuring devices have been presented. The article presents the results of the energy consumption of the citi bus in the test SORT 2. The results obtained were referred to results in the case other electric and conventional buses.

Key words: *electric, diesel, CNG, buses, SORT tests*

1. Introduction

According to ACEA [2] the worldwide fleet of electrical vehicles (BEV and PHEV) in 2016 exceeded 2 million cars, of which 575 thousand in the US, 650 thousand in China, 157 thousand in Japan, 597 thousand in Europe and 84 thousand in remaining regions in the world. The sales of electrical cars increased from 548 thousand in 2015 to 775 thousand in 2016 (in the US from 115 to 159 thousand, in China from 208 to 352 thousand, in Europe from 188 thousand to 209 thousand, and in Japan it fell slightly from 25 thousand to 23 thousand).

According to UITP [1] buses perform 83% of public transport in the world (450 billion trips). A statistic bus passenger uses 1/3 of fuel required for a passenger car. At present in Europe there are over 500 buses used with electric drive, of which 90% account for fully-electrical buses. The greatest number of those buses is used in the UK (130), Poland (78), the Netherlands (57), Germany (45), Sweden (39), France (31) and Spain (26). It should be borne in mind that the exhaust emission of CO_2 from electrical buses depends on the source of electrical energy and for a standard bus is equal to 17 gCO_2e/kWh in case of wind energy, 122 gCO_2e/kWh in case of Swiss energy mix and 579 gCO_2e/kWh in case of German energy mix and 1005 gCO_2e/kWh for the Polish energy mix.

The study of energy consumption by city buses is performed in the country – among others – in SORT track tests.

2. SORT Standardised on-road test cycles

The SORT project arose as an initiative of the UITP Bus Committee. The main aim of the SORT project is to design reproducible test cycles for on-road tests of buses in order to measure their fuel consumption [5].

Comparing the SORT cycles with this data shows a good match with reality. SORT 1 (heavy urban) with a standstill time of 40% and roughly 6 stops per kilometre fits very well for typical inner-city traffic situations (e.g. central Paris, France or London, UK). SORT 2 (easy urban) with 35% standstill time and roughly 3 stops per kilometre is closer to the situation of certain routes in Madrid, Spain or Munich, Germany. And last, SORT 3 (easy suburban) is representative of traffic in smaller cities (e.g. Klagenfurt, Austria or the suburban areas of Paris, France) – Figs 1–3.

The SORT 1 cycle, which is only 520 m, must be run trough at least twice in succession (= 1040 m). The SORT 2 (920 m) and SORT 3 (1,450 m) cycles need to be run trough, at least once.

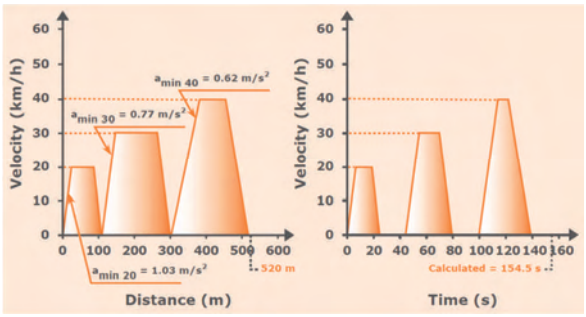

Fig. 1. SORT 1 [5]

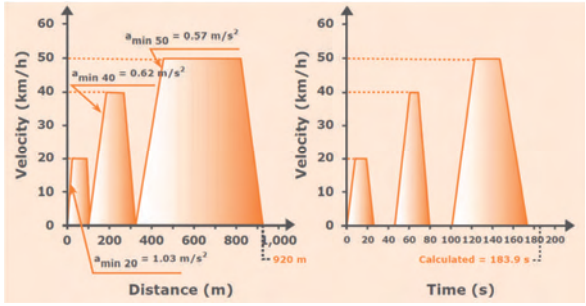

Fig. 2. SORT 2 [5]

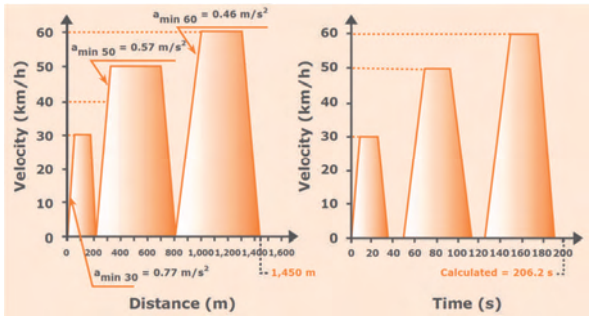

Fig. 3. SORT 3 [5]

The consumption measurements for each respective are to be repeated until 3 measurement lie within an accuracy

requirement 2%. To calculate the accuracy, the difference between the maximum and minimum consumption values of the three measurements is divided by the minimum value ($(C_{max} - C_{min})/C_{min}$ x 100).

The tolerance for trapezoidal target speed is ±1 km/h. During the transition from acceleration phase to the phase of driving at a constant speed, a maximum deviation of +3 km/h is permitted for a brief period. No more than 10 minutes should elapse between each measurement [6]. The above requirements were respected.

Wind speed was below 3 m/s, external temperature was range between 0°C and 30°C, humanidity level was below 95% in all conducted tests. Other requirements of SORT procedure were also met as required.

3. Tested vehicles

The tested vehicles consisted of 12-metre city buses:

– a bus marked as A1 with SI engine, fuelled with CNG with nominal power of 222 kW;
– a bus marked as A2 with a SI engine fuelled with diesel fuel, with nominal power 209 kW.
– a bus marked as A3, the so-called BEV, powered/driven by two electrical engines with nominal power of 2 x 182 kW (limited to 2 x 110 kW).

The mass of buses A1, A2 and A3 was equal to respectively 12,260 kg, 10,600 kg, 11,300 kg.

4. Test equipment

The tests of buses were performed with the use of the following testing equipment: KMA Mobile Fuel Flow Meter to measure the consumption of diesel fuel, CMF 025M Mass Flow Meter From Emerson to measure the consumption of CNG, Yokogawa WT 1800E Power Analyzer to measure the consumption of electrical energy and Datron mEEP20 used – among others – to measure the velocity and displacement of buses.

The universal system for fuel consumption measurement – AVL KMA Mobile is used to measure the fuel consumption in vehicles and on the engine test benches.

Basic parameters:

– measuring range: 0.35–150 dm^3/h 0.26–110 kg/h (with the fuel density: 0.75 g/cm^3)
– density meter: 500–2000 kg/m^3
– density measurement uncertainty: 1 kg/m^3
– measurement uncertainty (repeatability of the sensor calibration coefficients): ±1% (readout)
– measurement media (measuring module): petrol, fuels of standard and super quality (leader petrol/unleaded) also with alcohol admixtures; methanol, ethanol etc. to 100%; diesel oil; biodiesel.

Fig. 4 presents KMA Mobile Fuel Flow Meter used in tests.

Mass flow meter for gas fuel consumption measurement is shown in the Fig. 5. Used to measure a mass of gas consumption in vehicles and on the engine test bench. It also allows for measuring gas density. The software used allows for recording the momentary values of the parameters measured.

Basic parameters:

– maximum mass flow intensity: 2180 kg/h
– accuracy of mass flow intensity measurement: ±0.35%
– repeatability of mass flow intensity measurement: ±0.20%
– measurement media: gas fuels, also in liquid form (for example LNG).

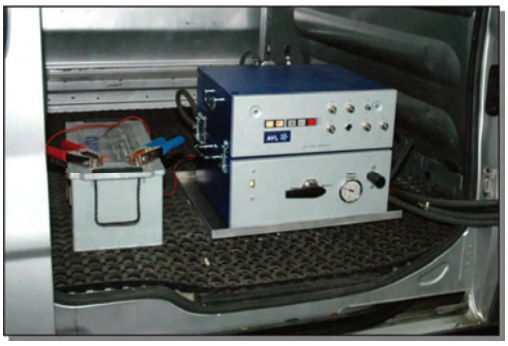

Fig. 4. KMA Mobile Fuel Flow Meter

Fig. 5. CMF 025M Mass Flow Meter From Emerson

Fig. 6 shows Yokogawa WT 1800E Power Analyzer.

The WT 1800E is a versatile instrument, unlocking precision power measurement capabilities for researches, designers and engineers working on a wide variety of applications in energy efficiency and conservation and renewable energy. Key applications include: Electric, Hybrid Electric and Plug-in Hybrid Electric. The WT 1800E guarantees a power accuracy of 0.05% of reading plus 0.05% of range and is capable of harmonics analysis up to the 500th order of a 50/60 Hz fundamental frequency. The stability of the WT 1800E ensures that precision measurements can be made today and over the long term.

Fig. 6. Yokogawa WT 1800E Power Analyzer

Figure 7 presents Datron mEEP20 recorder with optical head allows the registration of the vehicle traffic conditions on the road.

Multi-channel recorder allows simultaneous recording of multiple analogue signals such as weight, digital and frequency signals. Basic parameters:
– speed measuring range: 0.5–400 km/h
– repeatability: ±0.5%
– linearity of speed and road measurement: ±0.25%

Fig. 7. Datron mEEP20

5. Results and analysis of tests

During the tests of consumption of fuel and electrical energy for all three buses all requirements of SORT procedure have been fulfilled with regard to ambience conditions (temperature, pressure and air humidity, wind speed), testing track or method of replicating the tracking cycle. One of the exceptions was the different method of determining additional load for a bus with an electrical drive.

The weight of additional load to be used for the tested bus was calculated for buses fuelled with diesel and CNG according to the requirements of SORT procedure.

The said procedure assumes that measurements are carried out with half of the bus load capacity and the weight is assumed equal to 3200 kg, adjusted because of the bus size and number of seats or fuel tank capacity.

Thus, the calculated weight of the load does not correspond precisely with half of the actual load capacity of the tested bus. In case of tests of buses with electrical drive, the weight of additional load was calculated based on half of the product of the total number of passengers and weight per passenger equal to 68 kg. The difference in the adopted method of determining the weight of additional load was due to the fact that the SORT procedure has not been yet established for buses with electrical drive. If the method were to be applied to determine the weight of additional load in the current version of SORT procedure, the weight of the bus could be inflated or understated during the tests as one of the elements taken into consideration in the calculations is the fuel tank capacity.

According to SORT procedure the fuel tank capacity of a model bus is 200 dm^3, i.e. the weight of diesel fuel in such bus amounts to 168 kg. Depending on whether the tank of the tested bus has a smaller or bigger capacity, the weight of additional load is adjusted by taking away or adding the weight resulting from the difference between the mass of fuel in the tested bus and 169 kg. In case of buses with electrical drive there is no container for liquid fuel. Such tanks are traditional batteries, the weight of which is considerably greater than the weight of diesel fuel in the bus, and depending of their capacity it can differ significantly, influencing the weight of the bus and total number of passengers.

For example, the weight of traditional batteries in the tested electrical bus ranged from 1920 to 2520 kg, the weight of the bus – from 11,709 kg to 12,309 kg and the total number of passengers from 83 to 76.

The tests were performed in accordance with SORT 2 procedure.

Figure 8 presents a good performance of SORT 2 test as regards its replication in case of one of the tested buses. The bus drives – whenever possible – at velocities of trapeses – as marked on the graph – in general without or just slightly exceeding the maximum speed in each trapeze. A similarly good performance of SORT 2 test occurred in case of the remaining tested buses.

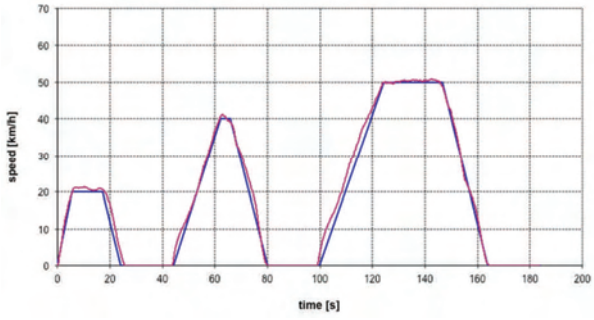

Fig. 8. SORT 2 chart (bus A2)

Table 1 presents the results as regards the consumption of fuel and electrical energy per route in SORT 2 cycle for the tested 12-metre buses.

Table 1. Results of consumption of fuel and electrical energy per route in SORT 2 cycle for tested 12-metre buses

Specification of buses	Fuel/ drive	Fuel consumption/Electric energy consumption per 100 km	Fuel consumption/Electric energy consumption per 1 km
A1	CNG	49.2 Nm^3/100 km	4.98 kWh/km
A2	Diesel fuel	39.4 dm^3/100 km	3.90 kWh/km
A3	Electric	94.9 kWh/100 km	0.95 kWh/km

According to Table 1 the consumption of energy per route (kWh/km) in case of a bus with an engine fuelled with CNG is almost 5 times greater and in case of diesel-fuelled bus is almost 4 times greater than the consumption of energy per route of an electrical bus.

The first experience in annual use of electrical buses in Warsaw by Miejskie Zakłady Autobusowe in the capital city (10 buses along the highly loaded urban line 222 (heavy-duty line SORT 1), with water heating system and an additional combustion aggregate fuelled with diesel) show that while average consumption of electrical energy per route comes to 103 kWh/100 km, the consumption of electrical energy per air-conditioning accounts for approx.

25% per route (25 kWh/100 km), and the use of electrical energy for the heating system accounts for c.a. 150% of energy consumption per route, i.e. approx. 170 kWh/100 km (SORT 1, 24 h temperature from –10 to –15°C) [3, 4].

Moreover, the use of an electrical heating system may – in low temperatures of the ambience – reduce the range of the bus three times and the total energy consumption at –10 to –15°C comes to approx. 300 kWh/100 km [4].

In such case the aforesaid differences in the consumption of energy in the tested buses fuelled with CNG or diesel are not considerably greater compared to the consumption of energy by an electrical bus. Nevertheless, electrical energy consumption by an electrical bus is still the lowest.

At the same time, attention must be given to the fact that in the light of data presented in [4] the technical readiness ratio for electrical buses compared to conventional bus fuelled with diesel is lower (on average for example in the period from July 2015 to April 2016 – respectively 0.883 and 0.981).

Based on prices of fuels and electrical energy the cost per 1 km was compared for the tested buses in terms of fuel/energy consumption. The price of diesel fuel and electrical energy was provided by one of the major domestic carriers, the price of CNG was calculated according to an average price quoted by PGNiG within the period from May 2015 to April 2016. The results of the comparison are shown in Table 2.

Table 2. Comparison of costs per 1km in tested buses in terms of fuel/energy consumption

Bus	Fuel/drive	Net price of fuel/electrical energy	Cost of 1 km
A1	CNG	2.58 zł/m^3	1.27 zł/km
A2	ON	3.33 zł/dm^3	1.31 zł/km
A3	electrical	0.36 zł/kWh	0.34 zł/km

Prices of fuel/electrical energy do not include value added taxon respective fuels.

6. Summary

The resulting values of consumption of diesel fuel are confirmed in actual use. According to MZA [3] on the routes corresponding to traffic conditions defined in SORT 2 the average consumption of diesel fuel of a 12-metre bus is equal to 39 dm^3/100 km [3]. However, for buses with electrical drive the consumption of electrical energy may differ considerably compared to the intended value due to the use of additional devices consuming power or ambient temperature.

Nevertheless, the tests prove that electrical buses characterise with lower energy consumption than buses with conventional engines powered with CNG or diesel fuel.

Lower are also costs per 1km by electrical buses which result only from the consumption of fuel/electrical energy.

Nomenclature

ACEA European Automobile Manufacturers Association
BEV battery electric vehicle
CNG compressed natural gas
ON diesel fuel
PGNiG Polish Oil and Gas Company
PHEV plug-in hybrid electric vehicle
SI spark ignition
SORT standardised on-road test
UITP Association of Public Transport

Bibliography

[1] BRUGE, P. UITP Vision. 5th European Battery. *Hybrid and Fuel Cell Electric vehicle Congress* (EEVC-2017). Geneva, 14-16 March 2017.
[2] DOLEJSI, P. ACEA perspective on alternatively powered vehicles. 5th European Battery. *Hybrid and Fuel Cell Electric vehicle Congress* (EEVC-2017). Geneva, 14-16 March 2017.
[3] KUŹMIŃSKI, J. Koszty eksploatacji autobusów elektrycznych. MZA Sp. z o.o. *Konferencja E-bus*. "Praktyczne aspekty elektryfikacji transport publicznego". Ministerstwo Rozwoju, 30.03.2017, Warszawa.
[4] KUŹMIŃSKI, J., GOGACZ, R., BARTOSIŃSKI, T. Doświadczenia w rocznej eksploatacji autobusów elektrycznych w Warszawie. *Autobusy. Technika, Eksploatacja, Systemy Transportowe*. 2016, **7-8**.
[5] Projekt UITP „SORT". Znormalizowane cykle testów jezdnych. UITP, 2013.
[6] UITP PROJECT 'SORT'. Standardised On-Road Test Cycles. International Association of Public Transport, 2014.

Wojciech Gis, DSc., DEng. – Motor Transport Institute.
e-mail: *Wojciech.Gis@its.waw.pl*

Stanisław Kruczyński, DSc., DEng. – Motor Transport Institute.
e-mail: *Stanislaw.Kruczynski@its.waw.pl*

Andrzej Wierzejski, MEng. – Motor Transport Institute.
e-mail: *Andrzej.Wierzejski@its.waw.pl*

Sławomir Taubert, MEng. – Motor Transport Institute.
e-mail: *Slawomir.Taubert@its.waw.pl*

Article citation info:
MONIETA, J. Modelling of the fuel injection of medium speed marine diesel engines. *Combustion Engines*. 2017, **170**(3), 139-146.
DOI: 10.19206/CE-2017-324

Jan MONIETA

CE-2017-324

Modelling of the fuel injection of medium speed marine diesel engines

The article presents the stages of fuel injection modeling of the four-stroke marine diesel engines as a set of functional blocks the of the fuel waves flow. The elaborated model includes the values of changing pressures in the combustion chamber and the course of changes of the pressure in spaces of the injection pump, injection pipe and the injector. Linear and local losses, as well as the conditions for the functioning were taken into account in stages of the fuel flow.

The influence of different values of the engine load on the pressure course of the in individual spaces of injection apparatus and in the engine cylinder during the working cycle depending on the crank angle of rotation of the crankshaft have been simulated. The mathematical relationships were selected and the structural and experimental data are used, allowing the calculation of the parameters of interest for the simulated process.

Key words: *marine engines, injection subsystem, injection course, modeling*

1. Introduction

Modeling is the first step in the formal description of problems related to functioning analysis and the synthesis of research objects. Modeling allows you to approximate the principles of organization, as well as how the object works, resulting in information about modelled system. It also allows you to reduce the cost and time research.

The model is a tool that allows you to describe the object and its behavior in different conditions of the external and internal using relations on a set of input and output sizes. The purpose of modeling is to obtain reliable mathematical model that allows you to trace the ways of behavior of the test object under the influence of extorting factors.

The essence of the simulation research of the fuel injection process is the development of models that allow understanding the physical phenomena that determine the quality of the injection. Conducting experiments on a real object in the laboratory is expensive and time consuming, and sometimes impossible, especially for large marine engines, and exploitation examinations are hampered on account of staying ships in seas and oceans where conditions of investigations are dependent from transient transport situations.

The utility and ecological parameters are largely determined by the combustion rate, characterized by the process of heat release and pressure changes. The combustion process efficiency is mainly conditioned by the quality of fuel-air mixture preparation. Among many factors influencing these processes, and connected with the injection system, the following ones should be specified [4]:

– beginning, duration and rate of injection fuel dose;
– pressure course and speed of fuel injection;
– location of fuel jet in the combustion chamber.

The validity of applying models is determined by the degree of conformity of the model with the real system of the fuel injection. Applying models is determined by the degree of conformity of the model with the real system of the fuel injection.

2. State of knowledge in the scope of the modeling of the fuel injection process

One of the factors determining macrostructure and microstructure in injection molding is the fuel distribution in time called injection [4, 15, 17]. Due to the short duration of injection (in milliseconds), its course occurs in closed spaces at high pressures and interactions of one phase with another. These processes have not been fully studied.

Basic equations of dynamics of fuel were formulated for the general model with applying three main principles of behaviour mechanics [5, 10, 17]:

– mass,
– momentum and the angular momentum,
– energy.

In the computational model of the pumping subsystem additional factors were taken into account [5, 10, 15]:

– changes in supply pressure as the result of the hydraulic impacts occurring during the pressing;
– elastic deformation of the injection pump drive;
– changes of the coefficient of fuel flow through throttling holes, depending on the hole cross section;
– injection subsystem leakage;
– movement resistance of the discharge valve head;
– damping the retaining surfaces of the head at the socket and the bumper;
– the elasticity of valve head and valve seat.

In previous models of the process of fuel injection simplifying assumptions were made, where it is possible to notice the dominance of applying finite element methods, geometric models, complicated mathematical descriptions and relations applied in practice.

The shortening of the optimum solutions obtainment time can be achieved by the formulated of mathematical models of injection subsystems of feed system and calculation of the parameters of interest in the numerical simulation methods. Many simulations of the diesel engine fuel injection subsystem are carried out in order to find the optimum fuel injection parameters [9]. The characteristics and the finite difference method have been applied to solve the governing equations. According to the author [7] recent studies show that finite difference method is superior to the method of characteristics concerning computation time and nonlinearity.

Methods proposed in literature of modeling of the injection process require selection at the preliminary stage and experimental verification.

The development of engines nowadays is conditioned mostly by a implementation of the stricter ecological standards, but for obvious reasons also fuel economy and movement parameters are taken into consideration.

3. Methodology of examinations

3.1. Object of examinations

The object of the study was a four-stroke diesel marine engine the drive Sulzer company of the drive generator with conventional fuel injection subsystem. Each cylinder is supplied the diesel oil by its individual fuel injection pump.

Up to now, research has been done on two types of engines, which limits the randomness of the results. The modeling object is the classic injection subsystem of Sulzer's four-stroke marine engine. In the so far commonly used conventional fuel systems the course of injection process is controlled in the very narrow range. On marine vessels the accumulator systems are still not implemented, there are major problems with the injection apparatus, and the costs of fuel were dominating in the profitability of ships. As regulation parameters there are the fuel dose and the change in the injection angle.

This system consists of the following elements (Fig. 1):

– the injection pump with the adjustment of the productivity with the pumping overflow valve,
– of the injection conduit,
– the injector with the multi-hole nozzle.

Each cylinder is powered with diesel oil using individual injection pump. Characteristic data of the investigated engine and elements of the injection subsystem was placed in Table 1.

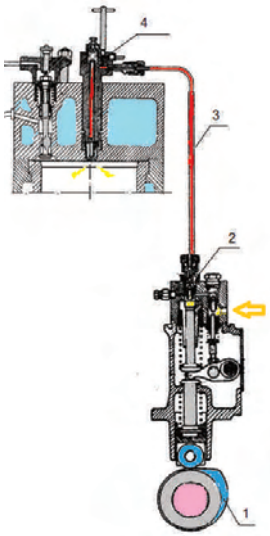

Fig. 1. Scheme of the injection subsystem of the four-stroke internal combustion engine: 1 – fuel cam, 2 – delivery valve, 3 – injection line, 4 – injector valve

Table 1. The main specifications of test injection subsystem

On.	Characteristics	Technical specification
1	Cylinder bore	220 mm
2	Piston stroke	320 mm
3	Rotational speed (constant)	500 rpm
4	Maximum engine power	220 kW
5	Pump type	With the regulation of dose on pumping
6	Plunger diameter	17 mm
7	Opening fuel valve pressure	215 bar
8	Fuel pipe inner diameter	2 mm
9	Nozzle hole number	6
10	Nozzle hole diameter	0.3 mm
11	Needle lift (maximal)	0.4
12	Nozzle hole angle	130 deg

3.2. Method of experimental investigations

For experimental studies he was used resistance sensors of the course of pressures in a combustion chamber. He also mounted a resistance pressure sensor on the discharge of the injection pump, and signals were visualized and analyzed using a portable computer (Fig. 2). In addition, recorded the top dead center. The analysis of these signals was run by time and crank angle of crankshaft domain using DaqView program [13]. Relative load the team was being carried out with the water resistor in the period from 0 to 100% with relative load the team was being carried out with the water resistor in the period from 0 up to the 100% with stepping every 25%.

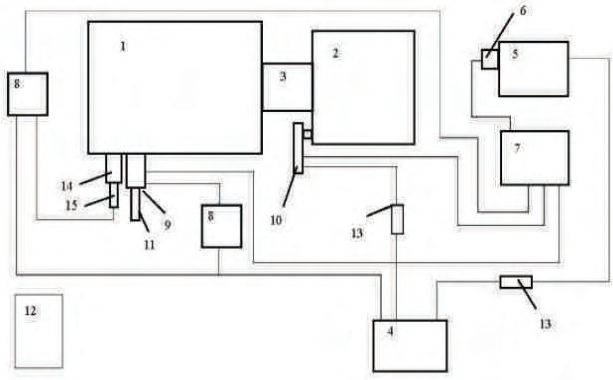

Fig. 2. Measuring circuit of investigations: 1 – internal combustion engine, 2 – generator, 3 – shaft with clutch the permanent clutch, 4 – power supply, 5 – portable computer, 6 – measuring card analog-digital, 8 – signal amplifier, 9 – injection pump, indicators valves, 10 – crankshaft position sensor, 11 – pressure sensor in the injection pump, pressure sensor, 12 – weather monitoring device, 13 – power supply 14–cylinder indicator valve, 15 – pressure sensor in the combustion chamber

On Figure 3 the course of the pressure indicates in the combustion chamber for one cylinder at burdening the 0%. Some results of experimental studies were used for calculations in the model, as: fuel feed pressure of injection pump, charge air pressure, course in-cylinder pressure of engine.

3.3. Modeling method

A physical model is a theoretical concept mapping processes and phenomena that occur in the real object. The degree of simplification of the actual object arises from modeling conditions, as the state of the art and the need and implementation conditions.

Two kinds of hardware models were builded. The model of the post of the injection subsystem was one of them apart from the engine with real elements. The second type is a virtual physical model which imitates elements of the comprehensive subsystem injection, enabling to take chosen phenomena into account (Fig. 4). Elements of the model are geometric models elaborated based on limited design data, protected by the producer, supplemented with geometrical measurements of new and exploited parts [6, 14]. The

functional model includes sequences of closed cycles, where the end of one circulation is the beginning of the next circulation of the engine. The shape of the fuel cam was determined based on geometrical measurements of the real cam (Fig. 5).

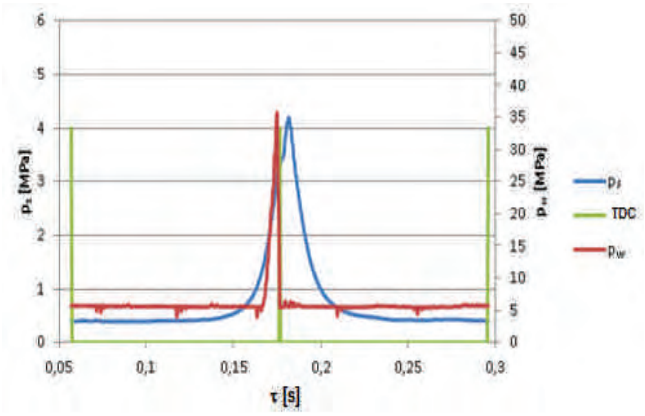

Fig. 3. Course of the pressure in a combustion chamber and the injection pump of the cylinder for one cycle at engine load of the 0%: p_s – pressure course in the combustion chamber, TDC – top dead centre, p_w – pressure in the injection pump

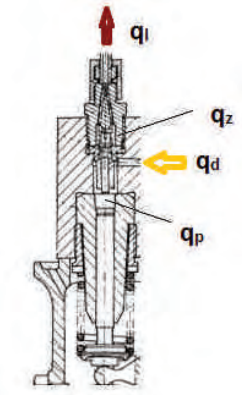

Fig. 4. Structural subsystem of the injection pump: q_d – stream of fuel reaching the injection pump,: q_t – stream of fuel pumped by the crowd, q_z – stream of fuel flowing through the delivery valve, q_l – stream of fuel flowing into the injection pipe

On Figure 6 an edge geometric model drawn up for the purposes of this work with the SolidWorks computer program was introduced. Similarly a geometry of the wire of the injection pump and the injection pipe was determined [14].

Fig. 5. The image the fuel cam of the inspected engine

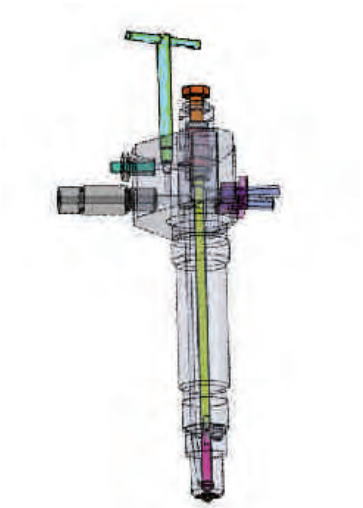

Fig. 6. Edge geometric model of the injector of the investigated engine [11]

In the article the mathematical simulation of the fuel injection process runs in the single-cylinder injection pump is presented. The verification of the model was done in correlation with the results obtained on a real engine. An analysis of presented results of the mathematical simulation gives good reason for ascertains that results correctly reproduce course of characteristics.

During the modelling of the process of the fuel injection the following computer programs were used: AutoCAD, Microsoft Excel, Matlab, COMSOL Multiphysics, SolidWorks.

In this paper, it was decided to take into account the effect of the course of the pressure in the engine cylinder on the course of the fuel injection which not all authors took into account, and of changes of medium parameters. The calculations include the influence of pressure and temperature on the parameters of the pumped fuel such: density, kinematic viscosity and modulus of elasticity.

4. Modeling results

4.1. Introductory remarks

Basic fuel dynamics equations were formulated for the general model using the basic principles of behavior mechanics [3, 17]:

- mass,
- momentum and the angular momentum,
- energy.

Mathematical model of injection subsystem includes the description of its geometrical and physical features as well as characteristic mathematical relations describing dynamics of hydraulic phenomena and structural elements. The design of the injection subsystem and the different assumptions for the individual components of this subsystem necessitate dividing it into three construction units and the corresponding three groups of equations describing the processes occurring. Due to the limited volume of the article, only examples of injection pumps were given.

An attempt to solve the problem more quickly and more cheaply was made with numerical way using data from experimental studies. It sought to bring the results of the modeling results to the experimental studies which was

checked by comparison. The work of the injection pump is controlled by the cam, being on the camshaft. Motion of pump piston depends on the lifts of fuel cam and camshaft position $h_p = h_p(\alpha_w)$. The change of transferring the piston pump in individual time intervals allows to the determine speed values of the lifts of the plunger in characteristic points:

$$v_t = \frac{dh_p}{d\tau} \tag{1}$$

The lift course of the piston of the injection pump and the speed of the piston in the fuel forcing phase, for the investigated engine, were described in Fig. 7. These values were appointed based on the outline of the fuel cam on the camshaft.

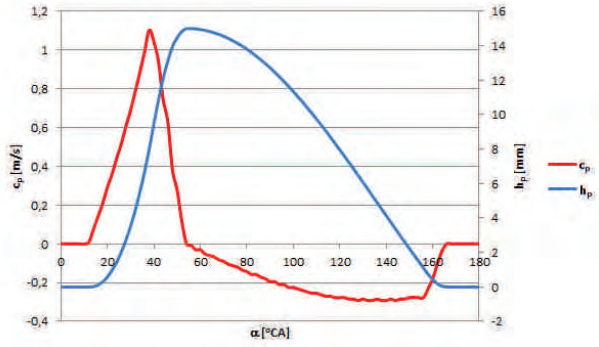

Fig. 7. Lift and velocity of plunger of the injection pump

Fuel injection pump with the valve with strain relief h_r working stroke is preceded by stroke h_o arising from needs to supplement the volume of fuel injection subsystem, released by relief stroke calculated with the formula:

$$h_o = \frac{4V_o}{\pi d_p^2} \tag{2}$$

Working stroke is calculated with the formula h_r:

$$h_r = \frac{4V_p}{\pi d_p^2} \tag{3}$$

4.2. Modelling of hydrodynamic phenomena in the pressing subsystem of the injection pump

The following types of equations were used to describe these phenomena. Fuel flow continuity equation for individual spaces of the pumping subsystem:

$$\frac{V}{E}\frac{dp}{d\tau} = \Sigma q \tag{4}$$

where: V – volume of the chamber taken into consideration of the pumping subsystem, E – modulus of elasticity of fuel, p – pressure of fuel in the considered space, Σ q – sum of inlet and outlet streams of fuel to and from the space.

Equation of motion of delivery valve, being the balance of the dynamic forces acting on the valve in the form of:

$$m\frac{d^2h}{d\tau^2} = \sum P \tag{5}$$

where: m – mass of the moving element, Σ P – the sum of the forces acting on the delivery valve.

Equation describing the stream of the fuel flow q through considered holes with cross sections A:

$$q = \mu A\sqrt{\frac{2}{\rho}(p_1 - p_2)} \tag{6}$$

where: μ – flow coefficient, A – the geometric cross section to flow, ρ – fuel density, $p_1 - p_2$ – pressure difference on both sides of the hole.

Equation of swelling pressure in the inlet or outlet of the flow hole as the result of the change of the volume stream q flowing through the opening [17]:

$$dp = \pm sign(q)\frac{\rho a}{A}dq \tag{7}$$

where: sign – plus or minus, a – speed of sound in fuel.

Continuity equations for the space above the injection pump plunger can be written as [5]:

$$A_p\left[c_p - w_{pw}(\alpha)A_p\frac{dp_p}{d\tau}\right] = w_{sl}\mu_o A_o j\sqrt{\frac{2}{\rho}|p_p - p_d|} - A_{zc}\frac{dh_z}{d\tau}$$

$$- w_{s2}\mu_z A_z\sqrt{\frac{2}{\rho}|p_p - p_l|} - A_z\frac{dh_g}{d\tau} + \frac{V_p}{E}\frac{dp_p}{d\tau} + q_u \tag{8}$$

where: A_p – active cross section of the pump piston, c_p – the actual speed of the injection pump piston, with regard the elastic deformations, $w_{pw}(\alpha)$ – camshaft deformability factor, $s_l\mu_o A_o j\sqrt{\frac{2}{\rho}|p_p - p_d|}$ – stream of fuel flowing through the intake hole in the injection pump, j – nozzle hole number, $p_p - p_d$ – difference pressures between the chamber in the injection pump cylinder and the inlet space, q_u – stream of leakages of fuel as the result of the leakiness of the pumping element, w_{s1} – control indicator equal 1 or – 1 depending on the sign of the pressure difference $p_p - p_d$, $w_{s2}\mu_z A_z\sqrt{\frac{2}{\rho}|p_p - p_l|}$ – stream of fuel flowing through the discharge valve, $A_z(h_g)$ – the cross-section between the socket and the head of discharge valve, $p_p - p_l$ – differential pressure between chamber in the cylinder of the injection pump and fuel injection pipe, w_{s2} – the control indicator equal is 1 or – 1 depending the sign of differential pressure, $p_p - p_l$, c_z – velocity of the inlet fuel stream, $\frac{V_p}{E}\frac{dp_p}{d\tau}$ – stream of fuel accumulated in the V_p volume of the cylinder as the result of the change of the prevailing pressure.

Boundary conditions in pumping subsystem of injection pump determine the equation of head of discharge valve [5]:

$$m_z\frac{d^2h_z}{d\tau^2} = A_z(p_p - p_l) - w_{or}\frac{dh_z}{d\tau} - (P_z + k_z h_z) \tag{9}$$

where: $m_z\frac{d^2h_z}{d\tau^2}$ – inertia force working on the moving elements of the valve (mass of head and one third mass of

the spring), A_z – cross-section of discharge valve, k_z – spring constant, P_z – force of preliminary of the valve spring tension, w_{or} – motion resistance coefficient.

Continuity equation for the flow for chambers in discharge connector of the injection pump is possible to calculate according to the pattern:

$$\frac{V_2}{E}\frac{dp_k}{dt} = w_{s2}\mu_z A_z\sqrt{\frac{2}{\rho}\left|p_p - p_k\right|} + A_z\frac{dh_g}{d\tau} - A_k c_k \qquad (10)$$

where: $A_k c_k$ – fuel stream flowing from the pumping subsystem of the injection pump to the chamber of injection pump with the cross-section area and injection speed c_k, $\frac{V_2}{E}\frac{dp_k}{dt}$ – fuel stream accumulated in the volume V_k capacity of the connector tube of injection pump the result of the move of the valve head pumping as the result of the pressures change.

Residual pressure values p_{sc} are possible to measure or approximately can be calculated according to the formula:

$$p_{sc} = p_{ow} - \Delta p = p_{ow} - E\frac{V_{hp} - V_o}{V_{hp}} \qquad (11)$$

where: p_{ow} – injector opening pressure, Δp – pressure drop caused by the opening of the injector nozzle, E – modulus of fuel elasticity, V_{hp} – volume of the high pressure part of the system injection subsystem, V_o – relief volume.

In the papers geometric models were swapped over based on design requirements and measurements of real elements of injection apparatus [6, 14]. In the paper [12] a functional model drawn up was elaborated for the different type of the medium-speed marine engine.

4.3. Regard into account the changeability of parameters of fuel

The fuel is a perfectly springy liquid and defers to the Hooke's law, which determines the change of the length of the element triggered with change of the pressure [5]:

$$\varepsilon_c = \frac{dp}{E} = -\frac{dx}{x} = -\frac{dV}{V} \qquad (12)$$

where: ε_c – unit change in length of the element of the liquid, dx – change the length of the fuel element, dV – change of the volume of the fuel element.
Assuming that the mass of the element due to pressure increase will not change, it can be written as:

$$dV = d\left(\frac{m}{\rho}\right) = -\frac{m}{\rho^2}d\rho \qquad (13)$$

where ρ is density of the fuel.

The speed of the propagation of the pressure wave $a_{p,t}$ in the injection subsystem is determined by the elasticity of E fuel, the elasticity of material of the injection pipe according to the formula:

$$a_{p,t} = \frac{1}{\sqrt{\rho_{p,t}\left(\frac{1}{E_{p,t}} + \frac{1}{E_s}\frac{d_{wl}}{s_l}\right)}} \qquad (14)$$

$E_{p,t}$ – modulus of elasticity of fuel at pressure p and temperature t, E_s – modulus of elasticity of the material injection, d_{wl} – internal diameter of injection pipes, s_l – injection pipe wall thickness.

Sebyła based on experimental studies formulated the equation on $E_{p,t}$ in the form [5]:

$$E_{p,t} = E_{ot} + 9.375p - 0.00625p^2 \qquad (15)$$

where: E_{ot} – modulus of elasticity at the atmospheric pressure and the given temperature. On the Fig. 8. the course of the modulus of elasticity of fuel was shows for one circulation of the engine changing depending on the pressure and the temperature.

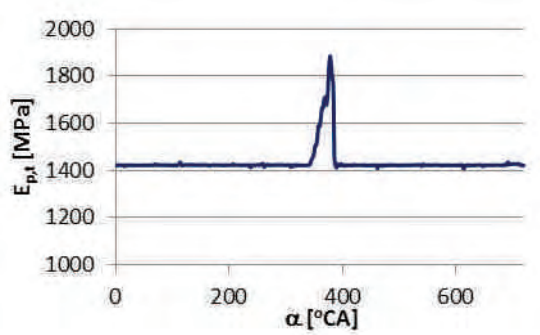

Fig. 8. The course of the modulus of elasticity of fuel was shows for one circulation of the engine

The influence of inlet liquid fuel temperature and pressure on direct-injection diesel engines can be significant. The primary fuel temperature effects on the injection parameters come from the fuel elasticity modulus of elasticity and the density with the fuel viscosity less significant as the injector subsystem flow is usually in a turbulent region [2].

Increasing the fuel temperature by 1 K in the x place caused by the pressure increase of 10 MPa [5], which can be written as:

$$t_{px} = t_d + (p_{px} - p_o)/10 \qquad (16)$$

where: t_{px} – pressure of fuel in the x place, t_d – temperature of the inlet of fuel, p_{px} – pressure of fuel in the x place, p_o – ambient pressure.

The density of fuel is being changed with the change of temperature and pressures. Individual authors are giving different relations, and according to Dowa and the Finn determine the pattern [5]:

$$\rho_{p,t} = \rho_o(1 + mp - np^2) \qquad (17)$$

where: m, n – the factors dependent on the temperature, ρ – density of fuel in current terms, p – pressure of fuel.

It is hard at deriving equations describing the movement of fuel in the wire to include constant changes of the pressure, flows of fuel, but adoption of their constant value is an significant error [4, 14]. On Fig. 9 the course of the density of fuel was showed within one circulation.

Dynamic viscosity varies with temperature and fuel pressure, and it was calculated according to the relation:

$$\eta_{p,t} = \eta_{20}\left(\frac{20}{t}\right)^{w_t} e^{w_p} \qquad (18)$$

where: η_{20} – absolute viscosity of fuel at the atmospheric pressure and the environmental temperature, absolute viscosity of fuel at the atmospheric, w_t – temperature coefficient, w_p – pressure coefficient.

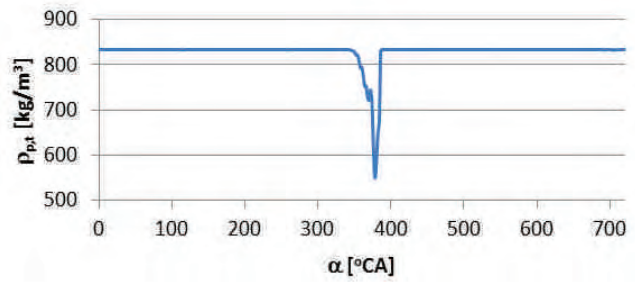

Fig. 9. Change of the fuel density of $\rho_{p,t}$ depending on the pressure and the temperature

The kinematic viscosity can be calculated from the relation:

$$\nu_{p,t} = \frac{\eta_{p,t}}{\rho_{p,t}} \tag{19}$$

or from the empirical model [5].

4.4. Calculating losses and coefficients

During the model calculations a number of losses and simplifications were assumed. The stream of leaked fuel from injection pump can be calculated with the formula [8]:

$$q_{pp} = \frac{p_t w_{sc} \delta^3}{12 \eta_{p,t}} \tag{19}$$

w_{sc} – factor in determining the ratio of the width to the length of slot, δ – radial clearance between piston and sleeve.

Radial clearance between the plunger and the cylinder fuel injection pump and nozzle body and needle for was determined for operated state by the geometric measurements [6, 14]. The flow coefficient depends on the substantial amount of factors as: shapes of holes, radii of the edge, state of the surface, geometrical dimensions, Reynolds number, parameters of flowing fuel [5, 6]. Yomaoka and others gave the formula for empirical coefficient of discharge valve in the form [18]:

$$\mu_z = 0.26 \, \mathrm{tg}^{-1}\left[(4p + 500)\left(h_z - \frac{0.0144}{\sqrt[3]{p}}\right)\right] + 0.15 \tag{20}$$

where: h_z lift of the delivery valve.

In the forces acting on the moving parts of delivery valves and injector valves should be taken of the strength of the opposition's force of movement which results from the viscosity of fuel filling room up on the circumference of the element. This force is proportional to the lateral surface of the element and the gradient of the fuel speed:

$$P = \eta_{p,t} \pi d_m l_e \frac{dc}{dn} \tag{21}$$

where: d_m – diameter of the movable element, l_e – the length of the element movable, n – normal coordinate to the direction of movement of the movable element.

$$P = \eta_{p,t} \frac{\pi d_m l_e}{\delta} c = w_{or} \frac{dx}{d\tau} \tag{22}$$

where: $w_{or} = \eta \frac{\pi d_m l_e}{\delta}$ coefficient of resistance of the move of the element of valve head, δ – layer thickness of fuel between the movable element and the wall of the body.

The friction losses in rectilinear or gently bent pipes are calculated from the formula [3]:

$$h_{stl} = \frac{\Delta p}{\gamma} = \lambda_l \frac{lc^2}{2gd_l}, \ \lambda = \lambda(\mathrm{Re}, r/d_l) \tag{23}$$

where: Δp – drop of the pressure, γ – specific gravity of liquid, λ_l – coefficient of linear losses on friction, r/d_l – relative roughness of the internal wall of the pipe, Re – Reynolds number.

The line loss factor is calculated depending on the type of flow [3]:

– for flow in the Reynolds number range 3000 to 80 000:

$$\lambda_l = \frac{0.316}{\mathrm{Re}^{0.25}} \tag{24}$$

– for larger number of Reynolds number 100 000 to 1 600 000 according to the formula Schilera-Herman:

$$\lambda_l = 0.0054 + 0.396 \, \mathrm{Re}^{-0.3} \tag{25}$$

At flows under pressure local losses associated with sudden changes of the diameter and direction which the viscosity of liquid is causing are appearing in wires and they depend on the Reynolds number. The height of the local losses is expressed by the formula:

$$h_{stl} = \xi_l \frac{c^2}{2g} \tag{26}$$

where: ζ – dissipation local factor, g – gravitational acceleration.

The following local loss cases were accounted in the injection subsystem of the tested engine [1]: knee and inflection of the injection line, sudden constriction at the outlet of the injection pump and entry into the spray opening, inlet with rounded edges, tees, etc.

4.5. Comparison of the calculated and measured results

Due to the limited volume of this article, only the examples of the injection pump were give. The relation of the set of functional elements is shown in Figure 1.

The stream of fuel pumped by individual holes of the injection subsystem can be transformed in order to appoint the pressure course of fuel in spaces of the injection subsystem. The pressure sensor in the experimental study was placed at the point where the pressure in the injection pump cylinder was measured. The formula for the fuel stream flowing through the delivery valve is of the form (equation 8):

$$q_z = w_{s2}\mu_z A_z \sqrt{\frac{2}{\rho}|p_p - p_l|} \tag{26}$$

The fuel stream pumped by the plunger of the injection pump depends on the diameter d_p of the piston of the pump and the pumping speed of c_p and perhaps to be calculated as:

$$q_p = \frac{\pi d_p^2 c_p}{4} \tag{27}$$

This stream should be reduced by the losses shown in chap. 4.4. Fig. 10 illustrates exemplary of the pressure

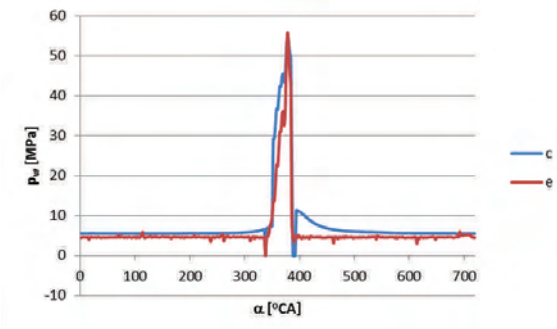

Fig. 10. The pressure course of in the injection pump measured in experimental studies (e) and calculated (c) for the 100% of the engine load

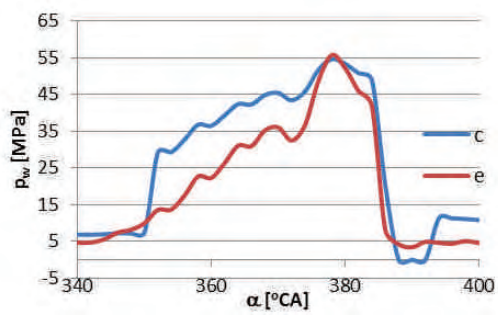

Fig. 11. Fragment of pressure courses in the injection pump measured in experimental studies (e) and calculated (c) for the 100% of the engine load

course of fuel pumped in the injection pump, appointed based on calculations and from experimental investigated and at the rotation speed of camshaft at 250 rpm. The figure shows that the waveforms are similar.

For a better comparison of the courses studied, the part of the waveforms was shown where the fuel injection occurred (Fig. 11). The figure shows that the maximum values of the waveforms are the same, while the values of the experimental pressure are generally lower. At the end of fuel injection, there are also differences in residual pressure.

5. Conclusions

The mathematical model for numerical simulation of injection processes was developed and verified by experiments under several operating load regimes. Estimated courses of the pressure in chambers of the injection subsystem are similar to courses occurring in the experimental road in laboratory tests of the real engine. Presented model requires correcting to the purpose increasing of pressure course in injection subsystem calculated to experimental.

Elaborated geometric and functional model of injector subsystem and used mathematical relations, enable to conduct the wide scope of research of the fuel injection process.

The input variables can be: fuel setting, fuel inlet pressure of injection pump, opening pressure of the injector, engine parameters and operating conditions of the injector. Features of the technical state can be design features of the elements of injection subsystem, changed according to the value of design solutions and processes of wear and damages.

Currently operated the conventional injection systems may be also optimized thanks to the modelling from the point of view of useful engine parameters and diagnosis methods, and especially under the angle of ecological requirements which must to fulfil. The elaborated model out makes possible the quick simulation of this process in different variants, without the construction of prototypes or time-consuming experimental investigations.

Acknowledgements

This research outcome has been achieved under the research project Ecological and economic aspects of the operation of selected elements of marine power systems No. 1/S/IESO/2014 financed from a subsidy of the Ministry of Science and Higher Education for statutory activities.

Nomenclature

a	speed of sound propagation in fuel
A_p	area of cross-section of the plunger
A_z	area of cross-section of the in-valve chamber
c	velocity
d_p	piston diameter
E	modulus of fuel elasticity
H_p	position of the piston of injection pump
l	pipe length
m	mass
m_z	mass of moving elements in the valve
p	pressure
P	force
p_p	pressure in chamber of pumping section
p_z	pressure in chamber of the delivery valve
q	streams of fuel flowing into and out of space
t	temperature
V	volume
V_p	volume of fuel pressed by the injection pump
x	length of the liquid element
α	crank angle
λ	dissipation factor linear to the friction
μ	flow coefficient
η	instantaneous dynamic viscosity coefficient of fuel
ρ	density of the fuel
τ	time

Bibliography

[1] BUKOWSKI, J. Mechanika płynów, *PWN*, Warszawa 1975.

[2] CHEN, G. Study of fuel temperature effects on fuel injection, combustion, and emissions of direct-injection diesel engines. *Trans. ASME. J. Eng. Gas Turbines and Power.* 2009, **2**, 022802/1-022802/8.

[3] CIAŁKOWSKI, M. Mechanika płynów, *Wyd. Politechniki Poznańskiej*, Poznań 2000.

[4] CYGAN, S., SZYMAŃSKI J. Podstawowe problemy doboru aparatury wtryskowej silników wysokoprężnych. *WKiŁ*, Warszawa 1979.

[5] FALKOWSKI, H., HAUSER, G., JANISZEWSKI, T., JASKUŁA A. Układy wtryskowe silników wysokoprężnych. Modelowanie. *WKiŁ*, Warszawa 1989, cz. 2.

[6] JERMAK, C., MAJCHROWSKI, R., MONIETA, J. The application of geometric measurement and analysis of images for mapping geometric model marine engine injection equipment. *Combustion Engines*. 2011, **146**(3), 71-72.

[7] KEGL, B. Numerical analysis of injection characteristics using biodiesel fuel, *Energy & Fuel*. 2006, **22**(2), 2377-2378.

[8] KIIJÄRVI, J. Diesel fuel injection system simulation. Publications of the Internal Combustion Engine Laboratory Helsinki University of Technology Teknillisen korkeakoulun polttomoottori laboratorion julkaisuja Espoo 2003.

[9] KOLADE, B., BOGHOSIAN, M., REDDY P., GALLAGHER S. Development of a general-purpose, thermal-hydraulic software and its application to fuel injection systems. *SAE Technical Paper.* 2003, 2003-01-0702.

[10] LEONARSKI, P. Opracowanie modeli diagnostycznych wybranego okrętowego silnika spalinowego. *Praca dyplomowa inżynierska*. Akademia Morska w Szczecinie, Wydział Mechaniczny, Szczecin 2016.

[11] LEJDA, K., USTRZYCKI, A. Modelling of injection characteristic with in-line type injection pump in diesel engines. *III International Scientific-Technical Conference EXPLODIESEL & GAS TURBINE'03, Gdańsk – Międzyzdroje – Lund.* 5-9.05.2003, 369-374.

[12] MONIETA, J. Functional model of injector of medium-speed marine diesel engine. *Journal of KONES 2007 Powetrain and Transport.* 2007, **14**(3), 423-428.

[13] MONIETA, J. The application in-cylinder pressure course in different domains for diagnostics of medium speed marine diesel engines in operation conditions. *Combustion Engines*. 2013, **154**(3), 153-160.

[14] MONIETA, J. Zastosowanie pomiarów geometrycznych i analizy obrazów do odwzorowania modelu geometrycznego pomp wtryskowych silnika okrętowego. *XXXIII Symposium of Power Plant, SYMSO 2012*, Gdynia 2012, 37, cd. 1-8.

[15] PIASECZNY, L., KAFAR, I. Simulation researches of evaporation and combustion of a single drop of fuel in CI engine. *Journal of Kones. Combustion Engines*. 2001, **8**(1-2), 312-319.

[16] SABAU, A., BARHALESCU, M.L., OANTA, E. Modeling of high-pressure fuel injection systems. *Annals of DAAAM for 2012 & Proceedings of the 23rd International DAAAM Symposium*, Vienna, Austria, 2012, 1019-1022.

[17] SOBIESZCZAŃSKI, M. Modelowanie procesów zasilania w silnikach spalinowych. *WKiŁ*, Warszawa 2000.

[18] YOMAOKA, K., SAITO, A., OKAZAKI, M. Analysis or by-pas control type fuel injection system for small diesel engine by digital computer. *Bulletin of the JSME.* 1972, **82**.

Jan Monieta, DEng. – Faculty of Mechanical Engineering at Maritime University of Szczecin.

e-mail: *J.Monieta@am.szczecin.pl*

Article citation info:
SOCHACZEWSKI, R., CZYŻ, Z., SIADKOWSKA, K. Modeling fuel injector two-stroke diesel engine. *Combustion Engines*. 2017, **170**(3), 147-153. DOI: 10.19206/CE-2017-325

Rafał SOCHACZEWSKI
Zbigniew CZYŻ
Ksenia SIADKOWSKA

CE-2017-325

Modeling a fuel injector for a two-stroke diesel engine

This paper discusses the modeling of a fuel injector to be applied in a two-stroke diesel engine. A one-dimensional model of a diesel injector was modeled in the AVL Hydsim. The research assumption is that the combustion chamber will be supplied with one or two spray injectors with a defined number of nozzle holes. The diameter of the nozzle holes was calculated for the defined options to provide a correct fuel amount for idling and the maximum load. There was examined the fuel mass per injection and efficient flow area. The studies enabled us to optimize the injector nozzle, given the option of fuel injection into the combustion chamber to be followed.

Key words: *diesel engine, two-stroke, fuel injector, modeling*

1. Introduction

The targeted measures to decrease fuel efficiency, emissions and improve power-to-density ratio are important not only in internal combustion engines in automotive applications but also engines in aviation applications. So, research is continued to introduce innovative technologies or upgrade the so far known ones that due to their materials or unconventional solutions could not be applied before. One of them is the opposed-piston two-stroke diesel engine [10, 13, 18]. When compared with standard engines, it shows many advantages, including:

– its combustion chamber is the space limited by two pistons reciprocating in a single cylinder line, which means no need to use heads and reduces heat loss,
– no valve mechanism and no loss due to its driving,
– reciprocating cylinders favor engine balance.

Its disadvantages are:

– a gearbox connecting two crankshafts or a complex crank system with a single shaft,
– a fuel injector inside a liner is perpendicular to the axis of the cylinder – a nozzle is selected for a given combustion chamber.

A special combustion chamber requires a new design of a fuel nozzle. Defining an injector nozzle is expensive and long-term. To speed up optimization and reduce the number of experiments, a technique of numerical modeling is applied. The literature describes many models of operation of injectors in a commona rail system: identifying capabilities of multiple injection to reduce the emissions of particulates and nitrogen oxides [1], macro- and microscopic behavior of the dynamics of multiple injection [5, 7], modeling a control valve to describe the impact of cavitation on losses in flow [2, 9, 17]. There are also strength tests of injector's elements to specify stresses and deformations in the injector due to injection-generated external loads [11], [15]. Both individual elements [1, 5, 7, 9] and the entire fuel injection systems [12, 17, 20, 21] are modeled.

When a fuel injector for a given combustion chamber is designed, previously specified nozzle parameters should be optimized by simulation. For given operating conditions (fuel pressure, amount of fuel injected, injection time, etc.), the number and diameter of nozzle holes should be determined first. These parametrs can be determined mathematically from the correlation of mass flow rate. Another method is the simulation to specify more parameters that have an impact on injector mass flow rate. The so obtained research results, e.g. mass flow rate of fuel injected can be used as an input for the next stage of combustion research.

One of the tools to model injection systems is AVL software of BOOST-HYDSIM. This is a program dedicated to the dynamic analysis of hydraulic and hydro-mechanical and control systems [3, 4, 6, 19]. It is based on the theory of fluid dynamics and vibration of multi-body systems. The main application area of BOOST Hydsim is the simulation of fuel injection.

This research combines a mathematical analysis and modeling to correctly select an injector nozzle for an opposed-piston two-stroke diesel engine. The research enables us to specify a diameter and number of nozzle holes to inject enough fuel at idling and the maximum load.

2. Principles of the model

The minimum and maximum amounts of fuel were determined from the AVL Boost calculations for an engine cooperating with a given propeller (third-degree curve) that can load of 100 kW at 4000 rpm. As a result, there was created fuel vs. power characteristics (Fig. 1) and the characteristics of compression pressure, maximum pressure and mean cylinder pressure (Fig. 2) vs. crankshaft speed. The research results are given in Table 1.

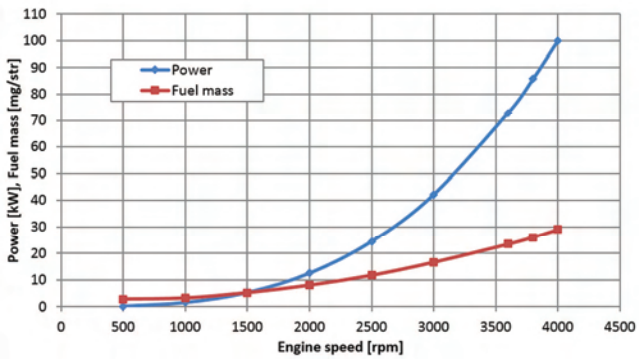

Fig. 1. Fuel amount and engine power vs. crankshaft speed

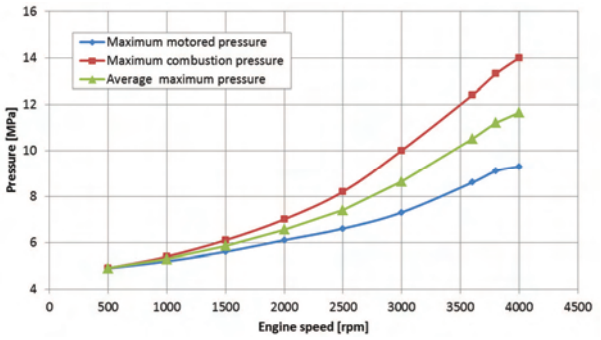

Fig. 2. Maximum motored pressure, maximum combustion pressure and average maximum pressure vs. crankshaft speed

Table 1. Research results of the propeller-loaded engine

Rotational speed	Power	Fuel mass per cylinder	Max. motored pressure	Max. combustion pressure	Average max. pressure
[rpm]	[kW]	[mg]	[MPa]	[MPa]	[MPa]
500	0.2	2.8	4.9	4.9	4.90
1000	**1.6**	**3.2**	**5.2**	**5.4**	**5.30**
1500	5.3	5.2	5.6	6.1	5.85
2000	12.5	8.0	6.1	7.0	6.55
2500	24.4	11.7	6.6	8.2	7.40
3000	42.2	16.6	7.3	10.0	8.65
3600	72.9	23.4	8.6	12.4	10.50
3800	85.7	26.0	9.1	13.3	11.20
4000	**100.0**	**29.0**	**9.3**	**14.0**	**11.65**

The results enable us to specify the boundary amounts of fuel to be injected: at idling at a crankshaft speed of 1000 rpm and for a maximum power at a crankshaft speed of 4000 rpm. Also, the boundary conditions for a cylinder, i.e. air pressure in the cylinder, into which fuel is injected were specified as mean compression pressure and the maximum pressure. The research data are given in Table 2.

Table 2. Simulation parameters

Type of operation	Rotational speed	Power	Fuel mass	Mean cylinder pressure
	[rpm]	[kW]	[mg/cylinder]	[MPa]
idle	1000	1.6	3.2	5.30
max. load	4000	100	29	11.65

To achieve a favorable air-fuel mixture, i.e. the largest possible contact surface of fuel injected with air, the fuel is assumed to be injected with one or two injectors of the number of nozzle holes as in Table 3.

Table 3. Options of the number of nozzle holes

Number of injectors per combustion chamber	Number of nozzle holes			
	2	3	4	6
1			•	•
2	•	•	•	

3. Model of an injector

Our research uses a Common Rail system injector design controlled with a solenoid valve because of the overall dimensions of the injector that define its weight and the ease of installation and arrangement of injectors on the engine. Fig. 3 depicts a model of the injector created in the Boost Hidsim.

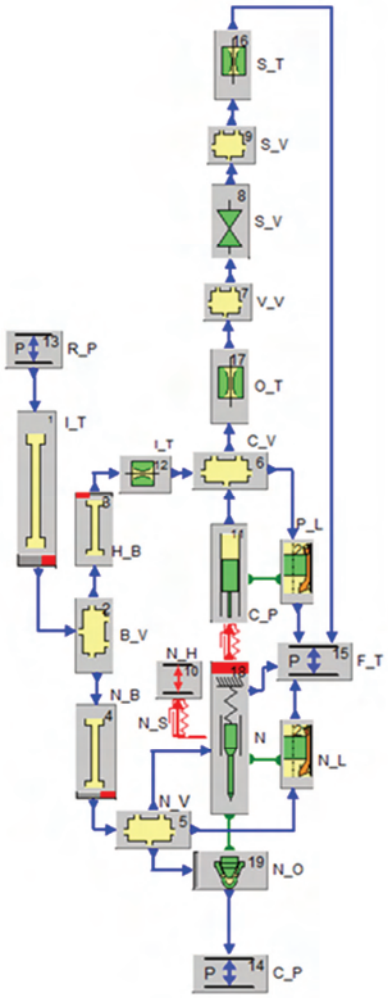

Fig. 3. Model of the injector in the Boost Hidsim

We modeled a valve closes orifice nozzle of a real geometry in which its efficient flow field is calculated from the height of the nozzle needle. The coefficient of through-the-injector-hole-flow loss is as 0.83, given that a correlation of an edge rounding and a hole diameter as r/d = 0.2 [8]. A control valve was modelled as a throttle in which the flow field is a function of time. In cooperating elements like a needle with a nozzle body and a control piston with a cylinder, there is assumed a loss due to fuel leaks. The model of fuel leaks is based on the Hagen-Poiseuille law, given a laminar flow through Annular Gap which changes according to fuel pressure [3].

A given amount of fuel is injected by estimating the minimum flow field for assumed parameters of injection and properties of the fuel. This is possible using sophisticated hydraulic models [14]. Approximate dependence was used in the studies [13]:

$$\dot{m}_e = c_d \cdot A_n \cdot \sqrt{2 \cdot \rho_f \cdot \Delta p} \tag{1}$$

where $\dot{m}_e$ – fuel mass flow rate [mg/cycle], c_d – outflow coefficient, A_n – minimal flow field [mm^2], ρ_f – fuel density [kg/m^3], $\Delta p = (p_2 - p_1)$ – pressure difference [MPa], p_1 – combustion chamber air pressure, p_2 – injected fuel pressure. The relationship was transformed to the following formula for the minimum injection field of a single nozzle hole:

$$A_{ni} = \frac{m \cdot 360 \cdot n}{\Delta\Theta \cdot c_d \cdot i \cdot i_1 \cdot \sqrt{2 \cdot \rho_f \cdot \Delta p}} \quad (2)$$

where m – fuel mass [mg/cylinder], n – rotational speed [r/s], A_{ni} – minimum flow field of a single nozzle hole [mm^2]; $A_n = A_{ni} \cdot i \cdot i_i$; i – number of injectors per cylinder, i_i – number of nozzle holes, $\Delta\Theta$ – injection time [°CA].

The diameters were determined, given that the flow through each of the injection nozzles is quasi static, incompressible and one-dimensional. The reduced diameter range was used to perform Boost Hydsim calculations. So, these were the conditions (Table 4) to investigate the injector's mass flow rate. It was assumed that there are two doses of fuel (t_1 – pilot and t_2 – main) to be injected at idling and injection pressure to be as 30 MPa. If the maximum load, there is one dose of the fuel injected at a pressure range of 100–180 MPa.

Table 4. Injection times and pressures

Number of nozzle holes	Nozzle hole diameter [mm]	Injection time [ms]	Injection pressure [MPa]
One injector			
4	$d_4 = \begin{cases} 0.14 \\ 0.16 \end{cases}$	b.j $\begin{cases} t_1 = 0.30 - 0.40 \\ t_2 = 0.40 - 0.70 \end{cases}$ max. load t_2 = 1.00	30 – idle; 100 – 180 – max. load
6	$d_6 = \begin{cases} 0.12 \\ 0.14 \end{cases}$		
Two injectors			
2	like for d_4	b.j $\begin{cases} t_1 = 0.30 - 0.40 \\ t_2 = 0.40 - 0.70 \end{cases}$ max. load t_2 = 1.00	30 – idle; 100 – 180 – max. load
3	like for d_6		
4	d_{42} = 0.10		

4. Research results

4.1. Idle

One injector

Given the values of the parameters and the calculated hole diameters, the minimal injection time when the injector completely opens was calculated. An outflow is limited by a field of injector hole but not the gap between the needle and the seat in the nozzle. The injector will not operate within a range of ballistic amounts of fuel. There are the research results of the injector operating in idling conditions. The maximum efficient flow field was compared (Fig. 5 and Fig. 7) to the flow field due to the injector hole diameter and the fuel mass per injection (Fig. 4 and Fig. 6). Table 5 and 6-hole nozzles.

4 holes

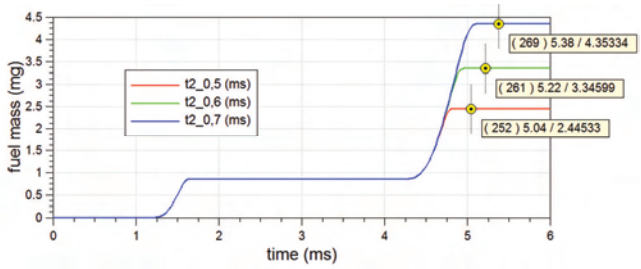

Fig. 4. Fuel mass (4-hole nozzle, t_1 = 0.4 ms; d_4 = 0.14 mm) at injection times of a main fuel dose t_2 = 0.5; 0.6; 0.7 ms

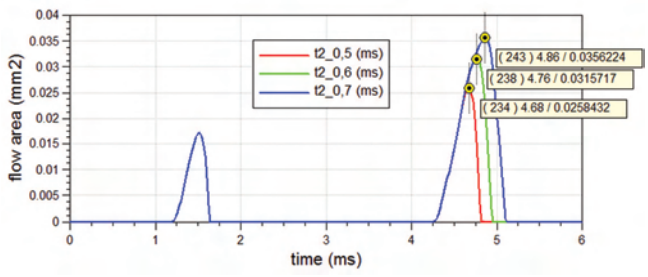

Fig. 5. Flow area (4-hole nozzle, t_1 = 0.4 ms; d_4 = 0.14 mm) at injection times of a main fuel dose t_2 = 0.5; 0.6; 0.7 ms

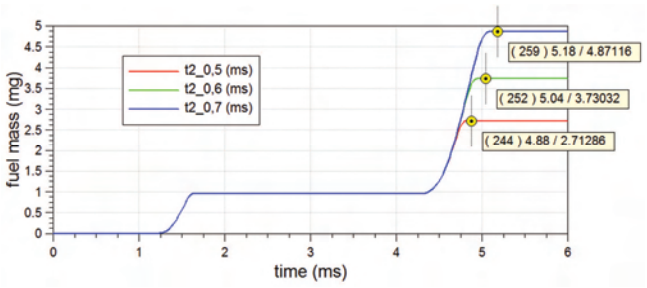

Fig. 6. Fuel mass (4-hole nozzle, t_1 = 0.4 ms; d_4 = 0.16 mm) at injection times of a main fuel dose t_2 = 0.5; 0.6; 0.7 ms

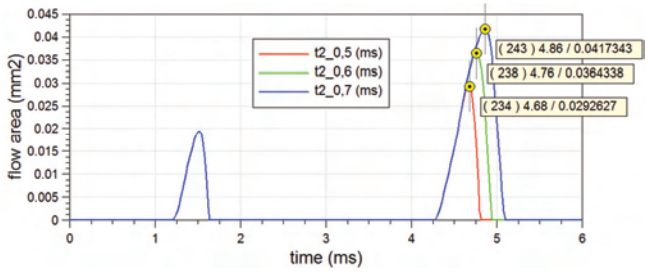

Fig. 7. Flow area (4-hole nozzle, t_1 = 0.4 ms; d_4 = 0.16 mm) at injection times of a main fuel dose t_2 = 0.5; 0.6; 0.7 ms

Table 5. Simulation for a 4-hole nozzle

Hole diameter d_4	Injection times of main fuel dose t_2	Minimum flow area	Calculated flow area	Required fuel mass	Calculated fuel mass
[mm]	[ms]	[mm^2]	[mm^2]	[mg]	[mg]
0.14	0.50	0. 01485	0.02584	3.20	2.44
	0.60		0.03157		3.35
	0.70		0.03562		4.35
0.16	0.50	0. 02186	0.02926	3.20	2.71
	0.60		0.03643		3.73
	0.70		0.04173		4.87

Given the diameters as d_4 = 0.14 and 0.16 mm and injection times of main fuel doses as t_2, the flow field is minimal in the assumed range. This means that the main doses are injected within a non-ballistic range. At the same time, if injecting the pilot dose t_1 = 0.40 ms and the main dose $t_2 \approx 0.60$ ms, the required dose at idle is achieved.

6 holes

Given the diameters d_6 = 0.12 and 0.14 mm and injecting the main fuel doses of t_2, the flow field is minimal in the assumed range. This means that the main doses are injected within a non-ballistic range. At the same time, if injecting the pilot dose t_1 = 0.40 ms and the main dose $t_2 \approx 0.5$–0.60 ms, the required dose at idle is achieved.

Table 6. Simulation for a 6-hole nozzle

Hole diameter d_6	Injection times of main fuel dose t_2	Minimum flow area	Calculated flow area	Required fuel mass	Calculated fuel mass
[mm]	[ms]	[mm^2]	[mm^2]	[mg]	[mg]
0.12	0.50	0.01221	0.03152	3.20	3.00
	0.60		0.03815		4.11
	0.70		0.04258		5.36
0.14	0.40	0.01457	0.02358	3.20	2.29
	0.50		0.03647		3.36
	0.60		0.04533		4.65

Then, the injection of a dose at the maximum load for the given variations should be investigated.

a) Two injectors

2 and 3 holes

Given the number of nozzle holes as 2, 3 and 4, the nozzle hole diameter to inject a fuel dose at idle as 1,6 mg/injector was calculated. By changing the correlation between the number of injectors and the number of nozzle holes, identical nozzle hole diameters were achieved. This fact refers to a 2- and 3-hole nozzle. The difference may be due to the fact that for a less number of nozzle holes, the minimum flow field can be achieved at a less elevated nozzle needle so shorter injection times. Accordingly, there was verification calculation for the given hole diameter of 2- and 3-hole nozzles, injection times, idling pressure and maximum load. The research results are given in Table 7 and Table 8.

Table 7. Simulation for a 2-hole nozzle

Hole diameter	Injection times of main fuel dose t_2	Minimum flow area	Calculated flow area	Required fuel mass	Calculated fuel mass
[mm]	[ms]	[mm^2]	[mm^2]	[mg]	[mg]
0.14	0.50	0. 01485	0.01382	1.60	1.35
	0.55		0.01533		1.57
	0.60		0.01647		1.82
0.16	0.50	0.02186	0.01585	1.60	1.51
	0.55		0.01775		1.77
	0.60		0.01930		2.05

The minimum flow field is achieved for both hole diameters when injecting the main dose $t_2 > 0.55$ ms, whereas an idling dose is achieved by injecting the pilot dose $t_1 = 0.40$ ms and the main dose $t_2 \approx 0.55$–0.6 ms.

The calculations for a 6-hole nozzle show that it is possible to inject an idling dose if nozzle diameters are $d_6 = 0.12$ and 0.14 mm. However, for a dose at the maximum load for the diameter of $d_6 = 0.14$ mm, injection pressure and injection time of the main dose t_2 should be significantly increased (Fig. 13, Table 11). Accordingly, one type of a hole diameter, i.e. $d_3 = 0.12$ mm only was assumed for a 3-hole nozzle. The injection time of the main dose was also reduced. The research results are given in Table 8.

Table 8. Simulation for a 3-hole nozzle

Hole diameter	Injection times of main fuel dose t_2	Minimum flow area	Calculated flow area	Required fuel mass	Calculated fuel mass
[mm]	[ms]	[mm^2]	[mm^2]	[mg]	[mg]
0.12	0.40	0. 01138	0.01203	1.60	1.17
	0.45		0.01480		1.42
	0.50		0.01702		1.69

Given the diameter $d_3 = 0.12$ mm and injecting the main fuel doses $t_2 > 0.40$ ms, the flow field is minimal. At the same time, if injecting the pilot dose of $t_1 = 0.40$ ms and the main dose of $t_2 \approx 0.5$ ms, the required dose at idle is achieved.

4 holes

Analogue calculations as for a 1-nozzle injector were performed for a 4-hole injector. A hole diameter for a 4-hole nozzle was calculated as $d_4 = 0.10$ mm and calculations for idling were performed. The main dose injection times were as $t_2 = 0.40$; 0.45; 0.50 ms. The research results are depicted Fig. 8, Fig. 9 and Table 9.

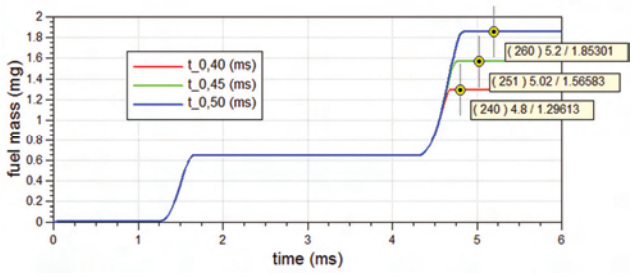

Fig. 8. Fuel mass (4-hole nozzle, $t_1 = 0.4$ ms; $d_4 = 0.10$ mm) at injection times of a main fuel dose $t_2 = 0.40$; 0.45; 0.50 ms

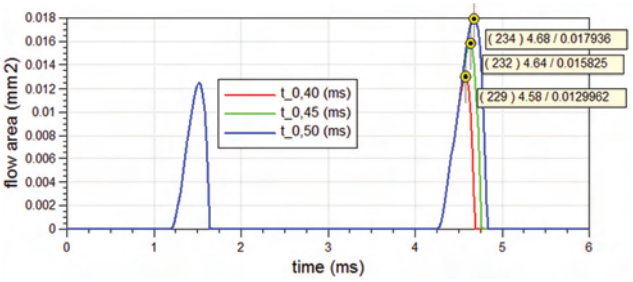

Fig. 9. Flow area (4-hole nozzle, $t_1 = 0.4$ ms; $d_4 = 0.10$ mm) at injection times of a main fuel dose $t_2 = 0.40$; 0.45; 0.50 ms

Table 9. Simulation for a 4-hole nozzle

Hole diameter	Injection times of main fuel dose t_2	Minimum flow area	Calculated flow area	Required fuel mass	Calculated fuel mass
[mm]	[ms]	[mm^2]	[mm^2]	[mg]	[mg]
0.10	0.40	0.00796	0.01300	1.60	1.27
	0.45		0.01583		1.57
	0.50		0.01794		1.85

Given the diameter $d_4 = 0.10$ mm and injecting the pilot dose at $t_1 = 0.40$ ms and the main dose at $t_2 > 0.40$ ms, the minimal flow field and the required dose at idle are achieved.

4.2. Maximum load

a) One injector

4 holes

Given the nozzle hole diameters calculated at idling, the mass flow rate of an injector at the maximum load was calculated. The amount of fuel under such conditions is about 29 mg/cylinder injected as a single dose. The calculation principles are as follows: fuel injection is as injecting the main dose, main dose injection time is $t_2 = 1.0$ ms, fuel injection pressure is p = 120–180 MPa.

The simulation results are given in Fig. 10, Fig. 11 and Table 10.

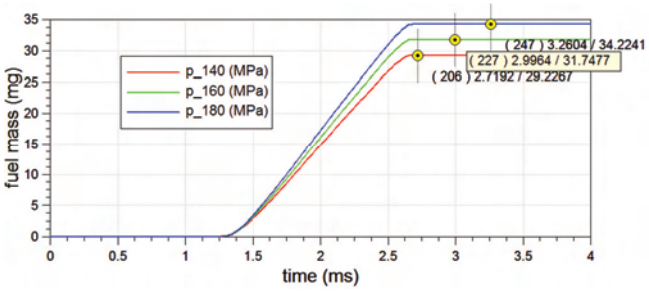

Fig. 10. Fuel mass (4-hole nozzle, t_2 = 1.0 ms; d_4 = 0.14 mm) at injection pressures as p = 140, 160, 180 MPa

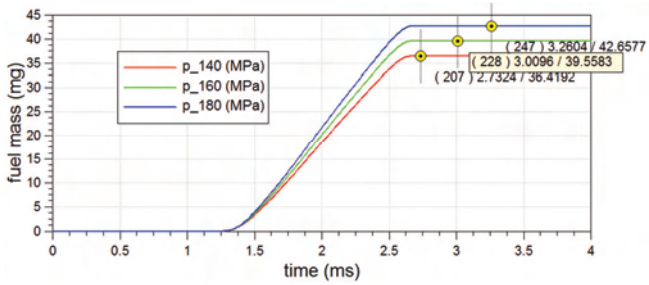

Fig. 11. Fuel mass (4-hole nozzle, t_2 = 1.0 ms; d_4 = 0.16 mm) at injection pressures as p = 140, 160, 180 MPa

Table 10. Simulation for a 4-hole nozzle

Hole diameter	Fuel pressure	Required fuel mass	Calculated fuel mass
[mm]	[MPa]	[mg]	[mg]
0.14	140	29.00	29.23
	160		31.75
	180		34.22
0.16	140		36.42
	160		39.56
	180		42.66

For the maximum load, it is better to use the hole diameter in a 4-hole nozzle as d_4 = 0.14 mm. Due to the large mass flow rate for a diameter nozzle as d_4 = 0.16 mm, fuel injection pressure or main dose injection time should be reduced.

6 holes

The hole diameters in a 6-hole injector are d_6 = 0.12 and 0.14 mm. The mass flow rates for this type of injector at the maximum load were calculated at injection pressures of 120 to 180 MPa according to the nozzle hole diameters. Fig. 12 and Fig. 13 show the mass of injected fuel for the different injection pressures. The research results are given in Table 11.

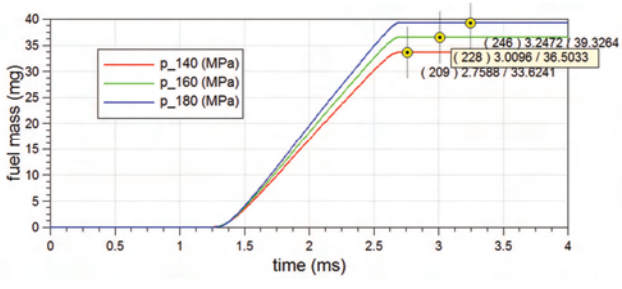

Fig. 12. Fuel mass (6-hole nozzle, t_2 = 1.0 ms; d_6 = 0.12 mm) at injection pressures as p = 140, 160, 180 MPa

Due to the large mass flow rates (d_6 = 0.12 mm) for the diameter nozzle d_6 = 0.14 mm, injection pressure was reduced to 120–140 MPa.

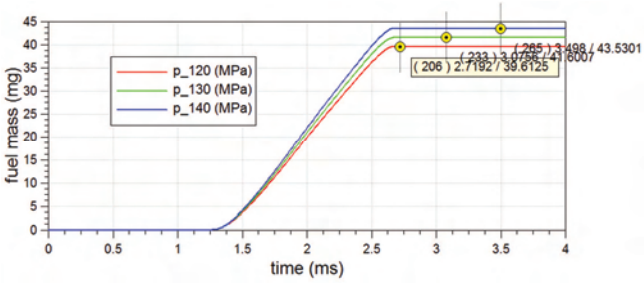

Fig. 13. Fuel mass (6-hole nozzle, t_2 = 1.0 ms; d_6 = 0.14 mm) at injection pressures as p = 140, 160, 180 MPa

Table 11. Simulation for a 6-hole nozzle

Hole diameter	Fuel pressure	Required fuel mass	Calculated fuel mass
[mm]	[MPa]	[mg]	[mg]
0.12	140	29.00	33.62
	160		36.50
	180		39.33
0.14	120		39.61
	130		41.60
	140		43.53

For the maximum load, it is better to use a nozzle hole diameter in a 6-hole nozzle as d_6 = 0.12 mm. For a diameter nozzle as d_4 = 0.16 mm, fuel injection pressure or main dose injection time should be reduced.

b) Two injectors

2 and 3 holes

Given nozzle hole diameters in a 2-hole injector calculated for idling as d_4 = 0.14 and 0.,16 mm, mass flow rates at the maximum load were calculated. The amount of fuel per injector injected under these conditions is about 14.5 mg as a single dose. The principles behind the calculations are identical as in those for a single injector.

Fig. 14 and Fig. 15 show the fuel mass for the hole diameters d_4 varied due to injection pressure. The research results are given in Table 12.

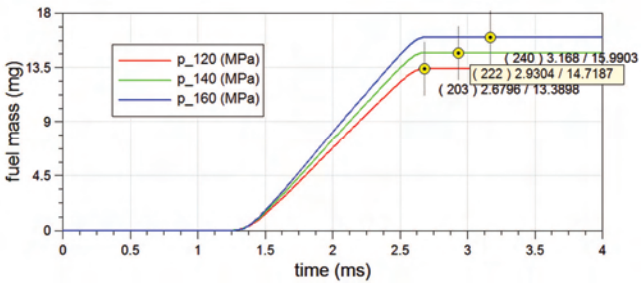

Fig. 14. Fuel mass (2-hole nozzle, t_2 = 1.0 ms; d_2 = 0.14 mm) at injection pressures as p = 120, 140, 160 MPa

A nozzle with the hole diameter of 0.16 mm, despite its low injection pressure as 100 MPa, shows a larger than required mass flow rate. Accordingly, the hole diameter of d_4 = 0.14 mm should be used in the two types of injectors with a 2-hole nozzle.

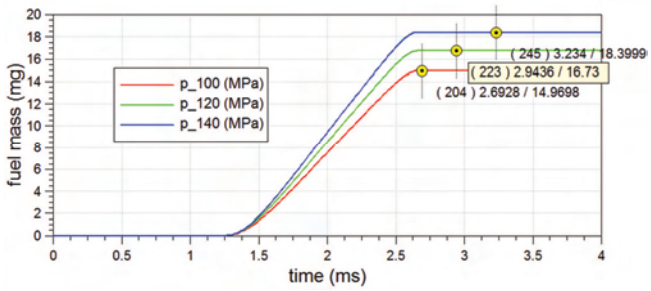

Fig. 15. Fuel mass (2-hole nozzle, t_2 = 1.0 ms; d_4 = 0.16 mm) at injection pressures as p = 120, 140, 160 MPa

Table 12. Simulation for a 2-hole nozzle

Hole diameter	Fuel pressure	Required fuel mass	Calculated fuel mass
[mm]	[MPa]	[mg]	[mg]
0.14	120	14.50	13.39
	140		14.72
	160		15.99
0.16	100		14.97
	120		16.73
	140		18.40

A mass of injected fuel for the 3-hole nozzle of a hole diameter of d_3 = 0.12 mm and injection pressures as p = 120, 140, 160 MPa (Fig. 16) was calculated At the maximum load, the required dose is achieved at the injection pressure of 120 MPa. For higher pressures, main dose injection time should be reduced (Table 13).

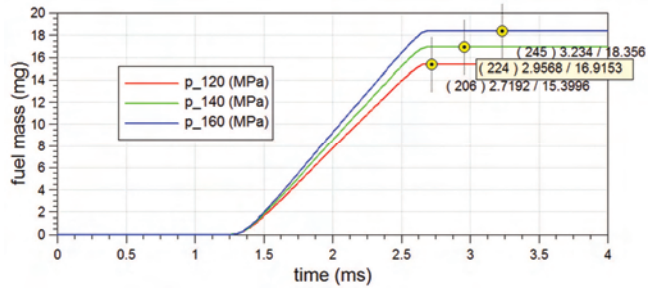

Fig. 16. Fuel mass (3-hole nozzle, t_2 = 1.0 ms; d_3= 0.12 mm) at injection pressures as p = 120, 140, 160 MPa

Table 13. Simulation for a 3-hole nozzle

Hole diameter	Fuel pressure	Required fuel mass	Calculated fuel mass
[mm]	[MPa]	[mg]	[mg]
0.12	120	14.50	15.40
	140		16.92
	160		18.36

4 holes

It was calculated a mass of injected fuel for the 4-hole nozzle of the hole diameter of d_{42} = 0.10 mm and injection pressures as p = 120, 140, 160 MPa (Fig. 16). At the maximum load, the required dose is achieved at the injection pressure of 120 MPa. For higher pressures, main dose injection time should be reduced (Table 13).

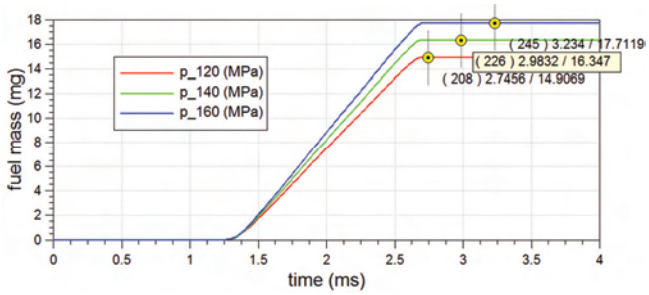

Fig. 17. Fuel mass (4-hole nozzle, t_2 = 1.0 ms; d_{42} = 0.10 mm) at injection pressures as p = 120, 140, 160 MPa

Table 14. Simulation for a 4-hole nozzle

Hole diameter	Fuel pressure	Required fuel mass	Calculated fuel mass
[mm]	[MPa]	[mg]	[mg]
0.10	120	14.50	14.91
	140		16.35
	160		17.71

Summary

Two options of injection were investigated while modeling an injector. For an input parameter, i.e. the fuel mass required at idling and the maximum load, the assumption is that the fuel is injected into the cylinder with one or two injectors. Depending on the option, the number of nozzle holes was assumed to be from 2 to 6 so the number and diameter of hole nozzles for the options were determined as follows:

a) one injector

- a 4-hole injector of a hole diameter as d_4 = 0.14 mm or optionally d_4 = 0.16 mm at reduced injection pressure or time,
- a 6-hole injector of a hole diameter as d_6 = 0.12 mm

b) two injectors

- 2-hole injectors of a hole diameter as d_2 = 0.14 mm,
- 3-hole injectors of a hole diameter as d_3 = 0.12 mm,
- 4-hole injectors of a hole diameter as d_4 = 0.10 mm.

The research results will be used to create the geometry to develop nozzles for a given fuel injector to perform bench tests. Such research will enable us to determine the mass flow rate and characteristics of the injectors. The mass flow rated calculated will be entered into the AVL Fire to optimize the combustion process.

Acknowledgement

This work has been realized in the cooperation with The Construction Office of WSK "PZL-KALISZ" S.A." and is part of Grant Agreement No. POIR.01.02.00-00-0002/15 financed by the Polish Nation-al Centre for Research and Development.

Bibliography

[1] AMOIA, V., FICARELLA, A., LAFORGIA, D., DE MATTHAEIS, S. A theoretical code to simulate the behavior of an electro-injector for diesel engines and parametric analysis. *SAE Transaction*. 1997, 970349.

[2] ARCOUMANIS, C., GAVAISES, M., ABDUL-WAHAB, E., MOSER, V. Modeling of advanced high pressure systems for passenger car diesel engines. *SAE Technical Paper*. 1999, 1999-01-0910.

[3] AVL BOOST Hydsim Primer, Version 1.2013.

[4] AVL BOOST Hydsim User Guide.

[5] BIANCHI, G., PELLONI, P., CORCIONE, F., LUPPINO, F. Numerical analysis of passenger car HSDI diesel engines with the 2nd generation of common rail injection systems: the effect of multiple injections on emissions. *SAE Technical Paper*. 2001, 2001-01-1068.

[6] CAIKA, V., SAMPL, P. Nozzle flow and cavitation modeling with coupled 1D-3D AVL software tools. *SAE Technical Paper*. 2011, 2011-24-0006.

[7] CATALANO, L., TONDOLO, V., DADONE, A. Dynamic rise of pressure in the common-rail fuel injection system. *SAE Technical Paper*. 2002, 2002-01-0210.

[8] DONGIOVANNI, C., COPPO, M. Accurate modelling of an injector for common rail systems. doi: 10.5772/9728, 2010.

[9] FICARELLA, A., LAFORGIA, D., LANDRISCINA, V. Evaluation of instability phenomena in a common rail injection system for high speed diesel engines. *SAE Technical Paper*. 1999, 1999-01-0192.

[10] FRANKE, M., HUANG, H., LIU, J.P. et al. Opposed piston opposed cylinder (opoc™) 450 hp engine: performance development by CAE simulations and testing [C]. *SAE Technical Paper*. 2006, 2006-01-0277.

[11] GANCARCZYK, T., KNEFEL, T. Modelowe analizy pompy wysokiego ciśnienia układu Common Rail. *Mechanik*. 2013, **2**.

[12] GAUTIER, C., SENAME, O., DUGARD, L., MEISSONNIER, G. Modelling of a diesel engine common rail injection system. *IFAC 16th Word Congress*. Prague, 2005.

[13] HEYWOOD, J.B. Internal combustion engine fundamentals. *McGraw-Hill International Editions*. 1988.

[14] HIROYASU, H. Diesel engine combustion and its modeling. In Diagnostics and Modeling of Combustion in Reciprocating Engines. 53-75, *COMODIA 85, Preceedings of Symposium.* Tokyo 1985.

[15] KNEFEL, T., GANCARCZYK, T. Dynamic and strength analysis of injector of common rail injection system. *Combustion Engines*. 2013, **154**(3), 953-959.

[16] LINO, P., MAIONE, B., PIZZO, A. Nonlinear modelling and control of a common rail injection system for diesel engines. *Applied Mathematical Modelling*. 2007, **31**, 1770-1784.

[17] PAYRI, R., CLIMENT, H., SALVADOR, F., FAVENNEC, A. Diesel injection system modelling. Methodology and application for a first-generation common rail system. *Proceedings of the Institution of Mechanical Engineering*. 2004, **218**, Part D.

[18] PIRAULT, J.-P., FLINT, M. Opposed piston engines: evolution, use, and future applications. *SAE International*. Warrendale. 2009, doi:10.4271/R-378.

[19] PIROOZ, A. Effects of injector nozzle geometry on spray characteristics, an analysis. *Indian J.Sci.Res*. 2014, **5**(1), 354-361.

[20] SEYKENS, X.L.J., SOMERS, L.M.T., BAER, R.S.G. Detailed modeling of common rail fuel injection process. *Journal of Middle European Construction and Design of Cars*. 2005, **III**, 30-39.

[21] SEYKENS, X.L.J., SOMERS, L.M.T., BAER, R.S.G. Modelling of common rail fuel injection system and influence of fluid properties on injection process. *Proceedings of VAFSEP*. Dublin, 2004.

[22] ZHANG, Z., ZHAO, C., XIE, Z. et al. Study on the effect of the nozzle diameter and swirl ratio on the combustion process for an opposed-piston two-stroke diesel engine. *Energy Procedia*. 2014, **61**, 542-546.

Rafał Sochaczewski, DEng. – Faculty of Mechanical Engineering at the Lublin University of Technology.

e-mail: *R.Sochaczewski@pollub.pl*

Zbigniew Czyż, MEng. – Faculty of Mechanical Engineering at the Lublin University of Technology.

e-mail: *Z.Czyz@Pollub.Pl*

Ksenia Siadkowska, MEng. – Faculty of Mechanical Engineering at the Lublin University of Technology.

e-mail: *K.Siadkowska@pollub.pl*

Article citation info:
KRUCZYŃSKI, S., ŚLĘZAK, M., GIS, W. et al. Problems in fuelling spark ignition engines with dimethyl ether. *Combustion Engines*. 2017, **170**(3), 154-158. DOI: 10.19206/CE-2017-326

Stanisław KRUCZYŃKI
Marcin ŚLĘZAK
Wojciech GIS
Piotr ORLIŃSKI
Andrzej KULCZYCKI
Wojciech DZIĘGIELEWSKI
Mateusz BEDNARSKI

CE-2017-326

Problems in fuelling spark ignition engines with dimethyl ether

This paper discusses briefly the production technology of dimethyl ether, taking into account plant raw materials and the physical and chemical properties of DME as compared to diesel fuel. The benefits and disadvantages of DME as a fuel are presented and changes in the emission of harmful substances characterised as compared to the combustion of diesel fuel. Also, basic usage problems are addressed, e.g. the wear of engine's elements, cavity and leakages in the fuel system.

Key words: *alternative fuels*, *fuel system*

1. Introduction

Extensive development of vehicle transport over the past decades has resulted in bigger consumption of engine fuels and rapid degradation of the environment. The need to ensure fuel supply – matching the growing demand – on world markets, combined with depleting crude oil resources brought a greater interest in alternative fuels. The selection of alternative fuels is determined by four criteria:

- availability of raw material,
- degree to which the production technology is available,
- impact on the degradation of environment throughout the entire life cycle (WtW),
- feasibility in terms of powering modern-day engines.

One of the alternative fuels that according to the aforesaid criteria appears more advantageous than a number of biofuels is dimethyl ether (DME) [2, 5, 11]. Its production has been developed chiefly in Asian countries – a major worldwide producer of DME is China, where coal is the basic raw material. In Europe there are several pilot installations, among others in Sweden and Denmark. Raw materials used for DME production may include:

- coal,
- natural gas,
- solid biomass,
- liquid biomass,
- biogas,
- waste, e.g. waste plastics.

High diversity of the raw materials that may be used stems from the method of producing the said fuel. Raw materials containing in their structure carbon and hydrogen, regardless of the manner of their bonding in particles are transformed into syngas, i.e. a combination of CO and H_2 in adequate proportions. In the next phase syngas is used for the synthesis of methanol, of which DME is ultimately produced. Below are presented chemical reactions occurring in respective phases of DME synthesis.

Hydrogen essential for adjusting the composition of syngas is usually the product of conversion of carbon oxide into vapour:

$$CO + H_2O \longrightarrow CO_2 + H_2 \qquad \Delta H = -40.9 \text{ kJ/mol}$$

Pyrolysis Gasification

raw material (C, H) → pyrolytic gas → CO, H_2 (syngas)

Gasification

→ CO, H_2 (syngas)

Syngas – a combination of CO and H_2 in proportion suitable for the synthesis is the product of combining purified products of gasification with hydrogen:

$$CO + 2H_2 \longrightarrow CH_3OH \qquad \Delta H = -90.7 \text{ kJ/mol}$$

$$CO_2 + 3\,H_2 \longrightarrow CH_3OH + H_2O \qquad \Delta H = -49.5 \text{ kJ/mol}$$

$$2\,CH_3OH \longrightarrow H_3COCH_3 + H_2O$$

The aggregate process of DME synthesis from syngas is as follows:

$$3CO + 3H_2 \longrightarrow CH_3OCH_3 + CO_2 \qquad \Delta H = 246.0 \text{ kJ/mol}$$

The formula of DME synthesis reaction is unrelated to the raw material. In technological practice raw material has considerable impact on the chemical composition of gasification products, which must be purified from sulphur compounds (mainly SO_3), partly CO_2, non-combusted hydrocarbons and a number of other chemical pollutants. In case of certain raw materials this process is very problematic in terms of effective production of syngas of a particular purity and a specified CO/H_2 proportion.

Methane or bio-methane is another raw material attractive for DME/bioDME synthesis. If DME is synthetized from natural gas or biogas, the process chart is similar as the one presented above. The only difference takes place in the initial phase, where methane (biogas) is directly processed into syngas. Those technologies have been developed by BP Chemicals and Haldor Topsoe, and also several Japanese companies, in collaboration with Total oil and gas company. Another important aspect as regards the implementation and use of bioDME is the reduction of CO_2 emissions in the fuel consumption chain. In accordance

with Directive 2009/28/EC [6] bioDME is considered to reduce CO_2 emission in the life cycle at the level of 92-92%, depending on the biomass material.

Due to its properties, DME may be stored and transported as LPG. Usually DME is stored in aboveground or underground containers with a horizontal axis and transported by road or railway tanks.

2. DME physical and chemical parameters

Dimethyl ether (DME), with a structure described by CH_3-O-CH_3 formula in standard conditions (0.1 MPa pressure, temperature of 273.15 K) is a colourless gas with a characteristic odour. Compressed under pressure higher than 0.6 MPa, it undergoes condensation. In such form it is considered as fuel for SI combustion engines [35]. Basic physical and chemical parameters of liquid DME compared to diesel fuel are presented in Table 1. There are references in literature to other values of parameters corresponding to DME properties.

Table 1. Chosen physical and chemical parameters of DME [10, 24, 27]

Parameter	Unit	DME	ON
Molar mass	g/mol	46.07	c.a.170
Carbon content	% w/w	13	14
Hydrogen content	% w/w	13	14
Oxygen content	% w/w	34.8	0
Hydrogen content	% w/w	13	14
Oxygen content	% w/w	34.8	0
Density	kg/m^3	667	831
Cetane number		> 55	40–50
Auto-ignition temperature	K	508	523
Lower calorific value	MJ/kg	27.6	42.5
Kinematic viscosity at 40º C	mm^2/s	< 0.1	3
AFR		9.0	14.6
Boiling point at 1013,25 hPa	K	248.1	450–643
Vapour enthalpy	kJ/kg	467.13	300
Surface tension at temp. 298 K	N/m	0.012	0.027
Bulk modulus	N/m^2	$6.37 \cdot 10^8$	$14.86 \cdot 10^8$
Vapour pressure at 298 K	kPa	530	< 10

3. Benefits of DME as fuel for SI engines

Low boiling temperature. The boiling temperature of DME is much lower than that of diesel fuel. Because of this parameter, liquid fuel injected to the engine's cylinder is promptly vaporised and therefore the self-ignition delay is shorter. With quick evaporation it is possible to use low injection pressure of (20–30) MPa [3], even in condition of the engine's high rotational speed.

Large cetane number. The cetane number indicating the combustion speed is higher for DME than for diesel fuel. Thus, compared to diesel fuel, DME has a much shorter self-ignition delay and in result the emission of nitrogen oxides [10] is reduced.

Mastered methods of storage and distribution. Because of similar physical and chemical properties of DME and the condensed mixture of propane and butane (LPG), the matter of their storage and distribution is considered well studied. DME can be stored in liquid form in condition of moderate pressure – above 0.6 MPa [10]. According to the results of studies conducted by High Pressure Gas Safety of Japan [15], due to chemical stability during storage, the diffusion ratio and the risk of the tank's explosion in the course of heating are similar for DME and LPG.

Very low toxicity. DME is a volatile organic compound, with no carcinogenic or mutagen properties. Its toxicity is considered very low or insignificant [22]. Also, it is considered that DME does not have any hazardous impact on human health [18].

Non-corrosive for metals. DME does not have any corrosive effect on metals used in the construction of fuel systems in combustion engines [**Błąd! Nie można odnaleźć źródła odwołania.**0].

4. Disadvantages of DME as fuel for SI engines

Low calorific value. Because of the particle structure in DME which contains oxygen, its calorific value accounts for approx. 65% of the calorific value of diesel fuel [14]. Moreover, considering that the density of liquid DME comes to 80% of diesel fuel's density – to achieve a similar calorific effect, a twice greater quantity (in terms of volume) of DME must be injected to the engine's cylinder than that of diesel fuel [21].

Low viscosity. Compared to diesel fuel, DME characterises with very low (at least twenty times lower [31]) viscosity and in consequence also poorer lubricity. Those unfavourable properties cause leakages from the fuel system and also worsen the workability of its movable elements, thus making them more prone to wear due to greater friction [10].

Low bulk modulus. Liquid DME is two to four times more compressible than diesel fuel [30]. For this reason, in fuel systems in SI engines not adapted to the characteristics of liquid DME fuel pressure may be decreased in high-pressure areas of injection systems.

Aggressive towards certain plastics. DME shows corrosive action in most elastomers, damaging sealing elements and other components of fuel systems made of elastomers [7,10, 34].

4. Emission of harmful products of DME combustion

DME produced on an industrial scale from methane can be also derived from renewable resources, e.g. wood. Combustion gases from DME-fuelled engines – compared to those powered with diesel fuel – contain less harmful substances, including particular matter, sulphur oxides and hydrocarbons. The emission of nitrogen oxides and carbon oxide may be smaller or greater, depending on the conditions of engine's operation [**Błąd! Nie można odnaleźć źródła odwołania.**0, 20]. Because of greater volatility of DME than that of diesel fuel, in case of leakage DME rapidly outflows to atmosphere, and thus does not contaminate soil.

Engines fuelled with DME [8, 13, 14] prove to emit less noise and less particular matter, THC and nitrogen oxides. Fuel consumption vs the generated energy is comparable with diesel oil. Studies on a one-cylinder AVL engine with engine displacement equal to 2000 cm^3 with turbocharger and a charge-air cooler proved the following differences in emission compared to diesel fuel combustion – presented in Table 2 [24].

Table 2. Comparison of parameters of SI engine fuelled with diesel fuel and DME [24]

	Diesel fuel	DME
Max. power and torque	comparable	
Fuel consumption	comparable	
Emission		
NO_x (g/[kW·h])	2.83	1.19
THC (g/[kW·h])	0.22	0.22
PM (g//[kW·h])	0.06	0.015
Smoke levels	5%	0%
Noise dB(A)	88	78

Due to high oxygen content and the lack of bonds between carbon atoms (C-C) in a DME particle, the use of that fuel in SI engines helps to reduce PM emission significantly compared to such emission in diesel-fuelled engines [8, 17]. Particular matter present in exhaust gases from DME-fuelled engines is mainly the product of combustion of grease and additives in DME that improve its viscosity [1, [23]]. For this reason, the exhaust cleaning systems in SI engines fuelled with DME usually do not require any PM filtration systems.

The emission of nitrogen oxides resulting from the combustion of DME is not conclusive. It is assumed that because of a shorter self-ignition delay and also a smaller part of the fuel combusted before its full mixing, the emission of nitrogen oxides is lower [14]. The factors listed below reduce the maximum temperature in the combustion chamber and therefore reduce NO_x emission. Nevertheless, increased NO_x emission as compared to a diesel-fuelled engine is possible. This is because of the extended period of the highest temperature throughout the combustion process [3].

The emission of hydrocarbons [4, 16, 19, 23, 26, 28] manifests in cases of a rich mixture, whether local or global. In case of DME, which contains oxygen particles in its structure, the occurrence of a rich mixture locally is limited owing to incomplete fuel & air mixing. As regards carbon monoxide, an increase in the emission is recorded occasionally – compared to diesel fuel which may be attributed to longer injection while at the same time its pressure is lower and the diameter of openings in the fuel injection system is greater. However, reducing HC and CO emissions is relatively easy owing to popular oxidising catalytic reactors.

Because of a shorter self-ignition delay and the resulting slower increase of pressure inside the combustion chamber, a reduction of noise levels generated by the combustion engine is observed [8, 15].

There are several compounds that should be considered, even though they are not regulated, in fuelling SI engines with DME. The emission of formaldehydes [32, 33] is greater and also moderate emission of sulphur dioxide, polycyclic aromatic hydrocarbons, benzene, toluene and xylene [32, 33] may be expected.

Laboratory research has been conducted to evaluate the reactivity and ozone forming potential [12, 17, 24] when fuelling engines with DME. In a typical urban atmosphere the DME reactivity is equal to or lesser than in case of conventional fuel. Therefore, it is reasonable to assume that the use of DME – compared to conventional fuel – may have positive impact on ozone levels in urban agglomerations. DME resilience in troposphere has been estimated to last 5–6 days.

5. Usage problems relating to SI engines fuelled with DME

Pure DME cannot be considered as a substitute of diesel fuel. Its use for fuelling combustion engines requires a modification of the fuel system and the use of additives improving certain physical and chemical properties of DME.

Critical problems concerning the use of SI engines fuelled with DME are discussed below:

Excessive wear of elements of the fuel system due to greater friction. The relatively low viscosity of DME implies poor greasing properties of the fuel. This results in greater friction between the movable parts of certain elements of the fuel system such as injection pumps, pumps in Common Rail and injectors [**Błąd! Nie można odnaleźć źródła odwołania.**0], thus accelerating their wear.

Low viscosity of DME may be resolved by additives improving the lubricity, a change in materials used in the fuel systems and processing of surfaces exposed to greater wear because of friction [31]. Among those solutions the most effective may be considered additives enriching DME.

Positive results have been proved in using commercial additives for DME [9], mainly those improving its lubricating properties. Those additives can be added in an amount ranging from 100 to 1000 mg/kg. Moreover, as fuel constituents improving its lubricity, added may be substances such as diesel, castor oil, vegetable oils and related esters [7, 15, 27, 29].

Fig. 1 presents examples of results of a lubricity study on DME, where DME is enriched with various additives, based on Medium Frequency Pressurised Reciprocating Rig [27], which is a modification of the standard HFRR method (High Frequency Reciprocating Rig), wherein the grease properties of fuel are expressed as the diameter of wear scad measured with precision up to 1 μm. DME additives included methyl esters of colza oil, castor oil and Lubrizol 539. For comparison, ill. 1 also shows additional lubricity criteria for diesel fuel.

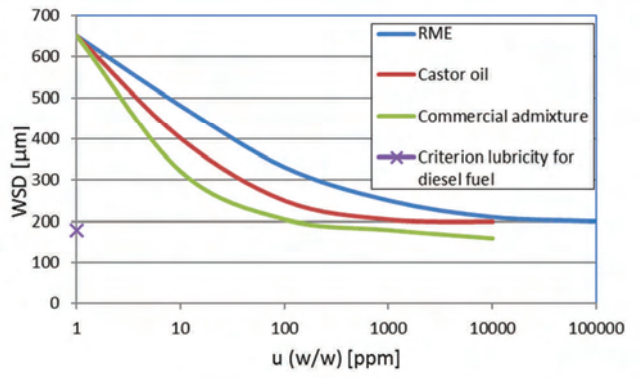

Fig. 1. Results of DME lubricity study – DME enriched with methyl esters of colza oil, castor oil and WSD (wear scad diameter) [27]

As illustrated by the above, even a small amount added of a substance improving lubricity changes DME properties considerably. According to the cited studies [2, 14], the

commercial additive proved to be the most effective. A dose of 800 ppm is sufficient to achieve lubricity comparable with that of diesel fuel. It should be noted that methyl esters of colza oil and castor oil, which are cheaper than commercial additives, also allow for improving the lubricity of DME.

Leaks from the fuel system. Factory fuel systems of SI engines fuelled with diesel are not adapted for DME because of great likelihood of leakages. Literature refers to two main causes of such leakages: low viscosity of DME and aggressive action of DME on sealing elements. Even in conditions of atmospheric pressure, DME leakage may be considerable, even if lack of tightness occurs between elements moving between each other, e.g. piston – cylinder in injection pumps, coming to as much as (40 ÷50)% of the fuel quantity [11]. Greater leakages are observed in case of engines intended for trucks and machinery equipment than in light-duty vehicles [9].

Leakages from the DME fuel systems may be prevented also by increasing its viscosity by applying suitable additives, as discussed earlier and also by exchanging sealing elements prone to corrosion into elements covered with Teflon or made of PTFE [10, 7, 34].

Cavity in the injection system. Due to high vapour pressure of DME cavity may develop in injection systems in engines fuelled with DME. Cavity results in hindered flow of fuel and corrosion of the system's elements. The intensity of cavity increases with the increase of fuel's temperature and occurs more frequently in areas of non-defined, dynamic fuel flow. An effective method of preventing cavity in DME injection systems is to maintain fuel pressure in the system above (1.2–3) MPa [11, 31].

Nomenclature

DME	dimethyl ether	SI	self-ignition engine
bioDME	dimethyl ether of plant origin	WSD	wear scad diameter

Bibliography

[1] ARCOUMANIS, C., BAE, C., CROOKES, R., KINOSHITA, E. The potential of di-methyl ether (DME) as an alternative fuel for compression-ignition engines: A review. *Fuel*. 2008, **87**, 1014-1030.

[2] BOLLON, F. DME standardization, DME/LPG blends. Mat. *Konf. POLBIOF'2007*. Kraków 2007.

[3] CIPOLAT, D. Combustion aspects of a compression ignition engine fueled on DME. *Proceedings of the seventh international conference on energy for a clean environment;* 2003, **156**.

[4] CROOKES, R., BOB-MANUEL, K. Di-methyl ether or rapeseed methyl ester: a preferred alternative fuel option for future diesel engine operation. *Proceedings of the fifth international colloquium on fuels*. 2005, 181-187.

[5] CURRAN, H.J., FISCHER, E.M., GLAUDE, P.A. et al. Detailed chemical kinetic modeling of diesel combustion with oxygenataed fuels. *SAE Technical Paper*. 2001, 2001-01-0653.

[6] Dyrektywa Parlamentu Europejskiego i Rady 2009/28/WE z dnia 23 kwietnia 2009 r. w sprawie promowania stosowania energii ze źródeł odnawialnych zmieniająca i w następstwie uchylająca dyrektywy 2001/77/WE oraz 2003/30/WE.

[7] EDGAR, B., DIBBLE, R.W., NAEGELI, D.W. Autoignition of di-methyl ether and di-methoxy methane sprays at high pressures. SAE Technical Paper. 1997, 971677.

[8] FLEISCH, T.H., MEURER, C. DME, the diesel fuel for the 21st Century? *AVL conference engine and environment*. 1995.

[9] GOTO, S., OGUMA, M., SUZUKI, S. Research and development of a medium duty DME truck. *SAE Technical Paper*. 2005, 2005-01-2194.

[10] GÓRSKI, W., JABŁOŃSKA, M. Eter dimetylowy – uniwersalne, ekologiczne paliwo XXI wieku. *Nafta-Gaz*. 2012, **9**, 631-641.

[11] GÓRSKI, W., KULCZYCKI, A. Dimethyl ether. A future fuel for diesel engine? *Przemysł Chemiczny*. 2009, **88**(5), 222-227.

[12] KAORU, F. DME handbook, *Japan DME Forum*. 2007.

[13] KAPUS, P., OFNER, H. Development of fuel injection equipment and combustion system for DI diesels operated on di-methyl ether. *SAE International Journal of Fuels and Lubricants*. 1995, **104**(4), 54-59.

[14] KAPUS, P.E., CARTELLIERI, W., ULEV potential of a DI/TCI diesel passenger car engine operated on di-methyl ether. *SAE Technical Paper*. 1995, 952754.

[15] MILLIS, A. Status and future opportunities for conversion of synthesis gas to liquid fuels. *Fuel*. 1994, **73**, 1243-1279.

[16] MINGFA, Y., ZUNQUING, Z., SIDU, X., MAOLING, F. Experimental study on the combustion process of dimethyle ether (DME). *SAE Trans J Fuel Lubr*. 2003, **112**(4), 2422-2429.

[17] MIYAMOTO, H., OGAWA, H., ARIMA, T., MIUAKIWA, K. Improvement of diesel combustion and emissions with various oxygenated fuel additives. *SAE Technical Paper*. 1996, 962115.

[18] OGAWA, T., INOUE, N., SHIKADA, T., OHNO, Y. Direct dimethyl ether synthesis. *Journal of Natural Gas Chemistry*. 2003, **12**, 219-227.

[19] PANA, C., NEGURUESCU, N., POPA, M.G. et al. Performance of a DME fueled diesel engine. *Proceedings of the fifth international colloquium on fuels*. 2005.

[20] PARK, S.H., LEE, C.S. Applicability of dimethyl ether (DME) in a compression ignition engine as an alternative fuel. *Energy Conversion and Management*. 2014, **86**, 848-863.

[21] SATO, Y., LEE, S., TAKAYANAGI, T. et al. Research and development of heavy-duty truck fueled with DME – development and performance of a DME engine. 2005.

[22] SEMELSBERGER, T.A., BORUP, R.L., GREENE, H.L. Dimethyl ether (DME) as an alternative fuel. *Journal of Power Sources*. 2006, **156**(2), 497-511.

[23] SIDHU, S., GRAHAM, J., STRIEBICH, R. Semi-volatile and particulate emissions from the combustion of alternative diesel fuel. *Chemosphere*. 2001, **42**, 681-690.

[24] SINIOR, J.E. Consultants, fundamental aspects of dimethyl ether. *U.S. Department of Energy*. 1998, Washington.

[25] SIVEBAEK, I.M. End-report of annex XX of the IEA/AMF of the IEA. *DME as an Automotive Fuel II*. Part 2. DTU 2001.

[26] SONG, J., HUANG, Z., QIAO, X., WANG, W. Performance of a controllable premixed combustion engine fueled

with dimethyl ether. *Energy Convers Manage*. 2004, **45**, 2223-2232.
[27] SORENSON, S.C., GLENSVIG, M., ABATA, D. Di-metyl ether in diesel fuel injection systems. *SAE International Journal of Fuels and Lubricants*. 1998, **107**(4), 438-449.
[28] SORENSONS, S.C., MIKKELSEN, S. Performance and emissions of a 0.273 l direct injection diesel engine fuelled with neat dimethyl ether. *SAE Trans J Fuel Lubr*. 1995, **104**(4), 80-90.
[29] SORENSONS, S.C. Dimethyl ether, in: Alternative fuels for transportation, Ramadhas A. S. (red.). *CRC Press*, Boca Raton 2010.
[30] TENG, H., MCCANDLESS, J.C., SCHNEYER, J.B. Thermo-chemical characteristics of di-methyl ether – an alternative fuel for compression-ignition engines. *SAE Trans J Fuel Lubr*. 2001, **110**(4), 96-106.
[31] TSUCHIYA, T., SATO, Y. Development of DME engine for heavy-duty truck. *SAE Technical Paper*. 2006, **52**(1).
[32] VERBEEK, R.P., VAN DOOM, A., VAN WALWIJK, M. Global assessment of di-methyl ether as an automotive fuel. second ed., 96.OR.VM.029. 1/RV, *TNO Road-Vehicles Research Institute*, 1996.
[33] WESTBROOK, C.K. Chemical kinetic modeling of oxygenated diesel fuels in advanced petroleum-based and alternative fuels. *DOE Report*. 1999.
[34] YU, J., BAE, C. Dimethyl ether (DME) spray characteristics compared to diesel in a common-rail fuel injection system. *J Autom Eng Proc IMechE Pt D*. 2003, **217**, 1135-1144.

Prof. Stanisław Wojciech Kruczyński, DSc., DEng. – Motor Transport Institute.
e-mail: *Stanislaw.Kruczynski@its.waw.pl*

Andrzej Kulczycki, DSc., DEng. – Air Force Institute of Technology.
e-mail: *klucza@itwl.pl*

Marcin Ślęzak, DSc., DEng. – Motor Transport Institute.
e-mail: *Marcin.Slezak@its.waw.pl*

Wojciech Dzięgielewski, DEng. – Air Force Institute of Technology.
e-mail: *Wojciech.Dziegelewski@itwl.pl*

Wojciech Gis, DSc., DEng. – Motor Transport Institute.
e-mail: *Wojciech.Gis@its.waw.pl*

Mateusz Bednarski, MEng – Institute of Vehicles, Warsaw University of Technology.
e-mail: *Mateusz.Bednarski@simr.pw.edu.pl*

Piotr Orliński, DSc., DEng. – Institute of Vehicles, Warsaw University of Technology.
e-mail: *P.Orlinski@simr.pw.edu.pl*

Article citation info:
MAZURUK, P., WOJS, M.K., ORLIŃSKI, P., SIKORA, M. Detection of damage to the power supply system of diesel engine under field conditions. *Combustion Engines*. 2017, **170**(3), 159-163. DOI: 10.19206/CE-2017-327

Paweł MAZURUK
Marcin K. WOJS
Piotr ORLIŃSKI
Mieczysław SIKORA

CE-2017-327

Detection of damage to the power supply system of diesel engine under field conditions

Fuel injection system damages is a major problem for internal combustion engines. Approximately 70% of the injection system malfunction is due to injector damages. Authors of the article tested an uniqe method of diagnosis injectors by using an acoustic emission. The acoustic emission signal (EA) is a phenomenon used in various field of technology and it is a wave generated in solid materials. The EA signal was measured during operation of damaged and undamaged injectors body in a few series, analized and verified in term of result obtain in response signals. The relationship between the acoustic emission signal and the injectors operating phases has been determined. On base of coefficient variation of the duration in the third phase the value of which increases substantially when the injectors are damaged were found in ranges of 45%. For corect working injectors value of coefficient variation were found in range from 21% to 37%.

Key words: *acoustic emissions, common rail, combustion engine, injector diagnostics*

1. Introduction

Common rail is mostly used in the construction of industrial compression ignition engines. This is one of the ways to meet increasingly stringent criteria for the emission of toxic substances. Common Rail has many advantages that greatly affect engine performance but also has some disadvantages too. In case of inadequate fuel quality, with high precision of system components, it is very susceptible to damage. Injection system damages are major operational problem for any engine, regardless of its brand, application, power or service life. According to research conducted by the authors about 70% of the injection system malfunction is due to damage to the injectors [2, 5, 8].

The reason for allowing injectors to work, the abnormal operation of which is not visible in the form of symptoms related to a problematic start-up or a perceptible inadequate operation of the engine is the inability to precisely investigate the technical condition of the injectors at the machine stoppage. As a result, there are emissions of toxic substances to the atmosphere, particulate filter is accelerated filling, power output is reduced and, in many cases, this is sudden and unwanted stopping of the engine [2, 3].

2. Aim of the study

Adduced arguments on the need for the diagnosis of injectors in real conditions the engine indicate that there is a need to develop a new, noninvasive method that can be applied in the diagnosis of injectors of common rail while the engine is running. The relationship between the signal of acoustic emission and operation phases of the injector is the aim of the study.

3. Acoustic emission in the diagnosis of combustion engines

The industry is using the phenomenon of acoustic emission to diagnose the state of facilities and equipment engineering for many years [1, 7, 9, 11, 14–16]. Acoustic emission (EA) is a passive method and it does not generate additional energy in the test object or it does not interfere with his work. Therefore it is a non-invasive method. The sources of acoustic emission in solid materials are processes that generate and propagate elastic waves in the material [12, 13]. There is an acoustic emission source signal that reflects the phases of the processes occurring in the Common Rail injectors and it is related to their technical state. The way the technical use of the EA included in ISO 22096, which proposed the use of signal EA for the diagnosis of specified devices, including combustion engines. However, existing methods indication, performed on the engine is running are vague, unreliable and uneconomical.

4. Stand for experimental research

The test stand was the diesel engine Perkins whose schematic (including the high pressure circuit) is shown in Figure 1. A diagnostic computer was connected to the engine. Computer monitors selected parameters of its work during the study [4, 6, 10].

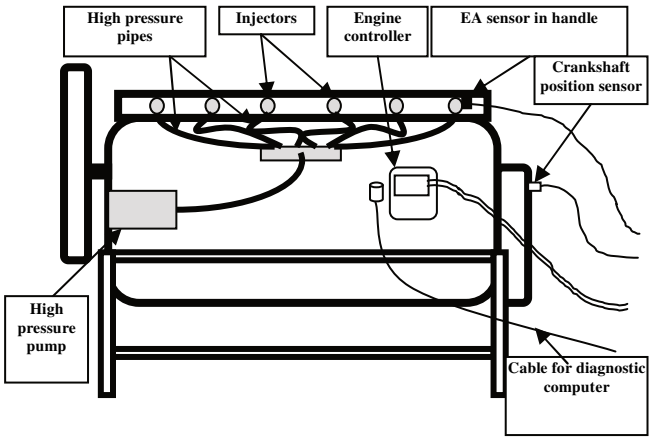

Fig. 1. A simplified diagram of the engine used for testing together with the instrumentation

The basic parameters of the engine used in the tests that are certified according to EU 97/68 / EC Stage IIIA are shown in Table 1.

Table 1. Basic parameters of the tested engine

Number of cylinders	4
Cylinder diameter	Ø105 mm
Piston stroke	127 mm
Engine capacity	4400 cm^3
Maximum power at 2200 rpm	102 kW
Maximum torque at 1400 rpm	536 Nm
Compression ratio	16.2:1
Supply system	Turbocharged with end cooling of the charging air

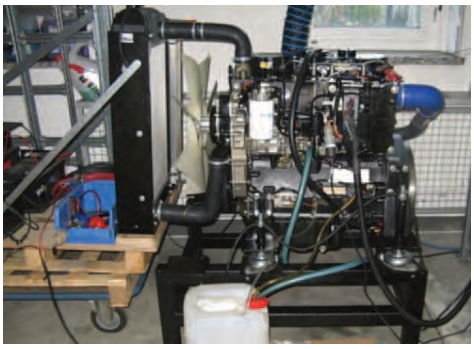

Fig. 2. A view of the PERKINS engine used for experimental research

Each tested injector was mounted on the same cylinder, to achieve a uniform condition during the EA signal measurement for all injectors. The remaining cylinders were fitted with properly functioning, factory-new injectors. The engine was in "perfect" condition (tested, brand new), which allowed us to exclude signals coming from the malfunction of its other functional systems.

The malfunction of most engines can be seen by testing his work at full load. Typical symptoms seen in this way include vibrations, strokes, intermittent work, excessive smoke, lack of power, etc. Those symptoms are usually invisible or impossible to test with the engine idling (while trying engine diagnostics in the field). Therefore, the aim of the research is to diagnose the injector malfunction by means of an acoustic emission already at idle speed of the engine. Detecting anomaly of the injector at idle speed could be done effectively even in the field, at the stoppage of the machine.

An important element of the test is the measurement channel acoustic emission, whose basic elements are shown in Fig. 3.

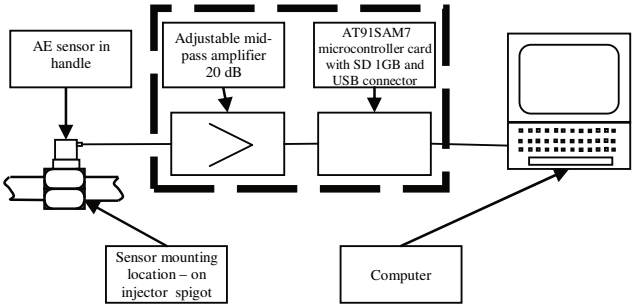

Fig. 3. Simplified schematic of the acoustic emission measurement track

5. Results of studies

The best reference point for the EA injection time sequence is the current signal in the injector electrical coil since it is often not possible to use the TDC position sensor on the engine running and the variability of injection maps that depend on the momentary load or conditions environment.

Figure 4 shows the dependence of the measured EA signal with respect to the control signal for the injection process. The injection consists of two phases: Pre-injection and main injection – blue line on the graph. Referring to the principle of the Common Rail (C-R) injector, it is possible to infer what processes in the injector overlap and which ones are reflected in the EA signal.

In Figure 4 the signal of the EA signal that depends on the injector solenoid coil is shown. The coil control signal during the main injection is divided into the coil excitation phase and then the coil spring, which is mainly related to charging the capacitor. On the basis of the analysis of the injection process on the total acoustic emission graph and the injector coil opening current, the following sectors of the injector can be selected (Fig. 4):

- sector A – the injector does not work, the control chamber and the spray chamber are constant pressure, the coil is not energized and the injector is ready for operation;
- sector B – the injector coil is energized, the anchor lift and fuel flow out of the control chamber, then the injector spur is erected and this is the start of the injection process;
- Sector C – the controller switches off the current signal to the coil, the drain choke closes,
- This is the beginning of the pressure equalization process in the control chamber;
- Sector D – the drain choke from the control chamber is closed by the anchor.

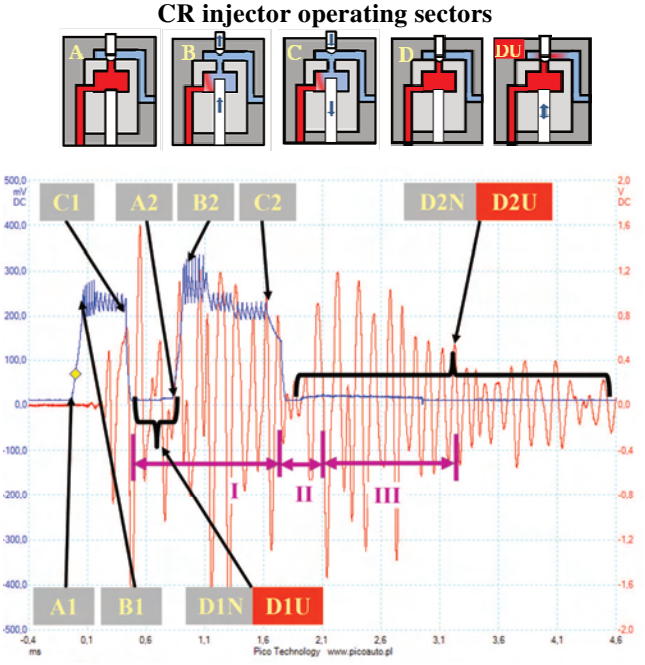

Fig. 4. EA injector signal divide into phases

In a new injector, the sector marked DN (Sector D New Injector) illustrates the pressure equalization in the control chamber, the needle closure, and the injection end. In a damaged injector, the sector described by the DU symbol (sector D defective injector) shows a leaking control chamber, an overflow to the overflow, a longer fuel pressure stabilization period in the control chamber, and an oscillation of the injector spindle.

The analysis of Fig. 4 allows for two phases forced by the current signal (pre-injection and primary injection) in the working injector. After the response, obtained three basic phases of signal EA (denoted by Roman numerals), which contain the following information:

Phase I – it determinates the value of the signal above the accepted threshold of detection and it contains information from processes pre-injection and the opening of the anchor (the beginning of the injection of basic and closing anchor). In this phase include the sectors A1, B1, C1, D1 and A2, B2 and C2 (figure 1 concerns pre-injection, the numeral 2 refers to the basic injection).

Phase II – it is a separate part of the EA signal containing information relating equalizing the pressure in the control chamber. The graph is characterized by low amplitude, because it does not generate the elastic wave originating from striking elements of the injector. Define only the beginning of the sector D2.

Phase III - it illustrates the process of closing the injector needle and it contains most of the sector D2. The duration of this phase depends on the correctness of the closure of the needle and it is generated in the shock of the needle slot elastic waves.

Table 2. Average values of the duration of each phase in the fuel injection signal. Δ is the coefficient of variation of the parameter under investigation

Lp.	Source signal-Injector number	Mean duration of phase I for k = 60			Mean duration of phase II for k = 60			Mean duration of phase III for k = 60		
		t [ms]	Standard deviation σ	Δ [%]	t [ms]	Standard deviation σ	Δ [%]	t [ms]	Standard deviation σ	Δ [%]
1	NN1	0.86	0.07	8,66	0,48	0,31	64,50	0,63	0,16	24,82
2	NN2	1.05	0.16	15,24	0,67	0,60	89,12	0,60	0,14	24,05
3	NN3	0.81	0.04	5,29	1,03	0,78	75,38	0,56	0,13	23,24
4	NN4	0.82	0.05	5,90	0,83	0,30	36,14	0,58	0,14	24,09
5	NN5	1.12	0.14	12,07	0,45	0,26	57,43	0,61	0,19	31,52
6	NN6	1.06	0.11	10,09	0,42	0,20	47,01	0,78	0,17	21,56
7	NN7	1.03	0.18	17,91	0,46	0,75	164,7	0,59	0,13	22,44
8	NN8	1.18	0.15	12,42	0,24	0,29	123,5	0,86	0,20	23,77
9	NN9	0.98	0.10	9,97	0,68	0,50	73,48	0,58	0,17	28,78
10	NN10	1.23	0.20	15,94	0,26	0,22	84,47	0,80	0,29	35,73
11	NN11	0.95	0.07	7,64	0,51	0,39	77,20	0,71	0,26	37,25
12	NN12	0.89	0.08	9,38	0,90	0,64	71,30	0,58	0,16	27,41
13	UU1	0.98	0,26	26,09	0,18	0,43	245,8	0,87	0,42	47,86
14	UU2	0.96	0.14	15,11	0,49	0,55	111,4	0,87	0,43	49,45
15	UU3	0.96	0.21	21,85	0,19	0,39	203,7	0,76	0,34	45,03
16	UU4	0.92	0.20	21,37	0,17	0,29	171,6	0,75	0,35	46,45
17	UU5	0.82	0.04	5,18	0,74	0,77	56,53	0,52	0,07	14,07
18	UU6	0.89	0.16	17,79	0,41	0,60	145,9	0,69	0,31	44,57

In order to visualize described above, significant from the point of view of diagnosis phases of the injector, used Look50_60 program, used for direct analysis of signal EA. Determined durations of the individual phases of the signal produced when the fuel injection are presented in Table 2.

An important parameter is the coefficient of variation of the duration of the third phase, the value of which increases substantially when the injectors are damaged (named UU…) and ranges in the area of 45%. For efficient injectors (named NN…) it ranges from 21% to 37%. The exception is the UU5 defective injector for which the Phase III variation coefficient adopts an extremely low value, even lower than the new injectors. In case of injuring the injector in the form of seizure of the needle (UU5), after the injection process ends, the impact of the needle is lost at the socket. Due to the constant leakage, the diagnostic tool reads relatively stable signals whose standard deviation is exceptionally low spread. Therefore, in the interpretation of the results, it should be taken into account that the phase variation factor III below 20% may indicate that the injector is malfunctioning.

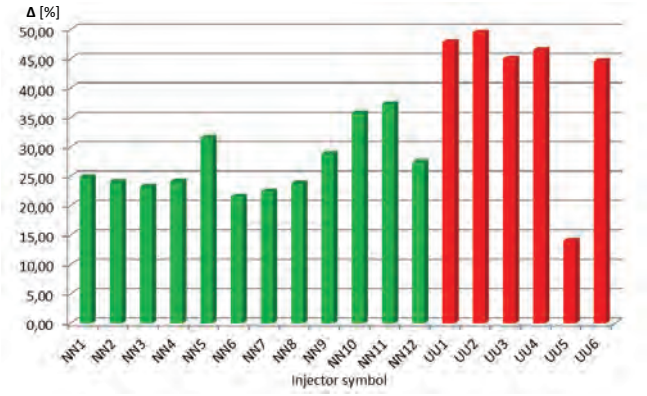

Fig. 5. A summary of the phase-change coefficients of phase III measurements

6. Spectral density function of the EA signal

By definition, spectral density is a function of the frequency defined in a set of positive real numbers, which is a set of process execution spectra and is represented in terms of power or energy per unit frequency. When analyzing spectral density charts, significant differences can be observed between spectral density characteristics for undamaged and damaged injectors.

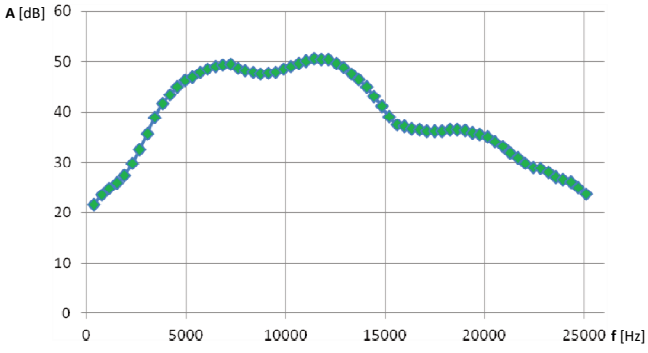

Fig. 6. Mean spectral density values for the new injector NN1–NN12

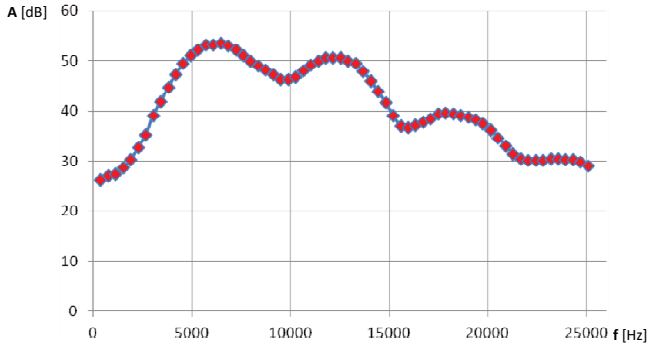

Fig. 7. Mean spectral density values for the set of UU1–UU6 damaged injectors with the exception of UU5

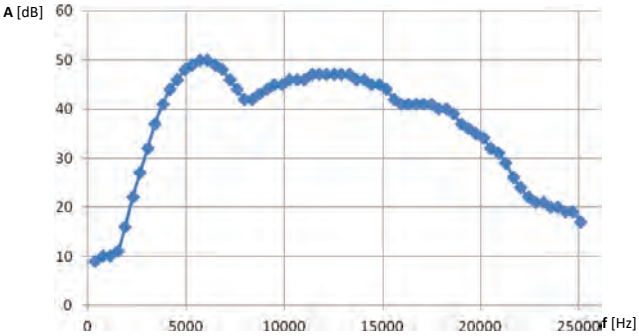

Fig. 8. Spectral density value of the UU5 damaged injector

On the graph of spectral density, the undamaged injectors have two visible maxima, the amplitude of the second being higher than the first and are in the range of 11–12 kHz. Another situation is in the graph of damaged injectors, where is possible to distinguish three distinct and decreasing peaks, wherein the first largest is in the range of approx. 6 kHz. This begs the conclusion that analyzing the shape of the spectral density on the basis of the read quantity of peaks and locations of the largest peaks can adequately predict the likely state of the injector. The different shape of the curve was determined for the UU5 injector but the feature is the same as for the damaged injectors. The first peak is of the highest amplitude and occurs at around 6 kHz.

7. Conclusions

The development of any system that improves the accuracy of the diagnosis of the failure of compression-ignition engine components (especially related to its injection system and combustion process) will be of interest to both specialist repair services and engine manufacturers. Analyzing the results of this study it is possible to specify the following conclusions:

1. Operating CR injectors of compression ignition engines are the source of acoustic emission signals.
2. It is possible to identify and classify injectors into one of two classes of the technical condition: 0 – undamaged, 1 – damaged.
3. There is an acoustic emission source signal that reflects the phases of the processes occurring in the running Common Rail injectors.
4. There is a relation of certain parameters of signal EA from the state of the injector (0 – no damage; 1 – is damaged).
5. It is possible to specify the times of the individual phases of the injector signal produced when the fuel injection.

Nomenclature

EA acoustic emission
CR Common Rail

Bibliography

[1] BEJGER, A. Zastosowanie fal sprężystych emisji akustycznej do diagnozowania układów wtryskowych okrętowych silników spalinowych. *Wydawnictwo Fotobit.* Kraków 2012.

[2] BEJGER, A., MAZURUK, P. Praktyczne sposoby wykrywania niesprawności układów wtryskowych silników Common-Rail. Nadieżnost i Efiektiwnost Tiechniczieskich Sistiem. *Mieżdunarodnyj Sbornik Trudow*. Kaliningrad 2009.

[3] MAZURUK, P. Diagnostyka zasobnikowych układów paliwowych na podstawie fazowości procesu wtrysku. *Rozprawa doktorska*. 2013.

[4] MAZURUK, P. Nowoczesne silniki Perkins Tier 4. *Zeszyty Naukowe Instytutu Pojazdów*. Politechnika Warszawska. 2011, **1**(82).

[5] MAZURUK, P. Diagnostyka wtryskiwaczy Common Rail z wykorzystaniem emisji akustycznej. *Zeszyty Naukowe Instytutu Pojazdów*. Politechnika Warszawska. 2012, **1**(87).

[6] ORLIŃSKI, P., WOJS, M.K., MAZURUK, P. Budowa stanowiska do badań paliw eksperymentalnych płynnych wykorzystującego silnik rolniczy o zapłonie samoczynnym. *Zeszyty Naukowe Instytutu Pojazdów*. Politechnika Warszawska. 2013, **1**(92).

[7] RANACHOWSKI, Z., PAWEŁEK, A., JASIEŃSKI, Z. et al. Durability and wear of engine parts – new methods of testing of alloys and composites. *Scientific Journals Maritime University of Szczecin*. 2013, **35**.

[8] MAZURUK, P., KRUCZYŃSKI, P., ADAMCZYK, H. Wpływ czynników eksploatacyjnych na uszkodzenia nowoczesnych układów paliwowych przemysłowych silników o zapłonie samoczynnym. *XXI Ogólnopolskie Sympozjum Naukowe Motoryzacyjne Problemy Ochrony Środowiska*. SiMR, Warszawa, 6.12.2013.

[9] OLSZOWSKI, S., MARCZAK, M. Diagnostics of new generation diesel engines. *Diagnostyka*. 2008, **4**(48).

[10] ORLIŃSKI, P, WOJS, M.K., SIKORA, M. Wpływ kąta wyprzedzenia wtrysku na emisję substancji toksycznych w silniku rolniczym o ZS zasilanym ciekłymi paliwami alternatywnymi. *Zeszyty Naukowe Instytutu Pojazdów*. Politechnika Warszawska. 2014, **1**(97).

[11] RANACHOWSKI, Z. Metody pomiaru i analiza sygnału emisji akustycznej. *Prace IPPT PAN*. Warszawa. 1997, **1**(11).
[12] RINDORF, H. Acoustic emission source location. *Brüel & Kjaer Technical Review*. 1981, **2**, 3-32.
[13] Katalog Polskich Norm: PN EN 1330-9:2002 Terminologia: Terminy stosowane w badaniach emisji akustycznej; PN EN 13477-1:2002 Emisja akustyczna. Charakteryzowanie aparatury. Opis aparatury; PN EN 13477-2:2010 Emisja akustyczna. Charakteryzowanie aparatury. Weryfikacja działania; PN EN 13554:2011 Emisja akustyczna. Zasady ogólne.
[14] PARMAR, D. Non-destructive bridge testing and monitoring with acoustic emission (AE) sensor technology. Final Report. *Hampton University*. 2011.
[15] RANACHOWSKI, Z., BEJGER, A. Application of light weight acoustic emission analyzer for diagnostic of the fuel injection system of medium power marine diesel engines. *Polish Journal of Environmental Studies*. 2009, **18**(2A) Supplement.
[16] RAUSCHER, F. Defect detection by acoustic emission examination of metallic pressure vessels. *Journal of Acoustic Emission*. 2004, **22**.

Paweł Mazuruk, DEng. – Motor Transport Institute in Warsaw. Engine application Manager in BU Power Systems Polska/Perkins Poland.

e-mail: *Mazuruk.Pawel@gmail.com*

Piotr Orliński, DSc., DEng. – Faculty of Automotive and Construction Machinery Engineering, Warsaw University of Technology.

e-mail: *P.Orlinski@simr.pw.edu.pl*

Marcin Krzysztof Wojs, DEng. – Faculty of Automotive and Construction Machinery Engineering at Warsaw University of Technology.

e-mail: *MWojs@simr.pw.edu.pl*

Mieczysław Sikora, MSc. – Faculty of Automotive and Construction Machinery Engineering at Warsaw University of Technology.

e-mail: *MSikora@simr.pw.edu.pl*

Article citation info:
WOLFF, A. Influence of piston ring pack configuration on blowby and friction losses in a marine two-stroke engine. Combustion Engines. 2017, 170(3), 164-170. DOI: 10.19206/CE-2017-328

Andrzej WOLFF

CE-2017-328

Influence of piston ring pack configuration on blowby and friction losses in a marine two-stroke engine

In the paper a comprehensive model of a piston ring pack motion on an oil film has been presented. The local thickness of the oil film can be compared to height of the combined surface roughness of a cylinder liner and piston rings. Equations describing the mixed lubrication problem based on the empirical mathematical model formulated in works of Patir, Cheng and Greenwood, Tripp have been combined and used in this paper. In addition a model of gas flow through the labyrinth seal of piston rings has been developed. The main parts of the model and software have been experimentally verified abroad by the author at the marine engine designing centre.

For the selected two-stroke marine engine, the influence of the number of piston rings used and the type of the top ring lock (straight or overlapped) on blowby to piston underside and on friction losses of the piston-ring-cylinder (PRC) system have been investigated. The developed model and software can be useful for optimization of the PRC system design.

Key words: *marine engines, piston rings, gas dynamics, hydrodynamic lubrication, mixed friction*

1. Introduction

Piston rings are important part of internal combustion engines. Commonly a set of piston rings is used to form a dynamic gas seal between the piston and cylinder wall [5, 6, 13]. The sliding motion of the piston forms a thin oil film between the ring land and cylinder wall, which lubricates the sliding components [2, 4, 11]. The hydrodynamic force generated by this thin oil film is opposed by a combination of the gas pressure acting on the back side of each ring and the ring stiffness. Due to the dynamic nature of these forces, each individual ring is periodically compressed and extended as the piston runs through its cycle. The problem of studying this interaction is further complicated by the high temperatures involved, as these result in low oil viscosity and subsequently very low oil film thickness. The oil film is typically thick enough to expect the existence of mixed lubrication, so this phenomenon should also be taken into account [2, 7, 8, 12, 13]. The use of modern oil of low viscosity, working at a high temperature causes the existence of a very thin oil film thickness comparable to the value of the liner surface roughness. In such conditions, the possibility of direct contact between the ring and cylinder liner surface exists. Therefore the numerical simulation of these processes, which take place in a typical piston ring pack operation, is important from practical point of view.

The purpose of this paper is to present numerical calculations concerning an influence of the number of piston rings used and the type of the top ring lock (straight or overlapped) on blowby to piston underside and on friction power losses of the PRC system.

2. Modelling of piston ring pack operation

2.1. Developed sub-models

A combined model of piston rings operation has been developed. It consists of two main models: a) model of gas flow through the labyrinth seal piston-rings-cylinder (PRC), b) model of oil flow in the lubrication gap between the ring and cylinder liner. The two aforementioned models are coupled. In addition, sub-models of the following mechanical phenomena have been used: a contact of rough surfaces, an axial movement of rings within piston grooves and an elastic torsional deformation of piston rings. All the sub-models are described in detail in publications [15–18] of the author. In this paper only the sub-models of gas flow [18] and mixed lubrication [3, 9, 18] are shortly presented.

2.2. Model of gas flow through the labyrinth seal of piston rings

The gas flow model [16, 18] consists of several volume regions V_1, V_2, …, V_9, which are connected by orifices with cross-section areas A_1, A_2, …, A_{12} (Fig. 3). The volumes V_3, V_5, V_7 correspond to volumes between the piston rings, while volumes V_2, V_4, V_6, V_8 correspond to groove volumes behind rings. Orifices with cross-section areas A_1, A_4, A_7, A_{10} correspond to the ring end gaps, whereas orifices with cross-sections A_2, A_3, A_5, A_6, A_8, A_9, A_{11}, A_{12} correspond to ring-side crevices.

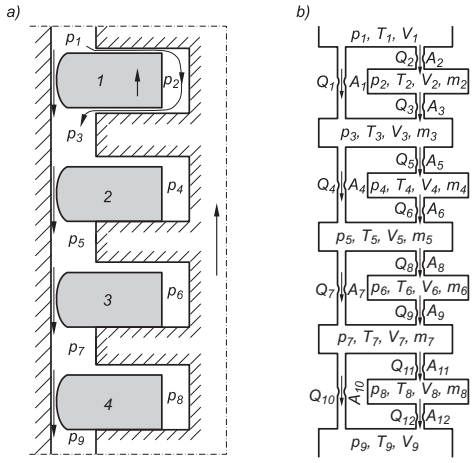

Fig. 1. Scheme of gas flow through the labyrinth seal of PRC system and the applied physical model for the ring pack of four piston rings

It was also assumed that the gas flow through orifices is isentropic (depending on pressure ratio – subsonic or sonic). The heat transfer between gas volume regions and surrounding walls was taken into account.

Thermal expansion of the piston and the cylinder liner and wear of the cylinder liner were taken into account. Leaks between piston rings and cylinder liner were defined

by flow areas of ring end gaps, which depend on the position of the piston in cylinder.

In addition, mathematical description takes into account changes of gas volume regions and cross-section areas between the rings and the piston grooves (due to axial movement of the rings) [5, 6, 13, 18].

In the mathematical model of these phenomena equations of the following physical laws are utilized (here given for a gas volume number *k*):

Equation of mass balance:

$$dm_k = \sum_i dm_{In_i} - \sum_j dm_{Out_j} \tag{1}$$

Equation of energy balance:

$$\sum_i dm_{In_i} \cdot i_{In_i} - \sum_j dm_{Out_j} \cdot i_{Out_j} - \delta Q_{Wall} = d(m_k \cdot u_k) + p_k \cdot dV_k \tag{2}$$

Gas state equation in differential form:

$$dT_k = T_k \cdot \left(\frac{dp_k}{p_k} + \frac{dV_k}{V_k} - \frac{dm_k}{m_k} \right) \tag{3}$$

where: m – gas mass, p – gas pressure, T – gas temperature, u – internal gas energy, i – gas enthalpy, Q – heat transferred through cylinder walls: index: In – gas inflow, Out – gas outflow, i – number of inflow channel, j – number of outflow channel, k – number of gas volume.

2.3. Model of oil flow in a gap (with rough surfaces) between the ring and cylinder

Two main cases of oil flow in the system piston ring – cylinder liner are presented in Fig. 4.

A one dimensional form of the modified Reynolds equation developed by Patir and Cheng [9] has been used to calculate hydrodynamic forces in the case of rough gap surfaces. This equation is applicable to any general roughness structure and takes the following form:

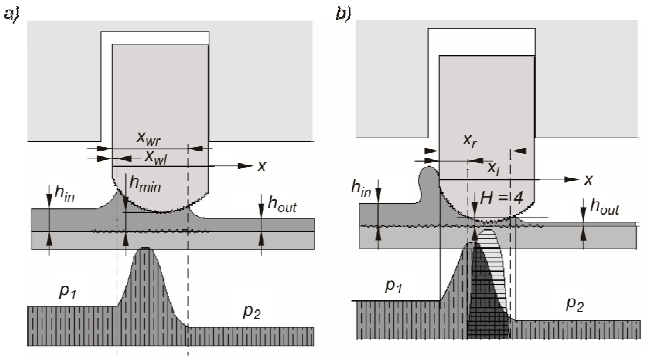

Fig. 2. Scheme of gap between the ring face and cylinder liner in the case of: a) fluid and b) mixed friction

A one dimensional form of the modified Reynolds equation developed by Patir and Cheng [9] has been used to calculate hydrodynamic forces in the case of rough gap surfaces. This equation is applicable to any general roughness structure and takes the following form:

$$\frac{\partial}{\partial x}\left(\phi_x \frac{h^3}{12\mu} \frac{d\bar{p}}{dx} \right) = \frac{U}{2} \frac{d\bar{h}_T}{dx} + \frac{U}{2} \sigma \frac{d\phi_S}{dx} + \frac{d\bar{h}_T}{dt} \tag{4}$$

where: t – time; x – coordinate along cylinder liner; h – nominal oil film thickness; h_T – average gap (ring-cylinder); p – hydrodynamic pressure; U – axial ring velocity; μ – dynamic oil viscosity; $v = \partial h_T / \partial t$ – radial ring velocity, σ – composite root mean square roughness of sliding surfaces.

The significance and mathematical description of empirical coefficients ϕ_x , ϕ_S and boundary conditions of equation (4) are presented in [9] and also in [18].

The effects of interacting asperities of piston ring and cylinder liner surfaces were modelled using the mathematical model developed by Greenwood and Tripp [3]. In this case the asperity contact force per unit circumference is given by

$$F_C = 16\sqrt{\frac{2}{15}}\pi(\eta\beta\sigma)^2 E' \sqrt{\left(\frac{\sigma}{\beta}\right)} \int_{x_l}^{x_r} F_{5/2}\left(\frac{h}{\sigma}\right) dx \tag{5}$$

where the integration limits x_l and x_r define a continuous interval, $x_l \le x \le x_r$ in which $h/\sigma \le 4$ and: E' – composite elastic modulus (for cylinder liner and piston ring); η – asperity density; β – asperity radius of curvature; σ – composite root mean square roughness of sliding surfaces.

The form of function $F_{5/2}$ can be found in article [3]. The model is also described in detail in publication [18] of the author of this article.

3. Experimental verification of developed model

A verification of the simulation model has been done by the author for a two- and four-stroke marine engine [15, 16, 18]. The experimental verification of the model of gas flow through the labyrinth seal of piston rings was carried out using measurements of unsteady gas pressure in the cylinder, between the piston rings and under piston performed by piezoelectric sensors mounted in the piston. A satisfactory qualitative and quantitative compatibility of the analyzed pressure variations has been achieved. The maximal relative differences between measured and calculated pressure values have not exceeded 15% [15, 18]. On the other hand, the experimental verification of the hydrodynamic model of piston rings involved measurement results of scraped oil volumes by a gland-box of a two-stroke marine engine. Unfortunately, similar measurements for piston ring packs of tested engines have not been carried out. Examination of scraped oil volumes by the ring pack (of the gland-box of marine internal combustion engine) proves a satisfactory quantitative agreement between numerical and experimental results. The maximal relative differences between measured and calculated values have not exceeded 10% [15, 18].

4. Calculation results

4.1. Main data of chosen engine

The computer program incorporating the presented model has been used for simulation of two-stroke Diesel engine (Tab. 1) operating at full load. The type of ring set

considered is common in marine engines. The piston ring pack consists of four rings (Figs 1 and 3). The package includes conventional straight ring end gaps.

Table 1. Main data of the marine engine under consideration [14]

Cylinder bore	580 mm
Piston stroke	2416 mm
Engine rotational speed	105 rpm

The surface geometry of the piston ring package, with vertical dimensions magnified by factor of 1000 relative to the horizontal ones, is depicted in Fig. 1. All the rings have the same asymmetrical barrel shape (Tab. 2).

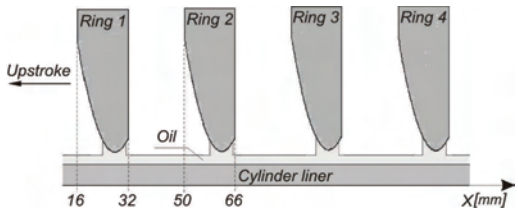

Fig. 3. Ring pack geometry under consideration

In order to ensure very low wear of profiled surfaces, the piston rings are coated (for example the top ring has chromium ceramic coating) [1, 10]. As a consequence, even hydrodynamic conditions during a long period of piston rings operation can be ensured.

Table 2. Basic geometric parameters of piston rings: 1, 2, 3, 4

Axial height of piston ring	H = 16 mm
Radius of parabolic sliding surface	R = 750 mm
Offset of parabolic sliding surface	O_f = 12 mm
Distance between piston rings	L_p = 18 mm

4.2. Calculation results for chosen types of the top ring

The following two types of the top ring lock have been investigated (Fig 4): a) straight-cut (SC), b) gas-tight (GT) with overlapped joint.

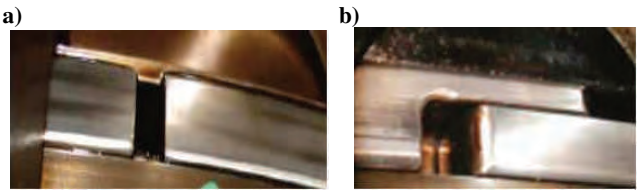

Fig. 4. Lock of the top piston ring: a) straight-cut (SC), b) gas-tight (GT) with overlapped joint (Copyright Winterthur Gas & Diesel Ltd.)

In this subchapter two characteristic piston ring pack configurations have been analysed and compared. The first one indicated as 4xSC consists of 4 piston rings with straight-cut locks. The second one indicated as GT+3xSC consist of gas-tight top ring (with overlapped joint) and 3 piston rings with straight-cut locks.

Typically, the figures that will follow show variation of some physical parameters as a function of the crankshaft rotation angle, beginning from the piston bottom dead centre (BDC) of the two-stroke engine operation (0°). In this case the end of compression phase is at 180° of crank angle (piston top dead centre – TDC). All the presented results correspond to full engine load.

In Fig. 5 calculated gas pressures $\boldsymbol{p_i}$ (i = 1, 3, 5, 7) for the main volume regions of the labyrinth seal (Fig. 1) as a function of crank angle are shown. The first case corresponding to 4xSC piston ring pack configuration is presented in Fig. 5a, and the second one corresponding to GT+3xSC configuration is shown in Fig. 5b.

Figure 5 presents the pressure variation between piston rings, calculated on the basis of known cylinder pressure variation and simulated gas leakage through the labyrinth sealing of the piston ring pack (orifices corresponding to ring end gaps and ring-side crevices – Fig. 1). Generally, the gas pressure in the cylinder and all the inter-ring gas pressures increase during the piston upstroke (compression phase) and decrease during a certain part of the piston downstroke (expansion phase). In Fig. 5a the following maximum gas pressure values can be seen: nearly 16 MPa in cylinder, over 8 MPa between the 1st and 2nd piston ring, about 5 MPa between the 2nd and 3rd ring and approximately 3 MPa between the 3rd and 4th ring.

On the piston underside a relatively low scavenging air pressure is noticed. At the piston ring pack location near scavenging ports (i.e. between 300° and 310° of crank angle) all inter-ring gas pressures are visibly reduced.

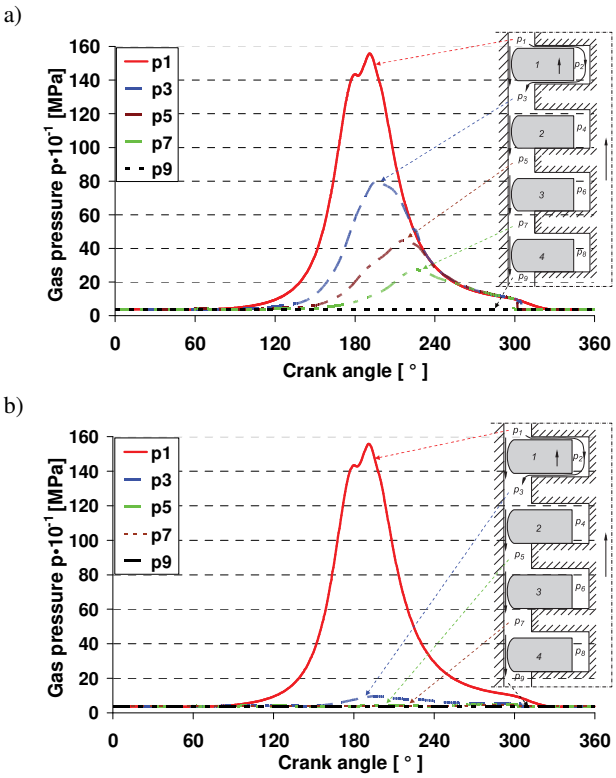

Fig. 5. Calculated gas pressure variations p_i in all the volume regions versus crank angle. Gas pressure nomenclature: p_1 – in combustion chamber, p_3 – between the 1st and 2nd piston ring, p_5 – between the 2nd and 3rd piston ring, p_7 – between the 3rd and 4th piston ring, p_9 – under the piston. Piston ring pack configuration: a) 4xSC, b) GT+3xSC

Figure 5b presents the calculation result corresponding to GT+3xSC piston ring pack configuration. Due to gas-tight top piston ring much higher pressure drop between the 1st and 2nd piston ring can be noticed. Gas pressure between the 1st and 2nd piston ring reaches the maximum value be-

low 1 MPa. For this reason the 2nd, 3rd and 4th piston ring are considerably less strongly pressed against the cylinder surface than in the case of the 4xSC configuration (compare Figs 5a and 5b). It should be noted that the top piston ring is not treated as quite gas-tight. It has been assumed that the leakage between the bottom side of this ring and the piston groove equals about 0.1% of the maximum possible axial ring lift. The mentioned leakage parameter has been evaluated during the verification of the gas flow model.

The hydrodynamic force acts in the radial direction on the ring and is counteracted by the spring force, gas force and friction force in the piston groove. The inertia force in the radial direction has been neglected due to very small values of the radial ring acceleration. Figure 6 presents the hydrodynamic force F_h for each piston ring (Figs. 1 and 3) necessary for compensating both the gas pressure and radial forces resulting from the ring stiffness [18]. All the forces are referenced to unit circumference of the piston ring (unit forces [N/m]). The first case corresponding to 4xSC piston ring pack configuration is presented in Fig. 6a, and the second one corresponding to GT+3xSC configuration is shown in Fig. 6b. The variations of hydrodynamic forces look similar to variations of inter-ring gas pressures (compare Figs 5 and 6). First of all, the 1st ring (top ring) is strongly pressed against the cylinder liner surface. The higher is the ring number (Figs 1 and 3), meaning more distant from the top, the less is the ring loaded. It should be added that hydrodynamic forces generated in oil gaps of the 2nd, 3rd and 4th piston ring reach significantly less values than in the case of the 4xSC configuration (compare Figs. 6a and 6b).

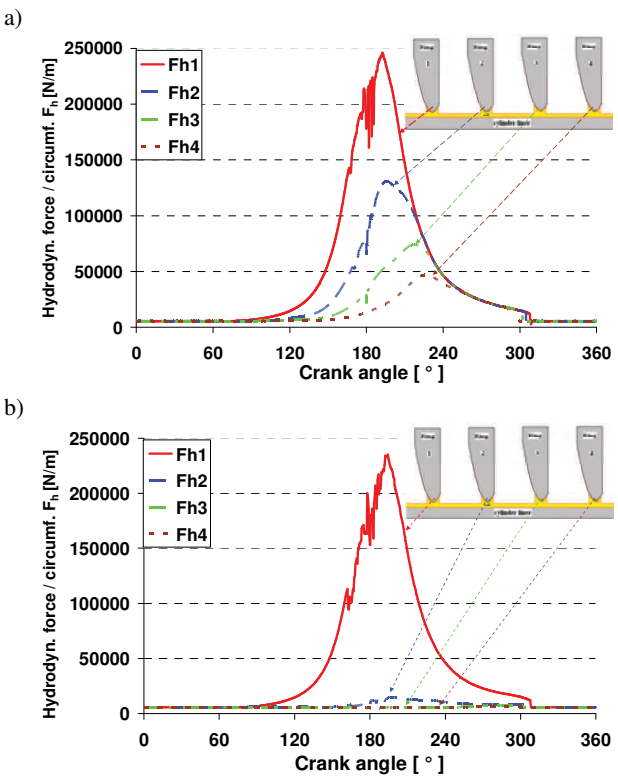

Fig. 6. Variation in hydrodynamic force F_{h_i} generated by each piston ring (i – ring number) versus crank angle. Piston ring pack configuration: a) 4xSC, b) GT+3xSC

Additionally, in the mixed lubrication cases the elastic radial contact forces are anticipated [18]. In Fig. 7 variations in aforementioned forces are shown. These forces occur in the case of a high gas pressure and low oil viscosity caused by high temperature near the top dead centre. It should be noticed that the values of elastic contact forces F_c are much lower than hydrodynamic forces F_h acting on rings (compare Figs 6 and 7).

The first case corresponding to 4xSC piston ring pack configuration is presented in Fig. 7a, and the second one corresponding to GT+3xSC configuration is shown in Fig. 7b. In both cases the highest value of the contact force F_c is generated by the 1st ring (top ring). The higher is the ring number (Figs 1 and 3), the less is the radial contact force. It should be noted that these forces generated by the 2nd, 3rd and 4th piston ring reach significantly less values than in the case of the 4xSC configuration (compare Figs 7a and 7b).

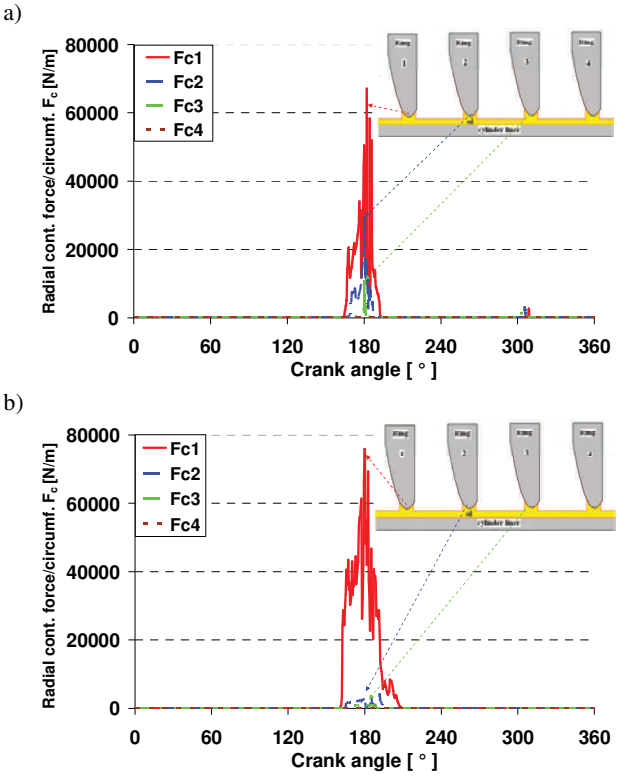

Fig. 7. Variation in radial component of contact force F_{c_i} for each piston ring (i – ring number) versus crank angle. Piston ring pack configuration: a) 4xSC, b) GT+3xSC

Analysing the presented results it can be concluded that hydrodynamic forces (Fig. 6) are generated by relatively low pressure acting on a large surface in contrast to high local contact pressure concentrated on a very small area of elastic contact (Fig. 7). Due to that the elastic contact seems to be responsible for the wear process.

Near the top dead centre (at high oil temperature) the additional tangential components of elastic contact forces (friction forces) F_{cx} for each piston ring should be noticed (Fig. 8). But exactly at this piston reverse point the axial velocity of piston rings decreases to zero, which means the simultaneous drop of aforementioned forces to zero value.

The sign change of these forces at TDC results from the sign change of piston velocity.

The first case corresponding to 4xSC piston ring pack configuration is presented in Fig. 8a, and the second one corresponding to GT+3xSC configuration is shown in Fig. 8b. In both cases the highest value of the tangential contact force $\boldsymbol{F_{cx}}$ is generated by the 1st ring (top ring). The higher is the ring number (Figs 1 and 3), the less is the tangential contact force. It should be added that these forces generated by the 2nd, 3rd and 4th piston ring reach significantly less values than in the case of the 4xSC configuration (compare Figs 8a and 8b).

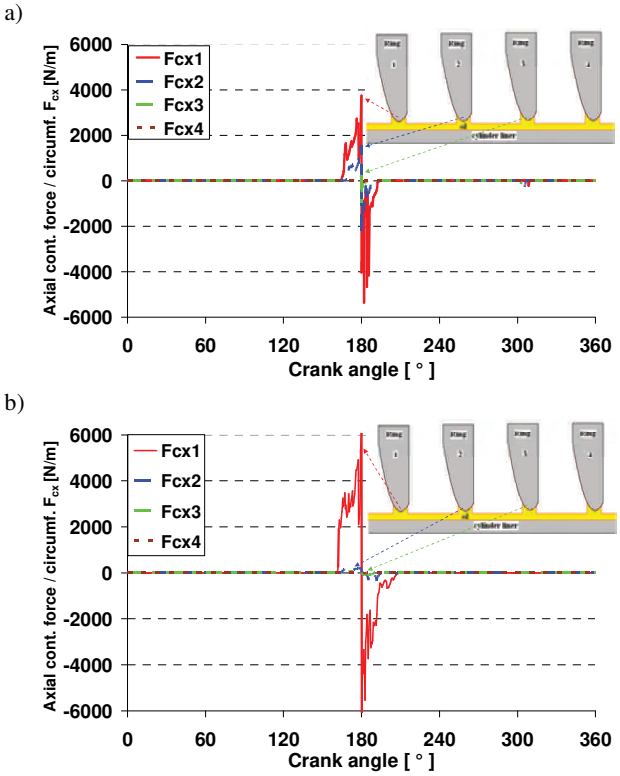

Fig. 8. Variation in tangential component of contact force F_{cx_i} for each piston ring (i – ring number) versus crank angle. Piston ring pack configuration: a) 4xSC, b) GT+3xSC

The motion of the ring pack scraping and distributing oil on the cylinder liner leaves the oil film profile shown in Fig. 9. This profile is formed after a few cycles of operation. An uneven oil film distribution along the cylinder liner can be clearly seen. Low film thickness near TDC and in the other part of cylinder liner at the location of scavenging air ports should be noticed. The minimum oil film thickness at TDC is about 0.2–0.3 μm and is comparable with root mean square (RMS) roughness of the cylinder liner that equals 0.22 μm [18]. The very low local film thickness values near TDC can be explained by occurrence of high gas pressure and high temperature in this area during the compression and working phases of engine operation. Due to high gas forces piston rings are strongly pressed against the cylinder surface. On the other hand, high temperature reduces the oil viscosity.

There are two places of oil supply for the cylinder liner of long-stroke IC engine located below TDC. Two peaks of oil film thickness at these places can be clearly seen in Fig. 9.

In a marine two-stroke engine the location of scavenging air ports is also important for cylinder lubrication. Their presence simply reduces the area of the mating surface between piston rings and cylinder liner. In this area a simplified approach was applied. The oil film thickness was assumed to be reduced at this location reflecting the reduced sliding surface.

Due to low gas pressure and oil temperature the greatest oil film thickness can be seen between scavenging air ports and the bottom dead centre (BDC).

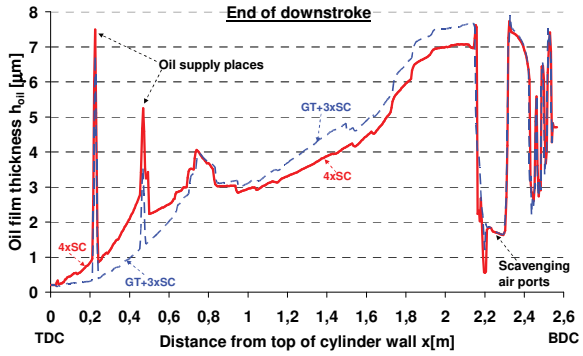

Fig. 9. Comparison of the oil film thickness h_{oil} left by the ring pack along cylinder wall concerning piston ring pack configurations 4xSC and GT+3xSC

Near the piston top dead centre (TDC) a considerably bigger oil film thickness is noticed in the case of the ring pack configuration indicated as 4xSC than in the case of GT+3xSC configuration. For this reason the lubrication conditions near TDC are better in the first case. Therefore lower value of the tangential contact force F_{cx} is generated by the top ring (compare Figs 8a and 8b).

But from the middle of the cylinder wall to the location of scavenging air ports an opposite situation is observed, i.e. lower oil film thickness is noticed in the case of 4xSC ring pack configuration than in the case of GT+3xSC configuration (Fig. 9).

4.3. Calculation results for chosen piston ring pack configurations

Complementary another four piston ring pack configurations have been analysed and compared with those described in the previous chapter (i.e. 4xSC and GT+3xSC). The total number of piston rings has been reduced to 2 or 3, but in a real engine less than 3 rings have not been used. Firstly, two configurations of piston rings with all straight-cut locks indicated as 2xSC and 3xSC have been taken into account. Secondly, two configurations with gas-tight top ring and 1 or 2 piston rings with straight-cut locks indicated as GT+SC and GT+2xSC have been analysed.

Multiplying friction forces (due to hydrodynamic and mixed lubrication) of all the rings by piston velocity, friction power losses can be calculated. In Fig 10 a comparison of results concerning mean values of total power losses for all the aforementioned piston ring pack configurations is shown. It should be noted that in any case the application of gas-tight top ring causes a certain increase of friction power

loss compared with the use of the top ring with straight-cut lock. In addition, the larger the number of piston rings the greater the friction power loss can be noticed.

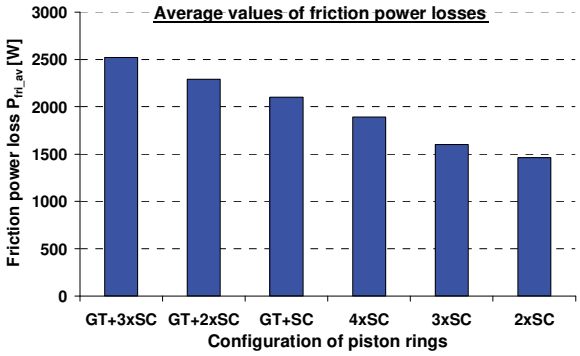

Fig. 10. Average values of total power loss $\mathbf{P_{fri\_av}}$ (due to hydrodynamic and mixed lubrication) for different piston ring pack configurations. Lock of the top piston ring: SC – straight-cut, GT – gas-tight

Then a comparison of gas blowby into piston underside for different piston ring pack configurations is shown (Fig. 11). It can be concluded that in any case the application of gas-tight top ring (configurations: GT+SC, GT+2xSC, GT+3xSC) causes an appreciable reduction of blow-down compared with the use of the top ring with straight-cut lock (configurations: 2xSC, 3xSC, 4xSC). Consequently improved fuel efficiency can be expected. The greater the number of piston rings the lower the blow-down can be noticed for the configurations of piston rings with all straight-cut locks. In the case of configurations with gas-tight top ring (GT+SC, GT+2xSC, GT+3xSC), the gas blowby into piston underside is almost not influenced by the number of conventional piston rings with straight-cut locks. These rings are simply slightly pressed by the gas forces against the cylinder surface (Fig. 6b).

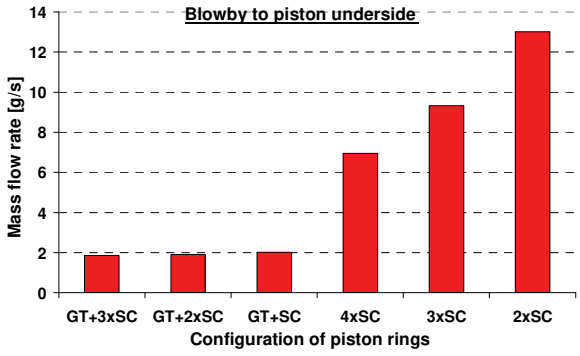

Fig. 11. Comparison of blowby for different ring pack configurations. Lock of the top piston ring: SC – straight-cut, GT – gas-tight

5. Conclusions

The major conclusions that may be drawn from the results are as follows:

1. The developed mathematical model and simulation programme give a lot of practical information that would be more complicated and expensive to obtain using experimental methods.
2. At first two characteristic piston ring pack configurations indicated as 4xSC and GT+3xSC have been compared. If the gas-tight (GT) top ring is applied (instead of the SC ring) then the following main phenomena can be noticed:
   – much higher pressure drop between the 1st and 2nd piston ring (Fig. 5), and consequently the 2nd, 3rd and 4th piston ring are significantly less strongly pressed against the cylinder surface (Fig. 6),
   – higher radial and tangential components of elastic contact force acting on the top piston ring (Figs. 7, 8),
   – significantly lower radial and tangential components of elastic contact force acting on the 2nd, 3rd and 4th piston ring (Figs. 7, 8),
   – slightly lower oil film thickness near the piston top dead centre (TDC) and an opposite situation from the middle of the cylinder liner to the location of scavenging air ports (Fig. 9),
   – more friction power loss of the piston ring pack (Fig. 10), but appreciable reduction of gas blowby to the piston underside (Fig. 11).
3. In addition four piston ring pack configurations indicated as 2xSC, 3xSC, GT+SC and GT+2xSC have been analysed. In mentioned cases the following phenomena can be observed:
   – the greater the number of piston rings the more friction power loss (Fig. 10), but the lower the blow-down for configurations of piston rings with all straight-cut locks (Fig. 11),
   – in the case of configurations GT+SC, GT+2xSC and GT+3xSC, the gas blow-down is almost not influenced by the number of SC piston rings (Fig. 11).
4. The main aim of simulation of piston rings operation is to predict lubrication conditions, define areas of the possible cylinder liner wear and finally determine the gas leakage through the sealing ring set. Further investigation of these phenomena should be recommended.

Acknowledgements

The author expresses his gratitude to *Wärtsilä's* R&D engine centre (nowadays: *Winterthur Gas & Diesel Ltd.*) in Winterthur (Switzerland) for having the opportunity to work on projects concerning mathematical modelling and numerical simulation of tribological systems of piston rings during several research periods at this company.

Abbreviations

PRC	piston-ring-cylinder
SC	straight-cut lock of piston ring
GT	gas-tight lock of top piston ring (overlapped joint)
TDC	top dead centre
BDC	bottom dead centre
RMS	root mean square

Bibliography

[1] DEMMERLE, R., BARROW, S., TERRETTAZ, F., JAQUET, D. New insights into the piston running behaviour of "Sulzer" large bore diesel engines. *CIMAC Congress*. 2001, Hamburg.

[2] DOWSON, D. Piston assemblies; background and lubrication analysis, engine tribology. Taylor C.M. (editor). *Elsevier Science*. 1993, 213-240.

[3] GREENWOOD, J., TRIPP, J.H. The contact of two nominally flat rough surfaces. *Proc Inst. Mech. Eng*. 1971, **185**, 625-633.

[4] ISKRA, A. Parametry filmu olejowego w węzłach mechanizmu tłokowo–korbowego silnika spalinowego. Poznań. *Wydawnictwo Politechniki Poznańskiej*, 2001.

[5] KOSZAŁKA, G. Application of the piston-rings-cylinder kit model in the evaluation of operational changes in blowby flow rate. *Eksploatacja i Niezawodność – Maintenance and Reliability*. 2010, **4**, 72-81.

[6] KOSZAŁKA, G., GUZIK, M. Mathematical model of piston ring sealing in combustion engine. *Polish Maritime Research*. 2014, **4**(84), 66-78.

[7] LIVANOS, G.A., KYRTATOS, N.P. Friction model of a marine diesel engine piston assembly. *Tribology International*. 2007, **40**, 1441-1453.

[8] OFFNER, G. Friction power loss simulation of internal combustion engines considering mixed lubricated radial slider, axial slider and piston to liner contacts. *Tribology Transactions*. 2013, **56**(3), 503-515.

[9] PATIR, N., CHENG, H.S. Application of average flow model to lubrication between rough sliding surfaces. *Transactions of ASME*. 1979, **101**.

[10] RÄSS, K., AMOSER, M. Progressive development of two-stroke engine tribology. *CIMAC Congress*. 2007, **83**, Vienna.

[11] SERDECKI, W. Badania współpracy elementów układu tłokowo-cylindrowego silnika spalinowego. *Wydawnictwo Politechniki Poznańskiej*. Poznań 2002.

[12] TAMMINEN, J., SANDSTRÖM, C.-E., ANDERSSON, P. Influence of load on the tribological conditions in piston ring and cylinder liner contacts in a medium-speed diesel engine. *Tribology International*. 2006, **39**, 1643-1652.

[13] TIAN, T. Dynamic behaviors of piston rings and their practical impact – part II: oil transport, friction, and wear of ring/liner interface and the effects of piston and ring dynamics. *Proc. I. Mech. E, Part J: Journal of Engineering Tribology*. 2002, **216**, 229-247.

[14] Wärtsilä Technology Review, information materials concerning IC engines designed at Wärtsilä company.

[15] WOLFF, A. Experimental verification of the model of piston ring pack operation of an internal combustion engine. *The Archive of Mechanical Engineering*. 2009, **LVI**(1), 73-90.

[16] WOLFF, A. Numerical analysis of piston ring pack operation of a marine two-stroke engine. *Combustion Engines*. 2011, **146**(3).

[17] WOLFF, A. Influence of engine load on piston ring pack operation of a marine two-stroke engine. *Journal of KONES Powertrain and Transport*. 2012, **19**(2), 557-569.

[18] WOLFF, A. Simulation based study of the system piston-ring-cylinder of a marine two-stroke engine. *Tribology Transactions*. 2014, **57**(4), 653-667.

Andrzej Wolff, DSc., DEng. – Faculty of Transport of Warsaw University of Technology.

e-mail: *Wolff@wt.pw.edu.pl*

Article citation info:
NOWAKOWSKI, J., BRZOZOWSKI, K., KNEFEL, T. Formulation of a task to control of harmful exhaust emissions from compression ignition engine. *Combustion Engines*. 2017, **170**(3), 171-175. DOI: 10.19206/CE-2017-329

Jacek NOWAKOWSKI
Krzysztof BRZOZOWSKI
Tomasz KNEFEL

CE-2017-329

Formulation of a task to control of harmful exhaust emissions from compression ignition engine

This paper presents a possibility of control a harmful exhaust emissions from compression ignition engine based on computationally efficiently model of the working cycle a compression ignition engine. Parameters of the model are identified on the basis of experimental measurements carried out for a CI engine with Common Rail system. In this study is considered the control task aimed at minimization of nitrogen oxides emission for a fixed operating point of the engine.

Key words: *compression ignition engine, control of exhaust emissions, numerical model*

1. Introduction

Observed in the years 1980s significant increase in number of road going vehicles equipped with compression ignition engines and resulting from it increased negative environmental impact of harmful exhaust emissions has resulted in commenced research work on methods of restriction of harmful components from exhaust gases generated by the compression ignition engines, and at the same time on a possibilities of obtaining assumed operational parameters of the engines.

Operational parameters of the engines, including engine efficiency, thermal and mechanical loading of its components, and emission of harmful components of exhaust gases are determined by process of heat release, which depends mainly on control parameters of the engine. Introduction of microprocessor technologies and digital methods to controlling technical processes, as well as development of accumulative fuel supply systems of Common Rail type have created a new opportunities in controlling area of injection system operation in compression ignition engines, and thus controlling processes of fuel injection and heat release [5]. Modern supercharged compression ignition engines are equipped with complex systems to controlling of fuel dose and course of fuel injection, pressure of the fuel in high-pressure part of the system, injection advance angle, recirculation rate of exhaust gases, temperature and pressure of the charge in the inlet manifold and swirl of the air flowing into the cylinder. To controlling temperature and pressure of the charge are currently used turbo compressors with changing geometry of turbine, coolers of supercharged air and coolers in recirculation circuits of exhaust gases. As complementary or alternative solution is also used a throttling on the inlet system. This is accomplished by installation of air throttle in the engine inlet system, or installation of group as such throttles.

Introduction of electronically controlled Common Rail systems has enabled controlling of fuel injection process. As result, it is possible to control individual combustion phases in compression ignition engine, including phase of kinetic combustion and phase of diffusion combustion – percentage of the phases of kinetic and diffusion combustion is directly related to methods how the fuel injection course is accomplished [4]. To a large degree it is possible to control the heat release course in the engine, and therefore it is possible to have effect on temperature and pressure course of the working medium in the cylinder, and on characteristic parameters of the process, such as: maximal pressure and maximal temperature of the working medium, or average indicated pressure or thermal efficiency.

2. Concept of the controlling

Within range of partial engine loads and under a given operational conditions exists a real possibility of selection of control parameters of the engine without change of engine torque, with simultaneous assurance of not exceeded allowable mechanical and thermal loads of engine components. Mutual correlation of fueling parameters and phenomena occurring in the engine's cylinder causes that their analysis, from engine's operational parameters point of view, including engine efficiency, thermal and mechanical load of its components, emission of harmful components of exhaust gases, requires significant amount of time and costs. To solve the above problems, therefore, a computational analysis supported by experimental research, connected with searching for optimal with a given criterion, set of control parameters is increasingly used.

Searched values of the control parameters must be possible to be attained in practice, and thus:

$$x_{i\min} \le x_i \le x_{i\max} \quad \text{for } i = 1,...,r \tag{1}$$

where $x_{i\min}, x_{i\max}$ are respectively minimal and maximal allowable values of x_i.

Limitation of the form of (1) means that searched values of control parameters should not exceed a preset boundary values, which can be different in a particular point of engine operation. For instance, allowable increase of fuel dose (and hence also its higher maximal value) will be higher for medium and high engine loads than in case when the control concerns conditions of low engine load.

The control task can be formulated in relation to all possible, or only to selected characteristic parameters with or without consideration of emission of harmful compounds of exhaust gases. In the general form, the control task can be formulated as a multi-criterion problem, in form of weighted sum of individual criteria:

$$\overline{\Omega}(X)=\sum_{i=1}^{k} C_i^F \cdot F_i^* + \sum_{i=1}^{q} C_i^L \cdot l_i \tag{2}$$

where: l_i – functionals of continuous functions $u_i(\varphi)$ describing courses of: mass, pressure, temperature and volume of the cylinder, F_i^* – emission of i-th component of exhaust gases, e.g.: carbon monoxide, hydrocarbons, nitrogen oxide and smoke, C_i^F, C_i^L – weight factors, directly connected with emission of i-th component and value of i-th functional.

The following functionals can used as the control criteria

– mean indicated pressure:

$$p_i = \frac{\int_V p dV}{V_s} \tag{3}$$

where V_s – swept capacity of the cylinder,

– thermal efficiency of the working cycle:

$$\eta_c = \frac{\int_V p dV}{B_0 W_0} \tag{4}$$

where: B_0 – fuel dose, W_0 – fuel caloric value.

– maximal pressure and temperature in the cycle:

$$\xi_{max} = \max_{0\le\varphi\le 4\pi}\{\xi(\varphi)\}, \quad \xi \in \{p, T\} \tag{5}$$

– maximal growth rate of pressure and temperature:

$$l_\xi = \max_{0\le\varphi\le 4\pi}\left\{\frac{d\xi}{d\varphi}\right\}, \quad \xi \in \{p, T\} \tag{6}$$

Moreover, the control task (2) is supplemented by boundary conditions having general form of:

$$F_{i\min}^* \le F_i^* \le F_{i\max}^* \text{ for } i = 1,...,k \tag{7}$$

$$l_{i\min} \le l_i \le l_{i\max} \text{ for } i = 1,...,q \tag{8}$$

defining respectively minimal and maximal values for each from the values important from controlling point of view.

In the control task formulated in such way, calculation of the objective function in each optimization step requires usage of the working cycle's model to evaluation of continuous functions $u_i(\varphi)$ $\varphi \in \langle 0, 4\pi \rangle$. It is necessary in each iteration, therefore, to integrate equations of the model, what requires adoption of numerically effective model of engine's working cycle.

3. Model of the working cycle

Requirement to ensure suitable computational efficiency of the model of the working cycle is pointing at a necessity of usage of simplified zero- or one-dimensional model. Let's consider, therefore, use of theoretical-empirical zero-dimensional model proposed in the study [2, 4]. Such type calculations model, after performed proceedings of identification of values of the model's parameters, allows to calculate characteristic parameters of the working cycle for any vector of control parameters. The model used in the controlling can be written in the general form:

$$M_i[X, E, G, p, m, T] = 0 \text{ for } i = 1,...,l \tag{9}$$

where: M_i – differential operator or function, l – number of equations,
together with dependencies for vector of model's parameters and vector of auxiliary parameters, respectively:

$$E = f_{(I,II)}(X) \tag{10}$$

and

$$G = f_{(I,II)}(X) \tag{11}$$

where $f_{(I,II)}(X)$ denotes mapping accomplished by neutral networks [2].

Integration of the equations describing the model leads directly to determination of the functions describing continuous courses of: mass, pressure, temperature and transient volume of cylinder, and their derivatives, what during the next step enables to determine values of individual functionals, defined in the control task in form of (2).

In scope of estimation of harmful compounds emissions like carbon monoxide, hydrocarbons, nitrogen oxide and smoke, implemented model is supplemented by relevant dependencies of the form [3]:

$$F_i^* = f_i(X) \tag{12}$$

where $i \in \{CO, HC, NO_x, D\}$.

4. Control task

In this study is considered the control task aimed at minimization of nitrogen oxides emission for a fixed operating point of the engine. This task therefore has the objective function in form of:

$$\overline{\Omega}_{NO_x}(X) = C_{NO_x}^F F_{NO_x}^* \tag{13}$$

where coefficient $C_{NO_x}^F$ can be taken as:

$$C_{NO_x}^F = \left[F_{NO_x,0}^*\right]^{-1} \tag{14}$$

where $F_{NO_x,0}^*$ denotes emissions of nitrogen oxides for factory settings.

Objective of the control formulated in such way should be attained for a considered point of engine operation with simultaneous fulfillment of additional constraints, with respect to:

– not exceeded allowable emission levels of other harmful components of exhaust gases:

$$F_i^* \le \delta_i F_{i,0}^* \text{ for } i \in \{CO, HC, D\} \tag{15}$$

where δ_i are coefficients assigned for a given operational point of the engine, while $F_{i,0}^*$ denotes emission or smoke of i-th component for factory settings,

– not exceeded allowable changes in parameters of characteristic working cycle:

$$l_i = l_{i,0} \text{ for } i \in \{p_i\} \tag{16}$$

$$\gamma l_{i,0} \le l_i \text{ for } i \in \{\eta_c\} \tag{17}$$

$$l_i \le \zeta_i l_{i,0} \text{ for } i \in \{p_{max}, T_{max}\} \tag{18}$$

where γ, ζ_i are coefficients assigned for a given point of engine operation, while $l_{i,0}$ is value of i-th functional (parameter of characteristic working cycle) for the initial conditions (at factory settings).

Solution of the control task formulated in form of (13) was performed for selected points of engine operation, the same as currently used by manufacturers to powering of passenger cars. Parameters of the engine are presented in the Table 1.

Table 1. The engine's technical data

Engine	Compression ignition engine supercharged by a turbo compressor with direct injection equipped with an electronically controlled Common Rail system
Layout of cylinders	4 in line
Number of valves per cylinder	4
Bore	70 mm
Stroke	82 mm
Total displacement	1.3 dm^3
Compression ratio	16.8
Maximum power	55 kW/4000 rpm
Maximum torque	200 N·m/1500 rpm

In order to evaluate the operating points for which the control task will be performed, a road tests of a vehicle equipped with such engine in conditions of real road traffic have been planned and accomplished. A number of drives were performed within framework of the tests, the cars were driven both in urban traffic conditions and on extra-urban roads. Parameters of vehicle's motion, engine speed and degree of engine load were recorded during the tests comprising in total eight hours of the driving. The recording was carried out with use of computer connected to OBD system of tested car. Read-out of motion parameters with frequency 1 Hz was performed with use of ELM327 Interface (OBD $\rightarrow$ RS232 Interpreter) and authorial software enabling simultaneous archiving of data downloaded from engine's ECU. All operating points of the engine recorded in course of the performed road tests [1] are presented in the Fig. 1.

Analysis of the road test results is pointing at dominating range of engine speed from interval of 2000-3000 rpm, and engine loads up to 75% of maximal torque at a given rotational speed. On this basis, four different engine loads for rotational speed of 2500 rpm have been chosen as the points for which the control task was solved. Summary of analyzed operating points from the control task presented in this study is given in the Table 2. Therefore, selected points of engine operation correspond to conditions often found in real conditions of engine operation.

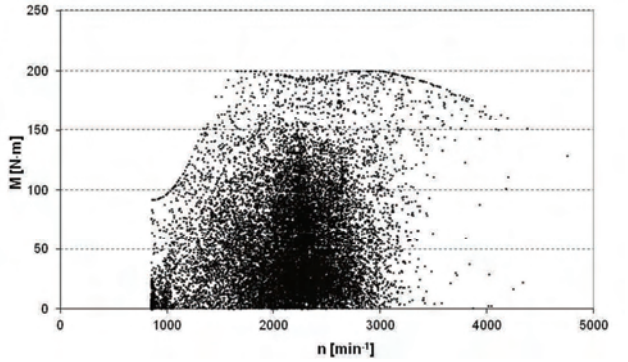

Fig. 1. Operating points of the engine recorded during accomplished road tests

Table 2. The engine's operating points considered in the control task

Load	0.25 $M_{max(2500\ rpm)}$	0.50 $M_{max(2500\ rpm)}$	0.75 $M_{max(2500\ rpm)}$	0.90 $M_{max(2500\ rpm)}$
Torque	48 N·m	95 N·m	143 N·m	171 N·m

Evaluation of permissible emissions of a given compound, and thus imposing limitations assumed in the control task, require analysis of exhaust gases' level emitted by tested engine, with respect to emission levels from other compression ignition engines, having comparable performance and displacement. Similarly, making benchmarking it is possible to define limitations related to thermal efficiency, mechanical and thermal engine loads. In this way the coefficients values present in the constraints (15–18) and shown in the Table 3 were evaluated.

Table 3. Values of coefficients $\delta_i, \gamma, \zeta_i$ taken to definition of boundary conditions in the control task

δ_{CO}	δ_{HC}	δ_D	γ	$\zeta_{p_{max}}$	$\zeta_{T_{max}}$
1.3	1.2	1.5	0.95	1.1	1.1

The Nelder-Mead method (downhill simplex method) was used to solve optimization task of the form with limitations. As result of performed optimization computations, new vectors of adjusting parameters were evaluated for each from analyzed operating points. Comparison with the parameters corresponding to factory settings is shown in the Table 4.

Table 4. Factory parameters and optimum parameters

	Engine load	B_0 [g]	φ_w [°OWK]	X_{EGR} [%]
Factory settings X_0	0.25 M_{max}	$0.9790 \cdot 10^{-2}$	356	20
	0.50 M_{max}	$1.7213 \cdot 10^{-2}$	354.4	11
	0.75 M_{max}	$2.4490 \cdot 10^{-2}$	353	0
	0.90 M_{max}	$2.8907 \cdot 10^{-2}$	352.5	0
Settings evaluated for assumed objective function (13) X_{OPT}	0.25 M_{max}	$1.0769 \cdot 10^{-2}$	356.6	24
	0.50 M_{max}	$1.729 \cdot 10^{-2}$	357.8	11
	0.75 M_{max}	$2.4561 \cdot 10^{-2}$	354	0
	0.90 M_{max}	$2.895 \cdot 10^{-2}$	353.6	0

Use of calculated adjustment parameters $\mathbf{X}_{OPT}$ leads to changes in the emissions (Table 5) and simultaneously satisfies, with sufficiently big margin, accepted limitations imposed on allowable changes in characteristic points of the working cycle.

Analysis of the data summarized in the Table 5 confirms possibility of significant reduction of emissions of nitrogen oxides, up to about 30% depending on point of engine operation, with simultaneous maintaining of assumed limitations with respect to other harmful compounds of exhaust gases and smokiness. Comparison of the values of medium indicated pressure, thermal efficiency of the working cycle, maximal pressure and temperature of the working cycle, obtained for factory set adjusting parameters, and after the modification, are presented in the Fig. 2.

Table 5. Emissions of harmful exhaust gases in analyzed points of engine operation

	Engine load	F_{CO} [%]	F_{HC} [ppm]	F_{NO_x} [ppm]	F_D [FSN]
Factory settings $\mathbf{X}_0$	0.25 M_{max}	0.068	265	97	0.3
	0.50 M_{max}	0.017	80	253	0.8
	0.75 M_{max}	0.007	50	769	0.2
	0.90 M_{max}	0.007	44	898	0.2
Settings evaluated for assumed objective function (13) $\mathbf{X}_{OPT}$	0.25 M_{max}	0.089	303	70	0.36
	0.50 M_{max}	0.021	74	175	1.21
	0.75 M_{max}	0.009	48	697	0.24
	0.90 M_{max}	0.008	43	812	0.28

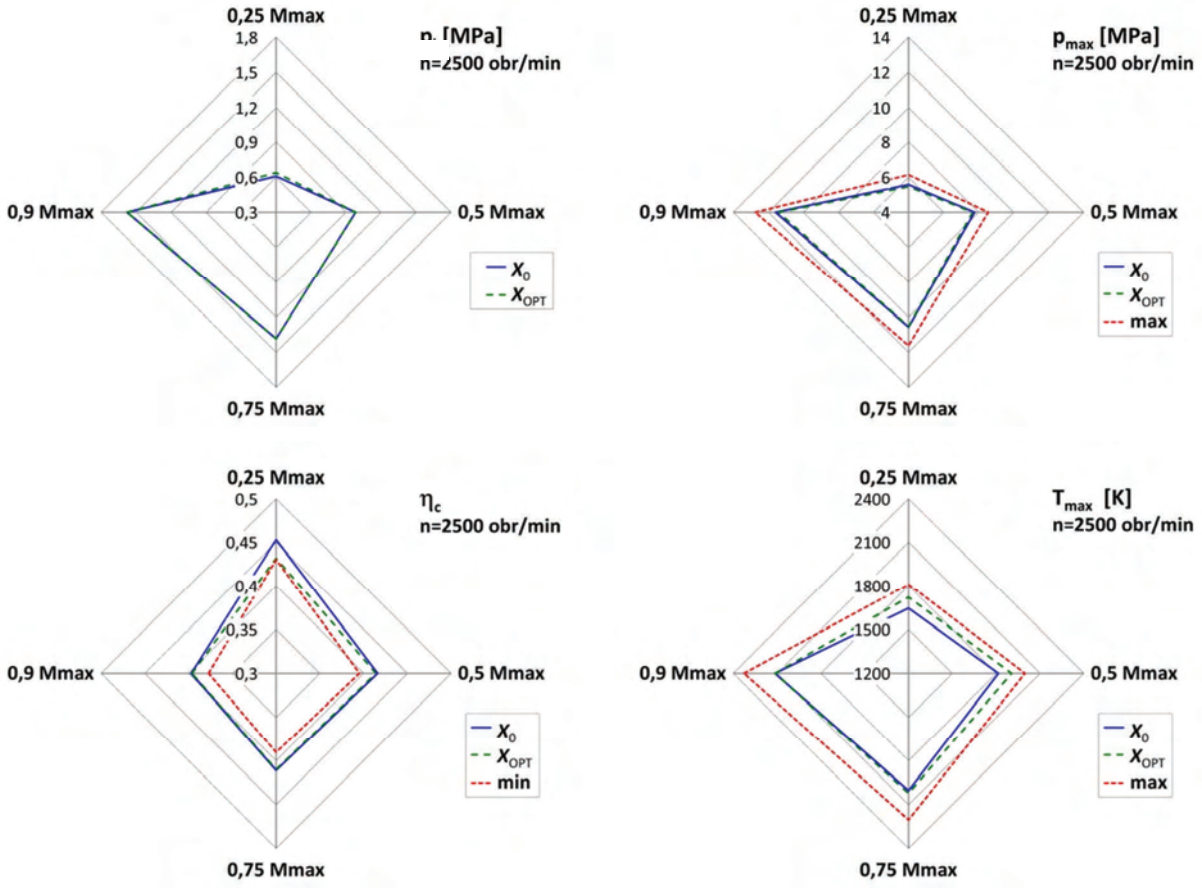

Fig. 2. Values of medium indicated pressure, thermal efficiency of working cycle, maximal pressure and temperature of the working cycle after application of calculated adjusting parameters $\mathbf{X}_{OPT}$ in relation to values of factory settings $\mathbf{X}_0$

5. Conclusions

Obtained solutions of the task aimed at selection of adjusting parameters in selected points of engine operation, obtained due to criterion of minimization of nitrogen oxides emission can be assessed on the basis of many criteria, which can be grouped within framework of three cumulative categories:

– environmental impact (emission of individual compounds of exhaust gases),
– utility (overall efficiency of the cycle),
– requirements of durability (maximal pressure and maximal temperature in the cylinder).

Due to significant environmental burden of harmful emissions of exhaust gases from traction vehicles, and taking into account increase in fleet of road going vehicles, the environmental criterion can be assumed as absolutely dominant over criterion of durability, and significantly preferred over criterion representing utility.

Nomenclature

X	vector of control parameters
X_{EGR}	degree of exhaust gas recirculation
E	vector of model parameters
G	vector of auxilary parameters
φ	crank angle
φ_w	injection advance angle
m	mass of the medium in cylinder
p	pressure in cylinder
T	temperature in cylinder

Bibliography

[1] ADAMSKI, W., BRZOZOWSKI, K., NOWAKOWSKI, J., PRASZKIEWICZ, T. Rzeczywista eksploatacja trakcyjna silnika a warunki przyjmowane w teście homologacyjnym. *Autobusy. Technika, Eksploatacja, Systemy Transportowe*. 2014, **5**, 37-40.

[2] BRZOZOWSKI, K., NOWAKOWSKI, J. Model for calculating compression ignition engine performance. *Eksploatacja i Niezawodnosc – Maintenance and reliability*. 2014, **3**, 407-414.

[3] BRZOZOWSKI, K., NOWAKOWSKI, J. Toxicity of exhaust gases of compression ignition engine under conditions of variable load for different values of engine control parameters. *Eksploatacja i Niezawodnosc – Maintenance and Reliability*. 2011, **4**, 56-62.

[4] HEYWOOD, J.B. International combustion engine fundamentals. *New York: Mc-Graw-Hill*, 1988.

[5] KNEFEL, T. Problematyka kształtowania sygnału sterującego wtryskiwaczem zasobnikowego układu zasilania w paliwo. *Wydawnictwo Naukowe Akademii Techniczno-Humanistycznej*, Bielsko-Biala, 2013.

Jacek Nowakowski, DSc., DEng. – Department of Combustion Engines and Vehicles at Faculty of Mechanical Engineering and Computer Science at University of Bielsko-Biala.

e-mail: *JNowakow@ath.bielsko.pl*

Tomasz Knefel, DSc., DEng. – Department of Combustion Engines and Vehicles at Faculty of Mechanical Engineering and Computer Science at University of Bielsko-Biala.

e-mail: *TKnefel@ath.bielsko.pl*

Krzysztof Brzozowski, DSc., DEng. – Department of Transport at Faculty of Management and Transport at University of Bielsko-Biala.

e-mail: *KBrzozowski@ath.bielsko.pl*

Article citation info:
TARTAKOVSKY, L., FLEISCHMAN, R. DPF retrofit program in Israel – effects of diesel particle filters on performance of in-use buses. *Combustion Engines*. 2017, **170**(3), 176-178. DOI: 10.19206/CE-2017-330

Leonid TARTAKOVSKY
Rafael FLEISCHMAN

CE-2017-330

DPF retrofit program in Israel – effects of diesel particle filters on performance of in-use buses

A long service life of heavy-duty diesel vehicles results in a large number of older-technology trucks and buses of various types running on roads nowadays. Cleaning up exhaust gases of these older vehicles gives an opportunity to improve air quality at affordable costs. Retrofitting older buses with diesel particulate filters (DPF) is a cost-effective measure to quickly and efficiently reduce particulate matter (PM) emissions and contribute to mitigation of air pollution in urban conglomerates.

In this paper, the milestones on a way to wide-scale retrofitting of heavy-duty vehicles with DPF are discussed on the example of Israel DPF retrofit program. Crucial importance of a balanced governmental approach combining regulation and economic incentives, together with collaboration of government, academia and vehicle operators, is underlined. Main results of the one-year pilot project focused on urban and intercity buses are discussed. Impact of DPF retrofitting on particulate emissions and engine performance and maintenance aspects of in-use diesel buses is analyzed. Very high particle filtration efficiency (in average, about 97%) together with relatively low fuel economy penalty (0.6–1.8%, depending on the bus type) are proved. Vital importance of careful monitoring and correct maintenance of DPF-equipped vehicles is underlined.

Key words: *particle emissions; diesel particle filter; heavy-duty vehicles; DPF retrofit*

1. Introduction

Climate change challenges require substantial improvement of vehicles' energy efficiency. However, this improvement must be achieved without compromising a continuous quest to zero-impact emissions [1]. It is well-known that combustion-generated particles formed in large quantities in diesel engines are of major concern to human health [2, 3]. In 2012, World Health Organization officially recognized diesel-originated particles as a most dangerous carcinogenic substance (group 1) like asbestos [4]. The published scientific data provide an evidence that ultrafine particles (UFP) are more harmful to human health than larger ones because UFP penetrate cell membranes and are transferred with the blood stream to all human organs, like brain, liver, etc. [5–7].

In the effort to mitigate PM emissions from the transportation sector, several aftertreatment technologies have been proposed and developed, while the most efficient of them has been shown to be a DPF [8]. Due to the relative simplicity of installing this device on in-use vehicles, massive DPF retrofit is performed worldwide, especially in heavy-duty trucks and buses, which can be kept in service for more than 15 years [9]. DPF retrofit has reportedly led to great PM reduction, up to 99% or even more [10, 11].

This paper reports on the main findings and lessons of DPF Retrofit Program in Israel with a main focus on the required interaction of scientific efforts and governmental willingness to make a change, and effects of diesel particle filters on real-world performance of in-use buses

2. Methodology

Despite a great number of successful examples of DPF retrofit in heavy-duty vehicles, decision makers always prefer to have a positive evidence at the local scene, thus making necessary and very important a pilot test carried out in the typical for a considered case conditions and with the vehicle models representative for a considered fleet. For this reason, a pilot test with 18 in-use urban and intercity buses was carried out during a period of 12 months to pave a road for the wide-scale DPF retrofit of heavy-duty vehicles in Israel. All relevant topography conditions were covered in the test, to provide the decision makers with as much as possible information.

There is a large variety of DPF types and technologies, with different characteristics, which could be installed in buses. To choose the DPF technology most suitable for retrofitting in the tested buses, exhaust gas temperature profiles have been measured during real-world operating conditions of intercity and urban buses. For this purpose, thermocouples were installed in the exhaust manifold, before the bus silencer, of the selected buses of the pilot group. The temperature was monitored for a couple of months prior the installation of the DPF.

A typical example of the measured temperature profile is shown in Figure 1. The horizontal axis in the Figure shows temperature ranges, and the vertical axis shows the percentage of time the exhaust gases were found to lie under each designated temperature range.

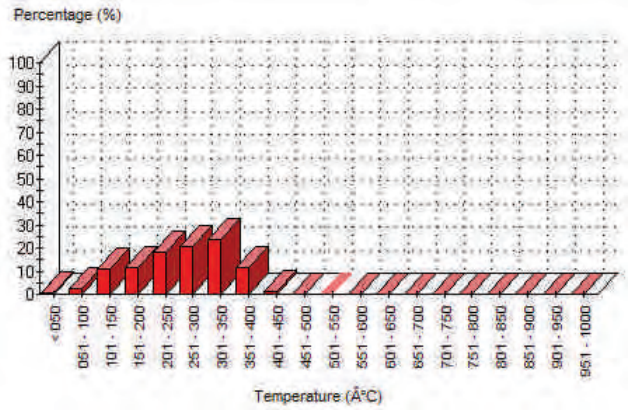

Fig. 1. Exhaust gas temperature profile of an intercity bus (in degrees Celsius)

As can be seen, the exhaust gas temperature of the considered in-use buses was higher than 100°C, 200°C, 300°C and 400°C during 97%, 75%, 36% and 1% of total usage time, respectively. The mean temperature during engine operation was found to be 258°C. The most suitable regeneration mechanism for this temperature profile is the NO2-based soot oxidation implemented in the Continuous Regeneration Trap (CRT) technology, developed for the first time by Johnson Matthey [12, 13]. Based on the obtained temperature profiles, three different DPF types (all of CRT technology) were selected in a close cooperation with VERT from the VERT-list of Best Available Technology (BAT) filters.

The buses (both urban and intercity) of the most popular in the local fleet manufacturers (in case of Israel – MAN and Mercedes) were selected for the pilot test. All the vehicles were produced under the Euro III emission standards, and had travelled a distance compatible with their age. Every vehicle had an original engine and had been appropriately maintained before and during the experiments.

UFP measurements were performed three times with each bus of the pilot group during the 12-months period after DPF retrofit. The measurements were carried out using the TSI-made Engine Exhaust Particle Sizer (EEPS) Spectrometer 3090 model. To assess particle number filtration efficiency PNFE, particle number concentrations (PNC) were measured upstream and downstream the DPF for each bus.

To evaluate DPF influence on the buses fuel economy, an additional group of buses of the same type and age running in the similar conditions was identified and designated as a control group. Fuel consumption data were gained for the period of 31 months for all 36 considered buses (18 of the control group and 18 of the pilot group). The data on fuel consumption before DPF retrofit allow us to estimate fuel economy deterioration due to natural aging. The data on fuel consumption of buses after DPF retrofit made possible assessment of fuel economy deterioration due to joint influence of aging and DPF itself. Knowing both number enables assessment of a sole DPF effect on fuel economy.

During the whole pilot duration, backpressure behavior in each retrofitted bus and maintenance operations were carefully monitored.

3. Results and discussion

The obtained results confirm known data on extremely high particle number filtration efficiency of DPFs. The averaged values of PNFE as were measured at different operation modes are shown in Fig. 2. As can be seen, PNFE of about 97% was measured at all engine operating regimes excluding low idle. The latter is not recommended for PNFE assessment due to substantially lower engine operation stability at this operation mode. The lower PNFE values at low idle are the result of higher particle agglomeration because of longer residence times due to low gas flow rates.

Figure 3 presents a histogram of the PNFE values obtained. Blue rectangles express the number of times that a result was obtained between a specific interval. The orange line expresses the cumulative percentage of measures.

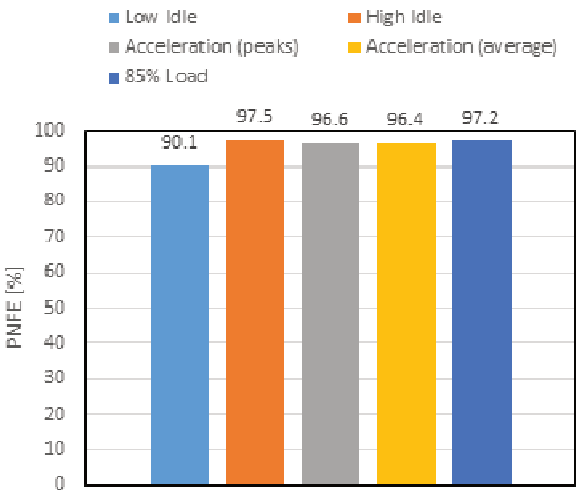

Fig. 2. PNFE as a function of engine operating regime

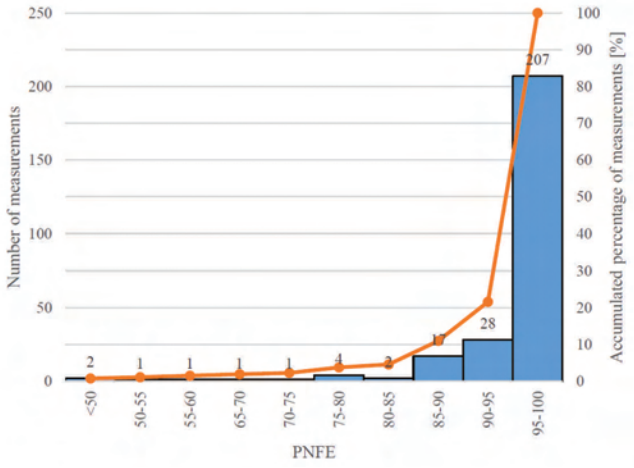

Fig. 3. PNFE histogram

As can be seen from Figure 3, all the results where PNFE values lower than 95% were measured comprise approximately 20% only of the total measurements and most probably are the result of various experimental uncertainties. It is important to note that PNFE values higher than 98% were obtained in 2/3 of the total measurement cases.

An analysis of buses fuel economy performed in accordance with the explained above methodology showed that fuel economy deterioration due to DPF retrofit is lower than frequently mentioned: 0.6 and 1.8 percent only for urban and intercity buses, respectively. A careful analysis of lubricant oil quality and maintenance events during the pilot test does reveal any influence of DPF retrofit on buses maintenance routine. Of course, at some moment filters cleaning due to ash accumulation will be required. Based on the gained values of backpressure during 12 months of the pilot test (did not exceed 75 mbar), we may estimate a frequency of filter cleaning as 2–2.5 years in average. It is clear that an exact need in DPF cleaning should be identified based on backpressure monitoring results.

Based on the success of the pilot test, the government of Israel has decided to invest 6 million USD in 2017 to retrofit of DPFs in heavy-duty diesel vehicles in Haifa region and in garbage trucks – nationwide. From August 2017, a

use of garbage trucks that do not meet at least Euro IV requirements will be forbidden. An appropriate legislative environment and retrofitting infrastructure are developed. To make the process of retrofitting clear for vehicle owners, a detailed instruction on DPF installation procedure was published by the Israeli Ministry of Transportation. The successful pilot also triggered a decision on Low Emission Zones (LEZ) formation in Israel with the first LEZ to be opened in Haifa (the whole city).

Conclusions

A pilot test demonstrating feasibility of DPF retrofit in heavy-duty vehicles is necessary as a pre-requisite of the successful retrofit program. Development of the public and governmental awareness to importance of DPF retrofit as an efficient and quick way of air pollution reduction is required. This can be done through scientific conferences, meetings with stakeholders and any other possible ways.

Air quality monitoring that includes measurement of black carbon or/and particle number concentrations is necessary to evaluate influence of DPF retrofit and other emissions reduction measures on air pollution. Another important factor affecting the overall success of any retrofit or another emissions mitigation program is an effective roadworthiness program. The latter must include PNC diagnostics, because standard opacity control technologies are not effective anymore in diagnostics of DPF-equipped vehicles.

Acknowledgements

A financial support of the bus operator Egged is gratefully acknowledged. The authors are grateful to the Israeli Ministry of Environmental Protection for support and fruitful cooperation.

Bibliography

[1] TARTAKOVSKY, L., GUTMAN, M., MOSYAK, A. Energy efficiency of road vehicles – trends and challenges. Chapter 3 in the edited collection "Energy efficiency: methods, limitations and challenges", Emmanuel F. Santos Cavalcanti and Marcos Ribeiro Barbosa (editors). *Nova Science Publishers*. 2012. 63-90.

[2] DOCKERY, D.W., POPE, C.A., XU, X. et al. An association between air pollution and mortality in six US cities. *N. Engl. J. Med.* 1993, **329**, 1753-1759.

[3] POPE III, C., DOCKERY, D. Health effects of fine particulate air pollution: lines that connect. *J. Air Waste Manage. Assoc.* 2006, **56**, 709-742.

[4] International Agency for Research on Cancer, IARC, 2012. *Diesel engine exhaust carcinogenic*. Press Release No 213, IARC, WHO, www.iarc.fr/en/media-centre/pr/2012/pdfs/pr213_E.pdf.

[5] SLEZAKOVA, K., MORAIS, S., PEREIRA, M. Atmospheric nanoparticles and their impacts on public health. In: Rodrigues-Morales, A. (Ed.), *Current Topics in Public Health*. INTECH, 2013, 503-529.

[6] KNIBBS, L.D., COLE E HUNTER, T., MORAWSKA, L. A review of commuter exposure to ultrafine particles and its health effects. *Atmos. Environ.* 2011, **45**, 2611-2622.

[7] HOET, P.H.M., BRÜSKE-HOHLFELD, I., SALATA, O.V. Nanoparticles – known and unknown health risks. *J. Nanobiotechnology*. 2004, **2**, 12.

[8] MAYER, A., CZERWINSKI, J., MATTER, U. et al. VERT: diesel nano-particulate emissions: properties and reduction strategies. *SAE Technical Paper*. 1998, 980539.

[9] BOUDART, J., FIGLIOZZI, M. Key variables affecting decisions of bus replacement age and total costs. *Transp. Res. Rec. J. Transp. Res. Board*. 2012, **2274**, 109-113.

[10] MAYER, A. (ed.) Particle filter retrofit for all diesel engines. *Expert Verlag*. 2008.

[11] TARTAKOVSKY, L., BAIBIKOV, V., COMTE, P. et al. Ultrafine particle emissions by in-use diesel buses of various generations at low-load regimes. *Atmos. Environ.* 2015, **107**, 273-280.

[12] COOPER, B.J., JUNG, H.J., THOSS, J.E. *US Patent* US4902487. 1990.

[13] ALLANSSON, R., BLAKEMAN, P.G., COOPER, B.J. et al. The use of the continuously regenerating trap (CRTTM) to control particulate emissions: minimising the impact of sulfur poisoning. *SAE Technical Paper*. 2002, 2002-01-1271.

Leonid Tartakovsky, DEng. – Faculty of Mechanical Engineering, Technion – Israel Institute of Technology, Haifa, Israel.

e-mail: *Tartak@technion.ac.il*

Rafael Fleischman – Faculty of Mechanical Engineering, Technion – Israel Institute of Technology, Haifa, Israel.

Article citation info:
CZERWINSKI, J., COMTE, P., GUEDEL, M., BONSACK, P. Nanoparticle emissions from gasoline vehicles DI & MPI. *Combustion Engines*. 2017, **170**(3), 179-187. DOI: 10.19206/CE-2017-331

Jan CZERWINSKI
Pierre COMTE
Martin GUEDEL
Peter BONSACK

CE-2017-331

Nanoparticle emissions from gasoline vehicles DI & MPI

The nanoparticles (NP) count concentrations are limited in EU for all Diesel passenger cars since 2013 and for gasoline cars with direct injection (GDI) since 2014. For the particle number (PN) of MPI gasoline cars there are still no legal limitations. In the present paper some results of investigations of nanoparticles from five DI and four MPI gasoline cars are represented. The measurements were performed at vehicle tailpipe and in CVS-tunnel. Moreover, five variants of "vehicle – GPF" were investigated. The PN-emission level of the investigated GDI cars in WLTC without GPF is in the same range of magnitude very near to the actual limit value of 6.0×10^{12} 1/km. With the GPF's with better filtration quality, it is possible to lower the emissions below the future limit value of 6.0×10^{11} 1/km. The modern MPI vehicles also emit a considerable amount of PN, which in some cases can attain the level of Diesel exhaust gas without DPF and can pass over the actual limit value for GDI (6.0×10^{12} 1/km). The GPF-technology offers in this respect further potentials to reduce the PN-emissions of traffic.

Key words: *particle number (PN), gasoline direct injection (GDI), multipoint port injection (MPI), gasoline particle filter (GPF)*

1. Introduction

The invisible nanoparticles (NP) from combustion processes penetrate easily into the human body through the respiratory and olfactory pathways and carry numerous harmful health effects potentials. The nanoaerosol in vehicle exhaust is known to be a complex mixture of different volatile and non-volatile species often showing a bimodal particle size distribution with a nucleation mode smaller than 20 nm and a larger accumulation mode that mainly contains aggregates of primary particles.

The larger accumulation mode is usually composed of more graphitic soot particles with an elemental carbon (EC) structure, whereas the particles in the nucleation mode are reported to be mainly volatile organics, especially when sulphur is absent from fuel and lubrication oil [1–4]. However, recent studies detected also low-volatility particle fractions in the ultrafine size range when sampling was carried out according to PMP protocol at 300°C [5–7].

These particles are suspected to be nucleated metal oxides originating from metal additives in lubrication oil or fuels [8–11]. The formation of this particulate fraction was especially observed when the soot content was low as in idle condition of diesel vehicles. These particles mainly appear in the ultrafine size rage < 23 nm. While the mass contribution of these ultrafine particles in vehicle emissions is very low, their contribution to the number concentration is significant. Moreover, these ultrafine particles may contribute to the surface composition of the aerosol and have therefore a significant impact on health effects associated with pollution.

Knowledge about the emission level, chemistry and formation mechanisms of these particles is an important objective in order to assess their toxic potential, and to propose effective measures to reduce these emissions.

Studies for gasoline fueled internal combustion engines pointed out that also this vehicle class can emit remarkable amounts of particles [6, 12, 13]. Especially gasoline direct injection technology (GDI) shows particle number (PN) emissions significantly higher than modern diesel cars equipped with best available DPF technology. Since the trend for gasoline vehicles with GDI technology is increasing, a significant rise in emission is predicted in the near future.

The nanoparticles emissions are produced especially at cold start and warm-up conditions and at a dynamic engine operation [14]. The lube oil contributes to this emission in the sense of number concentrations in nuclei mode and composition [8–10].

The investigations of morphology of the nanoparticles from gasoline direct injection engine revealed principally graphitic structures, which can store some metal oxides in certain conditions and can be overlapped by condensates [15, 16].

Car manufacturers and suppliers of exhaust aftertreatment technology offer several mature solutions of GPF for efficient elimination of the nanoparticles from DI SI-engines [17, 18].

There is also nanoparticles emission of gasoline vehicles with MPI (multipoint port injection). Some of them emitting high amount of PN and PM. In a study of AFHB, [19], an older model with MPI was found to emitting at stationary part load operation up to 4 orders of magnitude more nanoparticles, than a lower emitting GDI car. The main reason for this increased PN-emission was attributed to the increased lube oil consumption. Never-theless an inferior quality of mixture preparation cannot be excluded.

The MPI technology has a big share of the worldwide market because of its lower costs and simplicity and in several countries this technology will still stay as primary option for several years to come.

From this perspective and taking account of the progressing exhaust gas legislation aiming an increased care about health and environment protection it is necessary to include the cars with MPI in the efforts to reduce PN & PM.

Some investigations in present paper were performed at AFHB (Laboratories for IC-Engines and Exhaust Emission Control of the Berne University of Applied Sciences, Biel

CH) as a part of the network project GasOMeP, together with the Swiss Research Institutions: EMPA, FHNW and PSI.

This paper presents: comparisons of NP-emissions of five GDI vehicles and four MPI vehicles at steady state (SMPS) and at transient (CPC) operation, as well as the emissions reduction potentials with different gasoline particle filters (GPF's) on some GDI cars.

Table 1a. Data of investigated cars

Vehicles ①②③	Volvo V60 T4F ①	Opel Insignia 1.6 EcoFlex ②	Mitsubishi Carisma 1.8 GDI ③
Number and arrangement of cylinders	4 / in line	4 / in line	4 / in line
Displacement cm^3	1596	1598	1834
Power kW	132 @ 5700 rpm	125 @ 6000 rpm	90 @ 5500 rpm
Torque Nm	240 @ 1600 rpm	260 @ 1650-3200 rpm	174 @ 3750 rpm
Injection type	DI	DI	DI
Curb weight kg	1554	1701	1315
Gross vehicle weight kg	2110	2120	1750
Drive wheel	Front-wheel drive	Front-wheel drive	Front-wheel drive
Gearbox	a6	m6	m5
First registration	27.01.2012	2014	05.2001
Exhaust	EURO 5a	EURO 5b+	EURO 3
Aftertreatment	TWC	TWC	TWC/Ox.Cat

Table 1b. Data of investigated cars

Vehicles ④⑤⑥	Opel Zafira Tourer ④	VW Golf Plus ⑤	Diesel Peugeot 4008 1.6HDi STT ⑥
Number and arrangement of cylinders	4 / in line	4 / in line	4 / in line
Displacement cm^3	1598	1390	1560
Power kW	125 @ 6000 rpm	118 @ 5800 rpm	84 @ 3600 rpm
Torque Nm	260 @ 1650 - 3200 rpm	240 @ 1500 rpm	270 @ 1750 rpm
Injection type	DI	DI	DI
Curb weight kg	1678	1348 - 1362	1462
Gross vehicle weight kg	2360	1960 - 1980	2060
Drive wheel	Front-wheel drive	Front-wheel drive	Front-wheel drive
Gearbox	m6	m6	m6
First registration	22.07.2014	01.02.2010	12.04.2013
Exhaust	EURO 5b+	EURO 4	EURO 5b
Aftertreatment	TWC	TWC	DPF

2. Tested vehicles

Table 1 summarizes the most important GDI vehicle data. As a reference of the best available technology, concerning the reduction or elimination of PM- and PN-emissions a modern Diesel passenger car with a high-quality DPF was included in the tests (vehicle ⑥).

Table 2 shows the most important data of the investigated MPI vehicles. It can be remarked that the vehicle ⑧ in this group is the only one with turbocharger and vehicle ⑩ is equipped with 2 injectors per cylinder intake port.

Table 2. Data of investigated MPI vehicle

Vehicles ⑦⑧⑨⑩	Opel Adam ⑦	Fiat Panda 4x4 Twin Air ⑧	Ford KA 1.2i ⑨	Suzuki Baleno 1.2 Hybrid⑩
Number and arrange-ment of cylinders	4 / in line	2 / in line	4 / in line	4 / in line
Displace-ment cm^3	1398	875	1242	1242
Power kW	64 @ 6000 min^{-1}	62.5 @ 5500 min^{-1}	85 @ 5500 min^{-1}	66 @ 6000 min^{-1}
Torque Nm	130 @ 4000 min^{-1}	145 @ 1900 min^{-1}	102 @ 3000 min^{-1}	120 @ 4400 min^{-1}
Injection type	MPI	MPI	MPI	MPI
Curb weight kg	1195	1170	989	1010
Gross vehicle weight kg	1465	1550	1320	1405
Drive wheel	Front-wheel drive	4x4	Front-wheel drive	Front-wheel drive
Gearbox	m5	m6	m5	m5
First registra-tion	5.3.13	2.12.15	30.5.16	29.4.16
Exhaust	EURO 5b	EURO 6b	EURO 6b	EURO 6b
After-treatment	TWC	TWC	TWC	TWC + EGR

3. Fuels and lube oils

The gasoline used was from the Swiss market, RON 95, according to SN EN228. A bigger charge of gasoline was purchased for the project and it was analysed at INTERTEC Laboratory. The most important data are given in Table 3.

The lube oils for GDI-vehicles were also analysed at EMPA Laboratory, Table 4, which shows the 9 most prominent metals and the sums of all analysed 21 metals. For all GDI-vehicles, except of vehicle ②, the same lube oil was applied.

For the Diesel car as well as for the MPI cars the lube oils were not changed and not analysed.

Table 3. Data of gasoline

Property	Unit	Result
Density (at 15°C)	kg/m^3	736.1
Vapor pressure (at 37.8°C)	kPa	67.3
Research Octan Number (RON)	–	95.6
Oxygen content	% (m/m)	1.0
Sulfur content	mg/kg	<1.0
Pb Leed	mg/L	<1.0
Ca Calcium	mg/kg	<1.0
Fe Iron	mg/kg	<1.0
Mg Magnesium	mg/kg	<1.0
Mn Manganese	mg/kg	<1.0
P Phosphorus	mg/kg	<1.0
Zn Zink	mg/kg	<1.0
Na Natrium	mg/kg	<1.0
K Potasium	mg/kg	<1.0
Distillation (at 101.3 kPa)		
• start	°C	34
• 10% Vol	°C	48
• 50% Vol	°C	75
• 90% Vol	°C	142
• end	°C	174

Table 4. Data of the utilized lube oils (* analysis, others: specifications)

Property (typical value)	Vehicles ①③④⑤ Castrol Magnatec	Vehicle ② dexos 2	Unit
Viscosity kin 40°C	72.0	72.0	mm^2/s
Viscosity kin 100°C	12.2	12.1	mm^2/s
Viscosity index	166	165	(–)
Density 15°C	852	854	kg/m^3
Pour point	–39	–36	°C
Flash point (PMCC)	207	>201	°C
Total Base Number TBN		7.5	mg KOH/g
Sulphated ash	0.8	0.8	%wt
Na *	4.7	434	µg/g
Mg *	17	9.2	µg/g
Al *	32	5.4	µg/g
Ca *	2240	2300	µg/g
Mn *	0.20	24	µg/g
Fe *	17	34	µg/g
Cu *	0.07	27	µg/g
Zn *	760	630	µg/g
Mo *	36	0.81	µg/g
Sum metals	3109.56	3481.48	µg/g

4. Test methods and instrumentation

The vehicles were tested on a chassis dynamometer at constant speeds and in the dynamic driving cycles WLTC, with cold & warm engine start.

4.1. Chassis dynamometer – following test systems were used:

- roller dynamometer: AFHB GSA 200
- driver conductor system: Tornado, version 3.3.
- CVS dilution system: Horiba CVS-9500T with Roots blower
- air conditioning in the hall automatic (intake- and dilution air).

The driving resistances of the test bench were set according to the legal prescriptions, responding to the horizontal road.

4.2. Nanoparticle analysis

The measurements of NP size distributions were conducted with different SMPS-systems, which enabled different ranges of size analysis at steady state operation:

SMPS: DMA TSI 3081 & CPC TSI 3772 (10–429 nm)
nSMPS: nDMA TSI 3085 & CPC TSI 3776 (2–64 nm)

For the dilution and sample preparation an ASET system from Matter Aerosol was used (ASET aerosol sampling & evaporation tube). This system contains:

- Primary dilution – MD19 tunable rotating disc minidiluter (Matter Eng. MD19-2E)
- Secondary dilution – dilution of the primary diluted and thermally conditioned sample gas on the outlet of evaporative tube.
- Thermoconditioner (TC) – sample heating at 300°C

This sample preparation system fulfills the requirements of PMP and it was used for all measurements. At steady state operation (SSC see next section) this system worked with summary dilution factors DF = 100 to 500.

The estimated accuracy of PN-measurement in the size range of 80–120 nm, with DF = 100 is ±6%.

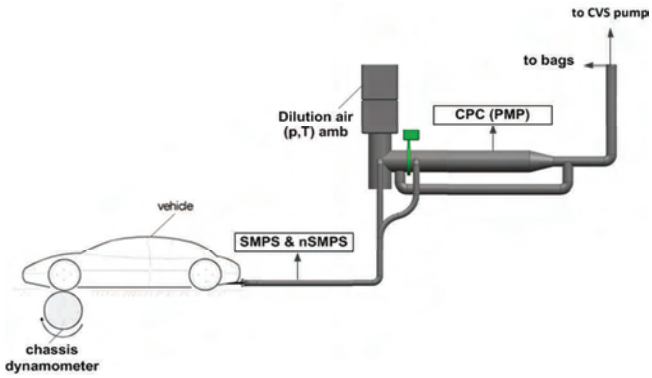

Fig. 1. Set-up of exhaust gas sampling for PN-analysis

For the measurements of summary PN at transient operation a CPC TSI 3790 (PMP conform) was used.

In the tests the gas sample for the NP-analysis was taken from the undiluted exhaust gas at tailpipe for stationary operation (SMPS) or from the diluted exhaust gas in CVS-tunnel at transient operation (CPC). The schematic of the general sampling set up is represented in Fig. 1.

4.3. Driving cycles

The vehicles were tested on a chassis dynamometer at constant speeds (SSC) and in the dynamic driving cycles.

The steady state cycle (SSC) consists of 20 min-steps at 95, 45 km/h and idling, performed in the sequence from the highest to the lowest speed.

Fig. 2 shows the steady state cycle (SSC) with the resulting tailpipe temperatures (t_{exh}) for gasoline vehicle ⑦ (MPI). This gives the magnitude of the temperatures at the particulate sampling point "tailpipe" during steady state measurements (SMPS).

The approach to find a homogenized world-wide driving cycle was successfully finished with the development of the homogenized WLTP world-wide light duty test procedure. The WLTC (world-wide light duty test cycle) represents typical driving conditions around the world.

This cycle (Fig. 3) has been used also in this study. It represents different driving conditions: urban, rural, highway and extra-highway.

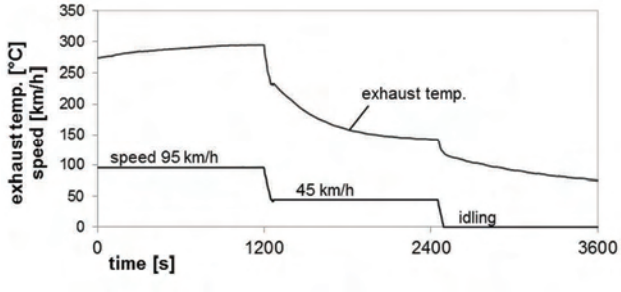

Fig. 2. Steady State Cycle (SSC) and tailpipe temperature of vehicle 7 (MPI)

In the test program with MPI vehicles the cycles RTS 95 and ADAC 130 were used. The RTS95 is a short chassis dynamometer test cycle representing aggressive driving and used for development purposes as short procedure replacing WLTC. The ADAC 130 cycle represents the high-way

driving and for the investigated vehicles class requires some full load accelerations.

Fig. 3 shows the time-courses and Table 5 summarizes the most important data of these driving cycles.

Table 5. Date of the driving cycles

Cycle	Duration s	Distance m	v_{max} km/h	a_{max} m/s^2	a_{min} m/s^2
WLTC	1800	23'262	131	1.58	–1.49
RTS95	886	12'927	134	2.61	–2.63
ADAC130	740	18'755	130	6.94	–5.00

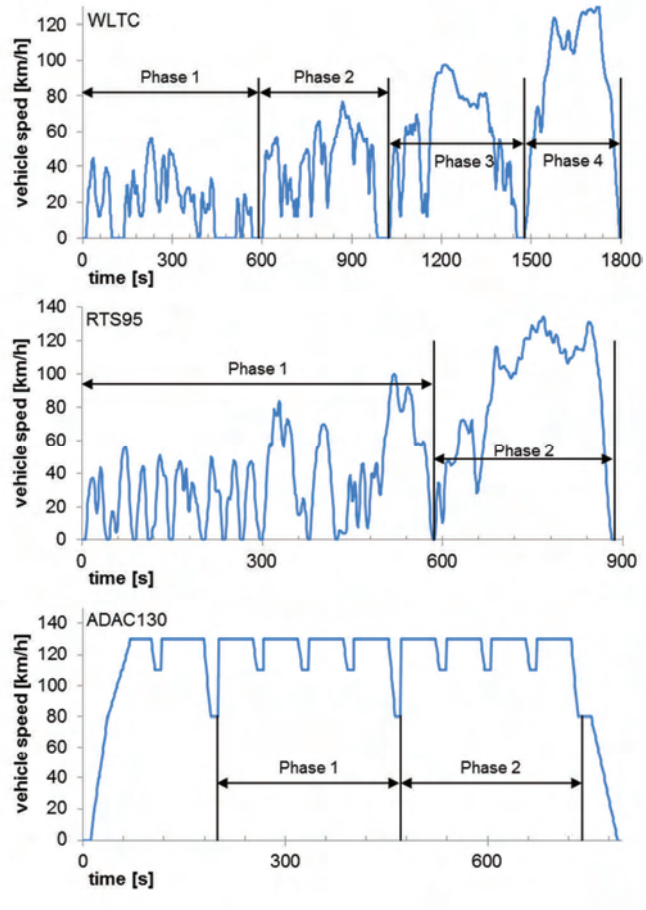

Fig. 3. Transient driving cycles WLTC, RTS 95 and ADAC 130

5. Results with GDI vehicles

5.1. Steady state operation (SSC)

The considerations of particle size distributions at steady state operation give a basic view on the PN-concentrations at tailpipe and allow some reflections about the nanoparticle production. Nevertheless, this is not a legal measuring procedure and therefore the results do not have to be compared with the legal PN limit values.

Fig. 4 represents exemplary the SMPS particle size distributions (PSD) of all tested vehicles (V1 to V5) at tailpipe without GPF at the same constant speeds and idling.

At 95 and 45 km/h the maxima of PSD's show in certain cases the particle counts concentrations (PC) in the range of 10^6 to 10^7 1/cm^3, which is similar as for Diesel engines (without DPF). At idling, the PC values are roughly one order of magnitude lower.

For vehicle ③, strong fluctuations of the PC-concentration during the period of scanning (over the size range) are visible. During the constant speed operation of this vehicle (at 95 and 45 km/h), periodic fluctuations of gaseous emissions (CO, HC, NO_x) were observed (not represented here) and confirmed a continuous switching of the operation between lean and rich. This means that for this vehicle, changing between the stratified, or homogenous (lean) and homogenous (rich) operating strategies, it also implies the switching of parameters, like ignition timing, injection timing, injection quantity and eventually EGR. This can have the influences on NP-emissions as demonstrated.

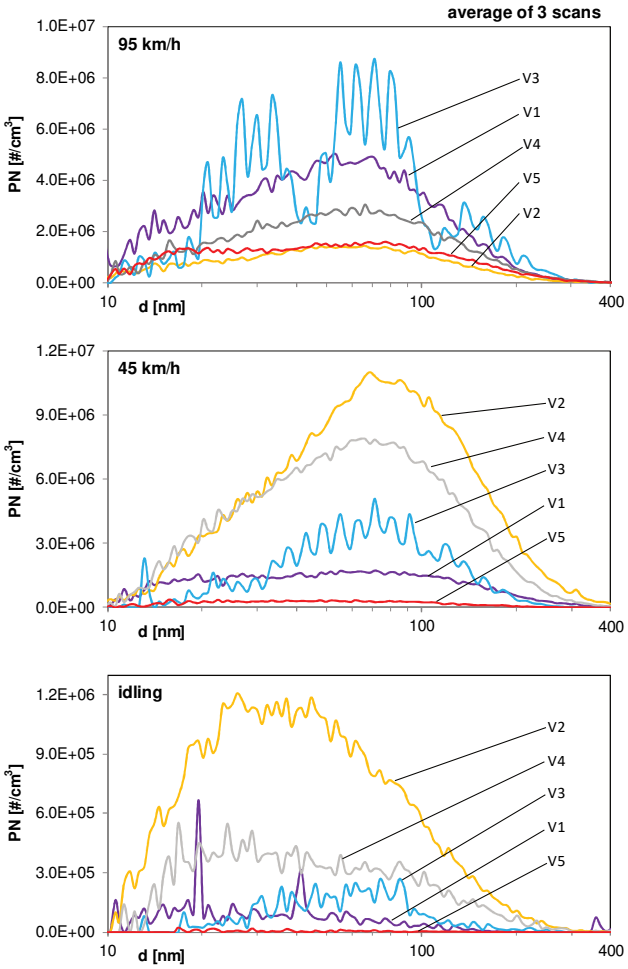

Fig. 4. SMPS particle size distributions at constant speeds with different GDI vehicles (w/o GPF)

The relationships of NP-emissions between different vehicles can vary depending on operating condition. As example: vehicle ② has at 95 km/h the lowest and at 45 km/h and idling the highest particle counts concentrations. This is also visible in the summary representation of integral PN-emissions at all tested constant speeds, Fig. 5.

There are different interacting processes during mixture preparation, combustion and gas flow in the exhaust system, which sensitively influence the generation of nanoparticle emissions. The following discussion gives some ideas and hypotheses about the reasons of the observed differences of PN-results between the different vehicles.

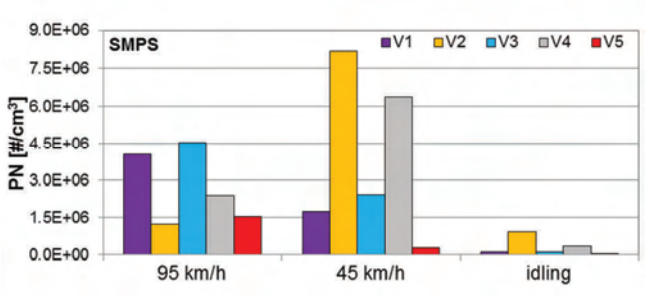

Fig. 5. Integral PN emissions at constant speeds with different GDI vehicles (w/o GPF)

Important question is the mixture preparation: the ideal mixture preparation should atomize and evaporate all the used fuel and bring it as homogenously premixed, as possible into the combustion chamber.

For MPI there is usually a portion of fuel deposited on the walls of the intake port, which can, especially at transient operation, arrive in the combustion chamber as liquid non-premixed droplets. A part of this "unprepared" fuel burns heterogeneously and is a source of soot-production.

These effects are stronger in DI technology and especially, when the liquid fuel arrives at the wall and, what is also possible, interacts with the lube oil layer, the production of nanoparticles is particularly increased [20, 21].

The chemistry of oil and fuel, their HC-matrix and additive packages have a significant influence on the NP's.

Further to consider are: the passage of aerosol through the exhaust system, the history of temperature drop, catalysis, chemistry, spontaneous condensation and store/release effects in the exhaust system. All of them have finally influences on "what will be measured at tailpipe".

The processes influencing NP-production depend on engine operating conditions. With no doubt the NP-emissions vary with the operating point and are increased at transient operation.

The measurements of all PSD's at constant speeds were simultaneously performed with two systems SMPS (size range 10–429 nm) and nano-SMPS (size range 2–64 nm).

Fig. 6 shows, as example, the particle size distributions measured with SMPS and with nSMPS for the higher (vehicle ④) and for the lower (vehicle ②) emitting vehicles at 95 km/h.

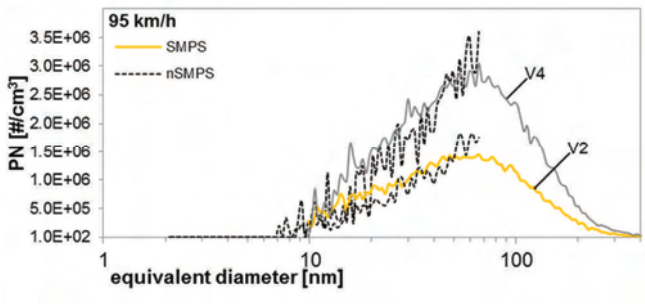

Fig. 6. SMPS & nSMPS particle size distributions at 95 km/h with GDI V2 & V4 (w/o GPF)

There are no PC in the sizes below 6 nm and the PC in the size range 6 to 10 nm can be considered as negligible.

Generally there is a very good accordance of PSD's measured with both systems SMPS and nSMPS in the common size range (10–64 nm).

Fig. 7 shows an example of scans with and without GPF. It confirms the excellent accordance of scans with both systems, it also confirms very good particle count filtration efficiency (PCFE) of the tested GPF and it particularly shows the total elimination of nanoparticles with sizes below 30 nm.

The opinion of the authors, resulting from these tests as well as from previous experiences with GDI-vehicles [19], is that additional research, or discussions about NP's with sub-10 nm-sizes and more restrictions of the legislation for sub-23nm-sizes, are not necessary.

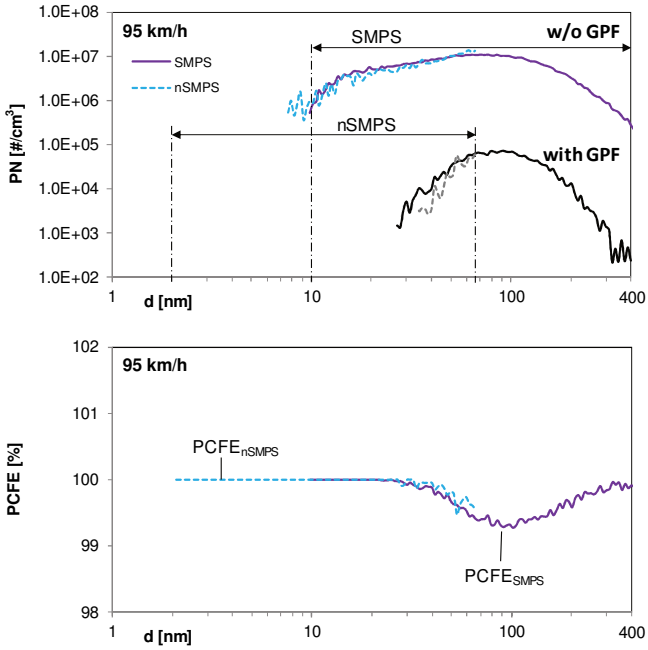

Fig. 7. Example of PSD's with SMPS & nSMPS and particle counts filtration efficiency (PCFE) with V1, GPF 1 at 95 km/h

Five variants "vehicle – GPF" were tested. The GPF's were randomly obtained for the tests and they were mounted in the exhaust systems of the cars approximately 60 cm downstream of the TWC. They were neither developed, nor optimized for this application. The specific data of the GPF's are not available.

Fig. 8 summarizes the filtration efficiencies (PCFE) obtained at the constant speeds. The PCFE-values are between 91% and 100%. GPF3 and GPF4 represent clearly lower filtration efficiency than GPF1 and GPF2. This result indicates that the filtration efficiencies can be adapted by optimizing the substrate to fulfil different objectives or requirements.

In comparison, the quality requirements for DPF retrofitting are: for the Swiss Confederation OAPC PCFE $\geq$ 97% and of the VERT Association PCFE $\geq$ 99%. This is in the sense of "best available technology for health protection".

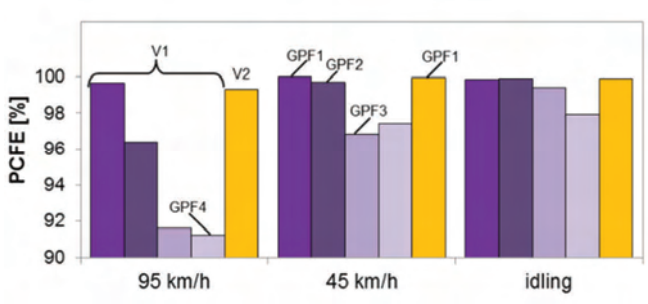

Fig. 8. Filtration efficiencies PCFE at constant speeds with different GPF's (SMPS data)

5.2. Transient operation

The results at transient operation are obtained with CPC (according to PMP) at the end of CVS-dilution tunnel. These results can be compared with the legal PN limit values.

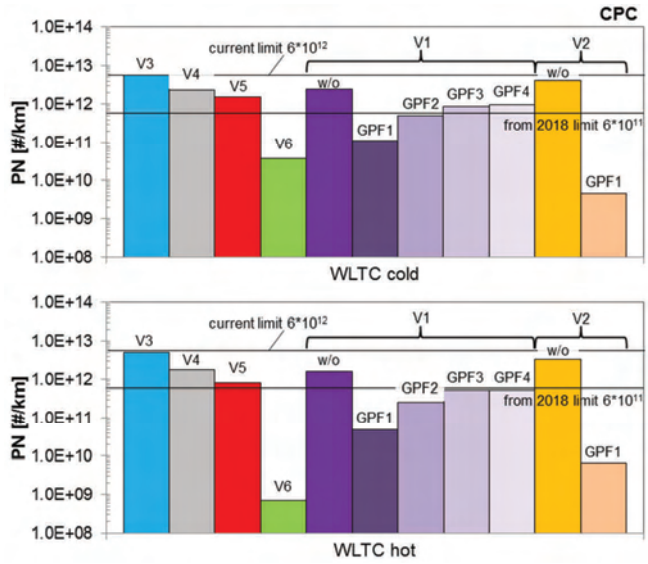

Fig. 9. Comparison of PN-emissions in WLTC cold and hot for different vehicles

All mechanisms influencing the NP-production in combustion chambers and in the exhaust system are at transient operation variable and mostly overlapping each other. A known and accepted fact is that the peak values of NP-emissions coincide with the acceleration, or deceleration events in the driving cycle.

Fig. 9 summarizes the average PN emissions in WLTC cold and hot. The emission level of "hot" cycles is generally lower than the emission level of "cold" cycles. Vehicles which are equipped with GPF have, as expected, lower PN-emissions. Vehicle ⑥ is a Diesel car with original DPF of a very good quality; it sets a quality level, which is only roughly attained by the vehicle ② with GPF1.

From all variants with GPF's the GPF3 and GPF4 have the highest emissions. These two filters also have the lowest average filtration efficiencies, Fig. 10.

Finally, it can be concluded that the PN-emission level of the investigated GDI cars in WLTC without GPF is in the same range of magnitude very near to the actual limit value of 6.0×10^{12} 1/km. With the GPF's with better filtration quality it is possible to lower the emissions below the future limit value of 6.0×10^{11} 1/km.

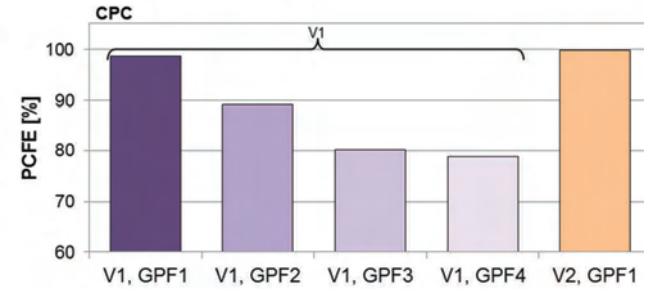

Fig. 10. PCFE's of the investigated GPF's in WLTC hot

6. Results with MPI vehicles

6.1. Steady state operation (SSC)

Fig. 11 gives an example of the SMPS-particle size distributions (PSD) with the MPI vehicles at 95 km/h and at idling. The indicated particle counts concentrations are mostly in the range of ambient background level (10^2 to 10^4 1/cm^3). Nevertheless, there are some exceptions such as a clearly higher PN-emission with vehicle ⑧ at 95 km/h and a higher PN-emission with vehicle ⑨ at idling.

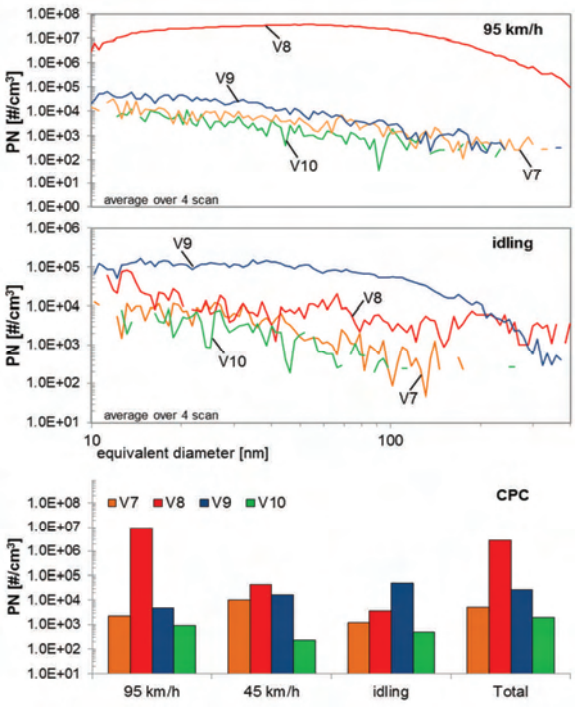

Fig. 11. SMPS particle size distribution at constant speeds with different MPI vehicles

At the highest speed (95 km/h) vehicle ⑧ causes the particle count concentrations, which are up to 3 ranges of magnitude higher, then with the other vehicles.

Fig. 12 compares the PSD's measured with SMPS and with nSMPS with the highest emitting vehicle ⑧ and with the lowest emitting vehicle ⑩ at 95 km/h.

For vehicle ⑧ there is a very good correlation of results obtained with nSMPS and with SMPS in the common size

range (10–64 nm). The particle numbers in the size spectrum below 10 nm are zero, or negligible.

For vehicle ⑩ there is no clearly pronounced size distribution, but random indications of particle counts in the ambient level. There is also a very good accordance of both measuring systems.

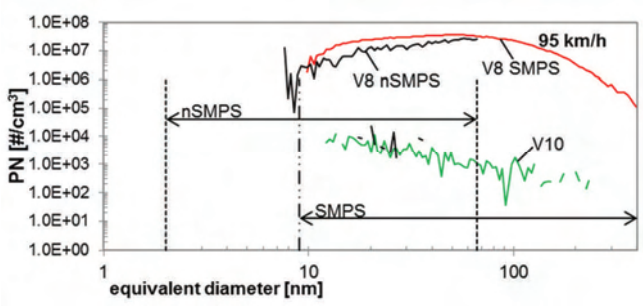

Fig. 12. Particle size distribution of MPI vehicles (min/max emissions)

6.2. Transient operation

The legal emission limits are established for the transient operation, which causes higher PN-values. The particle counts are measured as summary of all particle sizes in the diluted exhaust in CVS tunnel, by means of CPC.

Fig. 13 summarizes the integral PN-results of the four MPI vehicles in all transient cycles. It can be remarked that the relationships of emission level are for all vehicles in all driving cycles the same.

In the driving cycle with cold start the PN-emissions are higher than with warm start. One of the vehicles would not pass the present limit value of 6×10^{12} 1/km and three of the vehicles would not pass the future limit value of 6×10^{11} 1/km.

The following points have to be mentioned:

– in the cycle RTS95 vehicle ⑧ had to be accelerated at full load to follow the driving conductor cycle trace,
– at higher speeds and acceleration there is particularly higher PN-emission with vehicle ⑧,
– at the ADAC130 high speed cycle none of the vehicles could follow the cycle; all vehicles were fully accelerated; this caused very high CO-emissions – in one case with vehicle ⑧ CO in the bag came in over range,
– vehicle ⑩ with two injection valves per cylinder yielded the lowest PN-emissions – it can be supposed, that a better mixture preparation and lower portion of liquid fuel film deposited in the intake channels contributed much to this improvement.

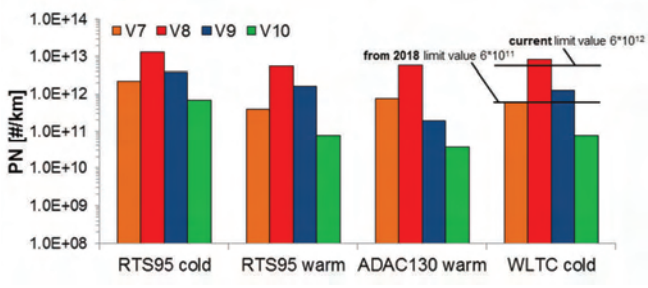

Fig. 13. PN results in all driving cycles

Fig. 14 impressively illustrates the residues on PM-measuring filters of two vehicles in all driving cycles. There is a high carbonaceous part of the particle emission of the high-emitting vehicle ⑧.

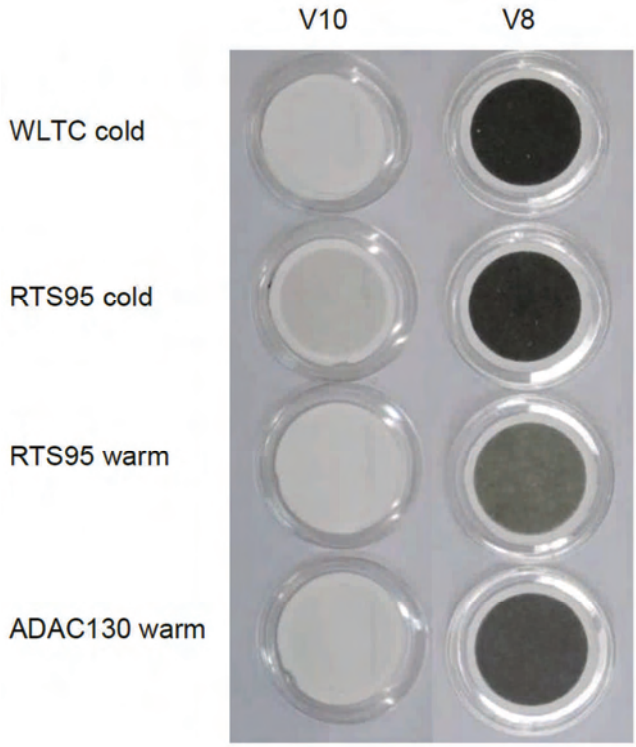

Fig. 14. PM-results of the lowest & highest emitting vehicles in different transient cycles

RTS95, which has higher accelerations, than WLTC, produces with cold start the highest amount of black carbon emission. Comparing all four vehicles in WLTC cold an increase of blackness of the filter residue in the sequence: V10 < V7 < V9 < V8 can be remarked. This is the same sequence, like for the increase of PN-emissions.

7. Conclusions

The most important statements of this work can be summarized as follows:

– The PN-emission level of the investigated GDI cars in WLTC without GPF is in the same range of magnitude and very near to the actual limit value of 6.0×10^{12} 1/km.
– With the GPF's with better filtration quality it is possible to lower the emissions below the future limit value of 6.0×10^{11} 1/km.
– The filtration efficiency of GPF can attain 99% but it can also be optimized to lower values – in this respect the requirement of "best available technology for health protection" should be considered.
– The present work demonstrated that the modern SI-vehicles with MPI also emit a considerable amount of PN and PM. In an extreme case the PN-emission was in the range of Diesel car (without DPF).
– The relationships of NP-emissions between different vehicles can vary depending on operating conditions.

– Generally there is a very good accordance of PSD's measured with both systems SMPS and nSMPS in the common size range (10–64 mm).
– For the investigated vehicles with gasoline DI and MPI, there is no increase of PC's in nuclei mode (below 10 nm) at the measured constant speeds, the particle counts below 10 nm are negligible.
– Due to the electronic regulation of the engine the NP-emission of some vehicles (here vehicle ③) are periodically fluctuating. The present paper focuses solely on solid nanoparticle emissions. The tested GDI cars, except of vehicle ③, were with homogenous combustion concept and all of them (GDI & MPI) represented a modern TWC technology. According to that the emissions of gaseous legislated components (CO, HC, NO_x) were very low.

The present research on MPI vehicles, showed some tendencies of significantly increased PN-emissions. With this knowledge and taking into consideration the immense multiplication factor of MPI vehicles worldwide the legal PN-limitations for MPI should be quickly progressed.

The present high filtration quality of Diesel vehicles (DPF) set's high requirements on the filtration quality in the gasoline sector (GPF).

Acknowledgements

The authors want to express their gratitude to the institutions, which financially supported the activities: Swiss Federal Office of Environment, Swiss Federal Office of Energy, Swiss Oil and Swiss Lubes.

For technical discussions, inspirations and help thanks are due to the GasOMeP partners: Dr. Norbert Heeb, EMPA; Prof. Dr. Heinz Burtscher, FHNW and Dr. André Prévot, PSI.

Nomenclature

AFHB	Abgasprüfstelle FH Biel, CH
ASET	aerosol sampling & evaporation tube
BAFU	Bundesamt für Umwelt, (see FOEN)
CLA	chemiluminescent analyzer
CPC	condensation particle counter
CVS	constant volume sampling
DF	dilution factor
DI	direct injection
DMA	differential mobility analyzer
DPF	diesel particle filter
EC	elemental carbon European Community
EGR	exhaust gas recirculation
EMPA	Eidgenössische Material Prüf- und Forschungsanstalt
FHNW	Fachhochschule Nord-West Schweiz
FOEN	Federal Office for Environment
GasOMeP	gasoline organic & metal particles
GDI	gasoline direct injection
GPF	gasoline particle filter
GRPE	EC Groupe Rapporteurs Pollution & Energy
MD	minidiluter
MFS	mass flow sensor
MPI	multipoint port injection
NP	nanoparticles < 999 nm
nSMPS	nano SMPS
OAPC	CH: Ordinance of Air Protection Control
PC	particle counts (integrated)
PM	particle mass
PN	particle numbers
PMP	Particle Measuring Program of the GRPE
PSD	particle size distribution
PSI	Paul Scherrer Institute
SMPS	scanning mobility particle sizer
SSC	steady state cycle
TC	thermoconditioner
TTM	Technik Thermische Maschinen
TWC	three way catalyst
V	vehicle
VERT	verification of emission reduction technologies
WLTC	worldwide light duty test cycle

Bibliography

[1] SGRO, L.A. et al. Investigating the origin of nuclei particles in GDI engine exhausts. *Combustion and Flame.* 2012, **159**(4), 1687-1692.
[2] BURTSCHER, H. Physical characterization of particulate emissions from diesel engines: a review. *Journal of Aerosol Scienc.* 2005, **36**(7), 896-932.
[3] ULRICH, A. WICHSER, A. Analysis of additive metals in fuel and emission aerosols of diesel vehicles with and without particle traps. *Analytical and Bioanalytical Chemistry.* 2003, **377**(1), 71-81.
[4] HU, S. et al. Metals emitted from heavy-duty diesel vehicles equipped with advanced PM and NO_x emission controls. *Atmospheric Environment.* 2009, **43**(18), 2950-2959.
[5] MAYER, A., CZERWINSKI, J.; ULRICH, A.; MOONEY, J.J. Metal-oxide particles in combustion engine exhaust. *SAE Technical Paper.* 2010, 2010-01-0792.
[6] MAYER, A., CZERWINSKI, J., KASPER, M. et al. Metal oxide particle emissions from diesel and petrol engines. *SAE Technical Paper.* 2012, 2012-01-0841.
[7] ULRICH, A. et al. Particle and metal emissions of diesel and gasoline engines are particle filters appropriate measures? *Proceedings of the 16th ETH Conference on Combustion Generated Nanoparticles*. 2012.
[8] BUCHHOLZ, B.A., DIBBLE, R.W., RICH, D., CHENG, A.S. (ed). Quantifying the contribution of lubrication oil carbon to particulate emissions from a diesel engine. *SAE Technical Paper. 2003,* 2003-01-1987.
[9] SONNTAG, D.B., BAILEY, CH.R., FULPER, C.R., BALDAUF, R.W. Contribution of lubricating oil to particulate matter emissions from light-duty gasoline vehicles in Kansas City. *Environment Science & Technology.* 27.02.2012.
[10] HADLER, J., LENSCH-FRANZE, CH., GOHL, M., MINK, T. Emission reduction a solution of lubricant composition,

calibration and mechanical development. *MTZ.* September 2015.
[11] YINHUI, W., RONG, Z., YANHONG, Q. et al. The impact of fuel compositions on the particulate emissions of direct injection gasoline engine. *Fuel.* 2016, **166**, 543-552.
[12] BACH, C. Emissionsvergleich verschiedener Antriebsarten in aktuellen Personenwagen.
Untersuchung der Emissionen von aktuellen Personenwagen mit konventionellen und direkteingespritzten Benzinmotoren, Dieselmotoren mit und ohne Partikelfilter, sowie Erdgasmotoren (Empa Final Report for Novatlantis and Bundesamt für Umwelt BAFU), in Empa Report 2007 (Novatlantis).
[13] BIELACZYC, P., SZCZOTKA, A., WOODBURN, J. An overview of particulate matter emissions from modern light duty vehicles. *Combustion Engines*. 2013, **153**(2), 101-108.
[14] HAN, T.W., MELOCHE, E., KUBSH, J. et al. Impact of ambient temperature on gaseous and particle emissions from a direct injection gasoline vehicle and its implications on particle filtration. *SAE Technical Paper.* 2013, 2013-01-0527.
[15] MATHIS, U., KAEGI, R., MOHR, M., ZENOBI, R. TEM analysis of volatile nanoparticles from particle trap equipped diesel and direct-injection spark-ignition vehicles. *Atmospheric Environment.* 2004, **38**, 4347-4355.
[16] LEE, K.O., SEONG, H., SAKAI, S. et al. Detailed morphological properties of nanoparticles from gasoline direct injection engine combustion of ethanol blends. *SAE Technical Paper.* 2013, 2013-24-0185.
[17] KÖNIGSTEIN, A., FRITZSCHE, J., KETTENRING, K. et al. Alternatives to meet future particle emission standards with a boosted SIDI engine. *24th Aachen Colloquium Automobile and Engine Technology,* Oct. 2015, 1301.
[18] KERN, B., KUNERT, S. The potential of comprehensive emission control for gasoline DI-engines – a comparison of different exhaust system options and an outlook on future requirements. *24th Aachen Colloquium Automobile and Engine Technology,* Oct. 2015, 1267.
[19] CZERWINSKI, J., COMTE, P., HEEB, N., MAYER, A. Experiences from nanoparticle research on four gasoline cars. *SAE Technical Paper.* 2015, 2015-01-1079.
[20] WINKLHOFER, E., HOPFNER, W., KAPUS, P. Euro VI Partikelgrenzwerte – Entwicklungsmethoden für GDI Motoren. AVL List GmbH, Graz, Österreich, *7. Tagung HDT*, Berlin, Dez. 2010.
[21] DYCKMANS, J., ARNDT, S., RAATZ, T. et al. Laseroptische Untersuchungen zur Gemischbildung und Verbrennung in Verbindung mit dem Einsatz von Alkoholen als alternativer Krafstoff bei der Benzindirekteinspritzung. Robert Bosch GmbH, Stuttgart. TU Braunschweig, *7. Tagung HDT*, Berlin, Dez. 2010.

Jan Czerwinski, Dr. Dipl. Ing., – IC-Engines & Exhaust Emissions Laboratory, Bern University of Applied Sciences (BFH-TI), Switzerland.
e-mail: *Jan.Czerwinski@bfh.ch*

Pierre Comte, Dipl. Ing. HTL – IC-Engines & Exhaust Emissions Laboratory, Bern University of Applied Sciences (BFH-TI), Switzerland.
e-mail: *Pierre.Comte@bfh.ch*

Martin Güdel, Bc. Sc. FH – IC-Engines & Exhaust Emissions Laboratory, Bern University of Applied Sciences (BFH-TI), Switzerland.
e-mail: *Martin.Guedel@bfh.ch*

Peter Bonsack, Dipl. Ing. FH – Federal Office for the Environment FOEN, Air Pollution Control and Chemicals Division, Switzerland.
e-mail: *Peter.Bonsack@bafu.admin.ch*

Article citation info:
ROSTEK, E., BABIAK, M. Thermogravimetric analysis in the synthetic engine oil 5W-30. *Combustion Engines*. 2017, **170**(3), 188-192. DOI: 10.19206/CE-2017-332

Ewa ROSTEK
Maciej BABIAK

CE-2017-332

Thermogravimetric analysis in the synthetic engine oil 5W-30

Engine oils undergo oxidative degradation and wears out during service. Hence it is important to characterize ageing of engine oils at different simulated conditions to evaluate the performance of existing oils and also design new formulations. This work focuses on characterizing the thermo-oxidative degradation of synthetic engine oils 5W-30. Thermogravimetric analysis of fresh and degraded oil samples at different temperatures and ageing intervals was performed in STA 449 F3 Jupiter® coupled with the FTIR spectrometer. The temperature regime provided that the samples were heated to the temperature of 600°C at the heating rate of 10 K/min. Gases (nitrogen, argon) were used with flow rates of 60 mL/min. The results, along with discussion, are presented in graphs – TG curves and IR spectrum.

Key words: *synthetic oil, degradation, oxidation, thermogravimetry, differential scanning calorimetry*

1. Introduction

Engine oils are carefully engineered for use in today's sophisticated engines by blending with various additives. Engine oils reduce friction between moving surfaces and also aids in transportation of contaminants and other particles away from moving parts. Oils are prone to thermal and oxidative degradation during service in internal combustion engines as they are exposed to extremely high temperatures (up to ca. 800°C in cylinder walls) and pressures (up to ca. 1000 psi in the bearings) under air environment [6]. The degree of degradation depends on engine conditions, cycle time and duration of its use.

Some of the desirable characteristics of lubricants include reduction of friction, high boiling point, optimum viscosity and thermal stability, corrosion retardation and resistance to oxidation. As engine oils are designed with a mixture of base oil and performance augmented additives such as friction modifiers, antioxidants, dispersants and detergents, and viscosity index improvers [6, 7, 9], it is necessary to understand the thermal stability of engine oils under various operating conditions in order to evaluate the performance of specific additive's package and to design better additive formulations.

Thermo(oxidative) degradation of engine oils in conventional thermogravimetric analyzer (TGA) and differential scanning calorimeter (DSC) are fundamental techniques to evaluate the stability of engine oils under isothermal and dynamic heating conditions [1, 3, 4, 8]. Importantly, the data obtained from this analysis coupled with the standard engine tests gives a better understanding of the stability of the engine oils [2]. Santos et al. [8] evaluated the rheological and thermo-analytical properties of automotive mineral lubricants and found that increasing the temperature of degradation from 150 to 210°C resulted in thixotropic and pseudo-plastic behavior of the oils. The increase in viscosity of the lubricants was found to be due to the polymerization process along with formation of insoluble high molecular weight products.

Thermogravimetric analysis in air resulted in three decomposition steps while only one decomposition step was observed in nitrogen atmosphere. Gamlin et al. [4] studied the effects of viscosity and base oil class of mineral, fully synthetic and semi-synthetic oils on the thermal stability of base oils. The mechanism of base oil degradation was examined using isothermal, non-isothermal and modulated TGA analysis. It was concluded that base oils with higher viscosity within the same category tend to degrade at higher temperatures. The base oils of natural/mineral origin were more resistant to oxidation than semi-synthetic and fully synthetic oils due to naturally occurring antioxidants, which can inhibit the oxidation process.

Oxidation is the primary mechanism by which oil degradation occurs in an engine. The process of oxidation occurs in three stages. The first stage corresponds to the depletion of antioxidant and antiwear additives, followed by oxidative degradation of the base oil [7, 9]. During this stage, the formation of polar organic compounds in oil (such as ketones, alcohols, carboxylic acids and esters) is more pronounced. The final stage corresponds to an increase in viscosity of the oil owing to polymerization.

The recombination of long chain radicals, Aldol and Claisen condensation reactions of carbonyl, carboxylic acid and alcohols that are formed via oxidative degradation in the second stage are the main reactions leading to higher molecular weight molecules [10]. Besides oxidation, during combustion, with the engine running at full load or with improper air/fuel ratios, other reactions that lead to the formation of nitrogen oxides and organic nitrates may occur. Similarly, the presence of sulfur may lead to the formation of SO_x, organic sulfones and sulfoxides via oxidation, and sulfurous acid esters when SO_x reacts with organic compounds present in oil. Therefore, a comprehensive understanding of engine oil ageing in terms of oxidation, nitration and sulfation, along with thermal stability and rheological properties is required.

Apparent activation energy of oxidation of oils is usually evaluated using TGA under dynamic heating rate in presence of air. Isoconversional methods are utilized to evaluate the variation of apparent activation energy of oxidative degradation of oils with conversion [3, 4]. Crnkovic et al. [3] evaluated the oxidative degradation kinetics of Brazilian fuel oils using TGA in presence of air, and the apparent activation energy was correlated to the ignition delay.

2. Materials and methods

Thermogravimetric testing of engine oil was conducted on the Simultaneous Thermal Analyser STA 449 *F3 Jupi-*

ter®, which was coupled with the FTIR spectrometer. In the analyser mentioned above the samples (S and R) were placed symmetrically in identical measuring vessels (Pt/Rh crucibles) in the same furnace whose temperature was regulated according to an assumed temperature regime, regardless of the changes in the properties of the samples during the measurement. The temperature regime provided that the samples were heated to the temperature of 600°C at the heating rate of 10 K/min. Gases (nitrogen, argon) were used with flow rates of 60 mL/min.

Differential scanning calorimetry (DSC) means a technique in which the change of the difference in the heat flow rate to the sample and to the reference sample is analysed while they are subjected to a temperature regime, or a technique where the change of the difference in the heat flow rate to the sample and to the reference material is measured as a function of temperature.

$$\Delta\Phi_{SR} = \Phi_S - \Phi_R \tag{1}$$

where: *S* – sample, *R* – reference sample.

The thermal analyser measured the difference in temperatures between the samples:

$$\Delta T_{SR} = T_S - T_R \tag{2}$$

When the analyser furnace is heated and the system is thermally symmetric, an identical heat flux flows to both samples and their difference in temperature is then zero. If this state of dynamic equilibrium was disturbed by a change in either sample, or if there was thermal asymmetry of the system caused by a difference in the heat capacity of the samples, the DSC measurement showed differences in temperature, $\Delta T_{SR} \neq 0$, in proportion to the differences in the heat fluxes to the sample and to the reference sample, and then

$$\Delta\Phi_{SR} = -k\Delta T_{SR} \tag{3}$$

where: *k* proportionality constant with the nature of the inverse of thermal resistance.

Used as raw materials in experiments was Engine Oil samples – fully synthetic engine oil 5W-30 (Castrol EDGE) for Audi, VW, BMW, Mercedes-Benz, Porsche, Skoda and Seat cars. This oil with Fluid Strenght Technology is most advanced engine oil, engineered with an adaptive strenght ready to perform however the engine and drive demands. Weight of the samples, depending on the experiment, the limits ranged from 20–24 mg.

A majority of the TG experiments were repeated three times, and the standard deviation of Tmax, the temperature corresponding to maximum mass loss rate, as observed in the differential thermogram, was within ±2°C for all the runs.

3. Results and discussion

Synthetic engine oil 5W-30 was degraded between 200 and 500°C. Figures 1–4 depicts the thermograms and differential thermograms of synthetic engine oils. The results of the measurement made with the use of the DSC technique were DSC curves – the dependence of the measured difference in the heat fluxes on time/temperature. The graphs in Fig. 1 present the course of derivatographic curves; the TG curve for fresh full synthetic engine oil are marked in red and the curve for used full synthetic oil are marked with a green.

The graphs in Fig. 2–3 present the DSC curves in a argon and nitrogen atmosphere. And the graph Fig. 4 present DDSC curves for fresh and used full synthetic engine oils in a argon atmosphere.

In the process of thermal decomposition of the full synthetic oils sample in the different atmosphere (nitrogen, argon) the following stages can be isolated:

– evaporation of water with heat absorbed from the system (50.3ºC for the oils sample in a argon atmosphere and 70. ºC for the oils sample in a nitrogen atmosphere),
– two distinct weight loss regimes are evident from the TGA profiles of the engine oils. The first regime is from 180 to 35 °C and the second regime is from 360 to 500°C for all the types of engine oils (fresh and used). Based on mass spectrometric measurements, Lehrle et al. [5] confirmed that in the temperature range of 180 to 350°C, both evaporation of hydrocarbons present in the low end of the molecular weight distribution, and degradation of base oil components occur. The former occurs at temperatures lesser than 250°C, while the onset of degradation occurs in the range of 275–300°C. The second weight loss regime can be attributed to the decomposition of long chain hydrocarbons.
– as fresh synthetic oils contained a lot of oxygenated organics including alcohols, diols, esters, sulfurous acid esters and other oxygenated functional groups, accelerated degradation of the these organics and base oil stock is justified in the temperature range of 275–300°C.
– in many experiments, fresh the oils pyrolyzed completely before 500°C without any formation of residue, while in certain cases less than 4 wt% residue was observed at 500°C.

The graphs in Fig. 2 and 3 present the TGA curves obtained by means of the DSC method. An exothermic effect with an enthalpy of –77.26 J/g (in a argon atmosphere) and –140.9 J/g (in a nitrogen atmosphere) during the first mass loss step which is due to the release of moisture, was observed. For a sample in nitrogen two overlapping exothermic effects with an entire enthalpy of –4.01 J/g and –9.905 J/g occurred during the remaining mass loss steps which reflect the pyrolytic decomposition of oil sample. Second exothermic effect with an enthalpy of –23.56 J/g (in a argon atmosphere) and –16.81 J/g (in a nitrogen atmosphere) was started at 336.7°C and 368.7°C. Gasification reactions starter above 430ºC.

A collection of all detected absorbance a oils sample in a different atmosphere are shown as a 3-dimensional cube in Figure 5. Additionally the TG-signal at the side face of the cube shows the communication between the two software.

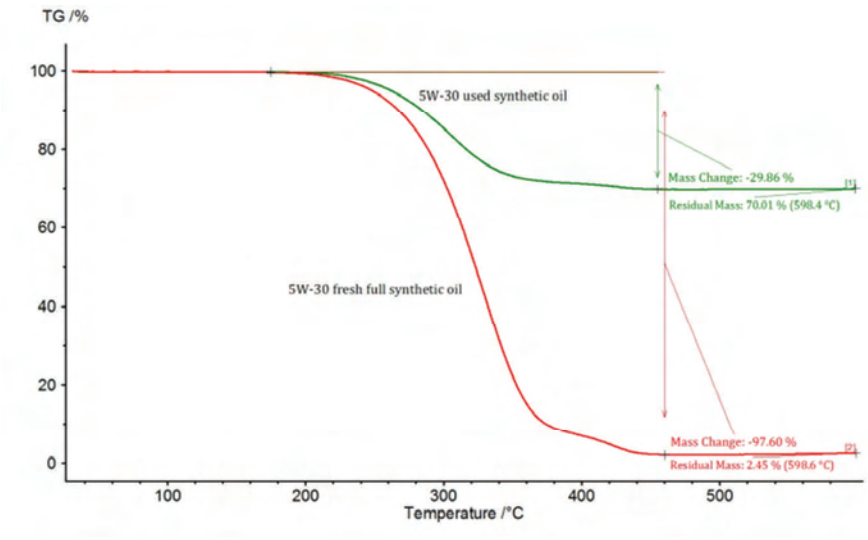

Fig. 1. Thermogravimetric analysis of full synthetic engine oils (fresh and used) conducted in a argon atmosphere

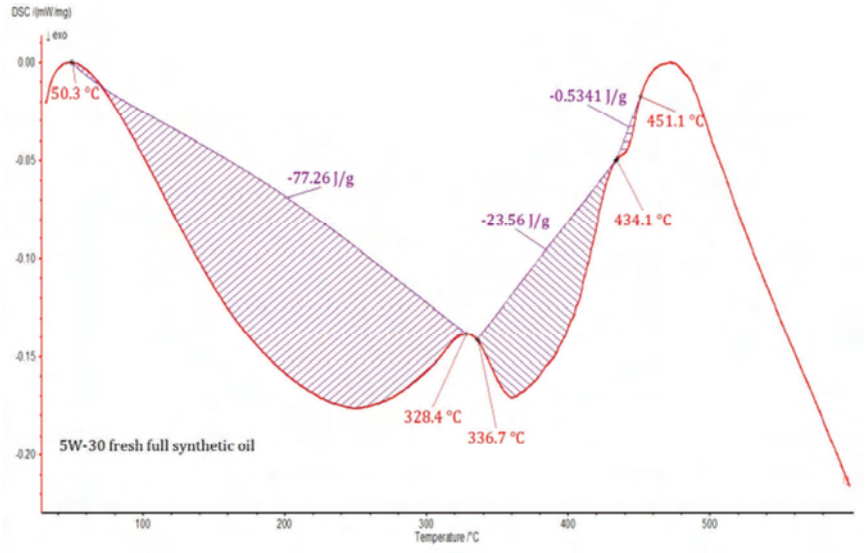

Fig. 2. Thermogravimetric analysis of fresh full synthetic engine oil conducted in a argon atmosphere

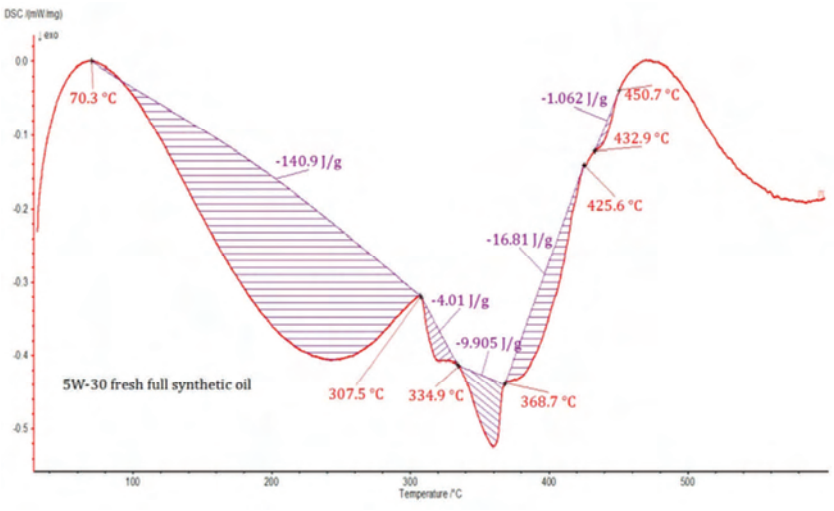

Fig. 3. Thermogravimetric analysis of fresh full synthetic engine oil conducted in a nitrogen atmosphere

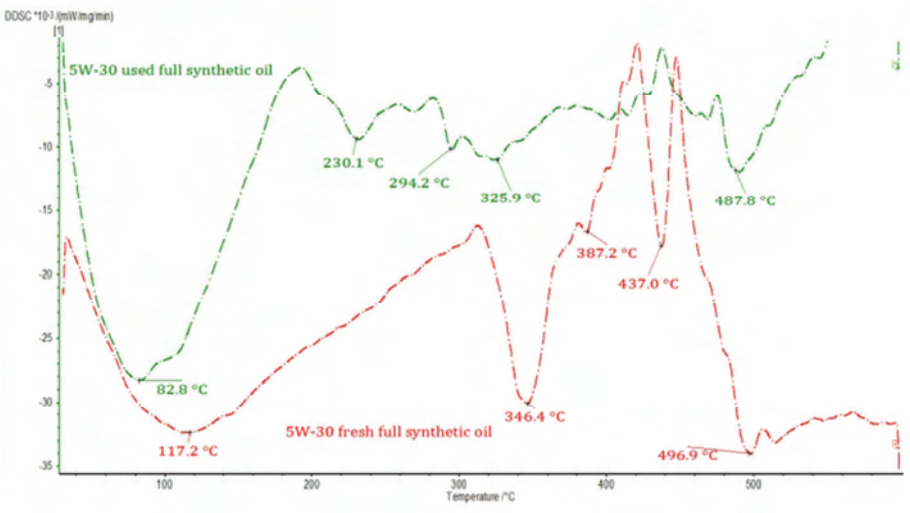

Fig. 4. DDSC curves of fresh and used full synthetic oils conducted ina a argon atmosphere

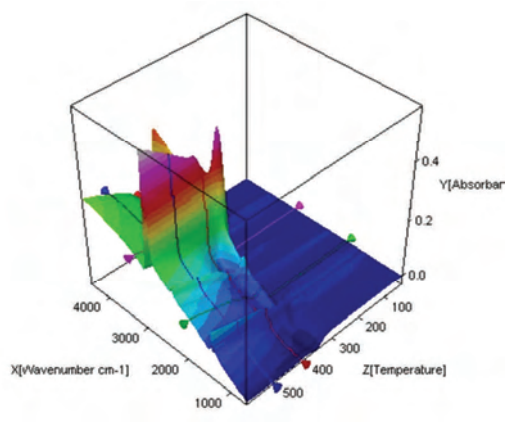

Fig. 5. 3D view of FTIR spectra – wavenumber versus temperature including the TG results at the side face of oils samples conducted in a argon atmosphere

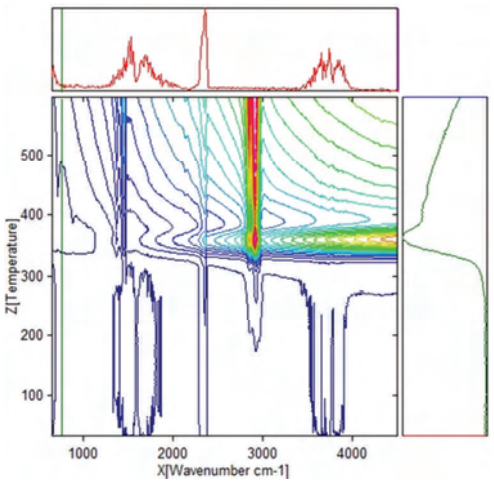

Fig. 6. IR spectrum of the full synthetic engine oil conducted in argon atmosphere

4. Conclusions

In this study, a characterization of oxidative degradation of full synthetic engine oils at different atmosphere. Based on the kinetic analysis of synthetic engine oils degraded at different temperatures, the following conclusions can be drawn:

1. At an oxidation temperature about of 120°C, synthetic oil loses stability in the initial time period, while it gains stability at longer ageing periods.
2. At an ageing temperature of 200°C, both synthetic fresh and used engine oils exhibit similar trends in variation of a E. The oils lose their thermal stability, while the stability is regained at long ageing periods. The gain in stability may be correlated with the decrease in oxidation index of synthetic oil. The increase in viscosity is due to the formation of long chain hydrocarbons.
3. Around 72–96 h, the oils lose their thermal stability, while the stability is regained at long ageing periods. The gain in stability may be correlated with the decrease in oxidation index of synthetic oil after 96 h of ageing and increase in kinematic viscosity of synthetic oil with ageing time. The increase in viscosity is due to the formation of long chain hydrocarbons. The oils rapidly lose their lubricity, as evidenced by the high rate of decrease of viscosity index.
4. The physicochemical characterization of fresh and used engine oils discussed in this work will be useful to develop distributed activation energy models with pseudo components taking part in a multistep mechanism. The apparent activation energies can be used as initial estimates for a more robust semi-mechanistic model of engine oil oxidation.

Nomenclature

DSC	differential scanning calorimetry
DDSC	first derivative DSC
FTIR	Fourier transform infrared spectroscopy
TGA	thermogravimrtric analysis

Bibliography

[1] ADHVARYU, A., PEREZ, J.M., SINGH, I.D. Application of quantitative NMR spectroscopy to oxidation kinetics of base oils using a pressurized differential scanning calorimetry technique. *Energy Fuels*. 1999, **13**, 493-498.

[2] BAKER, A.E. Hand book of lubrication. Theory and practice of tribology. Booser, E.R., Ed.; *CRC press*: Boca Raton, FL, USA, 1983, **1**, 481.

[3] CRNKOVIC, P.M., LEIVA, C.R.M, DOS SANTOS, A.M., MILIOLI, F.E. Kinetic study of the oxidative degradation of Brazilian fuel oils. *Energy Fuels*. 2007, **21,** 3415-3419.

[4] GAMLIN, C.D., DUTTA, N.K., CHOUDHURY, N.R. et al. Evaluation of kinetic parameters of thermal and oxidative decomposition of base oils by conventional, isothermal and modulated TGA, and pressure DSC. *Termochimica Acta.* 2002, **393,** 357-369.

[5] LEHRLE, R.S., DUNCAN, R., LIU, Y. et al. Mass spectrometric methods for assessing the thermal stability of liquid polymers and oils: study of some liquid polyisobutylenes used in the production of crankcase oil additives. *J. Anal. Appl. Pyrol.* 2002, **64,** 207-227.

[6] LISTON, T.V. Engine lubricant additives. What they are and how they function? *Lubr. Eng*. 1992, **48,** 389-397.

[7] MORTIER, R.M., ORSZULIK, S.T. Chemistry and technology of lubricants. *VCH Publisher*: New York, NY, USA, 1992.

[8] SANTOS, J.C.O., DOS SANTOS, I.M.G., SOUZA, A.G. et al. Thermoanalytical and rheological characterization of automotive mineral lubricants after thermal degradation. *Fuel.* 2004, **83,** 2393-2399.

[9] SYED, R. Lubricant additives. A comprehensive review of lubricants chemistry, technology, selection, and design. *ASTM International*: West Conshohocken, PA, USA. 2009.

[10] WOOTON, D. The lubricant's nemesis – oxidation. *Practicing Oil Analysis*. 2007. Available online: www.machinerylubrication.com/Articles/Print/999.

Ewa Rostek, MSc. – Motor Transport Institute in Warsaw.

e-mail: *Ewa.Rostek@its.waw.pl*

Babiak Maciej, DEng. – Faculty of Machines and Transport at Poznan University of Technology.

e-mail: *Maciej.Babiak@put.poznan.pl*

INSTYTUT TECHNICZNY WOJSK LOTNICZYCH

ul. Księcia Bolesława 6, 01-494 Warszawa, skr. poczt. 96
tel.: 261 851 300; tel./faks: 261 851 313
www.itwl.pl e-mail: poczta@itwl.pl

Tomograf komputerowy (CT) – badanie nieniszczące NDT

Instytut Techniczny Wojsk Lotniczych oferuje usługi z zakresu badań tomografem komputerowym. Badania prowadzone są na tomografie typu v/tome/x m 300 firmy GE o max. mocy lampy 300kV/500W. Urządzenie posiada również lampę do nanotomografii o mocy 80kV/15W.

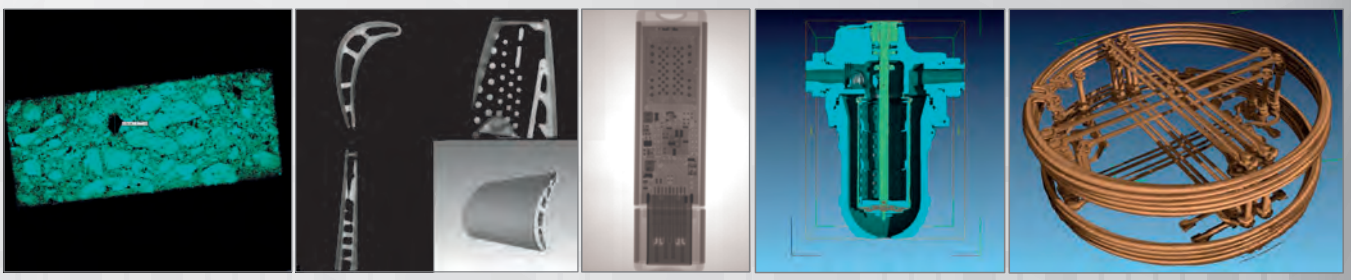

Prowadzimy prace badawcze obejmujące swym zakresem materiały takie jak:

- stopy tytanu
- stale
- materiały kompozytowe
- beton
- guma

Urządzenie umożliwia prowadzenie badań z zakresu:

- wykrywania defektów o rozmiarach powyżej 0,5 µm z wykorzystaniem lampy 180 kV
- materiałów o bardzo dużej gęstości (np. łopatki turbin silników lotniczych) z wykorzystaniem lampy o mocy 300 kV
- układy elektroniczne (scalone)
- materiały pirotechniczne
- złożone agregaty lotnicze

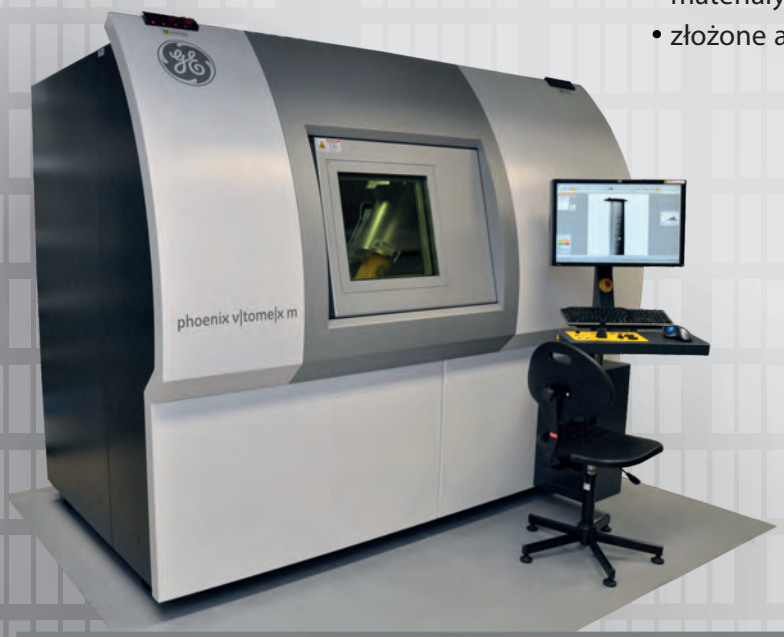

Masa badanych elementów do 50 kg.
Wymiary orientacyjne 50×50×60 cm.

Posiadamy wysoko wykwalifikowany, certyfikowany personel.

Kontakt bezpośredni:
Zakład Silników Lotniczych
tel.: +48 261 851 334; fax: +48 261 851 338
e-mail: jaroslaw.spychala@itwl.pl

Zapraszamy do współpracy!

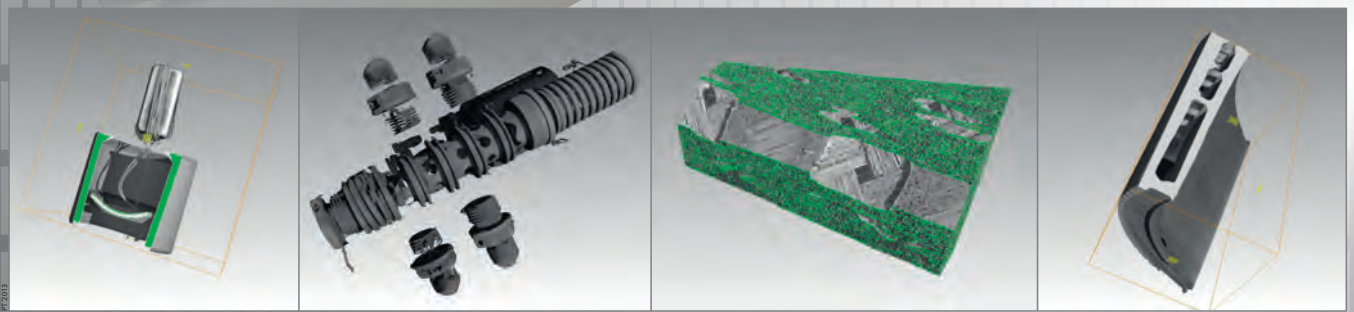

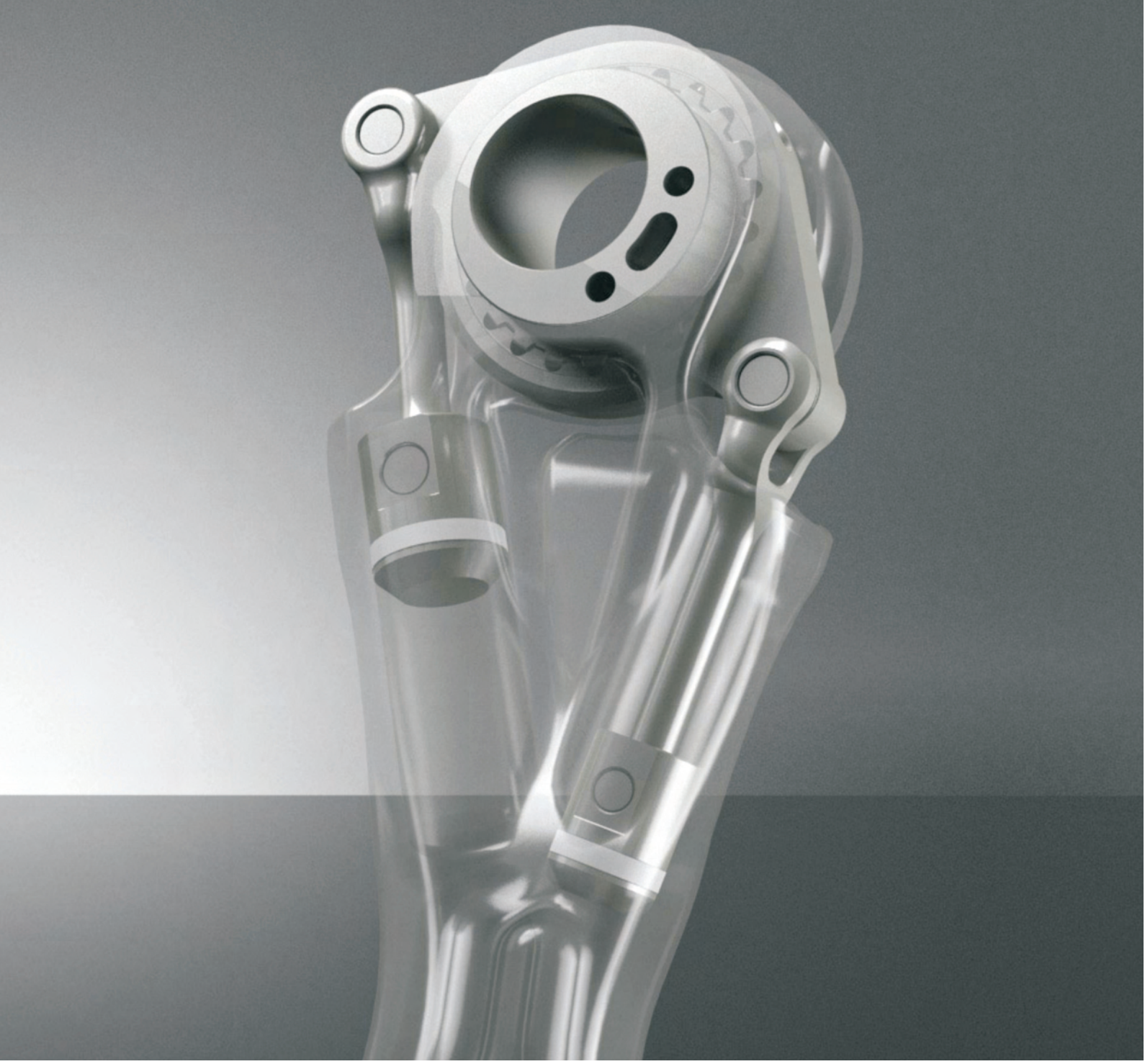

Publisher:

Polish Scientific Society of Combustion Engines

Combustion Engines

Polskie Towarzystwo Naukowe Silników Spalinowych

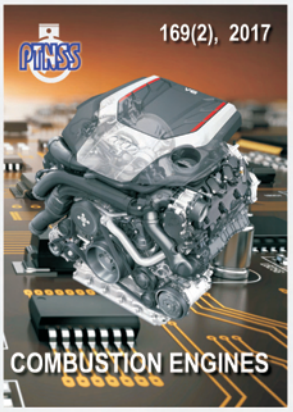

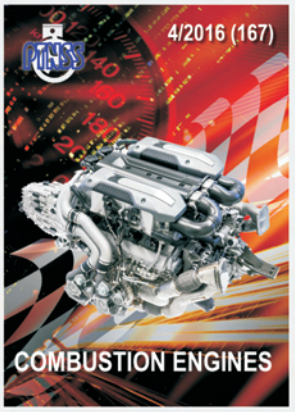

ISSN: 2300-9896

www.combustion-engines.eu